MOLECULAR MECHANISMS AND NEW THERAPEUTIC TARGETS IN EPITHELIAL TO MESENCHYMAL TRANSITION (EMT) AND FIBROSIS, VOLUME II

EDITED BY: Cecilia Battistelli, Marc Diederich, Timothy Joseph Keane, Pilar Sandoval, Sergio Valente and Raffaele Strippoli

PUBLISHED IN: Frontiers in Pharmacology

frontiers Research Topics

frontiers

ISSN 1664-8714
ISBN 978-2-83250-256-3
DOI 10.3389/978-2-83250-256-3

About Frontiers

Frontiers is more than just an open-access publisher of scholarly articles: it is a pioneering approach to the world of academia, radically improving the way scholarly research is managed. The grand vision of Frontiers is a world where all people have an equal opportunity to seek, share and generate knowledge. Frontiers provides immediate and permanent online open access to all its publications, but this alone is not enough to realize our grand goals.

Frontiers Journal Series

The Frontiers Journal Series is a multi-tier and interdisciplinary set of open-access, online journals, promising a paradigm shift from the current review, selection and dissemination processes in academic publishing. All Frontiers journals are driven by researchers for researchers; therefore, they constitute a service to the scholarly community. At the same time, the Frontiers Journal Series operates on a revolutionary invention, the tiered publishing system, initially addressing specific communities of scholars, and gradually climbing up to broader public understanding, thus serving the interests of the lay society, too.

Dedication to Quality

Each Frontiers article is a landmark of the highest quality, thanks to genuinely collaborative interactions between authors and review editors, who include some of the world's best academicians. Research must be certified by peers before entering a stream of knowledge that may eventually reach the public - and shape society; therefore, Frontiers only applies the most rigorous and unbiased reviews.
Frontiers revolutionizes research publishing by freely delivering the most outstanding research, evaluated with no bias from both the academic and social point of view. By applying the most advanced information technologies, Frontiers is catapulting scholarly publishing into a new generation.

What are Frontiers Research Topics?

Frontiers Research Topics are very popular trademarks of the Frontiers Journals Series: they are collections of at least ten articles, all centered on a particular subject. With their unique mix of varied contributions from Original Research to Review Articles, Frontiers Research Topics unify the most influential researchers, the latest key findings and historical advances in a hot research area! Find out more on how to host your own Frontiers Research Topic or contribute to one as an author by contacting the Frontiers Editorial Office: frontiersin.org/about/contact

MOLECULAR MECHANISMS AND NEW THERAPEUTIC TARGETS IN EPITHELIAL TO MESENCHYMAL TRANSITION (EMT) AND FIBROSIS, VOLUME II

Topic Editors:
Cecilia Battistelli, Sapienza University of Rome, Italy
Marc Diederich, Seoul National University, South Korea
Timothy Joseph Keane, Imperial College London, United Kingdom
Pilar Sandoval, Spanish National Research Council (CSIC), Spain
Sergio Valente, Sapienza University of Rome, Italy
Raffaele Strippoli, Sapienza University of Rome, Italy

Citation: Battistelli, C., Diederich, M., Keane, T. J., Sandoval, P., Valente, S., Strippoli, R., eds. (2022). Molecular Mechanisms and New Therapeutic Targets in Epithelial to Mesenchymal Transition (EMT) and Fibrosis, Volume II. Lausanne: Frontiers Media SA. doi: 10.3389/978-2-83250-256-3

Table of Contents

frontiers | Frontiers in Pharmacology

TYPE Editorial
PUBLISHED 06 September 2022
DOI 10.3389/fphar.2022.1008955

OPEN ACCESS

EDITED AND REVIEWED BY
Paola Patrignani,
University of Studies G. d'Annunzio Chieti and Pescara, Italy

*CORRESPONDENCE
Raffaele Strippoli,
raffaele.strippoli@uniroma1.it

SPECIALTY SECTION
This article was submitted to Inflammation Pharmacology, a section of the journal Frontiers in Pharmacology

RECEIVED 01 August 2022
ACCEPTED 15 August 2022
PUBLISHED 06 September 2022

CITATION
Battistelli C, Diederich M, Keane TJ, Sandoval P, Valente S and Strippoli R (2022), Editorial: Molecular mechanisms and new therapeutic targets in epithelial to mesenchymal transition (EMT) and fibrosis, volume II.
Front. Pharmacol. 13:1008955.
doi: 10.3389/fphar.2022.1008955

Editorial: Molecular mechanisms and new therapeutic targets in epithelial to mesenchymal transition (EMT) and fibrosis, volume II

Cecilia Battistelli[1], Marc Diederich[2], Timothy Joseph Keane[3], Pilar Sandoval[4], Sergio Valente[5] and Raffaele Strippoli[1,6]*

[1]Department of Molecular Medicine, Sapienza University of Rome, Rome, Italy, [2]Department of Pharmacy, College of Pharmacy, Seoul National University, Seoul, South Korea, [3]Department of Materials, Imperial College London, London, United Kingdom, [4]Severo Ochoa Molecular Biology Center (CSIC-UAM), Madrid, Spain, [5]Department of Chemistry and Technologies of Drugs, Sapienza University of Rome, Rome, Italy, [6]Istituto Nazionale per le Malattie Infettive Lazzaro Spallanzani (IRCCS), Rome, Italy

KEYWORDS

EMT, epigenetics, fibrosis, natural compound, non-coding RNAs, therapeutic targets

Editorial on the Research Topic
Molecular mechanisms and new therapeutic targets in epithelial to mesenchymal transition (EMT) and fibrosis, volume II

The induction of inflammatory epithelial-mesenchymal transition (EMT)/fibrosis requires a complex cellular reprogramming process involving epithelial, stromal, and immune cells and has important implications on cell survival, plasticity, and migratory/invasive abilities.

A wide array of extracellular stimuli, including soluble mediators, cell-to-cell interactions, and binding to the extracellular matrix (ECM), drive changes in resident cells towards a mesenchymal-like/profibrotic phenotype.

The classical EMT/fibrosis pathways induced by transforming growth factor (TGF)-β, the central profibrotic mediator, as well as by tumor necrosis factor (TNF)α and epidermal growth factor (EGF) are well known. Here we focused on the roles of new intracellular mechanisms involved in the modulation of EMT/fibrosis. Moreover, a better understanding of the crosstalk between classical EMT/fibrosis pathways and stress signaling pathways, such as autophagy and unfolded protein response (UPR) become increasingly important in the field.

Epigenetic processes, including histone acetylation and DNA/histone methylation, were shown to be essential modulators of the persistence of a new mesenchymal-like state or the reversion to an epithelial-like phenotype. Recent single-cell RNA-sequencing (scRNA-seq) experiments revealed that EMT transition is a transcriptional continuum of

numerous epithelial-mesenchymal states rather than a binary epithelial vs. mesenchymal model. These recent insights considerably enhanced the understanding of the complexity and cell-specificity of this essential physio-pathological process.

However, despite considerable efforts in the field, new mechanisms remain to be elucidated, and cell-type specificities have yet to be fully characterized.

In this Research Topic, Sara Lovisa provided an updated overview of the recent debate on the definition of EMT, analyzing the impact of new technologies such as single cell transcriptomics. Moreover, the author summarized the different strategies used to define EMT in fibrotic disorders.

Brasier et al. analyzed the mechanisms leading to changes in pulmonary cell plasticity induced by aeroallergens and respiratory viruses, leading to pathological airway remodeling. In particular, the authors elucidated the complex interplay between the hexosamine pathway, UPR, the inflammatory inhibitor of IκB kinase (IKK)-nuclear factor (NF)-κB pathway, and the regulation of epigenetic changes mediated by the recruitment of bromodomain-containing protein (BRD)4.

Li et al. used an experimental model of murine silicosis to study the capacity of metformin, a biguanide antidiabetic drug against type 2 diabetes, to attenuate lung fibrosis. The authors also co-cultured human macrophages and human bronchial epithelial cells treated with silica particles and metformin. Mechanistically, the manuscript elucidates the effect of metformin on autophagy regulated by the AMP-activated protein kinase (AMPK) - mammalian target of rapamycin (mTOR) pathway, leading to reduced silica particle-induced fibrosis.

Liu et al. investigated the importance of autophagy in murine peritoneal fibrosis (PF). Autophagy inhibitor 3-methyl adenine (3-MA) alleviated PF by inhibiting EMT. The authors observed the activation of multiple EMT-related pathways such as TGF-β/mothers against decapentaplegic homolog (SMAD)3, epidermal growth factor receptor (EGFR)/extracellular regulated kinase (ERK)1/2, and transcription factors signal transducer and activator of transcription (STAT)3 and NF-κB. Moreover, inhibition of autophagy attenuated peritoneal angiogenesis in the injured peritoneum.

This Research Topic describes different pharmacological approaches to preventing PF. Kopytina et al. focused on peritoneal dialysis (PD) fluid biocompatibility in the genesis of PF. The choice of PD fluid can lead to fibrosis, and PF represents the main cause of PD discontinuation in patients with end-stage kidney disease. Kopytina et al. analyzed steviol glycoside (SG)-based fluids compared to high and low glucose-based dialytic fluids. SG-based PD fluids increased biocompatibility and reduced induction of mesothelial to mesenchymal transition (MMT), a mesothelium-specific form of EMT.

Xie et al. analyzed the protective role of the hormonal peptides ELABELA (ELA) and aplin in MMT. ELA is a polypeptide hormone secreted by the vascular endothelium and the kidneys. Aplin is another hormone known to have a protective effect on organ fibrosis. Both hormones were modulated in patients exposed to PD fluids.

Treatment with the active proprotein of 32 amino acids, ELA-32, reversed the TGF-β1-induced reduction of the epithelial cell markers and suppressed the expression of mesenchymal cell markers by inhibiting the phosphorylation of SMAD2/3, ERK1/2, and protein kinase B (AKT).

Liu et al. analyzed the role of histone deacetylase (HDAC)-6 in MMT. The authors describe that the HDAC6 inhibitor tubastatin or genetic silencing of HDAC6 maintained the expression of E-cadherin but suppressed mesenchymal gene expression. Accordingly, HDAC6 inhibition maintained the epithelial/mesothelial phenotype in mesothelial cells treated with interleukin (IL)-6. Mechanistically, tubastatin suppressed the expression of TGF-β receptor I (TGFβRI), the phosphorylation of SMAD3, and the activation of Janus kinase (JAK)2 and STAT3.

Another non-tumor fibrosis model studied in this Research Topic is kidney fibrosis. Kidney fibrosis results from a wide array of inflammatory insults implicating both stromal and immune responses.

Zhang et al. analyzed the effect of a combination of mycophenolate and rapamycin (MR) on kidney fibrosis in a murine lupus nephritis experimental system. Mycophenolate is an immunosuppressant drug, whereas rapamycin is a known mTOR inhibitor. The authors found that the combination of these drugs at reduced doses resulted in reduced glomerular sclerosis and tubular atrophy, amelioration of kidney dysfunction, and improved survival. MR treatment reduced the expression of TGF-β1, IL-6, α-smooth muscle actin (α-SMA), fibronectin, and collagen I and III.

Martinez-Salgado et al. analyzed the role of activin receptor-like kinase 1 (ALK1) in tissue fibrosis and angiogenesis in a murine model of unilateral ureteral obstruction (UUO). Through a heterozygous mouse experimental system, ALK1 was demonstrated to promote vascular rarefaction and maturation and the emergence of myofibroblasts of vascular origin.

He et al. focused on the physiopathology of tubular epithelial cells (TECs). These cells play a role in kidney fibrosis undergoing partial EMT (pEMT), characterized by co-expression of both epithelial and mesenchymal markers and production of extracellular mediators favoring fibrogenesis in the interstitium. The authors discussed how wingless-related integration site (Wnt)/β-catenin inhibition by natural compounds, specific inhibitors, or genetic intervention might attenuate tubular EMT and fibrosis.

Systemic sclerosis (SSc) is a multi-system rheumatic disease characterized by vascular dysfunction, autoimmune abnormalities, and progressive organ fibrosis.

Dai et al. summarized the current knowledge regarding immune and stromal cells in SSc patients discussing their

potential roles in SSc pathogenesis and focusing on recent advances in identifying new cellular subtypes by scRNA-seq.

Overall, more profound knowledge of physio-pathological mechanisms controlling EMT dynamics and the validation of new pharmacological approaches will help develop future regenerative medicine strategies to improve the personalized control of EMT and fibrotic responses in specific and localized manners.

Author contributions

All authors listed have made a substantial, direct, and intellectual contribution to the work and approved it for publication.

Conflict of interest

The authors declare that the research was conducted in the absence of any commercial or financial relationships that could be construed as a potential conflict of interest.

Publisher's note

frontiers in Pharmacology

ORIGINAL RESEARCH
published: 09 August 2021
doi: 10.3389/fphar.2021.719589

Metformin Attenuates Silica-Induced Pulmonary Fibrosis by Activating Autophagy *via* the AMPK-mTOR Signaling Pathway

Shu-xian Li[1†], Chao Li[1†], Xin-ru Pang[1†], Juan Zhang[1], Gong-chang Yu[2], Abrey J. Yeo[3], Martin F. Lavin[3], Hua Shao[1], Qiang Jia[1]* and Cheng Peng[4]**

[1]Shandong Academy of Occupational Health and Occupational Medicine, Shandong First Medical University and Shandong Academy of Medical Sciences, Jinan, China, [2]Neck-Shoulder and Lumbocrural Pain Hospital of Shandong First Medical University, Shandong First Medical University and Shandong Academy of Medical Sciences, Jinan, China, [3]University of Queensland Centre for Clinical Research (UQCCR), Brisbane, QLD, Australia, [4]Queensland Alliance for Environmental Health Sciences (QAEHS), The University of Queensland, Brisbane, QLD, Australia

OPEN ACCESS

Edited by:
Raffaele Strippoli, Sapienza University of Rome, Italy

Reviewed by:
Hany Hamdy A. Arab, Cairo University, Egypt
Marco Cordani, IMDEA Nanociencia, Spain

***Correspondence:**
Gong-chang Yu
yugongchang@sdfmu.edu.cn
Qiang Jia
jiaqiang5632@163.com
Cheng Peng
c.peng@uq.edu.au

[†]These authors have contributed equally to this work and share first authorship

Specialty section:
This article was submitted to Experimental Pharmacology and Drug Discovery, a section of the journal Frontiers in Pharmacology

Received: *02 June 2021*
Accepted: *26 July 2021*
Published: *09 August 2021*

Citation:
Li S, Li C, Pang X, Zhang J, Yu G, Yeo AJ, Lavin MF, Shao H, Jia Q and Peng C (2021) Metformin Attenuates Silica-Induced Pulmonary Fibrosis by Activating Autophagy via the AMPK-mTOR Signaling Pathway. Front. Pharmacol. 12:719589. doi: 10.3389/fphar.2021.719589

Long-term exposure to crystalline silica particles leads to silicosis characterized by persistent inflammation and progressive fibrosis in the lung. So far, there is no specific treatment to cure the disease other than supportive care. In this study, we examined the effects of metformin, a prescribed drug for type || diabetes on silicosis and explored the possible mechanisms in an established rat silicosis model *in vivo*, and an *in vitro* co-cultured model containing human macrophages cells (THP-1) and human bronchial epithelial cells (HBEC). Our results showed that metformin significantly alleviated the inflammation and fibrosis of lung tissues of rats exposed to silica particles. Metformin significantly reduced silica particle-induced inflammatory cytokines including transforming growth factor-β1 (TGF-β1), tumor necrosis factor-α (TNF-α) and interleukin-1β (IL-1β) in rat lung tissue and HBEC culture supernatant. The protein levels of Vimentin and α-smooth muscle actin (α-SMA) were significantly decreased by metfomin while expression level of E-cadherin (E-Cad) increased. Besides, metformin increased the expression levels of phosphorylated adenosine 5′-monophosphate (AMP)-activated protein kinase (p-AMPK), microtubule-associated protein (MAP) light chain 3B (LC3B) and Beclin1 proteins, and reduced levels of phosphorylated mammalian target of rapamycin (p-mTOR) and p62 proteins *in vivo* and *in vitro*. These results suggest that metformin could inhibit silica-induced pulmonary fibrosis by activating autophagy through the AMPK-mTOR pathway.

Keywords: silica, metformin, pulmonary fibrosis, AMPK-mTOR, autophagy

INTRODUCTION

Silicosis is an important occupational disease and characterized by persistent lung inflammation and progressive fibrosis, which may eventually cause respiratory failure (Sayan and Mossman, 2016; Li et al., 2017). Inhaled silica particles can cause injury of lung macrophages and epithelial cells triggering an inflammatory response. Inflammation is a critical a pathogenic process of silicosis. Repeated inflammatory reactions lead to the recruitment and accumulation of inflammatory cells which secrete high levels of proinflammatory and profibrotic cytokines, such as transforming growth factor-β1 (TGF-β1), tumor necrosis factor-α (TNF-α) and interleukin-1β (IL-1β) (Fujimura, 2000;

Dong and Ma, 2016). Higher level of cytokines further induces epithelial-mesenchymal transition (EMT), a process in which epithelial cells gradually lose their epithelial characteristics and acquire the mesenchymal phenotype, such as down-regulation of E-cadherin (E-Cad) and up-regulation of Vimentin. EMT is one of the important driving forces behind fibrosis through promoting the abnormal deposition of extracellular matrix (ECM) and consequent tissue remodeling and fibrotic scarring (Camara and Jarai, 2010; Stone et al., 2016; Rout-Pitt et al., 2018; Sun et al., 2019).

Autophagy is a vital regeneration process to maintain the balance of the intracellular environment through cleaning the own damaged cellular components and participating in cell proliferation and apoptosis (Mizushima et al., 2011). Autophagy has been found to play a vital role in myocardial, skin, liver, and renal fibrosis, especially in lung fibrosis (Chen S. et al., 2015). Recent studies suggested that autophagy can reduce the expression of fibrogenic factors and inhibit the deposition of collagen in fibroblasts (Hernandez-Gea et al., 2012). In addition, autophagy alleviates the silica-induced pulmonary fibrosis by decreasing apoptosis of alveolar epithelial cells in silicosis (Chen S. et al., 2015).

Autophagy and mitochondrial homeostasis are modulated by AMP-activated protein kinase (AMPK) which is a serine/threonine-protein kinase. It has been found that the AMPK signaling pathway coordinates the induction of autophagy by inhibiting mammalian target of rapamycin (mTOR) (Mihaylova and Shaw, 2011). AMPK inhibits mTORC1-dependent ULK activity by phosphorylating S317 and S777, leading to the activation of autophagy (Lawrence and Nho, 2018) and suppressing mTORC1 *via* its phosphorylation activates autophagy indirectly (Tavakol et al., 2019).

AMPK has been recognized as a cellular bioenergy sensor and metabolic regulator on the various metabolic stresses (Ha et al., 2015; Herzig and Shaw, 2018; Rangarajan et al., 2018). AMPK has been found to be a pivotal molecule that modulate the fibrogenesis by inhibiting inflammatory injury, ECM secretion, and the induction of effector cells (Jiang et al., 2017).

Drug repurposing or repositioning for different common and rare diseases is an efficient way for drug discovery because of low cost in drug development by avoiding clinical trials and de-risked compounds (Pushpakom et al., 2019). Metformin is a common biguanide antidiabetic drug for type 2 diabetes treatment. Mechanistically, metformin elicits pleiotropic effects mainly *via* activating AMPK (Tsaknis et al., 2012; Sato et al., 2016). Evidence has shown that metformin has anti-inflammatory effects and anti-fibrosis effects. Metformin has been found to be able to inhibit cardiac fibrosis induced by pressure overload *in vivo* and reduce collagen synthesis in cardiac fibrosis probably *via* inhibition of the TGF-β/Smad3 signaling pathway (Xiao et al., 2010). Moreover, metformin prevents airway remodeling in a mouse model of bronchial asthma, indicating its potential anti-fibrotic properties (Park et al., 2012). A recent study found that metformin can effectively reverse bleomycin-induced pulmonary fibrosis, suggesting that metformin has effects on idiopathic pulmonary interstitial fibrosis (Gamad et al., 2018). Since silicosis is characterized mainly by pulmonary fibrosis, we speculated that metformin may have therapeutic effects on this disease.

In this study, we explored the effects of metformin on the silicosis for which we established the rat silicosis model as well as an *in vitro* co-culture system harboring a human macrophages cells and human bronchial epithelial cells treated the with silica particles and metformin. We then investigated the pathological changes in silicosis rat and cell co-cultured model with and without metformin treatment and examined the inflammatory responses, EMT and particularly the autophagy pathways using ELISA and Western blotting. Results showed that metformin regulates autophagy through the AMPK-mTOR pathway to reduce silica particle-induced fibrosis.

METHODS AND MATERIAL

Reagents and Antibodies

Silica particles (0.5–10 μm) were purchased from Sigma Aldrich (S5631, Shanghai, China). Standard suspensions of 50 mg/ml silica particles were prepared in 0.9% normal saline and autoclaved at 120°C for 2 h. Metformin was purchased from Sino-US Shanghai Squibb Pharmaceutical Co., Ltd. (Shanghai, China), and dissolved in 0.9% physiological saline by gavage. RIPA buffer, PMSF, BCA Protein Assay kit and Ad-GFP-LC3B were purchased from Beyotime Biotechnology (C3006, Shanghai, China). Compond C was purchased from Selleck Chemicals (S7840, Houston, United States). Goat anti-rabbit IgG H&L (Alexa Fluor® 488) and Goat anti-mouse IgG H&L (Alexa Fluor® 594) and primary antibodies α-SMA (ab32575), Beclin1 (ab207612) were purchased from Abcam (Cambridge, United Kingdom), E-cadherin (14472), Vimentin (5741S), LC3B (3868), mTOR (2983S), p-mTOR (2971S), AMPK (5831S), p-AMPK (50081S) were purchased from CST (Beverly, MA, United States). IRDye 680RD Goat anti rabbit (926-68071) and IRDye 800RD Goat anti Mouse (926-32210) secondary antibodies were purchased from Li-COR (Nebraska, United States).

In Vivo Experiment

Animals and Teatment

Forty-eight male Wistar rats (200–220 g, 6–8 weeks old) were purchased from Jinan Pengyue Experimental Animal Breeding Co., Ltd. (Jinan, China). All animals were housed under specific pathogen-free (SPF) conditions with free access to water and food. The ethical committee of Shandong Academy of Occupational Health and Occupational Medicine and the Frist Medical University approved the use of the experimental animals. The animal care and experimental protocol was approved by the ethical committee of Shandong Academy of Occupational Health and Occupational Medicine and Shandong First Medical University. Rats were randomly divided into six groups with eight rats in each, maintained under 12:12 h light-dark conditions at 23 ± 2°C and relative humidity 40–70%. Appropriate measures were taken using pain management protocol to reduce pain in animals, and the relief of pain and distress received careful attention during the experiment.

Based on reported toxicity of metformin in rats (Quaile et al., 2010) and a previous study (Gamad et al., 2018), all rats were randomly divided into six groups with eight rats in each including: negative control group, metformin control group (400 mg/kg/day), silica modal group and three metformin treatment groups (100, 200, 400 mg/kg/day). The μm-sized silica particles were prepared with normal saline as a 50 mg/ml silica suspension. The silica model group and three metformin treatment groups were injected with 1 ml (50 mg/kg) silica suspension into the lung once using a non-exposed tracheal intubation, and the rats in the negative control group and metformin control group were injected with the same volume of normal saline solution. In our previous studies, we found the treatment regime with dosage of silica particle at 50 mg/kg for 28 days yields clear manifestation of silicosis in rats (Sai et al., 2019; Pang et al., 2021). After being exposed to silica for 28 days, the rats in three metformin treatment groups were given a daily intragastric administration of 100, 200, 400 mg/kg metformin and metformin control group were given a daily intragastric administration of 400 mg/kg metformin for another 28 days. The rats in the negative control and silica model groups were treated with saline only. After treatment with metformin for 28 days, all the rats in each group were euthanized with an overdose of 150 mg/kg sodium pentobarbital (Merck and Co., Inc.) *via* intraperitoneal injection, and death in all rats was *via* observation of the cessation of respiration and palpation of the heartbeat. The lungs of each rat were harvested and used for the animal experiment (**Supplementary Figure S1A**).

Histopathological Observation

The lung tissues of rats in each group were isolated and fixed by 4% formaldehyde embedded in paraffin followed by dehydration, embedding in paraffin, and slicing onto 5 μm thick sections. Then the slides were stained with Hematoxylin and Eosin (H&E) and Masson trichrome. The pathological changes were observed under an optical microscope to examine the inflammatory infiltration, the integrity of the alveolar structure and collagen deposition under an optical microscope. The degree of alveolitis and pulmonary fibrosis was evaluated according to the scoring system outlined in Szapiel et al. (1979). Alveolitis was graded using the following criteria: None (0), no alveolitis; mild (1+), thickening of the alveolar septum by a mononuclear cell infiltrate; moderate (2+), a more widespread alveolitis; severe (3+), a diffuse alveolitis. The extent of fibrosis was graded using the following criteria: none (0), no fibrosis; mild (1+), focal regions of fibrosis, alveolar architecture has some distortion; moderate (2+), more extensive fibrosis and fibrotic still focal; severe (3+), widespread fibrosis, confluent lesions with extensive derangement of parenchymal architecture.

Immunohistochemistry of Lung Tissue

The lung tissue sections were deparaffinized, and antigen retrieved using citrate buffer solution. The sections were incubated with 3% H_2O_2 for 20 min at room temperature to eliminate endogenous peroxidase activity. After blocked with 3% BSA for 30 min, tissue sections were incubated with primary antibodies specific to E-Cad, α-SMA, Vimentin and LC3 overnight at 4°C, followed by incubation with horseradish peroxidase (HRP) labeled secondary antibody for 1 h at room temperature. After using a DAB kit for color development, the sections were counterstained with hematoxylin for 3 min, the image was observed by a fluorescence microscope (Olympus Co., Tokyo, Japan). The staining results were analyzed by Image-Pro Plus software. Integrated optical density summation (IOD SUM) of Vimentin, E-Cad, α-SMA and LC3 protein were measured by Image-Pro Plus software.

Enzyme-Linked Immunosorbent Assay

The homogenate samples of rat lung tissue in each group were centrifuged at 9,000 g at 4°C for 20 min. The supernatant samples were analyzed for the concentrations of TGF-β1 (ER10-96), TNF-α (ER02-96) and IL-1β (ER01-96) (Biokits Technologies Inc., Beijing, China) using rat ELISA assay kits following manufacturer's instructions. And the total protein concentration determined were standardized using the Coomassie blue staining kit (Nanjing Institute of Biological Engineering, Nanjing, China). The absorbance was measured at 450 and 570 nm using a spectrophotometer. The results were expressed in pg/mg protein.

Western Blot Analysis

Total protein was extracted by homogenization in ice-cold RIPA buffer with 1 mM PMSF. Homogenates were centrifuged for 15 min at 12,000 g. Protein concentrations in the supernatants were calculated using a BCA Protein Assay kit. The protein extracted was separated by SDS-PAGE and then electrotransferred to PVDF membrane (Merck KGaA, Darmstadt, Germany). The membranes were initially blocked with 5% non-fat dry milk in phosphate-buffered solution (PBS) for 1 h, and subsequently incubated with primary antibody against, including α-SMA (1:1,000), E-Cad (1:1,000), Vimentin (1:1,000), Beclin1(1:1,000), LC3B (1:1,000), mTOR (1:1,000), p-mTOR (1:1,000), AMPK (1:1,000), p-AMPK (1:1,000) incubated overnight at 4°C. Blots were washed for three times with Tris-Buffered Saline and 0.1% Tween 20 (TBST) and followed by IRDye 680RD (1:5,000) and IRDye 800RD (1:5,000) secondary antibodies for 1 h at room temperature. Finally, the densities were scanned by Li-Cor and quantified using the Image Studio Software.

In Vitro Experiment

Cell Culture

The bronchial epithelial cell line HBEC was presented by the Centre for Clinical Research of Queensland, Australia. And the THP-1 cell line was obtained from the American Type Culture Collection (ATCC) (Manassas, VA, United States), and were maintained at 37°C with 5% CO_2. The HBEC was cultured in PneumaCult-ExPlus Medium (05401, Stemcell Technologies, Canada) supplemented 1% Antibiotic-Antimycotic (Gibco, United States) and 0.1% Hydrocortisone Stock Solution (Stemcell Technologies, Canada). The THP-1 cell was cultured in RPMI 1640 (Gibco, United States) supplemented 10% FBS (BI, Israel) and 1% Antibiotic-Antimycotic.

Cell Counting Kit-8 Assay

4×10^3/well HBEC were seeded in 96-well plates and incubated overnight, and the medium was changed to the presence of

various doses of metformin (0, 0.1, 0.25, 0.5, 1, 2, 5, 10 mM) at various time points (24, 48, and 72 h). The selection of treatment concentrations was based previous studies (Wang et al., 2015; Mishra and Dingli, 2019). Cell viability was measured using the CCK-8 assay kits (CK04, Dojindo Laboratories, Kyushu, Japan) in accordance with the manufacturer's instructions. The absorbance at 450 nm was measured using a microplate reader.

THP-1 Differentiation and Co-Culture

THP-1 cells (1×10^6/well) were plated in transwell inserts (Corning, Lowell, United States) with a membrane pore size of 4 μm and were treated with 100 ng/ml phorbol 12-myristate 13-acetate (PMA, Sigma, MO, United States) for 72 h to differentiate into macrophage-like forms. HBEC (4×10^4/well) were cultured alone at the bottom of 6-well plate for 2 days. Then, the cell culture inserts containing THP-1 macrophages were transferred to the plates containing HBEC. To confirm if the metformin regulates the EMT process of HBECs by AMPK-dependent activation of autophagy, we added metformin and compound C (CC) an AMPK Inhibitor. The experiment was divided into six groups: control group (Control), metformin control group (Met), silica group (Silica), silica and metformin intervention group (Silica + Met), silica and CC intervention group (Silica + CC) and silica, metformin and CC intervention group (Silica + Met + CC).

With macrophages differentiated from THP-1 cells already seeded, 100 μg/ml of silica solution was introduced into the insert in the silica particle group, silica and metformin group, silica and CC group and silica, metformin and compound C group. Meanwhile, in the metformin control group and silica and metformin intervention group, 0.5 mM metformin solution was added to the bottom, silica and CC group was added 1 μM CC, metformin and CC group was added 0.5 mM metformin and 1 μM CC. The control group had no intervention. Each sample was cultured in duplicate, and each co-culture experiment was repeated 3 times (**Supplementary Figure S1B**).

Immunofluorescence Staining

Cell slides were placed in the culture chamber. After 72 h of co-culture treatment, the HBEC were washed three times with phosphate-buffered saline (PBS), fixed with 4% paraformaldehyde, and then blocked with blocking buffer (P0260, Beyotime biotechnology, Shanghai, China) for 1 h at room temperature. The cells were then incubated with E-Cad, Vimentin and α-SMA at a dilution of 1:200 overnight at 4°C, followed by incubation with secondary antibodies (1:500) for 1 h at room temperature. 4′,6-diamidino-2-phenylindole (DAPI) was used for nuclear staining. Finally, cells were observed and photographed by a fluorescence microscope (Olympus, Tokyo, Japan). The mean fluorescence was detected by the ImageJ software.

Enzyme-Linked Immunosorbent Assay

After receiving the indicated interventions for 72 h, the levels of TGF-β1 (EH03-96), TNF-α (EH02-96) and IL-1β (EH18-96, Biokits Technologies Inc., Beijing, China) in the cell supernatant of HBEC in each group were determined using ELISA as per the manufacturer's instructions. Then the total protein concentration was determined and standardized using the Coomassie blue staining kit (Nanjing Institute of Biological Engineering, Nanjing, China). The absorbance was measured at 450 and 570 nm using a spectrophotometer. The results were expressed in pg/mg protein.

Ad-GFP-LC3 Transfection

HBECs (4×10^4/well) were cultured alone at the bottom of 6-well plate for 24 h. After a wash with fresh culture medium, cells were transfected with Ad-GFP-LC3 adenovirus at a MOI of 100 in 2 ml culture medium for 48 h at 37°C. And after 72 h intervention by co-culture system, HBEC cells were observed and photographed by a fluorescence microscope.

Western Blotting Analysis

After the cell co-culturing, HBEC were washed with cold phosphate-buffered saline (PBS). The proteins were extracted using RIPA buffer with 1 mM PMSF. Protein concentrations were calculated using a BCA Protein Assay kit. Samples containing equivalent amounts of lysate protein (30 μg) were separated on SDS-PAGE and transferred to a PVDF membrane. Western Blotting was used to detect the effect of the co-culture model of silicosis on the expression of EMT-related proteins (E-Cad, Vimentin, α-SMA), autophagy-related proteins (LC3B, Beclin1, p62) and AMPK, p-AMPK, mTOR and p-mTOR.

Statistical Analysis

Statistical analyses were performed using SPSS 22.0 software (IBM Corp.). All data are shown as the mean ± SD. And all data were checked for normality and homoscedasticity, differences between groups were performed using one-way ANOVA followed by LSD-test, while Dunnett's method was used for variance differences. Non-parametric data was represented by median and to analyze the data using Kruskal-Wallis analysis of variance. When statistical significance is obtained, the rank-based Mann–Whitney *U*-test be used to compare the groups. The p values < 0.05 were regarded as statistically significant.

RESULTS

Metformin Moderates the Effects of Silica Exposure on Body Weight and Lung Organ Coefficient

The weight of the rats after exposed to silica particles was considerably reduced (about 15%) when compared with that in rats from control group. Compared with the silica group, the weight of animals in the metformin treatment groups increased significantly ($p < 0.05$). The lung organ coefficient of the silica group was significantly higher than the control group, while the lung organ coefficient was significantly reduced after metformin treatment ($p < 0.05$) (**Figure 1**).

Metformin Effectively Alleviates Pulmonary Inflammation and Fibrosis Mediated by Silicon Dioxide in Rats

HE staining results showed that the rats in the negative control group and the metformin control group have an intact lung structure, with normal alveolar septa and no obvious inflammatory changes (**Figure 2A**: a-b). However, the lung tissues of the rats from silica group (**Figure 2A**: c) showed a severe inflammatory response indicated by the thickness of alveolar septal increased considerably, neutrophils infiltration and monocytes around the alveolar stroma, mainly macrophages. In contrast, after metformin treatment for 28 days, alveolitis was significantly reduced, the alveolar structure was significantly improved, and alveolar inflammation was also significantly relieved (**Figure 2A**: d-f). Using the Szapiel (Szapiel et al., 1979) method, we quantified alveolar inflammation and the results showed that the alveolar score of the silica group was almost 2 times higher than the rats from negative control group. However, after metformin treatment, even at the concentration of 100 mg/kg, the alveolar inflammation score was about 25% lower than in the silica group ($p < 0.05$). The inflammation scores were decreased in a dose-repose pattern (**Figure 2C**). Masson staining indicates the degree of pulmonary fibrosis by staining collagen fibers. Collagen deposition (blue areas) in the lungs of rats from the silica group was significantly increased, compared with the control and metformin group (**Figure 2B**: c). However, with metformin treatment, inflammatory cells and the accumulation of collagen fibers were significantly reduced (**Figure 2B**: d-f). Quantitative analysis showed that the pulmonary fibrosis score of the silica group was significantly higher than the negative control group. However, the pulmonary fibrosis scores decreased from 2.8 of the silica group to 2, 1.8, and 1.5 after treatment with metformin at 100, 200, and 400 mg/kg ($p < 0.05$). (**Figure 2D**).

Metformin Reduces Silica Particle-Induced Inflammation by Inhibiting Inflammatory Cytokines TGF-β1, TNF-α, and IL-1β in Lung Tissues

As shown in **Figures 3A-C**, TGF-β1, TNF-α and IL-1β in lung tissues of rats from control and metformin group showed a basal level less than 500 pg/mg protein. Exposure to silica particles caused significantly increase of these cytokines on the 56th days ($p < 0.05$). However, metformin treatment led to a dose-response reduction of the inflammatory cytokines ($p < 0.05$). Metformin treatment at 100 mg/kg led to about 30, 20, and 40% reduction of TGF-β1, TNF-α, and IL-1β, respectively. Higher concentration of metformin (400 mg/kg) caused over 50% reduction of these cytokines. This indicates that metformin inhibits the expression of inflammatory cytokines in rat lung tissue caused by silica, thereby reducing alveolar inflammation.

Metformin Reversed Silica-Induced EMT in the Lung of Rats

E-Cad, α-SMA and Vimentin which are hallmark proteins for EMT were measured by the Western Blot and Immunohistochemistry. Rats with Metformin treatment only showed similar level of these proteins in lung tissues as that in control group. In the lung tissue of rats from the silica group, the expression level of E-Cad was reduced about three quarters while α-SMA and Vimentin were increased about 3 and 4 times, respectively, compared with the rats from control group. However, in silicosis rats treated with metformin, the expression level of E-Cad but α-SMA and Vimentin were significantly recovered in a dose-response relation with the concentration of metformin compared with the silica group ($p < 0.05$) (**Figures 3D,E**). These suggested that metformin could inhibit the process of EMT.

Metformin Inhibits Pulmonary Fibrosis by Activating Autophagy *via* the AMPK-mTOR Signaling Pathway

Recent studies have suggested the contribution of autophagy to the benefit of metformin. Therefore, we explored the involvement of autophagy in the effects of metformin on silicosis by assessing the expression of p62, Beclin 1 and LC3. The results showed silica dust treatment almost 30% decrease of p62 and, 30% increase of Beclin1 and LC3, respectively, in comparison with rats from control group. Treatment of metformin led to further significant reduction of p62 and increase of Beclin1 and LC3 ($p < 0.05$). These results indicate that silica exposure could induce autophagy which was promoted further by metformin treatment.

And we then examined the p-AMPK, AMPK and p-mTOR, mTOR by WB. The results showed that there was no difference between the rats in control and metformin only group in the protein level of p-AMPK and p-mTOR. Rats from silica dust group showed lower level of p-AMPK but higher in p-mTOR compared with rats from the control and metformin only group ($p < 0.05$). However, metformin treatment resulted in one time increase of the expression level of p-AMPK. And meanwhile p-mTOR was obviously decreased in a dose-response manner compared with the silica group ($p < 0.05$) (**Figure 4A**).

Metformin Inhibit EMT Process *in vitro*

To identify suitable dosage levels, we first tested the cytotoxicity of metformin on HBECs with different concentrations of metformin (0, 0.1, 0.25, 0.5, 1, 2, 5, 10 mM) for 24, 48, and 72 h. The dosage selection was referred to previous studies (Wang et al., 2015; Guo et al., 2016), in which the cytotoxicity of metformin was tested at the concentration 0–50 mM. As shown in **Figure 5A**, metformin at 0.1–0.5 mM had no significant effect on cell growth at all time intervals. Compared with control group, the viability of HBEC incubated with 1, 2, 5, and 10 mM of metformin were both significantly reduced and less than 85% on the 24, 48 and 72 h ($p < 0.05$). Therefore, 0.1, 0.25, and 0.5 mM of metformin were used for following *in vitro* experiments. After THP-1 cells differentiated into macrophages, 100 μg/ml of silica solution was introduced into the insert in the silica group and metformin group. Meanwhile 0.1, 0.25 and 0.5 mM metformin was added to the bottom in metformin group. The cells were cultured for 72 h. E-Cad, α-SMA and Vimentin were measured to assess the effect of metformin on EMT. The WB results showed silica

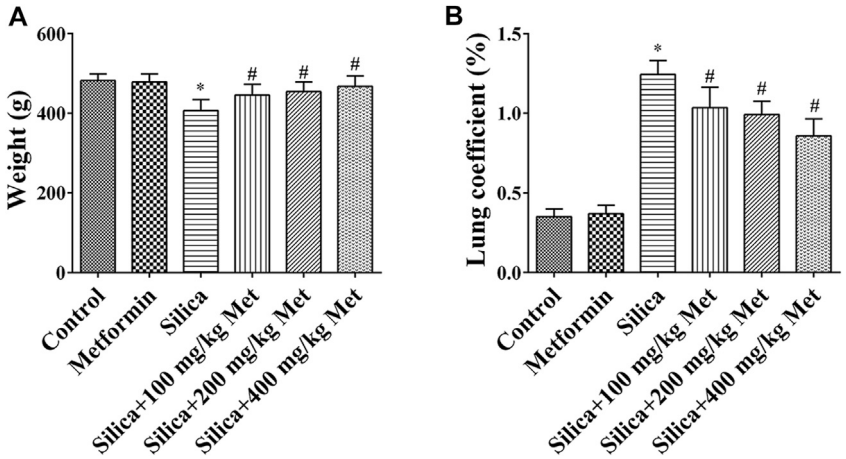

FIGURE 1 | Metformin moderates the effects of silica exposure on rat body weight and lung organ coefficient. The **(A)** body weight and **(B)** lung coefficient of the rats exposed to silica particles considerably reduced (about 15%) and significantly increased, respectively, when compared with that in rats from control group. Metformin treatment recovered the body weight and lung coefficient with significant changes. All the data are presented as mean ± SD (n = 8 for each group). $^{*}p < 0.05$, compared to the control group; $^{\#}p < 0.05$, compared to silica group.

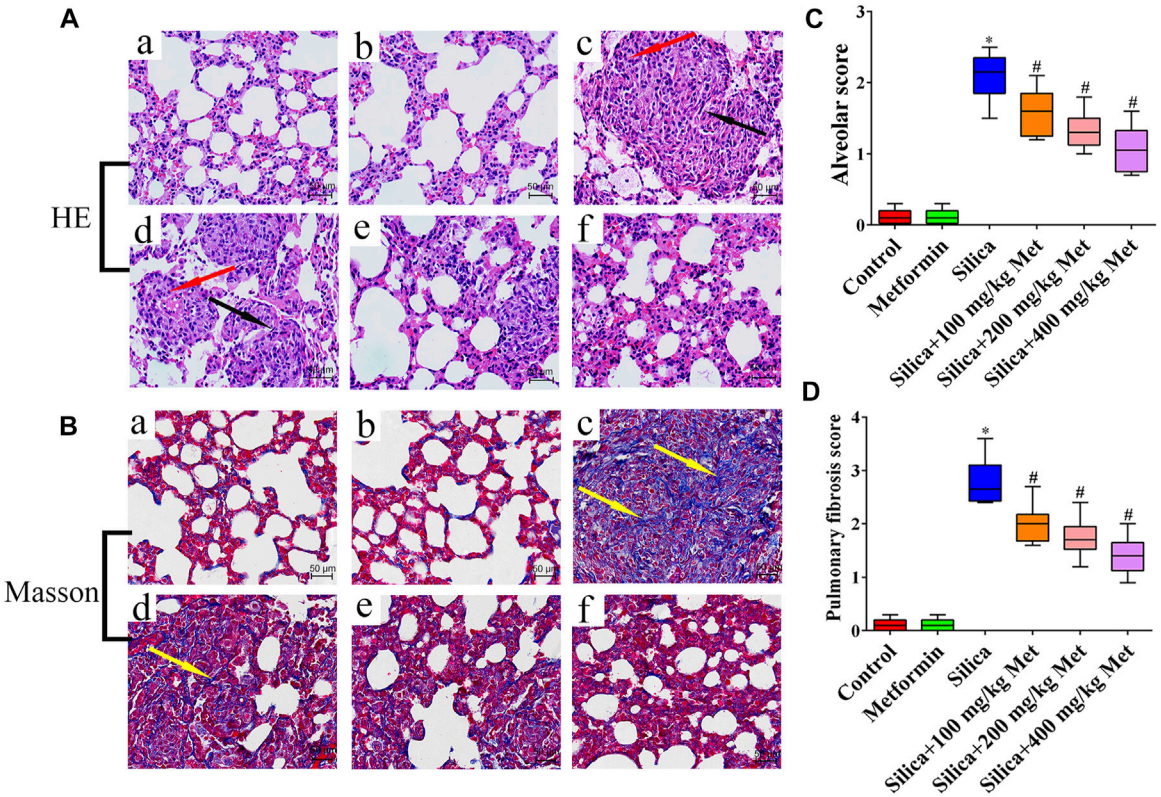

FIGURE 2 | Metformin reduces the inflammation and collagen accumulation in the lung tissue of silicosis rat caused by silica. **(A)** HE staining of lung tissues (200 × mag.) The red arrows point to the inflammatory cells. The fibroblasts are labeled with black arrows. **(B)** Masson trichrome staining of collagen on lung sections (200 × mag.). The yellow arrow points to the collagen. **(C-D)** Quantitative analysis of rat alveolitis and fibrosis score. **a** Control group; **b** Metformin treatment group; **c** Silica group; **d** Silica+100 mg/kg metformin group; **e** Silica+200 mg/kg metformin group; **f** Silica+400 mg/kg metformin group. $^{*}p < 0.05$, compared to the control group; $^{\#}p < 0.05$, compared to silica group.

caused an over 70% decrease of E-Cad which was recovered significantly by treatment of metformin. Compared with control cells, the expression of α-SMA and Vimentin was increased more than 2 times by silica treatment. However, co-treatment of metformin at 0.1, 0.25 and 0.5 mM led to a significant decrease of these two proteins in a dose-response manner (**Figure 5B**).

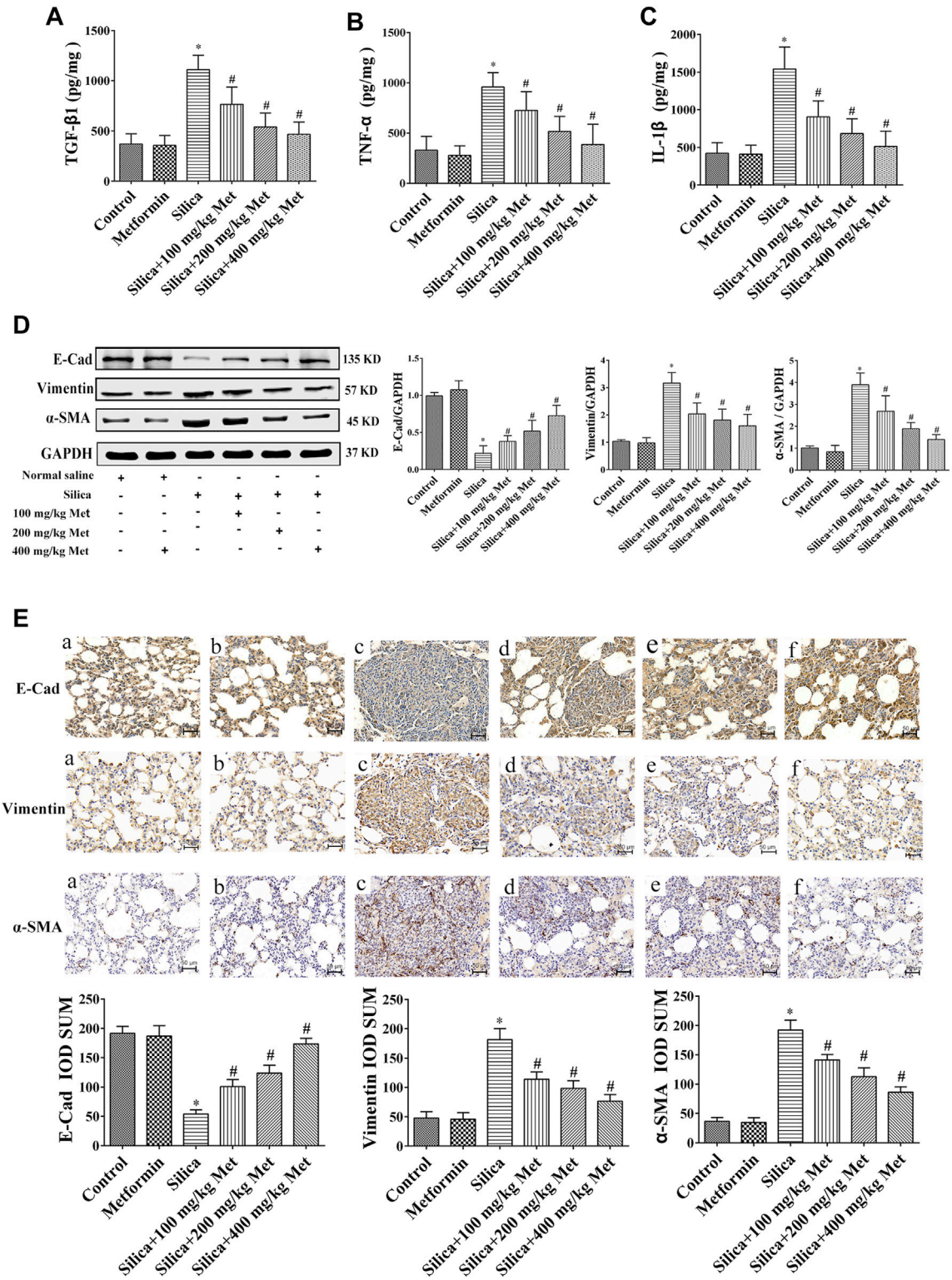

FIGURE 3 | Metformin reduces the expression level of inflammatory factors and alleviates silicosis fibrosis induced by silica particles in rat lung tissue. The expression level of **(A)** TGF-β1, **(B)** TNF-α and **(C)** IL-1β detected by ELISA. **(D)** The expressions of EMT-associated proteins expression level in the lung tissue of rats were detected by Western blot and **(E)** Immunohistochemistry (200 × mag.). **a** Control group; **b** Metformin treatment group; **c** Silica group; **d** Silica+100 mg/kg metformin group; **e** Silica + 200 mg/kg metformin group; **f** Silica + 400 mg/kg metformin group. All the data are presented as mean ± SD ($n = 8$ for each group). $^{*}p < 0.05$, compared to the negative control group; $^{\#}p < 0.05$, compared to silica group. TGF-β1, transforming growth factor-β1; TNF-α, tumor necrosis factor-α; IL-1β, interleukin-1β; Pro, protein; EMT, epithelial-mesenchymal transition; E-cad, E-Cadherin; α-SMA, α-Smooth muscle actin; Met, metformin.

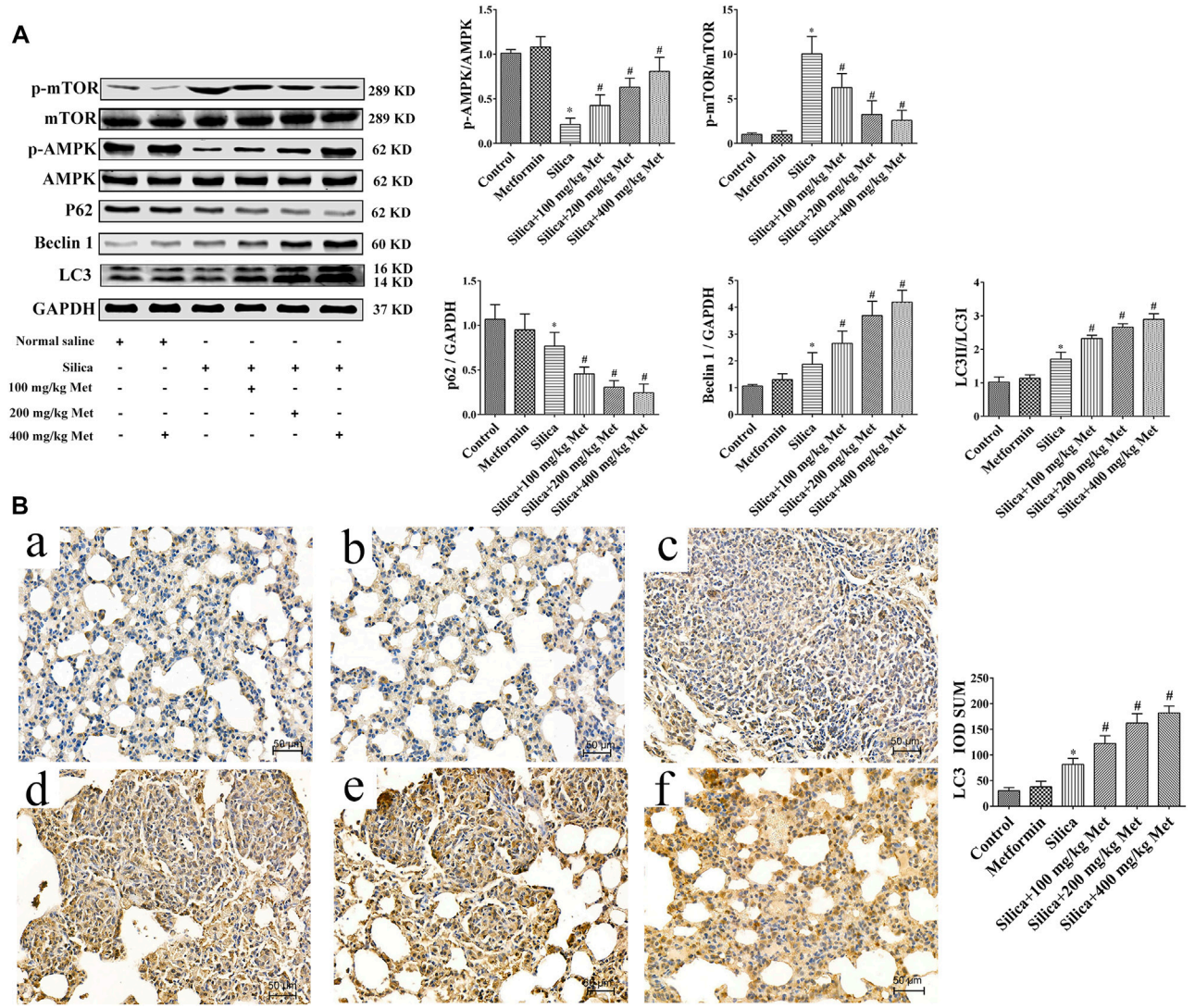

FIGURE 4 | Metformin activates autophagy *via* the AMPK-mTOR signaling pathway. **(A)** The protein levels of AMPK, p-AMPK, mTOR and p-mTOR, p62, Beclin1, and LC3 in lung tissues of rats by western blot. **(B)** The protein levels of LC3 was determined by Immunohistochemistry (200 × mag.). **a** Control group; **b** Metformin treatment group; **c** Silica group; **d** Silica+100 mg/kg metformin group; **e** Silica+200 mg/kg metformin group; **f** Silica+400 mg/kg metformin group. All the data are presented as mean ± SD (n = 8 for each group). $^{*}p < 0.05$, compared to the negative control group; $^{\#}p < 0.05$, compared to silica group. AMPK, adenosine5′-monophosphate (AMP)-activated protein kinase; mTOR, mammalian Target of Rapamyc; LC3, microtubules associated protein 1 light chain 3; Met, metformin.

Metformin Reduces Silica Particle-Induced Inflammation in Human Bronchial Epithelial Cells by Inhibiting Inflammatory Cytokines TGF-β1, TNF-α, and IL-1β

The content of TGF-β1, TNF-α, and IL-1β in HBECs of the co-culture system was measured using ELISA. The levels of TGF-β1, TNF-α, and IL-1β in the silica group were significantly higher in silica treatment compared with the control group ($p < 0.05$). silica group with metformin treatment led to a 30, 50, and 40% reduction of TGF-β1, TNF-α, and IL-1β, respectively compared with that in the silica group ($p < 0.05$). To explore the role of AMPK in the effect of metformin, we measured the level of cytokines in cells treated with silica and CC, or silica, metformin and CC. The results showed co-treatment of silica and CC led to a 30% increase of these cytokines with the significant difference in comparison with that in silica group ($p < 0.05$). The increased level of cytokines was reduced significantly by treatment with metformin ($p < 0.05$) as shown in **Figure 6**.

Metformin Regulates the Expression of EMT-Related Proteins in Human Bronchial Epithelial Cells of Co-Culture System Exposed to Silica Particles

To further explore the role of AMPK in silica particle-induced EMT and the regulation of metformin, we examined the EMT proteins in cells treated with silica particles, metformin and CC

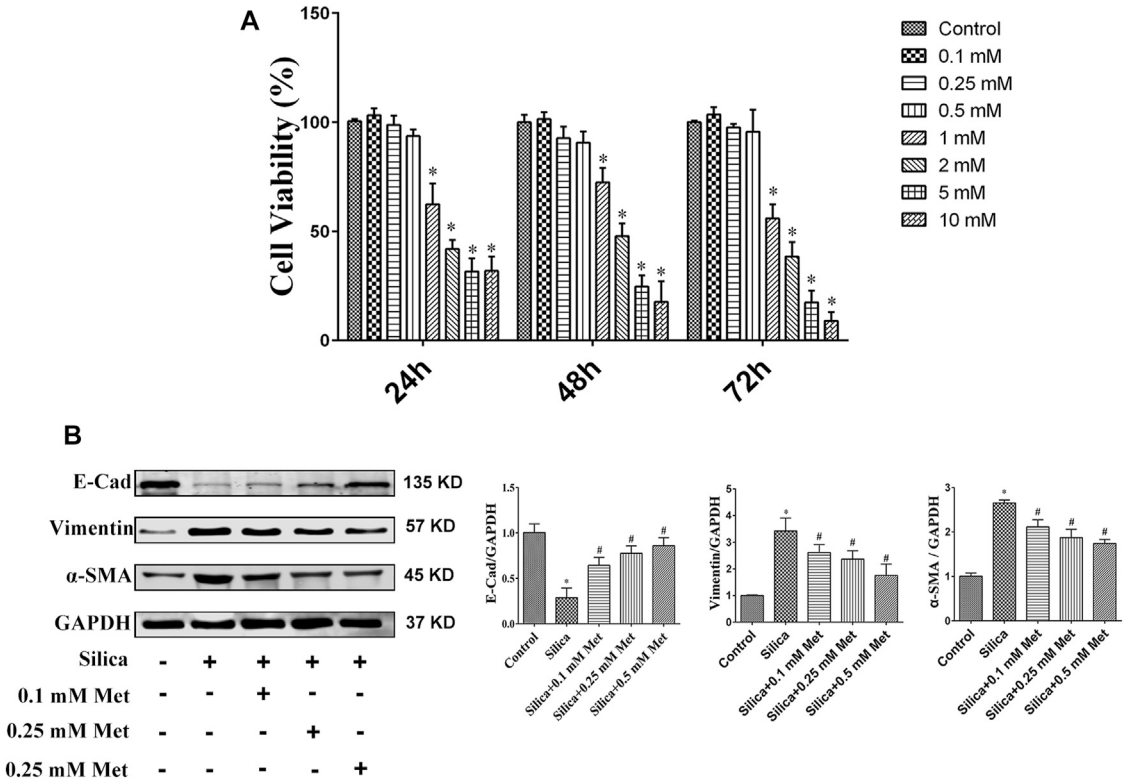

FIGURE 5 | Different concentrations of metformin affect cell viability and inhibit EMT process. **(A)** The viability of HBEC incubated with different concentrations of metformin was detected by the CCK-8 assay. **(B)** Western blotting results for the expressions level of EMT-associated proteins on HBEC after co-culture with different concentrations of metformin. All the data are presented as mean ± SD (n = 3 for each experimental group). *p < 0.05, compared to the control group; #p < 0.05, compared to silica group. EMT, epithelial-mesenchymal transition; E-cad, E-Cadherin; α-SMA, α-Smooth muscle actin; Met, metformin.

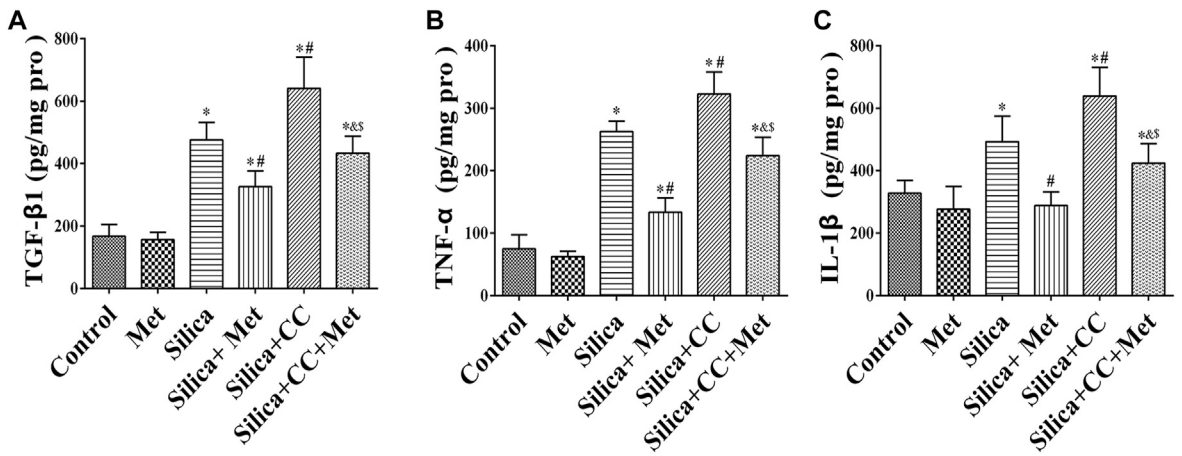

FIGURE 6 | Metformin reduces the expression level of inflammatory factors by silica particles in HBECs. The expression level of **(A)** TGF-β1, **(B)** TNF-α, and **(C)** IL-1β detected by ELISA. All the data are presented as mean ± SD (n = 3 for each experimental group). *p < 0.05, compared to the negative control group; #p < 0.05, compared to silica group; &p < 0.05, compared to Silica + Met group; $$p$ < 0.05, compared to Silica + CC group. TGF-β1, transforming growth factor-β1; TNF-α, tumor necrosis factor-α; IL-1β, interleukin-1β; Pro, protein; Met, metformin; CC, Compound C.

using Western Blot and Immunofluorescence. The results showed that in the silica group, the expression level of epithelial marker E-Cad in HBECs was reduced 30% and co-treatment of silica with CC reduced 50% of that in control cells. Treatment with CC promoted about 20% of silica-induced Vimentin and α-SMA, which was reduced to the similar degree by metformin with

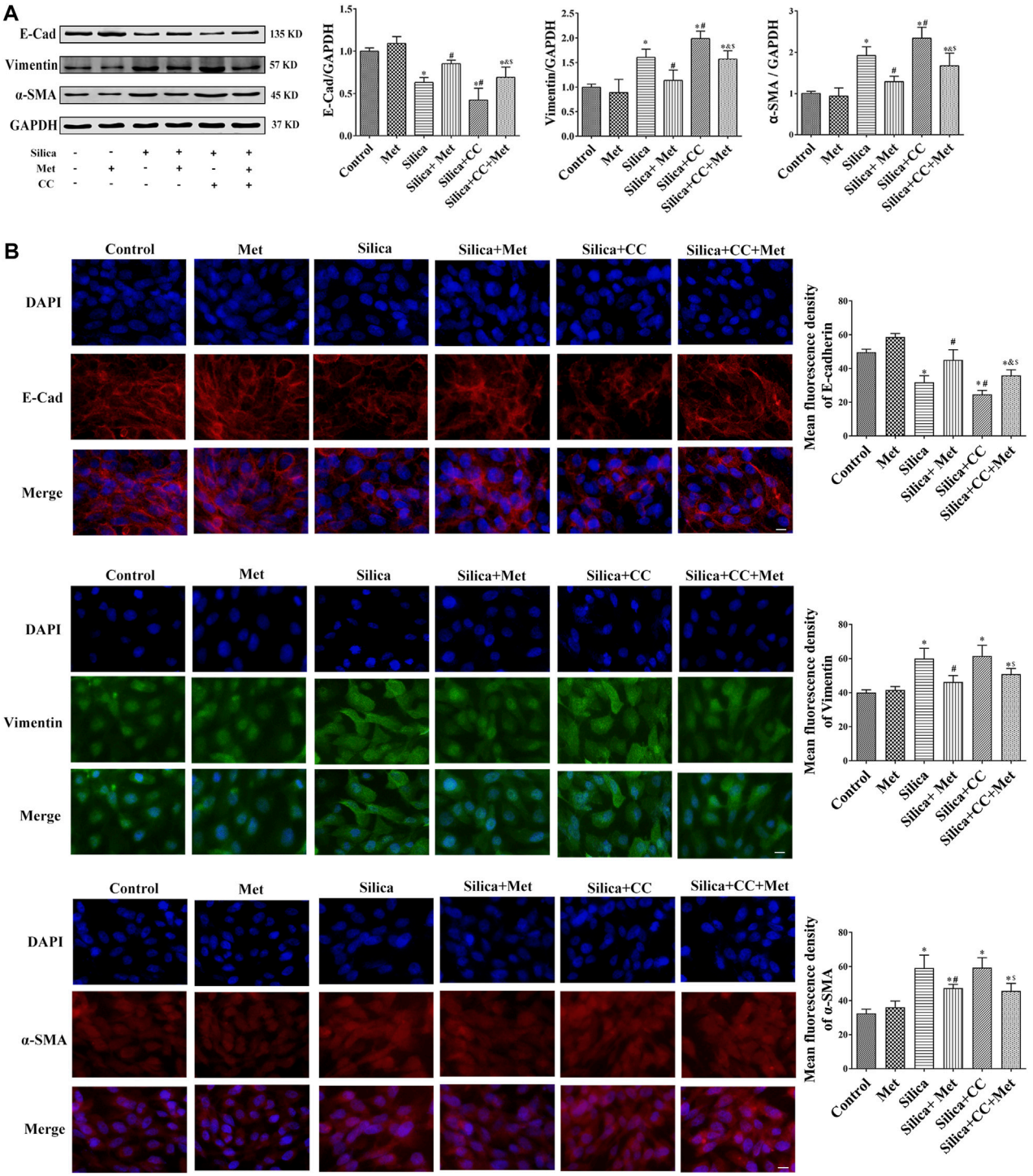

FIGURE 7 | Metformin regulates the expression of EMT-related proteins induced by silica particles. **(A)** The expression level of the expressions of EMT-associated proteins expression level in HBEC cells were detected by Western blot and the E-Cad, Vimentin and α-SMA were detected by **(B)** Immunofluorescence. Scale bar, 10 μm. All the data are presented as mean ± SD (n = 3 for each experimental group). $^{*}p < 0.05$, compared to the negative control group; $^{\#}p < 0.05$, compared to silica group; $^{\&}p < 0.05$, compared to Silica + Met group; $^{\$}p < 0.05$, compared to Silica + CC group. EMT, epithelial-mesenchymal transition; E-cad, E-Cadherin; α-SMA, α-Smooth muscle actin; Met, metformin; CC, Compound C.

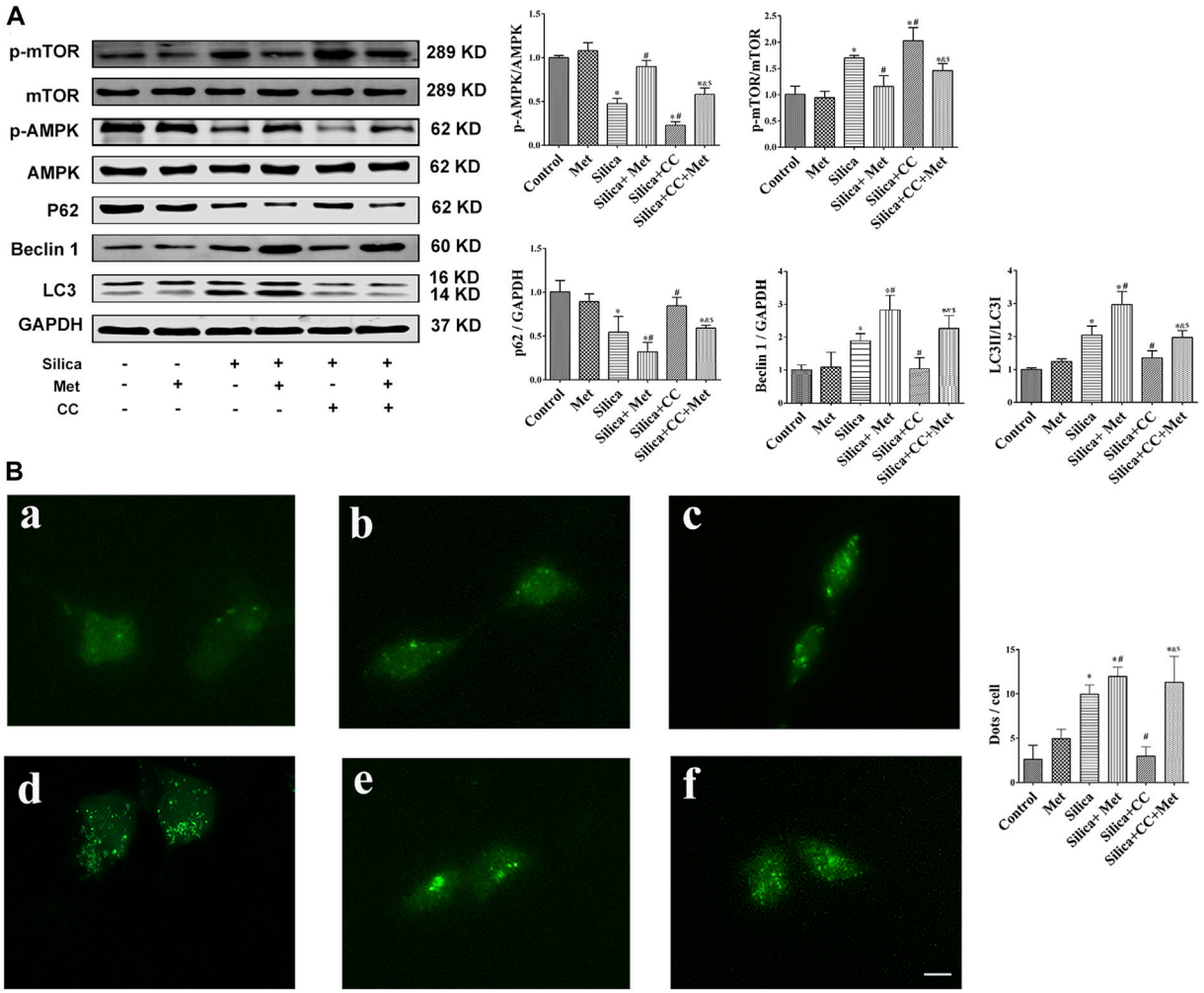

FIGURE 8 | Metformin activates autophagy *via* the AMPK-mTOR signaling pathway. **(A)** The protein levels of AMPK, p-AMPK, mTOR and p-mTOR, p62, Beclin1 and LC3 in HBEC were detected by western blot. **(B)** Fluorescence images of Ad-GFP-LC3 in HBEC cells after co-culture 72 h. GFP fluorescence indicated by green puncta. **a** Control group; **b** Met treatment group; **c** Silica group; **d** Silica+0.5 mM Met group; **e** Silica+0.1 μM CC group; **f** Silica+0.5 mM Met +0.1 μM CC group. Scale bars, 30 μm. All the data are presented as mean ± SD ($n = 3$ for each experimental group). $^{*}p < 0.05$, compared to the negative control group; $^{\#}p < 0.05$, compared to silica group; $^{\&}p < 0.05$, compared to Silica + Met group; $^{\$}p < 0.05$, compared to Silica + CC group. AMPK, adenosine5′-monophosphate (AMP)-activated protein kinase; mTOR, mammalian Target of Rapamyc; LC3, microtubules associated protein 1 light chain 3; Met, metformin; CC, Compound C.

significant difference ($p < 0.05$) when compared each other as shown in **Figures 7A,B**.

Metformin Activates AMPK-mTOR Signaling Pathway to Up-Regulate Autophagy-Related Proteins in the Silicosis Co-culture Model

To confirm if the regulation of metformin on the silica particle-induced EMT process is through AMPK-dependent activation of autophagy, we added metformin and CC, and examined the autophagy-related proteins p62, Beclin1 and LC3 by WB first. The results showed there is not much change of these proteins in HBECs of the co-culture system from control and metformin groups. Treatment with silica only led to a 30% decrease of p62 and 40% increases of Beclin1 and LC3, which was further reduced 20% for p62 and increased 25% for Beclin1 and LC3, by co-treatment with metformin. Cells co-treated with silica and CC showed higher level of p62 than that of silica group but similar to that in control cells. However, co-treatment with metformin, silica and CC led to a 25% decrease of p62 but increase in Beclin1 (50% increase) and LC3 (25% increase) in comparison with that in group of silica and CC as shown in **Figure 8A**.

Furthermore, we assessed autophagy by examining the formation of autophagosomes using HBECs transfected with GFP-LC3 adenovirus. As shown in Figure 8B-a and b, cells of control and metformin treatment only showed basal level of GFP-LC 3 foci. Cells treated with silica particles showed higher number of foci. (**Figure 8B**: c). As shown in **Figure 8B**: d, much more foci were found in cells treated with silica and metformin. In addition,

metformin enhanced LC foci in the cells treated with silica and CC.

Then, we measured the expression of p-AMPK, AMPK, p-mTOR and mTOR using WB. The results showed that the p-AMPK expression was decreased about 50%, while the p-mTOR expression was increased about 40% of control cells in the silica group, with statistically significant differences compared with the control group ($p < 0.05$). Treatment with CC with silica particles exacerbated the change of p-AMPK and p-mTOR expression with significant difference ($p < 0.05$). However, co-treatment Metformin with silica or silica and CC significantly recovered the level of these proteins.

DISCUSSION

Silicosis is one of the important occupational respiratory diseases caused by inhalation of respirable crystalline silica (Fernandez Alvarez et al., 2015). As one of the most common occupational disease, silicosis occurs not only in developing countries because of poor protection facility and regulations, but also in developed countries in recent years among the stone masons (Rees and Murray, 2007). Although great efforts have been made in prevention and treatment, there has been no effective therapeutic drugs so far and lung transplantation has been still the effective option for curing silicosis.

Silicosis is mainly caused by the deposition of silica particles in the alveoli. Accumulated silica particles in the lung alveoli stimulate lung microphages and epithelial cells leading to repeated inflammation and high expression of inflammatory cytokines such as TNF-α and IL-1, which then cause fibroblasts producing collagen, leading to fibrosis and silicon nodules (Pollard, 2016). For *in vivo* study, we set up the animal silicosis model by exposing rats to silica particles according to the method in our previous work (Sai et al., 2019). Firstly, we examined the effects of metformin on body weight of the rats treated with silica. Our results showed that after being exposed to silica for 56 days, the weight of the rats exposed to silica particles reduced about 15% compared with the rats of control group (**Figure 1A**), and the lung coefficient was significantly increased (**Figure 1B**). HE staining results showed that the lung tissues of the rats from silica group exhibited severe inflammation indicated by the destroyed alveolar structure and a large number of infiltrating inflammatory cells (**Figure 2A**). Masson staining of lung tissue sections showed that a large amount of collagen deposition and occurrence of silicotic nodule, indicating pulmonary fibrosis occurred after exposure to silica particles (**Figure 2B**). In addition, in order to simulate the process of silicosis, a modified co-culture cell model *in vitro* was established according to our published study (Pang et al., 2021). Treatment with silica caused an increased level of pro-inflammatory factors including TGF-β1, TNF-α and IL-1β in lung tissue of rats and medium of the co-culture system. These results indicted an obvious inflammatory response induced by silica particles (**Figures 3A–C**, **Figures 6A–C**).

Although the mechanism of silicosis fibrosis remains to be elusive, EMT is a recognized as a critical process leading to fibrotic changes. EMT plays an important role in many lung diseases such as chronic obstructive pulmonary disease and pulmonary fibrosis (Jolly et al., 2018). During EMT, epithelial cells undergo morphological changes including cell-cell adhesions loosed, epithelial markers down-regulated, mesenchymal markers up-regulated, and an elongated fibroblast-like morphology acquired (Gabasa et al., 2017; Li et al., 2018). EMT is complex process mediated by several key transcription factors and finely regulated through epigenetic and post-translational modifications (Serrano-Gomez et al., 2016). Despite the complex and transient nature of EMT, several hallmarks have been identified for EMT assessment including epithelial markers such as E-Cad and mesenchymal markers including Vimentin and α-SMA which were investigated in this study. The results showed that the expression of E-Cad decreased and mesenchymal markers Vimentin and α-SMA increased in rat lung tissues and HBEC cells exposed to silica (**Figure 3D**, **Figure 7**).

The inhaled silica particles are engulfed by alveolar macrophages and subsequently lead to the death of alveolar macrophages during which intracellular silica, cytotoxic oxidants and inflammatory cytokines are released (Davis et al., 1996; Yang et al., 2016; Barohn et al., 2019). These factors promote the proliferation of lung fibroblasts, the production of collagen and eventually lead to the formation of fibrosis (Guo et al., 2019). Autophagy may play an important role in the lung fibrosis (Racanelli et al., 2018), but the underlying mechanisms remain elusive. Autophagy is a fundamental intracellular catabolic process for recycling damaged organelles and proteins *via* the lysosome-mediated degradation pathway (Zhao et al., 2020). This process is essential for maintaining cellular homeostasis (Tseng et al., 2019). Beclin 1 is a mammalian homolog of yeast Atg6, which is the first mammalian autophagy protein to be described (Liang et al., 1998). Free Beclin 1 is an initiator of autophagy and thus extensively used as a marker for monitoring the onset of autophagy (Cao and Klionsky, 2007). Therefore, as an important regulator of autophagy, the expression level of Beclin 1 represents autophagy activity to some extent (Xu G. et al., 2019). LC3 is a mammalian homolog of yeast Atg8 and has LC3-I and LC3-II two subforms. The conversion of LC3-I into LC3-II is a key step in autophagosome formation (Mizushima et al., 2010). Therefore, the ration of LC3-II/LC3-I is commomly used to assess the autophagy activity. p62 has been known as one of the selective substrates for LC3. When autophagy occurs, p62 first binds to the ubiquitinated protein and then combines with LC3-II localized on the inner membrane of the autophagic vacuole to form a complex (Komatsu and Ichimura, 2010). In this study, we analyzed the expression of the autophagy-associated protein LC3-II/LC3-I, Beclin1 and p62 in lung tissues of the rats and HBEC cells. Our results showed that LC3 and Beclin1 in rats and HBECs were significantly increased and p62 decreased after being exposed to silica (**Figure 4**, **Figure 8A**). This result clearly indicated silica-induced autophagy activity. Supportively, Jessop et al. (2016) showed that silica exposure causes increased expression of LC3-II *in vitro* and enhanced autophagic activity in alveolar macrophages isolated from silica-exposed mice. Chen et al.

(2013) found that silica dust exposure can induce autophagy in the lung tissue of rats. Duan et al. (2014) demonstrated that Nano-SiO_2 could induce inflammatory response, activate autophagy, and eventually lead to endothelial dysfunction. Previous studies indicated that autophagy in the macrophages can be activated by silica, characterized as the accumulation of autophagosomes, which may be associated with the silicosis progression (Chen S. et al., 2015; Liu et al., 2016). (Cheng et al., 2019) found that SiO_2 induces activation of autophagy in human pulmonary fibroblasts cells. Recently, the activation of autophagy, a lysosome-dependent cell degradation pathway, by silica nanoparticles has been identified in alveolar epithelial cells (AECs) (Zhao et al., 2019). Additionally, Li et al. (2021) demonstrated that SiO_2 exposure can induce pulmonary fibrosis along with autophagy both *in vivo* and *in vitro*, and autophagy might play a protective role in the progression of pulmonary fibrosis.

AMPK is a key energy sensor and regulates cellular metabolism to maintain energy homeostasis and restore energy balance at the cellular and physiological levels during metabolic stress (Garcia and Shaw, 2017). mTOR is one of the downstream targets of AMPK, and activation of AMPK can result in inhibition of mTOR signaling (Xu et al., 2012). Studies had shown that AMPK activation could inhibit TNF-α, IL-1β, and IL-6 synthesis in macrophage (Sag et al., 2008; Yang et al., 2010; Galic et al., 2011). AMPK exerts a significant anti-inflammatory effect *via* suppression of the NF-κB signaling pathway (Salminen et al., 2011). In addition, emerging evidence indicated that AMPK plays an important role in autophagy (Bujak et al., 2015; Tamargo-Gomez and Marino, 2018) through the AMPK/mTOR signaling pathway (Kim et al., 2011; Wang et al., 2019). Recent studies found that AMPK functions are strongly associated with fibrogenesis (Jiang et al., 2017). Increasing evidence has revealed that AMPK protects against fibrosis in the heart (Zhang et al., 2011), liver (Yang et al., 2015), lung (King et al., 2012), kidney (Cavaglieri et al., 2015), and skin (Takata et al., 2014). In this respect, loss or reduction of AMPK has been implicated in diabetes mellitus, obesity and aging (Burkewitz et al., 2014; Southern et al., 2017; Rana et al., 2020). To explore the possible role of AMPK in silicosis, we investigated the expression of AMPK and mTOR. Our study showed that the p-AMPK expression was decreased, and then the autophagy regulatory protein p-mTOR was activated in silica group (**Figure 4A**, **Figure 8A**). Up to now, the role of AMPK in silicosis has not been reported. However, in IPF, within the regions of active fibrosis, a significant decrease in AMPK activity was observed together with reduced activation of the Thr172 (Rangarajan et al., 2018). It is noted that AMPK is a positive regulator of autophagy while in our study silica exposure caused an augment of the autophagy activity. The observed autophagy activity induced by silica may be attributed to several factors including engulfment of pre-autophagosomal structure, impaired autophagic degradation by silica. In addition, pro-fibrogenic factors BCL-binding component 3 (BBC3) and monocyte chemoattractant protein-1-induced protein 1 (MCP1P1) during fibrotic process may also contribute to the silica-induced autophagy (Liu et al., 2016; Liu et al., 2017). These factors may override the regulatory effects of AMPK and promote autophagy activity by silica. However, this speculation need to be confirmed by more research work.

Drug design and development are extremely expensive and time consuming. Recent studies showed that a drug may have effects on different diseases. Therefore, identification of new use or repurposing of an approved drug is becoming more attractive approach in disease treatment (Pushpakom et al., 2019). Derived from galegine, a natural product from the plant Galega officinalis, metformin is a commonly prescribed drug to treat type 2 diabetes globally. Interestingly, recent studies have found that metformin can effectively reverse bleomycin-induced pulmonary fibrosis (Gamad et al., 2018). Although the causes of silicosis and idiopathic pulmonary fibrosis are different, they share similarities in the pathological changes of lung tissue and common mechanism of pulmonary fibrosis. We speculated that metformin may have beneficial effects on silicosis. Therefore, in this study we investigated the effects of metformin on silicosis using *in vivo* and *in vitro* models.

As a unique anti-diabetic drug, metformin usually does not cause hypoglycemia (Nasri and Rafieian-Kopaei, 2014). Cassano et al. (Cassano et al., 2020) demonstrated that compared with the control group receiving a normal diet of rats, there was no statistical difference in the effect of metformin on blood glucose levels. And Luo et al. (2021) reported that after a daily intragastric administration of 500 mg/kg metformin for 35 days, there was no changes in blood glucose in rats, compared with the control group. We treated the rats with metformin at 100, 200, and 400 mg/kg/day for another 28 days. The dosage selection of metformin was based on reported toxicity of metformin in rats (Quaile et al., 2010) and a previous study (Gamad et al., 2018). The dosage range equals to human effective dose of 16, 32, and 64 mg/kg/day, respectively, according to the published conversion method (Nair and Jacob, 2016). We then examined the various parameters associated with inflammatory responses and fibrosis and compared them with those among the rats with different treatment. After treatment with different doses of metformin, the weight of the rats markedly increased, and the lung coefficient decreased to varying degrees. Metformin treatment only did not show any effects on body weight and lung coefficient. These results suggested that metformin recovered the general adverse health effects induced by silica particles. After metformin treatment, inflammatory cells and nodules and collagen fibers in the lung tissues were significantly reduced (**Figures 2A,B**). Quantitative analysis indicated metformin induced a 20–25% reduction of inflammation infiltration and fibrosis and the effects showed a dose-response manner among the rats received metformin at different concentration. The result suggested that metformin may have a positive therapeutic effect on silicosis (**Figures 2C,D**) through alleviating the inflammation and fibrosis, the hallmark processes leading to silicosis. We then examined the pathways involved in these processed to explore the mechanisms underlying the effects of metformin.

Macrophages ingestion of silica and release inflammatory cytokines, such as TNF-α, IL-1, and TGF-β. These in turn provoke recruitment of inflammatory cells into the alveolar wall and alveolar epithelial surface, initiating alveolitis and

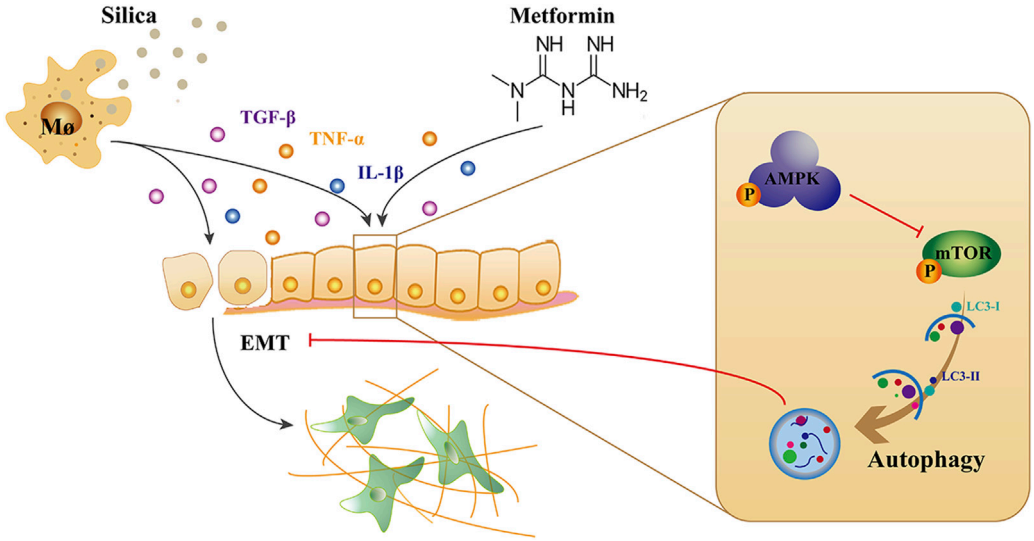

FIGURE 9 | The mechanism of action of metformin against silica-induced pulmonary fibrosis. Uptake of silica by alveolar macrophages release high level of inflammatory cytokines, and induced EMT which epithelial cells gradually lose their epithelial characteristics and acquire the mesenchymal phenotype. Metformin can activate AMPK and inhibit mTOR, leading to autophagy induction, thereby reducing the EMT process in silicosis.

inducing epithelial to mesenchymal transition (Mossman and Churg, 1998; Robledo and Mossman, 1999). Studies found that metformin attenuates PM2.5-induced inflammation (Gao et al., 2020) and inhibits TGF-β1-induced EMT (Yoshida et al., 2020). Our experimental results showed that after metformin treatment, the expression of pro-inflammatory factors TGF-β1, TNF-α, and IL-1β were significantly decreased (**Figures 3A–C**, **Figure 6**). This suggests that metformin alleviates the inflammatory response of silicosis through its anti-inflammatory effects. However, after metformin treatment, the protein expression of Vimentin and α-SMA was significantly down-regulated, while the E-Cad expression was up-regulated (**Figures 3D,E**, **Figure 7**). These results suggest that metformin may inhibit silica-mediated pulmonary fibrosis by inhibiting cellular pathways leading to EMT. In addition to fibrotic process, EMT has been implicated in cancer progression and metastasis. It is known that invasive properties and metastasis are controlled by EMT (Pearson, 2019). Cell invasion and metastasis are hallmarks of cancer development (Jiang et al., 2015). The inhibitive effect of metformin on EMT observed in this study suggest that metformin may have beneficial effect on cancer treatment. Indeed, metformin has been found to be able to inhibit the invasion and migration of various cancer cells (Chen X. et al., 2015; Chen et al., 2020).

Some evidence demonstrated that enhancing autophagy reduces silica-induced pulmonary fibrosis. MiR-326 inhibits inflammation and promotes autophagy activity to alleviate silica-induced pulmonary fibrosis (Xu T. et al., 2019). A study suggested that dioscin reduced silica-induced apoptosis and cytokine production by promoting autophagy, thereby exerted anti-fibrosis effects in silica-induced pulmonary fibrosis (Du et al., 2019). Rapamycin protects alveolar epithelial cells from apoptosis and attenuates silica-induced pulmonary fibrosis through the enhancement of autophagy in the mouse model (Zhao et al., 2019). Emerging evidence indicated that autophagy plays an import role in the beneficial effects of metformin (Bharath et al., 2020; Ren et al., 2020).Metformin attenuates lipopolysaccharide-induced epithelial cell senescence by activating autophagy (Wang et al., 2021). Bharath et al. (2020) showed that metformin enhances autophagy and normalizes mitochondrial function to alleviate aging-associated inflammation. Metformin alleviates oxidative stress and enhances autophagy in diabetic kidney disease (Ren et al., 2020). Metformin enhanced the autophagy as indicated by the up-regulated Beclin1 and LC3 and down-regulated the expression of p62 (**Figure 4A**). Immunohistochemistry results confirmed the increased expression of LC3 after treated with metformin (**Figure 4B**). The results from *in vitro* experiments in co-culture system also confirmed that the expression levels of LC3 and Beclin1 increased, and the expression of p62 decreased in HBECs (**Figure 8A**). In addition, we used GFP-LC3 cells to detect the accumulation of mature LC3 by which the GFP-LC3 signal becomes punctate (Bravo-San Pedro et al., 2017). The results from Ad-GFP-LC3 transfected cells demonstrated that metformin increased the number of GFP-LC3-foci (**Figure 8B**). Thus, the *in vivo* and *in vitro* studies confirmed the promoted autophagy by metformin.

Metformin was reported to activate AMPK. AMPK is a heterotrimeric complex consisting of an α catalytic subunit, scaffold protein β subunit, and regulatory γ non-catalytic subunit (Hardie et al., 2012). Metformin activates AMPK by increasing the phosphorylation of the catalytic a subunit at T172 (Shaw et al., 2005). Our results showed that after treatment with metformin, p-AMPK expression was significantly increased and p-mTOR expression decreased in silica stimulated rat lung tissues (**Figure 4A**). *In vitro* results showed that after 72 h of co-

cultivation with metformin, it was also showed that the increased expression of p-AMPK and decreased p-mTOR compared with silica group. On the contrary, after the intervention of CC, the expression of p-AMPK protein was significantly down-regulated and the expression of p-mTOR was up-regulated in HBEC cells (**Figure 8A**). To confirm the involvement of AMPK/mTOR pathway, we treated cells with CC, an AMPK inhibitor, together with silica particles or silica plus metformin. So far, CC remains the only small molecule that has been widely used to study AMPK signaling and various aspects of cell physiology, including cell proliferation, survival, and migration (Liu et al., 2020). Yan et al. (Yan et al., 2010) found that inhibition of AMPKα activity either by CC or by RNA interference markedly reduced the accumulation of LC3-II. Chiou et al. (2020) indicated that compound C treatments reduced AMPKα1 mRNA levels, which resulted in suppressed AMPKα protein expression and AMPKα phosphorylation in CC-treated cells. It should be noted that although CC has been used as AMPK inhibitor for over a decade, its inhibitive effect of CC is not specific to AMPK (Liu et al., 2014) which means others kinase may be affected. The non-specific effects generally occur at relatively high concentration (over 5 μM) (Dasgupta and Seibel, 2018) and in this study we used 1 μM to minimize the non-specific effects. Treatment of CC led to 50% decrease of p-AMPK and about 10% increase of p-mTOR. As expected, CC caused a depression of autophagy by up regulating p62 and down regulating Beclin1 and LC3B. Meanwhile immunofluorescent staining showed that CC decreased the number of GFP-LC3-containing puncta and the protein LC3B levels in HBEC cells (**Figure 8B**:e). However, GFP-LC3 foci regained after application of metformin (**Figure 8B**:e). Thus, all *in vivo* and *in vitro* data indicated that metformin exert its anti-silicotic effects through AMPK/mTOR medicated autophagy.

Drug repurposing has gained more and more attractions in identifying new therapeutic way. Metformin as a threptic drug for type 2 diabetics has been used for 60 years. Recent studies found that metformin have benefits for other diseases including liver, heart and renal diseases as well as cancer, obesity and even aging (Lv and Guo, 2020). The findings in this study will undoubtedly has clinical utility as an additional therapeutic option for patients with silicosis especially for those co-existing with type 2 diabetes or diseases mentioned above.

CONCLUSION

This study demonstrated that metformin has anti-silicotic potency in rats and *in vitro* cultured human cells. The effects of metformin may be due to its ability to alleviate the degree of alveolitis and pulmonary fibrosis, inhibit epithelial-mesenchymal transformation and alleviate the process of silica-induced pulmonary fibrosis. In addition, we showed that metformin can regulating autophagy through activating AMPK and inhibiting mTOR. Based on the results of our and others, we proposed the mechanism of action of metformin against silica particle-induced fibrosis as shown in **Figure 9**. The results from this study provide evidence that metformin may be potential therapeutic drug for effective treatment of silicosis.

DATA AVAILABILITY STATEMENT

The original contributions presented in the study are included in the article/**Supplementary Material**, further inquiries can be directed to the corresponding authors.

ETHICS STATEMENT

The animal study was reviewed and approved by The animal experiments were approved by Ethics Committee of Shandong Academy of Occupational Health and Occupational Medicine (approval no. 2019DL018).

AUTHOR CONTRIBUTIONS

G-CY, QJ, and CP conceived and designed the experiments; S-XL, CL, and X-RP performed the experiments and wrote the paper; AY and ML were responsible for the revision of the manuscript; JZ analyzed the data; and HS supervised the research. All authors read and approved the final manuscript.

FUNDING

This work was supported by National Natural Science Foundation of China (81872603, 81872575), National Major Scientific and Technological Special Project for "Significant New Drugs Development" (2018ZX09711001-011), Natural Science Foundation of Shandong Province (ZR2019MH102), Science and Technology Plan of Jinan City (201907061), the Innovation Project of Shandong Academy of Medical Sciences, Academic Promotion Programme of Shandong First Medical University (2019QL001), Tsung Cho Chang Education Foundation, Taiwan (UQ: 023142).

SUPPLEMENTARY MATERIAL

The Supplementary Material for this article can be found online at: https://www.frontiersin.org/articles/10.3389/fphar.2021.719589/full#supplementary-material

SUPPLEMENTARY FIGURE 1 | The schematic diagram of the procedure of animal experiments and cells co-culture. **(A)** In vivo animal experiments, all rats were divided into six groups, the silica model group and three metformin treatment groups were injected with silica suspension into the lung once using a non-exposed tracheal intubation, and the rats in the negative control group and metformin control group were both injected with normal saline solution. After exposed to silica for 28 days, the rats were given a daily intragastric administration for 28 days, respectively. **(B)** In vitro cell experiment, THP-1 cells were placed into the insert, where they were treated by PMA. HBEC cells were cultured alone at the bottom. Then, the cell culture inserts containing THP-1 macrophages were transferred to the plates containing HBECs and received the indicated interventions for 72 h.

REFERENCES

Barohn, R. J., Weir, S. J., and Simari, R. D. (2019). Progress in Drug Discovery in Academia and Persistent Challenges of "the Valley of Death". *Mayo Clinic Proc.* 94 (3), 391–393. doi:10.1016/j.mayocp.2019.01.014

Bharath, L. P., Agrawal, M., Mccambridge, G., Nicholas, D. A., Hasturk, H., Liu, J., et al. (2020). Metformin Enhances Autophagy and Normalizes Mitochondrial Function to Alleviate Aging-Associated Inflammation. *Cel Metab.* 32 (1), 44–55. e46. doi:10.1016/j.cmet.2020.04.015

Bravo-San Pedro, J. M., Pietrocola, F., Sica, V., Izzo, V., Sauvat, A., Kepp, O., et al. (2017). High-Throughput Quantification of GFP-Lc3+ Dots by Automated Fluorescence Microscopy. *Methods Enzymol.* 587, 71–86. doi:10.1016/bs.mie.2016.10.022

Bujak, A. L., Crane, J. D., Lally, J. S., Ford, R. J., Kang, S. J., Rebalka, I. A., et al. (2015). AMPK Activation of Muscle Autophagy Prevents Fasting-Induced Hypoglycemia and Myopathy during Aging. *Cel Metab.* 21 (6), 883–890. doi:10.1016/j.cmet.2015.05.016

Burkewitz, K., Zhang, Y., and Mair, W. B. (2014). AMPK at the Nexus of Energetics and Aging. *Cel Metab.* 20 (1), 10–25. doi:10.1016/j.cmet.2014.03.002

Câmara, J., and Jarai, G. (2010). Epithelial-mesenchymal Transition in Primary Human Bronchial Epithelial Cells Is Smad-dependent and Enhanced by Fibronectin and TNF-α. *Fibrogenesis Tissue Repair* 3 (1), 2. doi:10.1186/1755-1536-3-2

Cao, Y., and Klionsky, D. J. (2007). Physiological Functions of Atg6/Beclin 1: a Unique Autophagy-Related Protein. *Cell Res.* 17 (10), 839–849. doi:10.1038/cr.2007.78

Cassano, V., Leo, A., Tallarico, M., Nesci, V., Cimellaro, A., Fiorentino, T. V., et al. (2020). Metabolic and Cognitive Effects of Ranolazine in Type 2 Diabetes Mellitus: Data from an *In Vivo* Model. *Nutrients* 12 (2), 382. doi:10.3390/nu12020382

Cavaglieri, R. C., Day, R. T., Feliers, D., and Abboud, H. E. (2015). Metformin Prevents Renal Interstitial Fibrosis in Mice with Unilateral Ureteral Obstruction. *Mol. Cell Endocrinol.* 412, 116–122. doi:10.1016/j.mce.2015.06.006

Chen, S., Jin, Y. L., Yao, S. Q., Bai, Y. P., Fan, X. Y., Xu, Y. J., et al. (2013). Autophagy in Lung Tissue of Rats Exposed to Silica Dust. *Zhonghua Lao Dong Wei Sheng Zhi Ye Bing Za Zhi* 31 (8), 607–610. doi:10.3760/cma.j.issn.1001-9391.2018.12.002

Chen, S., Yuan, J., Yao, S., Jin, Y., Chen, G., Tian, W., et al. (2015a). Lipopolysaccharides May Aggravate Apoptosis through Accumulation of Autophagosomes in Alveolar Macrophages of Human Silicosis. *Autophagy* 11 (12), 2346–2357. doi:10.1080/15548627.2015.1109765

Chen, X., Hu, C., Zhang, W., Shen, Y., Wang, J., Hu, F., et al. (2015b). Metformin Inhibits the Proliferation, Metastasis, and Cancer Stem-like Sphere Formation in Osteosarcoma MG63 Cells *In Vitro*. *Tumor Biol.* 36 (12), 9873–9883. doi:10.1007/s13277-015-3751-1

Chen, Y. C., Li, H., and Wang, J. (2020). Mechanisms of Metformin Inhibiting Cancer Invasion and Migration. *Am. J. Transl Res.* 12 (9), 4885–4901.

Cheng, Y., Luo, W., Li, Z., Cao, M., Zhu, Z., Han, C., et al. (2019). CircRNA-012091/PPP1R13B-mediated Lung Fibrotic Response in Silicosis via Endoplasmic Reticulum Stress and Autophagy. *Am. J. Respir. Cel Mol Biol.* 61 (3), 380–391. doi:10.1165/rcmb.2019-0017OC

Chiou, J.-T., Huang, C.-H., Lee, Y.-C., Wang, L.-J., Shi, Y.-J., Chen, Y.-J., et al. (2020). Compound C Induces Autophagy and Apoptosis in Parental and Hydroquinone-Selected Malignant Leukemia Cells through the ROS/p38 MAPK/AMPK/TET2/FOXP3 axis. *Cell Biol Toxicol.* 36 (4), 315–331. doi:10.1007/s10565-019-09495-3

Dasgupta, B., and Seibel, W. (2018). Compound C/Dorsomorphin: Its Use and Misuse as an AMPK Inhibitor. *Methods Mol. Biol.* 1732, 195–202. doi:10.1007/978-1-4939-7598-3_12

Davis, G. S., Pfeiffer, L. M., Leslie, K. E., and Hemenway, D. R. (1996). Macrophage-lymphocyte Cytokine Interactions in Silicosis. *Chest* 109, 49S–50S. doi:10.1378/chest.109.3_supplement.49s

Dong, J., and Ma, Q. (2016). Myofibroblasts and Lung Fibrosis Induced by Carbon Nanotube Exposure. *Part. Fibre Toxicol.* 13 (1), 60. doi:10.1186/s12989-016-0172-2

Du, S., Li, C., Lu, Y., Lei, X., Zhang, Y., Li, S., et al. (2019). Dioscin Alleviates Crystalline Silica-Induced Pulmonary Inflammation and Fibrosis through Promoting Alveolar Macrophage Autophagy. *Theranostics* 9 (7), 1878–1892. doi:10.7150/thno.29682

Duan, J., Yu, Y., Yu, Y., Li, Y., Wang, J., Geng, W., et al. (2014). Silica Nanoparticles Induce Autophagy and Endothelial Dysfunction via the PI3K/Akt/mTOR Signaling Pathway. *Ijn* 9, 5131–5141. doi:10.2147/IJN.S71074

Fernández Álvarez, R., Martínez González, C., Quero Martínez, A., Blanco Pérez, J. J., Carazo Fernández, L., and Prieto Fernández, A. (2015). Guidelines for the Diagnosis and Monitoring of Silicosis. *Archivos de Bronconeumología (English Edition)* 51 (2), 86–93. doi:10.1016/j.arbres.2014.07.01010.1016/j.arbr.2014.07.002

Fujimura, N. (2000). Pathology and Pathophysiology of Pneumoconiosis. *Curr. Opin. Pulm. Med.* 6 (2), 140–144. doi:10.1097/00063198-200003000-00010

Gabasa, M., Duch, P., Jorba, I., Giménez, A., Lugo, R., Pavelescu, I., et al. (2017). Epithelial Contribution to the Profibrotic Stiff Microenvironment and Myofibroblast Population in Lung Fibrosis. *MBoC* 28 (26), 3741–3755. doi:10.1091/mbc.E17-01-0026

Galic, S., Fullerton, M. D., Schertzer, J. D., Sikkema, S., Marcinko, K., Walkley, C. R., et al. (2011). Hematopoietic AMPK β1 Reduces Mouse Adipose Tissue Macrophage Inflammation and Insulin Resistance in Obesity. *J. Clin. Invest.* 121 (12), 4903–4915. doi:10.1172/JCI58577

Gamad, N., Malik, S., Suchal, K., Vasisht, S., Tomar, A., Arava, S., et al. (2018). Metformin Alleviates Bleomycin-Induced Pulmonary Fibrosis in Rats: Pharmacological Effects and Molecular Mechanisms. *Biomed. Pharmacother.* 97, 1544–1553. doi:10.1016/j.biopha.2017.11.101

Gao, J., Yuan, J., Wang, Q. e., Lei, T., Shen, X., Cui, B., et al. (2020). Metformin Protects against PM2.5-induced Lung Injury and Cardiac Dysfunction Independent of AMP-Activated Protein Kinase α2. *Redox Biol.* 28, 101345. doi:10.1016/j.redox.2019.101345

Garcia, D., and Shaw, R. J. (2017). AMPK: Mechanisms of Cellular Energy Sensing and Restoration of Metabolic Balance. *Mol. Cel.* 66 (6), 789–800. doi:10.1016/j.molcel.2017.05.032

Guo, J., Yang, Z., Jia, Q., Bo, C., Shao, H., and Zhang, Z. (2019). Pirfenidone Inhibits Epithelial-Mesenchymal Transition and Pulmonary Fibrosis in the Rat Silicosis Model. *Toxicol. Lett.* 300, 59–66. doi:10.1016/j.toxlet.2018.10.019

Guo, Q., Liu, Z., Jiang, L., Liu, M., Ma, J., Yang, C., et al. (2016). Metformin Inhibits Growth of Human Non-small Cell Lung Cancer Cells via Liver Kinase B-1-independent Activation of Adenosine Monophosphate-Activated Protein Kinase. *Mol. Med. Rep.* 13 (3), 2590–2596. doi:10.3892/mmr.2016.4830

Ha, J., Guan, K.-L., and Kim, J. (2015). AMPK and Autophagy in Glucose/glycogen Metabolism. *Mol. Aspects Med.* 46, 46–62. doi:10.1016/j.mam.2015.08.002

Hardie, D. G., Ross, F. A., and Hawley, S. A. (2012). AMPK: a Nutrient and Energy Sensor that Maintains Energy Homeostasis. *Nat. Rev. Mol. Cel Biol.* 13 (4), 251–262. doi:10.1038/nrm3311

Hernández-Gea, V., Ghiassi-Nejad, Z., Rozenfeld, R., Gordon, R., Fiel, M. I., Yue, Z., et al. (2012). Autophagy Releases Lipid that Promotes Fibrogenesis by Activated Hepatic Stellate Cells in Mice and in Human Tissues. *Gastroenterology* 142 (4), 938–946. doi:10.1053/j.gastro.2011.12.044

Herzig, S., and Shaw, R. J. (2018). AMPK: Guardian of Metabolism and Mitochondrial Homeostasis. *Nat. Rev. Mol. Cel Biol* 19 (2), 121–135. doi:10.1038/nrm.2017.95

Jessop, F., Hamilton, R. F., Rhoderick, J. F., Shaw, P. K., and Holian, A. (2016). Autophagy Deficiency in Macrophages Enhances NLRP3 Inflammasome Activity and Chronic Lung Disease Following Silica Exposure. *Toxicol. Appl. Pharmacol.* 309, 101–110. doi:10.1016/j.taap.2016.08.029

Jiang, S., Li, T., Yang, Z., Yi, W., Di, S., Sun, Y., et al. (2017). AMPK Orchestrates an Elaborate cascade Protecting Tissue from Fibrosis and Aging. *Ageing Res. Rev.* 38, 18–27. doi:10.1016/j.arr.2017.07.001

Jiang, W. G., Sanders, A. J., Katoh, M., Ungefroren, H., Gieseler, F., Prince, M., et al. (2015). Tissue Invasion and Metastasis: Molecular, Biological and Clinical Perspectives. *Semin. Cancer Biol.* 35 (Suppl. l), S244–S275. doi:10.1016/j.semcancer.2015.03.008

Jolly, M. K., Ward, C., Eapen, M. S., Myers, S., Hallgren, O., Levine, H., et al. (2018). Epithelial-mesenchymal Transition, a Spectrum of States: Role in Lung Development, Homeostasis, and Disease. *Dev. Dyn.* 247 (3), 346–358. doi:10.1002/dvdy.24541

Kim, J., Kundu, M., Viollet, B., and Guan, K.-L. (2011). AMPK and mTOR Regulate Autophagy through Direct Phosphorylation of Ulk1. *Nat. Cel Biol* 13 (2), 132–141. doi:10.1038/ncb2152

King, J. D., Jr., Lee, J., Riemen, C. E., Neumann, D., Xiong, S., Foskett, J. K., et al. (2012). Role of Binding and Nucleoside Diphosphate Kinase A in the Regulation of the Cystic Fibrosis Transmembrane Conductance Regulator by AMP-Activated Protein Kinase. *J. Biol. Chem.* 287 (40), 33389–33400. doi:10.1074/jbc.M112.396036

Komatsu, M., and Ichimura, Y. (2010). Physiological Significance of Selective Degradation of P62 by Autophagy. *FEBS Lett.* 584 (7), 1374–1378. doi:10.1016/j.febslet.2010.02.017

Lawrence, J., and Nho, R. (2018). The Role of the Mammalian Target of Rapamycin (mTOR) in Pulmonary Fibrosis. *Ijms* 19 (3), 778. doi:10.3390/ijms19030778

Li, C., Lu, Y., Du, S., Li, S., Zhang, Y., Liu, F., et al. (2017). Dioscin Exerts Protective Effects against Crystalline Silica-Induced Pulmonary Fibrosis in Mice. *Theranostics* 7 (17), 4255–4275. doi:10.7150/thno.20270

Li, N., Shi, F., Wang, X., Yang, P., Sun, K., Zhang, L., et al. (2021). Silica Dust Exposure Induces Pulmonary Fibrosis through Autophagy Signaling. *Environ. Toxicol.* 36 (7), 1269–1277. doi:10.1002/tox.23124

Li, X., Yan, X., Wang, Y., Wang, J., Zhou, F., Wang, H., et al. (2018). NLRP3 Inflammasome Inhibition Attenuates Silica-Induced Epithelial to Mesenchymal Transition (EMT) in Human Bronchial Epithelial Cells. *Exp. Cel Res.* 362 (2), 489–497. doi:10.1016/j.yexcr.2017.12.013

Liang, X. H., Kleeman, L. K., Jiang, H. H., Gordon, G., Goldman, J. E., Berry, G., et al. (1998). Protection against Fatal Sindbis Virus Encephalitis by Beclin, a Novel Bcl-2-Interacting Protein. *J. Virol.* 72 (11), 8586–8596. doi:10.1128/JVI.72.11.8586-8596.1998

Liu, H., Cheng, Y., Yang, J., Wang, W., Fang, S., Zhang, W., et al. (2017). BBC3 in Macrophages Promoted Pulmonary Fibrosis Development through Inducing Autophagy during Silicosis. *Cell Death Dis.* 8 (3), e2657. doi:10.1038/cddis.2017.78

Liu, H., Fang, S., Wang, W., Cheng, Y., Zhang, Y., Liao, H., et al. (2016). Macrophage-derived MCPIP1 Mediates Silica-Induced Pulmonary Fibrosis via Autophagy. *Part. Fibre Toxicol.* 13 (1), 55. doi:10.1186/s12989-016-0167-z

Liu, X., Chhipa, R. R., Nakano, I., and Dasgupta, B. (2014). The AMPK Inhibitor Compound C Is a Potent AMPK-independent Antiglioma Agent. *Mol. Cancer Ther.* 13 (3), 596–605. doi:10.1158/1535-7163.MCT-13-0579

Liu, Y., He, H., Fan, L., Yuan, J., Huang, H., Yang, W., et al. (2020). Compound C Attenuates NLRP3 Inflammasome Despite AMPK Knockdown in LPS Plus Palmitate-Induced THP-1 Cells. *Naunyn-schmiedeberg's Arch. Pharmacol.* 393 (1), 67–76. doi:10.1007/s00210-019-01712-4

Luo, C., Wang, X., Huang, H.-X., Mao, X.-Y., Zhou, H.-H., and Liu, Z.-Q. (2021). Coadministration of Metformin Prevents Olanzapine-Induced Metabolic Dysfunction and Regulates the Gut-Liver axis in Rats. *Psychopharmacology* 238 (1), 239–248. doi:10.1007/s00213-020-05677-8

Lv, Z., and Guo, Y. (2020). Metformin and its Benefits for Various Diseases. *Front. Endocrinol.* 11, 191. doi:10.3389/fendo.2020.00191

Mihaylova, M. M., and Shaw, R. J. (2011). The AMPK Signalling Pathway Coordinates Cell Growth, Autophagy and Metabolism. *Nat. Cel Biol.* 13 (9), 1016–1023. doi:10.1038/ncb2329

Mishra, A. K., and Dingli, D. (2019). Metformin Inhibits IL-6 Signaling by Decreasing IL-6R Expression on Multiple Myeloma Cells. *Leukemia* 33 (11), 2695–2709. doi:10.1038/s41375-019-0470-4

Mizushima, N., Yoshimori, T., and Levine, B. (2010). Methods in Mammalian Autophagy Research. *Cell* 140 (3), 313–326. doi:10.1016/j.cell.2010.01.028

Mizushima, N., Yoshimori, T., and Ohsumi, Y. (2011). The Role of Atg Proteins in Autophagosome Formation. *Annu. Rev. Cel Dev. Biol.* 27, 107–132. doi:10.1146/annurev-cellbio-092910-154005

Mossman, B. T., and Churg, A. (1998). Mechanisms in the Pathogenesis of Asbestosis and Silicosis. *Am. J. Respir. Crit. Care Med.* 157, 1666–1680. doi:10.1164/ajrccm.157.5.9707141

Nair, A., and Jacob, S. (2016). A Simple Practice Guide for Dose Conversion between Animals and Human. *J. Basic Clin. Pharma* 7 (2), 27–31. doi:10.4103/0976-0105.177703

Nasri, H., and Rafieian-Kopaei, M. (2014). Metformin: Current Knowledge. *J. Res. Med. Sci.* 19 (7), 658–664.

Pang, X., Shao, L., Nie, X., Yan, H., Li, C., Yeo, A. J., et al. (2021). Emodin Attenuates Silica-Induced Lung Injury by Inhibition of Inflammation, Apoptosis and Epithelial-Mesenchymal Transition. *Int. Immunopharmacology* 91, 107277. doi:10.1016/j.intimp.2020.107277

Park, C. S., Bang, B.-R., Kwon, H.-S., Moon, K.-A., Kim, T.-B., Lee, K.-Y., et al. (2012). Metformin Reduces Airway Inflammation and Remodeling via Activation of AMP-Activated Protein Kinase. *Biochem. Pharmacol.* 84 (12), 1660–1670. doi:10.1016/j.bcp.2012.09.025

Pearson, G. W. (2019). Control of Invasion by Epithelial-To-Mesenchymal Transition Programs during Metastasis. *Jcm* 8 (5), 646. doi:10.3390/jcm8050646

Pollard, K. M. (2016). Silica, Silicosis, and Autoimmunity. *Front. Immunol.* 7, 97. doi:10.3389/fimmu.2016.00097

Pushpakom, S., Iorio, F., Eyers, P. A., Escott, K. J., Hopper, S., Wells, A., et al. (2019). Drug Repurposing: Progress, Challenges and Recommendations. *Nat. Rev. Drug Discov.* 18 (1), 41–58. doi:10.1038/nrd.2018.168

Quaile, M. P., Melich, D. H., Jordan, H. L., Nold, J. B., Chism, J. P., Polli, J. W., et al. (2010). Toxicity and Toxicokinetics of Metformin in Rats. *Toxicol. Appl. Pharmacol.* 243 (4), 340–347. doi:10.1016/j.taap.2009.11.026

Racanelli, A. C., Kikkers, S. A., Choi, A. M. K., and Cloonan, S. M. (2018). Autophagy and Inflammation in Chronic Respiratory Disease. *Autophagy* 14 (2), 221–232. doi:10.1080/15548627.2017.1389823

Rana, U., Callan, E., Entringer, B., Michalkiewicz, T., Joshi, A., Parchur, A. K., et al. (2020). AMP-kinase Dysfunction Alters Notch Ligands to Impair Angiogenesis in Neonatal Pulmonary Hypertension. *Am. J. Respir. Cel Mol Biol.* 62 (6), 719–731. doi:10.1165/rcmb.2019-0275OC

Rangarajan, S., Bone, N. B., Zmijewska, A. A., Jiang, S., Park, D. W., Bernard, K., et al. (2018). Metformin Reverses Established Lung Fibrosis in a Bleomycin Model. *Nat. Med.* 24 (8), 1121–1127. doi:10.1038/s41591-018-0087-6

Rees, D., and Murray, J. (2007). Silica, Silicosis and Tuberculosis. *Int. J. Tuberc. Lung Dis.* 11 (5), 474–484.

Ren, H., Shao, Y., Wu, C., Ma, X., Lv, C., and Wang, Q. (2020). Metformin Alleviates Oxidative Stress and Enhances Autophagy in Diabetic Kidney Disease via AMPK/SIRT1-FoxO1 Pathway. *Mol. Cell Endocrinol.* 500, 110628. doi:10.1016/j.mce.2019.110628

Robledo, R., and Mossman, B. (1999). Cellular and Molecular Mechanisms of Asbestos-Induced Fibrosis. *J. Cel Physiol* 180 (2), 158–166. doi:10.1002/(SICI)1097-4652(199908)180:2<158::AID-JCP3>3.0.CO;2-R

Rout-Pitt, N., Farrow, N., Parsons, D., and Donnelley, M. (2018). Epithelial Mesenchymal Transition (EMT): a Universal Process in Lung Diseases with Implications for Cystic Fibrosis Pathophysiology. *Respir. Res.* 19 (1), 136. doi:10.1186/s12931-018-0834-8

Sag, D., Carling, D., Stout, R. D., and Suttles, J. (2008). Adenosine 5′-Monophosphate-Activated Protein Kinase Promotes Macrophage Polarization to an Anti-inflammatory Functional Phenotype. *J. Immunol.* 181 (2), 8633–8641. doi:10.4049/jimmunol.181.12.8633

Sai, L., Yu, G., Bo, C., Zhang, Y., Du, Z., Li, C., et al. (2019). Profiling Long Non-coding RNA Changes in Silica-Induced Pulmonary Fibrosis in Rat. *Toxicol. Lett.* 310, 7–13. doi:10.1016/j.toxlet.2019.04.003

Salminen, A., Hyttinen, J. M. T., and Kaarniranta, K. (2011). AMP-activated Protein Kinase Inhibits NF-Kb Signaling and Inflammation: Impact on Healthspan and Lifespan. *J. Mol. Med.* 89 (7), 667–676. doi:10.1007/s00109-011-0748-0

Sato, N., Takasaka, N., Yoshida, M., Tsubouchi, K., Minagawa, S., Araya, J., et al. (2016). Metformin Attenuates Lung Fibrosis Development via NOX4 Suppression. *Respir. Res.* 17 (1), 107. doi:10.1186/s12931-016-0420-x

Sayan, M., and Mossman, B. T. (2016). The NLRP3 Inflammasome in Pathogenic Particle and Fibre-Associated Lung Inflammation and Diseases. *Part. Fibre Toxicol.* 13 (1), 51. doi:10.1186/s12989-016-0162-4

Serrano-Gomez, S. J., Maziveyi, M., and Alahari, S. K. (2016). Regulation of Epithelial-Mesenchymal Transition through Epigenetic and post-translational Modifications. *Mol. Cancer* 15, 18. doi:10.1186/s12943-016-0502-x

Shaw, R. J., Lamia, K. A., Vasquez, D., Koo, S. H., Bardeesy, N., Depinho, R. A., et al. (2005). The Kinase LKB1 Mediates Glucose Homeostasis in Liver and Therapeutic Effects of Metformin. *Science* 310 (5754), 1642–1646. doi:10.1126/science.1120781

Southern, B. D., Scheraga, R. G., and Olman, M. A. (2017). Impaired AMPK Activity Drives Age-Associated Acute Lung Injury after Hemorrhage. *Am. J. Respir. Cel Mol Biol.* 56 (5), 553–555. doi:10.1165/rcmb.2017-0023ED

Stone, R. C., Pastar, I., Ojeh, N., Chen, V., Liu, S., Garzon, K. I., et al. (2016). Epithelial-mesenchymal Transition in Tissue Repair and Fibrosis. *Cell Tissue Res.* 365 (3), 495–506. doi:10.1007/s00441-016-2464-0

Sun, J., Li, Q., Lian, X., Zhu, Z., Chen, X., Pei, W., et al. (2019). MicroRNA-29b Mediates Lung Mesenchymal-Epithelial Transition and Prevents Lung Fibrosis in the Silicosis Model. *Mol. Ther. - Nucleic Acids* 14, 20–31. doi:10.1016/j.omtn.2018.10.017

Szapiel, S. V., Elson, N. A., Fulmer, J. D., Hunninghake, G. W., and Crystal, R. G. (1979). Bleomycin-induced Interstitial Pulmonary Disease in the Nude, Athymic Mouse. *Am. Rev. Respir. Dis.* 120 (4), 893–899. doi:10.1164/arrd.1979.120.4.893

Takata, T., Motoo, Y., and Tomosugi, N. (2014). Effect of Saikokeishito, a Kampo Medicine, on Hydrogen Peroxide-Induced Premature Senescence of normal Human Dermal Fibroblasts. *J. Integr. Med.* 12 (6), 495–503. doi:10.1016/S2095-4964(14)60052-2

Tamargo-Gómez, I., and Mariño, G. (2018). AMPK: Regulation of Metabolic Dynamics in the Context of Autophagy. *Ijms* 19 (12), 3812. doi:10.3390/ijms19123812

Tavakol, S., Ashrafizadeh, M., Deng, S., Azarian, M., Abdoli, A., Motavaf, M., et al. (2019). Autophagy Modulators: Mechanistic Aspects and Drug Delivery Systems. *Biomolecules* 9 (10), 530. doi:10.3390/biom9100530

Tsaknis, G., Siempos, I. I., Kopterides, P., Maniatis, N. A., Magkou, C., Kardara, M., et al. (2012). Metformin Attenuates Ventilator-Induced Lung Injury. *Crit. Care* 16 (4), R134. doi:10.1186/cc11439

Tseng, Y.-J., Dong, L., Liu, Y.-F., Xu, N., Ma, W., Weng, S.-Q., et al. (2019). Role of Autophagy in Chronic Liver Inflammation and Fibrosis. *Cpps* 20 (8), 817–822. doi:10.2174/1389203720666190305165203

Wang, H., Liu, Y., Wang, D., Xu, Y., Dong, R., Yang, Y., et al. (2019). The Upstream Pathway of mTOR-Mediated Autophagy in Liver Diseases. *Cells* 8 (12), 1597. doi:10.3390/cells8121597

Wang, J., Gao, Q., Wang, D., Wang, Z., and Hu, C. (2015). Metformin Inhibits Growth of Lung Adenocarcinoma Cells by Inducing Apoptosis via the Mitochondria-Mediated Pathway. *Oncol. Lett.* 10 (3), 1343–1349. doi:10.3892/ol.2015.3450

Wang, Y., Chen, H., Sun, C., Shen, H., and Cui, X. (2021). Metformin Attenuates Lipopolysaccharide-induced Epithelial Cell Senescence by Activating Autophagy. *Cell Biol Int* 45 (5), 927–935. doi:10.1002/cbin.11536

Xiao, H., Ma, X., Feng, W., Fu, Y., Lu, Z., Xu, M., et al. (2010). Metformin Attenuates Cardiac Fibrosis by Inhibiting the TGFβ1-Smad3 Signalling Pathway. *Cardiovasc. Res.* 87 (3), 504–513. doi:10.1093/cvr/cvq066

Xu, G., Wang, X., Yu, H., Wang, C., Liu, Y., Zhao, R., et al. (2019a). Beclin 1, LC3, and P62 Expression in Paraquat-Induced Pulmonary Fibrosis. *Hum. Exp. Toxicol.* 38 (7), 794–802. doi:10.1177/0960327119842633

Xu, J., Ji, J., and Yan, X.-H. (2012). Cross-talk between AMPK and mTOR in Regulating Energy Balance. *Crit. Rev. Food Sci. Nutr.* 52 (5), 373–381. doi:10.1080/10408398.2010.500245

Xu, T., Yan, W., Wu, Q., Xu, Q., Yuan, J., Li, Y., et al. (2019b). MiR-326 Inhibits Inflammation and Promotes Autophagy in Silica-Induced Pulmonary Fibrosis through Targeting TNFSF14 and PTBP1. *Chem. Res. Toxicol.* 32 (11), 2192–2203. doi:10.1021/acs.chemrestox.9b00194

Yan, J., Yang, H., Wang, G., Sun, L., Zhou, Y., Guo, Y., et al. (2010). Autophagy Augmented by Troglitazone Is Independent of EGFR Transactivation and Correlated with AMP-Activated Protein Kinase Signaling. *Autophagy* 6 (1), 67–73. doi:10.4161/auto.6.1.10437

Yang, T., Wang, J., Pang, Y., Dang, X., Ren, H., Liu, Y., et al. (2016). Emodin Suppresses Silica-Induced Lung Fibrosis by Promoting Sirt1 Signaling via Direct Contact. *Mol. Med. Rep.* 14 (5), 4643–4649. doi:10.3892/mmr.2016.5838

Yang, Y., Zhao, Z., Liu, Y., Kang, X., Zhang, H., and Meng, M. (2015). Suppression of Oxidative Stress and Improvement of Liver Functions in Mice by Ursolic Acid via LKB1-AMP-Activated Protein Kinase Signaling. *J. Gastroenterol. Hepatol.* 30 (3), 609–618. doi:10.1111/jgh.12723

Yang, Z., Kahn, B. B., Shi, H., and Xue, B.-z. (2010). Macrophage α1 AMP-Activated Protein Kinase (α1AMPK) Antagonizes Fatty Acid-Induced Inflammation through SIRT1. *J. Biol. Chem.* 285 (25), 19051–19059. doi:10.1074/jbc.M110.123620

Yoshida, J., Ishikawa, T., Endo, Y., Matsumura, S., Ota, T., Mizushima, K., et al. (2020). Metformin Inhibits TGF-β1-induced E-pithelial-mesenchymal T-ransition and L-iver M-etastasis of P-ancreatic C-ancer C-ells. *Oncol. Rep.* 44 (1), 371–381. doi:10.3892/or.2020.7595

Zhang, C.-X., Pan, S.-N., Meng, R.-S., Peng, C.-Q., Xiong, Z.-J., Chen, B.-L., et al. (2011). Metformin Attenuates Ventricular Hypertrophy by Activating the AMP-Activated Protein Kinase-Endothelial Nitric Oxide Synthase Pathway in Rats. *Clin. Exp. Pharmacol. Physiol.* 38 (1), 55–62. doi:10.1111/j.1440-1681.2010.05461.x

Zhao, H., Wang, Y., Qiu, T., Liu, W., and Yao, P. (2020). Autophagy, an Important Therapeutic Target for Pulmonary Fibrosis Diseases. *Clinica Chim. Acta* 502, 139–147. doi:10.1016/j.cca.2019.12.016

Zhao, X., Wei, S., Li, Z., Lin, C., Zhu, Z., Sun, D., et al. (2019). Autophagic Flux Blockage in Alveolar Epithelial Cells Is Essential in Silica Nanoparticle-Induced Pulmonary Fibrosis. *Cel Death Dis.* 10 (2), 127. doi:10.1038/s41419-019-1340-8

Conflict of Interest: The authors declare that the research was conducted in the absence of any commercial or financial relationships that could be construed as a potential conflict of interest.

Publisher's Note: All claims expressed in this article are solely those of the authors and do not necessarily represent those of their affiliated organizations, or those of the publisher, the editors and the reviewers. Any product that may be evaluated in this article, or claim that may be made by its manufacturer, is not guaranteed or endorsed by the publisher.

frontiers in Pharmacology

ORIGINAL RESEARCH
published: 23 August 2021
doi: 10.3389/fphar.2021.724141

Blockade of Autophagy Prevents the Development and Progression of Peritoneal Fibrosis

*Yingfeng Shi[1†], Yan Hu[1†], Yi Wang[1], Xiaoyan Ma[1], Lunxian Tang[2], Min Tao[1], Andong Qiu[3], Shougang Zhuang[1,4] and Na Liu[1]**

[1]Department of Nephrology, Shanghai East Hospital, Tongji University School of Medicine, Shanghai, China, [2]Emergency Department of Critical Care Medicine, Shanghai East Hospital, Tongji University School of Medicine, Shanghai, China, [3]School of Life Science and Technology, Advanced Institute of Translational Medicine, Tongji University, Shanghai, China, [4]Department of Medicine, Rhode Island Hospital and Alpert Medical School, Brown University, Providence, RI, United States

Peritoneal fibrosis (PF) is a major cause of ultrafiltration failure in long-term peritoneal dialysis (PD) patients. Nevertheless, limited measures have been shown to be effective for the prevention and treatment of PF. Some views reveal that activation of autophagy ameliorates PF but others demonstrate that autophagy promotes PF. It is obvious that the role of autophagy in PF is controversial and further studies are needed. Here, we investigated the role of autophagy in rat models of PF and damaged cultured human peritoneal mesothelial cells (HPMCs). Autophagy was highly activated in fibrotic peritoneum from two PF rat models induced by 4.25% peritoneal dialysate fluid (PDF) and 0.1% chlorhexidine gluconate (CG). Blockade of autophagy with 3-MA effectively prevented PF in both models and reversed epithelial to mesenchymal transition (EMT) by down-regulating TGF-β/Smad3 signaling pathway and downstream nuclear transcription factors Slug and Snail. Treatment with 3-MA also inhibited activation of EGFR/ERK1/2 signaling pathway during PF. Moreover, 3-MA prominently decreased STAT3/NF-κB-mediated inflammatory response and macrophage infiltration, and prevented peritoneal angiogenesis through downregulation of β-catenin signal. In addition, TGF-β1 stimulation up-regulated autophagic activity as evidenced by the increased autophagosome *in vitro*. Exposure of HPMCs to TGF-β1 resulted in the induction of EMT and activation of TGF-β/Smad3, EGFR/ERK1/2 signaling pathways. Treatment with 3-MA blocked all these responses. In addition, delayed administration of 3-MA was effective in reducing EMT induced by TGF-β1. Taken together, our study indicated that autophagy might promote PF and 3-MA had anti-fibrosis effect *in vivo* and *in vitro*. These results suggest that autophagy could be a potential target on PF therapy for clinical patients with long-term PD.

Keywords: autophagy, peritoneal fibrosis, epithelial to mesenchymal transition, profibrotic signaling pathways, inflammation

OPEN ACCESS

Edited by:
Raffaele Strippoli, Sapienza University of Rome, Italy

Reviewed by:
Manuela Antonioli, Istituto Nazionale per le Malattie Infettive Lazzaro Spallanzani (IRCCS), Italy
Guadalupe González, Severo Ochoa Molecular Biology Center (CSIC-UAM), Spain

****Correspondence:***
Na Liu
naliubrown@163.com

†These authors share first authorship

Specialty section:
This article was submitted to Experimental Pharmacology and Drug Discovery, a section of the journal Frontiers in Pharmacology

Received: *12 June 2021*
Accepted: *09 August 2021*
Published: *23 August 2021*

Citation:
Shi Y, Hu Y, Wang Y, Ma X, Tang L, Tao M, Qiu A, Zhuang S and Liu N (2021) Blockade of Autophagy Prevents the Development and Progression of Peritoneal Fibrosis. Front. Pharmacol. 12:724141. doi: 10.3389/fphar.2021.724141

INTRODUCTION

Peritoneal dialysis (PD) is a well-established alternative therapy for patients with end-stage renal disease (ESRD). According to the last registry, PD is currently used by about 11% of dialysis patients with ESRD (Jain et al., 2012). In spite of the unique advantages such as preservation of residual renal function, stable hemodynamics, and higher quality of life for patients, compared to hemodialysis, PD

promotes continuous exposure of the peritoneal membrane to bioincompatible dialysis solutions, which leads to the alteration of normal peritoneal membrane structure and loss of ultrafiltration function, eventually causes the progressive development of peritoneal fibrosis (PF) and forces patients to withdraw from PD (Krediet and Struijk, 2013; Zhou et al., 2016a; Krediet, 2018). Therefore, exploring the mechanism of PF and effective prevention strategies are urgently needed.

Epithelial to mesenchymal transition (EMT) of peritoneal mesothelial cells (PMCs), also known as mesothelial to mesenchymal transition (MMT), is considered to be an important initiating factor in PF (Strippoli et al., 2016). Mounting evidence has demonstrated that transforming growth factor β1 (TGF-β1)-induced EMT is a pivotal process of progressive PF (Margetts et al., 2005). TGF-β1 signal exerts its biological effects through activating the phosphorylation of Smad2 and Smad3 by the type I TGF-β receptor (TGF-βRI), and then translocated into nucleus where they regulate gene transcription (Leask and Abraham, 2004). Previous study has confirmed that Smad3 knockout mice develop into mild PF by attenuating EMT and reducing collagen formation (Patel et al., 2010). Except for TGF-β1/Smad3 signaling pathway, activation of epidermal growth factor receptor (EGFR) pathway is another important mechanism during PF progress. Our research group demonstrated for the first time that EGFR and its downstream molecules participated in PF, and inhibition of EGFR blocked the development and progression of mouse PF induced by chlorhexidine gluconate (CG) (Wang et al., 2016).

Peritoneal inflammation is considered as an important event during the pathogenesis of PF (Zhang et al., 2017a). Peritoneal injury leads to the activation of signal transducer and activator of transcription 3 (STAT3) and nuclear factor kappa-B (NF-κB), promotes the release of multiple proinflammatory cytokines such as interleukin-6 (IL-6), monocyte chemoattractant protein-1 (MCP-1), tumor necrosis factor-α (TNF-α) and interleukin-1β (IL-1β) (Fan et al., 2013). NF-κB signaling pathway is also closely associated with the occurrence of EMT as well as macrophage recruitment (Kitterer et al., 2015). Macrophage has the ability to stimulate the production of connective tissue growth factor (CTGF), and has been involved in the activation of myofibroblasts (Wynn and Vannella, 2016). In addition, another important mechanism for PD-related PF is angiogenesis. The increase in angiogenesis is related to an increase in solute transport rate and a decline in the ultrafiltration capacity (Davies, 2004). The role of WNT/β-catenin signaling in peritoneal membrane angiogenesis has been recently clarified (Padwal et al., 2017; Padwal et al., 2018). Treatment with ICG-001, a β-catenin inhibitor, improved peritoneal angiogenesis in a mouse model of PF, and decreased levels of vascular endothelial growth factor (VEGF) (Padwal et al., 2018).

Autophagy is a self-protection mechanism to maintain the homeostasis of cellular environment, which is mediated by lysosome to degrade damaged proteins or organelles (Saha et al., 2018). Under physiological conditions, autophagy plays an vital role in ensuring the normal proliferation, differentiation and apoptosis of cells (Saha et al., 2018). However, autophagy is also involved in the pathophysiological mechanism of multiple diseases. Recent reports have shown that autophagy is closely related to pathogenesis and development of tissue fibrosis, such as heart (Zhao et al., 2018), liver (Meng et al., 2018), lung (Cabrera et al., 2015), and kidney (Zhao et al., 2019). For PF, autophagy has both positive and negative effects. The *in vitro* study demonstrated that initiation of autophagy could block the NLRP3-IL-1β mediated inflammasome activation, thus resisting the damage of high glucose (HG)-based peritoneal dialysis fluids on PMCs (Wu et al., 2016a). Only two animal experiments confirmed the protective role of autophagy against PF, and that autophagy down-regulation was observed in peritoneum from a HG-induced mouse peritoneal injury model (Yang et al., 2017; Li et al., 2019a). On the contrary, another research found that HG peritoneal dialysate induced autophagy in human peritoneal mesothelial cells (HPMCs), associated with fibrosis and apoptosis hallmarks (Wu et al., 2018). They indicated that autophagy promoted fibrosis and apoptosis in the peritoneum during long-term PD (Wu et al., 2018). Such dual character of autophagy has also been proved in renal fibrosis and hepatic fibrosis. Obviously, the role of autophagy in PF is still controversial, and it is very meaningful to conduct autophagy research on the progression of PF.

In this study, we examined the activation of autophagy in fibrotic peritoneum from two PF rat models injected with 4.25% peritoneal dialysate fluid (PDF) for 28 days and 0.1% CG for 21 days, and in TGF-β1-stimulated HPMCs. We also evaluated the effect of autophagy inhibition with 3-Methyladenine (3-MA) on fibrosis pathological changes *in vivo* and *in vitro*. Moreover, we clarified the mechanisms by which blockade of autophagy prevents the development of PF. This study elucidated the exact role and mechanism of autophagy in PF, and suggested that autophagy could be a potential target on PF therapy for clinical long-term PD patients.

MATERIALS AND METHODS

Antibodies and Reagents

3-MA was purchased from Selleckchem (Houston, TX, United States). Antibodies to Beclin-1 (#3738), p-Smad3 (#9520), Smad3 (#9523), E-cadherin (#14472), p-EGFR (#3777), EGFR (#4267), p-ERK1/2 (#4370), ERK1/2 (#4695), p-STAT3 (#9138), STAT3 (#9139), β-actin (#4970) and Snail (#3879) were purchased from Cell Signaling Technology (Danvers, MA, United States). Antibodies to GAPDH (sc-32233), Collagen I (sc-28654), TGF-βRI (sc-399), p-NF-κB (sc-166748), NF-κB (sc-8008), IL-1β (sc-52012), CD68 (sc-20060), CD31 (sc-376764), VEGF (sc-7269) were purchased from Santa Cruz Biotechnology (San Diego, CA, United States). Antibodies to Fibronectin (ab2413) and Slug (ab27568) were purchased from Abcam (Cambridge, MA, United States). Antibody to LC3 (NB100-2220) was purchased from Novus Biologicals (Littleton, CO). Antibody to β-catenin (610154) was purchased from BD Biosciences (San Diego, CA). Antibodies to CD34 (GB13013) and IL-6 (GB11117) were purchased from Servicebio (Wuhan, China). TGF-β1, IL-1β, MCP-1 enzyme-

linked immunosorbent assay (ELISA) kits and TGF-β1 protein were purchased from R&D Systems (Minneapolis, MN, United States). Beclin-1 siRNA was purchased from GenePharma (Shanghai, China). Lipofectamine 2000 was purchased from Invitrogen (Grand Island, NY, United States). 4.25% glucose peritoneal dialysis solution was purchased from Baxter Healthcare (Guangzhou, China). Antibody to α-SMA (A2547), chlorhexidine gluconate, DMSO and all other chemicals were obtained from Sigma-Aldrich (St. Louis, MO, United States).

Animal Models and Experimental Design

Male Sprague-Dawley rats (Shanghai Super-B&K Laboratory Animal Corp. Ltd., Shanghai, China) that weighed 200–220 g were housed under a 12 h light-dark cycle with food and water supplied ad libitum at the Experimental Animal Center of Tongji University. Two PF rat models were established respectively by intraperitoneal injection of 4.25% high glucose PDF (100 ml/kg) every day for 28 days (Xu et al., 2017; Shi et al., 2020) and 0.1% CG (10 ml/kg) dissolved in saline every other day for 21 days (Kokubo et al., 2012; Io et al., 2015; Shi et al., 2020). To investigate the anti-fibrosis effect of 3-MA on PF, rats were injected intraperitoneally with two doses of 3-MA (15 and 30 mg/kg) in warmed saline every day. 3-MA is administrated apart from the 10 ml/kg of CG or 100 ml/kg of PDF. Rats were randomly divided into four groups in each model: 1) Rats injected with an equivalent amount of saline intraperitoneally, defined as sham group ($n = 6$); 2) Rats injected with an equivalent amount of saline intraperitoneally and 3-MA, defined as sham + 3-MA group ($n = 6$); 3) Rats injected with 4.25% PDF or 0.1% CG and an equivalent amount of saline intraperitoneally, defined as PDF/CG group ($n = 6$); 4) Rats injected with 4.25% PDF or 0.1% CG and 3-MA, defined as PDF/CG+3-MA group ($n = 6$). At the end of 28 or 21 days, all rats were killed by exsanguination under anesthesia with inhaled 5% isoflurane in room air and the parietal peritoneum was collected from each group for further protein analysis and histological examination. The animal protocol was reviewed and approved by the Institutional Animal Care and Use Committee at Tongji University.

Cell Culture and Treatments

HPMCs (kind gifts from Haiping Mao at Sun Yat-Sen University, Guangzhou, China) were cultured in MEM medium containing 10% fetal bovine serum (FBS), 1% penicillin and streptomycin in an atmosphere of 5% CO2 and 95% air at 37°C. We passed the primary cells for three generations, obtained a stable phenotype, and then started the formal experiments. To examine the inhibitory effect of 3-MA on TGF-β1-induced EMT *in vitro*, subconfluent HPMCs were starved for 24 h in MEM medium containing 0.5% FBS and then exposed to TGF-β1 (2 ng/ml) in the presence of 3-MA (0, 1, 5 and 10 mM) for 36 h. After exposed for 36 h, cells were harvested for immunoblotting analyses and transmission electron microscope observation. To determine the effects of delayed treatment of 3-MA on TGF-β1-induced EMT, subconfluent HPMCs were starved for 24 h in MEM medium containing 0.5% FBS followed by stimulation with TGF-β1 (2 ng/ml) for 48 h and then incubated with 10 mM 3-MA for an additional 24 or 48 h, cells were harvested for immunoblotting analyses. All of the *in vitro* experiments were repeated for at least three times.

siRNA Transfection

The small interfering (si) RNA oligonucleotides targeted specially for Beclin-1 and non-targeting control siRNA were used in this study. The Beclin-1 siRNA (sense: 5′-CAGUUUGGCACAAUC AAUATT-3′ and antisense: 5′-UAUUGAUUGUGCCAAACU GTT-3′) were chemically synthesized by GenePharma (Shanghai, China). HPMCs were seed to 30–40% confluence in antibiotic-free medium and cultured for 24 h then transfected with Beclin-1 siRNA (100 pmol) with lipofectamine 2000 (Invitrogen, Grand Island, NY, United States) according to the manufacturer's instructions. In parallel, scrambled siRNA (100 pmol) was used as control for off-target changes in HPMCs. After transfection for 24 h, the original antibiotic-free medium was changed and cells were treated with TGF-β1 (2 ng/ml) for an additional 36 h before being harvested for the further experiments.

ELISA Analysis

ELISA detection of TGF-β1, IL-1β and MCP-1 proteins in peritoneal tissue from each group were performed in accordance with the manufacturer's instructions.

Immunoblot Analysis

Immunoblot analysis of rat peritoneal tissue and cell samples was conducted as described previously (Zhou et al., 2016b). The densitometry analysis of immunoblot results was conducted by using ImageJ software.

Morphologic Studies of Peritoneum

Formalin-fixed peritoneum was embedded in paraffin and cut into 3-μm-thick sections. For evaluation of PF, Masson's trichrome staining and Sirius red staining were performed according to the protocol provided by the supplier (Sigma-Aldrich). The positive area and thickness of the submesothelial tissue were measured, and the average of ten independent measurements were calculated for each section.

Immunohistochemical Staining

Sections cut at 3 μm thick were de-paraffinized and rehydrated, quenched with 3% H_2O_2, immersed in citrate buffer and heated in a microwave for retrieval of antigens as described in our previous study (Pang et al., 2009). Slides were viewed with a Nikon Eclipse 80i microscope equipped with a digital camera (DS-Ri1, Nikon, Shanghai, China).

Immunofluorescence Staining

Immunofluorescence staining was carried out according to the procedure described in our previous study (Pang et al., 2009). Formalin-Fixed Paraffin-Embedded (FFPE) sections (3 μm) were rehydrated and incubated with primary antibodies against Beclin-1, E-cadherin or Snail and then Texas Red- or FITC-labeled secondary antibodies (Invitrogen).

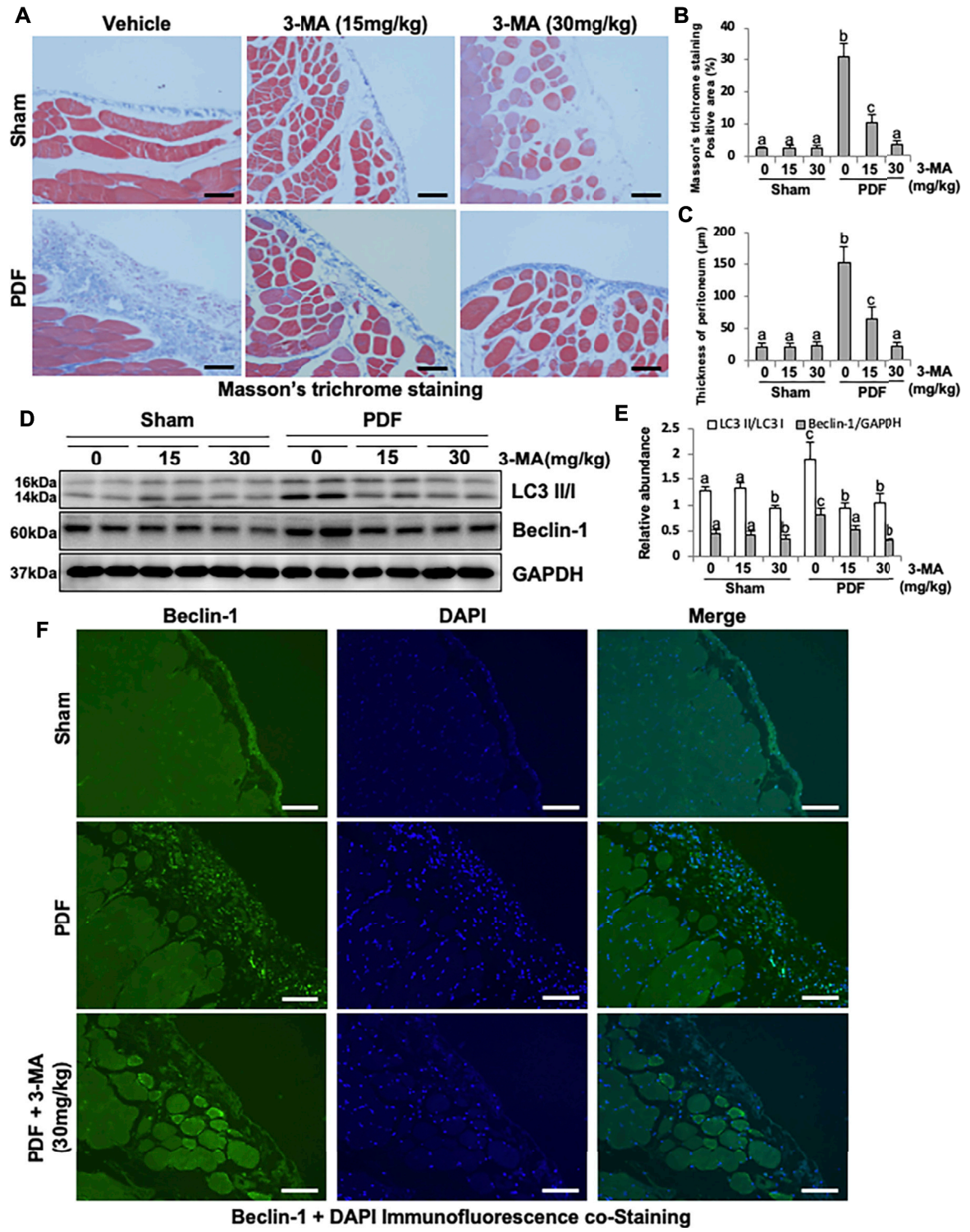

FIGURE 1 | Administration of 3-MA inhibits autophagy and prevents peritoneal fibrosis in 4.25% PDF-induced rat model. **(A)** Photomicrographs show Masson's trichrome staining of the peritoneum in each group. **(B)** Positive area of the Masson-positive submesothelial area (blue). **(C)** Thickness of the Masson-positive submesothelial area (blue). **(D)** Peritoneum tissue lysates were subjected to immunoblot analysis with specific antibodies against LC3, Beclin-1 and GAPDH. **(E)** Expression levels of LC3II and Beclin-1 were quantified by densitometry and normalized with LC3I and GAPDH respectively. **(F)** Photomicrographs show immunofluorescence co-staining of Beclin-1 and DAPI. Data are represented as the mean ± SEM. Means with different superscript letters are significantly different from one another ($p < 0.05$). All scale bars = 100 μm.

Transmission Electron Microscope

Transmission electron microscope (TEM) was performed to observe the morphology of autophagosome. After indicated treatments, cells were collected from each group for standard TEM processing. And various autophagic structures including phagophore, autophagosome, and autolysosome in HPMCs were revealed at high magnification from each cell and digital images with scale bars were taken.

Statistical Analysis

Data depicted in graphs represent the means ± SEM for each group. Intergroup comparison was made using one-way ANOVA. Multiple means were compared using Tukey's test. The differences between two groups were determined by Student's t-test. Statistically significant differences between mean values were marked in each graph. $p < 0.05$ was considered significant. The statistical analyses were conducted by using IBM SPSS Statistics 20.0 (Version X; IBM, Armonk, NY, United States).

RESULTS

Administration of 3-MA Inhibits Autophagy and Prevents PF in Both 4.25% PDF-Induced Rat Model and 0.1% CG-Induced Rat Model

To elucidate the role of autophagy in the development of PF, we first established a model of PF in rats by intraperitoneal injection with 4.25% high glucose peritoneal dialysate for 28 days and concurrently given 3-MA treatment (15 and 30 mg/kg). As shown in **Figure 1**, thickening of the submesothelial compact zone is demonstrated by Masson's trichrome staining. Treatment with 3-MA prevents PF in a dose-dependent manner as indicated by the significant reduction of Masson's trichrome staining positive area and the thickness of peritoneum (**Figures 1A–C**). Low homeostasis level of autophagy was detected in the normal rats with/without 3-MA injection, but it was significantly increased in the PF rats, as evidenced by the high level of LC3B II to I ratio and Beclin-1. Both dose of 3-MA could inhibit the anomalous up-regulation of autophagy caused by high glucose dialysate, as indicated in the decreased of LC3B II to I ratio and Beclin-1 (**Figures 1D,E**). Moreover, immunofluorescence co-staining showed that Beclin-1 was highly expressed in thickened peritoneum from PF rats, and mainly located in peritoneal mesothelial cells (**Figure 1F**).

Next, we established another rat model of PF by intraperitoneal injection of 0.1% CG every other day for 21 days, so as to verify the anti-peritoneal fibrosis effect of 3-MA again. Similarly, thickening of the submesothelial compact zone is demonstrated by the Masson's trichrome staining and Sirius red staining in PF rats, administration of 3-MA (30 mg/kg) significantly decreased thickness of the fibrotic submesothelial area and the quantified positive staining area (**Supplementary Figures S1A–D**). Consistent with PDF-model, increased expression of LC3 and Beclin-1 were observed in CG-induced PF rats, treatment with 3-MA remarkably blocked its expression (**Supplementary Figures S1E,F**). Taken together, these results indicate that autophagy is up-regulated in peritoneum in both PF models and 3-MA has the ability to prevent PF.

Blockade of Autophagy With 3-MA Prevents EMT in Both PF Rat Models

EMT occurs after peritoneal injury and is involved in the development of PF (Liu et al., 2015). To understand whether autophagy mediates PF by regulating the process of EMT, we examined the effect of 3-MA in both PF rat models. As shown in **Figures 2A–E** and **Supplementary Figure S2**, injection of PDF or CG caused a significant reduction of the protein levels of E-cadherin, an epithelial cell marker, and increased expression of α-SMA, Fibronectin, and Collagen I, three mesenchymal markers. Administrated with 3-MA in both dose of 15 mg/kg and 30 mg/kg could down-regulate the expression levels of three mesenchymal marker as mentioned above (**Figures 2A–D**). Moreover, 3-MA effectively restored the expression of E-cadherin in the damaged peritoneum, especially for the 30 mg/kg treatment group, whose expression level was similar to that of the normal rats (**Figures 2A,E**). In addition, both of Sirius red staining and Collagen I immunohistochemical staining further confirmed that 3-MA inhibited collagen formation and accumulation of the submesothelial compact zone, and markedly reduced quantitative positive area of them (**Figures 2F–H**). These data suggest that 3-MA prevents PF by inhibiting the process of EMT.

Inhibition of Autophagy With 3-MA Blocks EMT in PF Rats by Regulating TGF-β/Smad3 Signaling Pathway and Downstream Nuclear Transcription Factors: Slug and Snail

The production of TGF-β1, stimulated by high glucose and acid pH, is the main extracellular matrix (ECM) and collagen-producing factor during organ fibrosis (Massagué, 2012). To demonstrated whether PDF could induce TGF-β1 production in peritoneum, the secretion of TGF-β1 from peritoneum was determined by ELISA kit. As shown in **Figure 3A**, higher level of TGF-β1 was observed in injured peritoneum from PDF-model group than sham rats, administrated with 3-MA significantly reduced the production of TGF-β1. To further identify autophagy might be involved in the process of EMT by regulating TGF-β/Smad3 signaling pathway, Western blotting analysis was conducted. Immunoblot analysis showed that exposure to 4.25% PDF resulted in the activation of TGF-β/Smad3 signaling pathway, as evidenced by the significant increased expression of TGF-βRI and p-Smad3. Single dose of 3-MA decreased TGF-βRI and inhibited phosphorylation of Smad3, but had no impact on total Smad3 (**Figures 3B–D**). Immunohistochemical staining of p-Smad3 further confirmed inhibitory effect of 3-MA on Smad3 activation (**Figure 3E**). Furthermore, since TGF-β/Smad3 signaling pathway directly regulates Slug and Snail, two nuclear transcriptional repressors of E-cadherin, thus promoting EMT (Cano et al., 2000), we also examined the impact of 3-MA on their expressions. Basal levels of Slug and Snail were observed in the normal rats without PDF daily injection, while their expression levels were dramatically increased in

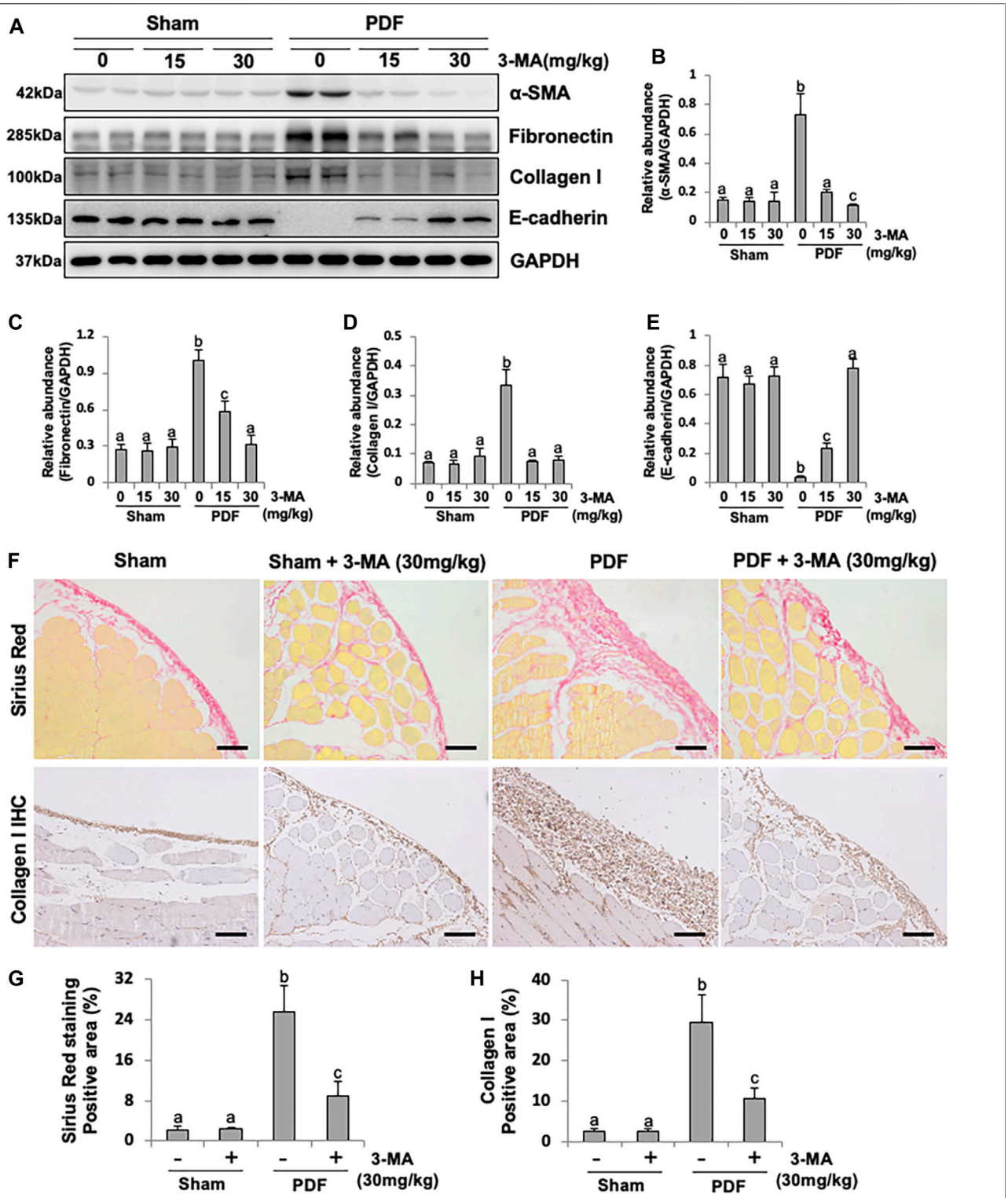

FIGURE 2 | Blockade of autophagy with 3-MA prevents EMT in a peritoneal fibrosis rat model. **(A)** Peritoneum tissue lysates were subjected to immunoblot analysis with specific antibodies against α-SMA, Fibronectin, Collagen I, E-cadherin and GAPDH. **(B–E)** Expression levels of α-SMA, Fibronectin, Collagen I and E-cadherin were quantified by densitometry and normalized with GAPDH. **(F)** Photomicrographs illustrate Sirius Red staining and immunohistochemistry staining of Collagen I from peritoneal tissues. **(G)** Positive area of Sirius Red-positive submesothelial area. **(H)** Positive area of Collagen I. Data are represented as the mean ± SEM. Means with different superscript letters are significantly different from one another ($p < 0.05$). All scale bars = 100 μm.

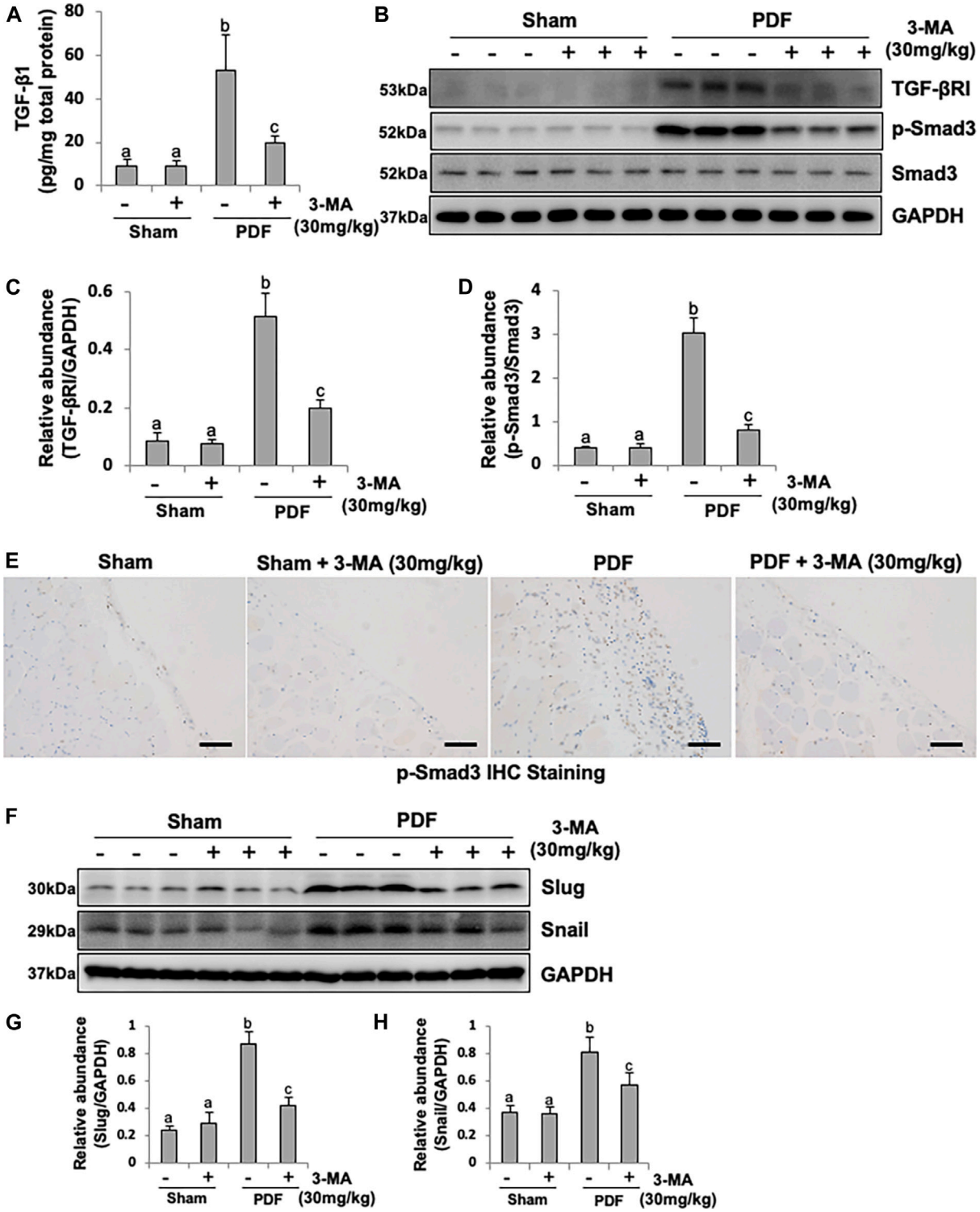

FIGURE 3 | Inhibition of autophagy with 3-MA blocks EMT in PF rats by regulating TGF-β/Smad3 signaling pathway and downstream nuclear transcription factors: Slug and Snail. **(A)** TGF-β1 level in peritoneum from each group by ELISA kit detection. **(B)** Peritoneum tissue lysates were subjected to immunoblot analysis with specific antibodies against TGF-βRI, p-Smad3, Smad3 and GAPDH. **(C)** Expression level of TGF-βRI was quantified by densitometry and normalized with GAPDH. **(D)** Expression level of p-Smad3 was quantified by densitometry and normalized with Smad3. **(E)** Photomicrographs illustrate immunohistochemistry staining of p-Smad3 from peritoneal tissues. **(F)** Peritoneum tissue lysates were subjected to immunoblot analysis with specific antibodies against Slug, Snail and GAPDH. **(G, H)** Expression levels of Slug and Snail were quantified by densitometry and normalized with GAPDH. Data are represented as the mean ± SEM. Means with different superscript letters are significantly different from one another ($p < 0.05$). All scale bars = 100 μm.

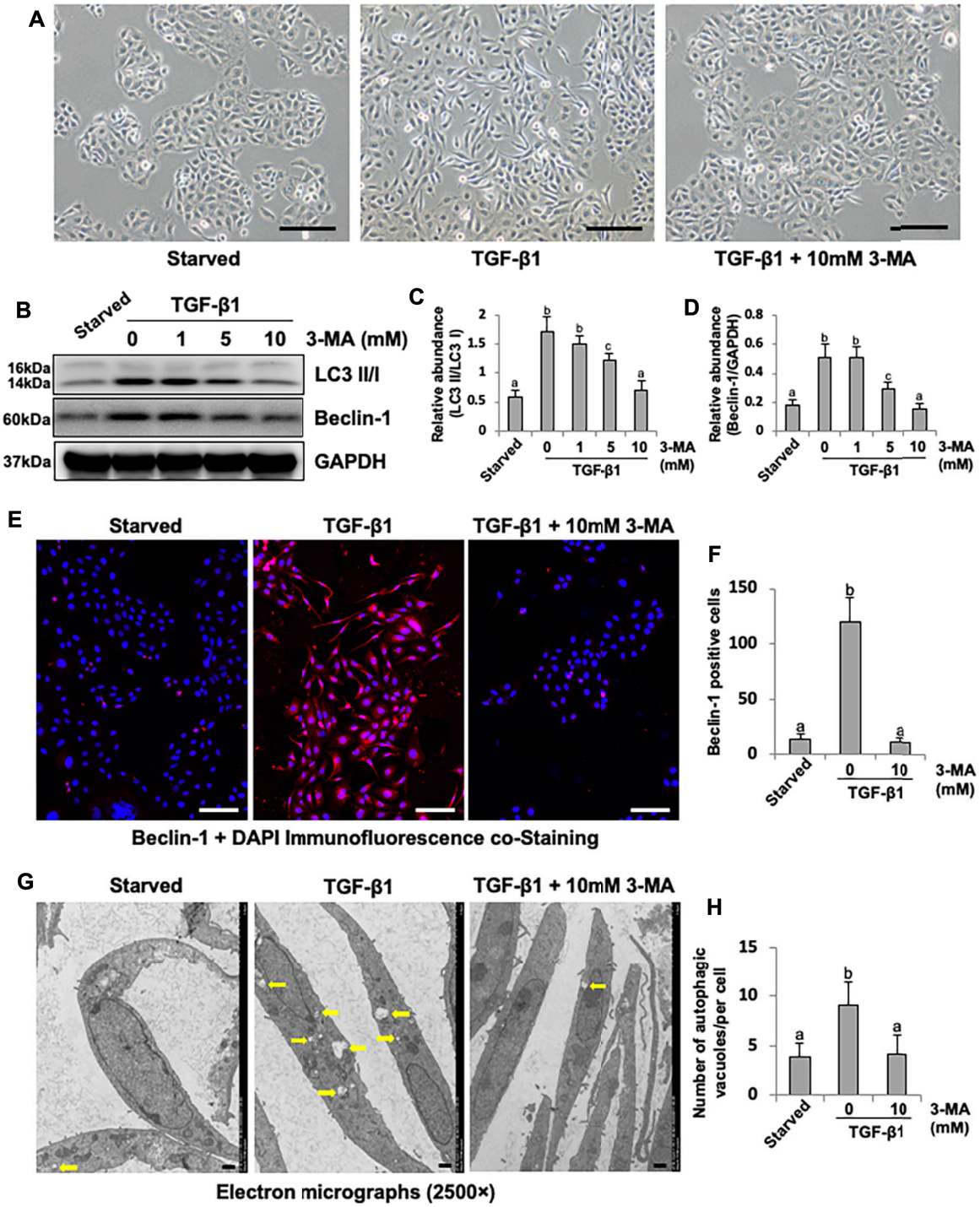

FIGURE 4 | 3-MA decreases autophagic activity in cultured human peritoneal mesothelial cells. **(A)** Photomicrographs illustrate light microscope observation of HPMCs. **(B)** Cell lysates were subjected to immunoblot analysis with specific antibodies against LC3, Beclin-1 and GAPDH. **(C, D)** Expression levels of LC3II and Beclin-1 were quantified by densitometry and normalized with LC3I and GAPDH respectively. **(E)** Photomicrographs show immunofluorescence co-staining of Beclin-1 and DAPI. **(F)** The count of Beclin-1-positive cells. **(G)** Transmission electron microscopy images of autophagosome (Yellow arrows) in HPMCs following TGF-β1 (2 ng/ml) stimulation in the presence/absence of 3-MA. **(H)** Quantitation of the number of autophagic vacuoles per cell. Data are represented as the mean ± SEM. Means with different superscript letters are significantly different from one another ($p < 0.05$). Scale bars in **(A)** = 500 μm, **(E)** = 100 μm, **(F)** = 10 μm.

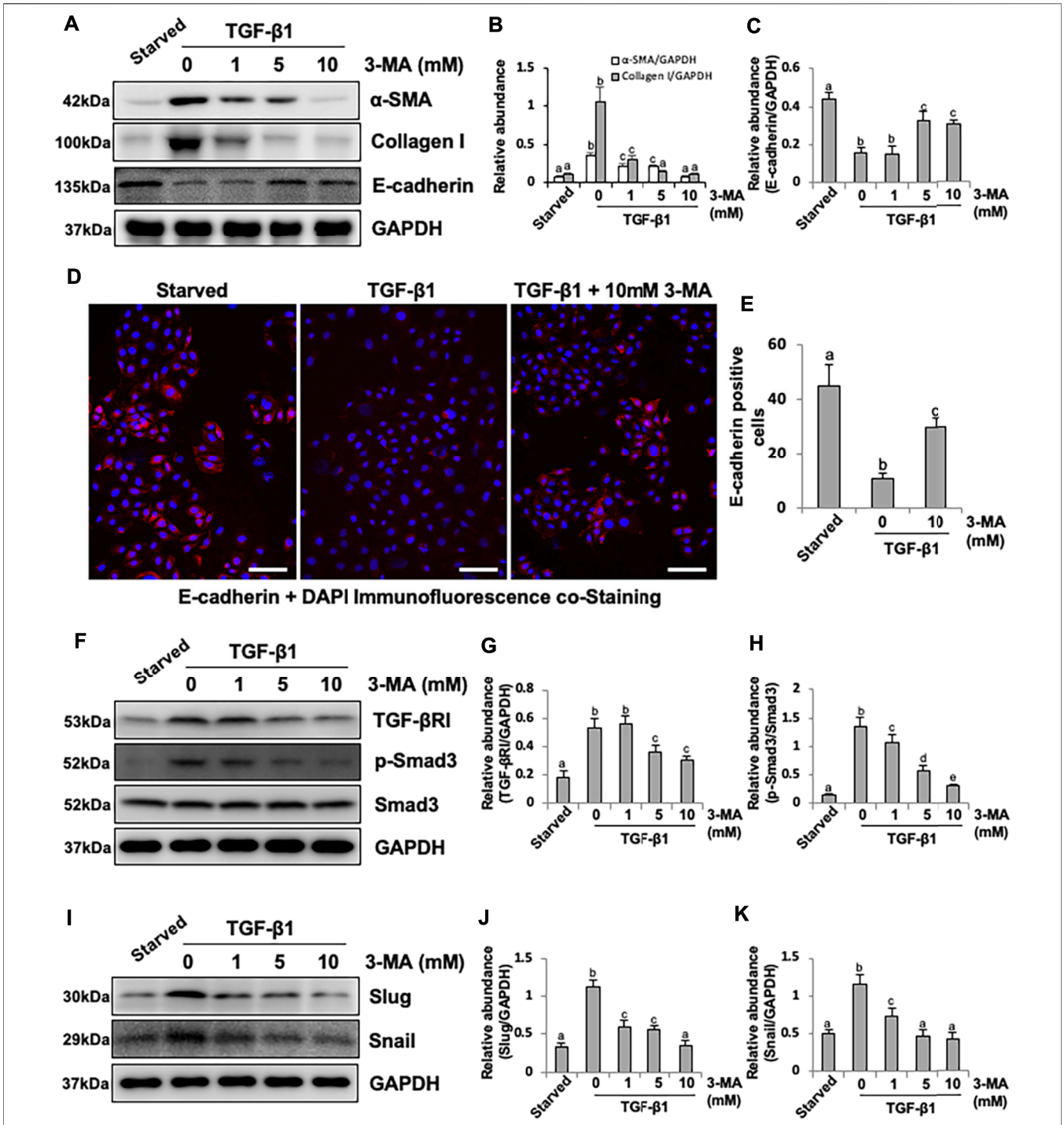

FIGURE 5 | Inhibition of autophagy with 3-MA blocks EMT in HPMCs by regulating TGF-β/Smad3 signaling pathway and downstream nuclear transcription factors: Slug and Snail. **(A)** Cell lysates were subjected to immunoblot analysis with specific antibodies against α-SMA, Collagen I, E-cadherin and GAPDH. **(B, C)** Expression levels of α-SMA, Collagen I and E-cadherin were quantified by densitometry and normalized with GAPDH. **(D)** Photomicrographs show immunofluorescence co-staining of E-cadherin and DAPI. **(E)** The count of E-cadherin-positive cells. **(F, I)** Cell lysates were subjected to immunoblot analysis with specific antibodies against TGF-βRI, p-Smad3, Smad3, Slug, Snail and GAPDH. **(G)** Expression level of TGF-βRI was quantified by densitometry and normalized with GAPDH. **(H)** Expression level of p-Smad3 was quantified by densitometry and normalized with Smad3. **(J, K)** Expression levels of Slug and Snail were quantified by densitometry and normalized with GAPDH. Data are represented as the mean ± SEM. Means with different superscript letters are significantly different from one another ($p < 0.05$). All scale bars = 100 μm.

PF rats. Treatment with 3-MA restored Slug to the normal level and lowered Snail to half percent (**Figures 3F–H**). Therefore, 3-MA could inhibit EMT during PF through inactivation of TGF-β/Smad3 signaling pathway and E-cadherin transcriptional inhibition by down-regulating Slug and Snail.

3-MA Decreases Autophagic Activity in Cultured Human Peritoneal Mesothelial Cells

Cultured HPMCs were stimulated by TGF-β1 and treated with 3-MA at different doses (1, 5, 10 mM). TGF-β1 was found to induce the morphological transition of HPMCs, which stimulated HPMCs to lose their epithelial shape to an elongated shape, treatment with 3-MA prevented the above morphologic changes of cultured HPMCs (**Figure 4A**). In addition, TGF-β1 also triggered a significant up-regulation of LC3B II to I ratio and Beclin-1. 3-MA dose-dependently suppressed these responses (**Figures 4B–D**). Immunofluorescence assay showed that the expression of Beclin-1 was significantly increased in response to TGF-β1, 3-MA treatment inhibited its expression (**Figures 4E,F**). As a gold standard to observe autophagosome, images from TEM revealed accumulation of autophagy-related vacuoles in TGF-β1-stimulated HPMCs compared to control cells. Administration with 3-MA significantly prevented the autophagic activity (**Figures 4G,H**). Above-mentioned results point out that autophagic activity is activated by TGF-β1 stimulation in cultured HPMCs.

Inhibition of Autophagy With 3-MA Blocks EMT in HPMCs by Regulating TGF-β/Smad3 Signaling Pathway and Downstream Nuclear Transcription Factors: Slug and Snail

Since our previous studies have proved that TGF-β1 stimulation could cause EMT of HPMCs, which imitates the early stage of PMC injury during PD process (Xu et al., 2017; Shi et al., 2020), we also examined the effect of 3-MA on the EMT of cultured HPMCs in response to TGF-β1. Exposure of HPMCs to TGF-β1 at 2 ng/ml resulted in increased expression of α-SMA and Collagen I and decreased expression of E-cadherin, administrated with 3-MA inhibited TGF-β1-induced upregulation of α-SMA and Collagen I and downregulation of E-cadherin in a dose dependent manner (**Figures 5A–C**). Immunofluorescence assay further confirmed that the expression of E-cadherin was significantly reduced in response to TGF-β1, treatment with 3-MA increased the level of E-cadherin (**Figures 5D,E**). Mechanistically, 3-MA significantly reduced the expression of TGF-βRI and inhibited Smad3 phosphorylation, but made no difference on total Smad3 (**Figures 5F–H**). Additionally, 3-MA also down-regulated two nuclear transcription factors, Slug and Snail, involved in TGF-β1/Smad3-related EMT (**Figures 5I–K**). In summary, these results reiterate the inhibitory effect of 3-MA on the process of EMT by regulating TGF-β/Smad3 signaling pathway and downstream nuclear transcription factors *in vitro*.

Furthermore, to determine the effects of delayed treatment of 3-MA on TGF-β1-induced EMT, we designed a treatment scheme as shown in **Supplementary Figure S3A**. At 24 h after pretreatment with TGF-β1, expression of α-SMA and Collagen I was induced, and further increased at 48 h. The expression of E-cadherin decreased at 24 h and further inhibited at 48 h. However, delayed treatment with 3-MA suppressed further increases of α-SMA and Collagen I and decreases of E-cadherin (**Supplementary Figures S3B–E**). These data suggest that delayed administration of 3-MA is effective in reducing EMT induced by TGF-β1.

Since 3-MA is not a specific autophagy inhibitor, specifically, 3-MA is a generic inhibitor of PI3Ks. To determine whether 3-MA effects on autophagy dominating among others, we downregulated the expression of the autophagic gene, Beclin-1 by using Beclin-1 siRNA in HPMCs to investigate the effect on TGF-β/Smad3, EGFR/ERK1/2 and STAT3/NF-κB signaling pathways. As shown in **Supplementary Figure S4**, reduction of Beclin-1 expression by its specific siRNA decreased TGF-β1 stimulated expression of α-SMA and Collagen I (**Supplementary Figures S4A,B**). Mechanistically, downregulation of Beclin-1 resulted in decreased of expression of p-Smad3, p-ERK1/2, and p-STAT3 without alteration of total Smad3, ERK1/2, and STAT3 (**Supplementary Figures S4C–H**). However, downregulation of Beclin-1 had no impact on p-EGFR and p-NF-κB (Data not show). It is reported that EGFR signaling can be activated by ATG genes (Zhang et al., 2019), we speculate that downregulation of ATG genes in HPMCs may affect the expression of p-EGFR and p-NF-κB. Collectively, these data suggest that inhibition of Beclin-1 by siRNA can remarkably inhibited TGF-β1 induced activation of Smad3/ERK1/2/STAT3 pathway in HPMCs.

3-MA Inhibits Activation of EGFR/ERK1/2 Signaling Pathway *in vivo* and *in vitro*

Besides TGF-β/Smad3 signaling pathway involved in PF, EGFR together with its downstream signal molecule ERK1/2 are also participated in the development of fibrogenesis. Thus, we set out to examined the effect of 3-MA on the activation of EGFR and ERK1/2 by immunoblotting assays. As shown in **Figures 6A–C**, phosphorylated EGFR and ERK1/2 were largely increased in the peritoneal membrane exposure to PDF. Inhibition of autophagy down-regulated phosphorylation of EGFR and decreased the ratio between p-EGFR and EGFR, as well as p-ERK1/2 and ERK1/2. Both total EGFR and ERK1/2 were increased after peritoneal injury, but not affected by 3-MA administration (**Figures 6A–C**). Moreover, we further examined whether EGFR/ERK1/2 signaling pathway would play an important role in TGF-β1-stimulated HPMCs *in vitro*. Exposure of HPMCs to TGF-β1 induced expression of p-EGFR and p-ERK1/2, treatment with 3-MA blocked all these responses, but had no impact on the expression of total EGFR and total ERK1/2 (**Figures 6D,E**). Collectively, these data demonstrate that 3-MA may prevent PF by inactivation of EGFR/ERK1/2 signaling pathway.

3-MA Prevents Inflammation and Macrophage Infiltration in PDF-Induced PF Rats

Considering the pivotal role of inflammation in PF, we further explored the anti-inflammatory effect of 3-MA. STAT3 and NF-

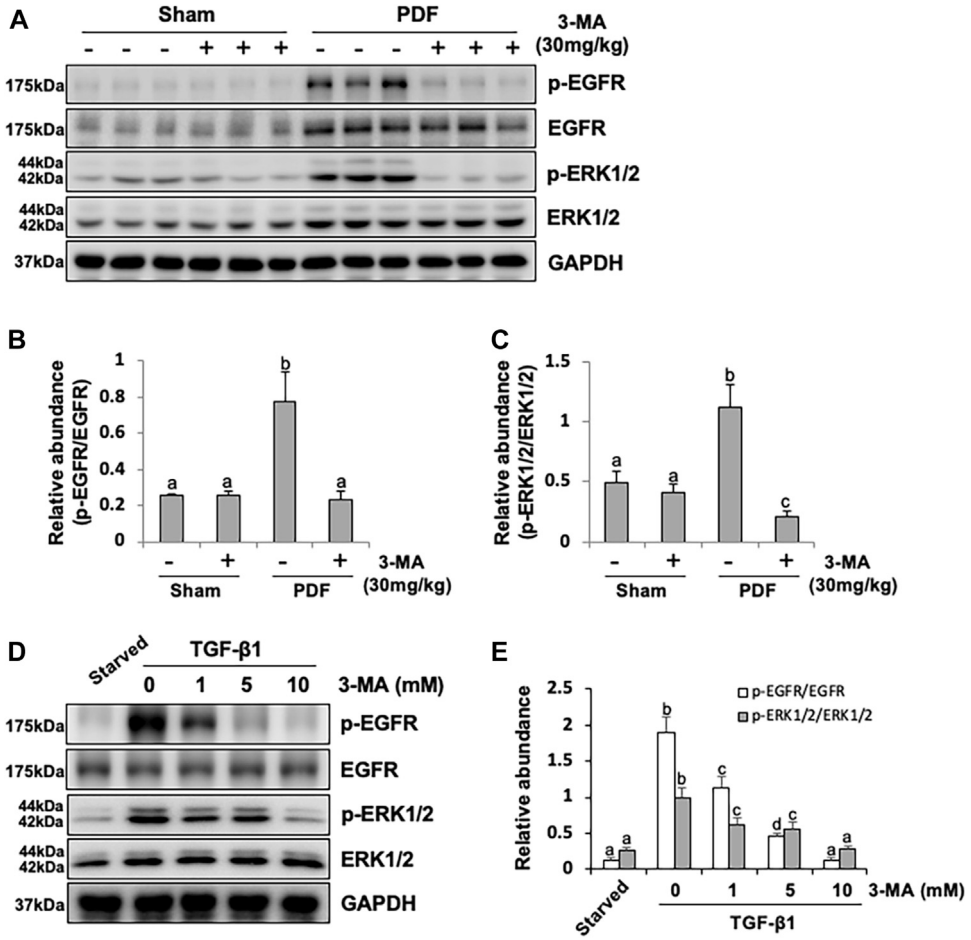

FIGURE 6 | 3-MA inhibits activation of EGFR/ERK1/2 signaling pathway *in vivo* and *in vitro*. **(A)** Peritoneum tissue lysates were subjected to immunoblot analysis with specific antibodies against p-EGFR, EGFR, p-ERK1/2, ERK1/2 and GAPDH. **(B, C)** Expression levels of p-EGFR and p-ERK1/2 were quantified by densitometry and normalized with EGFR and ERK1/2 respectively. **(D)** Cell lysates were subjected to immunoblot analysis with specific antibodies against p-EGFR, EGFR, p-ERK1/2, ERK1/2 and GAPDH. **(E)** Expression levels of p-EGFR and p-ERK1/2 were quantified by densitometry and normalized with EGFR and ERK1/2 respectively. Data are represented as the mean ± SEM. Means with different superscript letters are significantly different from one another ($p < 0.05$).

κB-induced inflammatory signaling pathways were evidently activated after exposure to non-biocompatible peritoneal dialysate for 28 days. Combination therapy with 3-MA down-regulated phosphorylated STAT3 and NF-κB (**Figures 7A–D**). The phosphorylation of NF-κB triggers the release of large number of inflammatory factors such as MCP-1, IL-1β and IL-6 (Choi et al., 2017). As a result, we further evaluated the effect of 3-MA on the expression of some inflammatory cytokines by ELISA kit analysis and immunohistochemical staining. As demonstrated in **Figures 7E–G**, all levels of these inflammatory factors were increased in the peritoneum of rats administrated with 4.25% PDF and inhibited by 3-MA treatment. In addition, increased macrophage infiltration in the peritoneal membrane was also involved in PF (Wang et al., 2016). To explore whether autophagy was involved in this process, we examined the level of CD68, one of macrophage markers, by conducting immunoblot analysis. Injection of 4.25% PDF significantly increased the expression of CD68, treatment with 3-MA effectively decreased its expression (**Figures 7H,I**). Furthermore, we examined CD68 expression by immunohistochemistry and showed that the number of CD68 positive cells was elevated in the peritoneum exposure to PDF and largely reduced after 3-MA treatment (**Figure 7J**). Thus, these results demonstrated that inflammation inhibition is also one of the mechanisms by which 3-MA prevents PF.

3-MA Suppresses Peritoneal Angiogenesis Through Inhibiting β-Catenin Signaling Pathway

Angiogenesis is a critical change of peritoneal structure in long term PD patients, which is associated with ultrafiltration failure (Shi et al., 2017). VEGF acted directly on the vascular endothelial cell mitogen, leading to the formation of new blood vessels. To further understand whether autophagy is involved in peritoneal angiogenesis, we examined the effect of 3-MA on PF rats. Exposure of peritoneum to 4.25% PDF promoted peritoneal angiogenesis as evidenced by the up-regulation of CD31,

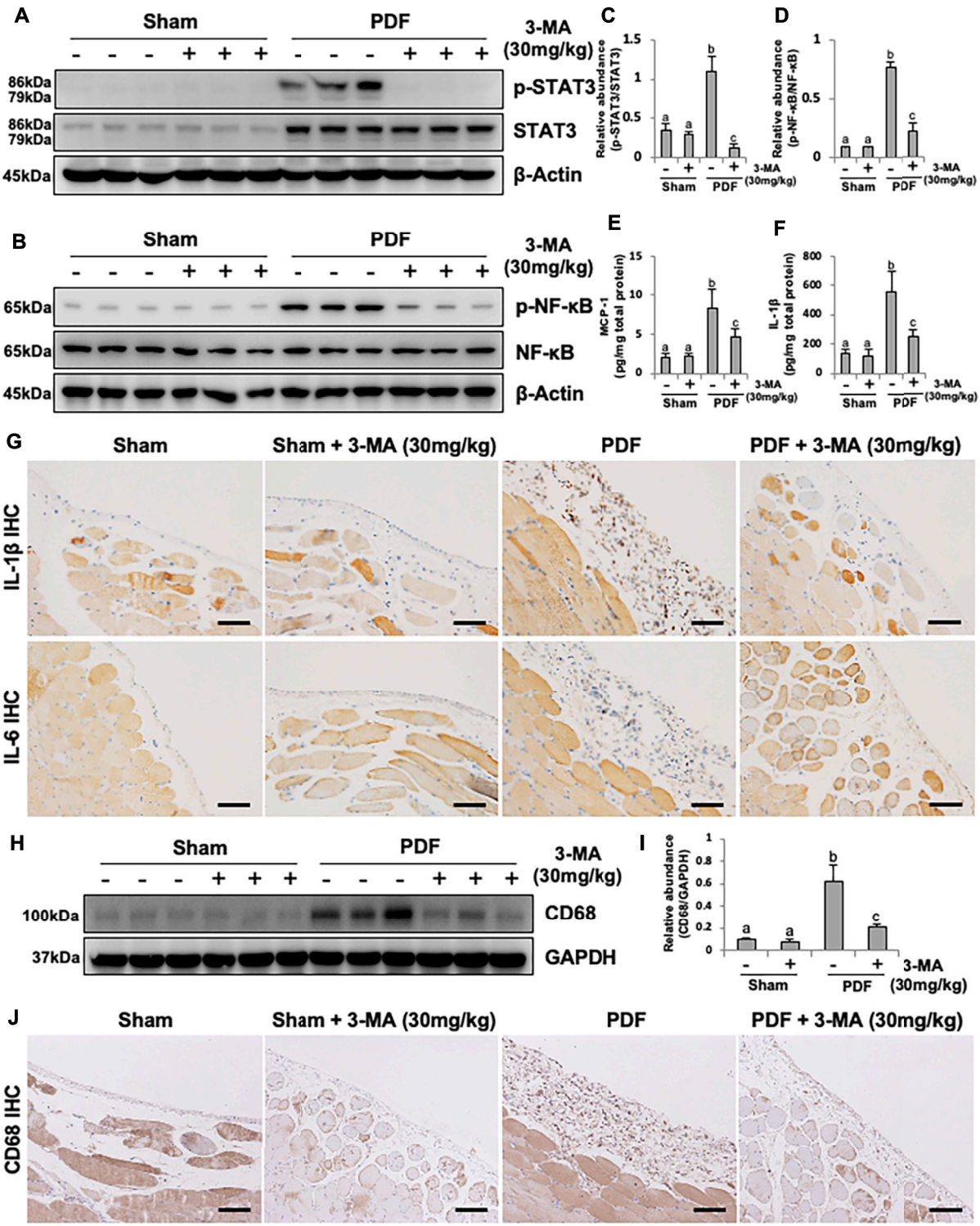

FIGURE 7 | 3-MA prevents inflammation and macrophage infiltration in PDF-induced PF rats. **(A, B)** Peritoneum tissue lysates were subjected to immunoblot analysis with specific antibodies against p-STAT3, STAT3, p-NF-κB, NF-κB and β-actin. **(C, D)** Expression levels of p-STAT3 and p-NF-κB were quantified by densitometry and normalized with STAT3 and NF-κB respectively. **(E, F)** The levels of MCP-1 and IL-1β in peritoneum from each group were detected by ELISA kit. **(G)** Photomicrographs illustrate immunohistochemistry staining of IL-1β and IL-6 from peritoneal tissues. **(H)** Peritoneum tissue lysates were subjected to immunoblot analysis with specific antibodies against CD68 and GAPDH. **(I)** Expression level of CD68 was quantified by densitometry and normalized with GAPDH. **(J)** Photomicrographs illustrate immunohistochemistry staining of CD68 from peritoneal tissues. Data are represented as the mean ± SEM. Means with different superscript letters are significantly different from one another ($p < 0.05$). All scale bars = 100 μm.

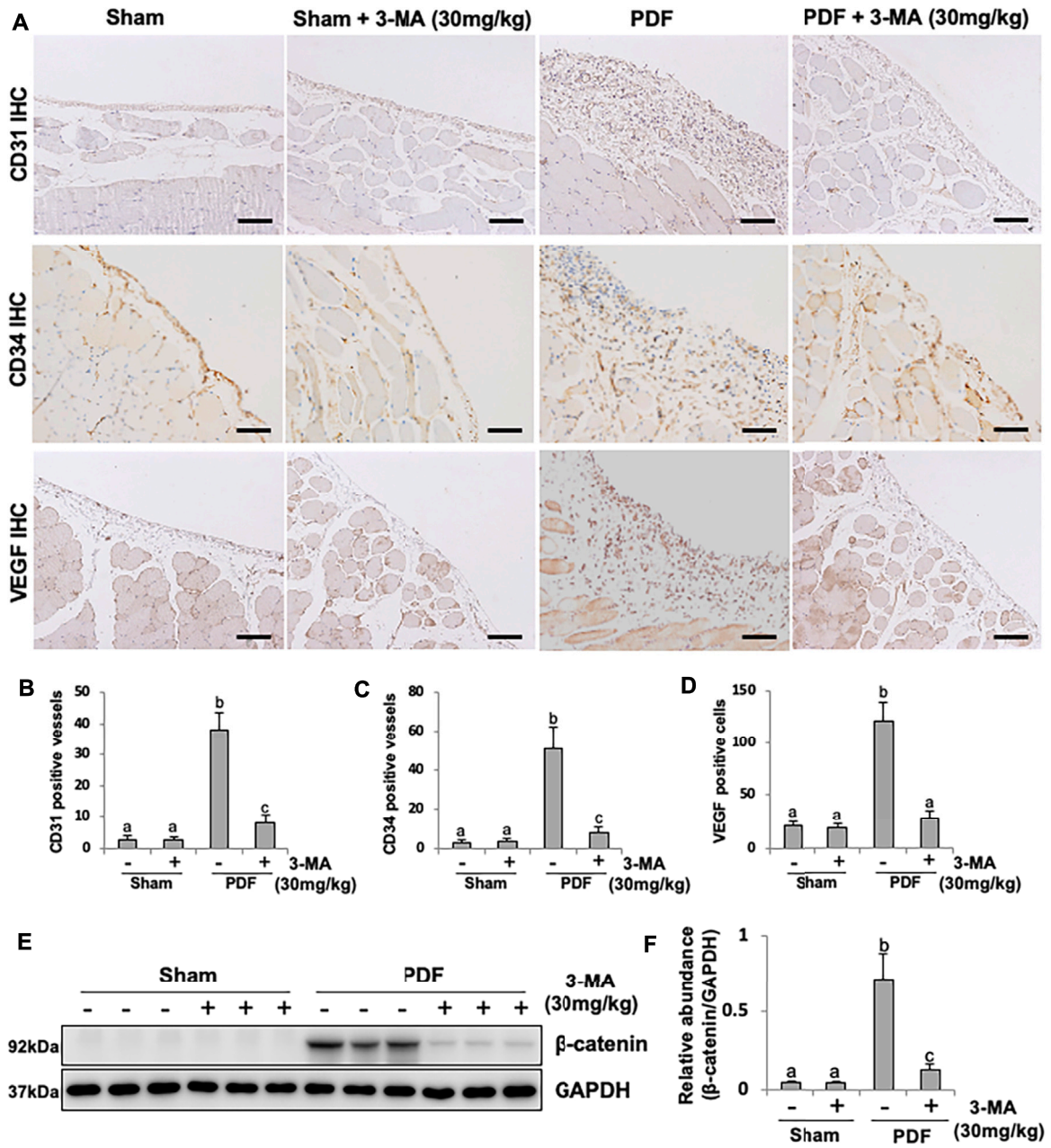

FIGURE 8 | 3-MA suppresses peritoneal angiogenesis through inhibiting β-catenin signaling pathway. **(A)** Photomicrographs illustrate immunohistochemistry staining of CD31, CD34 and VEGF from peritoneal tissues. **(B-D)** The count of CD31-positive vessels, CD34-positive vessels and VEGF-positive cells. **(E)** Cell lysates were subjected to immunoblot analysis with specific antibodies against β-catenin and GAPDH. **(F)** Expression level of β-catenin was quantified by densitometry and normalized with GAPDH. Data are represented as the mean ± SEM. Means with different superscript letters are significantly different from one another ($p < 0.05$). All scale bars = 100 μm.

CD34 and VEGF, three common markers of blood vessels. Administration of 3-MA could blockade this pathological change and decrease the number of CD31-and CD34-positive vessels, as well as VEGF-positive endothelial cells (**Figures 8A–D**). Mechanistically, it was reported that β-catenin signaling pathway plays an important role in peritoneal angiogenesis (Padwal et al., 2018). Our immunoblotting analysis demonstrated that β-catenin pathway was dramatically activated in PF rats, treatment with 3-MA remarkably decreased the expression of β-catenin in fibrotic peritoneum (**Figures 8E,F**). Taken together, these data suggest that 3-MA suppresses peritoneal angiogenesis by inhibiting β-catenin signaling pathway.

Actually, the mechanisms of autophagy promoting peritoneal fibrosis are complicated. In the present study, we found that high glucose and TGF-β can stimulate the activation of autophagy.

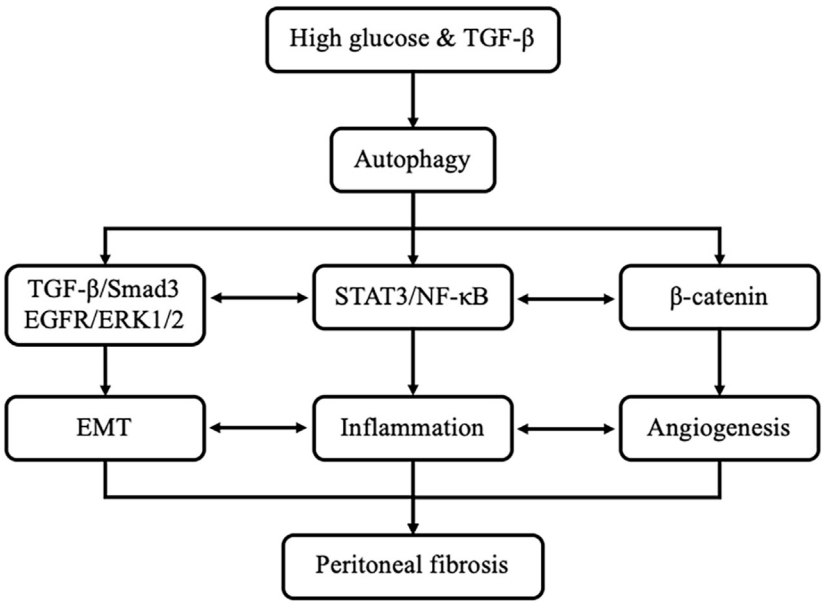

FIGURE 9 | Signaling pathways of autophagy promotes PF. Exposure of high glucose or TGF-β can induce the activation of autophagy *in vivo* and *in vitro*, respectively. Activation of autophagy leads to EMT, induction of proinflammatory responses and triggering angiogenesis by regulating TGF-β/Smad3, EGFR/ERK1/2, STAT3/NF-κB and β-Catenin axis, eventually caused peritoneal fibrosis. In addition, EMT also implicated in inflammation and angiogenesis. Inflammatory responses also induce EMT and angiogenesis.

Inhibition of autophagy with 3-MA prevents peritoneal fibrosis by regulating TGF-β/Smad3, EGFR/ERK1/2, STAT3/NF-κB and β-Catenin axis both *in vivo* and *in vitro* systems. Interestingly, a previous study shown that TGF-β induces EMT, which is also implicated in inflammation and angiogenesis due to the cytokines released by mesothelial cells that suffered EMT after exposition to glucose or TGF-β. Inflammatory cells recruited to the peritoneal cavity also induce EMT and angiogenesis (Tzavlaki and Moustakas, 2020). It can be seen that the crosstalk and interplay among multiple pathways associated with autophagy and peritoneal fibrosis, such as EMT, inflammation, and angiogenesis are complicated (**Figure 9**).

DISCUSSION

PF is one of the most common complications for long-term PD patients (Zhou et al., 2016; Krediet, 2018). At present, there is no effective intervention and treatment strategies for PF. Autophagy is a cellular process of the formation of autophagosomes by bulk degradation of cytoplasmic components. In addition to its bona fide function of catabolism, autophagy also plays important roles in fibrotic diseases (Saha et al., 2018). The role of autophagy in PF remains largely unclear and the findings from recent researches are inconsistent and very controversial (Yang et al., 2017; Wu et al., 2018; Li et al., 2019a). Using pharmacological inhibitory approach, our study has determined the regulation of PF by autophagy in two PF rat models induced by 4.25% PDF and 0.1% CG and *in vitro* model of TGF-β1 stimulated HPMCs. Blockade of autophagy by pharmacological inhibitor 3-MA effectively prevented PF by inhibiting EMT and the activation of TGF-β/Smad3, EGFR/ERK1/2 signaling pathways. 3-MA also prevented inflammation and macrophage infiltration by regulating the STAT3 and NF-κB signaling pathway. Moreover, inhibition of autophagy blockaded peritoneal angiogenesis in the injured peritoneum. In consistent with Wu et al. (2018), our conclusion based on the present research also demonstrated that autophagy contributed to PF. Taken together, 3-MA is effective in preventing the development of PF and autophagy might be a therapeutic target for long-term PD patients.

Despite the emerging evidence showing the induction of autophagy during PF, the upstream signaling leading to autophagy activation remains unclear. It is generally known that peritoneal dialysate currently used in PD patients usually contains high glucose, advanced glycation end products (AGEs) and glucose degradation products (GDPs). In this study, we demonstrated that high glucose PDF increased TGF-β1 production. Accumulating data have indicated that TGF-β1 induces autophagy under different pathological conditions (Ding and Choi, 2014; Sureshbabu et al., 2016; Zhang et al., 2017b). TGF-β1 stimulation increases autophagosomes accumulation and autophagic flux activation, and up-regulates autophagy-related genes such as Atg5, Atg7, LC3, Beclin-1 and Death-associated protein kinase (DAPK) (Kiyono et al., 2009; Ding and Choi, 2014; Sureshbabu et al., 2016). Similarly, our *in vitro* study showed that TGF-β1 (2 ng/ml) stimulation increased autophagic activity in cultured HPMCs with the up-regulation of LC3 and Beclin-1. As a gold standard to observe autophagosome, images from TEM revealed accumulation of autophagy-related

structures in TGF-β1-stimulated cells compared to starved cells. TGF-β1 has been shown to activate PI3K/Akt/mTOR pathway (Lamouille and Derynck, 2007), which is important to mediate autophagy. Therefore, high glucose PDF stimulates the production of TGF-β1 might induce autophagy by regulating PI3K/Akt/mTOR pathway. Additionally, AGEs can activate autophagy as well. Biological function of extracellular AGEs mainly depends on the interaction with receptor for AGEs (RAGE). After that, the AGEs in league together with intracellular AGEs induce oxidative stress and increase generation of reactive oxygen species (ROS) dependent or independent on protein kinase C (PKC) activity, finally leading to autophagy (Ding and Choi, 2015). Moreover, the other two pathways, ERK-DAPK-Beclin1-hVps34 and CaMKKβ-AMPK are also activated by AGEs and focus on autophagy (Xie et al., 2013). Recent study also confirmed that autophagy was highly up-regulated in peritoneal membrane from long-term PD patients, as evidenced by increased expression of LC3 and autophagosomes, which was related to PF (Wu et al., 2018). Collectively, these data suggest that long-term PD induce the activation of autophagy.

Considering that autophagy is activated in long-term PD patients during PF, it is worth to explore the possible fibrogenesis mechanisms associated with autophagy. EMT plays an initial role in the process of fibrosis and subsequent functional deterioration of the peritoneal membrane. In this regard, we determined the relationship between autophagy and EMT in this study. Our study showed that inhibition of autophagy with 3-MA decreased the expression of EMT-related makers including α-SMA, Fibronectin, and Collagen I *in vivo* and *in vitro*. Mechanistically, we further demonstrated that inhibition of autophagy with 3-MA blocks EMT by regulating TGF-β/Smad3 signaling pathway and downstream nuclear transcription factors. Consistently in the current study, activation of EMT by autophagy was also shown in hepatocellular carcinoma cells, which associated with the activation of TGF-β/Smad3 signaling (Li et al., 2013). It can be seen that in addition to the positive role of TGF-β on autophagy, up-regulated autophagy can act back on TGF-β expression as well. Hu et al. found that autophagy-mediated phosphodiesterase 4A (PDE4A) degradation could activate CAMP/PKA/CREB signaling, which contributed to TGF-β production (Hu et al., 2018). However, the relationship between autophagy and EMT is complicated, a recent study demonstrated that autophagy could promote EMT in both TGF-β-dependent and independent manner (Bao et al., 2020), which indicates that there might be other pathway involved in the 3-MA-mediated inhibition of EMT. In this respect, our current study also found that EGFR/ERK1/2 signaling was upregulated in PF rats during EMT, administrated with 3-MA significantly inhibited the activation of this signaling pathway. Zhang et al. demonstrated that the loss-of-function in ATG genes may activate EGFR signaling by driving the accumulation of activated, Krn-bound EGFR complexes in Rab11 recycling endosomes and/or at the plasm membrane, such that constitutively activating downstream ERK signaling in cancers (Zhang et al., 2019). Whether the dysfunction of autophagy may trigger hyperactivation of EGFR/ERK1/2 signaling through this mechanism during EMT in PF model is still needed further exploration. Taken together, our results suggest that autophagy might promote EMT through multiple mechanisms.

Though the mechanism is not fully clarified, the crosstalk between autophagy and inflammation has recently become an interesting topic. On the one hand, autophagy directly affects the development, homeostasis and survival of several inflammatory cells, such as macrophages, neutrophils and lymphocytes (T cells and B cells), and influencing the transcription, processing and secretion of inflammatory factors (Qian et al., 2017). On the other hand, autophagy is regulated by inflammatory cytokines as well (Wu et al., 2016b). In this study, we observed an elevation of multiple proinflammation cytokines, including MCP-1, IL-1β, and IL-6, as well as macrophage infiltration of the peritoneum in PDF rats, inhibition of autophagy with 3-MA blocked all these responses. Mechanistically, it is well-established that NF-κB signaling is a critical transduction pathway that regulates cell stress and inflammatory responses (Mendis et al., 2008). In this study, we observed that NF-κB signaling pathway was evidently activated after exposure to non-biocompatible peritoneal dialysate. Combination therapy with 3-MA down-regulated phosphorylated NF-κB. Since our previous studies have already confirmed that inflammatory response is one of the key pathologic processes involved in PF during long-term PD (Wang et al., 2016; Shi et al., 2020), thus we can draw a conclusion that autophagy contributes to PF by mediating inflammatory responses, which may associate with NF-κB pathway. In fact, although our current study suggests that autophagy can mediate the NF-κB signaling, existing studies have shown that the NF-κB signaling pathway can in turn regulate autophagy (Levine et al., 2011; Xu et al., 2021). Obviously, there is an interaction between the activation of autophagy and the NF-κB signaling pathway, the relationships in detail need to further elucidate.

Inhibition of peritoneal angiogenesis may also be a mechanism by which 3-MA prevents PF. In this study, peritoneal angiogenesis was more serious in 4.25% PDF-model group than control group, treatment with 3-MA significantly blocked the peritoneal angiogenesis as evidenced by the decreased of CD31- and CD34-positive vessels, as well as VEGF-positive endothelial cells. In consistent with our observations, Liang et al. showed that rapamycin-mediated autophagy enhanced the pro-angiogenic effect, and 3-MA effectively attenuated angiogenesis evidenced by decreased proliferation and migration of human umbilical vein endothelial cells (HUVECs), and formation of tube-like structures (Liang et al., 2018). The role of WNT/β-catenin signaling in peritoneal membrane angiogenesis has been recently clarified. Our study found that β-catenin pathway was dramatically activated in PF rats, treatment with 3-MA remarkably decreased the expression of β-catenin in fibrotic peritoneum. The activation of autophagy could augment the WNT/β-catenin signaling pathway (Liu et al., 2021), as a result, β-catenin binds to the T cell factor/lymphoid enhancer-binding factor (TCL/LEF) family in the nucleus, and changes the expression of crucial mediators of angiogenesis, such as VEGF (Liu et al., 2021). In addition, autophagy also regulates pigment epithelium derived factor (PEDF) expression, an endogenous VEGF inhibitor, and increases VEGF/PEDF ratio, promoting the formation of neovascularization (Li et al., 2019b). Collectively, 3-MA prevents peritoneal angiogenesis in PF rat model through inhibiting autophagy-mediated VEGF production, and suppressing the activation of β-catenin signaling. Autophagy may become a

therapeutic target in the clinical treatment of angiogenesis for long-term PD patients.

Though the role of autophagy in PF is still controversial, our current study also has some strengths. Firstly, we determined the role of autophagy in PF using two rat models induced by 4.25% PDF and 0.1% CG, both were well-documented animal models used for studying chronic peritoneal changes (Wang et al., 2016; Xu et al., 2017), and considered to be ideal models to examine the efficacy of potential therapeutic regents for treating PF (Yoshio et al., 2004). Similar results were observed in both models, that is, autophagy promotes the development of PF, it makes the conclusion draw from the current study more convincing. Secondly, since 3-MA has not yet been approved clinically for the treatment of PF, we evaluated the effect of 3-MA on fibrosis pathological changes *in vivo* and *in vitro*, which provides the preclinical evidence for the anti-fibrotic effect of 3-MA in PF. Finally, we used two doses in exploring the anti-fibrotic effect of 3-MA and found that 30 mg/kg is more effective than 15 mg/kg. Although it is acknowledged that 3-MA is not a specific autophagy inhibitor and it is likely that a higher dosage of 3-MA may have adverse effects, our research shown that higher dosage of 3-MA (30 mg/kg) have no bad effect on normal rats. Nevertheless, efficacy and safety of 3-MA for the treatment of PF are still need to further study.

In conclusion, we confirmed that autophagy promotes PF, and pharmacological blockade of autophagy protects against peritoneal injury. Autophagy was highly activated in fibrotic peritoneum from two PF rat models induced by 4.25% PDF and 0.1% CG, and in cultured HPMCs after TGF-β1 stimulation. Treatment with 3-MA significantly prevents PF through inhibiting EMT, inactivating fibrogenesis signaling pathways, down-regulating inflammation, and reducing peritoneal angiogenesis. Therefore, autophagy inhibition may have a potential therapeutic benefit for long-term PD patients.

DATA AVAILABILITY STATEMENT

The original contributions presented in the study are included in the article/**Supplementary Material**, further inquiries can be directed to the corresponding author.

ETHICS STATEMENT

The animal study was reviewed and approved by Institutional Animal Care and Use Committee at Tongji University.

AUTHOR CONTRIBUTIONS

Participated in research design: NL. Conducted experiments: YS, YH, YW, XM, LT, and MT. Contributed new reagents or analytic tools: YS, YW, and XM. Performed data analysis: YS. Wrote or contributed to the writing of the manuscript: YS, YH, AQ, SZ, and NL.

FUNDING

This study was supported by the National Nature Science Foundation of China grants (82070791, 81670690, 81470991 and 81200492 to NL, 82070700, 81830021 and 81670623 to SZ, 81970072 and 81500059 to LT), the Shanghai Scientific Committee of China (20ZR1445800 and 13PJ1406900 to NL), the Key Discipline Construction Project of Pudong Health Bureau of Shanghai (PWZxk2017-05 to NL), the key program of Science Foundation of Jiangxi Province (2018ACB 20016 to LT), the leading medical talent project of Shanghai Pudong heath bureau (PWRI2019-05 to LT), and the Branch Grant of National Key R&D Program of China (2018YFA0108802 to SZ).

SUPPLEMENTARY MATERIAL

The Supplementary Material for this article can be found online at: https://www.frontiersin.org/articles/10.3389/fphar.2021.724141/full#supplementary-material

Supplementary Figure S1 | Administration of 3-MA inhibits autophagy and attenuates peritoneal fibrosis in 0.1% CG -induced rat model. **(A, B)** Masson's trichrome staining of the peritoneum and its positive area. **(C, D)** Sirius Red staining of the peritoneum and its positive area. **(E)** Peritoneum tissue lysates were subjected to immunoblot analysis with specific antibodies against LC3, Beclin-1 and GAPDH. **(F)** Expression levels of LC3II and Beclin-1 were quantified by densitometry and normalized with LC3I and GAPDH respectively. Data are represented as the mean ± SEM. Means with different superscript letters are significantly different from one another ($p < 0.05$). All scale bars = 100 μm.

Supplementary Figure S2 | Inhibition of autophagy with 3-MA blocks EMT in 0.1% CG -induced rat model. **(A)** Peritoneum tissue lysates were subjected to immunoblot analysis with specific antibodies against α-SMA, Fibronectin, Collagen I, E-cadherin and GAPDH. (**B–E**) Expression levels of α-SMA, Fibronectin, Collagen I and E-cadherin were quantified by densitometry and normalized with GAPDH. Data are represented as the mean ± SEM. Means with different superscript letters are significantly different from one another ($p < 0.05$).

Supplementary Figure S3 | Delayed administration of 3-MA inhibits TGF-β1-induced EMT in HPMCs. **(A)** Diagram depicts treatment scheme with 3-MA. **(B)** Cell lysates were subjected to immunoblot analysis with specific antibodies against α-SMA, Collagen I, E-cadherin and GAPDH. **(C–E)** Expression levels of α-SMA, Collagen I and E-cadherin were quantified by densitometry and normalized with GAPDH. Data are represented as the mean ± SEM. Means with different superscript letters are significantly different from one another ($p < 0.05$).

Supplementary Figure S4 | siRNA-mediated silencing of Beclin-1 inhibits TGF-β1 induced activation of Smad3/ERK1/2/STAT3 pathway in HPMCs (**A**) Cell lysates were subjected to immunoblot analysis with specific antibodies against Beclin-1, α-SMA, Collagen I and GAPDH. **(B)** Expression levels of Beclin-1, α-SMA and Collagen I were quantified by densitometry and normalized with GAPDH. **(C)** Cell lysates were subjected to immunoblot analysis with specific antibodies against p-Smad3, Smad3 and GAPDH. **(D)** Expression level of p-Smad3 was quantified by densitometry and normalized with Smad3. **(E)** Cell lysates were subjected to immunoblot analysis with specific antibodies against p-ERK1/2, ERK1/2 and GAPDH. **(F)** Expression levels of p-ERK1/2 was quantified by densitometry and normalized with ERK1/2. **(G)** Cell lysates were subjected to immunoblot analysis with specific antibodies against p-STAT3, STAT3 and GAPDH. **(H)** Expression levels of p-STAT3 was quantified by densitometry and normalized with STAT3. Data are represented as the mean ± SEM. Means with different superscript letters are significantly different from one another ($p < 0.05$).

REFERENCES

Bao, Y., Ding, Z., Zhao, P., Li, J., Chen, P., Zheng, J., et al. (2020). Autophagy Inhibition Potentiates the Anti-EMT Effects of Alteronol through TGF-β/Smad3 Signaling in Melanoma Cells. *Cell Death Dis.* 11 (4), 223. doi:10.1038/s41419-020-2419-y

Cabrera, S., Maciel, M., Herrera, I., Nava, T., Vergara, F., Gaxiola, M., et al. (2015). Essential Role for the ATG4B Protease and Autophagy in Bleomycin-Induced Pulmonary Fibrosis. *Autophagy* 11 (4), 670–684. doi:10.1080/15548627.2015.1034409

Cano, A., Pérez-Moreno, M. A., Rodrigo, I., Locascio, A., Blanco, M. J., del Barrio, M. G., et al. (2000). The Transcription Factor Snail Controls Epithelial-Mesenchymal Transitions by Repressing E-Cadherin Expression. *Nat. Cel. Biol.* 2 (2), 76–83. doi:10.1038/35000025

Choi, S. Y., Ryu, H. M., Choi, J. Y., Cho, J. H., Kim, C. D., Kim, Y. L., et al. (2017). The Role of Toll-like Receptor 4 in High-Glucose-Induced Inflammatory and Fibrosis Markers in Human Peritoneal Mesothelial Cells. *Int. Urol. Nephrol.* 49 (1), 171–181. doi:10.1007/s11255-016-1430-9

Davies, S. J. (2004). Longitudinal Relationship between Solute Transport and Ultrafiltration Capacity in Peritoneal Dialysis Patients. *Kidney Int.* 66 (6), 2437–2445. doi:10.1111/j.1523-1755.2004.66021.x

Ding, Y., and Choi, M. E. (2015). Autophagy in Diabetic Nephropathy. *J. Endocrinol.* 224 (1), R15–R30. doi:10.1530/joe-14-0437

Ding, Y., and Choi, M. E. (2014). Regulation of Autophagy by TGF-β: Emerging Role in Kidney Fibrosis. *Semin. Nephrol.* 34 (1), 62–71. doi:10.1016/j.semnephrol.2013.11.009

Fan, Y., Mao, R., and Yang, J. (2013). NF-κB and STAT3 Signaling Pathways Collaboratively Link Inflammation to Cancer. *Protein Cell* 4 (3), 176–185. doi:10.1007/s13238-013-2084-3

Hu, S., Wang, L., Zhang, X., Wu, Y., Yang, J., and Li, J. (2018). Autophagy Induces Transforming Growth Factor-β-dependent Epithelial-Mesenchymal Transition in Hepatocarcinoma Cells through cAMP Response Element Binding Signalling. *J. Cel. Mol. Med.* 22 (11), 5518–5532. doi:10.1111/jcmm.13825

Io, K., Nishino, T., Obata, Y., Kitamura, M., Koji, T., and Kohno, S. (2015). SAHA Suppresses Peritoneal Fibrosis in Mice. *Perit. Dial. Int.* 35 (3), 246–258. doi:10.3747/pdi.2013.00089

Jain, A. K., Blake, P., Cordy, P., and Garg, A. X. (2012). Global Trends in Rates of Peritoneal Dialysis. *J. Am. Soc. Nephrol.* 23 (3), 533–544. doi:10.1681/asn.2011060607

Kitterer, D., Latus, J., Ulmer, C., Fritz, P., Biegger, D., Ott, G., et al. (2015). Activation of Nuclear Factor of Activated T Cells 5 in the Peritoneal Membrane of Uremic Patients. *Am. J. Physiol. Ren. Physiol.* 308 (11), F1247–F1258. doi:10.1152/ajprenal.00617.2014

Kiyono, K., Suzuki, H. I., Matsuyama, H., Morishita, Y., Komuro, A., Kano, M. R., et al. (2009). Autophagy Is Activated by TGF-Beta and Potentiates TGF-Beta-Mediated Growth Inhibition in Human Hepatocellular Carcinoma Cells. *Cancer Res.* 69 (23), 8844–8852. doi:10.1158/0008-5472.can-08-4401

Kokubo, S., Sakai, N., Furuichi, K., Toyama, T., Kitajima, S., Okumura, T., et al. (2012). Activation of P38 Mitogen-Activated Protein Kinase Promotes Peritoneal Fibrosis by Regulating Fibrocytes. *Perit. Dial. Int.* 32 (1), 10–19. doi:10.3747/pdi.2010.00200

Krediet, R. T., and Struijk, D. G. (2013). Peritoneal Changes in Patients on Long-Term Peritoneal Dialysis. *Nat. Rev. Nephrol.* 9 (7), 419–429. doi:10.1038/nrneph.2013.99

Krediet, R. T. (2018). Ultrafiltration Failure Is a Reflection of Peritoneal Alterations in Patients Treated with Peritoneal Dialysis. *Front. Physiol.* 9, 1815. doi:10.3389/fphys.2018.01815

Lamouille, S., and Derynck, R. (2007). Cell Size and Invasion in TGF-Beta-Induced Epithelial to Mesenchymal Transition Is Regulated by Activation of the mTOR Pathway. *J. Cel. Biol.* 178 (3), 437–451. doi:10.1083/jcb.200611146

Leask, A., and Abraham, D. J. (2004). TGF-beta Signaling and the Fibrotic Response. *FASEB J.* 18 (7), 816–827. doi:10.1096/fj.03-1273rev

Levine, B., Mizushima, N., and Virgin, H. W. (2011). Autophagy in Immunity and Inflammation. *Nature* 469 (7330), 323–335. doi:10.1038/nature09782

Li, J., Yang, B., Zhou, Q., Wu, Y., Shang, D., Guo, Y., et al. (2013). Autophagy Promotes Hepatocellular Carcinoma Cell Invasion through Activation of Epithelial-Mesenchymal Transition. *Carcinogenesis* 34 (6), 1343–1351. doi:10.1093/carcin/bgt063

Li, R., Du, J. H., Yao, G. M., Yao, Y., and Zhang, J. (2019a). Autophagy: a New Mechanism for Regulating VEGF and PEDF Expression in Retinal Pigment Epithelium Cells. *Int. J. Ophthalmol.* 12 (4), 557–562. doi:10.18240/ijo.2019.04.05

Li, S., Peng, F., Gong, W., Wu, J., Wang, Y., Xu, Z., et al. (2019b). Dimethylaminomicheliolide Ameliorates Peritoneal Fibrosis through the Activation of Autophagy. *J. Mol. Med.* 97 (5), 659–674. doi:10.1007/s00109-019-01757-1

Liang, P., Jiang, B., Li, Y., Liu, Z., Zhang, P., Zhang, M., et al. (2018). Autophagy Promotes Angiogenesis via AMPK/Akt/mTOR Signaling during the Recovery of Heat-Denatured Endothelial Cells. *Cel. Death Dis.* 9 (12), 1152. doi:10.1038/s41419-018-1194-5

Liu, B., Zhou, H., Zhang, T., Gao, X., Tao, B., Xing, H., et al. (2021). Loss of Endothelial Glucocorticoid Receptor Promotes Angiogenesis via Upregulation of Wnt/β-Catenin Pathway. *Angiogenesis* 24, 631–645. doi:10.1007/s10456-021-09773-x

Liu, Y., Dong, Z., Liu, H., Zhu, J., Liu, F., and Chen, G. (2015). Transition of Mesothelial Cell to Fibroblast in Peritoneal Dialysis: EMT, Stem Cell or Bystander? *Perit. Dial. Int.* 35 (1), 14–25. doi:10.3747/pdi.2014.00188

Margetts, P. J., Bonniaud, P., Liu, L., Hoff, C. M., Holmes, C. J., West-Mays, J. A., et al. (2005). Transient Overexpression of TGF-{beta}1 Induces Epithelial Mesenchymal Transition in the Rodent Peritoneum. *J. Am. Soc. Nephrol.* 16 (2), 425–436. doi:10.1681/asn.2004060436

Massagué, J. (2012). TGFβ Signalling in Context. *Nat. Rev. Mol. Cel. Biol.* 13 (10), 616–630. doi:10.1038/nrm3434

Mendis, E., Kim, M. M., Rajapakse, N., and Kim, S. K. (2008). Suppression of Cytokine Production in Lipopolysaccharide-Stimulated Mouse Macrophages by Novel Cationic Glucosamine Derivative Involves Down-Regulation of NF-kappaB and MAPK Expressions. *Bioorg. Med. Chem.* 16 (18), 8390–8396. doi:10.1016/j.bmc.2008.08.037

Meng, D., Li, Z., Wang, G., Ling, L., Wu, Y., and Zhang, C. (2018). Carvedilol Attenuates Liver Fibrosis by Suppressing Autophagy and Promoting Apoptosis in Hepatic Stellate Cells. *Biomed. Pharmacother.* 108, 1617–1627. doi:10.1016/j.biopha.2018.10.005

Padwal, M., Cheng, G., Liu, L., Boivin, F., Gangji, A. S., Brimble, K. S., et al. (2018). WNT Signaling Is Required for Peritoneal Membrane Angiogenesis. *Am. J. Physiol. Ren. Physiol.* 314 (6), F1036–f1045. doi:10.1152/ajprenal.00497.2017

Padwal, M., Siddique, I., Wu, L., Tang, K., Boivin, F., Liu, L., et al. (2017). Matrix Metalloproteinase 9 Is Associated with Peritoneal Membrane Solute Transport and Induces Angiogenesis through β-catenin Signaling. *Nephrol. Dial. Transpl.* 32 (1), 50–61. doi:10.1093/ndt/gfw076

Pang, M., Kothapally, J., Mao, H., Tolbert, E., Ponnusamy, M., Chin, Y. E., et al. (2009). Inhibition of Histone Deacetylase Activity Attenuates Renal Fibroblast Activation and Interstitial Fibrosis in Obstructive Nephropathy. *Am. J. Physiol. Ren. Physiol.* 297 (4), F996–f1005. doi:10.1152/ajprenal.00282.2009

Patel, P., Sekiguchi, Y., Oh, K. H., Patterson, S. E., Kolb, M. R., and Margetts, P. J. (2010). Smad3-dependent and -independent Pathways Are Involved in Peritoneal Membrane Injury. *Kidney Int.* 77 (4), 319–328. doi:10.1038/ki.2009.436

Qian, M., Fang, X., and Wang, X. (2017). Autophagy and Inflammation. *Clin. Transl. Med.* 6 (1), 24. doi:10.1186/s40169-017-0154-5

Saha, S., Panigrahi, D. P., Patil, S., and Bhutia, S. K. (2018). Autophagy in Health and Disease: A Comprehensive Review. *Biomed. Pharmacother.* 104, 485–495. doi:10.1016/j.biopha.2018.05.007

Shi, J., Yu, M., and Sheng, M. (2017). Angiogenesis and Inflammation in Peritoneal Dialysis: The Role of Adipocytes. *Kidney Blood Press. Res.* 42 (2), 209–219. doi:10.1159/000476017

Shi, Y., Tao, M., Wang, Y., Zang, X., Ma, X., Qiu, A., et al. (2020). Genetic or Pharmacologic Blockade of Enhancer of Zeste Homolog 2 Inhibits the Progression of Peritoneal Fibrosis. *J. Pathol.* 250 (1), 79–94. doi:10.1002/path.5352

Strippoli, R., Moreno-Vicente, R., Battistelli, C., Cicchini, C., Noce, V., Amicone, L., et al. (2016). Molecular Mechanisms Underlying Peritoneal EMT and Fibrosis. *Stem Cell Int.* 2016, 3543678. doi:10.1155/2016/3543678

Sureshbabu, A., Muhsin, S. A., and Choi, M. E. (2016). TGF-β Signaling in the Kidney: Profibrotic and Protective Effects. *Am. J. Physiol. Ren. Physiol.* 310 (7), F596–f606. doi:10.1152/ajprenal.00365.2015

Tzavlaki, K., and Moustakas, A. (2020). TGF-β Signaling. *Biomolecules* 10 (3), 487. doi:10.3390/biom10030487

Wang, L., Liu, N., Xiong, C., Xu, L., Shi, Y., Qiu, A., et al. (2016). Inhibition of EGF Receptor Blocks the Development and Progression of Peritoneal Fibrosis. *J. Am. Soc. Nephrol.* 27 (9), 2631–2644. doi:10.1681/asn.2015030299

Wu, J., Li, X., Zhu, G., Zhang, Y., He, M., and Zhang, J. (2016a). The Role of Resveratrol-Induced Mitophagy/autophagy in Peritoneal Mesothelial Cells Inflammatory Injury via NLRP3 Inflammasome Activation Triggered by Mitochondrial ROS. *Exp. Cel. Res.* 341 (1), 42–53. doi:10.1016/j.yexcr.2016.01.014

Wu, J., Xing, C., Zhang, L., Mao, H., Chen, X., Liang, M., et al. (2018). Autophagy Promotes Fibrosis and Apoptosis in the Peritoneum during Long-Term Peritoneal Dialysis. *J. Cel. Mol. Med.* 22 (2), 1190–1201. doi:10.1111/jcmm.13393

Wu, T. T., Li, W. M., and Yao, Y. M. (2016b). Interactions between Autophagy and Inhibitory Cytokines. *Int. J. Biol. Sci.* 12 (7), 884–897. doi:10.7150/ijbs.15194

Wynn, T. A., and Vannella, K. M. (2016). Macrophages in Tissue Repair, Regeneration, and Fibrosis. *Immunity* 44 (3), 450–462. doi:10.1016/j.immuni.2016.02.015

Xie, J., Méndez, J. D., Méndez-Valenzuela, V., and Aguilar-Hernández, M. M. (2013). Cellular Signalling of the Receptor for Advanced Glycation End Products (RAGE). *Cell Signal* 25 (11), 2185–2197. doi:10.1016/j.cellsig.2013.06.013

Xu, L., Liu, N., Gu, H., Wang, H., Shi, Y., Ma, X., et al. (2017). Histone Deacetylase 6 Inhibition Counteracts the Epithelial-Mesenchymal Transition of Peritoneal Mesothelial Cells and Prevents Peritoneal Fibrosis. *Oncotarget* 8 (51), 88730–88750. doi:10.18632/oncotarget.20982

Xu, X., Xu, H., Ren, F., Huang, L., Xu, J., and Li, F. (2021). Protective Effect of Scorpion Venom Heat-Resistant Synthetic Peptide against PM2.5-induced Microglial Polarization via TLR4-Mediated Autophagy Activating PI3K/AKT/NF-κB Signaling Pathway. *J. Neuroimmunol.* 355, 577567. doi:10.1016/j.jneuroim.2021.577567

Yang, L., Fan, Y., Zhang, X., Liu, J., and Ma, J. (2017). Effect of 1,25(OH)2D3 on High Glucose-induced Autophagy Inhibition in Peritoneum. *Mol. Med. Rep.* 16 (5), 7080–7085. doi:10.3892/mmr.2017.7408

Yoshio, Y., Miyazaki, M., Abe, K., Nishino, T., Furusu, A., Mizuta, Y., et al. (2004). TNP-470, an Angiogenesis Inhibitor, Suppresses the Progression of Peritoneal Fibrosis in Mouse Experimental Model. *Kidney Int.* 66 (4), 1677–1685. doi:10.1111/j.1523-1755.2004.00935.x

Zhang, P., Holowatyj, A. N., Roy, T., Pronovost, S. M., Marchetti, M., Liu, H., et al. (2019). An SH3PX1-Dependent Endocytosis-Autophagy Network Restrains Intestinal Stem Cell Proliferation by Counteracting EGFR-ERK Signaling. *Dev. Cel.* 49 (4), 574–589. doi:10.1016/j.devcel.2019.03.029

Zhang, Y., Alexander, P. B., and Wang, X. F. (2017a). TGF-β Family Signaling in the Control of Cell Proliferation and Survival. *Cold Spring Harb. Perspect. Biol.* 9 (4), a022145. doi:10.1101/cshperspect.a022145

Zhang, Z., Jiang, N., and Ni, Z. (2017b). Strategies for Preventing Peritoneal Fibrosis in Peritoneal Dialysis Patients: New Insights Based on Peritoneal Inflammation and Angiogenesis. *Front. Med.* 11 (3), 349–358. doi:10.1007/s11684-017-0571-2

Zhao, X. C., Livingston, M. J., Liang, X. L., and Dong, Z. (2019). Cell Apoptosis and Autophagy in Renal Fibrosis. *Adv. Exp. Med. Biol.* 1165, 557–584. doi:10.1007/978-981-13-8871-2_28

Zhao, X. D., Qin, R. H., Yang, J. J., Xu, S. S., Tao, H., Ding, X. S., et al. (2018). DNMT3A Controls miR-200b in Cardiac Fibroblast Autophagy and Cardiac Fibrosis. *Inflamm. Res.* 67 (8), 681–690. doi:10.1007/s00011-018-1159-2

Zhou, Q., Bajo, M. A., Del Peso, G., Yu, X., and Selgas, R. (2016a). Preventing Peritoneal Membrane Fibrosis in Peritoneal Dialysis Patients. *Kidney Int.* 90 (3), 515–524. doi:10.1016/j.kint.2016.03.040

Zhou, X., Zang, X., Ponnusamy, M., Masucci, M. V., Tolbert, E., Gong, R., et al. (2016b). Enhancer of Zeste Homolog 2 Inhibition Attenuates Renal Fibrosis by Maintaining Smad7 and Phosphatase and Tensin Homolog Expression. *J. Am. Soc. Nephrol.* 27 (7), 2092–2108. doi:10.1681/asn.2015040457

Conflict of Interest: The authors declare that the research was conducted in the absence of any commercial or financial relationships that could be construed as a potential conflict of interest.

Publisher's Note: All claims expressed in this article are solely those of the authors and do not necessarily represent those of their affiliated organizations, or those of the publisher, the editors and the reviewers. Any product that may be evaluated in this article, or claim that may be made by its manufacturer, is not guaranteed or endorsed by the publisher.

GLOSSARY

AGEs advanced glycation end products
CG chlorhexidine gluconate
CTGF connective tissue growth factor
DAPK Death-associated protein kinase
DMSO dimethyl sulfoxide
ECM extracellular matrix
EGFR epidermal growth factor receptor
ELISA enzyme-linked immunosorbent assay
ERK1/2 extracellular signal–regulated kinase 1/2
EMT epithelial to mesenchymal transition
ESRD end-stage renal disease
FBS fetal bovine serum
FFPE Formalin-Fixed Paraffin-Embedded
GAPDH glyceraldehyde 3-phosphate dehydrogenase
GDPs glucose degradation products
HG high glucose
HUVECs human umbilical vein endothelial cells
HPMCs human peritoneal mesothelial cells
IL-1β interleukin-1β
IL-6 interleukin-6
LC3 light chain 3
LEF lymphoid enhancer-binding factor
MMT mesothelial to mesenchymal transition
MCP-1 monocyte chemoattractant protein-1
3-MA 3-methyladenine
NF-κB nuclear factor-κB
PKC protein kinase C
PDE4A phosphodiesterase 4A
PEDF pigment epithelium derived factor
PF peritoneal fibrosis
PD peritoneal dialysis
PDF peritoneal dialysate fluid
ROS reactive oxygen species
STAT3 signal transducer and activator of transcription 3
α-SMA α-smooth muscle actin
TCL T cell factor
TEM transmission electron microscope
TNF-α tumor necrosis factor-α
TGF-β transforming growth factor-β
TGF-βRI type I TGF-β receptor
VEGF vascular endothelial growth factor

frontiers in Pharmacology

ORIGINAL RESEARCH
published: 30 August 2021
doi: 10.3389/fphar.2021.722638

Requirement of Histone Deacetylase 6 for Interleukin-6 Induced Epithelial-Mesenchymal Transition, Proliferation, and Migration of Peritoneal Mesothelial Cells

*Yingfeng Shi[1†], Min Tao[1†], Jun Ni[1,2†], Lunxian Tang[3], Feng Liu[1], Hui Chen[1], Xiaoyan Ma[1], Yan Hu[1], Xun Zhou[1], Andong Qiu[4], Shougang Zhuang[1,5] and Na Liu[1]**

[1]Department of Nephrology, Shanghai East Hospital, Tongji University School of Medicine, Shanghai, China, [2]Department of Immunology and Microbiology, Shanghai Institute of Immunology, Shanghai Jiao Tong University School of Medicine, Shanghai, China, [3]Emergency Department of Critical Care Medicine, Shanghai East Hospital, Tongji University School of Medicine, Shanghai, China, [4]School of Life Science and Technology, Advanced Institute of Translational Medicine, Tongji University, Shanghai, China, [5]Department of Medicine, Rhode Island Hospital and Alpert Medical School, Brown University, Providence, RI, United States

OPEN ACCESS

Edited by:
Raffaele Strippoli,
Sapienza University of Rome, Italy

Reviewed by:
George Hsiao,
Taipei Medical University, Taiwan
Clemens Zwergel,
Sapienza University of Rome, Italy

***Correspondence:**
Na Liu
naliubrown@163.com

†These authors have contributed equally to this work

Specialty section:
This article was submitted to Experimental Pharmacology and Drug Discovery, a section of the journal Frontiers in Pharmacology

Received: 09 June 2021
Accepted: 31 July 2021
Published: 30 August 2021

Citation:
Shi Y, Tao M, Ni J, Tang L, Liu F, Chen H, Ma X, Hu Y, Zhou X, Qiu A, Zhuang S and Liu N (2021) Requirement of Histone Deacetylase 6 for Interleukin-6 Induced Epithelial-Mesenchymal Transition, Proliferation, and Migration of Peritoneal Mesothelial Cells. Front. Pharmacol. 12:722638. doi: 10.3389/fphar.2021.722638

Aims: Influenced by microenvironment, human peritoneal mesothelial cells (HPMCs) acquired fibrotic phenotype, which was identified as the protagonist for peritoneal fibrosis. In this study, we examined the role of histone deacetylase 6 (HDAC6) for interleukin-6 (IL-6) induced epithelial-mesenchymal transition (EMT), proliferation, and migration of HPMCs.

Methods: The role of HDAC6 in IL-6-elicited EMT of HPMCs was tested by morphological observation of light microscope, immunoblotting, and immune-fluorescence assay; and the function of HDAC6 in proliferation and migration of HPMCs was examined by CCK-8 assay, wound healing experiment, and immunoblotting.

Results: IL-6 stimulation significantly increased the expression of HDAC6. Treatment with tubastatin A (TA), a highly selective HDAC6 inhibitor, or silencing of HDAC6 with siRNA decreased the expression of HDAC6. Moreover, TA or HDAC6 siRNA suppressed IL-6-induced EMT, as evidenced by decreased expressions of α-SMA, Fibronectin, and collagen I and the preserved expression of E-cadherin in cultured HPMCs. Mechanistically, HDAC6 inhibition suppressed the expression of transforming growth factor β (TGFβ) receptor I (TGFβRI), phosphorylation of Smad3, secretion of connective tissue growth factor (CTGF), and transcription factor Snail. On the other hand, the pharmacological inhibition or genetic target of HDAC6 suppressed HPMCs proliferation, as evidenced by the decreased optical density of CCK-8 and the expressions of PCNA and Cyclin E. The migratory rate of HPMCs also decreased. Mechanistically, HDAC6 inhibition blocked the activation of JAK2 and STAT3.

Abbreviations: HPMCs, human peritoneal mesothelial cells; HDAC6, histone deacetylase 6; IL-6, interleukin-6; EMT, epithelial-mesenchymal transition; TA, tubastatin A; α-SMA, α-smooth muscle actin; TGFβ, transforming growth factor β, TGFβRI; TGF-β receptor I; CTGF, connective tissue growth factor; PD, peritoneal dialysis; PF, peritoneal fibrosis.

Conclusion: Our study illustrated that IL-6-induced HDAC6 not only regulated IL-6 itself downstream JAK2/STAT3 signaling but also co-activated the TGF-β/Smad3 signaling, leading to the change of the phenotype and mobility of HPMCs. HDAC6 could be a potential therapeutic target for the prevention and treatment of peritoneal fibrosis.

Keywords: histone deacetylase 6, interleukin-6, epithelial-mesenchymal transition, proliferation, migration, peritoneal mesothelial cells

INTRODUCTION

Peritoneal dialysis (PD) is an effective and home-based renal replacement therapy for end-stage renal disease (ESRD) patients (Li et al., 2017). Peritoneal fibrosis (PF) is the main factor for ultrafiltration loss and treatment failure in PD patients, and it is characterized by the loss of mesothelial cells (MCs) and increase of myofibroblasts in submesothelial areas, where epithelial-mesenchymal transition (EMT) occurs (Zhou Q. et al., 2016).

The EMT process refers to the *trans*-differentiation of epithelial cells into motile mesenchymal cells, which is regulated by related transcriptional factors, such as Snail and Twist, resulting in upregulation of mesothelial cell markers (i.e., α-SMA, Collagen I, and Fibronectin) and downregulation of epithelial cell markers (i.e., E-cadherin and ZO-1) (Lamouille et al., 2014). Meanwhile, peritoneal mesothelial cells under phenotypic transformation often acquire the capacity of proliferation and invasiveness and secrete more cell cycle associated proteins, such as proliferating cell nuclear antigen (PCNA) and Cyclin E (He et al., 2015). Traditionally, this process is triggered *via* the activation of the canonical transforming growth factor-β (TGF-β) pathway (Zhou Q. et al., 2016). However, peritoneal fibrosis has two cooperative parts, the fibrosis process itself and the inflammation (Zhou Q. et al., 2016; Balzer, 2020). The link between them is frequently bidirectional, with each one inducing the other (Balzer, 2020). Thus, the noncanonical inflammatory cytokines-elicited EMT also arouses the attention of researchers.

Particularly for IL-6, it is a multifunctional cytokine produced by a variety of cells such as lymphoid and non-lymphoid cells and by normal and transformed cells, including macrophages, mesothelial cells, and mesenchymal cells (Choy et al., 2020). The prospective clinic studies show that significant amounts of IL-6 in drained dialysate are in much higher concentrations than in serum under stable conditions (Lopes Barreto et al., 2011; Yang et al., 2014; Yang et al., 2018). The dialysate IL-6 level is increased shortly before the onset of and during the peritoneal fibrosis and several months after the clinically cured peritonitis, suggesting its local production and reflecting an intraperitoneal fibrosis and inflammatory state (Yang et al., 2014; Yang et al., 2018). However, the cellular mechanisms initiating an IL-6-related fibrosis response are still unclear. The current study aims to investigate the mechanism of IL-6-directed EMT, proliferation, and migration of MCs from an epigenetic point of view.

Epigenetics refers to heritable changes in gene expression which does not involve changes to the underlying DNA sequences (Guo et al., 2019). Acetylation is an important epigenetics modification in histone tail, which is regulated by histone acetyltransferases (HATs) and histone deacetylases (HDACs) (West and Johnstone, 2014). Histone deacetylase 6 (HDAC6) belongs to class IIb and primarily resides in the cytoplasm, while its deacetylase activity controls both cytoplasmic and nuclear functions (Pulya et al., 2021). The best characterized substrate for HDAC6 is α-tubulin (Hubbert et al., 2002). HDAC6 deacetylates α-tubulin *via* a process that requires its second HDAC domain and leads to an increase in the cell motility (Hubbert et al., 2002). Moreover, we and other research groups found that, unlike classes I, IIa, and III HDACs knockout mice, the homozygous HDAC6-deficient mice, which presented hyperacetylated tubulin in quite a lot tissues, were viable and fertile (Zhang et al., 2008; Chen et al., 2020). This indicated that HDAC6-specific inhibitors could be a safer and better tolerated medicine than pan-HDAC inhibitors. Recently, some of HDAC6 selective inhibitors, such as ACY-1215 (IC50 = 4.8 nM) and ACY-241 (IC50 = 2.6 nM), had been underwent the Phase I/II clinical trials in the field of tumors treatment (Porter et al., 2017; Pulya et al., 2021). Comparing these molecules, tubastatin A (TA) inhibited HDAC6 with an IC50 of 15 nM. Even so, TA was still a potential candidate because of its high selectivity. TA was found to have about 1093 fold selectivity towards HDAC6 over class I HDACs, while ACY-1215 and ACY-241 had 12-fold and 18-fold selectivity, respectively (Porter et al., 2017; Pulya et al., 2021). Thus, TA was adopted and administrated at different concentrations in the current study.

Notably, previous studies reported that HDAC6 promoted kidney and lung fibrosis, mainly through its regulation and activation on growth factor receptors (Deribe et al., 2009; Saito et al., 2017; Chen et al., 2020). However, the role of HDAC6 in the inflammatory factor IL-6 signaling pathway remains unexplored. IL-6 was accounted for a significant concentration in the drained dialysate and thus adopted to stimulate human peritoneal mesothelial cells (HPMCs). Interestingly, we observed that HDAC6 was overexpressed after stimulation; meanwhile HPMCs tended to EMT, proliferation, and migration. What is the role of this IL-6-induced deacetylase for cell phenotype and mobility? Does it have a modification on the downstream signaling of IL-6? Could it be a linker between IL-6 and TGF-β signaling?

In this study, we first assessed the effect of TA on the IL-6-induced change of the phenotype and the mobility of HPMCs and

further investigated the signaling regulatory mechanism, in order to provide evidence for future clinical trials in the field of peritoneal fibrosis.

MATERIALS AND METHODS

Antibodies and Reagents

Tubastatin A and MG132 were purchased from Selleckchem (Houston, TX, United States). Antibodies to HDAC6 (#7612), Acetyl Histone H3 (Lys9) (#9649), Histone H3 (#9717), Acetyl α-Tubulin (Lys40) (#5335), α-Tubulin (#3873), ZO-1 (#13663), Smad3 (#9523), p-Smad3 (#9520), JAK2 (#3230), p-JAK2 (#3771), STAT3 (#9139), p-STAT3 (#9138), CTGF (#86641), E-cadherin (#14472), Cyclin E (#20808) and Snail (#3879) were purchased from Cell Signaling Technology (Danvers, MA, United States). Antibody to Fibronectin (ab2413) was purchased from Abcam (Cambridge, MA). Antibodies to GAPDH (sc-32233), Collagen I (A2) (sc-28654), TGFβRI (sc-399), Smad7 (sc-365846), and PCNA (sc-71858) were purchased from Santa Cruz Biotechnology (San Diego, CA, United States). IL-6 protein was purchased from R&D Systems (Minneapolis, MN, United States). HDAC6 siRNA was purchased from GenePharma (Shanghai, China). Lipofectamine 2000 was purchased from Invitrogen (Grand Island, NY, United States). The Cell Counting Kit-8 (CCK-8) proliferation assay kit was purchased from Beyotime Biotechnology (Haimen, China). Antibody to α-SMA (A2547) and all other chemicals were obtained from Sigma-Aldrich (St. Louis, MO, United States).

Mesothelial Cell Culture

Human peritoneal mesothelial cells (HPMCs) (Jennio Biotechnology, Guangzhou, China) were cultured in MEM containing 10% fetal bovine serum (FBS) and 1% penicillin and streptomycin in an atmosphere of 5% CO_2 and 95% air at 37°C. To determine the effect of HDAC6 inhibition on EMT induced by IL-6, the HPMCs were starved for 24 h with 0.5% FBS in MEM and then exposed to IL-6 (100 ng/ml) for 36 h in the presence or absence of different concentrations of TA (5, 10, and 20 μM) or MG132 (5 μM) before cell harvesting. All of the *in vitro* experiments were repeated for at least three times.

siRNA Transfection

The small interfering (si) RNA oligonucleotides targeted specially for HDAC6 were used to downregulate the HDAC6 level in the cultured human peritoneal mesothelial cells. The HPMCs were seeded to 30–40% confluence in antibiotic-free medium and grown for 24 h and then were transfected with HDAC6 siRNA (50 nmol) with Lipofectamine 2000 according to the manufacturer's instructions. In parallel, scrambled siRNA (50 nmol) was used as control for the off-target changes in the HPMCs. After transfection for 24 h, the cells were treated with IL-6 (100 ng/ml) for an additional 36 h before being harvested for further experiments.

CCK-8 Proliferation Assay

The CCK-8 proliferation kit was used according to the manufacturer's instructions. The HPMCs were starved for 24 h with MEM containing 0.5% FBS and then exposed to IL-6 (100 ng/ml) in the presence or absence of TA (5, 10, and 20 μM). After 36 h, the original culture medium was removed, and 100 μl new MEM medium containing 10 μl CCK-8 was added to each well in a 96-well plate for 37°C incubation for an additional 4 h. The final optical density values were read at 450 nm.

Immunoprecipitations and Immunoblotting

Following an initial 24 h starvation, the HPMCs were exposed to IL-6 (100 ng/ml) for 36 h. The cell lysate was harvested by using ice-cold non-denaturing lysis buffer (Thermo Scientific, Rockford, IL). Co-immunoprecipitation (co-IP) was done using the Thermo Scientific Pierce co-IP kit (26149) following the manufacturer's protocol. Briefly, the HDAC6 or IgG antibody was first immobilized for 2 h using AminoLink Plus coupling resin. The resin was then washed and incubated with the cell lysate overnight. After incubation, the resin was again washed and the protein was eluted using the elution buffer. The samples were analyzed by immunoblotting using the antibodies of Smad3, HDAC6, and GAPDH. Immunoblotting was performed as previously described (Zhou X. et al., 2016). The densitometry analysis of immunoblotting results was conducted by using ImageJ software.

Wound Healing Assay

The HPMCs were seeded in a 6-well plate and allowed to reach 90% confluence. A scratch wound was created on the cell surface using a micropipette tip. Then, the cells were washed with PBS three times and incubated in serum-free MEM with IL-6 (100 ng/ml) in the presence or absence of TA (20 μM) and HDAC6 siRNA. The photomicrographs (× 40 objective magnification) of the migrating cells were taken at 0–36 h. The width of the wound was measured using ImageJ software (National Institutes of Health, Bethesda, MD, United States). The migratory rate was calculated as (A− B)/A × 100%, where A and B reflect the width of the wound at 0–36 h, respectively.

Immunofluorescence Staining

The cells grown on chamber slides were fixed for 15 min with 4% paraformaldehyde. The samples were permeabilized with 0.1% Triton X-100 for 30 min. Then, the samples were blocked with goat serum for 15 min. The primary antibodies against HDAC6, Acetyl Histone H3, α-SMA, Fibronectin, E-cadherin, and ZO-1 diluted in PBS (1:100) were added to the samples, respectively, and incubated overnight at 4°C. After PBS washing, the cells were incubated with the Texas Red-labeled secondary antibody (1:200, Beyotime, China) diluted in PBS for 1 h at room temperature. The nuclei were stained with DAPI. After additional washing for 5 min three times, the samples were sealed by the antifade reagent and visualized with an Olympus fluorescence microscope (at ×200 magnification).

Statistical Analysis

All the experiments were conducted at least three times. The data depicted in the graphs represent the means ± SEM for each group. The intergroup comparison was made using one-way analysis of

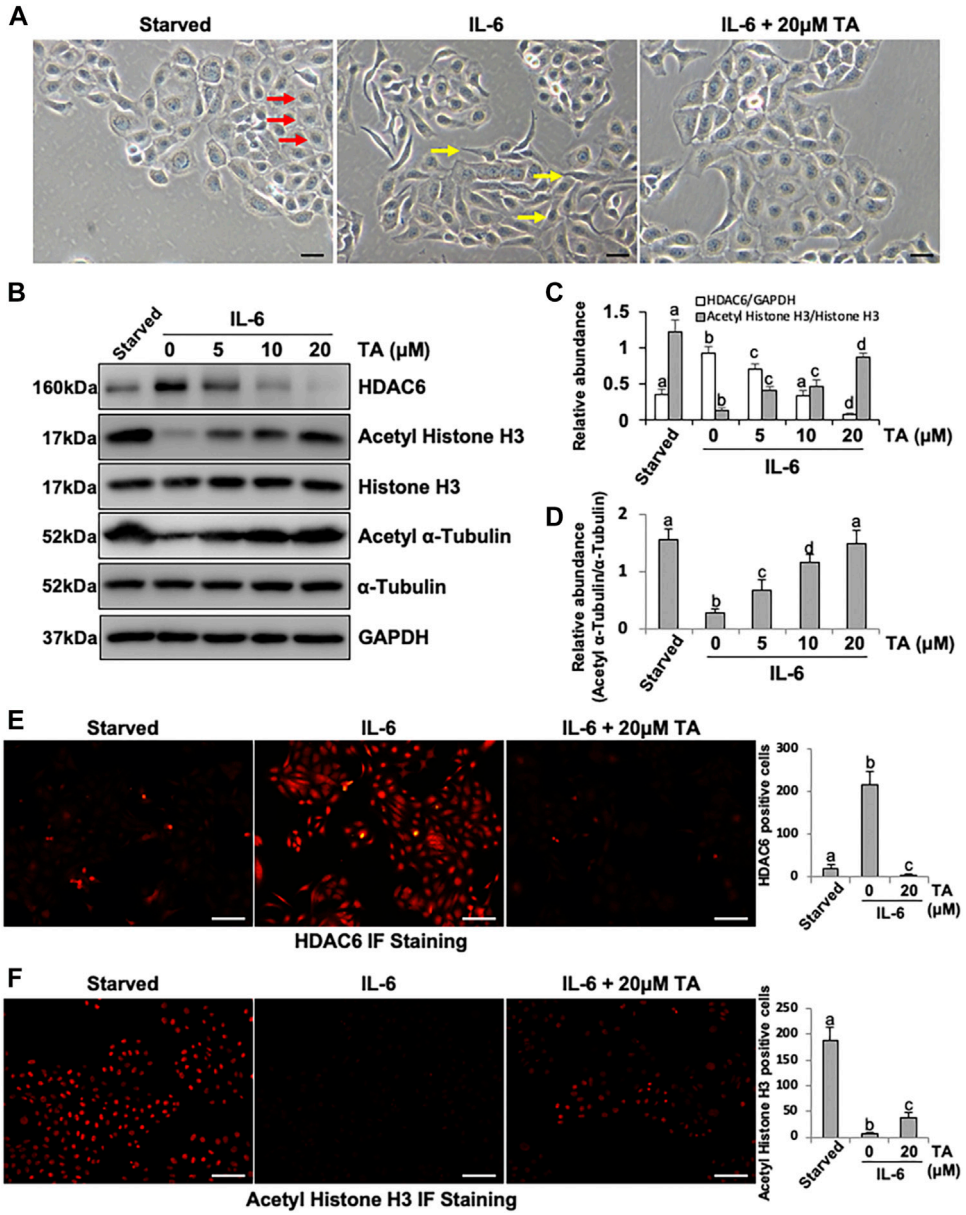

FIGURE 1 | IL-6 increases the expression of HDAC6 in cultured human peritoneal mesothelial cells. **(A)** Cell morphology was observed using light microscopy. Red arrows indicate the cobblestone-shaped cells and yellow arrows show the spindle-shaped cells. **(B)** Cell lysates were subjected to immunoblot analysis with antibodies against HDAC6, Acetyl Histone H3, Histone H3, Acetyl α-Tubulin, α-Tubulin, and GAPDH. **(C)** Expression levels of HDAC6 and Acetyl Histone H3 were quantified by densitometry and normalized with GAPDH and total Histone H3, respectively. **(D)** Expression level of Acetyl α-Tubulin was quantified by densitometry and normalized with total α-Tubulin. Immunofluorescence photomicrographs (×200) illustrate staining of HDAC6 **(E)** and Acetyl Histone H3 **(F)**. In the HPMCs under different treatment, the count of HDAC6 or Acetyl Histone H3 positive cells was calculated from 10 random fields of each cell sample. Data are represented as the mean ± SEM (n = 3). Means with different superscript letters are significantly different from one another ($p < 0.05$). All scale bars = 100 μm.

variance. Multiple means were compared using Tukey's test. The differences between the two groups were determined by Student's *t*-test. The statistical significant difference between the mean values was marked in each graph. $p < 0.05$ was considered significant. The statistical analyses were conducted by using IBM SPSS Statistics 20.0 (Version X; IBM, Armonk, NY, United States).

RESULTS

IL-6 Increases the Expression of HDAC6 in Cultured Peritoneal Mesothelial Cells

IL-6 was a canonical inflammation factor, which was highly expressed in the fibrotic peritoneum and the dialysis effluent from long-term PD patients (Lopes Barreto et al., 2011; Yang

et al., 2014; Yang et al., 2018). We aimed to investigate the mechanism by which IL-6 regulated the peritoneal fibrosis. Firstly, the human peritoneal mesothelial cells were stimulated by IL-6 *in vitro*. We found that the exposure of HPMCs to IL-6 at 100 ng/ml changed the cell morphology into fusiform or spindle shape (**Figure 1A**) and increased the expression level of HDAC6 and decreased the expression of Acetyl Histone H3 and Acetyl α-Tubulin in the cultured HPMCs (**Figures 1B–D**). The treatment of cells with TA, a highly selective inhibitor of HDAC6, at different concentrations (5, 10, and 20 μM) resulted in decreasing the expression of HDAC6 and increasing the expression of Acetyl Histone H3 (**Figures 1B,C**) and Acetyl α-Tubulin (**Figures 1B,D**) in a concentration-dependent manner, with a maximum effect at 20 μM. Neither IL-6 stimulation nor TA treatment had an impact on total expression of Histone H3 and α-Tubulin (**Figure 1B**). In addition, the immunofluorescent staining of HPMCs showed that HDAC6 was mainly expressed in both nucleus and the cytosol, while TA treatment decreased IL-6-induced HDAC6 and improved Acetyl Histone H3 (**Figures 1E,F**).

Notably, we found that TA not only inhibited the activity of HDAC6 but also reduced the expression of HDAC6. We suggested that TA induced the degradation of HDAC6 through the ubiquitin-proteasome pathway. It has been documented that MG132 is a specific inhibitor which can reduce the degradation of ubiquitin-conjugated proteins in mammalian cells (Longhitano et al., 2020). The HPMCs were exposed to IL-6 (100 ng/ml) and TA (20 μM) treatment in the presence or absence of MG132 (5 μM). Immunoblotting showed that TA significantly downregulated the expression of HDAC6, and further administration of MG132 resulted in upregulation of HDAC6 as indicated in **Supplementary Figure S1**. These data suggested that IL-6 increased the expression of HDAC6 in HPMCs, which was sensitive to TA and ubiquitination at least in part contributed to the downregulation of HDAC6.

Pharmacological Blockade of HDAC6 Inhibits IL-6 Induced EMT of Cultured Human Peritoneal Mesothelial Cells

Beside the canonical TGF-β-directed EMT pathway, inflammatory cytokine IL-6 also facilitated the EMT of the peritoneal mesothelial cells (Xiao et al., 2017), while the specific mechanism was still obscure. Considering the high expression of HDAC6 under the IL-6 stimulation, we hypothesized that HDAC6 would play an essential role in IL-6-trigged EMT of HPMCs. To test this hypothesis, we examined the effect of HDAC6 inhibition on IL-6-induced EMT of peritoneal mesothelial cells. As shown in **Figure 2**, exposure to IL-6 promoted the EMT of HPMCs, showing the increased expression of mesenchymal cell markers (α-SMA, Fibronectin, and Collagen I) and the decreased expression of epithelial cell marker, E-cadherin (Strippoli et al., 2016). Inhibition of HDAC6 with TA markedly suppressed IL-6-induced expression of α-SMA, Fibronectin, and Collagen I and prevented E-cadherin loss (**Figures 2A–C**). In parallel, immunofluorescent staining had a similar phenomenon. TA treatment downregulated the expressions of α-SMA and Fibronectin and upregulated the expressions of E-cadherin and ZO-1 (**Figures 2D–G**). The results indicated that the inhibition of HDAC6 by TA could effectively alleviate IL-6-induced EMT of HPMCs.

siRNA-Mediated Silencing of HDAC6 Inhibits EMT of Peritoneal Mesothelial Cells

To further verify the role of HDAC6 in EMT, we tested the effect of HDAC6 knockdown on the EMT of HPMCs using specific siRNA. As shown in **Figure 3A**, the cell morphology was slightly turned into oval or cobblestone shape after HDAC6 inhibition. siRNA-mediated silencing of HDAC6 recovered the abnormally low expression of Acetyl Histone H3 and Acetyl α-Tubulin induced by IL-6 but did not alter the level of total Histone H3 and α-Tubulin (**Figures 3B–D**). As expected, HDAC6 siRNA also downregulated α-SMA, Fibronectin, and Collagen I and upregulated the expression of E-cadherin (**Figures 3E–G**). These data further confirmed the importance of HDAC6 in mediating IL-6 induced EMT of peritoneal mesothelial cells.

HDAC6 Is Required for the Activation of the TGF-β Signaling Pathway in Peritoneal Mesothelial Cells

It was reported that IL-6 could trigger the activation of the TGF-β signaling pathway in the fibrosis process (Luckett-Chastain et al., 2017); however, the cross-talk mechanism was obscure. We speculated that IL-6-elicited HDAC6 was required for the activation of the TGF-β signaling pathway, leading to an increased secretion of growth factors, such as CTGF, and the increased expression of transcription factors, such as Snail. To test this hypothesis, we examined the expression of TGF-β type receptor I (TGFβRI) on the TA-inhibited peritoneal mesothelial cells. As shown in **Figures 4A,B**, the base level of TGFβRI was negligible in the starved cell. However, its expression level was substantially elevated after IL-6 stimulation, which was further inhibited by TA treatment in a dose-dependent manner. TA also suppressed the phosphorylation of Smad3, while it restored the expression of Smad7, which could block the activation of Smad2/3 by competitively binding with TGFβRI (Murayama et al., 2020). There was no impact on total Smad3 (**Figures 4A–D**). Moreover, the immunoblot results presented that TA decreased the secretion of the growth factor CTGF in the IL-6 stimulated HPMCs (**Figures 4E,F**); and the nuclear transcription factor Snail, which was responsible for transcription inhibition of E-cadherin (Zhang et al., 2018; Wang et al., 2020), also witnessed a decrease after TA treatment (**Figures 4G,H**). Similarly, HDAC6 siRNA inhibited accumulation of TGFβRI, phosphorylation of Smad3, and loss of Smad7 (**Figures 5A–D**). It also had an inhibition effect on the expressions of CTGF and Snail (**Figures 5E–H**). These results suggested that HDAC6 was required for the activation of the TGF-β/Smad3 signaling pathway, resulting in the secretion of CTGF and upregulation of Snail (**Figure 8**).

Additionally, we conducted the immunoprecipitation experiment to find the direct substrate of HDAC6

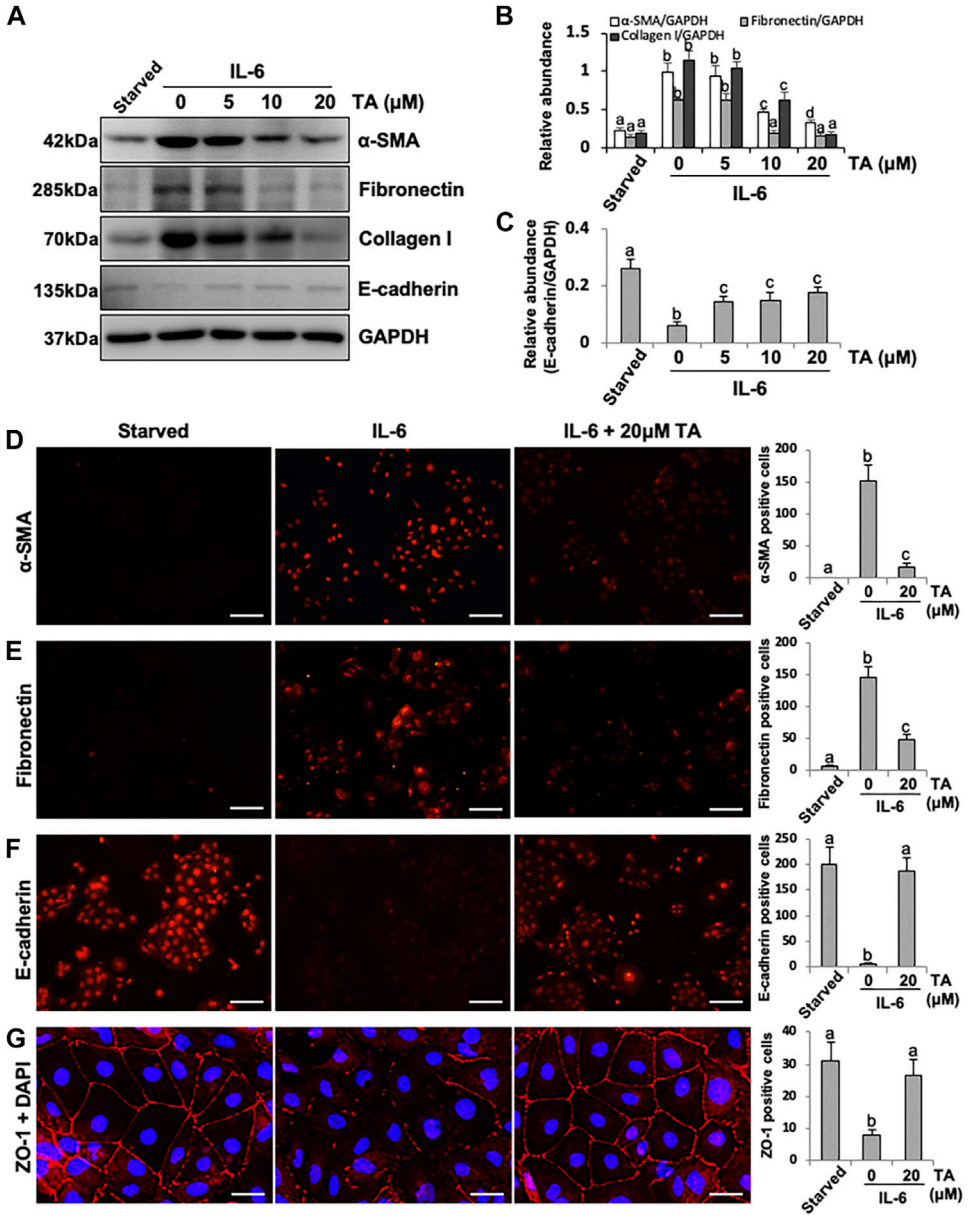

FIGURE 2 | Pharmacological blockade of HDAC6 inhibits IL-6-induced EMT of cultured human peritoneal mesothelial cells. **(A)** Cell lysates were subjected to immunoblot analysis with specific antibodies against α-SMA, Fibronectin, Collagen I, E-cadherin, and GAPDH. **(B)** Expression levels of α-SMA, Fibronectin, and Collagen I were quantified by densitometry and normalized with GAPDH. **(C)** Expression level of E-cadherin was quantified by densitometry and normalized with GAPDH. Immunofluorescence photomicrographs (×200) illustrate staining of α-SMA **(D)**, Fibronectin **(E)**, E-cadherin **(F)**, and ZO-1 **(G)** in HPMCs under different treatment. The count of α-SMA, Fibronectin, E-cadherin, and ZO-1 positive cells was calculated from 10 random fields of each cell sample. Data are represented as the mean ± SEM (n = 3). Means with different superscript letters are significantly different from one another ($p < 0.05$). The scale bars in **D**, **E**, and **F** = 100 μm and the scale bar in **G** = 25 μm.

(**Supplementary Figure S2**). The starved HPMCs were exposed to IL-6 (100 ng/ml) for 36 h and then harvested and prepared for immunoprecipitation and immunoblot. The result showed an interaction between HDAC6 and Smad3 in HPMCs treated with IL-6. Therefore, we speculated that HDAC6 directly interacted with Smad3 in the cytoplasm, and deacetylated Smad3 tended to nuclear localization and phosphorylation.

Inhibition of HDAC6 with TA or siRNA Alleviates Proliferation and Migration Through the JAK2/STAT3 Signaling Pathway in HPMCs.

It was reported that HPMCs underwent EMT acquired the ability of cell cycle progression, cell proliferation, and cell mobility (He et al., 2015). Thus, we assessed the role of HDAC6 in regulating

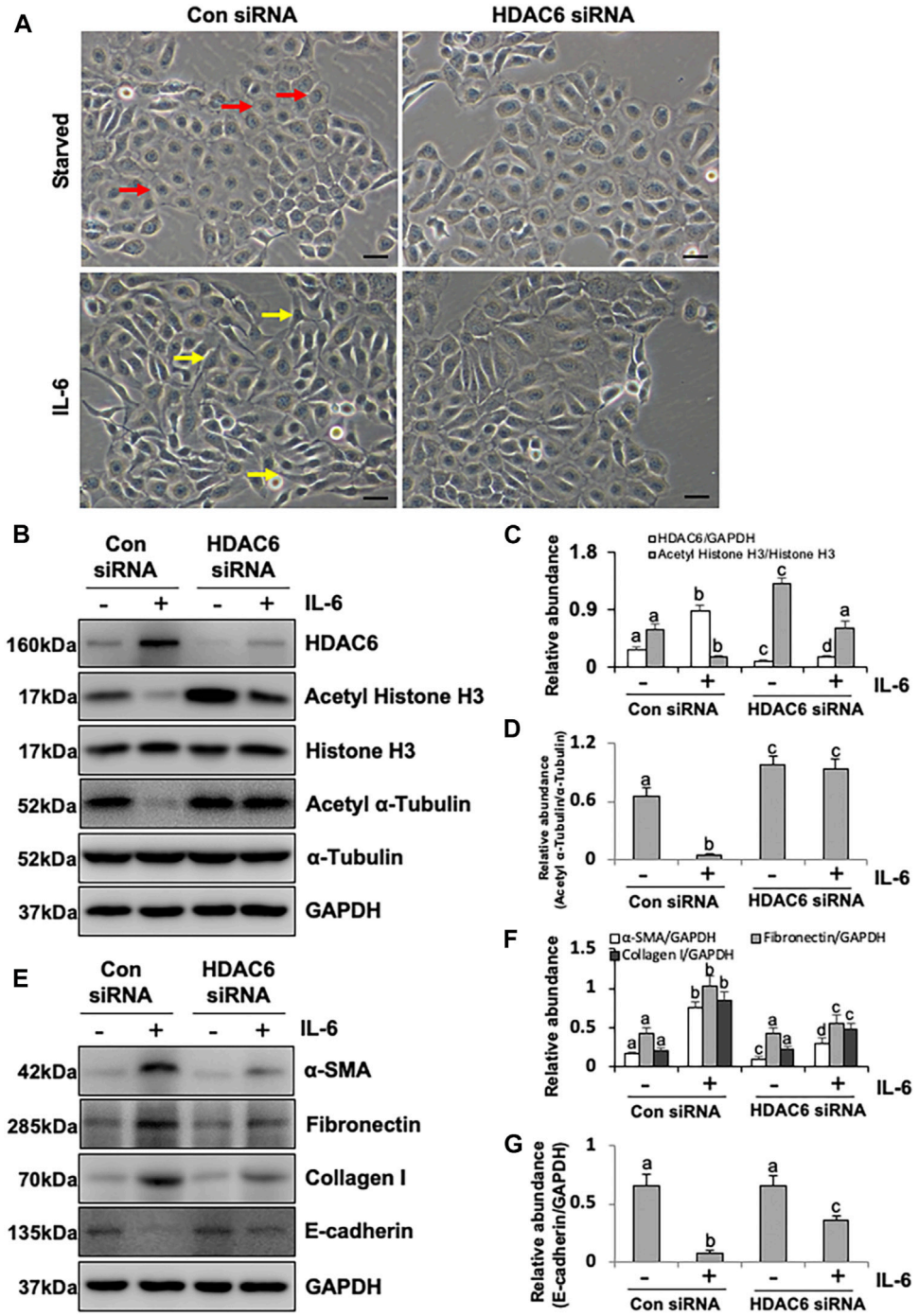

FIGURE 3 | siRNA-medicated silencing of HDAC6 inhibits EMT of peritoneal mesothelial cells. **(A)** Cell morphology was observed using light microscopy. The red arrows indicated the cobblestone-shaped cells and the yellow arrows showed the spindle-shaped cells. **(B)** Cell lysates were subjected to immunoblot analysis with antibodies against HDAC6, Acetyl Histone H3, Histone H3, Acetyl α-Tubulin, α-Tubulin, and GAPDH. **(C)** Expression levels of HDAC6 and Acetyl Histone H3 were quantified by densitometry and normalized with GAPDH and total histone H3, respectively. **(D)** Expression level of Acetyl α-Tubulin was quantified by densitometry and normalized with total α-Tubulin. **(E)** Cell lysates were subjected to immunoblot analysis with specific antibodies against α-SMA, Fibronectin, Collagen I, E-cadherin, and GAPDH. **(F)** Expression levels of α-SMA, Fibronectin, and Collagen I were quantified by densitometry and normalized with GAPDH. **(G)** Expression level of E-cadherin was quantified by densitometry and normalized with GAPDH. Data are represented as the mean ± SEM (n = 3). Means with different superscript letters are significantly different from one another ($p < 0.05$). All scale bars = 100 μm.

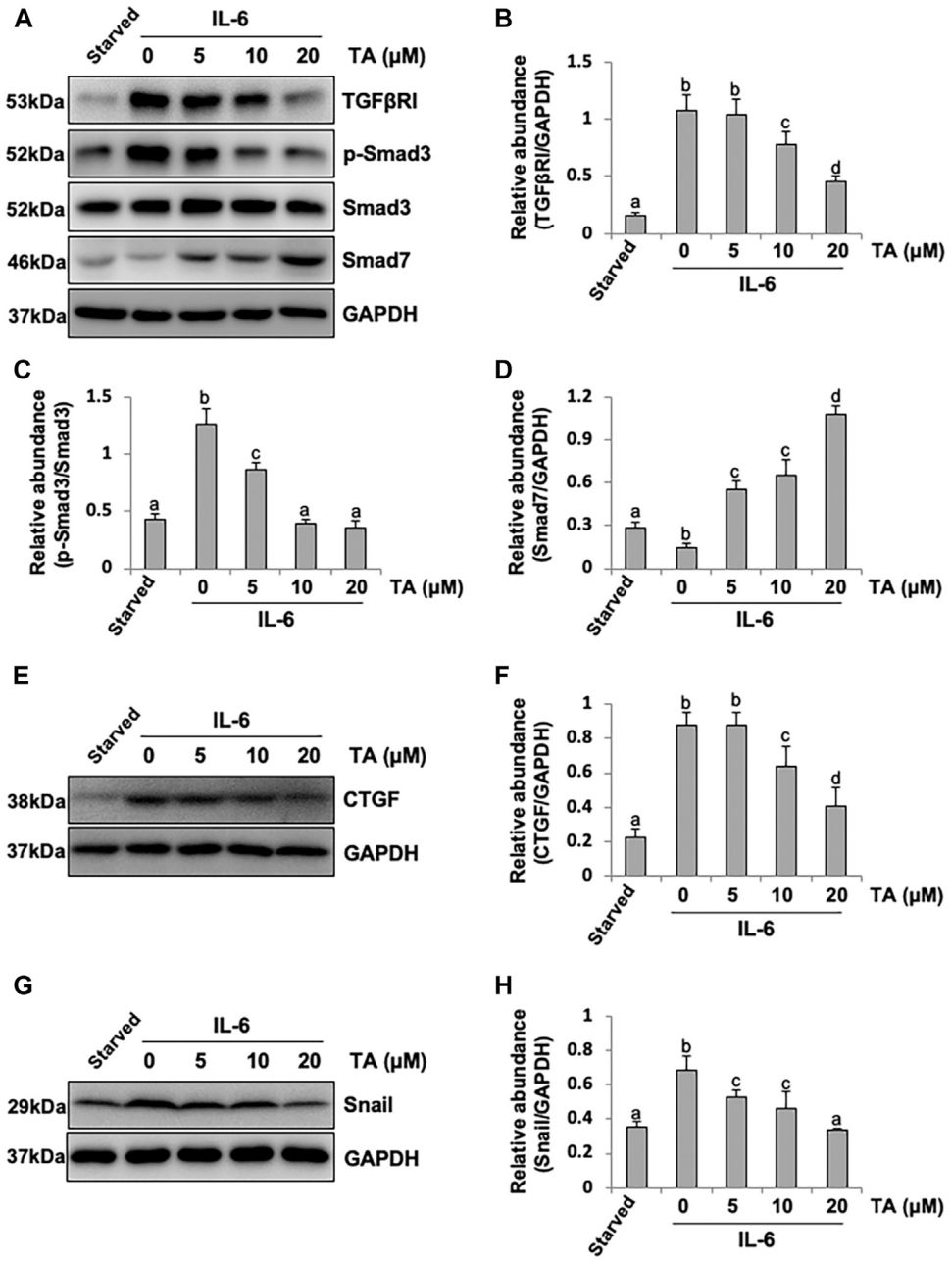

FIGURE 4 | Pharmacological blockade of HDAC6 inhibits the activation of the TGF-β signaling pathway and decreases the expression of CTGF and Snail in peritoneal mesothelial cells. **(A)** Cell lysates were subjected to immunoblot analysis with specific antibodies against TGFβRI, p-Smad3, Smad3, Smad7, and GAPDH. **(B)** Expression level of TGFβRI was quantified by densitometry and normalized with GAPDH. **(C)** Expression level of p-Smad3 was quantified by densitometry and normalized with Smad3. **(D)** Expression level of Smad7 was quantified by densitometry and normalized with GAPDH. **(E)** Cell lysates were subjected to immunoblot analysis with specific antibodies against CTGF and GAPDH. **(F)** Expression level of CTGF was quantified by densitometry and normalized with GAPDH. **(G)** Cell lysates were subjected to immunoblot analysis with specific antibodies against Snail and GAPDH. **(H)** Expression level of Snail was quantified by densitometry and normalized with GAPDH. Data are represented as the mean ± SEM (n = 3). Means with different superscript letters are significantly different from one another ($p < 0.05$).

the proliferation of HPMCs by the CCK-8 assay. The results showed that IL-6 at 100 ng/ml substantially stimulated the cell proliferation of HPMCs, compared with the simple starved group, while the TA treatment kept down the proliferation level, especially at the concentration of 20 μM (**Figure 6A**). The immunoblot analysis further confirmed the ability of TA in inhibiting cell proliferation, as indicated by decreased expression levels of PCNA and Cyclin E, two proliferating

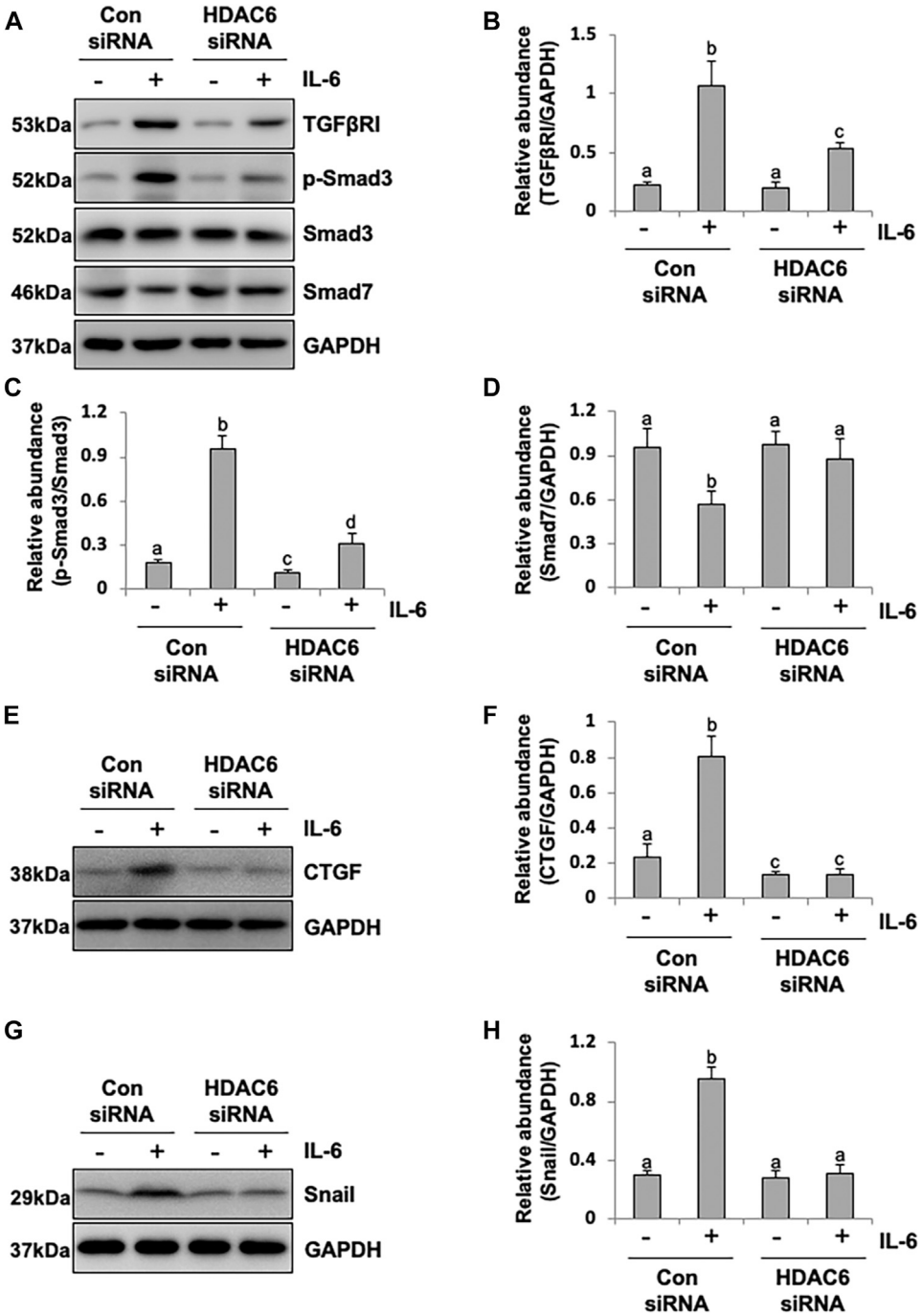

FIGURE 5 | siRNA-medicated silencing of HDAC6 inhibits the activation of the TGF-β signaling pathway and decreases the expression of CTGF and Snail in peritoneal mesothelial cells. **(A)** Cell lysates were subjected to immunoblot analysis with specific antibodies against TGFβRI, p-Smad3, Smad3, Smad7, and GAPDH. **(B)** Expression level of TGFβRI was quantified by densitometry and normalized with GAPDH. **(C)** Expression level of p-Smad3 was quantified by densitometry and normalized with Smad3. **(D)** Expression level of Smad7 was quantified by densitometry and normalized with GAPDH. **(E)** Cell lysates were subjected to immunoblot analysis with specific antibodies against CTGF and GAPDH. **(F)** Expression level of CTGF was quantified by densitometry and normalized with GAPDH. **(G)** Cell lysates were subjected to immunoblot analysis with specific antibodies against Snail and GAPDH. **(H)** Expression level of Snail was quantified by densitometry and normalized with GAPDH. Data are represented as the mean ± SEM (n = 3). Means with different superscript letters are significantly different from one another ($p < 0.05$).

hallmarks (**Figures 6B–D**). In addition, the cell migration test showed that TA suppressed the migratory rate of HPMCs (**Figures 6E,F**). To further reveal the mechanism in TA-downregulated proliferation and migration, we tested the expressions of JAK2 and STAT3 before and after the TA treatment in IL-6-stimulated HPMCs. The immunoblot

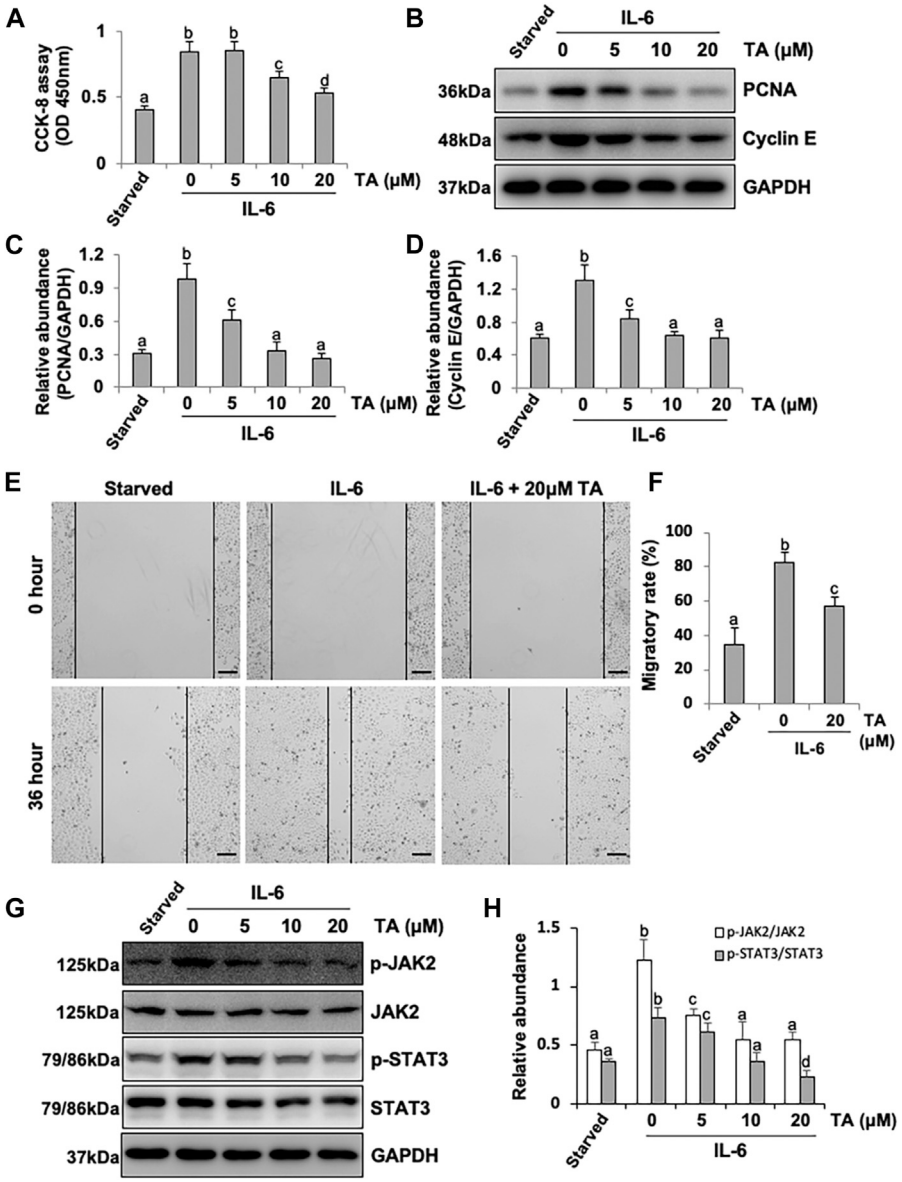

FIGURE 6 | Pharmacological blockade of HDAC6 alleviates proliferation and migration through the JAK2/STAT3 signaling pathway in human peritoneal mesothelial cells. **(A)** Cell proliferation was assessed by the CCK-8 assay. **(B)** Cell lysates were subjected to the immunoblot analysis with specific antibodies against PCNA, Cyclin E, and GAPDH. **(C)** Expression level of PCNA was quantified by densitometry and normalized with GAPDH. **(D)** Expression level of Cyclin E was quantified by densitometry and normalized with GAPDH. **(E)** Wound-healing assay of HPMCs treated with IL-6 (100 ng/ml) in the presence or absence of TA (20 μM). Photomicrographs of migrating cells were taken at 0 and 36 h. **(F)** The width of the wound was measured, and the migratory rate was calculated. **(G)** Cell lysates were subjected to the immunoblot analysis with specific antibodies against p-JAK2, JAK2, p-STAT3, STAT3, and GAPDH. **(H)** Expression levels of p-JAK2 and p-STAT3 were quantified by densitometry and normalized with JAK2 and STAT3, respectively. Data are represented as the mean ± SEM (n = 3). Means with different superscript letters are significantly different from one another ($p < 0.05$). All scale bars = 500 μm.

analysis showed that TA suppressed the phosphorylation of JAK2 and STAT3 in a concentration-dependent manner, while the total protein was not impacted (**Figures 6G,H**). Additionally, we found that siRNA-mediated silencing of HDAC6 achieved similar results (**Figure 7**). Taken together, these data illustrated that HDAC6 promoted the proliferation and migration of HPMCs through regulating the JAK2/STAT3 signaling (**Figure 8**).

DISCUSSION

The mesothelial cells which transferred to the mesenchymal phenotype acquired the increased capacity of proliferation, migration, and extracellular matrix (ECM) secretion, forming a fibrosis scar (Zhou Q. et al., 2016). Beside the canonical TGF-β, the inflammation factor IL-6 was also an important fibrosis inducer, which had a significant amount in the drained

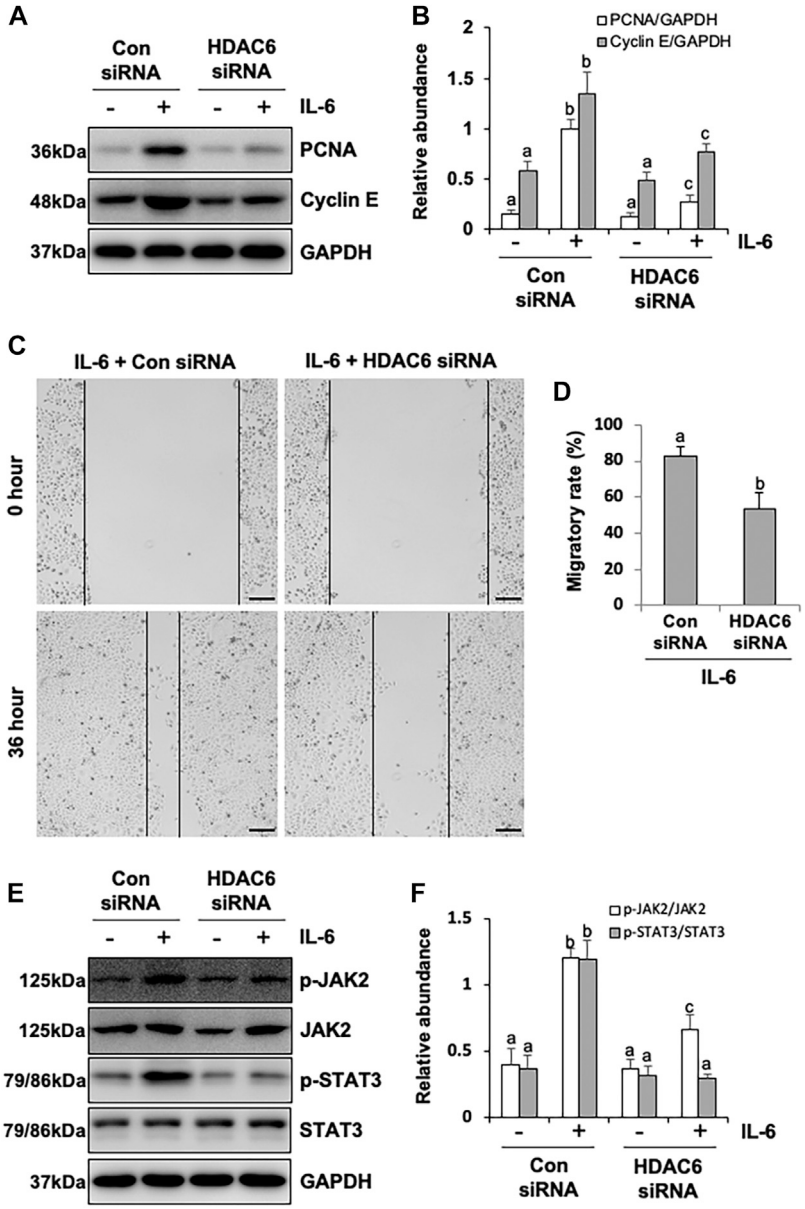

FIGURE 7 | siRNA-medicated silencing of HDAC6 inhibits proliferation and migration through the JAK2/STAT3 signaling pathway in human peritoneal mesothelial cells. **(A)** Cell lysates were subjected to the immunoblot analysis with specific antibodies against PCNA, Cyclin E, and GAPDH. **(B)** Expression levels of PCNA and Cyclin E were quantified by densitometry and normalized with GAPDH. **(C)** The wound-healing assay of the HPMCs treated with IL-6 (100 ng/ml) in the presence of HDAC6 siRNA or scrambled siRNA. Photomicrographs of migrating cells were taken at 0 and 36 h. **(D)** The width of the wound was measured, and the migratory rate was calculated. **(E)** Cell lysates were subjected to the immunoblot analysis with specific antibodies against p-JAK2, JAK2, p-STAT3, STAT3, and GAPDH. **(F)** Expression levels of p-JAK2 and p-STAT3 were quantified by densitometry and normalized with JAK2 and STAT3, respectively. Data are represented as the mean ± SEM (n = 3). Means with different superscript letters are significantly different from one another ($p < 0.05$). All scale bars = 500 μm.

dialysate from the PD patients (Lopes Barreto et al., 2011; Yang et al., 2014; Yang et al., 2018). However, the specific mechanism in the IL-6-induced cell phenotype change was still obscure. The current study firstly unravels a pivotal role of IL-6-elicited HDAC6 in signaling regulation and in EMT, proliferation, and migration of HPMCs.

It had been well established that TGF-β1 triggers EMT. Indeed, IL-6 also had this capacity, which was an indirect process through coactivating the TGF-β signaling pathway (Luckett-Chastain et al., 2017). Although the IL-6/TGF-β cooperation in the realm of ECM deposition had been documented (Luckett-Chastain et al., 2017; Epstein Shochet et al., 2020), their modulatory link was obscure. Our current study found that IL-6 stimulation induced the overexpression of HDAC6 in HPMCs. HDAC6 might be a vital linker between two signalings. The best characterized substrate for HDAC6

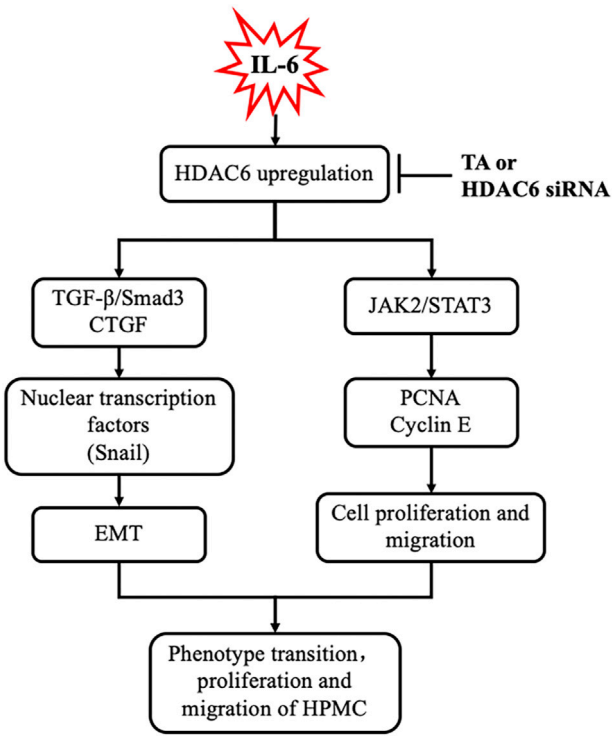

FIGURE 8 | Requirement of HDAC6 for IL-6 induced EMT, proliferation, and migration of peritoneal mesothelial cells resulted in an aggravation of peritoneal fibrosis. Exposure of IL-6 to the peritoneal mesothelial cells upregulates HDAC6, which leads to activation of TGF-β/Smad3 and JAK2/STAT3 signaling, subsequently inducing EMT (i.e., expression of CTGF and Snail), proliferation, and migration (i.e., production of PCNA and Cyclin E) response. All these responses are inhibited by TA or HDAC6 siRNA.

was α-Tubulin, an important component of the cytoskeleton, which had been reported to closely contact with clathrin, a receptor endocytosis-related protein (Rappoport et al., 2003; Montagnac et al., 2013). Evidence showed that clathrin moved along the microtubule cytoskeleton parallel to the cell surface (Rappoport et al., 2003; Montagnac et al., 2013). Acetylation of α-Tubulin tended to form a polymerization of microtubule and resulted in modest reduced endocytosis, while deacetylated α-Tubulin facilitated the insertion of the complexes in the clathrin-coated pits (Thomas et al., 2016; Melgari et al., 2020). Given that the TGF-β receptors were constitutively internalized *via* clathrin-dependent or lipid raft-dependent endocytic pathways (Kardassis et al., 2009), we suggested that IL-6 might modulate the activity of TGFβRI through upregulating deacetylase HDAC6, deacetylating α-Tubulin, and subsequent promoting clathrin internalization. This was evidenced by our present data demonstrating that HDAC6 inhibition increased the acetylation of α-Tubulin, decreased the expression of TGFβRI, and the activation of the TGF-β network in IL-6 treated HPMCs. But how does IL-6 increase the expression and activity of HDAC6? It might also work through an epigenetic mechanism. The detailed mechanism waited further investigation.

Our study also found that HDAC6 affected the activity of Smad3 in IL-6-treated HPMCs. The activation of Smad3 was not just the downstream effector of the TGF receptor. The emerging evidence implicated that the microtubule structure regulated the Smads activity (Dong et al., 2000; Zhu et al., 2004). Binding of Smads to microtubules kept Smads in their inactive stage, and TGF-β1 could trigger the release of Smads from microtubules and the subsequent phosphorylation of Smads (Dong et al., 2000; Zhu et al., 2004). Thus, one possible mechanism is that HDAC6 modulated the Smad3 activity through deacetylating α-Tubulin and promoting the release of Smad3. Another mechanism of Smad3 activation might be a direct acetylation modification by HDAC6 itself. A recent study reported the requirement of HDAC6 for the epidermal growth factor- (EGF-) triggered nuclear localization of β-catenin (Li et al., 2008). The deacetylation of lysine 49 in β-catenin was suggested to be essential for nuclear localization of β-catenin. It was conceivable that HDAC6 regulated nuclear localization of Smad3 *via* deacetylating Smad3 or Smad3-interacting proteins. As expected, the immunoprecipitation experiment confirmed a direct interaction between HDAC6 and Smad3 in HPMCs treated with IL-6. Subsequently, intranuclear Smad3 recruited and activated the transcription factor Snail and promoted the expression of the ECM protein and the secretion of CTGF. Our results showed that HDAC6 was required for the phosphorylation of Smad3, while it did not affect the total expression of Smad3. Interestingly, Smad7, a Smad3 blocker in the TGF-β network, encountered a significant increase following the HDAC6 inhibition. Collectively, we suggested that HDAC6 was required for IL-6-elicited TGF-β signaling transduction through upregulation of TGFβRI, activation of Smad3, and downregulation of Smad7. Nevertheless, the mechanisms underlying HDAC6-mediated Smad signaling need further investigation.

Another important transcription factor in IL-6 signaling was STAT3, which was responsible for cell proliferation and invasion (Cheng et al., 2020). We speculated that activation of JAK2/STAT3 might relate to deacetylation of α-Tubulin. Like many other transcription factors, STAT3 possessed a coiled-coil domain, which was found in a variety of tubulin-binding proteins (Zhang et al., 2000; Tala et al., 2014). In leukemia cells, STAT3 was mainly concentrated in the centrosome region where microtubules were more stable and hyperacetylated (Yan et al., 2015). It was possible that deacetylation of α-Tubulin promoted the activation and nuclear translocation of STAT3, which might generate a positive feedback and affect phosphorylation of JAK2, contributing to an amplifying IL-6/JAK2/STAT3 signaling. Thus, the cell cycle associated proteins (i.e., PCNA and Cyclin E) increased and resulted in cell proliferation. Moreover, HDAC6 also promoted the cell migration. It was documented that the interaction between deacetylated α-Tubulin and STAT3 changed the stability of microtubule and activated the small GTPase Rac-1 or Rho to control actin-dependent membrane ruffling and cell motility (Hubbert et al., 2002). Consistently, HDAC6 inhibition reduced the STAT3 response and blocked the feedback for JAK2, slowing down the proliferation and migration of HPMCs.

In conclusion, the current study firstly found that IL-6-induced deacetylase HDAC6 not only regulated IL-6 itself downstream the JAK2/STAT3 signaling but also co-activated the TGF-β/Smad3 signaling, leading to the change of the phenotype and mobility of cells. This finding partially interpreted the mechanism of the development of peritoneal fibrosis under the inflammation microenvironment. HDAC6 could be a potential therapeutic target for the prevention and treatment of peritoneal fibrosis.

DATA AVAILABILITY STATEMENT

The original contributions presented in the study are included in the article/**Supplementary Material**; further inquiries can be directed to the corresponding author.

ETHICS STATEMENT

The animal study was reviewed and approved by the Ethics Committee of Shanghai East Hospital, Tongji University School of Medicine of China.

AUTHOR CONTRIBUTIONS

NL participated in the research design. YS, JN, MT, LT, XM, FL, HC, YH, and XZ conducted the experiments. YS, MT, and JN contributed new reagents or analytic tools. YS and JN performed the data analysis. YS, MT, NL, AQ, and SZ wrote or contributed to the writing of the manuscript. All authors approved the final version of the manuscript.

FUNDING

This study was supported by the Shanghai Scientific Committee of China (20ZR1445800 and 13PJ1406900 to NL), the National Natural Science Foundation of China (Grants 82070791, 81670690, 81470991, and 81200492 to NL; 81700672 to JN; 81830021 and 81670623 to SZ; and 81970072 and 81500059 to LT), the Key Discipline Construction Project of Pudong Health Bureau of Shanghai (PWZxk 2017-05 to NL), the academic leader training plan of health system of Shanghai Pudong new area (PWRd 2019-13 to FL), the key program of Science Foundation of Jiangxi Province (2018ACB 20016 to LT), the leading medical talent project of Shanghai Pudong heath bureau (PWRI 2019-05 to LT), and Branch Grant of National Key R&D Program of China (2018YFA0108802 to SZ).

SUPPLEMENTARY MATERIAL

The Supplementary Material for this article can be found online at: https://www.frontiersin.org/articles/10.3389/fphar.2021.722638/full#supplementary-material

Supplementary Figure S1 | TA induces the degradation of HDAC6 through ubiquitin-proteasome pathway. **(A)** Cell lysates are subjected to immunoblot analysis with specific antibodies against HDAC6 and GAPDH. **(B)** Expression level of HDAC6 is quantified by densitometry and normalized with GAPDH. Data are represented as the mean ± S.E.M ($n = 3$). Means with different superscript letters are significantly different from one another ($p < 0.05$).

Supplementary Figure S2 | Smad3 is identified as a direct substrate of HDAC6. **(A)** Following an initial 24-h starvation, HPMCs are exposed to IL-6 (100 ng/ml) for 36 h. Total cellular proteins are harvested and immunoprecipitations are performed using HDAC6 or IgG antibody. And then immunoprecipitated proteins are immunoblotted with specific antibodies against Smad3, HDAC6 and GAPDH. An interaction between HDAC6 and Smad3 is found in HPMCs treated with IL-6.

REFERENCES

Balzer, M. S. (2020). Molecular Pathways in Peritoneal Fibrosis. *Cell Signal.* 75, 109778. doi:10.1016/j.cellsig.2020.109778

Chen, X., Yu, C., Hou, X., Li, J., Li, T., Qiu, A., et al. (2020). Histone Deacetylase 6 Inhibition Mitigates Renal Fibrosis by Suppressing TGF-β and EGFR Signaling Pathways in Obstructive Nephropathy. *Am. J. Physiology-Renal Physiol.* 319 (6), F1003–f1014. doi:10.1152/ajprenal.00261.2020

Cheng, M., Liu, P., and Xu, L. X. (2020). Iron Promotes Breast Cancer Cell Migration via IL-6/JAK2/STAT3 Signaling Pathways in a Paracrine or Autocrine IL-6-rich Inflammatory Environment. *J. Inorg. Biochem.* 210, 111159. doi:10.1016/j.jinorgbio.2020.111159

Choy, E. H., De Benedetti, F., Takeuchi, T., Hashizume, M., John, M. R., and Kishimoto, T. (2020). Translating IL-6 Biology into Effective Treatments. *Nat. Rev. Rheumatol.* 16 (6), 335–345. doi:10.1038/s41584-020-0419-z

Deribe, Y. L., Wild, P., Chandrashaker, A., Curak, J., Schmidt, M. H. H., Kalaidzidis, Y., et al. (2009). Regulation of Epidermal Growth Factor Receptor Trafficking by Lysine Deacetylase HDAC6. *Sci. Signal.* 2 (102), ra84. doi:10.1126/scisignal.2000576

Dong, C., Li, Z., Alvarez, R., Jr., Feng, X.-H., and Goldschmidt-Clermont, P. J. (2000). Microtubule Binding to Smads May Regulate TGFβ Activity. *Mol. Cel.* 5 (1), 27–34. doi:10.1016/s1097-2765(00)80400-1

Epstein Shochet, G., Brook, E., Bardenstein-Wald, B., and Shitrit, D. (2020). TGF-β Pathway Activation by Idiopathic Pulmonary Fibrosis (IPF) Fibroblast Derived Soluble Factors Is Mediated by IL-6 Trans-signaling. *Respir. Res.* 21 (1), 56. doi:10.1186/s12931-020-1319-0

Guo, C., Dong, G., Liang, X., and Dong, Z. (2019). Epigenetic Regulation in AKI and Kidney Repair: Mechanisms and Therapeutic Implications. *Nat. Rev. Nephrol.* 15 (4), 220–239. doi:10.1038/s41581-018-0103-6

He, L., Che, M., Hu, J., Li, S., Jia, Z., Lou, W., et al. (2015). Twist Contributes to Proliferation and Epithelial-To-Mesenchymal Transition-Induced Fibrosis by Regulating YB-1 in Human Peritoneal Mesothelial Cells. *Am. J. Pathol.* 185 (8), 2181–2193. doi:10.1016/j.ajpath.2015.04.008

Hubbert, C., Guardiola, A., Shao, R., Kawaguchi, Y., Ito, A., Nixon, A., et al. (2002). HDAC6 Is a Microtubule-Associated Deacetylase. *Nature* 417 (6887), 455–458. doi:10.1038/417455a

Kardassis, D., Murphy, C., Fotsis, T., Moustakas, A., and Stournaras, C. (2009). Control of Transforming Growth Factor β Signal Transduction by Small GTPases. *Febs j* 276 (11), 2947–2965. doi:10.1111/j.1742-4658.2009.07031.x

Lamouille, S., Xu, J., and Derynck, R. (2014). Molecular Mechanisms of Epithelial-Mesenchymal Transition. *Nat. Rev. Mol. Cel Biol.* 15 (3), 178–196. doi:10.1038/nrm3758

Li, P. K.-T., Chow, K. M., Van De Luijtgaarden, M. W. M., Johnson, D. W., Jager, K. J., Mehrotra, R., et al. (2017). Changes in the Worldwide Epidemiology of Peritoneal Dialysis. *Nat. Rev. Nephrol.* 13 (2), 90–103. doi:10.1038/nrneph.2016.181

Li, Y., Zhang, X., Polakiewicz, R. D., Yao, T.-P., and Comb, M. J. (2008). HDAC6 Is Required for Epidermal Growth Factor-Induced β-Catenin Nuclear Localization. *J. Biol. Chem.* 283 (19), 12686–12690. doi:10.1074/jbc.C700185200

Longhitano, L., Tibullo, D., Giallongo, C., Lazzarino, G., Tartaglia, N., Galimberti, S., et al. (2020). Proteasome Inhibitors as a Possible Therapy for SARS-CoV-2. *Ijms* 21 (10), 3622. doi:10.3390/ijms21103622

Lopes Barreto, D., Coester, A. M., Noordzij, M., Smit, W., Struijk, D. G., Rogers, S., et al. (2011). Variability of Effluent Cancer Antigen 125 and Interleukin-6 Determination in Peritoneal Dialysis Patients. *Nephrol. Dial. Transplant.* 26 (11), 3739–3744. doi:10.1093/ndt/gfr170

Luckett-Chastain, L. R., Cottrell, M. L., Kawar, B. M., Ihnat, M. A., and Gallucci, R. M. (2017). Interleukin (IL)-6 Modulates Transforming Growth Factor-β Receptor I and II (TGF-Bri and II) Function in Epidermal Keratinocytes. *Exp. Dermatol.* 26 (8), 697–704. doi:10.1111/exd.13260

Melgari, D., Barbier, C., Dilanian, G., Rücker-Martin, C., Doisne, N., Coulombe, A., et al. (2020). Microtubule Polymerization State and Clathrin-dependent Internalization Regulate Dynamics of Cardiac Potassium Channel. *J. Mol. Cell Cardiol.* 144, 127–139. doi:10.1016/j.yjmcc.2020.05.004

Montagnac, G., Meas-Yedid, V., Irondelle, M., Castro-Castro, A., Franco, M., Shida, T., et al. (2013). αTAT1 Catalyses Microtubule Acetylation at Clathrin-Coated Pits. *Nature* 502 (7472), 567–570. doi:10.1038/nature12571

Murayama, K., Kato-Murayama, M., Itoh, Y., Miyazono, K., Miyazawa, K., and Shirouzu, M. (2020). Structural Basis for Inhibitory Effects of Smad7 on TGF-β Family Signaling. *J. Struct. Biol.* 212 (3), 107661. doi:10.1016/j.jsb.2020.107661

Porter, N. J., Mahendran, A., Breslow, R., and Christianson, D. W. (2017). Unusual Zinc-Binding Mode of HDAC6-Selective Hydroxamate Inhibitors. *Proc. Natl. Acad. Sci. USA.* 114 (51), 13459–13464. doi:10.1073/pnas.1718823114

Pulya, S., Amin, S. A., Adhikari, N., Biswas, S., Jha, T., and Ghosh, B. (2021). HDAC6 as Privileged Target in Drug Discovery: A Perspective. *Pharmacol. Res.* 163, 105274. doi:10.1016/j.phrs.2020.105274

Rappoport, J. Z., Taha, B. W., and Simon, S. M. (2003). Movement of Plasma-Membrane-Associated Clathrin Spots along the Microtubule Cytoskeleton. *Traffic* 4 (7), 460–467. doi:10.1034/j.1600-0854.2003.00100.x

Saito, S., Zhuang, Y., Shan, B., Danchuk, S., Luo, F., Korfei, M., et al. (2017). Tubastatin Ameliorates Pulmonary Fibrosis by Targeting the TGFβ-Pi3k-Akt Pathway. *PLoS One* 12 (10), e0186615. doi:10.1371/journal.pone.0186615

Strippoli, R., Moreno-Vicente, R., Battistelli, C., Cicchini, C., Noce, V., Amicone, L., et al. (2016). Molecular Mechanisms Underlying Peritoneal EMT and Fibrosis. *Stem Cell Int.* 2016, 1–11. doi:10.1155/2016/3543678

TalaSun, X., Chen, J., Zhang, L., Liu, N., Zhou, J., et al. (2014). Microtubule Stabilization by Mdp3 Is Partially Attributed to its Modulation of HDAC6 in Addition to its Association with Tubulin and Microtubules. *PLoS One* 9 (3), e90932. doi:10.1371/journal.pone.0090932

Thomas, G. W., Rael, L. T., Hausburg, M., Frederick, E. D., Brody, E., and Bar-Or, D. (2016). The Low Molecular Weight Fraction of Commercial Human Serum Albumin Induces Acetylation of α-tubulin and Reduces Transcytosis in Retinal Endothelial Cells. *Biochem. Biophysical Res. Commun.* 478 (4), 1780–1785. doi:10.1016/j.bbrc.2016.09.026

Wang, H., Li, Q.-F., Chow, H., Choi, S., and Leung, Y.-C. (2020). Arginine Deprivation Inhibits Pancreatic Cancer Cell Migration, Invasion and EMT via the Down Regulation of Snail, Slug, Twist, and MMP1/9. *J. Physiol. Biochem.* 76 (1), 73–83. doi:10.1007/s13105-019-00716-1

West, A. C., and Johnstone, R. W. (2014). New and Emerging HDAC Inhibitors for Cancer Treatment. *J. Clin. Invest.* 124 (1), 30–39. doi:10.1172/jci69738

Xiao, J., Gong, Y., Chen, Y., Yu, D., Wang, X., Zhang, X., et al. (2017). IL-6 Promotes Epithelial-To-Mesenchymal Transition of Human Peritoneal Mesothelial Cells Possibly through the JAK2/STAT3 Signaling Pathway. *Am. J. Physiology-Renal Physiol.* 313 (2), F310–f318. doi:10.1152/ajprenal.00428.2016

Yan, B., Xie, S., Liu, Z., Luo, Y., Zhou, J., Li, D., et al. (2015). STAT3 Association with Microtubules and its Activation Are Independent of HDAC6 Activity. *DNA Cel Biol.* 34 (4), 290–295. doi:10.1089/dna.2014.2713

Yang, X., Tong, Y., Yan, H., Ni, Z., Qian, J., and Fang, W. (2018). High Intraperitoneal Interleukin-6 Levels Predict Peritonitis in Peritoneal Dialysis Patients: a Prospective Cohort Study. *Am. J. Nephrol.* 47 (5), 317–324. doi:10.1159/000489271

Yang, X., Zhang, H., Hang, Y., Yan, H., Lin, A., Huang, J., et al. (2014). Intraperitoneal Interleukin-6 Levels Predict Peritoneal Solute Transport Rate: a Prospective Cohort Study. *Am. J. Nephrol.* 39 (6), 459–465. doi:10.1159/000362622

Zhang, S., Huang, Q., Cai, X., Jiang, S., Xu, N., Zhou, Q., et al. (2018). Osthole Ameliorates Renal Fibrosis in Mice by Suppressing Fibroblast Activation and Epithelial-Mesenchymal Transition. *Front. Physiol.* 9, 1650. doi:10.3389/fphys.2018.01650

Zhang, T., Kee, W. H., Seow, K. T., Fung, W., and Cao, X. (2000). The Coiled-Coil Domain of Stat3 Is Essential for its SH2 Domain-Mediated Receptor Binding and Subsequent Activation Induced by Epidermal Growth Factor and Interleukin-6. *Mol. Cel Biol.* 20 (19), 7132–7139. doi:10.1128/mcb.20.19.7132-7139.2000

Zhang, Y., Kwon, S., Yamaguchi, T., Cubizolles, F., Rousseaux, S., Kneissel, M., et al. (2008). Mice Lacking Histone Deacetylase 6 Have Hyperacetylated Tubulin but Are Viable and Develop Normally. *Mol. Cel Biol.* 28 (5), 1688–1701. doi:10.1128/mcb.01154-06

Zhou, Q., Bajo, M.-A., Del Peso, G., Yu, X., and Selgas, R. (2016a). Preventing Peritoneal Membrane Fibrosis in Peritoneal Dialysis Patients. *Kidney Int.* 90 (3), 515–524. doi:10.1016/j.kint.2016.03.040

Zhou, X., Zang, X., Ponnusamy, M., Masucci, M. V., Tolbert, E., Gong, R., et al. (2016b). Enhancer of Zeste Homolog 2 Inhibition Attenuates Renal Fibrosis by Maintaining Smad7 and Phosphatase and Tensin Homolog Expression. *Jasn* 27 (7), 2092–2108. doi:10.1681/asn.2015040457

Zhu, S., Goldschmidt-Clermont, P. J., and Dong, C. (2004). Transforming Growth Factor-β-Induced Inhibition of Myogenesis Is Mediated through Smad Pathway and Is Modulated by Microtubule Dynamic Stability. *Circ. Res.* 94 (5), 617–625. doi:10.1161/01.res.0000118599.25944.d5

Conflict of Interest: The authors declare that the research was conducted in the absence of any commercial or financial relationships that could be construed as a potential conflict of interest.

Publisher's Note: All claims expressed in this article are solely those of the authors and do not necessarily represent those of their affiliated organizations or those of the publisher, the editors, or the reviewers. Any product that may be evaluated in this article, or claim that may be made by its manufacturer, is not guaranteed or endorsed by the publisher.

frontiers in Pharmacology

MINI REVIEW
published: 07 September 2021
doi: 10.3389/fphar.2021.737570

Epithelial-to-Mesenchymal Transition in Fibrosis: Concepts and Targeting Strategies

Sara Lovisa[1,2]*

[1]Department of Biomedical Sciences, Humanitas University, Pieve Emanuele (MI), Italy, [2]IRCCS Humanitas Research Hospital, Rozzano (MI), Italy

The epithelial-to-mesenchymal transition (EMT), an embryonic program relaunched during wound healing and in pathological conditions such as fibrosis and cancer, continues to gain the attention of the research community, as testified by the exponential trend of publications since its discovery in the seventies. From the first description as a mesenchymal transformation, the concept of EMT has been substantially refined as an in-depth comprehension of its functional role has recently emerged thanks to the implementation of novel mouse models as well as the use of sophisticated mathematical modeling and bioinformatic analysis. Nevertheless, attempts to targeting EMT in fibrotic diseases are at their infancy and continue to pose several challenges. The aim of this mini review is to recapitulate the most recent concepts in the EMT field and to summarize the different strategies which have been exploited to target EMT in fibrotic disorders.

Keywords: EMT, EMP, partial EMT, plasticity, fibrosis, epithelial-to-mesenchymal transition

OPEN ACCESS

Edited by:
Raffaele Strippoli,
Sapienza University of Rome, Italy

Reviewed by:
Manuel Lopez-Cabrera,
Consejo Superior de Investigaciones Científicas (CSIC), Spain
Ryuichi Ono,
National Institute of Health Sciences (NIHS), Japan

***Correspondence:**
Sara Lovisa
sara.lovisa@humanitasresearch.it

Specialty section:
This article was submitted to Inflammation Pharmacology, a section of the journal Frontiers in Pharmacology

Received: *07 July 2021*
Accepted: *12 August 2021*
Published: *07 September 2021*

Citation:
Lovisa S (2021) Epithelial-to-Mesenchymal Transition in Fibrosis: Concepts and Targeting Strategies. Front. Pharmacol. 12:737570. doi: 10.3389/fphar.2021.737570

EMT IN 2021: NOVEL REFINEMENTS OF AN OLD CONCEPT

Since its first description in the embryogenesis work by Elizabeth Hay in the 1970s (Hay, 1968; Hay, 1995), the concept of epithelial-to-mesenchymal transition (EMT) has expanded from the field of development and has been investigated in the fields of wound healing, fibrosis, and cancer (Nieto et al., 2016). With an average of 5,000 primary papers published per year in the 2016–2019 period (Yang et al., 2020; Hamidi et al., 2021), the topic of EMT continues to gain the interest of the scientific community and to provide novel insights into this phenomenon both in physiology and in disease.

EMT is traditionally defined as a cellular and molecular process through which cells lose their epithelial identity, defined by apical–basal polarity and stable intercellular junctions, and acquire a mesenchymal phenotype including cytoskeletal and morphological rearrangements, acquisition of fibroblast-like gene expression profile, migratory capacity, and ability to produce the extracellular matrix (ECM) (Kalluri, 2009; Kalluri and Weinberg, 2009; Zeisberg and Neilson, 2009). However, recent studies as well as the fervent town hall discussions during the 2017 and 2019 meetings of The EMT International Association (TEMTIA) have clearly highlighted the need to revise and expand the traditional definition of EMT in order to embrace newly discovered features such as the partial activation of the program and the existence of a continuous spectrum of hybrid EMT phenotype rather than a binary E–M model and have therefore introduced and encouraged the use of the term "epithelial-to-mesenchymal plasticity" (EMP) (Yang et al., 2020).

The appreciation that EMT exists as a hybrid phenotype in a continuum of epithelial and mesenchymal traits has emerged from the construction of mathematical algorithms modeling the existence of multiple intermediate steps with various degrees of E or M states (Lu et al., 2013; Jolly

et al., 2016; Tripathi et al., 2021), as well as from the pseudotemporal reconstruction of the EMT trajectory by single cell transcriptomics (Carstens et al., 2021; Deshmukh et al., 2021). The acquisition of this knowledge represents a great example of how crosstalk between different fields, such as mathematics and bioinformatics, can help in providing further understanding of the biology of EMT. In addition to the pure definition and the various criteria utilized to define this process, the functional role of EMT as defined by the type II and III classifications (Kalluri and Weinberg, 2009; Zeisberg and Neilson, 2009) requires to be updated in light of the most recent findings. In fact, the fibroblast-generating capacity of type II EMT during fibrosis has been rebutted (Ovadya and Krizhanovsky, 2015; Huang and Susztak, 2016; Lovisa et al., 2016), and the dispensability of type III EMT for metastasis has been questioned (Maheswaran and Haber, 2015; Brabletz et al., 2018).

This review aims to present the overview of recent concepts in EMT as well as novel insights as emerged from single cell transcriptomics, and to provide a summary of the strategies attempted to target EMT in the context of fibrotic diseases. So far, multiple approaches have been proposed to target EMT: from targeting the upstream inducing signaling pathways [which has been extensively reviewed in other recent reviews (Di Gregorio et al., 2020; Jonckheere et al., 2021)] to targeting EMT-transcription factors (TFs), promoting MET, and targeting EMT-induced vulnerabilities, the last being the strategy potentially leading to the most promising outcomes.

EMT CLASSIFICATION: TYPE II AND TYPE III REVISITED

In these past years, the two major EMT paradigms permeating the fibrosis and cancer fields, which are, respectively, the capacity to generate fibroblasts (type II EMT) and the indispensability in the metastatic cascade (type III EMT), have been interrogated and partially revised. Historically, the outstanding question in the fibrosis field has been the origin of the myofibroblasts responsible for the scarring of the tissue. Candidate cellular origins include the activation of tissue-resident fibroblasts, the differentiation from bone marrow precursors, and the *trans*-differentiation of epithelial, mesothelial, and endothelial cells, macrophages, pericytes, and adipocytes into myofibroblasts (Plikus et al., 2021).

In light of this major question, EMT and the cognate process of endothelial-to-mesenchymal transition (EndMT) were initially identified as the mechanisms generating these fibrosis-associated myofibroblasts (Okada et al., 1997; Kim et al., 2006; Zeisberg M. et al., 2007; Zeisberg E. M. et al., 2007; Zeisberg et al., 2008; Flier et al., 2010). However, novel genetically engineered knock-out mouse models coupled with lineage tracing strategies clearly demonstrated that, at least in the context of kidney fibrosis, EMT does not directly generate myofibroblasts nor confers migratory capacity and that EMT cells still reside within the epithelial basement membrane in a partial EMT (pEMT) state (LeBleu et al., 2013; Grande et al., 2015; Lovisa et al., 2015). This pEMT represents a damage response of the injured renal epithelium, which substantially impairs epithelial functionality and regenerative capacity. In fact, pEMT triggers an arrest of the tubular epithelial cell cycle at the G2/M phase, therefore impeding the regenerative potential, and induces loss of the expression and functionality of membrane transporters critical for the absorptive capacity of the kidney (Lovisa et al., 2015). Moreover, the activation of the mesenchymal program leads to the acquisition of a pro-inflammatory secretome profile which in turn fuels immune infiltration and further promotes fibrosis (Grande et al., 2015; Lovisa et al., 2015). Similarly, the contribution of EndMT to the myofibroblast pool was determined as minor while having a significant impact on vascular integrity (LeBleu et al., 2013; Lovisa et al., 2020).

Mesothelial cells, which line pleural, peritoneal, and pericardial cavities, represent an example of physiologic pEMT as, in the basal condition, they phenotypically display epithelial features although concomitantly expressing mesenchymal markers such as vimentin, a remnant of their mesoderm-derived embryonic origin (Mutsaers et al., 2015). In the pathological condition, these cells undergo an EMT analogous process termed "mesothelial-to-mesenchymal transition" (MMT), which was found to be responsible for causing peritoneal fibrosis (Yáñez-Mó et al., 2003; Yang et al., 2003; Del Peso et al., 2008). The functional consequences of MMT as well as other types of mesenchymal *trans*-differentiation such as the one undergone by macrophages [termed "macrophage-to-myofibroblast transition" (Meng et al., 2016; Wang et al., 2017; Tang et al., 2020)] appear to still be unquestionably linked to the full transition and generation of fibrosis-associated myofibroblasts, with a consequent more direct impact on the generation of fibrosis (Koopmans and Rinkevich, 2018).

The functional role of EMT in cancer has been similarly questioned. In fact, the metastasis dogma by which the metastasizing cells are those efficiently activating EMT to intravasate and extravasate and subsequently reverting to the epithelial state at distant sites through the process of mesenchymal-to-epithelial transition (MET) has been disproved at least in the context of breast (Fischer et al., 2015; Lourenco et al., 2020) and pancreatic cancers (Zheng et al., 2015; Chen et al., 2018; Carstens et al., 2021) and, since then, has been the subject of intense debate (Brabletz et al., 2018; Williams et al., 2019). The activation of EMT in cancer cells not only is connected with the metastatic potential but in these past years also has been clearly demonstrated to confer diverse advantageous properties such as resistance to chemotherapy, immune evading capacity, and rewiring of the cell metabolism (Kang et al., 2019; Lu and Kang, 2019; Bakir et al., 2020; Jia et al., 2021). All these concepts represent novel advancements in our knowledge on EMT which must be included in an updated classification (**Figure 1**). Moreover, these aspects highlight how dynamic and complex the EMT is and how the generation of new *in vivo* models coupled with technology advancement can provide a deeper understanding of this phenomenon which sometimes may lead to unexpected findings with respect to the original concepts.

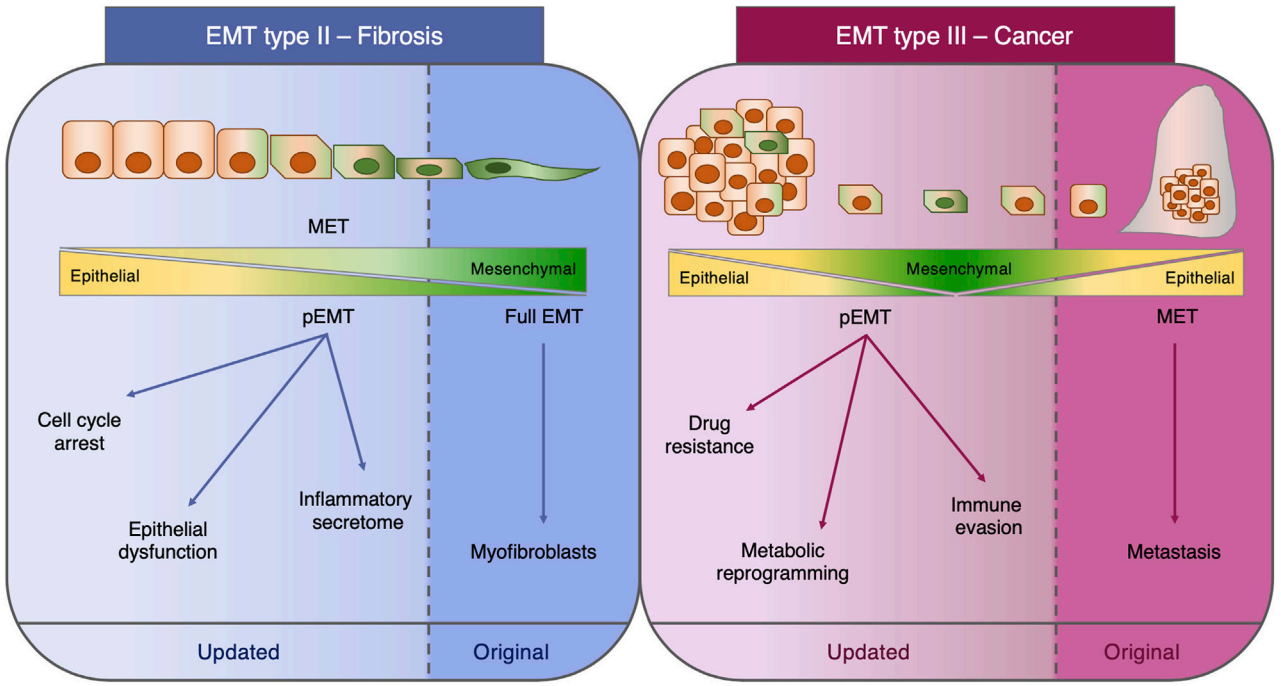

FIGURE 1 | Type II and type III EMT. Schematic representation of the functional role of EMT in fibrosis (type II EMT) and cancer (type III EMT). For each class of EMT, both the original concept and the most recent findings are depicted. EMT: epithelial-to-mesenchymal transition; MET: mesenchymal-to-epithelial transition; pEMT: partial EMT.

UNDERSTANDING EMT BY SINGLE CELL TRANSCRIPTOMICS

Our comprehension of the dynamics of EMT has significantly advanced thanks to the introduction of technologies such as single cell RNA-sequencing (scRNA-seq). A first study employing scRNA-seq and pseudospatial trajectory reconstruction of epithelial cells undergoing spontaneous or TGFβ-induced EMT revealed that the EMT is a transcriptional continuum of epithelial–mesenchymal states (McFaline-Figueroa et al., 2019). Interfering with signaling pathways by inhibiting transcription factors (TFs) or receptors impeded the progression along the EMT and caused cells to accumulate at defined points in the EMT continuum, thus revealing the existence of regulatory checkpoints (McFaline-Figueroa et al., 2019). This observation indicated that disabling key signaling pathways could enrich a particular gene expression profile, therefore giving the impression of a stable E/M intermediate phenotype.

By coupling scRNA-seq and mathematical modeling to a time course experiment of TGFβ-induced EMT in the MCF10A breast cell line, a recent study mapped the molecular changes and signaling cascades occurring during EMT progression (Deshmukh et al., 2021). Fundamental findings are the fact that many EMT regulatory pathways (Notch, Shh, Wnt, PI3K/Akt) were found to be activated simultaneously, possibly indicating that a crosstalk among multiple signaling pathways may occur in a temporal manner and that the rate of progression through EMT was not the same for all the cells, indicating a temporal heterogeneity in the activation of EMT. Even after 8 days of TGFβ treatment, half of the analyzed cells were in the hybrid E/M state, and the pseudotime analysis revealed the presence of twenty distinct EMT clusters (Deshmukh et al., 2021).

One recurrent issue in analyzing EMT at the transcriptional level has been the impossibility to distinguish the mesenchymal signature of the epithelium from the one in the stromal compartment, due to the promiscuous expression of the markers analyzed. Recently, a computational framework to decouple the true EMT signature of epithelial cells from the stromal mesenchymal signature in bulk RNA-seq data has been developed to characterize EMT across different types of tumors (Tyler and Tirosh, 2021). This method revealed that the expression of the classical EMT-transcription factors (except *SNAI2*) is very high in cancer-associated fibroblasts and therefore should not be used as a marker of partial EMT in bulk analysis. Certainly, a similar bioinformatic approach would be desirable for the bulk RNA-seq dataset of fibrotic disorders to analyze pEMT without the confounder of the fibrotic stroma.

A common concept emerging from different studies employing scRNA-seq is represented by the fact that the pEMT profile is highly context-specific (Cook and Vanderhyden, 2020; Tyler and Tirosh, 2021). This concept was, for example, highlighted by a multiplexed scRNA-seq of EMT time course induction in four different cell lines, using three distinct inducers (TGFβ1, TNF, EGF) and also including the analysis of EMT reversion by removal of the inducing signal (Cook and Vanderhyden, 2020). Pseudotemporal trajectories

confirmed that EMT is not just a linear progression but rather a multistep process characterized by a series of discrete transcriptional events. Surprisingly, the activity of TFs was also remarkably context specific, and TFs that have been implicated in EMT but are not the traditional core EMT-TFs were found differentially regulated in a context-specific manner (Cook and Vanderhyden, 2020). A combined bioinformatic and mathematical analysis on the same time-series scRNA-seq allowed to construct a context-specific EMT gene regulatory circuit (GRC) from transcriptomics data to identify activity dynamics of EMT-TFs (Ramirez et al., 2020). Although most of these scRNA-seq studies were conducted using tumor cell lines and, therefore, it cannot be assumed that the same findings apply to non-transformed epithelial cells activating pEMT as part of their injury-induced damage response, these studies provided novel insights into the dynamics of EMT which are worth to be taken into consideration when studying EMT in the context of fibrosis.

DIRECT TARGETING OF EMT-TFs: GENETIC DELETION AND SMALL MOLECULE INHIBITORS

The most compelling evidence that inhibition of EMT-driving TFs is an effective strategy for reducing fibrosis has been generated by using genetically engineered knock-out mouse models. In fact, renal epithelial cells' conditional deletion of the *Twist1* or *Snail1* genes, encoding, respectively, Twist1 and Snail EMT-TFs, using two distinct epithelial-driven Cre/lox models (γGT-Cre and Cdh16-Cre), proved to be effective in inhibiting the process of EMT and led to substantial reduction of kidney fibrosis (Grande et al., 2015; Lovisa et al., 2015). Epithelial-specific inducible activation of Snail was necessary and sufficient to induce fibrosis which could be reversed by deactivating or silencing Snail (Grande et al., 2015). Genetic deletion of these EMT-TFs efficiently reduced ECM deposition, myofibroblast accumulation, and immune infiltration and led to a significantly improved tubular epithelial functionality and regenerative capacity, therefore demonstrating that EMT inhibition leads to both epithelial recovery and suspension of the paracrine effect on mesenchymal and immune cells (Grande et al., 2015; Lovisa et al., 2015). A similar paracrine effect exerted on fibroblasts by epithelial cells undergoing EMT has been reported in lung fibrosis (Hill et al., 2019; Yao et al., 2019). Mice with conditional deletion of Snail in hepatocytes using the albumin-Cre model also display reduced ECM and immune infiltration during hepatic fibrosis, with no direct effects on hepatic stellate cell activation (Rowe et al., 2011).

Similarly, conditional deletion of Twist1 or Snail in endothelial cells (using Cdh5- and Tie1-Cre models) was recently shown to inhibit the cognate process of EndMT and protect from kidney fibrosis by limiting vascular leakage and the downstream hypoxia-driven metabolic rearrangements (Balzer and Susztak, 2020; Lovisa et al., 2020). Tie2-driven conditional deletion of Twist1 in the endothelium was also shown to be associated with reduction of lung fibrosis (Mammoto et al., 2013; Mammoto et al., 2016; Mammoto et al., 2018), while Tie2-driven deletion of Snail led to embryonic lethal vascular defects (Wu et al., 2014).

Based on this evidence, a pharmacological approach directly targeting EMT-TFs would theoretically represent an efficient strategy to inhibit EMT. Although, being transcription factors, Twist and Snail are usually considered undruggable and their pharmacological targeting remains challenging, there are reports of compounds derived from natural products that can target Twist, Snail, and Zeb1 (Pei et al., 2017; Avila-Carrasco et al., 2019; Feng et al., 2020). It is to be noted, however, that most of these studies attempt to target cancer-related EMT and these inhibitors are not fully specific for these TFs.

Alternative strategies include targeting protein effectors responsible for the post-translational control of TF stability. One example is a recent study reporting a small molecule which, by disrupting Snail–CBP/p300 interaction, promotes Snail proteasomal degradation and therefore reverses Snail-induced EMT and its associated tumor invasion and metastasis (Li et al., 2020). In the context of fibrosis, a recent study identified triptolide, a small molecule inhibitor targeting MEX3C, the E3 ligase responsible for PTEN polyubiquitination, as an EMT inhibitor (Li et al., 2019). High glucose–induced polyubiquitination of PTEN triggers phosphatase activity and favors the dephosphorylation of Twist and Snail, which in turn stabilizes these two TFs and induces EMT. The authors showed that triptolide treatment *in vitro* was able to reduce the glucose-induced protein expression of both Twist and Snail and successfully inhibited EMT and kidney fibrosis in both spontaneous and experimentally induced *in vivo* models (Li et al., 2019).

Recent advances in the use of nanoparticles and microvesicles such as exosomes have proven the efficacy and therapeutic application of siRNA delivery, and therefore, this could potentially be exploited as a strategy to target EMT, although the lack of cell specificity could represent a serious concern with this type of approach. In fact, aspects to be taken into consideration are the mutual interdependency of the EMT-TFs and their EMT-independent functions (Stemmler et al., 2019). Although in general these TFs are not expressed in adult tissues, there is evidence supporting their necessity in the adult process like Slug required in the process of cutaneous wound re-epithelialization (Hudson et al., 2009) and Twist2 expressed by a multipotent cell population generating cardiomyocytes in the adult heart (Min et al., 2018). Therefore, the extent to which these EMT-TFs are required for adult tissue homeostasis, cell identity, and fate determination is not completely known, and this might pose an obstacle for anti-EMT therapeutic strategies not targeted to a specific cell type.

REVERSING EMT: THE MESENCHYMAL-TO-EPITHELIAL TRANSITION

The mesenchymal-to-epithelial transition (MET) is a process employed during embryonic development to generate epithelia (Pei et al., 2019). Induction of MET has been associated with

amelioration of fibrosis. In fact, reversion of TGFβ-induced EMT in tubular epithelial cells (Zeisberg et al., 2003) and induction of MET in fibroblasts in the injured kidney (Zeisberg et al., 2005) were shown to result in reduction of fibrosis and promotion of kidney regeneration. Induction of MET by treatment with BMP-7 was shown to improve *in vivo* fibrosis in renal, cardiac, and intestinal models (Zeisberg et al., 2003; Zeisberg et al., 2007; Flier et al., 2010), and treatment with a BMP agonist was indeed able to revert established fibrosis (Sugimoto et al., 2012). These observations are completely in line with the requirement of MET for the reprogramming of fibroblasts into pluripotent stem cells (Li et al., 2010) and the role of BMPs in driving the initiation of such MET-mediated reprogramming (Samavarchi-Tehrani et al., 2010).

Induction of MET in cardiac fibroblasts by stimulation of the p53 pathway induced the regeneration of functional vessels, through a process called "mesenchymal-to-endothelial transition" (MEndT) (Miyake and Kalluri, 2014; Ubil et al., 2014). MEndT contributes to neovascularization in the injured heart, and its induction improved cardiac function (Ubil et al., 2014; Dong et al., 2020). Treatment with the small molecule RITA, which inhibits ubiquitin-mediated p53 degradation and enhances p53 signaling, increased MEndT, reduced cardiac fibrosis, and improved cardiac function, therefore mechanistically proving that p53-mediated activation of MEndT in cardiac fibroblasts is able to limit cardiac injury (Ubil et al., 2014).

Novel insights into mechanisms of MET are inferred from single cell transcriptomics (Cook and Vanderhyden, 2020). EMT and MET were investigated by scRNA-seq in four different cell lines by induction with TGFβ, TNF, or EGF for 7 days, followed by 3 days of withdrawal time which was sufficient to almost completely revert cells transcriptionally to the epithelial state. Analysis of the time-dependent shifts in the gene expression profile showed that while it is true that stimulus withdrawal led to MET reversibility, it is also clear that the trajectory of changes in the reversion expression profile did not match that of the EMT induction (Cook and Vanderhyden, 2020). Further bioinformatics and mathematical modeling confirmed that EMT and MET trajectories have two distinct paths which do not overlap (Ramirez et al., 2020). This certainly indicates that EMT and MET are not perfectly symmetric processes and MET should not be oversimplified as the equal and opposite process of EMT.

It was reported that alternates of EMT–MET are necessary to induce pluripotency in somatic cell reprogramming, so that EMT is necessary to favor the subsequent MET (Liu et al., 2013; Li et al., 2017). This implies two considerations: 1) targeting EMT might then not be strategic in the attempt to favor MET-mediated regeneration over injury and fibrosis and 2) if some degree of EMT favors the subsequent MET in pluripotent reprogramming, one could argue that this predisposition could potentially occur also in the context of injury. A recent study on mechanisms of cardiac repair shows that dedifferentiation and activation of an EMT-like program in adult cardiomyocytes, induced by the ectopic reactivation of ERBB2 and mediated by YAP, are indeed necessary for migration and subsequent redifferentiation of cardiomyocytes at the injured site (Aharonov et al., 2020; González-Iglesias and Nieto, 2020). A similar requirement for YAP-induced EMT in hepatocytes was reported promoting liver regeneration (Oh et al., 2018). Therefore, why injury-induced EMT fails to successfully prime cells for reprogramming and regeneration in some contexts, such as the kidney, is clearly an open question that requires deeper investigation.

TARGETING EMT-DEPENDENT METABOLIC VULNERABILITIES

The comprehension of the functional role of EMT beyond the mere generation of fibroblasts is potentially opening the opportunity to target EMT from a different perspective consisting in the identification of the EMT-induced cellular vulnerabilities mediated by druggable targets.

Disruption of the tissue metabolic homeostasis represents a hallmark of fibrosis, and targeting this metabolic dysregulation has started to emerge as a potential strategy for fibrosis treatment (Zhao et al., 2020). Defective fatty acid oxidation (FAO) was shown to induce renal fibrosis, and FAO inhibition provokes features of dedifferentiation, namely, the expression of mesenchymal markers, in the renal epithelium (Kang et al., 2015). FAO decrease and the consequent lipid accumulation were shown to induce an EMT expression profile in renal epithelial cells *in vitro* (Xu et al., 2014). FAO improvement by overexpression of the transcription factor PPARGC1A, which regulates the expression of all FAO rate-limiting enzymes, or by pharmacological treatment with fenofibrate was capable of protecting renal epithelial cells from TGFβ-induced dedifferentiation toward a mesenchymal profile (Kang et al., 2015). Conversely, *in vivo* inhibition of EMT during fibrosis was able to restore FAO and metabolic homeostasis, in association with improved epithelial health and functionality (Lovisa et al., 2015).

Reversion of the TGFβ-induced PPARγ inhibition by curcumin treatment was shown to inhibit EMT and ameliorate TNBS-induced intestinal fibrosis (Xu et al., 2017). Treatment with a PPARγ antagonist reverted the EMT inhibitory effect of curcumin, therefore further highlighting the existence of the FAO-EMT axis and the anti-fibrotic effects of the PPARγ agonists.

The interdependency of FAO metabolism and mesenchymal transition was also highlighted in the context of EndMT. Suppression of FAO by endothelial conditional deletion of the FAO enzyme CPT2 spontaneously induced amplification of the embryonic EndMT which resulted in the thickening of the cardiac valves and provoked EndMT with consequent abnormal vascular permeability in the kidney, spleen, and lung (Lovisa and Kalluri, 2018; Xiong et al., 2018). Inhibition of EndMT was proven to ameliorate fibrosis and restore the metabolic functionality of the kidney (Lovisa et al., 2020). In fact, the vascular leakage caused by the process of EndMT leads to a cascade of events characterized by a hypoxia-induced epithelial upregulation of the c-Myc transcription factor, which in turn is

TABLE 1 | Summary of the different strategies to target EMT in fibrosis.

Targeting strategy	Molecular targets		Approach	References
EMT-inducing pathways	TGFβ, Hedgehog, Hippo, Wnt, and Notch signaling pathways		Genetic deletion, antagonists, small molecule inhibitors, miRNAs, natural compounds	Avila-Carrasco et al. (2019); Di Gregorio et al. (2020); Jonckheere et al. (2021)
EMT-transcription factors	Twist, Snail		Genetic deletion in epithelial and endothelial cells	Rowe et al. (2011); Mammoto et al. (2013); Wu et al. (2014); Grande et al. (2015); Lovisa et al. (2015); Mammoto et al. (2016); Mammoto et al. (2018); Lovisa et al. (2020)
	Snail–CBP/p300 interaction		Small molecule inhibitor	Li et al. (2020) (cancer)
	MEX3C-mediated, PTEN-induced Twist and Snail phosphorylation		Small molecule inhibitor	Li et al. (2019)
	Twist, Snail, Slug, Zeb1		Natural compounds	Pei et al. (2017); Avila-Carrasco et al. (2019); Feng et al. (2020)
MET	BMP-7		Agonist	Zeisberg et al. (2003); Zeisberg et al. (2005); Zeisberg et al. (2007); Flier et al. (2010); Sugimoto et al. (2012)
	Ubiquitinated p53		Small molecule inhibitor	Ubil et al. (2014)
EMT-related metabolic vulnerabilities	FAO	PPARGC1A, PPARα, PPARɣ	Genetic induction, agonist, natural compound	Kang et al. (2015); Xu et al. (2017)
	Glycolysis	c-Myc	Genetic deletion in epithelial cells, transcriptional repression	Lovisa et al. (2020)
		HK2	Inhibitor	Lovisa et al. (2020); Yu et al. (2021)
		SGLT2	Inhibitor	Li et al. (2020)

EMT: epithelial-to-mesenchymal transition; MET: mesenchymal-to-epithelial transition; FAO: fatty acid oxidation.

responsible for a glycolytic switch of the renal metabolism which normally heavily depends on FAO (Lovisa et al., 2020). The increase in glycolysis was proved to be detrimental as the treatment with the glycolysis inhibitor 3-bromopyruvate ameliorated tissue fibrosis (Lovisa et al., 2020; Yu et al., 2021). Moreover, genetic or pharmacological targeting of c-Myc by treatment with the JQ1 inhibitor reduced fibrosis, preserved the epithelial parenchyma, and restored the metabolic homeostasis (Lovisa et al., 2020). Whether inhibition of glycolysis is able to reduce EMT was not investigated; however, it is possible as EMT cells switch their metabolism from oxidative phosphorylation to glycolysis and scRNA-seq confirmed the downregulation of genes of the mitochondrial oxidative phosphorylation (Deshmukh et al., 2021).

Additionally, high glucose itself was shown to induce EMT in renal tubular epithelial cells (Li et al., 2020). Inhibition of sodium-glucose cotransporter 2 (SGLT2) suppressed glucose-induced EMT and decreased renal fibrogenesis (Li et al., 2020). SGLT2 suppression in tubular epithelial cells was also able to suppress EndMT of the peritubular capillaries (Li et al., 2020), further highlighting the existence of an epithelial–endothelial crosstalk during tissue injury (Balzer and Susztak, 2020).

To unravel the interdependency between metabolism and EMP, the first step would be to perform a comprehensive analysis of the metabolome of EMT during fibrosis, including the analysis of single cell metabolism along the continuum of the EMT spectrum. Considering that targeting EMT through metabolic inhibitors has gained great attention in the cancer field (Ramesh et al., 2020), it would be logical to argue that this approach might be translated as well in fibrotic diseases, with repurposed metabolic inhibitors potentially becoming a valuable strategy to target fibrosis.

CONCLUDING REMARKS

Fibrosis is the final outcome of a cascade of events participating in an uncontrolled wound healing response which causes an exaggerated accumulation of ECM, eventually leading to tissue scarring and organ failure (Zeisberg and Kalluri, 2013; Distler et al., 2019; Henderson et al., 2020). Fibrosis can affect any organ, and it is estimated to be responsible for up to 45% of the deaths worldwide, therefore representing a major global healthcare burden which cannot be further ignored (Henderson et al., 2020). The gigantic effort to understand mechanisms of fibrosis pathogenesis using experimental models and cutting-edge techniques such as single cell sequencing has not yet been translated into effective clinical trials. The gap between the promising results obtained with *in vivo* experimental models and the failure faced when they are clinically translated is enormous and demands immediate action.

In the context of identifying cellular drivers of fibrosis, EMT was thought to be the major mechanism causing the accumulation of myofibroblasts (Kalluri and Weinberg, 2009). Although this might be true *in vitro*, where treatment with inflammatory cytokines forces epithelial cells to transition to an almost full mesenchymal phenotype, it appears that this is not the case *in vivo*. Instead, *in vivo* EMT cells reside in a hybrid partial EMT state which functionally participates in causing a detrimental damage response of the injured tissue. Although being in principle highly valuable (**Table 1**), targeting EMT has emerged as a challenging task. Multiple factors contribute to this difficulty in developing effective anti-EMT strategies, including the dynamic transition through the hybrid state, the theoretical infinity of the E/M intermediates, its orchestration

mainly at the transcriptional level, and the co-existence of multiple and partially overlapping EMT-inducing pathways.

EMT has been recently looked at as an attractive target in oncology (Marcucci et al., 2016). This interest is not quite reflected in the fibrosis field, but certainly cross-communication between these two areas of investigation could improve and optimize the effort toward targeting EMT. The interest of the cancer scientific community on EMT mainly regards targeting the possible metabolic alteration accompanying EMT (Ramesh et al., 2020). Focusing the attention on the EMT-induced vulnerabilities might indeed represent a promising strategy, which would circumvent all the difficulties associated with directly targeting the transcriptional drivers of EMT. Moreover, this strategy would open the possibility for therapeutic repurposing of metabolic drugs to fibrotic diseases. Persevering in our effort to better understand the biological basis of EMT will certainly help in identifying novel routes for therapeutic intervention.

AUTHOR CONTRIBUTIONS

SL conceptualized the review, performed literature research, wrote and edited the manuscript, and prepared the figure.

FUNDING

SL is supported by the European Union's Horizon 2020 research and innovation programme under Marie Sklodowska-Curie grant agreement #101029427 and Italian Association for Cancer Research (AIRC) Start-Up 2020 grant #24750. She was also supported by Fondazione Umberto Veronesi (2020 Post-Doctoral Fellowship).

ACKNOWLEDGMENTS

The author wishes to thank Raghu Kalluri (MD Anderson Cancer Center, Houston) and Valerie LeBleu (Northwestern University, Chicago) for their valuable guidance. The author is thankful to Julienne Carstens and Pedro Correa de Sampaio for their friendship, encouragement, and insightful discussions. The author also wishes to thank Gustavo Baldassarre (CRO Aviano, Italy), Giannicola Genovese (MD Anderson Cancer Center, Houston), Giulio Draetta (MD Anderson Cancer Center, Houston), and Silvio Danese (Humanitas Research Hospital, Italy) for their continued support.

REFERENCES

Aharonov, A., Shakked, A., Umansky, K. B., Savidor, A., Genzelinakh, A., Kain, D., et al. (2020). ERBB2 Drives YAP Activation and EMT-like Processes during Cardiac Regeneration. *Nat. Cel Biol* 22, 1346–1356. doi:10.1038/s41556-020-00588-4

Avila-Carrasco, L., Majano, P., Sánchez-Toméro, J. A., Selgas, R., López-Cabrera, M., Aguilera, A., et al. (2019). Natural Plants Compounds as Modulators of Epithelial-To-Mesenchymal Transition. *Front. Pharmacol.* 10, 715. doi:10.3389/fphar.2019.00715

Bakir, B., Chiarella, A. M., Pitarresi, J. R., and Rustgi, A. K. (2020). EMT, MET, Plasticity, and Tumor Metastasis. *Trends Cel Biol* 30, 764–776. doi:10.1016/j.tcb.2020.07.003

Balzer, M. S., and Susztak, K. (2020). The Interdependence of Renal Epithelial and Endothelial Metabolism and Cell State. *Sci. Signal.* 13, eabb8834. doi:10.1126/scisignal.abb8834

Brabletz, T., Kalluri, R., Nieto, M. A., and Weinberg, R. A. (2018). EMT in Cancer. *Nat. Rev. Cancer* 18, 128–134. doi:10.1038/nrc.2017.118

Carstens, J. L., Yang, S., Correa de Sampaio, P., Zheng, X., Barua, S., McAndrews, K. M., et al. (2021). Stabilized Epithelial Phenotype of Cancer Cells in Primary Tumors Leads to Increased Colonization of Liver Metastasis in Pancreatic Cancer. *Cell Rep* 35, 108990. doi:10.1016/j.celrep.2021.108990

Chen, Y., LeBleu, V. S., Carstens, J. L., Sugimoto, H., Zheng, X., Malasi, S., et al. (2018). Dual Reporter Genetic Mouse Models of Pancreatic Cancer Identify an Epithelial-To-Mesenchymal Transition-independent Metastasis Program. *EMBO Mol. Med.* 10, e9085. doi:10.15252/emmm.201809085

Cook, D. P., and Vanderhyden, B. C. (2020). Context Specificity of the EMT Transcriptional Response. *Nat. Commun.* 11, 2142. doi:10.1038/s41467-020-16066-2

Del Peso, G., Jiménez-Heffernan, J. A., Bajo, M. A., Aroeira, L. S., Aguilera, A., Fernández-Perpén, A., et al. (2008). Epithelial-to-mesenchymal Transition of Mesothelial Cells Is an Early Event during Peritoneal Dialysis and Is Associated with High Peritoneal Transport. *Kidney Int. Suppl.*, S26–S33. doi:10.1038/sj.ki.5002598

Deshmukh, A. P., Vasaikar, S. V., Tomczak, K., Tripathi, S., den Hollander, P., Arslan, E., et al. (2021). Identification of EMT Signaling Cross-Talk and Gene Regulatory Networks by Single-Cell RNA Sequencing. *Proc. Natl. Acad. Sci. U S A.* 118, 118. doi:10.1073/pnas.2102050118

Di Gregorio, J., Robuffo, I., Spalletta, S., Giambuzzi, G., De Iuliis, V., Toniato, E., et al. (2020). The Epithelial-To-Mesenchymal Transition as a Possible Therapeutic Target in Fibrotic Disorders. *Front Cel Dev Biol* 8, 607483. doi:10.3389/fcell.2020.607483

Distler, J. H. W., Györfi, A. H., Ramanujam, M., Whitfield, M. L., Königshoff, M., and Lafyatis, R. (2019). Shared and Distinct Mechanisms of Fibrosis. *Nat. Rev. Rheumatol.* 15, 705–730. doi:10.1038/s41584-019-0322-7

Dong, W., Li, R., Yang, H., Lu, Y., Zhou, L., Sun, L., et al. (2020). Mesenchymal-endothelial Transition-Derived Cells as a Potential New Regulatory Target for Cardiac Hypertrophy. *Sci. Rep.* 10, 6652. doi:10.1038/s41598-020-63671-8

Feng, Y. L., Chen, D. Q., Vaziri, N. D., Guo, Y., and Zhao, Y. Y. (2020). Small Molecule Inhibitors of Epithelial-Mesenchymal Transition for the Treatment of Cancer and Fibrosis. *Med. Res. Rev.* 40, 54–78. doi:10.1002/med.21596

Fischer, K. R., Durrans, A., Lee, S., Sheng, J., Li, F., Wong, S. T., et al. (2015). Epithelial-to-mesenchymal Transition Is Not Required for Lung Metastasis but Contributes to Chemoresistance. *Nature* 527, 472–476. doi:10.1038/nature15748

Flier, S. N., Tanjore, H., Kokkotou, E. G., Sugimoto, H., Zeisberg, M., and Kalluri, R. (2010). Identification of Epithelial to Mesenchymal Transition as a Novel Source of Fibroblasts in Intestinal Fibrosis. *J. Biol. Chem.* 285, 20202–20212. doi:10.1074/jbc.M110.102012

González-Iglesias, A., and Nieto, M. A. (2020). Proliferation and EMT Trigger Heart Repair. *Nat. Cel Biol* 22, 1291–1292. doi:10.1038/s41556-020-00594-6

Grande, M. T., Sánchez-Laorden, B., López-Blau, C., De Frutos, C. A., Boutet, A., Arévalo, M., et al. (2015). Snail1-induced Partial Epithelial-To-Mesenchymal Transition Drives Renal Fibrosis in Mice and Can Be Targeted to Reverse Established Disease. *Nat. Med.* 21, 989–997. doi:10.1038/nm.3901

Hamidi, S., Nagai, H., and Sheng, G. (2021). Partial EMT/MET: An Army of One. *Methods Mol. Biol.* 2179, 29–33. doi:10.1007/978-1-0716-0779-4_5

Hay, E. D. (1968). in *Epithelial-Mesenchymal Interactions*. Editors R. Fleischmajer and R. E. Billingham (Philadelphia, Pennsylvania, US: Williams & Wilkins), 31–55.

Hay, E. D. (1995). An Overview of Epithelio-Mesenchymal Transformation. *Acta Anat. (Basel)* 154, 8–20. doi:10.1159/000147748

Henderson, N. C., Rieder, F., and Wynn, T. A. (2020). Fibrosis: from Mechanisms to Medicines. *Nature* 587, 555–566. doi:10.1038/s41586-020-2938-9

Hill, C., Li, J., Liu, D., Conforti, F., Brereton, C. J., Yao, L., et al. (2019). Autophagy Inhibition-Mediated Epithelial-Mesenchymal Transition Augments Local Myofibroblast Differentiation in Pulmonary Fibrosis. *Cell Death Dis* 10, 591. doi:10.1038/s41419-019-1820-x

Huang, S., and Susztak, K. (2016). Epithelial Plasticity versus EMT in Kidney Fibrosis. *Trends Mol. Med.* 22, 4–6. doi:10.1016/j.molmed.2015.11.009

Hudson, L. G., Newkirk, K. M., Chandler, H. L., Choi, C., Fossey, S. L., Parent, A. E., et al. (2009). Cutaneous Wound Reepithelialization Is Compromised in Mice Lacking Functional Slug (Snai2). *J. Dermatol. Sci.* 56, 19–26. doi:10.1016/j.jdermsci.2009.06.009

Jia, D., Park, J. H., Kaur, H., Jung, K. H., Yang, S., Tripathi, S., et al. (2021). Towards Decoding the Coupled Decision-Making of Metabolism and Epithelial-To-Mesenchymal Transition in Cancer. *Br. J. Cancer* 124, 1902–1911. doi:10.1038/s41416-021-01385-y

Jolly, M. K., Tripathi, S. C., Jia, D., Mooney, S. M., Celiktas, M., Hanash, S. M., et al. (2016). Stability of the Hybrid Epithelial/mesenchymal Phenotype. *Oncotarget* 7, 27067–27084. doi:10.18632/oncotarget.8166

Jonckheere, S., Adams, J., De Groote, D., Campbell, K., Berx, G., and Goossens, S. (2021). Epithelial-Mesenchymal Transition (EMT) as a Therapeutic Target. *Cells Tissues Organs*, 1–26. doi:10.1159/000512218

Kalluri, R. (2009). EMT: when Epithelial Cells Decide to Become Mesenchymal-like Cells. *J. Clin. Invest.* 119, 1417–1419. doi:10.1172/JCI39675

Kalluri, R., and Weinberg, R. A. (2009). The Basics of Epithelial-Mesenchymal Transition. *J. Clin. Invest.* 119, 1420–1428. doi:10.1172/JCI39104

Kang, H., Kim, H., Lee, S., Youn, H., and Youn, B. (2019). Role of Metabolic Reprogramming in Epithelial-Mesenchymal Transition (EMT). *Int. J. Mol. Sci.* 20, 2042. doi:10.3390/ijms20082042

Kang, H. M., Ahn, S. H., Choi, P., Ko, Y. A., Han, S. H., Chinga, F., et al. (2015). Defective Fatty Acid Oxidation in Renal Tubular Epithelial Cells Has a Key Role in Kidney Fibrosis Development. *Nat. Med.* 21, 37–46. doi:10.1038/nm.3762

Kim, K. K., Kugler, M. C., Wolters, P. J., Robillard, L., Galvez, M. G., Brumwell, A. N., et al. (2006). Alveolar Epithelial Cell Mesenchymal Transition Develops *In Vivo* during Pulmonary Fibrosis and Is Regulated by the Extracellular Matrix. *Proc. Natl. Acad. Sci. U S A.* 103, 13180–13185. doi:10.1073/pnas.0605669103

Koopmans, T., and Rinkevich, Y. (2018). Mesothelial to Mesenchyme Transition as a Major Developmental and Pathological Player in Trunk Organs and Their Cavities. *Commun. Biol.* 1, 170. doi:10.1038/s42003-018-0180-x

LeBleu, V. S., Taduri, G., O'Connell, J., Teng, Y., Cooke, V. G., Woda, C., et al. (2013). Origin and Function of Myofibroblasts in Kidney Fibrosis. *Nat. Med.* 19, 1047–1053. doi:10.1038/nm.3218

Li, H. M., Bi, Y. R., Li, Y., Fu, R., Lv, W. C., Jiang, N., et al. (2020). A Potent CBP/p300-Snail Interaction Inhibitor Suppresses Tumor Growth and Metastasis in Wild-type P53-Expressing Cancer. *Sci. Adv.* 6, eaaw8500. doi:10.1126/sciadv.aaw8500

Li, J., Liu, H., Takagi, S., Nitta, K., Kitada, M., Srivastava, S. P., et al. (2020). Renal Protective Effects of Empagliflozin via Inhibition of EMT and Aberrant Glycolysis in Proximal Tubules. *JCI Insight* 5, e129034. doi:10.1172/jci.insight.129034

Li, Q., Hutchins, A. P., Chen, Y., Li, S., Shan, Y., Liao, B., et al. (2017). A Sequential EMT-MET Mechanism Drives the Differentiation of Human Embryonic Stem Cells towards Hepatocytes. *Nat. Commun.* 8, 15166. doi:10.1038/ncomms15166

Li, R., Liang, J., Ni, S., Zhou, T., Qing, X., Li, H., et al. (2010). A Mesenchymal-To-Epithelial Transition Initiates and Is Required for the Nuclear Reprogramming of Mouse Fibroblasts. *Cell Stem Cell* 7, 51–63. doi:10.1016/j.stem.2010.04.014

Li, Y., Hu, Q., Li, C., Liang, K., Xiang, Y., Hsiao, H., et al. (2019). PTEN-induced Partial Epithelial-Mesenchymal Transition Drives Diabetic Kidney Disease. *J. Clin. Invest.* 129, 1129–1151. doi:10.1172/JCI121987

Liu, X., Sun, H., Qi, J., Wang, L., He, S., Liu, J., et al. (2013). Sequential Introduction of Reprogramming Factors Reveals a Time-Sensitive Requirement for Individual Factors and a Sequential EMT-MET Mechanism for Optimal Reprogramming. *Nat. Cel Biol* 15, 829–838. doi:10.1038/ncb2765

Lourenco, A. R., Ban, Y., Crowley, M. J., Lee, S. B., Ramchandani, D., Du, W., et al. (2020). Differential Contributions of Pre- and Post-EMT Tumor Cells in Breast Cancer Metastasis. *Cancer Res.* 80, 163–169. doi:10.1158/0008-5472.CAN-19-1427

Lovisa, S., Fletcher-Sananikone, E., Sugimoto, H., Hensel, J., Lahiri, S., Hertig, A., et al. (2020). Endothelial-to-mesenchymal Transition Compromises Vascular Integrity to Induce Myc-Mediated Metabolic Reprogramming in Kidney Fibrosis. *Sci. Signal.* 13, eaaz2597. doi:10.1126/scisignal.aaz2597

Lovisa, S., and Kalluri, R. (2018). Fatty Acid Oxidation Regulates the Activation of Endothelial-To-Mesenchymal Transition. *Trends Mol. Med.* 24, 432–434. doi:10.1016/j.molmed.2018.03.003

Lovisa, S., LeBleu, V. S., Tampe, B., Sugimoto, H., Vadnagara, K., Carstens, J. L., et al. (2015). Epithelial-to-mesenchymal Transition Induces Cell Cycle Arrest and Parenchymal Damage in Renal Fibrosis. *Nat. Med.* 21, 998–1009. doi:10.1038/nm.3902

Lovisa, S., Zeisberg, M., and Kalluri, R. (2016). Partial Epithelial-To-Mesenchymal Transition and Other New Mechanisms of Kidney Fibrosis. *Trends Endocrinol. Metab.* 27, 681–695. doi:10.1016/j.tem.2016.06.004

Lu, M., Jolly, M. K., Levine, H., Onuchic, J. N., and Ben-Jacob, E. (2013). MicroRNA-based Regulation of Epithelial-Hybrid-Mesenchymal Fate Determination. *Proc. Natl. Acad. Sci. U S A.* 110, 18144–18149. doi:10.1073/pnas.1318192110

Lu, W., and Kang, Y. (2019). Epithelial-Mesenchymal Plasticity in Cancer Progression and Metastasis. *Dev. Cel* 49, 361–374. doi:10.1016/j.devcel.2019.04.010

Maheswaran, S., and Haber, D. A. (2015). Cell Fate: Transition Loses its Invasive Edge. *Nature* 527, 452–453. doi:10.1038/nature16313

Mammoto, T., Jiang, A., Jiang, E., and Mammoto, A. (2016). Role of Twist1 Phosphorylation in Angiogenesis and Pulmonary Fibrosis. *Am. J. Respir. Cel Mol Biol* 55, 633–644. doi:10.1165/rcmb.2016-0012OC

Mammoto, T., Jiang, E., Jiang, A., Lu, Y., Juan, A. M., Chen, J., et al. (2013). Twist1 Controls Lung Vascular Permeability and Endotoxin-Induced Pulmonary Edema by Altering Tie2 Expression. *PLoS One* 8, e73407. doi:10.1371/journal.pone.0073407

Mammoto, T., Muyleart, M., Konduri, G. G., and Mammoto, A. (2018). Twist1 in Hypoxia-Induced Pulmonary Hypertension through Transforming Growth Factor-β-Smad Signaling. *Am. J. Respir. Cel Mol Biol* 58, 194–207. doi:10.1165/rcmb.2016-0323OC

Marcucci, F., Stassi, G., and De Maria, R. (2016). Epithelial-mesenchymal Transition: a New Target in Anticancer Drug Discovery. *Nat. Rev. Drug Discov.* 15, 311–325. doi:10.1038/nrd.2015.13

McFaline-Figueroa, J. L., Hill, A. J., Qiu, X., Jackson, D., Shendure, J., and Trapnell, C. (2019). A Pooled Single-Cell Genetic Screen Identifies Regulatory Checkpoints in the Continuum of the Epithelial-To-Mesenchymal Transition. *Nat. Genet.* 51, 1389–1398. doi:10.1038/s41588-019-0489-5

Meng, X. M., Wang, S., Huang, X. R., Yang, C., Xiao, J., Zhang, Y., et al. (2016). Inflammatory Macrophages Can Transdifferentiate into Myofibroblasts during Renal Fibrosis. *Cel Death Dis* 7, e2495. doi:10.1038/cddis.2016.402

Min, Y. L., Jaichander, P., Sanchez-Ortiz, E., Bezprozvannaya, S., Malladi, V. S., Cui, M., et al. (2018). Identification of a Multipotent Twist2-Expressing Cell Population in the Adult Heart. *Proc. Natl. Acad. Sci. U S A.* 115, E8430–E8439. doi:10.1073/pnas.1800526115

Miyake, T., and Kalluri, R. (2014). Cardiac Biology: Cell Plasticity Helps Hearts to Repair. *Nature* 514, 575–576. doi:10.1038/nature13928

Mutsaers, S. E., Birnie, K., Lansley, S., Herrick, S. E., Lim, C. B., and Prêle, C. M. (2015). Mesothelial Cells in Tissue Repair and Fibrosis. *Front. Pharmacol.* 6, 113. doi:10.3389/fphar.2015.00113

Nieto, M. A., Huang, R. Y., Jackson, R. A., and Thiery, J. P. (2016). Emt: 2016. *Cell* 166, 21–45. doi:10.1016/j.cell.2016.06.028

Oh, S. H., Swiderska-Syn, M., Jewell, M. L., Premont, R. T., and Diehl, A. M. (2018). Liver Regeneration Requires Yap1-tgfβ-dependent Epithelial-Mesenchymal Transition in Hepatocytes. *J. Hepatol.* 69, 359–367. doi:10.1016/j.jhep.2018.05.008

Okada, H., Danoff, T. M., Kalluri, R., and Neilson, E. G. (1997). Early Role of Fsp1 in Epithelial-Mesenchymal Transformation. *Am. J. Physiol.* 273, F563–F574. doi:10.1152/ajprenal.1997.273.4.F563

Ovadya, Y., and Krizhanovsky, V. (2015). A New Twist in Kidney Fibrosis. *Nat. Med.* 21, 975–977. doi:10.1038/nm.3938

Pei, D., Shu, X., Gassama-Diagne, A., and Thiery, J. P. (2019). Mesenchymal-epithelial Transition in Development and Reprogramming. *Nat. Cel Biol* 21, 44–53. doi:10.1038/s41556-018-0195-z

Pei, H., Li, Y., Liu, M., and Chen, Y. (2017). Targeting Twist Expression with Small Molecules. *Medchemcomm* 8, 268–275. doi:10.1039/c6md00561f

Plikus, M. V., Wang, X., Sinha, S., Forte, E., Thompson, S. M., Herzog, E. L., et al. (2021). Fibroblasts: Origins, Definitions, and Functions in Health and Disease. *Cell* 184, 3852–3872. doi:10.1016/j.cell.2021.06.024

Ramesh, V., Brabletz, T., and Ceppi, P. (2020). Targeting EMT in Cancer with Repurposed Metabolic Inhibitors. *Trends Cancer* 6, 942–950. doi:10.1016/j.trecan.2020.06.005

Ramirez, D., Kohar, V., and Lu, M. (2020). Toward Modeling Context-specific EMT Regulatory Networks Using Temporal Single Cell RNA-Seq Data. *Front. Mol. Biosci.* 7, 54. doi:10.3389/fmolb.2020.00054

Rowe, R. G., Lin, Y., Shimizu-Hirota, R., Hanada, S., Neilson, E. G., Greenson, J. K., et al. (2011). Hepatocyte-derived Snail1 Propagates Liver Fibrosis Progression. *Mol. Cel Biol* 31, 2392–2403. doi:10.1128/MCB.01218-10

Samavarchi-Tehrani, P., Golipour, A., David, L., Sung, H. K., Beyer, T. A., Datti, A., et al. (2010). Functional Genomics Reveals a BMP-Driven Mesenchymal-To-Epithelial Transition in the Initiation of Somatic Cell Reprogramming. *Cell Stem Cell* 7, 64–77. doi:10.1016/j.stem.2010.04.015

Stemmler, M. P., Eccles, R. L., Brabletz, S., and Brabletz, T. (2019). Non-redundant Functions of EMT Transcription Factors. *Nat. Cel Biol* 21, 102–112. doi:10.1038/s41556-018-0196-y

Sugimoto, H., LeBleu, V. S., Bosukonda, D., Keck, P., Taduri, G., Bechtel, W., et al. (2012). Activin-like Kinase 3 Is Important for Kidney Regeneration and Reversal of Fibrosis. *Nat. Med.* 18, 396–404. doi:10.1038/nm.2629

Tang, P. M., Zhang, Y. Y., Xiao, J., Tang, P. C., Chung, J. Y., Li, J., et al. (2020). Neural Transcription Factor Pou4f1 Promotes Renal Fibrosis via Macrophage-Myofibroblast Transition. *Proc. Natl. Acad. Sci. U S A.* 117, 20741–20752. doi:10.1073/pnas.1917663117

Tripathi, S., Xing, J., Levine, H., and Jolly, M. K. (2021). Mathematical Modeling of Plasticity and Heterogeneity in EMT. *Methods Mol. Biol.* 2179, 385–413. doi:10.1007/978-1-0716-0779-4_28

Tyler, M., and Tirosh, I. (2021). Decoupling Epithelial-Mesenchymal Transitions from Stromal Profiles by Integrative Expression Analysis. *Nat. Commun.* 12, 2592. doi:10.1038/s41467-021-22800-1

Ubil, E., Duan, J., Pillai, I. C., Rosa-Garrido, M., Wu, Y., Bargiacchi, F., et al. (2014). Mesenchymal-endothelial Transition Contributes to Cardiac Neovascularization. *Nature* 514, 585–590. doi:10.1038/nature13839

Wang, Y. Y., Jiang, H., Pan, J., Huang, X. R., Wang, Y. C., Huang, H. F., et al. (2017). Macrophage-to-Myofibroblast Transition Contributes to Interstitial Fibrosis in Chronic Renal Allograft Injury. *J. Am. Soc. Nephrol.* 28, 2053–2067. doi:10.1681/ASN.2016050573

Williams, E. D., Gao, D., Redfern, A., and Thompson, E. W. (2019). Controversies Around Epithelial-Mesenchymal Plasticity in Cancer Metastasis. *Nat. Rev. Cancer* 19, 716–732. doi:10.1038/s41568-019-0213-x

Wu, Z. Q., Rowe, R. G., Lim, K. C., Lin, Y., Willis, A., Tang, Y., et al. (2014). A Snail1/Notch1 Signalling axis Controls Embryonic Vascular Development. *Nat. Commun.* 5, 3998. doi:10.1038/ncomms4998

Xiong, J., Kawagishi, H., Yan, Y., Liu, J., Wells, Q. S., Edmunds, L. R., et al. (2018). A Metabolic Basis for Endothelial-To-Mesenchymal Transition. *Mol. Cel* 69, 689–e7. doi:10.1016/j.molcel.2018.01.010

Xu, S., Jiang, B., Wang, H., Shen, C., Chen, H., and Zeng, L. (2017). Curcumin Suppresses Intestinal Fibrosis by Inhibition of PPARγ-Mediated Epithelial-Mesenchymal Transition. *Evid. Based Complement. Alternat Med.* 2017, 7876064. doi:10.1155/2017/7876064

Xu, Y., Huang, J., Xin, W., Chen, L., Zhao, X., Lv, Z., et al. (2014). Lipid Accumulation Is Ahead of Epithelial-To-Mesenchymal Transition and Therapeutic Intervention by Acetyl-CoA Carboxylase 2 Silence in Diabetic Nephropathy. *Metabolism* 63, 716–726. doi:10.1016/j.metabol.2014.02.010

Yáñez-Mó, M., Lara-Pezzi, E., Selgas, R., Ramírez-Huesca, M., Domínguez-Jiménez, C., Jiménez-Heffernan, J. A., et al. (2003). Peritoneal Dialysis and Epithelial-To-Mesenchymal Transition of Mesothelial Cells. *N. Engl. J. Med.* 348, 403–413. doi:10.1056/NEJMoa020809

Yang, A. H., Chen, J. Y., and Lin, J. K. (2003). Myofibroblastic Conversion of Mesothelial Cells. *Kidney Int.* 63, 1530–1539. doi:10.1046/j.1523-1755.2003.00861.x

Yang, J., Antin, P., Berx, G., Blanpain, C., Brabletz, T., Bronner, M., et al. (2020). Guidelines and Definitions for Research on Epithelial-Mesenchymal Transition. *Nat. Rev. Mol. Cel Biol* 21, 341–352. doi:10.1038/s41580-020-0237-9

Yao, L., Conforti, F., Hill, C., Bell, J., Drawater, L., Li, J., et al. (2019). Paracrine Signalling during ZEB1-Mediated Epithelial-Mesenchymal Transition Augments Local Myofibroblast Differentiation in Lung Fibrosis. *Cell Death Differ* 26, 943–957. doi:10.1038/s41418-018-0175-7

Yu, H., Zhu, J., Chang, L., Liang, C., Li, X., and Wang, W. (2021). 3-Bromopyruvate Decreased Kidney Fibrosis and Fibroblast Activation by Suppressing Aerobic Glycolysis in Unilateral Ureteral Obstruction Mice Model. *Life Sci.* 272, 119206. doi:10.1016/j.lfs.2021.119206

Zeisberg, E. M., Potenta, S. E., Sugimoto, H., Zeisberg, M., and Kalluri, R. (2008). Fibroblasts in Kidney Fibrosis Emerge via Endothelial-To-Mesenchymal Transition. *J. Am. Soc. Nephrol.* 19, 2282–2287. doi:10.1681/ASN.2008050513

Zeisberg, E. M., Tarnavski, O., Zeisberg, M., Dorfman, A. L., McMullen, J. R., Gustafsson, E., et al. (2007). Endothelial-to-mesenchymal Transition Contributes to Cardiac Fibrosis. *Nat. Med.* 13, 952–961. doi:10.1038/nm1613

Zeisberg, M., Hanai, J., Sugimoto, H., Mammoto, T., Charytan, D., Strutz, F., et al. (2003). BMP-7 Counteracts TGF-Beta1-Induced Epithelial-To-Mesenchymal Transition and Reverses Chronic Renal Injury. *Nat. Med.* 9, 964–968. doi:10.1038/nm888

Zeisberg, M., and Kalluri, R. (2013). Cellular Mechanisms of Tissue Fibrosis. 1. Common and Organ-specific Mechanisms Associated with Tissue Fibrosis. *Am. J. Physiol. Cel Physiol* 304, C216–C225. doi:10.1152/ajpcell.00328.2012

Zeisberg, M., and Neilson, E. G. (2009). Biomarkers for Epithelial-Mesenchymal Transitions. *J. Clin. Invest.* 119, 1429–1437. doi:10.1172/JCI36183

Zeisberg, M., Shah, A. A., and Kalluri, R. (2005). Bone Morphogenic Protein-7 Induces Mesenchymal to Epithelial Transition in Adult Renal Fibroblasts and Facilitates Regeneration of Injured Kidney. *J. Biol. Chem.* 280, 8094–8100. doi:10.1074/jbc.M413102200

Zeisberg, M., Yang, C., Martino, M., Duncan, M. B., Rieder, F., Tanjore, H., et al. (2007). Fibroblasts Derive from Hepatocytes in Liver Fibrosis via Epithelial to Mesenchymal Transition. *J. Biol. Chem.* 282, 23337–23347. doi:10.1074/jbc.M700194200

Zhao, X., Kwan, J. Y. Y., Yip, K., Liu, P. P., and Liu, F. F. (2020). Targeting Metabolic Dysregulation for Fibrosis Therapy. *Nat. Rev. Drug Discov.* 19, 57–75. doi:10.1038/s41573-019-0040-5

Zheng, X., Carstens, J. L., Kim, J., Scheible, M., Kaye, J., Sugimoto, H., et al. (2015). Epithelial-to-mesenchymal Transition Is Dispensable for Metastasis but Induces Chemoresistance in Pancreatic Cancer. *Nature* 527, 525–530. doi:10.1038/nature16064

Conflict of Interest: The author declares that the research was conducted in the absence of any commercial or financial relationships that could be construed as a potential conflict of interest.

frontiers in Pharmacology

REVIEW
published: 22 December 2021
doi: 10.3389/fphar.2021.808735

The Hexosamine Biosynthetic Pathway Links Innate Inflammation With Epithelial-Mesenchymal Plasticity in Airway Remodeling

Allan R. Brasier[1,2]*, *Dianhua Qiao*[1] and *Yingxin Zhao*[3]

[1]Department of Medicine, University of Wisconsin-Madison School of Medicine and Public Health (SMPH), Madison, WI, United States, [2]Institute for Clinical and Translational Research (ICTR), University of Wisconsin-Madison, Madison, WI, United States, [3]Department of Internal Medicine, University of Texas Medical Branch Galveston, Galveston, TX, United States

OPEN ACCESS

Edited by:
Pilar Sandoval,
Centre for Molecular Biology Severo Ochoa (CSIC), Spain

Reviewed by:
Marta Fierro Fernandez,
Centre for Molecular Biology Severo Ochoa (CSIC), Spain
Steven O'Reilly,
STipe Therapeutics, Denmark
Chad Slawson,
University of Kansas Medical Center Research Institute, United States

***Correspondence:**
Allan R. Brasier
abrasier@wisc.edu

Specialty section:
This article was submitted to Inflammation Pharmacology, a section of the journal Frontiers in Pharmacology

Received: 03 November 2021
Accepted: 07 December 2021
Published: 22 December 2021

Citation:
Brasier AR, Qiao D and Zhao Y (2021) The Hexosamine Biosynthetic Pathway Links Innate Inflammation With Epithelial-Mesenchymal Plasticity in Airway Remodeling. Front. Pharmacol. 12:808735. doi: 10.3389/fphar.2021.808735

Disruption of the lower airway epithelial barrier plays a major role in the initiation and progression of chronic lung disease. Here, repetitive environmental insults produced by viral and allergens triggers metabolic adaptations, epithelial-mesenchymal plasticity (EMP) and airway remodeling. Epithelial plasticity disrupts epithelial barrier function, stimulates release of fibroblastic growth factors, and remodels the extracellular matrix (ECM). This review will focus on recent work demonstrating how the hexosamine biosynthetic pathway (HBP) links innate inflammation to airway remodeling. The HBP is a core metabolic pathway of the unfolded protein response (UPR) responsible for protein N-glycosylation, relief of proteotoxic stress and secretion of ECM modifiers. We will overview findings that the IκB kinase (IKK)-NFκB pathway directly activates expression of the *SNAI-ZEB1* mesenchymal transcription factor module through regulation of the Bromodomain Containing Protein 4 (BRD4) chromatin modifier. BRD4 mediates transcriptional elongation of SNAI1-ZEB as well as enhancing chromatin accessibility and transcription of fibroblast growth factors, ECM and matrix metalloproteinases (MMPs). In addition, recent exciting findings that IKK cross-talks with the UPR by controlling phosphorylation and nuclear translocation of the autoregulatory XBP1s transcription factor are presented. HBP is required for N glycosylation and secretion of ECM components that play an important signaling role in airway remodeling. This interplay between innate inflammation, metabolic reprogramming and lower airway plasticity expands a population of subepithelial myofibroblasts by secreting fibroblastic growth factors, producing changes in ECM tensile strength, and fibroblast stimulation by MMP binding. Through these actions on myofibroblasts, EMP in lower airway cells produces expansion of the *lamina reticularis* and promotes airway remodeling. In this manner, metabolic reprogramming by the HBP mediates environmental insult-induced inflammation with remodeling in chronic airway diseases.

Keywords: fibrosis, epigenetics, EMT, innate inflammation, plasticity, hexosamine biosynthetic pathway (HBP)

INTRODUCTION: THE TRANSITION ZONE OF THE AIRWAY MEDIATES RESPONSE TO ENVIRONMENTAL STRESSORS

This manuscript will focus on the role of specialized epithelium in the "transition zone" of the lower airway that is emerging as a major driver in the initiation and maintenance of inflammation and airway remodeling (Burgel, 2011; Zhao et al., 2017; Tian et al., 2018c; Brasier, 2019; Skibba et al., 2021). Anatomically, the "transition zone" is a region between the gas-conducting bronchioles and the gas-exchanging alveoli. This zone is a pseudostratified columnar epithelium composed of at least five distinct epithelial phenotypes, as multi-ciliated cells, secretory/"Club" cells, mucin-producing goblet cells, ionocytes and basal cells (Adams et al., 2020; Deprez et al., 2020; Zaragosi et al., 2020). These cells differ from one another in secretory functions, self-renewal and mucociliary clearance properties. Underlying these are a basement membrane, *lamina reticularis,* composed of Collagen (COL I/III), fibronectin (FN1) and population of subepithelial fibroblasts. This unit is referred to as the "epithelial mesenchymal trophic unit" (EMTU). and is responsible for maintaining trophic effects on the epithelium (**Figure 1**) (Evans et al., 1999).

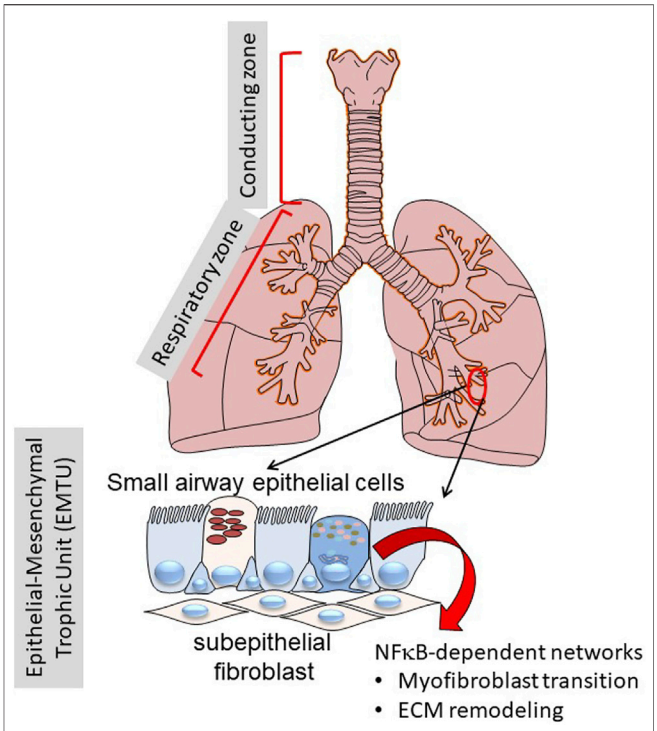

FIGURE 1 | Role of the transition zone in airway remodeling. Shown is a schematic view of the human lungs from the larynx to distal alveoli. The lungs can be functionally separated into the conducting zone (larynx, trachea) and the respiratory zone (small bronchioles and alveoli). Of focus for this work, the distinct epithelial cell types in the transition zone plays key roles in inflammation and remodeling through NF-κB regulated inducible gene expression programs.

Dynamic Responses of Lower Airway Epithelial Cells to Environmental Agents

Under normal conditions, cells in the lower airway epithelium exhibit much lower rate of cellular turnover than those in the conducting airways (Bowden, 1983). However, in response to environmental toxicants, epithelial cells rapidly undergo necrosis and shed, releasing damage-associated molecular patterns. Surviving adjacent epithelial cells respond by de-differentiation, enabling them to migrate to repopulate the injured area (Erjefalt et al., 1995). This epithelial injury-repair process is also activated by environmental oxidants, viruses and allergens, whose mechanisms are increasingly being elucidated.

Airway epithelial cells are poised for sensing and dynamically responding to viral attack through an arsenal of pattern recognition receptors (PRRs) monitoring the airway lumen, cellular cytoplasm, and subcellular organelles for the presence of pathogen-associated molecular patterns (PAMPs) (Whitsett and Alenghat, 2015). Luminal PAMPs of viral origin, double-stranded RNA and 5-phosphorylated RNA, are bound by membrane-associated Toll-like receptor 3 (TLR3) present on airway epithelial cells. In contrast, intracellular viral PAMPs are detected by members of the retinoic acid inducible gene -I (RIG-I)/melanoma differentiation-associated protein (MDA5) family. Upon binding their cognate PAMPs, PRRs function to recruit signaling adapters that trigger intracellular innate signaling. PRR-active innate signaling is an interconnected network of intracellular signaling pathways including the MyD88-IκB kinase (IKK) -NFκB, tank binding kinase (TBK)-interferon regulatory factor (IRF), mitogen activated protein kinase (MAPK) pathways and others (Rohmann et al., 2011). These cascades trigger a genomic response resulting in the secretion of danger signals, protective IFNs and cytokines (Bertolusso et al., 2014) as well as determining apoptotic cell fate decisions (Czerkies et al., 2018). Consequently, PRR-activated innate signaling produces rapid neutrophilic inflammation (Tian et al., 2017) and oxidative injury (Choudhary et al., 2016), disrupting cilia function, producing epithelial loss, and barrier disruption (Rezaee, 2011).

Another signaling response is mediated by protease activated receptors (PARs), members of the G protein receptor family (Shpacovitch et al., 2007). In contrast with classical receptors, PARs are activated by N-terminal proteolytic cleavage; the resulting N-termini is a tethered activation ligand that binds an extracellular domain and initiates receptor signaling. PARs are activated by endogenous serine proteases released from activated neutrophils and mast cells. PAR signaling also enhances leukocyte motility, adhesion and inflammatory molecule release through pathways determined by G protein *a* subtypes specific for each receptor (Shpacovitch et al., 2008). Of relevance here, PAR-2 signaling has been linked to TGFβ activation and mesenchymal gene expression [*COLI, a* smooth muscle cell actin (*αSMA*)] characteristic of epithelial plasticity and induction of pulmonary fibrosis (Lin et al., 2015).

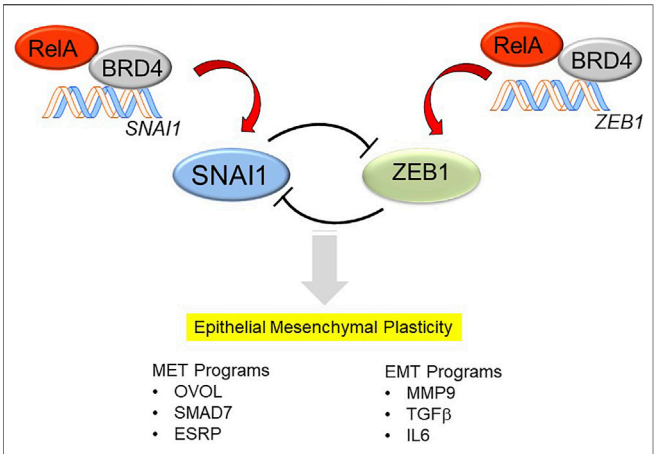

FIGURE 2 | Mechanisms how NFκB/RELA activates the SNAI/ZEB transcription factor module, triggering EMP. In differentiated airway epithelial cells, the core mesenchymal regulators SNAI1 and ZEB1 are suppressed by a double-negative feedback loop. SNAIL1 inhibits the expression of miR-34, which represses the translation of SNAI1, whereas ZEB represses the induction of miR-200, which inhibits the translation of ZEB1. The mutual trans-repression is disrupted by the effects of NFκB/RELA to trigger synthesis of SNAI1 and ZEB1. RELA recruits the BRD4 coactivator to directly activate SNAI and ZEB1 genes to trigger the transition into EMP. EMP is a bistable state characterized by expression of genes controlling MET (*OVOL, SMAD7, ESRP*) as well as those controlling EMT (*MMP9, TGFβ, IL6*).

EPITHELIAL PLASTICITY OF LOWER AIRWAY EPITHELIAL CELLS

Lower airway epithelial cells are programmed to produce distinct patterns of inflammatory and remodeling gene networks. Gene-profiling experiments have shown that lower airway cells produce greater amounts of T helper type 2 (Th2)-activating CCL-type chemokines than do conducting airway-derived epithelia (Olszewska-Pazdrak et al., 1998; Zhang et al., 2001). Systems levels proteomics studies using a highly sensitive unbiased secretome profiling technique found that small airway epithelial cells from the transition zones also produce greater amounts of myofibroblast growth factors (IL6 and TGFβ) Th2 polarizing cytokines (TSLP) and mucogenic cytokines (CCL-20) than do cells from the conducting airways (Zhao et al., 2017). These profiling experiments have been supported by function cell-type depletion experiments in mouse models. Mice depleted of RelA in the secretoglobin+/"Club cell" population have significantly reduced chemokine response, leukocytic inflammation, and airway obstruction in response to experimental RSV infection (Tian et al., 2018c), TLR3 stimulation (Tian et al., 2018a). Finally, recent studies found that the transition zone Club cells mediate allergic asthma-induced remodeling in response to *Aspergillosis* and cat dander allergens (Wiesner et al., 2020; Skibba et al., 2021). Collectively, this evidence points to the conclusion that the transition zone is critical to initiation and maintenance of airway inflammation and remodeling.

Injury-repair is a multi-step genomic and post-translational response involving a series of reversible cell-state transitions. The first step in the injury response pathway involves loss of cell-surface expression of epithelial cadherin (CDH1) via proteolysis and subsequent internalization, disrupting adherens junctions (Aiello et al., 2018) that play important role in the maintenance of epithelial barrier function. CDH1 loss produces a "hybrid" epithelial/mesenchymal (E/M) state, a reversible condition where cells can either revert to normal epithelium via mesenchymal-epithelial transition (MET) or transition into more stable mesenchymal-like states depending on cellular context and cues (Zhang et al., 2014; Jolly et al., 2016; Jolly et al., 2019). This hybrid E/M state, will be referred to as Epithelial-Mesenchymal Plasticity (EMP) by convention (Yang et al., 2020)]. EMP is a spectrum of mesenchymal-like states stabilized by SNAI2 expression (Subbalakshmi et al., 2021). EMP includes expression of a regulatory network that includes epithelial splicing regulatory protein 1 (ESRP1), the transcription factor Ovo Like Transcriptional Repressor 1 [OVOL (Jia et al., 2015)], and Mothers Against Decapentaplegic Homolog 7 [SMAD7 (Li et al., 2015)]. With the termination of injury, activity of this network promotes MET, reverting back to the Epithelial state. The mechanisms how this occurs is only partially understood. OVOL1 promotes MET through a regulatory feedback loop with suppression of ZEB1 in concert with ESRP1 (Roca et al., 2013). By contrast, SMAD7 is an effector of the BMP4 pathway important in maintaining the differentiated epithelial cell state.

With persistence of inflammation or injury, enhanced expression of the core Snail family repressor (SNAI) and Zinc Finger E-Box Binding Homeobox (ZEB1) transcription factor module, suppression of *CDH1* expression and loss of the MET program, cells transition to a mesenchymal phenotype (**Figure 2**). However, it is currently controversial whether primary (untransformed cells) undergo "complete" mesenchymal transition. Cell culture experiments of highly differentiated lower airway epithelial cells indicate that the cells remain in this bistable EMP even after prolonged stimulation with TGFβ and rapidly reverse with TGFβ removal (Tian et al., 2015). Of relevance, epithelial plasticity has been observed in chronic obstructive pulmonary disease asthma, idiopathic pulmonary fibrosis and viral pulmonary diseases (Holgate et al., 2000; Hogg et al., 2004; Harvey et al., 2007; Sohal et al., 2014; Tian et al., 2018c). Few of these studies have systematically examined whether MET restrictors are also being co-expressed, so the only conclusion that can be derived at this point is that epithelial plasticity is characteristic of these diseases.

MECHANISMS HOW ALLERGENS TRIGGER EPITHELIAL PLASTICITY

Although the mechanisms controlling the EMP to growth factors, such as TGFβ, are well-understood (Kalluri and Weinberg, 2009; Ijaz et al., 2014), less is known how aeroallergens trigger EMP. Aeroallergens are plant- and animal-derived products that modify the epithelial barrier function and activate innate signaling cascades (Lambrecht and Hammad, 2014). A number of common and important aeroallergens have been studied, summarized briefly below.

The house dust mite (HDM), *Dermatophagtoides pteronyssius* produces *a* complex aeroallergen containing bacterial cell wall products [lipopolysaccharide (LPS) and *ß*-glucan (Douwes et al., 2000)] as well as mite-produced proteases (Jacquet, 2011). Of these the *Der p1 is a* cysteine protease that disrupts epithelial tight junctions by cleavage of zona occludens (Heijink et al., 2010). At the mechanistic level, Der p1 activates the protease-activated receptor (PAR)-2 cleaving its NH_2 terminus, irreversibly activating signaling (Asokananthan et al., 2002). The cockroach allergen, Per a 10, also induces innate signaling by protease activity directed to PAR-2 (Arizmendi et al., 2011). In contrast, Ragweed pollen contains an endogenous NADPH-driven oxidase that disrupts the epithelial barrier by forming reactive oxygen species (Bacsi et al., 2005), producing CXCL2 release and neutrophilic inflammation (Hosoki et al., 2016). The *Aspergillus*-derived alkaline protease 1 (Alp1) is an aeroallergen that disrupts epithelial tight junctions by cleaving epithelial cadherin, producing IL33/CCL2 secretion and eosinophilia (Wiesner et al., 2020). Cat dander extracts (CDE) activate the MD2 co-receptor and TLR4, upstream of the Myd88-NFκB pathway (Hosoki et al., 2016; Hosoki et al., 2017b) producing CXCL2 secretion and neutrophil recruitment (Hosoki et al., 2017b) through a CD14/LPS-independent pathway (Hosoki et al., 2016; Hosoki et al., 2017a; Hosoki et al., 2017b). CDE triggers a coordinated time-dependent increase of TGFβ-1,-2 and -3 production, local SMAD3 and NFκB signaling and expression of the mesenchymal core regulatory proteins ZEB1/SNAI1 (Skibba et al., 2021).

VIRAL REPLICATION TRIGGERS PLASTICITY THROUGH THE IKK-NFκB PATHWAY

In addition to these actions triggered by common aeroallergens, activation of viral pattern recognition receptors trigger epithelial plasticity in transition zone epithelium. Here, we found that stimulation with selective TLR3 agonists activates epithelial plasticity, with features of chronic stress fiber formation, expression of the *SNAI1/ZEB* module, activation of mesenchymal intermediate filament *VIM*, and extracellular matrix proteins (*FN1, COL1A*) (Tian et al., 2017). At the mechanistic level, TLR3-mediated epithelial plasticity was prevented by silencing NFκB/RELA or administration of a small molecule IκB kinase (IKK) inhibitor (Tian et al., 2017), implicating the potent NFκB signaling pathway in virus-induced EMP (the mechanisms how NFκB triggers EMT and coactivators required are described in **Sections 5**,6 below). Based on this novel model of viral inflammation-induced airway remodeling, we concluded that NFκB is a major controller of EMP, a finding that has potentially important relevance to airway remodeling produced by repetitive viral infections.

Recent exciting work has extended the role of innate responses with EMP in response to Respiratory Syncytial Virus (RSV) infection. RSV is an *Orthopneumovirus* within the larger Paramyxoviridae family, responsible for seasonal outbreaks of respiratory tract infections worldwide (Borchers et al., 2013) and represents the most common cause of pediatric hospitalization in children (Stockman et al., 2012) and lower respiratory tract infections (Shi et al., 2017). Upon inoculation, RSV initially replicates in ciliated airway epithelial cells in the upper nasopharynx and conducting airways (Zhang et al., 2002; Liesman et al., 2014), producing epithelial sloughing, spreading into the lower airways (Jozwik et al., 2015). In contrast to the TLR3 intracellular signaling RSV activates the Retinoic acid inducible gene-I a cytoplasmic RNA helicase PRR (Liu et al., 2007). Activated RIG-I forms a signaling complex on the surface of mitochondria, triggering the IKK-NFκB signaling pathway (Liu et al., 2007; Liu et al., 2008), that activates the EMP program in an NFκB-dependent manner (Tian et al., 2018a; Tian et al., 2018c; Qiao et al., 2021). RSV infection induces the MET gene network *OVOL1* and *SMAD7* were also observed, providing direct evidence of the bistable E/M state (Xu et al., 2021b; Qiao et al., 2021).

Consistent with the central role of the transition zone in remodeling, RSV replication has been documented in bronchioles and alveolar epithelial cells of children with naturally acquired severe infections (Johnson et al., 2007) and in normal immune volunteers experimentally infected with RSV (Jozwik et al., 2015). In the small airways, inflammation-induced EMP producing mucosal thickening and reduced small airway diameter are primarily responsible for reduced expiratory airflow. Prospective observational studies show that children with severe RSV infections exhibit long-term decreased pulmonary function (Martinez, 2009; Fauroux et al., 2017). The interstitial lung disease associated with COVID-19 (Myall et al., 2021) and SARS (Hui et al., 2005) are other examples of viral induced airway remodeling that may involve transition zone innate signaling.

IKK-NFκB SIGNALING TRIGGERS SEQUENTIAL SIGNALING CASCADES IN EMP

EMP is the product of sequential multi-step signaling cascades (Zhang et al., 2014) converging on master transcription factors, functioning in synergistic "cliques", whose temporal expression and downstream gene regulatory networks coordinate productive EMP (Tian et al., 2015; Chang et al., 2016). A combined computational and RNA sequencing study of alveolar carcinoma cells illuminated the central role of precisely timed expression of the master transcription factors, ETS2, HNF4A and JUNB. These factors exhibited autoregulation and their synergistic interaction was required for transition of TGFβ "primed" cells to a stable mesenchymal-like state. This study also identified the critical role of BRD4-dependent superenhancers in maintenance of transcription factor hubs within chromatin for maintenance of EMT.

Superenhancers are extended chromatin regions (up to 10 kB in length) complexed with high levels of coactivators, enriched in activating histone acetylation marks, and have been implicated as mechanisms of epigenetic control of cell identity (Loven et al., 2013; Pott and Lieb, 2015). These domains are sites ("factories")

for gene transcription. Genes within these factories are bound by hypophosphorylated RNA polymerase II poised for rapid gene expression through regulated transcriptional elongation (Tian et al., 2016), a major mechanism for gene expression in epithelial plasticity. However, epithelial plasticity programs in transformed cells are substantially influenced by signaling effects of transforming oncogenes. We found that TGFβ-induced plasticity programs in primary cells are distinct from those in TGFβ-induced Ras-oncogene transformed cells (Tian et al., 2015), so these previous studies are of uncertain relevance to plasticity programs produced in primary cells.

To understand key regulatory pathways in primary small airway epithelial cells, we have applied systemic time-course of RNA-seq analysis (Tian et al., 2015; Tian et al., 2018b), protein expression studies and phosphoprotein profiling (Zhang et al., 2019; Zhao et al., 2021) to telomerase immortalized (but non oncogenically transformed) primary small airway epithelial cells. These studies have identified that a major component of regulatory gene networks are driven by IKK- NFκB signaling downstream of the initial TGFβ signal. TGFβ induces NFκB translocation and binding to core EMP regulators, including the SNAI1-ZEB1 module, growth factors and EMT regulators (Tian et al., 2018b). Importantly, deletion of RELA using siRNA or CRISPR/Cas9 genome editing blocks TGFβ-induced EMP (Tian et al., 2015; Tian et al., 2018b). These studies clearly identify RELA as a "master transcription factor" of EMP, controlling at least six clusters of essential EMP transcription factors, including: 1) the SNAI1/ZEB1 module; 2) the WNT/β-catenin morphogen pathway, 3) the JUN transcription factor and 4) the TGFβ/IL-6 autocrine regulatory module (Tian et al., 2018b).

Of these, the SNA1-ZEB1 transcription factor module is of special note and deserves elaboration. SNAI1 and ZEB1 are mesenchymal transcription factors regulated by a double-negative feedback loop with microRNA (miR) expression (**Figure 2**). In differentiated epithelial cells, SNA1 and ZEB1 are expressed at low levels. Here, SNAI1 inhibits the expression of miR-34, a miR that blocks translation of *SNAI1* mRNA (Siemens et al., 2011). In parallel, ZEB1 inhibits expression of miR-200, a miR that inhibits the translation of *ZEB1* mRNA (Ahn et al., 2012). Perturbation of this negative feedback loop occurs with stimulus-induced SNAI1 expression, this process inhibits miR-34 expression, allowing SNAI1 to be translated. With SNAI1 expression, SNAI1 directly activates ZEB1 abundance, promoting EMP transition (Lu et al., 2013).

Consequently, activation of the SNAI1 transcriptional co-repressor is the sine *qua non* of the "mature" mesenchymal-like state. In addition to its actions on ZEB, SNAI1 directly binds to regulatory promoter regions of *CDH1* and Zona Occludins (*Z O -1*), leading to their repression and subsequent cellular loss of apical-basal polarity (Vincent et al., 2009). Although its role in type II EMT is not fully understood, ZEB1 plays an important role in maintenance of the epigenetic landscape in cancer cells (Lindner et al., 2020), silencing *CDH1* and has been implicated in modulating the mucosal IFN response in primary small airway cells, perturbing the expression of the IRF1 transcription factor through an epigenetic mechanism involving transcription factor "exclusion" (Yang et al., 2017b). Our evidence that RELA directly binds to the *SNAI1* and *ZEB1* promoters, enhancing their expression (Tian et al., 2016) provides understanding how RELA functions as a master regulator of EMP in epithelial cells. These data are consistent with the role of cRel in driving fibroblast to myofibroblast transition in skin fibroblasts (Worrell et al., 2020).

Surprisingly to us, in TGFβ-induced EMP, the NFκB-dependent gene regulatory network is activated *prior* to significant RELA nuclear translocation. To better understand this phenomenon, we examined the role of the upstream IKK in TGFβ-induced EMP. Consistent with the earlier findings generated by RELA silencing, small molecule IKK inhibitors completely block TGFβ-induced EMP was blocked (Tian et al., 2015). Temporal proteomic studies revealed that IKK was required for the induction of 23 signaling pathways essential in EMP that exhibited time-dependent activation (**Figure 3**). These cascades included TGFβ signaling, p38 mitogen associate protein kinase (MAPK), Toll receptor signaling, and integrin pathways and others (Zhao et al., 2021). These findings illustrate the complex, temporally coordinated processes controlling EMP are controlled at multiple levels by the IKK-NFκB signaling pathway.

Through the IKK-NFκB pathway, TGFβ induces epithelial cells to express functional mesenchymal signatures, such as *αSMA* to enhance cytokinesis, intermediate filament *VIM* to produce motility, *COL1A, FN1* and *MMP9* to promote ECM formation and deposition (Knight and Holgate, 2003). We note that *MMP9* is an invariant gene expressed by diverse types of epithelial carcinoma cells undergoing mesenchymal transition (Peixoto et al., 2019).

THE UNFOLDED PROTEIN RESPONSE (UPR) IS A CORE PATHWAY DRIVING EMP

Although epithelial cells are not primary secretory cells, dynamic changes in ER protein load produced by TGFβ stimulation triggers the UPR. Two major UPR sensor/effectors that have been identified include inositol-requiring protein 1α (IRE1α) and protein kinase RNA-like ER kinase (PERK) (Kopp et al., 2019). Of these, IRE1α functions as the primary arm of the UPR linked to epithelial plasticity. In the presence of unfolded proteins accumulating in the ER, the HSPA5/BiP chaperone dissociates from IRE1α, resulting in a coupled dimerization-autotransphosphorylation reaction, triggering its rnase activity. The IRE1α rnase processes the mRNA encoding unspliced X box-binding protein 1 (*XBP1u*) to form spliced XBP1 (*XBP1s*) mRNA. Upon translation, XBP1s is a transcription factor that controls the transcription of genes encoding proteins involved in protein folding, ER-associated degradation (ERAD), protein quality control and phospholipid synthesis. In addition to splicing XBP1, certain cellular mRNAs undergo regulated IRE1-dependent decay (RIDD). Phosphorylated IRE1α also induces JUN N-terminal kinase (JNK) and IKK-NFκB

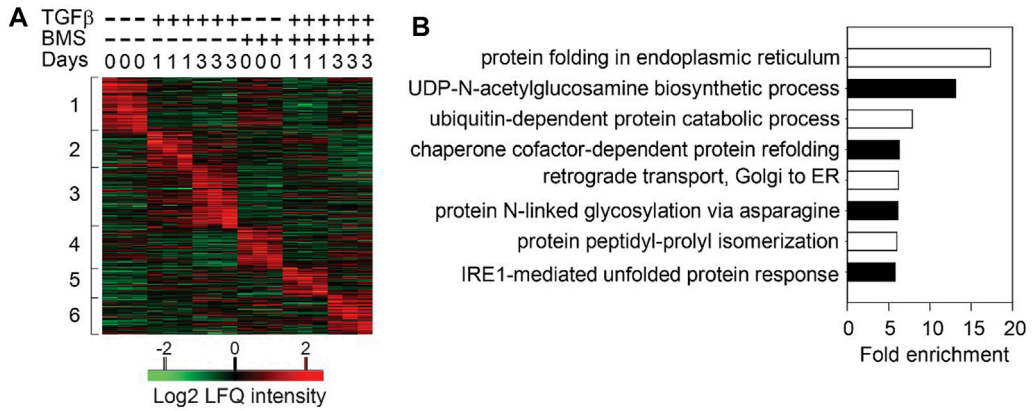

FIGURE 3 | Sequential cascades of IKK-mediated protein profiles **(A)** Time-series proteomics of hSAECs in response to TGFβ stimulation in the presence or absence of IKK inhibitor **(B)** Gene ontology biological process (GOBP) annotation enrichment of proteins that were upregulated after 3 days of TGFβ treatment and blocked by BMS-345541 (the proteins in Cluster three in and only UPR- and HBP-related annotations are shown. Reproduced with permission from (Zhao et al., 2021).

pathways through interactions with TRAF adapters, interfacing with the innate signaling pathway (Hetz, 2012). Through these arms, the UPR restores ER homeostasis by either increasing the protein folding capacity of the ER, reducing the influx of nascent proteins into the ER, and/or degradation through ERAD.

The amplitude and kinetics of UPR signaling are tightly regulated, a process increasingly recognized to play important roles in metabolic reprogramming and cell differentiation (Hetz, 2012). In the EMP, the upregulation of secreted ECM proteins (FN1, COL1) enhances produces ER stress, disrupts HSPA5-IRE1α interactions and activates the UPR (Feng et al., 2014; Zhang et al., 2019) via XBP1s formation (Zhao et al., 2016). XBP1s, in turn, activates expression of protein folding enzymes Prolyl 4-Hydroxylase (P4HB), Protein Disulfide isomerase Family A Member (PDIA)-4 and PDIA-6 to relieve ER stress.

Using integrated proteomic and transcriptomic studies, we observed that TGFβ stimulation induced ECM disassembly, collagen structure, lamellipodia formation, and focal adhesion (Zhang et al., 2019). Analysis of the secreted proteins showed that TGFβ stimulation increased secretion of 101 N-glycosylated ECM proteins. That the UPR was important in this process was revealed by studies inhibiting IRE1α, blocking XBP1s formation. Blockade of XBP1s significantly reduces the secretion of these N-glycosylated secreted proteins, including the key ECM components, FN1 and COL1. These studies indicated that the IRE1α-XBP1s pathway of the UPR is essential for ECM remodeling induced by epithelial plasticity.

CROSS-TALK OF THE IRE-XBP1S AND THE IKK-NFκB PATHWAYS IN HBP

An exciting finding recently published been that cross-talk IRE1α-XBP1s arm of the UPR has extensive cross-talk with the IKK-NFκB pathway (Zhao et al., 2021). In response to

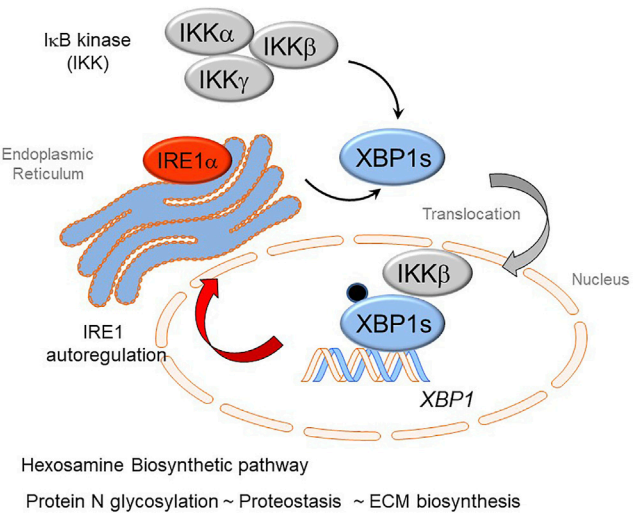

FIGURE 4 | Cross-talk of innate inflammation with the Unfolded Protein Response (UPR) regulates the Hexosamine Biosynthetic Pathway (HBP). The rnase activity of the IRE1α kinase mediates splicing of the XBP1 mRNA transcript forming XBP1s. Recent advances have shown that activation of the IκB kinase (IKK) interfaces with the UPR. Here IKK is required for phosphorylation of XBP1s on Ser 48 (pXBP1). In addition, IKKβ forms a complex with pXBP1s; the complex translocates into the nucleus. The IKK-pXPB1s complex is required for HBP activation, necessary for GFPT2 expression, restoration of proteostasis, and maintenance of *XBP1* expression through an autoregulatory loop.

TGFβ stimulation, IKKβ directly complexes with- and phosphorylates- XBP1s, which activates HBP and upregulates protein N-glycosylation, preventing transition cells from ER stress-induced apoptosis in EMP. Inhibition of IKK activity abolishes the phosphorylation of XBP1-Ser 47, blocks XBP1s nuclear translocation and inhibits the activation of HBP. These data suggest that the IKKβ-XBP1s-HBP crosstalk pathway couples inflammation and glucose metabolic reprogramming

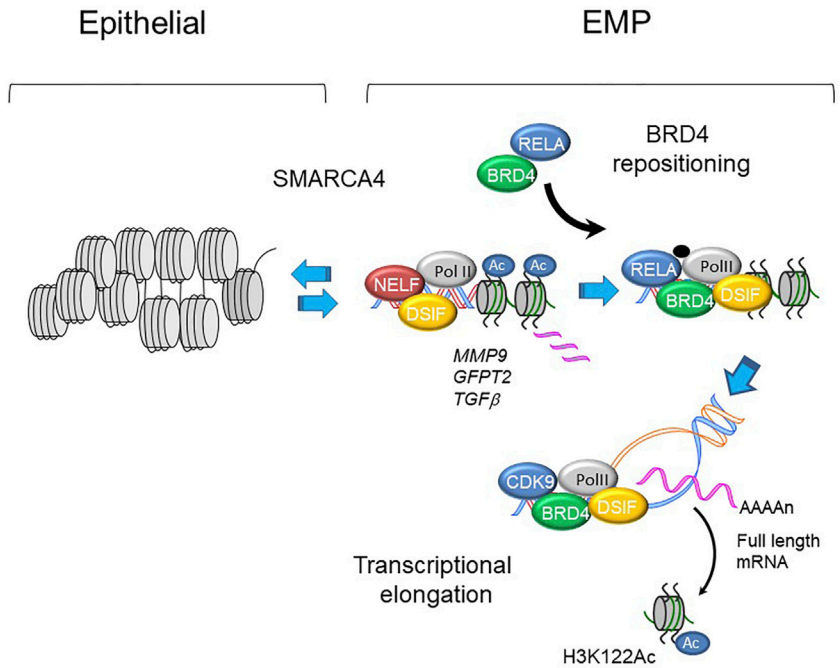

FIGURE 5 | BRD4 regulated transcription in EMP programs. Schematic view of MMP9, GFP2 and TGFb promoters in epithelial and mesenchymal-like (EMP) states. With activation of master transcription factors, BRD4 is repositioned from genomic sites including epithelial superenhancers to epithelial plasticity genes. Upon phosphorylation, plasticity genes are expressed through regulated transcriptional elongation, involving remodeling nucleosomes through BRD4-dependent HAT activity (Yang et al., 2005; Brasier et al., 2011; Devaiah et al., 2016a; Yang et al., 2017a).

in EMP (**Figure 4**). UPR is sustained through RSV by an autoregulatory loop where XBP1 enhances Pol II binding to its own promoter (Qiao et al., 2021). This autoregulation ensures a continuous supply of *XBP1* mRNA to maintain ER proteostasis and support EMP.

THE HEXOSAMINE BIOSYNTHETIC PATHWAY (HBP) IS A MAJOR METABOLIC ADAPTATION IN EMP

TGFβ is well-known to have potent effects on cellular metabolic adaptations, including the activation of glycolysis, glutaminolysis through a mechanism proposed by altering the NAD+/NADH ratio (Henderson and O'Reilly, 2021). Activation of epithelial plasticity by TGFβ produces substantial intracytoplasmic accumulation of N glycosylated proteins (Zhang et al., 2019). To further understand this process, we found that the key enzymes of the HBP, Glutamine-fructose-6-phosphate transaminase (GFPT)-1, -2, Glucosamine-phosphate N-acetyltransferase (GNPNAT), and phosphoglucomutase (PGM3) were up-regulated in the TGFβ-induced EMP state. GFPT converts D-fructose-6-phosphate (Fru-6-P) and L-glutamine to D-glucosamine-6-phosphate (GlcN-6-P) and L-glutamate. GlcN-6-P is an essential precursor of uridine 5′-diphosphate-N-acetyl-D-glucosamine (UDP-GlcNAc), a rate-limiting substrate of the O-GlcNAc transferase (OGT) in the HBP, a pathway required for glycoprotein formation (Akella et al., 2019). This finding was significant because activation of HBP and subsequent up-regulation of protein N-glycosylation is important in nascent protein folding and ER quality control, ER-associated apoptosis and secretion of ECM proteins. Together, our data suggest that HBP is an adaptive response activated in EMP to improve the folding and secretion of ECM proteins to restore proteostasis (**Figure 4**).

In parallel to the metabolic response to TGFβ, metabolic adaptations are also observed in viral induced innate inflammation. Metabolic profiling studies have shown that RSV replication upregulates glucose influx, aerobic glycolysis, increased lactic acid and UDP-GlcNAc generation (Zhao et al., 2019; Martín-Vicente et al., 2020). We found that paramyxovirus infections also produce ER accumulation of N-glycoproteins and intracellular accumulation of UDP-GlcNAc (Qiao et al., 2021). Mechanistic dissection of the UPR confirmed that viral replication primarily induced activation of the IRE1α kinase-XBP1s arm of the UPR. Intriguingly, the RSV-induced EMP regulatory network, including expression of the *SNAI1-ZEB1* module, *FN1* and *MMP9* were dependent on IRE1-XBP1, a finding confirmed by both small molecule inhibitors and gene-specific targeting experiments. Furthermore, our mechanistic studies showed that RSV enhances XBP1 binding to the super-enhancer of *GFPT2*, promoting RNA polymerase II engagement to the *GFPT2* gene (Qiao et al., 2021). The ability of paramyxovirus infection to activate the HBP and epithelial

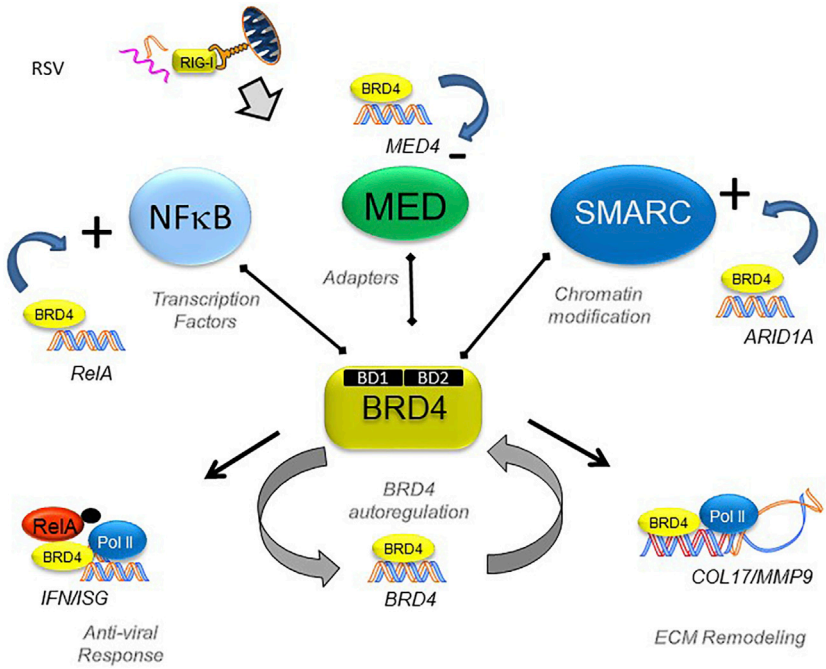

FIGURE 6 | BRD4's dynamically regulated gene networks. Schematic diagram of BRD4 dependent genes in RSV infection. Although BRD4 is required for innate signaling and expression of ECM remodeling proteins, this study provides evidence that BRD4 controls is own expression through an autoregulatory network. In addition, BRD4 controls expression of members of its interacting coactivators that bind the BD, including transcription factors, adaptors and chromatin remodeling complexes. Reproduced with permission from (Xu et al., 2021a).

plasticity via the IRE1-XBP1 pathway was confirmed in a mouse model of Sendai virus infection (Qiao et al., 2021). These findings suggest that RSV replication activates the HBP to enhance N glycosylation to promote native protein folding and ECM secretion, restoring ER proteostasis and epithelial plasticity (Zhang et al., 2019).

EPIGENETIC CONTROL OF EPITHELIAL PLASTICITY

Epigenetic reprogramming is central for how transcription factor cascades control gene expression important in epithelial plasticity (Kalluri and Weinberg, 2009; Peixoto et al., 2019). EMP regulatory epigenetics are mediated by post-translational modifications of histone side chains; these are produced by chromatin regulatory proteins, including Bromodomain-containing 4 (BRD4). BRD4 is a member of the bromodomain and extra-terminal domain (BET) family of proteins that plays essential roles in epigenetic control of inflammation-inducible gene expression (Nowak et al., 2008; Tian et al., 2019), maintenance of cellular identity (Loven et al., 2013) and chromatin compaction/conformation (Devaiah et al., 2016b). A body of work shows that BRD4 plays essential roles both in the maintenance of epithelial identity and in the genomic reprogramming underlying EMP through its activations in binding acetylated histones, functioning as an RNA polymerase II COOH terminal kinase, and as a histone acetyltransferase (Devaiah et al., 2012; Devaiah and Singer, 2012; Devaiah et al., 2016a). These roles include its direct role as a coactivator of master transcription factors in the EMP, and through its actions controlling cell-type identity genes via superenhancers. Interestingly, *XBP1* is one such gene under BRD4-dependent superhancer control (Loven et al., 2013).

In its role as a master transcription factor coactivator, BRD4 inducibly complexes with NFκB/RELA, JUN, and SMAD transcription factors mediating gene regulatory networks controlling epithelial plasticity. Of these, the interaction with RELA is most understood at the molecular level. It has been well-established that activated RELA undergoes a coupled phosphorylation/acetylation processing mediated by the IKK and p300/CBP, respectively (Nowak et al., 2008; Brasier et al., 2011). The BRD4 BD binds to the acetyl-K 310 residue of RELA, and the complex is recruited to a subset of NF-κB- and BRD4-dependent genes. Of these targets, RELA recruits BRD4 to the key EMP regulators, *SNA1I, ZEB1, Twist*, *IL6, FN1* and others (Tian et al., 2016). Here, BRD4-CDK9 complex functions to activate EMP programs through a process of regulated transcriptional elongation (Tian et al., 2016; Yang et al., 2017a) (**Figure 5**). In addition, BRD4 –SMAD3 complex also plays a key role in TGFβ-induced myofibroblast formation (Ijaz et al., 2017), and we have recently found that BRD4 forms complexes with members of the AP-1 complex (Mann et al., 2021). More work will be required to understand how these transcription factors function in a

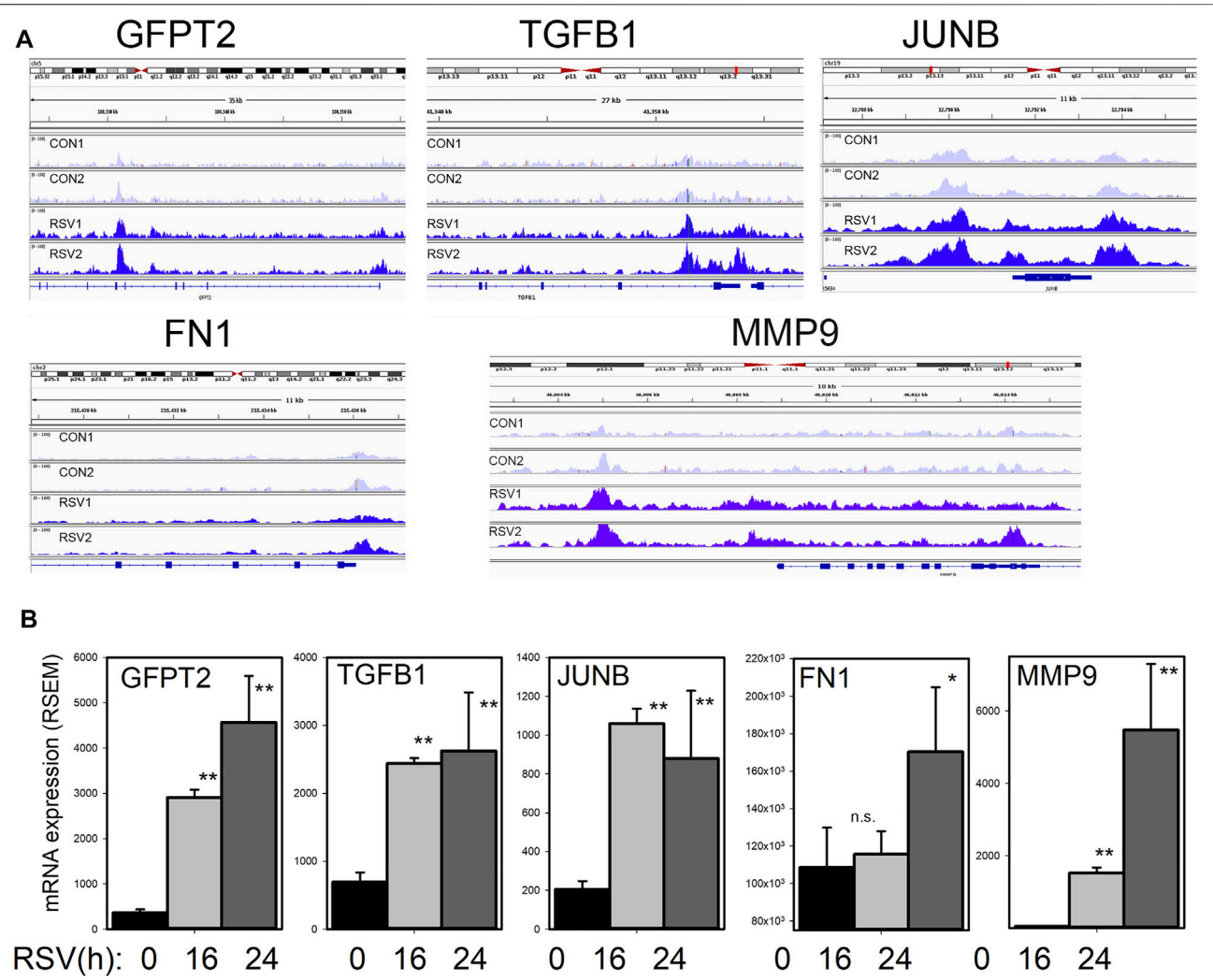

FIGURE 7 | RSV inducible chromatin changes in the TGFβ growth factor-ECM pathway **(A)** Integrated genomic viewer (IGV) of ATAC-Seq cleavage fragments mapped to the *GFPT2, TGFB1*, *JUNB*, and *FN1* genes in control and RSV-infected state. Note the increased transposase digestion of promoter elements after RSV infection **(B)** mRNA changes of each gene. Shown is mean ± SD ($n = 4$ independent RNA-seq reads quantified by RSEM). *, $p < 0.05$, **, $p < 0.01$ post hoc Tukey's test. Reproduced with permission from (Xu et al., 2020).

synergistic manner to reposition BRD4 to gene regulatory networks controlling EMP.

BRD4 REGULATES GROWTH FACTORS AND ECM REMODELING

Despite understanding that BRD4 is required for EMP, the BRD4-dependent gene regulatory network of non-transformed epithelial cells is incompletely understood. To help advance this topic, we recently investigated the effect of a specific competitive inhibitor of the BRD4 bromodomain (BD) on RSV-induced epithelial plasticity. We found that BRD4 activates RSV-inducible expression of major components of its functional interactome, including RELA, members of the Med coactivator complex, and SMARC subunits (**Figure 6**). Although BRD4 participates in transcriptional elongation (**Figure 5**), the global changes in chromatin accessibility seen in EMP suggests BRD4 may regulate gene programs through other mechanisms.

To address the question whether BRD4 dependent genes are regulated by changes in chromatin accessibility, we mapped the BRD4-dependent gene regulatory network to 1700 chromatin-accessible sites in the genome determined by Tn5 transposase-cleavage-next generation sequencing (ATAC-Seq) studies (Xu et al., 2020). Genome ontology and pathway enrichment indicated a substantial enrichment of genes controlling ECM biosynthesis and/or modification (Xu et al., 2021a). Specifically, we found that RSV produces nucleosome-free regions on *TGFB1/JUNB//FN1/MMP9* genes and *GFPT2* (Xu et al., 2020) (**Figure 7**). These studies indicate that BRD4 may play a critical role in mediating expression of this HBP-plasticity program through enhanced chromatin opening.

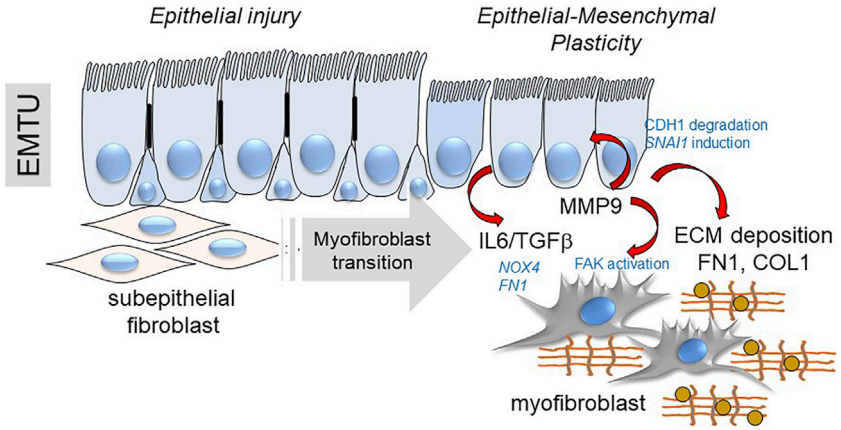

FIGURE 8 | EMP controls myofibroblast expansion. Shown is a schematic of the transition of the epithelial-mesenchymal trophic unit (EMTU) of the small airway. Under resting conditions, the small airway epithelium interacts with a thin sheath of subepithelial fibroblasts. In response to epithelial injury produced by respiratory viruses or aero-allergens, growth factors and matrix metalloproteinases released by injured epithelium trigger the subepithelial fibroblasts to acquire pro-fibrotic characteristics including expression of αSMA, FN1 and COL1 resulting in ECM expansion of the *lamina reticularis* of the airway.

RELATIONSHIP OF EMP TO SUBEPITHELIAL MYOFIBROBLAST EXPANSION

Although much of this work has focused on the mechanisms of EMP on the lower airway epithelial cell, how cell plasticity affects organ fibrosis are not fully understood. Noted earlier, epithelial cells do not themselves become myofibroblasts in the airway (Rock et al., 2011). However, epithelial plasticity may affect neighboring pro-fibrotic cells. Illustrated earlier in **Figure 1**, epithelial cells interact with subepithelial fibroblasts within an attenuated fibroblast sheath known as the EMTU (Evans et al., 1999). In response to aeroallergens or respiratory virus infection, subepithelial fibroblasts are one of several mesenchymal lineages that transition into αSMA and COL1-expressing myofibroblasts (Gizycki et al., 1997; Knight, 2001). Myofibroblasts are secretory phenotypes that produce ECM proteins and MMPs that contribute to *lamina reticularis* expansion in chronic airway disease (Brewster et al., 1990). Not only is this cell type primarily responsible for producing ECM and interstitial fibrosis (Hinz et al., 2007; Rock et al., 2011; Hung et al., 2013), these cells form the pathognomonic fibroblastic foci of human IPF (Hinz et al., 2007; Thannickal, 2012). With myofibroblast persistence, deposition of ECM stiffens the lungs, reducing normal elastic properties and pulmonary function.

The fibroblast-myofibroblast transition is mediated by growth factors (TGFβ, IL6), changes in ECM stiffness and matrix metalloproteinase secretion (Tian et al., 2017; Xu et al., 2021b); all initiated from EMP produced by epithelial injury/repair and sustained by the HBP. Epithelial barrier disruption induces secretion of epithelial growth factors (IL6, TGFβ, EGF) and fibrogenic cytokines (periostin, IL-17, IL-11) (Holgate et al., 2004). TGFβ activates signaling cascades that result in fibroblast motility, anti-apoptosis, and expression of ECM proteins, FN1 and COL1 (Ijaz et al., 2017).

Enhanced secretion of aberrantly glycosylated COL1 and FN proteoforms by epithelial and fibroblast plasticity result in changing the tensile strength of the ECM. Tensile strength is an important signal for pulmonary mesenchymal cell populations to acquire myofibroblast properties (Tomasek et al., 2002). In the presence of high ECM stress, FN1 splice products induce phosphorylation of focal adhesion kinases and αSMA replaces actin in stress fibers (Hinz et al., 2007). The effects of TGFβ and fibrogenic cytokines further stimulate metabolic adaptations in the myofibroblast population, leading to epigenetic changes resulting in enhanced production of ECM, resistance to apoptosis and migratory invasiveness (Horowitz et al., 2006; Henderson et al., 2019; Henderson and O'Reilly, 2021). Myofibroblasts also release inflammatory/profibrotic mediators that perpetuate epithelial injury and further promote ECM deposition (Powell et al., 1999).

Finally, MMPs released by EMP modify myofibroblast populations independently of changes in ECM composition. MMP9 has emerged as an important paracrine regulator of EMP in lung disease by its property to cleave CDH1 (Cowden Dahl et al., 2008), activating *SNAI1* expression (Lin et al., 2011) and through its paracrine effect expanding subepithelial myofibroblasts (Xu et al., 2021b). Intriguing studies have shown that MMP9 is directly recruited to the fibroblast membrane by lysyl hydroxylase three to activate αSMA expression and myofibroblast transition (Dayer and Stamenkovic, 2015). This mechanism plays an important role in RSV-induced remodeling and expansion of subepithelial myofibroblasts (**Figure 8**) (Brasier, 2020; Xu et al., 2021b). These intriguing data inform the hypothesis that innate inflammation in small airway epithelial cells is linked to EMP, and EMP triggers airway remodeling, in part through paracrine actions of MMP9.

CONCLUSION AND FUTURE DIRECTIONS

This review elaborates on the details of the hybrid E/M state, now referred to as "epithelial-mesenchymal plasticity". We illustrate mechanistic studies that have identified the innate NFκB pathway as a shared signaling pathway activated by aeroallergens and respiratory viruses. NFκB-IKK plays a central role in EMP by activating key gene regulatory networks controlling ECM synthesis, matrix modification and a core network of mesenchymal transcription factors by recruitment of the BRD4 coactivator that promotes transcriptional elongation and reprograms chromatin environment of growth factors and ECM genes. In addition, our exciting findings show that IKK participates in IRE1-XBPs pathway cross-talk, activating the hexosamine biosynthetic pathway. Here, IKK is responsible for phosphorylation, complex formation and stable nuclear retention of XBP1s. Action of the HBP is required for synthesis, folding and secretion of ECM modifying proteins, linked to myofibroblast expansion of subepithelial fibroblasts in the EMTU.

This work identifies key molecular pathways that can be modified to promote MET in response to common allergens and respiratory viruses to answer fundamental questions on the role of EMP in modification of airway immunity and remodeling.

AUTHOR CONTRIBUTIONS

Writing Editing, AB, DQ, and YZ.

FUNDING

NIAID 2P01AI062885 (ARB), U01 AI136994 (ARB), NCATS UL1TR002373 (ARB), NIAID 1R21AI133454 (YZ, ARB).

REFERENCES

Adams, T. S., Schupp, J. C., Poli, S., Ayaub, E. A., Neumark, N., Ahangari, F., et al. (2020). Single-Cell RNA-Seq Reveals Ectopic and Aberrant Lung-Resident Cell Populations in Idiopathic Pulmonary Fibrosis. *Sci. Adv.* 6 (28), eaba1983. doi:10.1126/sciadv.aba1983

Ahn, Y. H., Gibbons, D. L., Chakravarti, D., Creighton, C. J., Rizvi, Z. H., Adams, H. P., et al. (2012). ZEB1 Drives Prometastatic Actin Cytoskeletal Remodeling by Downregulating miR-34a Expression. *J. Clin. Invest.* 122 (9), 3170–3183. doi:10.1172/JCI63608

Aiello, N. M., Maddipati, R., Norgard, R. J., Balli, D., Li, J., Yuan, S., et al. (2018). Subtype Influences Epithelial Plasticity and Mode of Cell Migration. *Dev Cell.* 45 (6), 681–695. doi:10.1016/j.devcel.2018.05.027

Akella, N. M., Ciraku, L., and Reginato, M. J. (2019). Fueling the Fire: Emerging Role of the Hexosamine Biosynthetic Pathway in Cancer. *BMC Biol.* 17 (1), 52. doi:10.1186/s12915-019-0671-3

Arizmendi, N. G., Abel, M., Mihara, K., Davidson, C., Polley, D., Nadeem, A., et al. (2011). Mucosal Allergic Sensitization to Cockroach Allergens Is Dependent on Proteinase Activity and Proteinase-Activated Receptor-2 Activation. *J. Immunol.* 186 (5), 3164–3172. doi:10.4049/jimmunol.0903812

Asokananthan, N., Graham, P. T., Stewart, D. J., Bakker, A. J., Eidne, K. A., Thompson, P. J., et al. (2002). House Dust Mite Allergens Induce Proinflammatory Cytokines from Respiratory Epithelial Cells: The Cysteine Protease Allergen, Der P 1, Activates Protease-Activated Receptor (PAR)-2 and Inactivates PAR-1. *J. Immunol.* 169 (8), 4572–4578. doi:10.4049/jimmunol.169.8.4572

Bacsi, A., Dharajiya, N., Choudhury, B. K., Sur, S., and Boldogh, I. (2005). Effect of Pollen-Mediated Oxidative Stress on Immediate Hypersensitivity Reactions and Late-phase Inflammation in Allergic Conjunctivitis. *J. Allergy Clin. Immunol.* 116 (4), 836–843. doi:10.1016/j.jaci.2005.06.002

Bertolusso, R., Tian, B., Zhao, Y., Vergara, L., Sabree, A., Iwanaszko, M., et al. (2014). Dynamic Cross Talk Model of the Epithelial Innate Immune Response to Double-Stranded Rna Stimulation: Coordinated Dynamics Emerging from Cell-Level Noise. *PLoS ONE* 9 (4), e93396. doi:10.1371/journal.pone.0093396

Borchers, A. T., Chang, C., Gershwin, M. E., and Gershwin, L. J. (2013). Respiratory Syncytial Virus-Aa Comprehensive Review. *Clin. Rev. Allergy Immunol.* 45 (3), 331–379. doi:10.1007/s12016-013-8368-9

Bowden, D. H. (1983). Cell Turnover in the Lung. *Am. Rev. Respir. Dis.* 128 (2 Pt 2), S46–S48. doi:10.1164/arrd.1983.128.2P2.S46

Brasier, A. R., Tian, B., Jamaluddin, M., Kalita, M. K., Garofalo, R. P., and Lu, M. (2011). RelA Ser276 Phosphorylation-Coupled Lys310 Acetylation Controls Transcriptional Elongation of Inflammatory Cytokines in Respiratory Syncytial Virus Infection. *J. Virol.* 85 (22), 11752–11769. doi:10.1128/JVI.05360-11

Brasier, A. R. (2019). Mechanisms How Mucosal Innate Immunity Affects Progression of Allergic Airway Disease. *Expert Rev. Respir. Med.* 13 (4), 349–356. doi:10.1080/17476348.2019.1578211

Brasier, A. R. (2020). RSV Reprograms the CDK9*BRD4 Chromatin Remodeling Complex to Couple Innate Inflammation to Airway Remodeling. *Viruses* 12 (4), 472. doi:10.3390/v12040472

Brewster, C. E., Howarth, P. H., Djukanovic, R., Wilson, J., Holgate, S. T., and Roche, W. R. (1990). Myofibroblasts and Subepithelial Fibrosis in Bronchial Asthma. *Am. J. Respir. Cel Mol Biol* 3 (5), 507–511. doi:10.1165/ajrcmb/3.5.507

Burgel, P. R. (2011). The Role of Small Airways in Obstructive Airway Diseases. *Eur. Respir. Rev.* 20 (119), 23–33. doi:10.1183/09059180.00010410

Chang, H., Liu, Y., Xue, M., Liu, H., Du, S., Zhang, L., et al. (2016). Synergistic Action of Master Transcription Factors Controls Epithelial-To-Mesenchymal Transition. *Nucleic Acids Res.* 44 (6), 2514–2527. doi:10.1093/nar/gkw126

Choudhary, S., Boldogh, I., and Brasier, A. R. (2016). Inside-Out Signaling Pathways from Nuclear Reactive Oxygen Species Control Pulmonary Innate Immunity. *J. Innate Immun.* 8 (2), 143–155. doi:10.1159/000442254

Cowden Dahl, K. D., Symowicz, J., Ning, Y., Gutierrez, E., Fishman, D. A., Adley, B. P., et al. (2008). Matrix Metalloproteinase 9 Is a Mediator of Epidermal Growth Factor-dependent E-Cadherin Loss in Ovarian Carcinoma Cells. *Cancer Res.* 68 (12), 4606–4613. doi:10.1158/0008-5472.CAN-07-5046

Czerkies, M., Korwek, Z., Prus, W., Kochańczyk, M., Jaruszewicz-Błońska, J., Tudelska, K., et al. (2018). Cell Fate in Antiviral Response Arises in the Crosstalk of IRF, NF-Kb and JAK/STAT Pathways. *Nat. Commun.* 9 (1), 493. doi:10.1038/s41467-017-02640-8

Dayer, C., and Stamenkovic, I. (2015). Recruitment of Matrix Metalloproteinase-9 (MMP-9) to the fibroblast cell surface by Lysyl Hydroxylase-3 (LH3) triggers TGF-β activation and fibroblast differentiation. *J Biol Chem.* 22, 13763–78. doi:10.1074/jbc.M114.622274

Deprez, M., Zaragosi, L. E., Truchi, M., Becavin, C., Ruiz García, S., Arguel, M. J., et al. (2020). A Single-Cell Atlas of the Human Healthy Airways. *Am. J. Respir. Crit. Care Med.* 202 (12), 1636–1645. doi:10.1164/rccm.201911-2199OC

Devaiah, B. N., and Singer, D. S. (2012). Cross-Talk Among RNA Polymerase II Kinases Modulates C-Terminal Domain Phosphorylation. *J. Biol. Chem.* 287 (46), 38755–38766. doi:10.1074/jbc.M112.412015

Devaiah, B. N., Lewis, B. A., Cherman, N., Hewitt, M. C., Albrecht, B. K., Robey, P. G., et al. (2012). BRD4 Is an Atypical Kinase that Phosphorylates Serine2 of the RNA Polymerase II Carboxy-Terminal Domain. *Proc. Natl. Acad. Sci. U S A.* 109 (18), 6927–6932. doi:10.1073/pnas.1120422109

Devaiah, B. N., Case-Borden, C., Gegonne, A., Hsu, C. H., Chen, Q., Meerzaman, D., et al. (2016a). BRD4 Is a Histone Acetyltransferase that Evicts Nucleosomes from Chromatin. *Nat. Struct. Mol. Biol.* 23 (6), 540–548. doi:10.1038/nsmb.3228

Devaiah, B. N., Gegonne, A., and Singer, D. S. (2016b). Bromodomain 4: a Cellular Swiss Army Knife. *J. Leukoc. Biol.* 100 (4), 679–686. doi:10.1189/jlb.2RI0616-250R

Douwes, J., Zuidhof, A., Doekes, G., van der Zee, S. C., Wouters, I., Boezen, M. H., et al. (2000). (1-->3)-beta-D-glucan and Endotoxin in House Dust and Peak Flow Variability in Children. *Am. J. Respir. Crit. Care Med.* 162 (4 Pt 1), 1348–1354. doi:10.1164/ajrccm.162.4.9909118

Erjefält, J. S., Erjefält, I., Sundler, F., and Persson, C. G. (1995). *In Vivo* restitution of Airway Epithelium. *Cell Tissue Res* 281 (2), 305–316. doi:10.1007/BF00583399

Evans, M. J., Van Winkle, L. S., Fanucchi, M. V., and Plopper, C. G. (1999). The Attenuated Fibroblast Sheath of the Respiratory Tract Epithelial-Mesenchymal Trophic Unit. *Am. J. Respir. Cel Mol Biol* 21 (6), 655–657. doi:10.1165/ajrcmb.21.6.3807

Fauroux, B., Simões, E. A. F., Checchia, P. A., Paes, B., Figueras-Aloy, J., Manzoni, P., et al. (2017). The Burden and Long-Term Respiratory Morbidity Associated with Respiratory Syncytial Virus Infection in Early Childhood. *Infect. Dis. Ther.* 6 (2), 173–197. doi:10.1007/s40121-017-0151-4

Feng, Y. X., Sokol, E. S., Del Vecchio, C. A., Sanduja, S., Claessen, J. H., Proia, T. A., et al. (2014). Epithelial-to-mesenchymal Transition Activates PERK-eIF2α and Sensitizes Cells to Endoplasmic Reticulum Stress. *Cancer Discov.* 4 (6), 702–715. doi:10.1158/2159-8290.Cd-13-0945

Gizycki, M. J., Adelroth, E., Rogers, A. V., O'Byrne, P. M., and Jeffery, P. K. (1997). Myofibroblast Involvement in the Allergen-Induced Late Response in Mild Atopic Asthma. *Am. J. Respir. Cel Mol Biol* 16 (6), 664–673. doi:10.1165/ajrcmb.16.6.9191468

Harvey, B. G., Heguy, A., Leopold, P. L., Carolan, B. J., Ferris, B., and Crystal, R. G. (2007). Modification of Gene Expression of the Small Airway Epithelium in Response to Cigarette Smoking. *J. Mol. Med. (Berl)* 85 (1), 39–53. doi:10.1007/s00109-006-0103-z

Heijink, I. H., Postma, D. S., Noordhoek, J. A., Broekema, M., and Kapus, A. (2010). House Dust Mite-Promoted Epithelial-To-Mesenchymal Transition in Human Bronchial Epithelium. *Am. J. Respir. Cel Mol Biol* 42 (1), 69–79. doi:10.1165/rcmb.2008-0449OC

Henderson, J., and O'Reilly, S. (2021). The Emerging Role of Metabolism in Fibrosis. *Trends Endocrinol. Metab.* 32 (8), 639–653. doi:10.1016/j.tem.2021.05.003

Henderson, J., Distler, J., and O'Reilly, S. (2019). The Role of Epigenetic Modifications in Systemic Sclerosis: A Druggable Target. *Trends Mol. Med.* 25 (5), 395–411. doi:10.1016/j.molmed.2019.02.001

Hetz, C. (2012). The Unfolded Protein Response: Controlling Cell Fate Decisions under ER Stress and beyond. *Nat. Rev. Mol. Cel Biol* 13 (2), 89–102. doi:10.1038/nrm3270

Hinz, B., Phan, S. H., Thannickal, V. J., Galli, A., Bochaton-Piallat, M. L., and Gabbiani, G. (2007). The Myofibroblast: One Function, Multiple Origins. *Am. J. Pathol.* 170 (6), 1807–1816. doi:10.2353/ajpath.2007.070112

Hogg, J. C., Chu, F., Utokaparch, S., Woods, R., Elliott, W. M., Buzatu, L., et al. (2004). The Nature of Small-Airway Obstruction in Chronic Obstructive Pulmonary Disease. *N. Engl. J. Med.* 350 (26), 2645–2653. doi:10.1056/NEJMoa032158

Holgate, S. T., Davies, D. E., Lackie, P. M., Wilson, S. J., Puddicombe, S. M., and Lordan, J. L. (2000). Epithelial-Mesenchymal Interactions in the Pathogenesis of Asthma. *J. Allergy Clin. Immunol.* 105 (2 Pt 1), 193–204. doi:10.1016/s0091-6749(00)90066-6

Holgate, S. T., Holloway, J., Wilson, S., Bucchieri, F., Puddicombe, S., and Davies, D. E. (2004). Epithelial-Mesenchymal Communication in the Pathogenesis of Chronic Asthma. *Proc. Am. Thorac. Soc.* 1 (2), 93–98. doi:10.1513/pats.2306034

Horowitz, J. C., Cui, Z., Moore, T. A., Meier, T. R., Reddy, R. C., Toews, G. B., et al. (2006). Constitutive Activation of Prosurvival Signaling in Alveolar Mesenchymal Cells Isolated from Patients with Nonresolving Acute Respiratory Distress Syndrome. *Am. J. Physiol. Lung Cel Mol Physiol* 290 (3), L415–L425. doi:10.1152/ajplung.00276.2005

Hosoki, K., Boldogh, I., Aguilera-Aguirre, L., Sun, Q., Itazawa, T., Hazra, T., et al. (2016). Myeloid Differentiation Protein 2 Facilitates Pollen- and Cat Dander-Induced Innate and Allergic Airway Inflammation. *J. Allergy Clin. Immunol.* 137 (5), 1506–1513. doi:10.1016/j.jaci.2015.09.036

Hosoki, K., Brasier, A. R., Kurosky, A., Boldogh, I., and Sur, S. (2017a). Reply: Protease Plays a Role in Ragweed Pollen-Induced Neutrophil Recruitment and Epithelial Barrier Disruption. *Am. J. Respir. Cel Mol Biol* 56 (2), 272–273. doi:10.1165/rcmb.2016-0281LE

Hosoki, K., Redding, D., Itazawa, T., Chakraborty, A., Tapryal, N., Qian, S., et al. (2017b). Innate Mechanism of Pollen- and Cat Dander-Induced Oxidative Stress and DNA Damage in the Airways. *J. Allergy Clin. Immunol.* 140, 1436–e5. doi:10.1016/j.jaci.2017.04.044

Hui, D. S., Joynt, G. M., Wong, K. T., Gomersall, C. D., Li, T. S., Antonio, G., et al. (2005). Impact of Severe Acute Respiratory Syndrome (SARS) on Pulmonary Function, Functional Capacity and Quality of Life in a Cohort of Survivors. *Thorax* 60 (5), 401–409. doi:10.1136/thx.2004.030205

Hung, C., Linn, G., Chow, Y. H., Kobayashi, A., Mittelsteadt, K., Altemeier, W. A., et al. (2013). Role of Lung Pericytes and Resident Fibroblasts in the Pathogenesis of Pulmonary Fibrosis. *Am. J. Respir. Crit. Care Med.* 188 (7), 820–830. doi:10.1164/rccm.201212-2297OC

Ijaz, T., Pazdrak, K., Kalita, M., Konig, R., Choudhary, S., Tian, B., et al. (2014). Systems Biology Approaches to Understanding Epithelial Mesenchymal Transition (EMT) in Mucosal Remodeling and Signaling in Asthma. *World Allergy Organ. J.* 7 (1), 13. doi:10.1186/1939-4551-7-13

Ijaz, T., Jamaluddin, M., Zhao, Y., Zhang, Y., Jay, J., Finnerty, C. C., et al. (2017). Coordinate Activities of BRD4 and CDK9 in the Transcriptional Elongation Complex Are Required for TGFβ-Induced Nox4 Expression and Myofibroblast Transdifferentiation. *Cell Death Dis* 8 (2), e2606. doi:10.1038/cddis.2016.434

Jacquet, A. (2011). The Role of the House Dust Mite-Induced Innate Immunity in Development of Allergic Response. *Int. Arch. Allergy Immunol.* 155 (2), 95–105. doi:10.1159/000320375

Jia, D., Jolly, M. K., Boareto, M., Parsana, P., Mooney, S. M., Pienta, K. J., et al. (2015). OVOL Guides the Epithelial-Hybrid-Mesenchymal Transition. *Oncotarget* 6 (17), 15436–15448. doi:10.18632/oncotarget.3623

Johnson, J. E., Gonzales, R. A., Olson, S. J., Wright, P. F., and Graham, B. S. (2007). The Histopathology of Fatal Untreated Human Respiratory Syncytial Virus Infection. *Mod. Pathol.* 20 (1), 108–119. doi:10.1038/modpathol.3800725

Jolly, M. K., Tripathi, S. C., Jia, D., Mooney, S. M., Celiktas, M., Hanash, S. M., et al. (2016). Stability of the Hybrid Epithelial/mesenchymal Phenotype. *Oncotarget* 7 (19), 27067–27084. doi:10.18632/oncotarget.8166

Jolly, M. K., Somarelli, J. A., Sheth, M., Biddle, A., Tripathi, S. C., Armstrong, A. J., et al. (2019). Hybrid Epithelial/Mesenchymal Phenotypes Promote Metastasis and Therapy Resistance across Carcinomas. *Pharmacol. Ther.* 194, 161–184. doi:10.1016/j.pharmthera.2018.09.007

Jozwik, A., Habibi, M. S., Paras, A., Zhu, J., Guvenel, A., Dhariwal, J., et al. (2015). RSV-specific Airway Resident Memory CD8+ T Cells and Differential Disease Severity after Experimental Human Infection. *Nat. Commun.* 6, 10224. doi:10.1038/ncomms10224

Kalluri, R., and Weinberg, R. A. (2009). The Basics of Epithelial-Mesenchymal Transition. *J. Clin. Invest.* 119 (6), 1420–1428. doi:10.1172/JCI39104

Knight, D. A., and Holgate, S. T. (2003). The Airway Epithelium: Structural and Functional Properties in Health and Disease. *Respirology* 8 (4), 432–446. doi:10.1046/j.1440-1843.2003.00493.x

Knight, D. (2001). Epithelium-Fibroblast Interactions in Response to Airway Inflammation. *Immunol. Cel Biol* 79 (2), 160–164. doi:10.1046/j.1440-1711.2001.00988.x

Kopp, M. C., Larburu, N., Durairaj, V., Adams, C. J., and Ali, M. M. U. (2019). UPR Proteins IRE1 and PERK Switch BiP from Chaperone to ER Stress Sensor. *Nat. Struct. Mol. Biol.* 26 (11), 1053–1062. doi:10.1038/s41594-019-0324-9

Lambrecht, B. N., and Hammad, H. (2014). Allergens and the Airway Epithelium Response: Gateway to Allergic Sensitization. *J. Allergy Clin. Immunol.* 134 (3), 499–507. doi:10.1016/j.jaci.2014.06.036

Li, Y., Gong, W., Ma, X., Sun, X., Jiang, H., and Chen, T. (2015). Smad7 Maintains Epithelial Phenotype of Ovarian Cancer Stem-Like Cells and Supports Tumor Colonization by Mesenchymal-Epithelial Transition. *Mol. Med. Rep.* 11 (1), 309–316. doi:10.3892/mmr.2014.2714

Liesman, R. M., Buchholz, U. J., Luongo, C. L., Yang, L., Proia, A. D., DeVincenzo, J. P., et al. (2014). RSV-Encoded NS2 Promotes Epithelial Cell Shedding and Distal Airway Obstruction. *J. Clin. Invest.* 124 (5), 2219–2233. doi:10.1172/JCI72948

Lin, C. Y., Tsai, P. H., Kandaswami, C. C., Lee, P. P., Huang, C. J., Hwang, J. J., et al. (2011). Matrix Metalloproteinase-9 Cooperates with Transcription Factor Snail to Induce Epithelial-Mesenchymal Transition. *Cancer Sci.* 102 (4), 815–827. doi:10.1111/j.1349-7006.2011.01861.x

Lin, C., von der Thüsen, J., Daalhuisen, J., ten Brink, M., Crestani, B., van der Poll, T., et al. (2015). Protease-activated Receptor (PAR)-2 Is Required for PAR-1 Signalling in Pulmonary Fibrosis. *J. Cel Mol Med* 19 (6), 1346–1356. doi:10.1111/jcmm.12520

Lindner, P., Paul, S., Eckstein, M., Hampel, C., Muenzner, J. K., Erlenbach-Wuensch, K., et al. (2020). EMT Transcription Factor ZEB1 Alters the Epigenetic Landscape of Colorectal Cancer Cells. *Cel Death Dis* 11 (2), 147. doi:10.1038/s41419-020-2340-4

Liu, P., Jamaluddin, M., Li, K., Garofalo, R. P., Casola, A., and Brasier, A. R. (2007). Retinoic Acid-Inducible Gene I Mediates Early Antiviral Response and Toll-Like Receptor 3 Expression in Respiratory Syncytial Virus-Infected Airway Epithelial Cells. *J. Virol.* 81 (3), 1401–1411. doi:10.1128/JVI.01740-06

Liu, P., Li, K., Garofalo, R. P., and Brasier, A. R. (2008). Respiratory Syncytial Virus Induces RelA Release from Cytoplasmic 100-kDa NF-Kappa B2 Complexes via a Novel Retinoic Acid-Inducible Gene-I{Middle Dot}NF- Kappa B-Inducing Kinase Signaling Pathway. *J. Biol. Chem.* 283 (34), 23169–23178. doi:10.1074/jbc.M802729200

Lovén, J., Hoke, H. A., Lin, C. Y., Lau, A., Orlando, D. A., Vakoc, C. R., et al. (2013). Selective Inhibition of Tumor Oncogenes by Disruption of Super-enhancers. *Cell* 153 (2), 320–334. doi:10.1016/j.cell.2013.03.036

Lu, M., Jolly, M. K., Levine, H., Onuchic, J. N., and Ben-Jacob, E. (2013). MicroRNA-Based Regulation of Epithelial-Hybrid-Mesenchymal Fate Determination. *Proc. Natl. Acad. Sci. U S A.* 110 (45), 18144–18149. doi:10.1073/pnas.1318192110

Mann, M., Roberts, D. S., Zhu, Y., Li, Y., Zhou, J., Ge, Y., et al. (2021). Discovery of RSV-Induced BRD4 Protein Interactions Using Native Immunoprecipitation and Parallel Accumulation-Serial Fragmentation (PASEF) Mass Spectrometry. *Viruses* 13 (3), 454. doi:10.3390/v13030454

Martín-Vicente, M., González-Riaño, C., Barbas, C., Jiménez-SousaÁ., M. Á., Brochado-Kith, O., Resino, S., et al. (2020). Metabolic Changes during Respiratory Syncytial Virus Infection of Epithelial Cells. *PloS one* 15 (3), e0230844. doi:10.1371/journal.pone.0230844

Martinez, F. D. (2009). The Origins of Asthma and Chronic Obstructive Pulmonary Disease in Early Life. *Proc. Am. Thorac. Soc.* 6 (3), 272–277. doi:10.1513/pats.200808-092RM

Myall, K. J., Mukherjee, B., Castanheira, A. M., Lam, J. L., Benedetti, G., Mak, S. M., et al. (2021). Persistent Post-COVID-19 Interstitial Lung Disease. An Observational Study of Corticosteroid Treatment. *Ann. Am. Thorac. Soc.* 18 (5), 799–806. doi:10.1513/AnnalsATS.202008-1002OC

Nowak, D. E., Tian, B., Jamaluddin, M., Boldogh, I., Vergara, L. A., Choudhary, S., et al. (2008). RelA Ser276 Phosphorylation Is Required for Activation of a Subset of NF-KappaB-Dependent Genes by Recruiting Cyclin-Dependent Kinase 9/cyclin T1 Complexes. *Mol. Cel Biol* 28 (11), 3623–3638. doi:10.1128/MCB.01152-07

Olszewska-Pazdrak, B., Casola, A., Saito, T., Alam, R., Crowe, S. E., Mei, F., et al. (1998). Cell-specific Expression of RANTES, MCP-1, and MIP-1alpha by Lower Airway Epithelial Cells and Eosinophils Infected with Respiratory Syncytial Virus. *J. Virol.* 72, 4756–4764. doi:10.1128/JVI.72.6.4756-4764.1998

Peixoto, P., Etcheverry, A., Aubry, M., Missey, A., Lachat, C., Perrard, J., et al. (2019). EMT Is Associated with an Epigenetic Signature of ECM Remodeling Genes. *Cel Death Dis* 10 (3), 205. doi:10.1038/s41419-019-1397-4

Pott, S., and Lieb, J. D. (2015). What Are Super-Enhancers? *Nat. Genet.* 47 (1), 8–12. doi:10.1038/ng.3167

Powell, D. W., Mifflin, R. C., Valentich, J. D., Crowe, S. E., Saada, J. I., and West, A. B. (1999). Myofibroblasts. I. Paracrine Cells Important in Health and Disease. *Am. J. Physiol.* 277 (1), C1–C19. doi:10.1152/ajpcell.1999.277.1.C1

Qiao, D., Skibba, M., Xu, X., Garofalo, R. P., Zhao, Y., and Brasier, A. R. (2021). Paramyxovirus Replication Induces the Hexosamine Biosynthetic Pathway and Mesenchymal Transition via the IRE1α-XBP1s Arm of the Unfolded Protein Response. *Am. J. Physiol. Lung Cel Mol Physiol* 321 (3), L576–l594. doi:10.1152/ajplung.00127.2021

Rezaee, F., Meednu, N., Emo, J. A., Saatian, B., Chapman, T. J., Naydenov, N. G., et al. (2011). Polyinosinic:polycytidylic Acid Induces Protein Kinase D-dependent Disassembly of Apical Junctions and Barrier Dysfunction in Airway Epithelial Cells. *J. Allergy Clin. Immunol.* 128, 1216–1224. doi:10.1016/j.jaci.2011.08.035

Roca, H., Hernandez, J., Weidner, S., McEachin, R. C., Fuller, D., Sud, S., et al. (2013). Transcription Factors OVOL1 and OVOL2 Induce the Mesenchymal to Epithelial Transition in Human Cancer. *PloS one* 8 (10), e76773. doi:10.1371/journal.pone.0076773

Rock, J. R., Barkauskas, C. E., Cronce, M. J., Xue, Y., Harris, J. R., Liang, J., et al. (2011). Multiple Stromal Populations Contribute to Pulmonary Fibrosis without Evidence for Epithelial to Mesenchymal Transition. *Proc. Natl. Acad. Sci. U S A.* 108 (52), E1475–E1483. doi:10.1073/pnas.1117988108

Rohmann, K., Tschernig, T., Pabst, R., Goldmann, T., and Drömann, D. (2011). Innate Immunity in the Human Lung: Pathogen Recognition and Lung Disease. *Cel Tissue Res* 343 (1), 167–174. doi:10.1007/s00441-010-1048-7

Shi, T., McAllister, D. A., O'Brien, K. L., Simoes, E. A. F., Madhi, S. A., Gessner, B. D., et al. (2017). Global, Regional, and National Disease burden Estimates of Acute Lower Respiratory Infections Due to Respiratory Syncytial Virus in Young Children in 2015: a Systematic Review and Modelling Study. *Lancet* 390 (10098), 946–958. doi:10.1016/S0140-6736(17)30938-8

Shpacovitch, V., Feld, M., Bunnett, N. W., and Steinhoff, M. (2007). Protease-activated Receptors: Novel PARtners in Innate Immunity. *Trends Immunol.* 28 (12), 541–550. doi:10.1016/j.it.2007.09.001

Shpacovitch, V., Feld, M., Hollenberg, M. D., Luger, T. A., and Steinhoff, M. (2008). Role of Protease-Activated Receptors in Inflammatory Responses, Innate and Adaptive Immunity. *J. Leukoc. Biol.* 83 (6), 1309–1322. doi:10.1189/jlb.0108001

Siemens, H., Jackstadt, R., Hünten, S., Kaller, M., Menssen, A., Götz, U., et al. (2011). miR-34 and SNAIL Form a Double-Negative Feedback Loop to Regulate Epithelial-Mesenchymal Transitions. *Cell Cycle* 10 (24), 4256–4271. doi:10.4161/cc.10.24.18552

Skibba, M., Xu, X., Wiess, K., Huisken, J., and Brasier, A. R. (2021). Role of Secretoglobin+ (Club Cell) NFκB/RelA-Tgfβ Signaling in Aero-Allergen-Induced Epithelial Plasticity and Subepithelial Myofibroblast Transdifferentiation. *BMC Respir. Res. press*. doi:10.1186/s12931-021-01910-w

Sohal, S. S., Mahmood, M. Q., and Walters, E. H. (2014). Clinical Significance of Epithelial Mesenchymal Transition (EMT) in Chronic Obstructive Pulmonary Disease (COPD): Potential Target for Prevention of Airway Fibrosis and Lung Cancer. *Clin. Transl Med.* 3, 33. doi:10.1186/s40169-014-0033-2

Stockman, L. J., Curns, A. T., Anderson, L. J., and Fischer-Langley, G. (2012). Respiratory Syncytial Virus-Associated Hospitalizations Among Infants and Young Children in the United States, 1997-2006. *Pediatr. Infect. Dis. J.* 31 (1), 5–9. doi:10.1097/INF.0b013e31822e68e6

Subbalakshmi, A. R., Sahoo, S., Biswas, K., and Jolly, M. K. (2021). A Computational Systems Biology Approach Identifies SLUG as a Mediator of Partial Epithelial-Mesenchymal Transition (EMT). *Cells Tissues Organs* 10, 1–14. doi:10.1159/000512520

Thannickal, V. J. (2012). Mechanisms of Pulmonary Fibrosis: Role of Activated Myofibroblasts and NADPH Oxidase. *Fibrogenesis Tissue Repair* 5 (1), S23. doi:10.1186/1755-1536-5-s1-s23

Tian, B., Li, X., Kalita, M., Widen, S. G., Yang, J., Bhavnani, S. K., et al. (2015). Analysis of the TGFβ-Induced Program in Primary Airway Epithelial Cells Shows Essential Role of NF-κB/RelA Signaling Network in Type II Epithelial Mesenchymal Transition. *BMC Genomics* 16 (1), 529. doi:10.1186/s12864-015-1707-x

Tian, B., Zhao, Y., Sun, H., Zhang, Y., Yang, J., and Brasier, A. R. (2016). BRD4 Mediates NF-κb-Dependent Epithelial-Mesenchymal Transition and Pulmonary Fibrosis via Transcriptional Elongation. *Am. J. Physiol. Lung Cel Mol Physiol* 311 (6), L1183–l1201. doi:10.1152/ajplung.00224.2016

Tian, B., Patrikeev, I., Ochoa, L., Vargas, G., Belanger, K. K., Litvinov, J., et al. (2017). NF-κB Mediates Mesenchymal Transition, Remodeling, and Pulmonary Fibrosis in Response to Chronic Inflammation by Viral RNA Patterns. *Am. J. Respir. Cel Mol Biol* 56 (4), 506–520. doi:10.1165/rcmb.2016-0259OC

Tian, B., Liu, Z., Yang, J., Sun, H., Zhao, Y., Wakamiya, M., et al. (2018a). Selective Antagonists of the Bronchiolar Epithelial NF-Kb-Bromodomain-Containing Protein 4 Pathway in Viral-Induced Airway Inflammation. *Cell Rep* 23 (4), 1138–1151. doi:10.1016/j.celrep.2018.03.106

Tian, B., Widen, S. G., Yang, J., Wood, T. G., Kudlicki, A., Zhao, Y., et al. (2018b). The NFκB Subunit RELA Is a Master Transcriptional Regulator of the Committed Epithelial-Mesenchymal Transition in Airway Epithelial Cells. *J. Biol. Chem.* 293 (42), 16528–16545. doi:10.1074/jbc.RA118.003662

Tian, B., Yang, J., Zhao, Y., Ivanciuc, T., Sun, H., Wakamiya, M., et al. (2018c). Central Role of the NF-kappaB Pathway in the Scgb1a1-Expressing Epithelium in Mediating Respiratory Syncytial Virus-Induced Airway Inflammation. *J. Virol.* 92 (11), e00441. doi:10.1128/JVI.00441-18

Tian, B., Hosoki, K., Liu, Z., Yang, J., Zhao, Y., Sun, H., et al. (2019). Mucosal Bromodomain-Containing Protein 4 Mediates Aeroallergen-Induced Inflammation and Remodeling. *J. Allergy Clin. Immunol.* 143 (4), 1380–1394. doi:10.1016/j.jaci.2018.09.029

Tomasek, J. J., Gabbiani, G., Hinz, B., Chaponnier, C., and Brown, R. A. (2002). Myofibroblasts and Mechano-Regulation of Connective Tissue Remodelling. *Nat. Rev. Mol. Cel Biol* 3 (5), 349–363. doi:10.1038/nrm809

Vincent, T., Neve, E. P., Johnson, J. R., Kukalev, A., Rojo, F., Albanell, J., et al. (2009). A SNAIL1-Smad3/4 Transcriptional Repressor Complex Promotes TGF-Beta Mediated Epithelial-Mesenchymal Transition. *Nat. Cel Biol* 11 (8), 943–950. doi:10.1038/ncb1905

Whitsett, J. A., and Alenghat, T. (2015). Respiratory Epithelial Cells Orchestrate Pulmonary Innate Immunity. *Nat. Immunol.* 16 (1), 27–35. doi:10.1038/ni.3045

Wiesner, D. L., Merkhofer, R. M., Ober, C., Kujoth, G. C., Niu, M., Keller, N. P., et al. (2020). Club Cell TRPV4 Serves as a Damage Sensor Driving Lung Allergic Inflammation. *Cell Host Microbe* 27 (4), 614–628. doi:10.1016/j.chom.2020.02.006

Worrell, J. C., Leslie, J., Smith, G. R., Zaki, M. Y. W., Paish, H. L., Knox, A., et al. (2020). cRel Expression Regulates Distinct Transcriptional and Functional Profiles Driving Fibroblast Matrix Production in Systemic Sclerosis. *Rheumatology (Oxford)* 59 (12), 3939–3951. doi:10.1093/rheumatology/keaa272

Xu, X., Qiao, D., Mann, M., Garofalo, R. P., and Brasier, A. R. (2020). Respiratory Syncytial Virus Infection Induces Chromatin Remodeling to Activate Growth Factor and Extracellular Matrix Secretion Pathways. *Viruses* 12 (8), 804. doi:10.3390/v12080804

Xu, X., Mann, M., Qiao, D., Li, Y., Zhou, J., and Brasier, A. R. (2021a). Bromodomain Containing Protein 4 (BRD4) Regulates Expression of its Interacting Coactivators in the Innate Response to Respiratory Syncytial Virus. *Front. Mol. Biosciences* 8 (973), 728661. doi:10.3389/fmolb.2021.728661

Xu, X., Qiao, D., Dong, C., Mann, M., Garofalo, R. P., Keles, S., et al. (2021b). The SWI/SNF-Related, Matrix Associated, Actin-Dependent Regulator of Chromatin A4 Core Complex Represses Respiratory Syncytial Virus-Induced Syncytia Formation and Subepithelial Myofibroblast Transition. *Front. Immunol.* 12, 633654. doi:10.3389/fimmu.2021.633654

Yang, Z., Yik, J. H., Chen, R., He, N., Jang, M. K., Ozato, K., et al. (2005). Recruitment of P-TEFb for Stimulation of Transcriptional Elongation by the Bromodomain Protein Brd4. *Mol. Cel* 19 (4), 535–545. doi:10.1016/j.molcel.2005.06.029

Yang, J., Tian, B., and Brasier, A. R. (2017a). "Targeting Chromatin Remodeling in Inflammation and Fibrosis," in *Advances in Protein Chemistry and Structural Biology*. Editor R. Donev (Cambridge, MA: Elsevier).

Yang, J., Tian, B., Sun, H., Garofalo, R. P., and Brasier, A. R. (2017b). Epigenetic Silencing of IRF1 Dysregulates Type III Interferon Responses to Respiratory Virus Infection in Epithelial to Mesenchymal Transition. *Nat. Microbiol.* 2, 17086. doi:10.1038/nmicrobiol.2017.86

Yang, J., Antin, P., Berx, G., Blanpain, C., Brabletz, T., Bronner, M., et al. (2020). Guidelines and Definitions for Research on Epithelial-Mesenchymal Transition. *Nat. Rev. Mol. Cel Biol* 21 (6), 341–352. doi:10.1038/s41580-020-0237-9

Zaragosi, L. E., Deprez, M., and Barbry, P. (2020). Using Single-Cell RNA Sequencing to Unravel Cell Lineage Relationships in the Respiratory Tract. *Biochem. Soc. Trans.* 48 (1), 327–336. doi:10.1042/bst20191010

Zhang, Y., Luxon, B. A., Casola, A., Garofalo, R. P., Jamaluddin, M., and Brasier, A. R. (2001). Expression of Respiratory Syncytial Virus-Induced Chemokine Gene Networks in Lower Airway Epithelial Cells Revealed by cDNA Microarrays. *J. Virol.* 75 (19), 9044–9058. doi:10.1128/JVI.75.19.9044-9058.2001

Zhang, L., Peeples, M. E., Boucher, R. C., Collins, P. L., and Pickles, R. J. (2002). Respiratory Syncytial Virus Infection of Human Airway Epithelial Cells Is Polarized, Specific to Ciliated Cells, and without Obvious Cytopathology. *J. Virol.* 76 (11), 5654–5666. doi:10.1128/jvi.76.11.5654-5666.2002

Zhang, J., Tian, X. J., Zhang, H., Teng, Y., Li, R., Bai, F., et al. (2014). TGF-beta-induced Epithelial-To-Mesenchymal Transition Proceeds through Stepwise Activation of Multiple Feedback Loops. *Sci. Signal.* 7 (345), ra91. doi:10.1126/scisignal.2005304

Zhang, J., Jamaluddin, M., Zhang, Y., Widen, S. G., Sun, H., Brasier, A. R., et al. (2019). Type II Epithelial-Mesenchymal Transition Upregulates Protein N-Glycosylation to Maintain Proteostasis and Extracellular Matrix Production. *J. Proteome Res.* 18 (9), 3447–3460. doi:10.1021/acs.jproteome.9b00342

Zhao, Y., Tian, B., Sadygov, R. G., Zhang, Y., and Brasier, A. R. (2016). Integrative Proteomic Analysis Reveals Reprograming Tumor Necrosis Factor Signaling in Epithelial Mesenchymal Transition. *J. Proteomics* 148, 126–138. doi:10.1016/j.jprot.2016.07.014

Zhao, Y., Jamaluddin, M., Zhang, Y., Sun, H., Ivanciuc, T., Garofalo, R. P., et al. (2017). Systematic Analysis of Cell-type Differences in the Epithelial Secretome Reveals Insights into the Pathogenesis of Respiratory Syncytial Virus-Induced Lower Respiratory Tract Infections. *J. Immunol.* 198 (8), 3345–3364. doi:10.4049/jimmunol.1601291

Zhao, Y., Chahar, H. S., Komaravelli, N., Dossumekova, A., and Casola, A. (2019). Human Metapneumovirus Infection of Airway Epithelial Cells Is Associated with Changes in Core Metabolic Pathways. *Virology* 531, 183–191. doi:10.1016/j.virol.2019.03.011

Zhao, Y., Zhang, J., Sun, H., and Brasier, A. R. (2021). Crosstalk of the IκB Kinase with Spliced X-Box Binding Protein 1 Couples Inflammation with Glucose Metabolic Reprogramming in Epithelial-Mesenchymal Transition. *J. Proteome Res.* 20 (7), 3475–3488. doi:10.1021/acs.jproteome.1c00093

Conflict of Interest: The authors declare that the research was conducted in the absence of any commercial or financial relationships that could be construed as a potential conflict of interest.

Publisher's Note: All claims expressed in this article are solely those of the authors and do not necessarily represent those of their affiliated organizations, or those of the publisher, the editors and the reviewers. Any product that may be evaluated in this article, or claim that may be made by its manufacturer, is not guaranteed or endorsed by the publisher.

frontiers in Pharmacology

MINI REVIEW
published: 10 January 2022
doi: 10.3389/fphar.2021.830340

Emerging Therapeutic Strategies for Attenuating Tubular EMT and Kidney Fibrosis by Targeting Wnt/β-Catenin Signaling

Lichao Hu[†], *Mengyuan Ding*[†] *and Weichun He* [*‡]

Center for Kidney Disease, Second Affiliated Hospital, Nanjing Medical University, Nanjing, China

Epithelial-mesenchymal transition (EMT) is defined as a process in which differentiated epithelial cells undergo phenotypic transformation into myofibroblasts capable of producing extracellular matrix, and is generally regarded as an integral part of fibrogenesis after tissue injury. Although there is evidence that the complete EMT of tubular epithelial cells (TECs) is not a major contributor to interstitial myofibroblasts in kidney fibrosis, the partial EMT, a status that damaged TECs remain inside tubules, and co-express both epithelial and mesenchymal markers, has been demonstrated to be a crucial stage for intensifying fibrogenesis in the interstitium. The process of tubular EMT is governed by multiple intracellular pathways, among which Wnt/β-catenin signaling is considered to be essential mainly because it controls the transcriptome associated with EMT, making it a potential therapeutic target against kidney fibrosis. A growing body of data suggest that reducing the hyperactivity of Wnt/β-catenin by natural compounds, specific inhibitors, or manipulation of genes expression attenuates tubular EMT, and interstitial fibrogenesis in the TECs cultured under profibrotic environments and in animal models of kidney fibrosis. These emerging therapeutic strategies in basic researches may provide beneficial ideas for clinical prevention and treatment of chronic kidney disease.

Keywords: epithelial-mesenchymal transition, tubular epithelial cell, Wnt/β-catenin signaling, kidney fibrosis, myofibroblast

OPEN ACCESS

Edited by:
Pilar Sandoval,
Centre for Molecular Biology Severo Ochoa (CSIC), Spain

Reviewed by:
Dong Zhou,
University of Connecticut, United States

***Correspondence:**
Weichun He
heweichun@njmu.edu.cn

‡ORCID:
Weichun He
orcid.org/0000-0001-5685-7802

[†]*These authors have contributed equally to this work*

Specialty section:
This article was submitted to Inflammation Pharmacology, a section of the journal Frontiers in Pharmacology

Received: *07 December 2021*
Accepted: *20 December 2021*
Published: *10 January 2022*

Citation:
Hu L, Ding M and He W (2022) Emerging Therapeutic Strategies for Attenuating Tubular EMT and Kidney Fibrosis by Targeting Wnt/β-Catenin Signaling. Front. Pharmacol. 12:830340. doi: 10.3389/fphar.2021.830340

INTRODUCTION

Kidney fibrosis, a pathological process characterized by excessive deposition of extracellular matrix (ECM) in the interstitium accompanied by destruction of normal kidney architecture, is a hallmark and inevitable end point of all kinds of progressive chronic kidney disease (CKD). Myofibroblast is well known as the major type of matrix-producing cell, the source of which has long been controversial and remains a hot area of research in nephrology (Mack and Yanagita, 2015; Yuan et al., 2019). Based on much of the current data from studies using lineage tracing techniques, the main origins of myofibroblasts are accepted to be resident mesenchymal cells including fibroblast (Asada et al., 2011; Lebleu et al., 2013), pericyte (Humphreys et al., 2010; Gomez and Duffield, 2014), and mesenchymal stem cell (Kramann et al., 2015; El Agha et al., 2017; Kramann et al., 2017), and other precursors comprising circulating bone marrow-derived progenitor (Li et al., 2007; Lebleu et al., 2013), peritubular endothelial cell (Zeisberg et al., 2008;

Cruz-Solbes and Youker, 2017), and tubular epithelial cell (TEC) (Lebleu et al., 2013; Cruz-Solbes and Youker, 2017).

TEC, as a major component of renal parenchyma, is particularly vulnerable to damage during acute kidney injury (AKI) and is also a driving force for the progression of CKD. The involvement of epithelial-mesenchymal transition (EMT) in kidney fibrosis is widely concerned (Liu et al., 2018). EMT is traditionally defined as a phenotypic conversion programme in which the damaged TEC loses epithelial markers and acquires mesenchymal features (Liu, 2010; Cruz-Solbes and Youker, 2017). The contribution of this complete EMT to interstitial myofibroblasts appears to be very low (Lebleu et al., 2013), whereas the partial EMT is of more concern (Zhou and Liu, 2016; Sheng and Zhuang, 2020). Partial EMT refers to a status in which damaged TECs express both markers of epithelial and mesenchymal but remain inside tubules with G2/M phase cell cycle arrest, resulting in compromised regeneration and repair, impaired functionality, and altered secretome. EMT begins with stress responses of TEC to protect from damage and ultimately allows cells to acquire a secretory phenotype, leading to the release of pathological mediators that persistently activate various myofibroblast precursors. Partial EMT has been demonstrated to be an indispensable stage of fibrogenic progression, making inhibition of EMT one of the main strategies for restraining kidney fibrosis (Liu, 2010; Grande et al., 2015; Lovisa et al., 2015; Zhou and Liu, 2016).

EMT process is governed by sophisticated signal networks involving several developmental pathways, such as Wnt, Notch, and Hedgehog. Of them, the role of Wnt/β-catenin signaling is believed to be essential. Numerous studies have demonstrated that Wnt/β-catenin signaling is a potent mediator of EMT process. Hence, the intervention in EMT via modulating activity of this pathway is considered a promising therapeutic strategy against kidney fibrosis. In this mini review, we briefly discuss the mechanisms by which Wnt/β-catenin signaling regulates tubular EMT process, and summarize current strategies to interfere with EMT by modulating activity of this signaling.

WNT/β-CATENIN AND TUBULAR EMT

In canonical Wnt cascade, when Wnt ligands bind to receptors Frizzled protein (FZD) and lipoprotein receptor-related protein-5 or 6 (LRP5/6), Disheveled protein (Dvl) is recruited and a cytoplasmic destruction complex comprising proteins adenomatous polyposis coli (APC), Axin, casein kinase 1 (CK1), and glycogen synthase kinase 3β (GSK3β) is inhibited, resulting in de-phosphorylation, stabilization, and nuclear translocation of β-catenin. In the nucleus, the combination of β-catenin with T-cell factor and lymphoid enhancer-binding factor (TCF/LEF) initiates transcription of Wnt target genes (Clevers and Nusse, 2012; Nusse and Clevers, 2017). Wnt/β-catenin signaling seems quiescent in normal adult kidneys, whereas in injured kidneys, Wnt proteins are markedly induced. Transient activation of Wnt/β-catenin signaling favors cell regeneration and tissue repair after AKI, but its sustained activation aggravates kidney fibrosis in CKD progression (Zhou et al., 2013a; Zhou et al., 2013b; Tan et al., 2014; Schunk et al., 2021).

TECs are a main source of Wnt proteins in injured kidneys, and these ligands act in an autocrine or paracrine manner between several cell types. Activation of Wnt/β-catenin signaling induces transformation of TECs into a secretory phenotype with most partial EMT and a few complete EMT, induces proliferation, activation and differentiation of interstitial fibroblasts into myofibroblasts, and induces polarization M2 phenotype, and pro-inflammatory activation of macrophages. In turn, Wnt ligands derived from fibroblasts and macrophages can also target TECs directly (Schunk et al., 2021).

In TECs, Wnt/β-catenin signaling takes effects by inducing its target genes, some of which play the substantial roles in regulating tubular EMT process in the setting of CKD, such as fibroblast-specific protein 1 (FSP-1), fibronectin, matrix metalloproteinase 7 (MMP7), Snail, and Twist (Boutet et al., 2006; He et al., 2009; He et al., 2012; Tan et al., 2014; Ning et al., 2018). Concretely, FSP-1 and fibronectin are commonly used as EMT markers because they are not normally expressed in epithelial cells. FSP-1 is a marker for myofibroblasts, while fibronectin is a major component of ECM (Liu, 2011). MMP7, a secreted zinc- and calcium-dependent endopeptidase that acts on a variety of substrates to regulate various cellular processes, is a critical regulatory factor in EMT by mediating E-cadherin ectodomain shedding and proteolytic degradation (He et al., 2012; Zhou et al., 2017a; Liu et al., 2020). Snail and Twist are critical transcription factors that drive EMT programme. Conditional deletion of Snail or Twist1 in TECs inhibited EMT programme, which in turn alleviated interstitial fibrosis in several CKD models (Grande et al., 2015; Lovisa et al., 2015). We will briefly discuss the functions of the two proteins in controlling EMT in detail.

Snail is a member of the zinc finger 1 transcription factor family and is able to trigger the first step in EMT process by transcriptionally suppressing the expression of E-cadherin and disrupting adhesions between epithelial cells (Cano et al., 2000; Liu, 2004; Hao et al., 2011; Simon-Tillaux and Hertig, 2017). By repressing E-cadherin, Snail also releases β-catenin from the dissociating adherens junctions, thus further facilitating the cell to EMT programme, because in addition to intracellular β-catenin that can act as a signaling sensor after Wnt signal activation, β-catenin located near the cytoplasmic membrane can physically interact with E-cadherin (Wang et al., 2010). Moreover, Snail activates the production of alpha smooth muscle actin (α-SMA) and vimentin, two mesenchymal markers (Cano et al., 2000; Boutet et al., 2006), and induces Id1, a transcription antagonist that plays a crucial role in promoting EMT (Li et al., 2012). Besides being a transcriptional target of Wnt/β-catenin, Snail is post-transcriptionally modified by GSK3β and can cooperate with Wnt ligands to induce the signaling. Thus, when Wnt ligands initiate the signaling, the simultaneous activation of β-catenin, and Snail produces synergistic or additive effects in driving EMT (García de Herreros and Baulida, 2012; Schunk et al., 2021). In addition to EMT programming, Snail also controls other major biological processes responsible for renal fibrogenesis, such as

TABLE 1 | Potential modulations for inhibiting EMT and components of Wnt/β-catenin pathway involved.

Modulators or modulation methods for inhibiting tubular EMT	Factors that induce tubular EMT	Experimental models of CKD	Components of the pathway involved that are detected	References
Downregulation of β-Arrestin-1	β-arrestin-1; TGFβ1	UUO mice; TGFβ1-treated HK-2 cells	Wnt1, active β-catenin	Xu et al. (2018)
AGER1; Downregulation of RAGE; ICG-001	AOPP; Downregulation of AGER1	AOPP-treated HKC-8 cells	Wnt1, p-GSK3β, β-catenin, TCF4	Feng et al. (2020)
Overexpression of SIK1; Downregulation of β-catenin; Downregulation of Twist1	AA	AA-induced AKI-CKD transition mice; AA-treated HK-2 cells	Wnt1, p-β-catenin (Y654), nuclear β-catenin, Snail, Twist1	Hu et al. (2021)
U0126 (ERK1/2 inhibitor); Downregulation of ERK1/2	Uric acid	Hyperuricemic nephropathy rats	Wnt1, β-catenin	Liu et al. (2017), Tao et al. (2019)
Downregulation of MMP2; Minocycline (MMP inhibitor)	MMP2	UUO mice	Wnt1, β-catenin, Snail	Du et al. (2012)
25-O-methylalisol F (MAF)	TGFβ1; ANG	TGFβ1- or ANG-treated NRK-52E cells	Wnt1, active β-catenin, Snail1, Twist, MMP7, PAI-1, FSP-1	Chen et al. (2018a)
Vitexin	COM; Glyoxylate	Glyoxylate-induced nephrolithiasis mice; COM-treated HK-2 cells	Wnt1, p-β-catenin, β-catenin	Ding et al. (2021)
Astragaloside IV (AS-IV)	HG	Type 2 DKD rats; HG-treated HK-2 cells	Wnt1, β-catenin, nuclear β-catenin, GSK3β-APC-Axin protein complex	Wang et al. (2020)
Atractylenolide I (ATL-1)	TGFβ1	UUO mice; TGFβ1-treated NRK-52E cells	Wnt1, p-β-catenin/β-catenin	Guo et al. (2021)
Downregulation of WISP1	Uremia	Uremic rats	Wnt2b, c-Myc, cyclin D	Chen et al. (2019)
Downregulation of CRP	CRP; TGFβ1	STZ-induced DKD rats; TGFβ1 or CRP-treated HK-2 cells	Wnt3a, β-catenin	Zhang et al. (2019)
Overexpression of kallistatin	Downregulation of kallistatin; TGFβ1	TGFβ1-treated HK-2 cells; UUO mice	Wnt4, DKK1, Axin2, p-GSK3β (Ser9)/GSK3β, β-catenin, active β-catenin, fibronectin, Snail, PAI-1, Renin	Yiu et al. (2021)
Anti-FKN antibody; XAV939 (β-catenin inhibitor)	FKN; ANG	MRL/lpr mice; ANG-treated HK-2 cells	Wnt4, β-catenin, c-Myc, cyclin D1	Fu et al. (2019)
Downregulation of RSPO1; Downregulation of LGR4	RSPO1	High fat diet-induced obesity mice; Recombinant RSPO1-treated HK-2 cells	LRP6, p-GSK3β (Ser9)/GSK3β, active β-catenin, nuclear β-catenin	Carmon et al., 2011, Su et al., 2021
Overexpression of CFTR; iCRT14 (β-catenin inhibitor)	CFTR inhibitor (CFTRinh-172 or GlyH101); downregulation of CFTR	UUO mice; Hypoxia-treated MDCK cells and HK-2 cells	Dvl2, nuclear β-catenin, Axin2, Met, MMP7, MMP2, cyclin D2	Zhang et al. (2017)
Downregulation of DOCK4; Downregulation of USP36	USP36; HG	STZ-induced DKD mice; HG-treated HK-2 cells	β-catenin degradation complex, β-catenin	Zhu et al. (2021)
Overexpression of AMPKα2	Downregulation of AMPKα2	UUO mice; HKC cells with downregulated AMPKα2	β-catenin	Qiu et al. (2015)
Downregulation of FHL2	Overexpression of FHL2; TGFβ1	UUO mice; TGFβ1-treated NRK-52E cells	Active β-catenin, nuclear β-catenin, Snail, Twist, vimentin, PAI-1, MMP7	Cai et al. (2018)

RAGE, receptor of advanced glycation end-products; AGER1, advanced glycation end-products receptor 1; AOPP, advanced oxidative protein product; SIK1, salt inducible kinase 1; AA, aristolochic acid; ERK, extracellular signal-regulated kinase; MMP, matrix metalloproteinase; ANG, angiotensin II; COM, calcium oxalate monohydrate; HG, high glucose; DKD, diabetic kidney disease; GSK3β, glycogen synthase kinase-3β; APC, adenomatous polyposis coli; WISP1, Wnt-inducible signaling pathway protein-1; CRP, C-reactive protein; STZ, streptozotocin; FKN, fractalkine; RSPO1, R-spondin 1; LGR4, leucine-rich repeat-containing G protein coupled receptor 4; CFTR, cystic fibrosis transmembrane conductance regulator; MDCK, renal distal tubular Madin-Darby canine kidney; DOCK4, dedicator of cytokinesis 4; USP36, ubiquitin specific proteases 36; AMPK, AMP-activated protein kinase; FHL2, four and a half LIM domain protein 2.

interference of fatty acid metabolism, cell cycle arrest, and inflammation (Simon-Tillaux and Hertig, 2017). Furthermore, Snail-induced partial EMT could orchestrate p53-p21-mediated G2/M arrest via nuclear factor kappa B-mediated inflammation in CKD models (Qi et al., 2021).

Twist is a transcription factor of the basic helix-loop-helix class and is capable of not only repressing E-cadherin gene transcription by binding to the E-boxes in its promoter region but also inducing the expression of mesenchymal markers including fibronectin, vimentin, α-SMA, and N-cadherin (Howe et al., 2003; Yang et al., 2004; Kida et al., 2007). Additionally, Twist also regulates hypoxia-induced EMT in a hypoxia inducible factor-1 (HIF-1)-dependent manner in renal fibrosis (Bechtel and Zeisberg, 2009; Sun et al., 2009). Bmi1 is responsible for Twist1-induced EMT (Yang et al., 2010), and the promoter of Bmi1 contains potential binding sites for Twist1 and HIF-1α. Under hypoxic conditions, Twist1 and HIF-1α cooperatively enhanced Bmi1 transcriptional activation and controlled its downstream target genes including Snail and E-cadherin (Du et al., 2014; Ning et al., 2018).

In a short, sustained activation of Wnt/β-catenin signaling is a potent propeller of EMT. Therefore, it represents a promising therapeutic target to restrain tubular EMT process and mitigate kidney fibrosis.

EMERGING STRATEGIES TO SUPPRESS EMT BY TARGETING WNT/β-CATENIN

A great deal of strategies for hampering tubular EMT process and alleviating kidney fibrosis through inhibiting the activity of Wnt/β-catenin signaling in various animal or cellular models of CKD have been reported, in which the components of Wnt/β-catenin pathway were selectively or specifically detected for exploring the intrinsic relationship between the strategy and the change in the activity of the signaling. These studies are shown below based on the most upstream level of the components of the signaling pathway being examined and are summarized in **Table 1**.

Wnt1

β-Arrestin-1 is a negative adapter of G-protein-coupled receptors (GPCRs) and also acts as a scaffold protein that regulates various cellular functions independently of GPCR activation (Kendall and Luttrell, 2009). Xu et al. reported that β-arrestin-1 was induced in the fibrotic kidneys in mice with unilateral ureteral obstruction (UUO) and in the TGFβ1-treated TECs and renal fibroblasts. Gene silencing of β-arrestin-1 reduced EMT and fibroblasts activation and attenuated kidney fibrosis, as well as diminished the upregulation of Wnt1 mRNA and active β-catenin *in vivo* and *in vitro* (Xu et al., 2018).

Advanced oxidative protein product (AOPP), belonging to dityrosine-containing protein family, is a marker of protein glycoxidation closely related to oxidative stress. As a uremic toxin, AOPP has been found accumulation in patients with CKD. Chronic accumulation of AOPP aggravated kidney fibrosis in animal models (Shi et al., 2008). Feng et al. reported that AOPP induced EMT through activating receptor of advanced glycation end-products (RAGE)/Wnt/β-catenin pathway in the cultured TECs. Either ICG-001, an inhibitor of β-catenin, or RAGE knockout, or advanced glycation end-products receptor 1 (AGER1, an antagonist of RAGE), could inhibit AOPP-induced EMT. AOPP-induced upregulation of Wnt1, p-GSK3β, β-catenin, and TCF4 was suppressed by downregulation of RAGE (Feng et al., 2020).

Salt inducible kinase 1 (SIK1), a member of AMP-activated protein kinases (AMPKs) family, plays a key role in regulating metabolism, cell survival, and growth (Taub, 2019). Hu et al. reported that the expression of SIK1 was downregulated in the kidneys from mice with AKI-CKD transition induced by aristolochic acid (AA) and in AA-treated TECs, whereas upregulation of SIK1 alleviated EMT, inflammation and fibrogenesis, and impeded AKI-CKD transition. Mechanistically, overexpression of SIK1 inhibited AA-induced upregulation of Wnt1 and p-β-catenin (Y654), the increase in β-catenin nuclear translocation, and the upregulation of Snail and Twist1 (Hu et al., 2021).

Extracellular signal-regulated kinase-1 and 2 (ERK1/2) are serine/threonine kinases that have been found to be involved in uric acid-mediated EMT and the pathogenesis of hyperuricemic nephropathy (HN) (Liu et al., 2017). Tao et al. reported that inhibition of ERK1/2 by either U0126, a selective inhibitor of ERK1/2 pathway, or specific siRNA, mitigated EMT in the kidneys from HN rats through inactivation of multiple signaling pathways including Wnt/β-catenin. The induction of Wnt1 and β-catenin was remarkably suppressed by inhibition of ERK1/2 (Tao et al., 2019).

MMPs are a family of zinc-dependent proteases, and MMPs-mediated destruction of tubule basement membrane integrity was once believed to be a key step in promoting EMT (Cheng and Lovett, 2003; Cheng et al., 2006). Although the complete EMT is no longer considered a major contributor to interstitial myofibroblasts, MMPs still play a role in fibrogenesis. Du et al. reported that the activities of MMP2 and MMP9 were increased in the kidneys from UUO mice, while inactivation of MMP2 by either MMP2 knockout or minocycline, an inhibitor of MMPs, suppressed inflammation and EMT, and ameliorated kidney fibrosis. The upregulation of Wnt1, β-catenin, and Snail in the UUO kidneys were restrained by inhibition of MMP2 (Du et al., 2012).

Triterpenoid compounds are main active components in *Alismatis rhizoma*, a natural product with lipid-lowering and renoprotective effects (Tian et al., 2014; Ma et al., 2016). Chen et al. reported that 25-O-methylalisol F (MAF), a new triterpenoid compound, was able to inhibit TGFβ1- or angiotensin II (ANG)-induced EMT in TECs and renal fibroblast activation, respectively. The effect of MAF on EMT was related to its regulation of renin-angiotensin system, TGFβ1/Smad, and Wnt/β-catenin. TGFβ1- or ANG-induced upregulation of Wnt1, active β-catenin and downstream targets Snail1, Twist, MMP7, PAI-1, and FSP-1 were inhibited by MAF (Chen et al., 2018a).

Recurrent nephrolithiasis is a contributor to kidney fibrosis, and the pathogenesis involves oxidative stress, inflammation, apoptosis, and EMT (Khan et al., 2016). Vitexin (apigenin-8-C-β-D-glucopyranoside), a flavonoid monomer derived from *Ficus deltoidea*, bamboo, and dried hawthorn leaves, possesses biological effects including antivirus, anti-inflammatory, and anticancer (Xue et al., 2020; Yahaya et al., 2020). Ding et al. reported that vitexin alleviated crystal deposition and kidney injury in a mouse model of nephrolithiasis induced by glyoxylate and cell models of TECs and macrophages treated with calcium oxalate monohydrate (COM), and the protective role of vitexin was related to the inhibition of pyroptosis, apoptosis, EMT, and macrophage infiltration. The upregulation of Wnt1 and β-catenin and downregulation of p-β-catenin in COM-treated TECs were restrained by vitexin (Ding et al., 2021).

Astragaloside IV (AS-IV), a saponin extracted from *Astragalus membranaceus*, possesses rich pharmacological activities, including antioxidant stress, anti-inflammatory, anti-diabetes, and renal protection (Fu et al., 2014; Zhou et al., 2017b; Chen et al., 2018b). Wang et al. reported that AS-IV repressed EMT, fibrogenesis, oxidative stress, and inflammation by inactivating Wnt/β-catenin signaling in a rat model of type 2 diabetic kidney disease (DKD) and in high glucose (HG)-treated TECs. HG-induced upregulation of Wnt1 and β-catenin and an increase in nuclear β-catenin were inhibited by AS-IV. In addition, AS-IV could regulate the activity of Wnt/β-catenin signaling *via* binding to GSK3β-APC-Axin protein complex (Wang et al., 2020).

Atractylenolide I (ATL-1), a eudesmane-type sesquiterpenoid lactone derivative of *Rhizoma Atractylodis macrocephalae*,

possesses various biological activities including antioxidant and anticancer (Li et al., 2020). Guo et al. reported that ATL-1 inhibited EMT and fibroblasts activation in the kidneys from UUO mice and in TGFβ1-treated TECs and renal fibroblasts. ATL-1 suppressed the activities of several proliferation-related pathways including Wnt/β-catenin. The upregulation of Wnt1 and the decrease in p-β-catenin/β-catenin ratio in UUO kidneys were restrained by ATL-1 (Guo et al., 2021).

Wnt2b

Wnt-inducible signaling pathway protein-1 (WISP1, also known as CCN4), belonging to the CCN family of ECM proteins, is a downstream target of Wnt/β-catenin, and has been shown to be involved in fibrotic diseases (Murahovschi et al., 2015). Chen et al. reported that the expression of WISP1 was induced and Wnt/β-catenin signaling was activated in the kidneys from a rat model of uremia, while WISP1 gene silencing repressed tubular EMT through inhibiting Wnt/β-catenin signaling. The upregulation of Wnt2b, c-Myc, and cyclin D1 in uremia is inhibited by WISP1 deficiency (Chen et al., 2019).

Wnt3a

C-reactive protein (CRP), an acute phase plasma protein, is generally considered as a non-specific marker of inflammation (Pepys and Hirschfield, 2003), however, many studies have confirmed that CRP is involved in the pathogenesis of many diseases (Szalai, 2004; Zhang et al., 2015). Elevated CRP expression level has been found in DKD and CKD (Menon et al., 2005; Hayashino et al., 2014). Zhang et al. reported that CRP enhanced EMT in the kidneys from STZ-induced DKD rats and in the TGFβ1-treated TECs, and the effects of CRP on EMT involved Wnt/β-catenin and ERK signaling. CRP facilitated the upregulation of Wnt3a and β-catenin induced by TGFβ1 in TECs, whereas deficiency of CRP inhibited the induction of Wnt3a and β-catenin *in vivo* (Zhang et al., 2019).

Wnt4

Kallistatin is a serine protease inhibitor that regulates multiple pathways involving in various biological functions such as vasodilation, angiogenesis, oxidative stress, inflammation, and fibrosis (Huang et al., 2014; Chao et al., 2016; Yiu et al., 2016; Wang et al., 2017; Guo et al., 2018). Yiu et al. reported that kallistatin levels were markedly lower in the kidneys from CKD patients. In UUO mice, depletion of endogenous kallistatin resulted in aggravated tubular EMT and kidney fibrosis, while overexpression of kallistatin exerted kidney protective effects. Depletion of kallistatin increased the levels of Wnt4, p-GSK3β (Ser9)/GSK3β, Axin2, active β-catenin, and target genes of Wnt/β-catenin, whereas overexpression of kallistatin restrained the activation of Wnt/β-catenin. The regulatory effect of kallistatin on EMT and the activity of Wnt/β-catenin pathway in TGFβ1-treated TECs was similar to that *in vivo* (Yiu et al., 2021).

Fractalkine (FKN), also known as chemokine (C-X3-C motif) ligand 1, is a chemokine that regulates cell adhesion and growth and has been shown to be involved in the pathogenesis of inflammatory diseases including autoimmune disease (Ruchaya et al., 2014; Liao et al., 2017). Fu et al. reported that FKN was induced in the kidneys from MRL/lpr mice (a murine model of lupus nephritis). Treatment with an anti-FKN antibody suppressed EMT and fibrogenesis and improved renal function along with suppressing the activation of Wnt/β-catenin signaling, whereas the administration of recombinant FKN exhibited the opposite effects. The effect of FKN on EMT and the activation of Wnt/β-catenin in ANG-treated TECs was similar to that *in vivo*. Inactivation of Wnt/β-catenin by an antagonist XAV939 blockaded the enhancement of FKN overexpression to the EMT. The affected components of the pathway by FKN included Wnt4, β-catenin, c-Myc, and cyclin D1 (Fu et al., 2019).

LRP6

R-spondin1 (RSPO1), a member of secretory protein RSPOs family, possesses a high affinity with leucine-rich repeat-containing G protein coupled receptor 4 (LGR4). RSPO1 has been identified as an activator of Wnt/β-catenin signaling because the binding of LGR4 and RSPO1 enhanced Wnt-induced phosphorylation of LRP6 (Carmon et al., 2011). It has been found that circulating RSPO1 was remarkably elevated in patients with obesity and insulin resistant (Kang et al., 2019). Su et al. reported that the expression of RSPO1 was induced in the kidneys from obesity mice fed with high-fat diet, while knockdown of RSPO1 alleviated kidney injury and fibrogenesis. The recombinant RSPO1 facilitated EMT process by binding to LGR4 to activate Wnt/β-catenin signaling, represented by an increase in active β-catenin and nuclear β-catenin in TECs, whereas these effects of RSPO1 could be diminished by downregulation of LGR4 (Su et al., 2021).

Degradation Complex

Cystic fibrosis transmembrane conductance regulator (CFTR), a cAMP-activated Cl^- channel, is abundantly expressed at the apical surfaces of proximal, and distal tubules in normal kidneys (Kibble et al., 2000; Morales et al., 2000). Zhang et al. reported that the expression of CFTR was downregulated in the fibrotic kidneys from both CKD patients and UUO mice and in the TECs cultured under hypoxia condition. Suppression of CFTR function or expression by CFTR inhibitor, CFTRinh-172 or GlyH101, is sufficient to trigger EMT process *in vitro*. Knockdown of CFTR increased nuclear β-catenin, enhanced β-catenin-mediated transcriptional activity, and upregulated the expression of target genes, whereas iCRT14, a β-catenin inhibitor, blocked the effect of CFTR downregulation on EMT. Mechanistically, the interaction of CFTR and Dvl2 *via* PDZ domain appears to contribute to the inhibitory effect of CFTR on β-catenin activity (Zhang et al., 2017).

Dedicator of cytokinesis 4 (DOCK4), a guanine nucleotide exchange factor for Rac, has been reported to enhance the stability and activity of β-catenin and induce EMT by interacting with β-catenin degradation complex to increase the level of cellular β-catenin response to Wnt ligands (Upadhyay et al., 2008; Xie et al., 2020). Zhu et al. reported that the expression of ubiquitin specific proteases 36 (USP36), a member of deubiquitinating enzymes family, was induced in DKD in

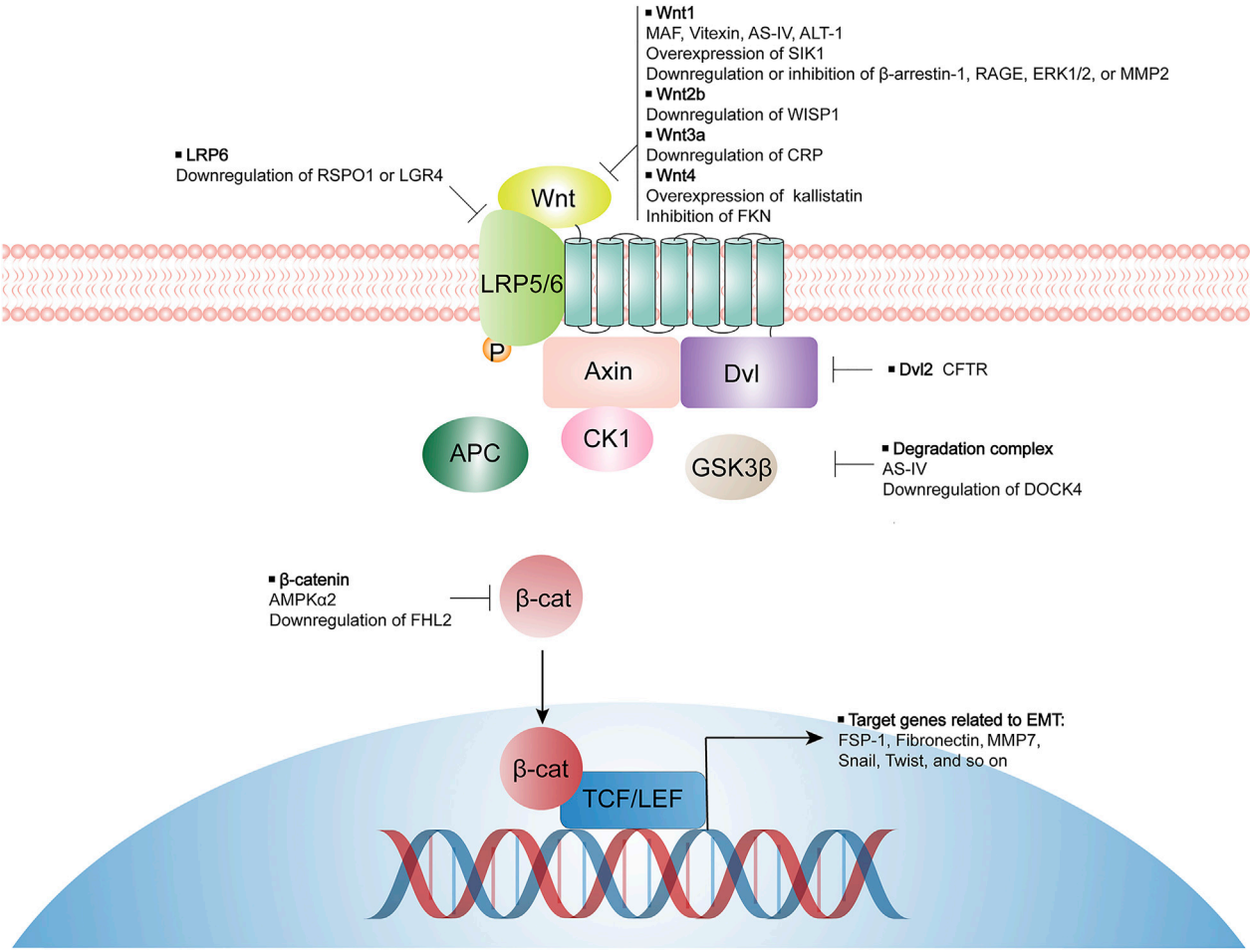

FIGURE 1 | Modulators for inhibiting tubular EMT and their potential targeted components of Wnt/β-catenin pathway. LRP, lipoprotein receptor-related protein; Dvl, disheveled; GSK3β, glycogen synthase kinase-3β; APC, adenomatous polyposis coli; MAF, 25-O-methylalisol F; AS-IV, Astragaloside IV; ATL-1, Atractylenolide I; SIK1, salt inducible kinase 1; RAGE, receptor of advanced glycation end-products; ERK, extracellular signal-regulated kinase; MMP, matrix metalloproteinase; WISP1, Wnt-inducible signaling pathway protein-1; CRP, C-reactive protein; FKN, fractalkine; RSPO1, R-spondin 1; LGR4, leucine-rich repeat-containing G protein coupled receptor 4; CFTR, cystic fibrosis transmembrane conductance regulator; DOCK4, dedicator of cytokinesis 4; AMPK, AMP-activated protein kinase; FHL2, four and a half LIM domain protein 2.

human and murine model and in HG-treated TECs, and the overexpression of USP36 enhanced EMT in TECs. Additionally, USP36 directly bound to and mediated the de-ubiquitination of DOCK4, whereas DOCK4 knockdown effectively abolished EMT induced by USP36 overexpression through suppressing Wnt/β-catenin signaling in TECs (Zhu et al., 2021).

β-Catenin

AMPK, a heterotrimeric serine/threonine protein kinase, functions as an energy sensor in response to stresses, and regulates cell energy balance and differentiation (Mihaylova and Shaw, 2011; Ruderman et al., 2013). Qiu et al. reported that knockdown of AMPKα, especially AMPKα2, enhanced EMT by activating Wnt/β-catenin and TGFβ/Smad signaling in TECs, and AMPKα2 deficiency exacerbated EMT and inflammation and promoted fibrogenesis in the kidneys from UUO mice. The results in this study demonstrated that AMPKα2 was able to decrease the expression of β-catenin in TECs (Qiu et al., 2015).

Four and a half LIM domain protein 2 (FHL2) belongs to the members of FHL subfamily that is included in LIM-only proteins family. FHL2 acts as a scaffold protein interacting with various intracellular protein partners, enabling it to regulate signaling pathways that involve a plethora of cellular tasks (Tran et al., 2016). We have reported that FHL2 was upregulated in the fibrotic kidneys in CKD patients and in UUO mice and in the TGFβ1-treated TECs (Cai et al., 2018; Duan et al., 2020). Overexpression of FHL2 promoted EMT, whereas downregulation of FHL2 suppressed EMT induced by TGFβ1. The interaction between FHL2 and β-catenin in TECs was increased by TGFβ1, and knockdown of FHL2 increased β-catenin phosphorylation and decreased nuclear localization of β-

catenin, β-catenin-mediated transcription and its target genes expression (Cai et al., 2018).

DISCUSSION

Although TECs undergoing conventional EMT are no longer recognized as a major constituent of interstitial myofibroblasts, the partial EMT has been demonstrated to exert the crucial functions in the fibrogenesis during kidney fibrosis progression. Given the importance of Wnt/β-catenin signaling in the regulation of EMT, targeting this pathway to restrain tubular EMT process has become a promising strategy for inhibiting kidney fibrosis, which has attracted numerous researchers to conduct relevant studies.

Data from animal models and cell experiments suggest that inhibiting Wnt/β-catenin signaling activity by either natural compounds, specific inhibitors, or manipulation of selective genes expression, may effectively suppress tubular EMT process and mitigate kidney interstitial fibrosis. Some of these studies have deeply investigated the mechanism by which Wnt/β-catenin activity is inhibited, while others have only observed the inhibitory effect of certain modulators on Wnt/β-catenin activity but not the mechanism of the signaling activity inhibition. Potential targeted components of Wnt/β-catenin pathway by various modulators are summarized in **Figure 1**. In conclusion, targeting Wnt/β-catenin signaling precisely to impede EMT process remains a challenge but one that carries great opportunities for the inhibition of kidney fibrosis and the therapy of CKD.

AUTHOR CONTRIBUTIONS

LH and MD wrote the article. WH conceived, wrote, and revised the article.

FUNDING

This work was supported by grants from the National Nature Science Foundation of China (81170659/H0509 and 31571169/C110201) to WH and the Postgraduate Research Practice Innovation Program of Jiangsu Province (SJCX21_0648) to MD.

REFERENCES

Asada, N., Takase, M., Nakamura, J., Oguchi, A., Asada, M., Suzuki, N., et al. (2011). Dysfunction of Fibroblasts of Extrarenal Origin Underlies Renal Fibrosis and Renal Anemia in Mice. *J. Clin. Invest.* 121, 3981–3990. doi:10.1172/JCI57301

Bechtel, W., and Zeisberg, M. (2009). Twist: a New Link from Hypoxia to Fibrosis. *Kidney Int.* 75, 1255–1256. doi:10.1038/ki.2009.102

Boutet, A., De Frutos, C. A., Maxwell, P. H., Mayol, M. J., Romero, J., and Nieto, M. A. (2006). Snail Activation Disrupts Tissue Homeostasis and Induces Fibrosis in the Adult Kidney. *EMBO J.* 25, 5603–5613. doi:10.1038/sj.emboj.7601421

Cai, T., Sun, D., Duan, Y., Qiu, Y., Dai, C., Yang, J., et al. (2018). FHL2 Promotes Tubular Epithelial-To-Mesenchymal Transition through Modulating β-catenin Signalling. *J. Cel Mol Med* 22, 1684–1695. doi:10.1111/jcmm.13446

Cano, A., Pérez-Moreno, M. A., Rodrigo, I., Locascio, A., Blanco, M. J., Del Barrio, M. G., et al. (2000). The Transcription Factor Snail Controls Epithelial-Mesenchymal Transitions by Repressing E-Cadherin Expression. *Nat. Cel Biol* 2, 76–83. doi:10.1038/35000025

Carmon, K. S., Gong, X., Lin, Q., Thomas, A., and Liu, Q. (2011). R-spondins Function as Ligands of the Orphan Receptors LGR4 and LGR5 to Regulate Wnt/beta-Catenin Signaling. *Proc. Natl. Acad. Sci. U S A.* 108, 11452–11457. doi:10.1073/pnas.1106083108

Chao, J., Bledsoe, G., and Chao, L. (2016). Protective Role of Kallistatin in Vascular and Organ Injury. *Hypertension* 68, 533–541. doi:10.1161/HYPERTENSIONAHA.116.07861

Chen, H., Yang, T., Wang, M. C., Chen, D. Q., Yang, Y., and Zhao, Y. Y. (2018a). Novel RAS Inhibitor 25-O-Methylalisol F Attenuates Epithelial-To-Mesenchymal Transition and Tubulo-Interstitial Fibrosis by Selectively Inhibiting TGF-β-Mediated Smad3 Phosphorylation. *Phytomedicine* 42, 207–218. doi:10.1016/j.phymed.2018.03.034

Chen, Q., Su, Y., Ju, Y., Ma, K., Li, W., and Li, W. (2018b). Astragalosides IV Protected the Renal Tubular Epithelial Cells from Free Fatty Acids-Induced Injury by Reducing Oxidative Stress and Apoptosis. *Biomed. Pharmacother.* 108, 679–686. doi:10.1016/j.biopha.2018.09.049

Chen, Y. Z., Sun, D. Q., Zheng, Y., Zheng, G. K., Chen, R. Q., Lin, M., et al. (2019). WISP1 Silencing Confers protection against Epithelial-Mesenchymal Transition of Renal Tubular Epithelial Cells in Rats via Inactivation of the Wnt/β-Catenin Signaling Pathway in Uremia. *J. Cel Physiol* 234, 9673–9686. doi:10.1002/jcp.27654

Cheng, S., and Lovett, D. H. (2003). Gelatinase A (MMP-2) Is Necessary and Sufficient for Renal Tubular Cell Epithelial-Mesenchymal Transformation. *Am. J. Pathol.* 162, 1937–1949. doi:10.1016/S0002-9440(10)64327-1

Cheng, S., Pollock, A. S., Mahimkar, R., Olson, J. L., and Lovett, D. H. (2006). Matrix Metalloproteinase 2 and Basement Membrane Integrity: a Unifying Mechanism for Progressive Renal Injury. *FASEB J.* 20, 1898–1900. doi:10.1096/fj.06-5898fje

Clevers, H., and Nusse, R. (2012). Wnt/β-catenin Signaling and Disease. *Cell* 149, 1192–1205. doi:10.1016/j.cell.2012.05.012

Cruz-Solbes, A. S., and Youker, K. (2017). Epithelial to Mesenchymal Transition (EMT) and Endothelial to Mesenchymal Transition (EndMT): Role and Implications in Kidney Fibrosis. *Results Probl. Cel Differ* 60, 345–372. doi:10.1007/978-3-319-51436-9_13

Ding, T., Zhao, T., Li, Y., Liu, Z., Ding, J., Ji, B., et al. (2021). Vitexin Exerts Protective Effects against Calcium Oxalate crystal-induced Kidney Pyroptosis *In Vivo* and *In Vitro*. *Phytomedicine* 86, 153562. doi:10.1016/j.phymed.2021.153562

Du, R., Xia, L., Ning, X., Liu, L., Sun, W., Huang, C., et al. (2014). Hypoxia-induced Bmi1 Promotes Renal Tubular Epithelial Cell-Mesenchymal Transition and Renal Fibrosis via PI3K/Akt Signal. *Mol. Biol. Cel* 25, 2650–2659. doi:10.1091/mbc.E14-01-0044

Du, X., Shimizu, A., Masuda, Y., Kuwahara, N., Arai, T., Kataoka, M., et al. (2012). Involvement of Matrix Metalloproteinase-2 in the Development of Renal Interstitial Fibrosis in Mouse Obstructive Nephropathy. *Lab. Invest.* 92, 1149–1160. doi:10.1038/labinvest.2012.68

Duan, Y., Qiu, Y., Huang, X., Dai, C., Yang, J., and He, W. (2020). Deletion of FHL2 in Fibroblasts Attenuates Fibroblasts Activation and Kidney Fibrosis via Restraining TGF-B1-Induced Wnt/β-Catenin Signaling. *J. Mol. Med. (Berl)* 98, 291–307. doi:10.1007/s00109-019-01870-1

El Agha, E., Kramann, R., Schneider, R. K., Li, X., Seeger, W., Humphreys, B. D., et al. (2017). Mesenchymal Stem Cells in Fibrotic Disease. *Cell stem cell* 21, 166–177. doi:10.1016/j.stem.2017.07.011

Feng, H., Hu, H., Zheng, P., Xun, T., Wu, S., Yang, X., et al. (2020). AGE Receptor 1 Silencing Enhances Advanced Oxidative Protein Product-Induced Epithelial-To-Mesenchymal Transition of Human Kidney Proximal Tubular Epithelial Cells via RAGE Activation. *Biochem. Biophys. Res. Commun.* 529, 1201–1208. doi:10.1016/j.bbrc.2020.06.144

Fu, D., Senouthai, S., Wang, J., and You, Y. (2019). FKN Facilitates HK-2 Cell EMT and Tubulointerstitial Lesions via the Wnt/β-Catenin Pathway in a Murine

Model of Lupus Nephritis. *Front. Immunol.* 10, 784. doi:10.3389/fimmu.2019.00784

Fu, J., Wang, Z., Huang, L., Zheng, S., Wang, D., Chen, S., et al. (2014). Review of the Botanical Characteristics, Phytochemistry, and Pharmacology of Astragalus Membranaceus (Huangqi). *Phytother Res.* 28, 1275–1283. doi:10.1002/ptr.5188

García de Herreros, A., and Baulida, J. (2012). Cooperation, Amplification, and Feed-Back in Epithelial-Mesenchymal Transition. *Biochim. Biophys. Acta* 1825, 223–228. doi:10.1016/j.bbcan.2012.01.003

Gomez, I. G., and Duffield, J. S. (2014). The FOXD1 Lineage of Kidney Perivascular Cells and Myofibroblasts: Functions and Responses to Injury. *Kidney Int. Suppl. (2011)* 4, 26–33. doi:10.1038/kisup.2014.6

Grande, M. T., Sánchez-Laorden, B., López-Blau, C., De Frutos, C. A., Boutet, A., Arévalo, M., et al. (2015). Snail1-induced Partial Epithelial-To-Mesenchymal Transition Drives Renal Fibrosis in Mice and Can Be Targeted to Reverse Established Disease. *Nat. Med.* 21, 989–997. doi:10.1038/nm.3901

Guo, Y., Chao, L., and Chao, J. (2018). Kallistatin Attenuates Endothelial Senescence by Modulating Let-7g-Mediated miR-34a-SIRT1-eNOS Pathway. *J. Cel Mol Med* 22, 4387–4398. doi:10.1111/jcmm.13734

Guo, Y., Xiao, Y., Zhu, H., Guo, H., Zhou, Y., Shentu, Y., et al. (2021). Inhibition of Proliferation-Linked Signaling Cascades with Atractylenolide I Reduces Myofibroblastic Phenotype and Renal Fibrosis. *Biochem. Pharmacol.* 183, 114344. doi:10.1016/j.bcp.2020.114344

Hao, S., He, W., Li, Y., Ding, H., Hou, Y., Nie, J., et al. (2011). Targeted Inhibition of β-catenin/CBP Signaling Ameliorates Renal Interstitial Fibrosis. *J. Am. Soc. Nephrol.* 22, 1642–1653. doi:10.1681/ASN.2010101079

Hayashino, Y., Mashitani, T., Tsujii, S., and Ishii, H. (2014). Diabetes, D., and Care Registry at Tenri Study, GSerum High-Sensitivity C-Reactive Protein Levels Are Associated with High Risk of Development, Not Progression, of Diabetic Nephropathy Among Japanese Type 2 Diabetic Patients: a Prospective Cohort Study (Diabetes Distress and Care Registry at Tenri [DDCRT7]). *Dia Care* 37, 2947–2952. doi:10.2337/dc14-1357

He, W., Dai, C., Li, Y., Zeng, G., Monga, S. P., and Liu, Y. (2009). Wnt/beta-catenin Signaling Promotes Renal Interstitial Fibrosis. *J. Am. Soc. Nephrol.* 20, 765–776. doi:10.1681/ASN.2008060566

He, W., Tan, R. J., Li, Y., Wang, D., Nie, J., Hou, F. F., et al. (2012). Matrix Metalloproteinase-7 as a Surrogate Marker Predicts Renal Wnt/β-Catenin Activity in CKD. *J. Am. Soc. Nephrol.* 23, 294–304. doi:10.1681/ASN.2011050490

Howe, L. R., Watanabe, O., Leonard, J., and Brown, A. M. (2003). Twist Is Up-Regulated in Response to Wnt1 and Inhibits Mouse Mammary Cell Differentiation. *Cancer Res.* 63, 1906–1913. doi:10.1016/s0165-7836(03)00126-7

Hu, J., Qiao, J., Yu, Q., Liu, B., Zhen, J., Liu, Y., et al. (2021). Role of SIK1 in the Transition of Acute Kidney Injury into Chronic Kidney Disease. *J. Transl Med.* 19, 69. doi:10.1186/s12967-021-02717-5

Huang, K. F., Huang, X. P., Xiao, G. Q., Yang, H. Y., Lin, J. S., and Diao, Y. (2014). Kallistatin, a Novel Anti-angiogenesis Agent, Inhibits Angiogenesis via Inhibition of the NF-Kb Signaling Pathway. *Biomed. Pharmacother.* 68, 455–461. doi:10.1016/j.biopha.2014.03.005

Humphreys, B. D., Lin, S. L., Kobayashi, A., Hudson, T. E., Nowlin, B. T., Bonventre, J. V., et al. (2010). Fate Tracing Reveals the Pericyte and Not Epithelial Origin of Myofibroblasts in Kidney Fibrosis. *Am. J. Pathol.* 176, 85–97. doi:10.2353/ajpath.2010.090517

Kang, Y. E., Kim, J. M., Yi, H. S., Joung, K. H., Lee, J. H., Kim, H. J., et al. (2019). Serum R-Spondin 1 Is a New Surrogate Marker for Obesity and Insulin Resistance. *Diabetes Metab. J.* 43, 368–376. doi:10.4093/dmj.2018.0066

Kendall, R. T., and Luttrell, L. M. (2009). Diversity in Arrestin Function. *Cell Mol Life Sci* 66, 2953–2973. doi:10.1007/s00018-009-0088-1

Khan, S. R., Pearle, M. S., Robertson, W. G., Gambaro, G., Canales, B. K., Doizi, S., et al. (2016). Kidney Stones. *Nat. Rev. Dis. Primers* 2, 16008. doi:10.1038/nrdp.2016.8

Kibble, J. D., Neal, A. M., Colledge, W. H., Green, R., and Taylor, C. J. (2000). Evidence for Cystic Fibrosis Transmembrane Conductance Regulator-dependent Sodium Reabsorption in Kidney, Using Cftr(tm2cam) Mice. *J. Physiol.* 526 (Pt 1), 27–34. doi:10.1111/j.1469-7793.2000.00027.x

Kida, Y., Asahina, K., Teraoka, H., Gitelman, I., and Sato, T. (2007). Twist Relates to Tubular Epithelial-Mesenchymal Transition and Interstitial Fibrogenesis in the Obstructed Kidney. *J. Histochem. Cytochem.* 55, 661–673. doi:10.1369/jhc.6A7157.2007

Kramann, R., Fleig, S. V., Schneider, R. K., Fabian, S. L., Dirocco, D. P., Maarouf, O., et al. (2015). Pharmacological GLI2 Inhibition Prevents Myofibroblast Cell-Cycle Progression and Reduces Kidney Fibrosis. *J. Clin. Invest.* 125, 2935–2951. doi:10.1172/JCI74929

Kramann, R., Wongboonsin, J., Chang-Panesso, M., Machado, F. G., and Humphreys, B. D. (2017). Gli1+ Pericyte Loss Induces Capillary Rarefaction and Proximal Tubular Injury. *J. Am. Soc. Nephrol.* 28, 776–784. doi:10.1681/ASN.2016030297

Lebleu, V. S., Taduri, G., O'connell, J., Teng, Y., Cooke, V. G., Woda, C., et al. (2013). Origin and Function of Myofibroblasts in Kidney Fibrosis. *Nat. Med.* 19, 1047–1053. doi:10.1038/nm.3218

Li, J., Deane, J. A., Campanale, N. V., Bertram, J. F., and Ricardo, S. D. (2007). The Contribution of Bone Marrow-Derived Cells to the Development of Renal Interstitial Fibrosis. *Stem cells* 25, 697–706. doi:10.1634/stemcells.2006-0133

Li, Y., Wang, Y., Liu, Z., Guo, X., Miao, Z., and Ma, S. (2020). Atractylenolide I Induces Apoptosis and Suppresses Glycolysis by Blocking the JAK2/STAT3 Signaling Pathway in Colorectal Cancer Cells. *Front. Pharmacol.* 11, 273. doi:10.3389/fphar.2020.00273

Li, Y., Wen, X., and Liu, Y. (2012). Tubular Cell Dedifferentiation and Peritubular Inflammation Are Coupled by the Transcription Regulator Id1 in Renal Fibrogenesis. *Kidney Int.* 81, 880–891. doi:10.1038/ki.2011.469

Liao, X., Ren, J., Reihl, A., Pirapakaran, T., Sreekumar, B., Cecere, T. E., et al. (2017). Renal-infiltrating CD11c+ Cells Are Pathogenic in Murine Lupus Nephritis through Promoting CD4+ T Cell Responses. *Clin. Exp. Immunol.* 190, 187–200. doi:10.1111/cei.13017

Liu, B. C., Tang, T. T., Lv, L. L., and Lan, H. Y. (2018). Renal Tubule Injury: a Driving Force toward Chronic Kidney Disease. *Kidney Int.* 93, 568–579. doi:10.1016/j.kint.2017.09.033

Liu, N., Xu, L., Shi, Y., Fang, L., Gu, H., Wang, H., et al. (2017). Pharmacologic Targeting ERK1/2 Attenuates the Development and Progression of Hyperuricemic Nephropathy in Rats. *Oncotarget* 8, 33807–33826. doi:10.18632/oncotarget.16995

Liu, Y. (2011). Cellular and Molecular Mechanisms of Renal Fibrosis. *Nat. Rev. Nephrol.* 7, 684–696. doi:10.1038/nrneph.2011.149

Liu, Y. (2004). Epithelial to Mesenchymal Transition in Renal Fibrogenesis: Pathologic Significance, Molecular Mechanism, and Therapeutic Intervention. *J. Am. Soc. Nephrol.* 15, 1–12. doi:10.1097/01.asn.0000106015.29070.e7

Liu, Y. (2010). New Insights into Epithelial-Mesenchymal Transition in Kidney Fibrosis. *J. Am. Soc. Nephrol.* 21, 212–222. doi:10.1681/ASN.2008121226

Liu, Z., Tan, R. J., and Liu, Y. (2020). The Many Faces of Matrix Metalloproteinase-7 in Kidney Diseases. *Biomolecules* 10, 960. doi:10.3390/biom10060960

Lovisa, S., Lebleu, V. S., Tampe, B., Sugimoto, H., Vadnagara, K., Carstens, J. L., et al. (2015). Epithelial-to-mesenchymal Transition Induces Cell Cycle Arrest and Parenchymal Damage in Renal Fibrosis. *Nat. Med.* 21, 998–1009. doi:10.1038/nm.3902

Ma, Q., Han, L., Bi, X., Wang, X., Mu, Y., Guan, P., et al. (2016). Structures and Biological Activities of the Triterpenoids and Sesquiterpenoids from Alisma Orientale. *Phytochemistry* 131, 150–157. doi:10.1016/j.phytochem.2016.08.015

Mack, M., and Yanagita, M. (2015). Origin of Myofibroblasts and Cellular Events Triggering Fibrosis. *Kidney Int.* 87, 297–307. doi:10.1038/ki.2014.287

Menon, V., Greene, T., Wang, X., Pereira, A. A., Marcovina, S. M., Beck, G. J., et al. (2005). C-reactive Protein and Albumin as Predictors of All-Cause and Cardiovascular Mortality in Chronic Kidney Disease. *Kidney Int.* 68, 766–772. doi:10.1111/j.1523-1755.2005.00455.x

Mihaylova, M. M., and Shaw, R. J. (2011). The AMPK Signalling Pathway Coordinates Cell Growth, Autophagy and Metabolism. *Nat. Cel Biol* 13, 1016–1023. doi:10.1038/ncb2329

Morales, M. M., Falkenstein, D., and Lopes, A. G. (2000). The Cystic Fibrosis Transmembrane Regulator (CFTR) in the Kidney. *Acad. Bras Cienc* 72, 399–406. doi:10.1590/s0001-37652000000300013

Murahovschi, V., Pivovarova, O., Ilkavets, I., Dmitrieva, R. M., Döcke, S., Keyhani-Nejad, F., et al. (2015). WISP1 Is a Novel Adipokine Linked to Inflammation in Obesity. *Diabetes* 64, 856–866. doi:10.2337/db14-0444

Ning, X., Zhang, K., Wu, Q., Liu, M., and Sun, S. (2018). Emerging Role of Twist1 in Fibrotic Diseases. *J. Cel Mol Med* 22, 1383–1391. doi:10.1111/jcmm.13465

Nusse, R., and Clevers, H. (2017). Wnt/β-Catenin Signaling, Disease, and Emerging Therapeutic Modalities. *Cell* 169, 985–999. doi:10.1016/j.cell.2017.05.016

Pepys, M. B., and Hirschfield, G. M. (2003). C-reactive Protein: a Critical Update. *J. Clin. Invest.* 111, 1805–1812. doi:10.1172/JCI18921

Qi, R., Wang, J., Jiang, Y., Qiu, Y., Xu, M., Rong, R., et al. (2021). Snai1-induced Partial Epithelial-Mesenchymal Transition Orchestrates P53-P21-Mediated G2/M Arrest in the Progression of Renal Fibrosis via NF-Kb-Mediated Inflammation. *Cell Death Dis* 12, 44. doi:10.1038/s41419-020-03322-y

Qiu, S., Xiao, Z., Piao, C., Zhang, J., Dong, Y., Cui, W., et al. (2015). AMPKα2 Reduces Renal Epithelial Transdifferentiation and Inflammation after Injury through Interaction with CK2β. *J. Pathol.* 237, 330–342. doi:10.1002/path.4579

Ruchaya, P. J., Antunes, V. R., Paton, J. F., Murphy, D., and Yao, S. T. (2014). The Cardiovascular Actions of fractalkine/CX3CL1 in the Hypothalamic Paraventricular Nucleus Are Attenuated in Rats with Heart Failure. *Exp. Physiol.* 99, 111–122. doi:10.1113/expphysiol.2013.075432

Ruderman, N. B., Carling, D., Prentki, M., and Cacicedo, J. M. (2013). AMPK, Insulin Resistance, and the Metabolic Syndrome. *J. Clin. Invest.* 123, 2764–2772. doi:10.1172/JCI67227

Schunk, S. J., Floege, J., Fliser, D., and Speer, T. (2021). WNT-β-catenin Signalling - a Versatile Player in Kidney Injury and Repair. *Nat. Rev. Nephrol.* 17, 172–184. doi:10.1038/s41581-020-00343-w

Sheng, L., and Zhuang, S. (2020). New Insights into the Role and Mechanism of Partial Epithelial-Mesenchymal Transition in Kidney Fibrosis. *Front. Physiol.* 11, 569322. doi:10.3389/fphys.2020.569322

Shi, X. Y., Hou, F. F., Niu, H. X., Wang, G. B., Xie, D., Guo, Z. J., et al. (2008). Advanced Oxidation Protein Products Promote Inflammation in Diabetic Kidney through Activation of Renal Nicotinamide Adenine Dinucleotide Phosphate Oxidase. *Endocrinology* 149, 1829–1839. doi:10.1210/en.2007-1544

Simon-Tillaux, N., and Hertig, A. (2017). Snail and Kidney Fibrosis. *Nephrol. Dial. Transplant.* 32, 224–233. doi:10.1093/ndt/gfw333

Su, X., Zhou, G., Tian, M., Wu, S., and Wang, Y. (2021). Silencing of RSPO1 Mitigates Obesity-Related Renal Fibrosis in Mice by Deactivating Wnt/β-Catenin Pathway. *Exp. Cel Res* 405, 112713. doi:10.1016/j.yexcr.2021.112713

Sun, S., Ning, X., Zhang, Y., Lu, Y., Nie, Y., Han, S., et al. (2009). Hypoxia-inducible Factor-1alpha Induces Twist Expression in Tubular Epithelial Cells Subjected to Hypoxia, Leading to Epithelial-To-Mesenchymal Transition. *Kidney Int.* 75, 1278–1287. doi:10.1038/ki.2009.62

Szalai, A. J. (2004). C-reactive Protein (CRP) and Autoimmune Disease: Facts and Conjectures. *Clin. Dev. Immunol.* 11, 221–226. doi:10.1080/17402520400001751

Tan, R. J., Zhou, D., Zhou, L., and Liu, Y. (2014). Wnt/β-catenin Signaling and Kidney Fibrosis. *Kidney Int. Suppl. (2011)* 4, 84–90. doi:10.1038/kisup.2014.16

Tao, M., Shi, Y., Tang, L., Wang, Y., Fang, L., Jiang, W., et al. (2019). Blockade of ERK1/2 by U0126 Alleviates Uric Acid-Induced EMT and Tubular Cell Injury in Rats with Hyperuricemic Nephropathy. *Am. J. Physiol. Ren. Physiol* 316, F660–F673. doi:10.1152/ajprenal.00480.2018

Taub, M. (2019). Salt Inducible Kinase Signaling Networks: Implications for Acute Kidney Injury and Therapeutic Potential. *Int. J. Mol. Sci.* 20, 3219. doi:10.3390/ijms20133219

Tian, T., Chen, H., and Zhao, Y. Y. (2014). Traditional Uses, Phytochemistry, Pharmacology, Toxicology and Quality Control of Alisma Orientale (Sam.) Juzep: a Review. *J. Ethnopharmacol* 158 (Pt A), 373–387. doi:10.1016/j.jep.2014.10.061

Tran, M. K., Kurakula, K., Koenis, D. S., and De Vries, C. J. (2016). Protein-protein Interactions of the LIM-Only Protein FHL2 and Functional Implication of the Interactions Relevant in Cardiovascular Disease. *Biochim. Biophys. Acta* 1863, 219–228. doi:10.1016/j.bbamcr.2015.11.002

Upadhyay, G., Goessling, W., North, T. E., Xavier, R., Zon, L. I., and Yajnik, V. (2008). Molecular Association between Beta-Catenin Degradation Complex and Rac Guanine Exchange Factor DOCK4 Is Essential for Wnt/beta-Catenin Signaling. *Oncogene* 27, 5845–5855. doi:10.1038/onc.2008.202

Wang, E., Wang, L., Ding, R., Zhai, M., Ge, R., Zhou, P., et al. (2020). Astragaloside IV Acts through Multi-Scale Mechanisms to Effectively Reduce Diabetic Nephropathy. *Pharmacol. Res.* 157, 104831. doi:10.1016/j.phrs.2020.104831

Wang, Q., Sun, Z. X., Allgayer, H., and Yang, H. S. (2010). Downregulation of E-Cadherin Is an Essential Event in Activating Beta-catenin/Tcf-dependent Transcription and Expression of its Target Genes in Pdcd4 Knockdown Cells. *Oncogene* 29, 128–138. doi:10.1038/onc.2009.302

Wang, T., Shi, F., Wang, J., Liu, Z., and Su, J. (2017). Kallistatin Suppresses Cell Proliferation and Invasion and Promotes Apoptosis in Cervical Cancer through Blocking NF-Kb Signaling. *Oncol. Res.* 25, 809–817. doi:10.3727/096504016X14799180778233

Xie, L., Zhai, R., Chen, T., Gao, C., Xue, R., Wang, N., et al. (2020). Panax Notoginseng Ameliorates Podocyte EMT by Targeting the Wnt/β-Catenin Signaling Pathway in STZ-Induced Diabetic Rats. *Drug Des. Devel Ther.* 14, 527–538. doi:10.2147/DDDT.S235491

Xu, H., Li, Q., Liu, J., Zhu, J., Li, L., Wang, Z., et al. (2018). β-Arrestin-1 Deficiency Ameliorates Renal Interstitial Fibrosis by Blocking Wnt1/β-Catenin Signaling in Mice. *J. Mol. Med.* 96, 97–109. doi:10.1007/s00109-017-1606-5

Xue, W., Wang, X., Tang, H., Sun, F., Zhu, H., Huang, D., et al. (2020). Vitexin Attenuates Myocardial Ischemia/reperfusion Injury in Rats by Regulating Mitochondrial Dysfunction Induced by Mitochondrial Dynamics Imbalance. *Biomed. Pharmacother.* 124, 109849. doi:10.1016/j.biopha.2020.109849

Yahaya, M. A. F., Zolkiffly, S. Z. I., Moklas, M. A. M., Hamid, H. A., Stanslas, J., Zainol, M., et al. (2020). Possible Epigenetic Role of Vitexin in Regulating Neuroinflammation in Alzheimer's Disease. *J. Immunol. Res.* 2020, 9469210. doi:10.1155/2020/9469210

Yang, J., Mani, S. A., Donaher, J. L., Ramaswamy, S., Itzykson, R. A., Come, C., et al. (2004). Twist, a Master Regulator of Morphogenesis, Plays an Essential Role in Tumor Metastasis. *Cell* 117, 927–939. doi:10.1016/j.cell.2004.06.006

Yang, M. H., Hsu, D. S., Wang, H. W., Wang, H. J., Lan, H. Y., Yang, W. H., et al. (2010). Bmi1 Is Essential in Twist1-Induced Epithelial-Mesenchymal Transition. *Nat. Cel Biol* 12, 982–992. doi:10.1038/ncb2099

Yiu, W. H., Li, Y., Lok, S. W. Y., Chan, K. W., Chan, L. Y. Y., Leung, J. C. K., et al. (2021). Protective Role of Kallistatin in Renal Fibrosis via Modulation of Wnt/β-Catenin Signaling. *Clin. Sci. (Lond)* 135, 429–446. doi:10.1042/CS20201161

Yiu, W. H., Wong, D. W., Wu, H. J., Li, R. X., Yam, I., Chan, L. Y., et al. (2016). Kallistatin Protects against Diabetic Nephropathy in Db/db Mice by Suppressing AGE-RAGE-Induced Oxidative Stress. *Kidney Int.* 89, 386–398. doi:10.1038/ki.2015.331

Yuan, Q., Tan, R. J., and Liu, Y. (2019). Myofibroblast in Kidney Fibrosis: Origin, Activation, and Regulation. *Adv. Exp. Med. Biol.* 1165, 253–283. doi:10.1007/978-981-13-8871-2_12

Zeisberg, E. M., Potenta, S. E., Sugimoto, H., Zeisberg, M., and Kalluri, R. (2008). Fibroblasts in Kidney Fibrosis Emerge via Endothelial-To-Mesenchymal Transition. *J. Am. Soc. Nephrol.* 19, 2282–2287. doi:10.1681/ASN.2008050513

Zhang, J. T., Wang, Y., Chen, J. J., Zhang, X. H., Dong, J. D., Tsang, L. L., et al. (2017). Defective CFTR Leads to Aberrant β-catenin Activation and Kidney Fibrosis. *Sci. Rep.* 7, 5233. doi:10.1038/s41598-017-05435-5

Zhang, L., Liu, S. H., Wright, T. T., Shen, Z. Y., Li, H. Y., Zhu, W., et al. (2015). C-reactive Protein Directly Suppresses Th1 Cell Differentiation and Alleviates Experimental Autoimmune Encephalomyelitis. *J. Immunol.* 194, 5243–5252. doi:10.4049/jimmunol.1402909

Zhang, L., Shen, Z. Y., Wang, K., Li, W., Shi, J. M., Osoro, E. K., et al. (2019). C-reactive Protein Exacerbates Epithelial-Mesenchymal Transition through Wnt/β-Catenin and ERK Signaling in Streptozocin-Induced Diabetic Nephropathy. *FASEB J.* 33, 6551–6563. doi:10.1096/fj.201801865RR

Zhou, D., and Liu, Y. (2016). Renal Fibrosis in 2015: Understanding the Mechanisms of Kidney Fibrosis. *Nat. Rev. Nephrol.* 12, 68–70. doi:10.1038/nrneph.2015.215

Zhou, D., Tan, R. J., Zhou, L., Li, Y., and Liu, Y. (2013a). Kidney Tubular β-catenin Signaling Controls Interstitial Fibroblast Fate via Epithelial-Mesenchymal Communication. *Sci. Rep.* 3, 1878. doi:10.1038/srep01878

Zhou, D., Tian, Y., Sun, L., Zhou, L., Xiao, L., Tan, R. J., et al. (2017a). Matrix Metalloproteinase-7 Is a Urinary Biomarker and Pathogenic Mediator of Kidney Fibrosis. *J. Am. Soc. Nephrol.* 28, 598–611. doi:10.1681/ASN.2016030354

Zhou, L., Li, Y., Zhou, D., Tan, R. J., and Liu, Y. (2013b). Loss of Klotho Contributes to Kidney Injury by Derepression of Wnt/β-Catenin Signaling. *J. Am. Soc. Nephrol.* 24, 771–785. doi:10.1681/ASN.2012080865

Zhou, X., Sun, X., Gong, X., Yang, Y., Chen, C., Shan, G., et al. (2017b). Astragaloside IV from Astragalus Membranaceus Ameliorates Renal Interstitial Fibrosis by Inhibiting Inflammation via TLR4/NF-κb *In Vivo* and *In Vitro*. *Int. Immunopharmacol* 42, 18–24. doi:10.1016/j.intimp.2016.11.006

Zhu, S., Hou, S., Lu, Y., Sheng, W., Cui, Z., Dong, T., et al. (2021). USP36-Mediated Deubiquitination of DOCK4 Contributes to the Diabetic Renal Tubular Epithelial Cell Injury via Wnt/β-Catenin Signaling Pathway. *Front Cel Dev Biol* 9, 638477. doi:10.3389/fcell.2021.638477

Conflict of Interest: The authors declare that the research was conducted in the absence of any commercial or financial relationships that could be construed as a potential conflict of interest.

Publisher's Note: All claims expressed in this article are solely those of the authors and do not necessarily represent those of their affiliated organizations, or those of the publisher, the editors and the reviewers. Any product that may be evaluated in this article, or claim that may be made by its manufacturer, is not guaranteed or endorsed by the publisher.

frontiers in Pharmacology

REVIEW
published: 03 February 2022
doi: 10.3389/fphar.2022.826839

Contributions of Immune Cells and Stromal Cells to the Pathogenesis of Systemic Sclerosis: Recent Insights

Bingying Dai[1], *Liqing Ding*[1], *Lijuan Zhao*[1], *Honglin Zhu*[1,2,3]* *and Hui Luo*[1,2,3]*

[1]*Department of Rheumatology and Immunology, Xiangya Hospital, Central South University, Changsha, China,* [2]*Provincial Clinical Research Center for Rheumatic and Immunologic Diseases, Xiangya Hospital, Changsha, China,* [3]*National Clinical Research Center for Geriatric Disorders, Xiangya Hospital, Changsha, China*

Systemic sclerosis (SSc) is a multisystem rheumatic disease characterized by vascular dysfunction, autoimmune abnormalities, and progressive organ fibrosis. A series of studies in SSc patients and fibrotic models suggest that immune cells, fibroblasts, and endothelial cells participate in inflammation and aberrant tissue repair. Furthermore, the growing number of studies on single-cell RNA sequencing (scRNA-seq) technology in SSc elaborate on the transcriptomics and heterogeneities of these cell subsets significantly. In this review, we summarize the current knowledge regarding immune cells and stromal cells in SSc patients and discuss their potential roles in SSc pathogenesis, focusing on recent advances in the new subtypes by scRNA-seq.

Keywords: systemic sclerosis, ScRNA-seq, immune cells, fibroblasts, endothelial cells

OPEN ACCESS

Edited by:
Raffaele Strippoli,
Sapienza University of Rome, Italy

Reviewed by:
Toshiyuki Yamamoto,
Fukushima Medical University, Japan
Steven O'Reilly,
STipe Therapeutics, Denmark

***Correspondence:**
Honglin Zhu
honglinzhu@csu.edu.cn
Hui Luo
luohui@csu.edu.cn

Specialty section:
This article was submitted to Inflammation Pharmacology, a section of the journal Frontiers in Pharmacology

Received: *01 December 2021*
Accepted: *04 January 2022*
Published: *03 February 2022*

Citation:
Dai B, Ding L, Zhao L, Zhu H and Luo H (2022) Contributions of Immune Cells and Stromal Cells to the Pathogenesis of Systemic Sclerosis: Recent Insights. Front. Pharmacol. 13:826839. doi: 10.3389/fphar.2022.826839

1 INTRODUCTION

Systemic sclerosis (SSc) is an autoimmune connective tissue disease that can be mainly divided into limited cutaneous SSc (lcSSc) and diffuse cutaneous SSc (dcSSc) according to the extent of skin involvement (LeRoy et al., 1988). In patients, lcSSc mainly manifests as a thickening and hardening of the distal acral skin, often related to positive anti-centromere antibodies. Whereas dcSSc in patients also involves the proximal limbs and trunk which are prone to develop visceral organ complications, commonly associated with positive anti-topoisomerase I (anti-Scl-70) or anti-RNA polymerase III antibodies (Steen 2005).

SSc has three major pathological characteristics, including vasculopathy, immune dysregulation, and connective tissue fibrosis. Dysfunction of endothelial cells (ECs) is a key event leading to SSc microangiopathy (Mostmans et al., 2017). Activated ECs are able to recruit inflammatory cells by secreting adhesion molecules and E-selectin or stimulate extracellular matrix (ECM) production by connective tissue growth factor (CTGF) or other pro-fibrotic mediators. Innate and adaptive immune responses play a prominent part in the progression of SSc (Lech and Anders 2013; Allanore et al., 2015). Substantial evidence uncovers the link between the immune system and fibrosis. For instance, specific serum autoantibodies and pro-fibrotic cytokines like IFN-α, IL-4, and IL-13 and the transforming growth factor-beta (TGF-β) secreted by inflammatory cells, as well as abnormal inflammatory signatures [such as type-I interferon (IFN) signature] appear in the blood or target organs of SSc patients (Allanore et al., 2015). In addition, *in situ* hybridization has found that fibroblasts adjacent to the infiltrated inflammatory cells are more likely to synthesize collagen, implying the recruitment to fibroblasts (Fleischmajer et al., 1977; Kähäri et al., 1988). In SSc, alteration of activation, proliferation, and differentiation in the fibroblast occupy kernel status in tissue fibrosis. These cells release different kinds of chemokines that promote or inhibit the

recruitment of circulating immune cells. Moreover, the activation of fibroblasts prevents T-cell apoptosis and enhances the sustainability of T-cell function (Pilling et al., 1999; O'Reilly et al., 2012). Interactions between the fibroblasts and immune cells often lead to the amplification of ECM production. In addition, abundant works have emphasized the process on injured ECs transdifferentiating toward myofibroblasts known as endothelial-to-mesenchymal transition (EndMT), which is also responsible for the expansion of the fibroblast pool (Xu et al., 2011; Jimenez 2013; Ebmeier and Horsley 2015).

In recent years, droplet-based single-cell RNA sequencing (scRNA-seq) has been developed at a rapid pace. In SSc, scRNA-seq reveals novel or rare cell types with great precision and characterizes their developmental trajectory. Profiling cell landscapes by scRNA-seq depicts the entire cell compositions under the conditions of physiology and pathology. Moreover, scRNA-seq allows researchers to discern the potential roles of differentially expressed genes in individual cells and their involvement in signaling pathways which sheds light on the pathogenic mechanism of SSc. There are currently plentiful studies on scRNA-seq targeting monocytes, macrophages, dendritic cells (DCs), T cells, fibroblasts, and ECs in SSc.

In this review, we primarily focus on the recent insights into the characteristics and functions of immune cells and stromal cells in various tissues including the blood, lungs, and skin in SSc patients by scRNA-seq and traditional methods. Therefore, it will greatly benefit to facilitate our comprehension of pathogenic mechanisms and the development of subsequent treatments.

2 INNATE IMMUNE CELLS

The innate immune system has been shown to be activated at various stages of SSc. Generally, pattern recognition receptors, such as Toll-like receptors (TLRs) in SSc, identify damage-associated molecular patterns and pathogen-associated molecular patterns, which trigger an inflammatory response (Martin 2014) and could lead to a fibrotic state ultimately (Dowson et al., 2017). Myeloid cells, such as monocytes, macrophages, and DCs, are representative of innate immunity and play a significant role in the onset and progression of SSc (Satoh et al., 2017; Ah Kioon et al., 2018; Bhandari et al., 2020). Monocytes participate in fibrosis progression by affecting inflammatory responses and differentiating into macrophage or fibroblast-like cells (Shi and Pamer 2011). The human monocytes can be divided into three subtypes according to the expression of membrane molecules: classical monocytes ($CD14^{++}CD16^{-}$), nonclassical monocytes ($CD14^{+}CD16^{++}$), and intermediate monocytes ($CD14^{+}CD16^{+}$) (Passlick et al., 1989; Auffray et al., 2007). Macrophages are significant mediators of tissue injury and the major source of TGF-β, which are involved in inflammation and fibrosis of SSc (Toledo and Pioli 2019). Traditionally, macrophages are divided into classically activated macrophages (M1) and alternately activated macrophages (M2), which have opposite functions of pro-inflammation and anti-inflammation (Mosser and Edwards 2008). DCs have two primary subtypes—conventional dendritic cells (cDCs) and plasmacytoid dendritic cells (pDCs), both derived from the common DC precursor (Liu et al., 2009). A third subset of DCs is derived from the monocyte precursor (Guilliams et al., 2014). cDCs are a class of powerful antigen-presenting cells and consist of two principal subsets (cDC1s and cDC2s) (Guilliams et al., 2014). These cells variably express the TLRs, which are able to initiate adaptive immune responses (Boltjes and van Wijk 2014). Moreover, pDCs play a critical role in innate immunity by producing type-I IFNs (Cella et al., 1999; Siegal et al., 1999; Guiducci et al., 2010; Swiecki and Colonna 2015).

2.1 Monocytes

Recently, both bulk RNA-seq and scRNA-seq had confirmed the presence of a cluster of monocytes ($CD16^{+}$ monocytes) closely related to SSc pathogenesis. Bulk RNA-seq is found as an inflammatory gene module, including *KLF10*, *JUNB*, *PLAUR*, and *JUND*, in the monocytes of the peripheral blood in SSc when compared with the healthy control (HC) (**Supplementary Table S1**). ScRNA-seq was further used to explore the details of monocytes, and seven subsets (PM0–PM6) were finally identified. The PM0 cluster typically expressed the abovementioned inflammatory co-expression genes and had similar transcriptomics with $IL1B^{+}$ $FCN1^{hi}$ monocytes in the lung tissue of SSc-associated interstitial lung disease (SSc-ILD) (Kobayashi et al., 2021) (**Table 1**). According to previous studies, *IL1B* could be a key pro-fibrotic mediator (Park et al., 2018), and $IL1B^{+}$ $FCN1^{hi}$ cells were involved in skin and lung fibrosis, indicating that the cluster might be a new therapeutic target for SSc (Aran et al., 2019). Similar results by flow cytometry showed that in addition to the activated phenotypic profile of monocytes in the peripheral blood in SSc, the number of $CD16^{+}$ monocytes were increased and related to ILD and modified Rodnan skin score (mRSS) (Lescoat et al., 2017; Schneider et al., 2021).

Recently, the whole-genome transcriptome analysis showed activated fibrotic pathway and increased fibronectin expression in circulating $CD14^{+}$ monocytes of SSc patients. Interestingly, in a pro-fibrotic milieu, $CD14^{+}$ monocytes were a source of ECM-producing cells, as they could differentiate into myofibroblast-like cells and produce type I collagen and α-SMA (Rudnik et al., 2021a) (**Figure 1**). One previous study described a monocyte population that secreted high levels of tissue inhibitor of metalloproteinases 1 (TIMP-1) protein, a potentially important regulator in fibrogenesis of SSc. TLR signaling had a key role in TIMP-1 secretion (Ciechomska et al., 2013). CD52 is a glycoprotein anchored to glycosylphosphatidylinositol (Xia et al., 1993; Hale 2001), and it is widely expressed on the monocytes, lymphocytes, and DCs (Ratzinger et al., 2003). Recently, a study has found that the expression of CD52 on circulating monocytes of SSc was reduced. The reduction of CD52 enhanced the adhesion between monocytes and ECs and then led to an increased recruitment of monocytes into the tissues. It is worth noting that the increased type-I IFN–related genes in SSc could downregulate the expression of CD52 in monocytes by histone deacetylase IIa (HDAC IIa). Targeting the IFN–HDAC–CD52 axis may bring a new strategy for early SSc patients (Rudnik et al., 2021b).

TABLE 1 | Immune cells and stroma cells in SSc by scRNA-seq.

Special subsets	Samples	Species	Diseases	Characters of special subsets	Ref.
$CD16^+$ monocytes	PB	Human	SSc	Similar to $IL1B^+FCN1^{hi}$ monocytes in the lung of SSc-ILD	Kobayashi et al. (2021)
$FCGR3A^+$ macrophages	Skin	Human	dcSSc	Derived from $CCR1^+$ and $MARCO^+$ macrophages both with characteristic of M1 and M2 macrophages	Xue et al. (2021)
$SPP1^{hi}$ macrophages	Lung	Human	SSc-ILD	Encoded OPN which predicted the deterioration of lung function	Gao et al. (2020)
$SPP1^{hi}$ and $FABP^{hi}$ macrophages	Lung	Human	SSc-ILD	Upregulated type-I IFN signaling	Valenzi et al. (2021)
$CX3CR1^+SiglecF^+$ macrophages	Lung	Mouse	Bleomycin-induced pulmonary fibrosis	Produced nutrient factor (PDGF-aa) of fibroblasts	Aran et al. (2019)
$Lyve1^{hi}MHCII^{lo}$ macrophages	Lung, fat, heart, and dermis	Mouse	—	Restrained induced tissue fibrosis	Chakarov et al. (2019)
FCN^+ mo-DCs	Skin	Human	dcSSc	Located in perivascular and related to severe skin fibrosis	Xue et al. (2021)
pDCs	Lung	Human	SSc-ILD	Upregulated multiple cellular stress pathways and increased the expression of type-I IFN receptor	Valenzi et al. (2021)
$CXCL13^+$ T cells	Skin	Human	dcSSc	Expressed Tfh-like genes and promoted B-cell responses	Gaydosik et al. (2021)
$SFRP2^{hi}WIF1^+$ fibroblasts	Skin	Human	dcSSc	Precursor of myofibroblasts	Tabib et al. (2021)
Actively proliferating myofibroblasts	Lung	Human	SSc-ILD	Highly expressed collagen and other pro-fibrotic genes	Valenzi et al. (2019)
$CTHRC1^+$ fibroblasts	Lung	Mouse	Bleomycin-induced pulmonary fibrosis	Expressed pathologic ECM genes and migrated into injured areas	Tsukui et al. (2020)
Activated fibroblasts	Lung	Mouse	Bleomycin-induced pulmonary fibrosis	Exhibited a myofibroblast-like gene expression signature	Peyser et al. (2019)
Endothelial cells	Lung	Human	dcSSc	Associated with ECM deposition, vascular injury, and EndMT	Apostolidis et al. (2018)

SSc, systemic sclerosis; scRNA-seq, single-cell RNA-sequencing; ILD, interstitial lung disease; PB, peripheral blood; OPN, osteopontin; Lyve1, lymphatic endothelium hyaluronan receptor-1; IFN, interferon; pDCs, plasmacytoid dendritic cells; Tfh, T follicular helper; IL, interleukin; SFRP, secreted frizzled-related protein; CTHRC, collagen triple helix repeat containing 1; ECM, extracellular matrix; EndMT, endothelial-to-mesenchymal transition.

2.2 Macrophages

Robert Lafyatis et al. found five clusters of macrophages in the skin lesions of SSc patients, three of which were parallelly described in HC, including $CCR1^+$, $MARCO^+$, and $TREM2^+$ macrophages. Additional macrophage clusters associated with SSc were proliferating macrophages and $FCGR3A^+$ macrophages, and the latter were probably derived from $CCR1^+$ and $MARCO^+$ macrophages based on pseudotime analysis. $FCGR3A^+$ macrophages expressed M2 macrophage activation markers *CD163* and *MS4A4A* and the macrophage scavenger receptor 1 (*MSR1*) and were characterized concomitantly by the enriched pathway–like "response to lipopolysaccharide" associated with M1 polarization (Xue et al., 2020; Xue et al., 2021).

The macrophages in the SSc-ILD lung tissue were divided into seven discrete subtypes (MP1–MP7). *SPP1* expression at a higher prevalence was noted in the MP1 cluster, and the chemokine CCL18 was relatively enriched in the MP7 cluster. *SPP1* encoded osteopontin, a potential predictor for lung function deterioration. The differentially upregulated genes of the two subtypes were mainly involved in the differentiation and migration of myeloid cells and responded to pro-inflammatory signals (Gao et al., 2020). Intriguingly, subsequent studies confirmed that in addition to $SPP1^{hi}$ macrophages, three other subsets including $FABP4^{hi}$ macrophages, monocyte-derived macrophages ($FCN1^{hi}$ macrophages), and proliferating macrophages also appeared in SSc-ILD lung tissues. Compared with idiopathic pulmonary fibrosis (a chronic pulmonary fibrosis disease) and the HC, the type-I IFN signaling was upregulated in $SPP1^{hi}$ and $FABP^{hi}$ macrophages of SSc-ILD. Concretely, the interferon-induced transmembrane proteins *IF35*, *EGR1*, and *ISG15* were upregulated in the $SPP1^{hi}$ macrophages, while *TBK1*, *PTPN11*, and *CHUK* were upregulated in the $FABP4^{hi}$ macrophages (Valenzi et al., 2021).

The subpopulations of macrophages showed the greatest discrimination between mice and humans. Macrophages in the lung tissues of bleomycin-induced fibrosis mice were classified into three types by scRNA-seq: alveolar macrophages, intermediate macrophages ($CX3CR1^+SiglecF^+$), and interstitial macrophages. The transitional subpopulation highly expressing MHCII molecules was located in aggregates adjacent to infiltrated $Pdgfra^+$ and $Pdgfrb^+$ fibroblasts and might be the source of Pdgf-aa (a nutrient factor of fibroblasts) in the fibrosis niche. In other words, the paracrine interactions between the macrophages and fibroblasts played a positive role in tissue fibrosis (Aran et al., 2019). Recently, $MHCII^{hi}CX3CR1^{hi}$ macrophages also have been systematically studied in the lung, fat, dermis, and heart tissues of mice with a low expression of lymphatic endothelial hyaluronan receptor-1 (*Lyve1*). $Lyve1^{lo}MHCII^{hi}CX3CR1^{hi}$ macrophages were conserved in these tissues and located adjacent to the fibers. The other conserved macrophages were $Lyve1^{hi}MHCII^{lo}CX3CR1^{lo}$ macrophages with a role to restrain induced tissue fibrosis (Chakarov et al., 2019).

The traditional paradigm implies the M2 pro-fibrotic properties of monocytes/macrophages in the blood and target

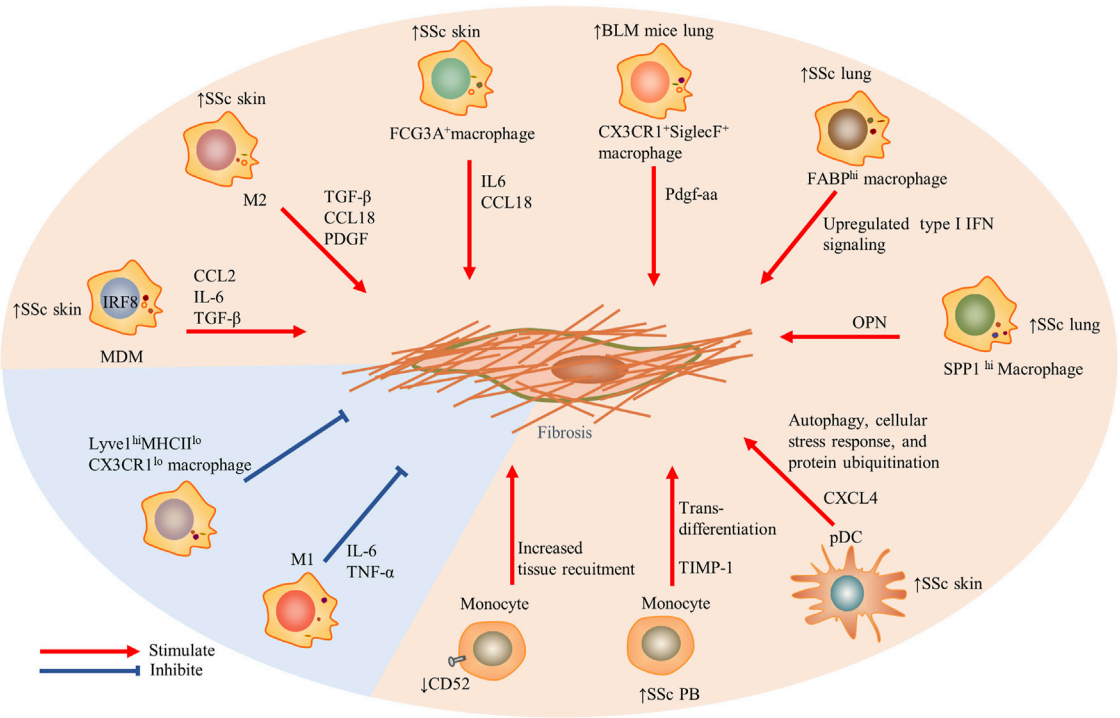

FIGURE 1 | The role of innate immune cells including monocytes, macrophages, and dendritic cells in the fibrosis in SSc. Particularly, Lyve1^{hi}MHCII^{lo}CX3CR1^{lo} macrophages restrained induced tissue fibrosis, and traditional M1 macrophages also prevented fibrosis. Red arrows indicate stimulation; blue blunted-ends indicate inhibition. SSc, systemic sclerosis; PB, peripheral blood; IRF, interferon regulatory factor 8; MDM, monocytes-derived macrophages; CCL, CC chemokine ligand; IL, interleukin; IFN, interferon; OPN, osteopontin; TIMP-1, tissue inhibitor of metalloproteinases 1; and Lyve1, lymphatic endothelium hyaluronan receptor-1.

organs of SSc patients. M1 macrophages exerted their effects primarily at the stage of the inflammatory responses by producing IL-1β, TNF-α, and IL-6 (Gordon 2003; Mosser 2003). Infiltrated M2 macrophages in the skin and peripheral blood have been observed in SSc with the putative marker CD163 (Higashi–Kuwata et al., 2010; Bielecki et al., 2013). M2 macrophages produced pro-fibrotic mediators such as TGF-β, CCL18, and the platelet-derived growth factor to promote fibroblast activation and collagen release (Jaguin et al., 2015; Shapouri–Moghaddam et al., 2018). However, in addition to the M1 and M2 macrophages, the circulating macrophage of SSc patients also included a confluent M1/M2 phenotype which has been reported to be associated with a more severe phenotype (SSc-ILD) (Trombetta et al., 2018) and arthritis or myalgia (Mohamed et al., 2021). Monocytes in the peripheral blood in SSc might differentiate into monocytes-derived macrophages (MDMs) during exposure to the soluble factors in the plasma and secret activation markers such as CCL2, IL-6, and TGF-β. Their activation has a pro-fibrotic property (Bhandari et al., 2020), which possibly involves the key transcription factor—interferon regulatory factor 8 (IRF8), a regulator of differentiation and function of the myeloid cells. On the one hand, MDMs show an M2 phenotype after silencing IRF8; on the other hand, skin fibrosis of mice with myeloid cell–specific knockout of IRF8 increased after bleomycin treatment (Ototake et al., 2021).

2.3 Dendritic Cells

The results of scRNA-seq showed that there were six DC subpopulations in skin biopsies of the HC, including cDC1 (*CLEC9A*$^+$ DCs), two subsets of cDC2 (*CXorf21*$^+$ DCs and *MCOLN2*$^+$ DCs), a novel DC subtype (*LAMP3*$^+$ DCs), a cluster of proliferating DCs (*KIAA0101*$^+$ DCs), and a Langerhans cell subset (*Langerin*$^+$ DCs). *FCN1*$^+$, the monocyte-derived DC marker, was related to cDC2 in the pseudo-time distribution and existed solely in dcSSc, which was associated with severe skin fibrosis and had been mentioned in previous studies (Kobayashi et al., 2021). In addition, pDCs derived from the lymphoid progenitor cells also appeared almost exclusively in the skin in dcSSc (Xue et al., 2020; Xue et al., 2021). The upregulated pathway, including autophagy, cellular stress response, and protein ubiquitination, showed the abnormal phenotypes of activation among the pDCs of SSc-ILD (Valenzi et al., 2021).

The assay of transposase-accessible chromatin using sequencing showed that the DCs occupied the greatest epigenetic difference between SSc skin lesions and the normal skin, and the disease-related single-nucleotide polymorphisms were significantly enriched in the DCs, indicating that it may be an important epigenetic driving factor of SSc (Liu et al., 2020). The proteome-wide analysis has proved that pDCs in SSc secreted chemokine CXCL4, a predictor of mRSS (van Bon et al., 2014). pDCs expressing IFNα and CXCL4 accumulated around the

vessels of the skin in SSc (van Bon et al., 2014; Ah Kioon et al., 2018). In a recent study, CXCL4, as a self-antigen, promoted the activation of type-I IFN signals by pDCs and anti-CXCL4 antibodies by B cells, which maintained the vicious circle of SSc IFN-I signature (Lande et al., 2020). Epigenetic factors such as the recent miR-126 and miR-139-5p (Chouri et al., 2021) and the previous miR-618 (Rossato et al., 2017) also contributed to the characteristics of type-I IFN in disease. Moreover, xenotransplantation of human pDCs into bleomycin-induced nonobese diabetic/severe combined immunodeficiency mice increased IFN-induced response to TLR agonist significantly and further demonstrated the key role of pDC in immune response and fibrosis degree (Ross et al., 2021).

3 T LYMPHOCYTES

T-cell heterogeneity is high in terms of expression and function of T-cell receptors. Antigen-specific oligoclonal T cells are related to the breakdown in self-tolerance (Laurent et al., 2018). Specific cytokine profiles have a significant impact on the functions of fibroblasts and ECs and can promote or inhibit collagen over-synthesis and vascular diseases (Hügle et al., 2013; Chizzolini and Boin 2015). T lymphocytes are divided into T helper (Th) cells, regulatory T (Treg) cells, cytotoxic T (CTL) cells, and $\gamma\delta$ T cells. All Th cells express CD4, mainly including Th1, Th2, Th17, Th9, Th22, and T follicular helper (Tfh) cells, and each subpopulation developed from naive T cells which responded to diverse microenvironmental stimuli. Treg cells primarily maintain immune tolerance. CTL cells mainly express CD8 to identify and kill abnormal target cells such as cancer cells and infected cells, but a few can also express CD4. The receptors of γδ T cell are γ chain and δ chain which permit recognition of antigens without MHC restriction. In addition, a new subset of T cells in SSc skin likely promoting B-cell responses has been fully revealed by scRNA-seq which provides a fuller framework for understanding the contribution of T lymphocytes to autoimmunity (Gaydosik et al., 2021).

3.1 T-Cell Subsets by scRNA-Seq

Currently, only one study in 2021 analyzed the skin-resident and recirculating T-cell subsets and their heterogeneity in dcSSc by scRNA-seq. According to differences in transcriptome profiles, skin T lymphocytes were divided into nine clusters. In addition to traditional $CD4^+$ T cells, $CD8^+$ T cells, and Treg cells, T cell clusters expressing IL-26, proliferation genes, *TRDC*, and *CXCL13* were also identified. Each T-cell cluster had activated and special molecular pathways. Especially, the mitochondrial, ERK/MAPK signaling, and oxidative phosphorylation pathways in $CXCL13^+$ T cells were all upregulated. $CXCL13^+$ T cells expanded in the skin of dcSSc with perivascular localization and were related to ILD significantly. Moreover, the subpopulation exhibited recirculating memory migratory phenotype ($CCR7^+SELL^-$), which implied a certain migration ability. *CXCL13* is a B-cell chemoattractant that helps to form tertiary lymphoid structures (TLOs) (Ansel et al., 2000). In this study, $CXCL13^+$ T cells were adjacent to $CD20^+$ B cells and expressed Tfh-related genes with lower levels like *ICOS* and *PD1* but not *BCL6* and *CXCR5*. Therefore, it may be a special Tfh subset, and treatment for $CXCL13^+$ T cells may prevent disease progression (Gaydosik et al., 2021) (**Figure 2**).

3.2 Th1 and Th2 Cells

Th1 cells mainly secrete cytokines such as IFN-γ, TNF-α, and IL-2, while Th2 cells mainly secrete cytokines such as IL-4, IL-5, and IL-13 (Wynn 2004). At present, most researchers agree with the view of skewed Th2 pattern in SSc effector T cells (O'Reilly et al., 2012; Chizzolini and Boin 2015; Distler et al., 2019; Zhang et al., 2020; Worrell and O'Reilly 2020). Therefore, targeted delivery to restore the balance between Th1 and Th2 cytokines should be further researched for limiting fibrosis (Gourh et al., 2009). Generally, IFN-γ mainly inhibited collagen synthesis by reducing the activity of fibroblasts or restraining the effect of cytokines IL-4 and IL-13 (Rosenbloom et al., 1986). Compared with the HC, cytokines IL-4 and IL-13 in the serum of SSc patients were increased (Gasparini et al., 2020). IL-13 inhibited the expression of matrix metalloproteinase-1 (MMP-1) through the PKB/AKT pathway in skin fibroblasts of HC and SSc patients (Brown Lobbins et al., 2018). Latest reports have discovered the new Th2 cytokine IL-31 was elevated in plasma and target organs (skin and lung) of SSc patients (Yaseen et al., 2020). IL-31 promoted skin and lung fibrosis and enhanced Th2 immune responses, which were ameliorated by the blockade of IL-31 or anti-IL-31RA antibody (Kuzumi et al., 2021).

3.3 Th17 Cells

Naive T cells differentiate into Th17 cells in the presence of IL-6, IL-21, IL-23, or IL-1 (Harrington et al., 2005; Park et al., 2005; Bettelli et al., 2006), which involve inflammation and autoimmune disease by secreting IL-17, IL-22, and MMPs (Korn et al., 2009; Zambrano–Zaragoza et al., 2014). The proportion of Th17 in the blood, skin, and bronchoalveolar lavage (BAL) of patients of SSc was increased and associated with disease activity (Kubo et al., 2019; Robak et al., 2019; Fox et al., 2021). Due to the plasticity of Th17 cells, a subpopulation of Th17 cells expressed the adhesion molecule CD146 and had a stronger ability to bind and cross vascular endothelium in peripheral blood (Gabsi et al., 2019). Moreover, IFN-γ^+IL-17^+ Th17 cells which differentiate from Th17 in the presence of IL-12 have recently been shown to enhance the collagen secretion of fibroblasts by producing IL-21 (Annunziato et al., 2007; Xing et al., 2020). In addition, a previous study reported a significantly higher ratio of Th17/Treg cells in the peripheral blood of SSc patients than in HC, which supported the deflection towards Th17-mediated inflammatory processes (Yang et al., 2021). The conversion of Treg to Th17 cells might contribute to this bias as the $CD4^+CD25^+FOXP3^{lo}CD45RA^-$ Treg subset produced high levels of IL-17 (Liu et al., 2013).

The key cytokine IL-17 has been extensively studied controversially. IL-17 was both elevated in serum and skin during the early and active stages of SSc (Yang et al., 2014; Tezcan et al., 2021). Mechanically, IL-17 induced inflammation of ECs, and promoted fibroblast proliferation (Kurasawa et al., 2000; Xing et al., 2013). However, other sounds published their

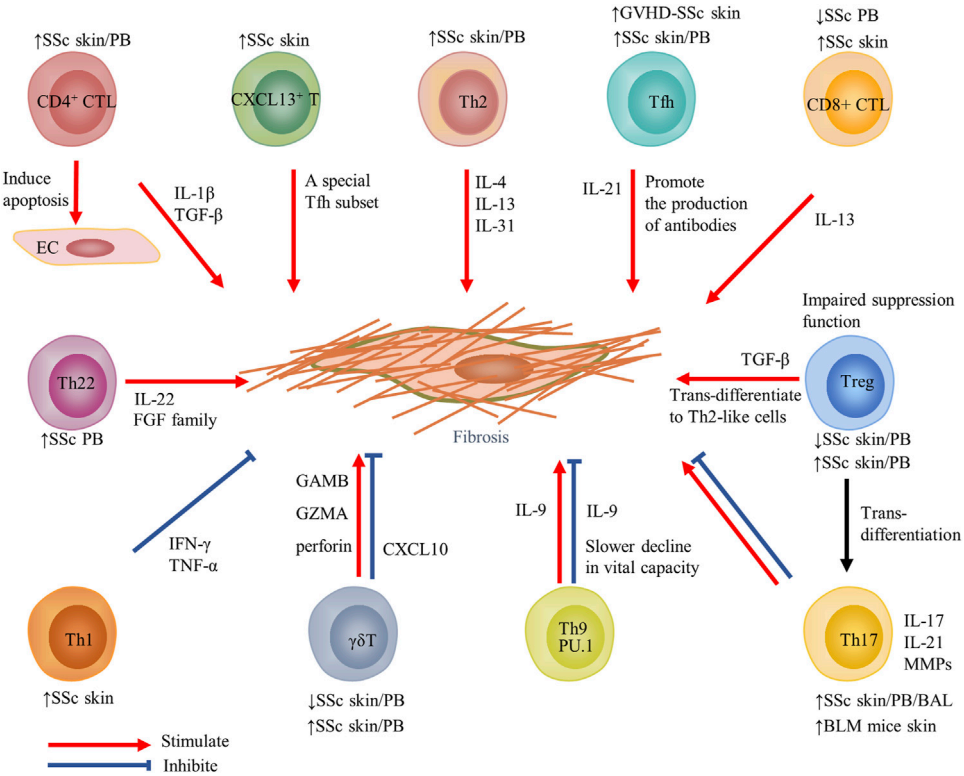

FIGURE 2 | Contribution of T-cell subsets and their cytokines to fibrosis in SSc. Changes in T-cell subsets of PB or target organs in SSc and fibrosis models are displayed above or below the cell. Red arrows indicate stimulation; blue blunted-ends indicate inhibition. SSc, systemic sclerosis; PB, peripheral blood; EC, endothelial cells; IL, interleukin; Tfh, T follicular helper; GVHD, graft-versus-host disease; and MMP, matrix metalloproteinase.

anti-fibrosis effect which reduced CTGF and type I collagen through the upregulation of miR-129-5p (Nakashima et al., 2012). More recently, a more refined organotypic model of human skin has been introduced; based on which IL-17 softened the skin by promoting inflammation and attenuating Wnt signaling (Dufour et al., 2020). It is to be noted that Th17 cells and IL-17 possessed a uniform effect in animal models which mediated fibrosis and SSc-like appearance in BLM mice and TSK-1 mice (Okamoto et al., 2012; Lei et al., 2016).

3.4 Th9 Cells

Th9 cells secrete IL-9 and IL-10 under the influence of pro-fibrosis factors (TGF-β, IL-4), and epithelial cytokine (thymic stromal lymphopoietin) (Veldhoen et al., 2008; Yao et al., 2013; Kaplan et al., 2015). IL-9 was highly expressed in the serum in both dcSSc and lcSSc and led to a lower degree of fibrosis and a slower decline in vital capacity at the earliest stage, which suggests IL-9 may be a protective molecule in pulmonary fibrosis (Yanaba et al., 2011). However, other studies elaborate increased IL-9 in the skin, and renal biopsy tissues were positively related to mRSS (Guggino et al., 2017). Furthermore, the Th9 transcription factor PU.1 activated the switch of pro-fibrotic fibroblast phenotype. When PU.1 was inactivated, skin and lung fibrosis in BLM-induced fibrotic mice became reduced (Wohlfahrt et al., 2019). The role of Th9 cells and IL-9 in the immune response of SSc individuals needs further research given the paucity of available results.

3.5 Th22 Cells

Although the existence of Th22 cells in SSc has been proved, less attention has been paid to their function. Th22 cells mainly produce IL-22 cytokine and express several members of the fibroblast growth factor (FGF) family, including FGF-1, FGF-5, and FGF-13 which play a role in tissue repair and fibrosis (Eyerich et al., 2009). It has been stressed that significantly increased circulating Th22 cells in SSc patients are related to SSc-ILD and CCR6 (a skin- and lung-homing chemokine receptor) (Truchetet et al., 2011). Furthermore, Th22 cells have been verified to participate in skin immunity because they promote keratinocyte activation induced by TNF and lead to fibroblasts obtaining a pro-inflammatory phenotype (Brembilla et al., 2016).

3.6 Tfh Cells

An increased frequency of Tfh cells related to disease severity in the peripheral blood of SSc patients has been observed, which promoted plasmablasts ($CD19^{+}CD27^{+}CD38^{hi}$) differentiation and antibody production through the IL-21 signaling pathway (Ricard et al., 2019). Furthermore, it has been particularly emphasized that circulating Tfh cells unbalanced toward the Tfh 1 subset in SSc may alter the function of B cells through

the IL-21 and IL-6 pathways. In addition, $CD4^+CXCR5^+$ Tfh cells also appeared in the skin of SSc patients (Ly et al., 2021). In the skin of graft-versus-host disease (GVHD)–SSc mice, increased $ICOS^+$ Tfh-like cells promoted skin fibrosis in IL-21 and MMP-12–dependent manner (Taylor et al., 2018). Therefore, inhibition of the Tfh cell subset or their cytokines like IL-21 (ruxolitinib) may bring good news to SSc patients.

3.7 Treg Cells

To date, there has been little agreement on the proportions of circulating changes of SSc Tregs (Gu et al., 2008; Zhu and Paul 2008; Antiga et al., 2010; Mathian et al., 2012; Ugor et al., 2017). The possible intrinsic explanation is the decreased expression of runt-related transcription factor 1 (*Runx1*) mRNA. *Runx1* mRNA and forkhead box transcription factor (*FoxP3*) form a transcription factor complex which is essential for eliciting the suppression function of Treg cells (Kataoka et al., 2015). In SSc patients, an inflammatory environment may be harmful to the immunosuppressive functions. For instance, the frequency of activated and inactivated Treg cells was lower in SSc than in the HC, but the immunosuppressive function of SSc Tregs was restored *in vitro* (Mathian et al., 2012). In addition, co-incubation of healthy Treg cells with the plasma of SSc patients could reduce the expression of CD69 and TGF-β of Tregs by some unknown factors in the plasma, thus reducing the functional response of Treg cells to effector T cells (Radstake et al., 2009). Some studies in the target organ of SSc also had confusing results (Klein et al., 2011; Yang et al., 2014). Particularly, the circulating Treg cells could migrate to the skin tissues and become Th2-like cells due to homing molecules that secreted a large number of cytokines IL-4 and IL-13, which might have driven the differentiation of fibroblasts and lead to fibrosis in SSc patients (MacDonald et al., 2015).

3.8 $CD8^+$ CTL Cells

Compared with HC, the proportion of circulating $CD8^+$ T cells in SSc patients in the early stage was decreased and related to the prolonged course of disease (Fox et al., 2021). Although according to a 2021 study, antigen-driven expansion of $CD8^+$ T cells had a high temporal persistence in the blood of SSc patients (Servaas et al., 2021). In addition, the $CD8^+$ T cells lacking CD28 expression in the peripheral blood in SSc and skin lesions have been detected. It is reasonable that cytotoxic $CD8^+CD28^-$ T cells exhibited a pro-fibrotic phenotype because these cells were linked to the degree of skin fibrosis and significantly produced IL-13 (Li et al., 2017).

In recent years, genome-wide results in skin biopsies have identified $CD8^+$ T cells–related genes (*CD8A*, *GraK*, *GraH*, and *GraB*) (Rice et al., 2016; Skaug et al., 2020). $CD8^+$ T cells had infiltrated the skin of patients with scleroderma, particularly in the early stage, and their cytokine IL-13 promoted the activation of signal transducer and activator of transcription 6 (STAT6) signal through highly expressed receptors in the monocytes and fibroblasts (Fuschiotti et al., 2013). The growth of ECs in the skin in SSc was restricted. To some extent, this may be attributed to perforin and granzyme B expressed by $CD8^+$ T cells (Kahaleh and Fan 1997; Li et al., 2017). When it comes to $CD8^+$ T cells of SSc patients with pulmonary fibrosis, their proportion in the bronchoalveolar lavage fluid and lung tissue was significantly higher than for $CD4^+$ T cells (Yurovsky et al., 1996; Luzina et al., 2009).

3.9 $CD4^+$ CTL Cells

$CD4^+$ CTL cells are a subset of $CD4^+$ T cells with cytotoxicity, which have been widely studied in the context of chronic viral infections such as cytomegalovirus and human immunodeficiency virus. At present, significant studies gradually focused on their potential role in immune-mediated fibrosis, which promoted cytokine release, including IL-1β and TGF-β (Mattoo et al., 2016). The lymphocytes, also referred to as $CD4^+CD319^+$(*SLAMF7*$^+$) lymphocytes, were increased significantly in the peripheral blood of early dcSSc patients compared to the HC (Fox et al., 2021). $CD4^+$ CTL cells labeled *GZMA* have recently been found to be the dominant infiltrating cells in the skin of patients with SSc compared with Th1, Th2, Tfh, and Tregs. Furthermore, these cells may induce apoptosis of ECs accompanied by an excessive tissue repair process leading to fibrosis and tissue dysfunction (Maehara et al., 2020), indicating the source of tissue damage mediators first discovered in skin lesions in SSc decades ago (Kahaleh and Fan, 1997).

3.10 γδ T Cells

The rare γδ T cells still have a place in the immune responses of the skin, intestine, and lung tissues. There were a decreased number of γδ T cells in the peripheral blood mononuclear cells (PBMCs) of scleroderma individuals, especially in patients with anti-Scl-70 antibodies and shorter disease duration (Holcombe et al., 1995). In another research, activated circulating γδ T cells of SSc patients was increased, and they could upregulate COL1A2 mRNA in co-cultured fibroblasts (Ueda-Hayakawa et al., 2013). CD27 is a co-stimulatory receptor that was very vital to the development and function of the γδ T cells. The increased pathogenicity of the $CD27^+$ γδ T cells had been verified because the subset upregulated the expression of granzyme B, granzyme A, or perforin (Henriques et al., 2016). In addition, the circulating $Vdelta1^+$ T cells (a γδ T subset) tended to accumulate in the skin tissues of SSc due to their expression of adhesion molecules and activation markers (Giacomelli et al., 1998). While in bleomycin-induced pulmonary fibrosis mice, γδ T cells promoted the alleviation of fibrosis by producing CXCL10 (Pociask et al., 2011). Exploring the role and potential mechanism of the minority T cell in the pathogenesis of fibrosis will be helpful for γδ T cell–based immunotherapy.

4 B CELLS

Abundant B-cell receptors (BCRs) repertoire is generated in the bone marrow through the rearrangement of immunoglobulin gene fragments (Zhang et al., 2004). B cells are a heterogeneous

population distinguished by cytokine production spectra or membrane surface molecules (Perez–Andres et al., 2010). A proliferation-inducing ligand and B-cell–activating factor (BAFF) (TNF family member) are indispensable for B-cell maturation and long-term maintenance (Mackay et al., 2003). Once naive B cells are activated by antigen or Th cells, they will differentiate into memory B cells and plasma cells which are associated with fibrosis through the production of cytokines and classical disease-specific autoantibodies in SSc, while regulatory B cells (Bregs) maintain self-tolerance primarily by cytokine IL-10 (Lee et al., 2021).

4.1 B-Cell Subsets by scRNA-Seq

Systematic analysis of B cells in the blood or target organs of SSc patients by scRNA-seq is a largely explored domain. We briefly describe a finding in systemic lupus erythematosus (SLE) patients. Nine clusters of B cells were identified in the PBMCs which included switched memory, naive with interferon signature (naive-Ifn), non–switched memory, switched memory-Ifn, double-negative 2 (DN2), DN2-Ifn, activated memory, naive, and plasmablast. The strong interferon signature in SLE patients may have resulted from the DN2 subset. The CD52 gene, which had a role in maintaining B-cell homeostasis, was significantly elevated in multiple B-cell clusters from SLE patients, especially in the most depleted clusters of non–switched memory B cells (Zhu et al., 2018; Bhamidipati et al., 2020).

4.2 Memory B Cells

Although the $CD19^{+}CD27^{+}$ memory B cells in the peripheral blood of SSc patients were decreased, the expression of their activation markers (CD80, CD95, HLA-DR) changed in the opposite direction (Forestier et al., 2018). Furthermore, recent findings have emphasized that the frequency of $CD19^{+}IgD^{-}CD27^{+}CD38^{-}CD95^{+}$–activated switched memory (ASM) B cells in the peripheral blood of patients with dcSSc was lower than that in the HC, mostly in individuals with anti–Scl-70 antibodies or pulmonary fibrosis, implying that the ASM B cells were associated with severe SSc (Simon et al., 2021). In fact, $CD21^{low}$ B cells were mainly composed of memory B cells such as the DN switched ($CD27^{-}IgD^{-}$) memory B cells and expressed high levels of activation markers. Beyond this, it was a possible indicator of new ulcers and visceral vascular damage (Marrapodi et al., 2020; Visentini et al., 2021).

4.3 Effector B Cells

Effector B cells (Beffs) participate in the immune response by secreting pro-fibrotic cytokine TGF-β (Dumoitier et al., 2017) and a variety of inflammatory markers, such as IL-4, IL-6, IL-12, TNF-α, and GM-CSF (Harris et al., 2000; Li et al., 2015; Shen and Fillatreau 2015). In the skin of SSc patients, infiltrated $CD20^{+}$ B cells and $CD138^{+}$ plasma cells were related to the early disease stage and disease progression (Bosello et al., 2018). The same discovery about the increases of B cells and plasma cells was verified by cutaneous transcriptome data (Whitfield et al., 2003; Streicher et al., 2018). As a classic pro-inflammatory cytokine, IL-6 promoted fibrosis by activating the downstream signaling molecule STAT3 and was also related to SSc disease severity (Sato et al., 2001). Tocilizumab (TCZ) is a humanized IL-6 receptor-α–blocking antibody (Mihara et al., 2011). Recently, the results of a phase 3 randomized controlled trial showed that TCZ stabilized the decline in forced vital capacity in SSc-ILD, whereas there was no change in mRSS (Khanna et al., 2021). The clinical end points of TCZ on skin fibrosis may be mediated only in part by the direct inhibition of fibrosis by TCZ (Khanna et al., 2018). In the bleomycin-induced scleroderma model, the BAFF inhibitor balanced the skew between Beffs and Bregs and alleviated skin and lung fibrosis (Matsushita et al., 2018). Consistent with this research, SSc patients treated with belimumab (binds with soluble BAFF with high affinity) achieved clinical improvements associated with reduced expression of B-cell activation and fibrosis-related genes in the skin (Gordon et al., 2018).

4.4 Regulatory B Cells

Compared with Treg cells, Bregs have relatively uniform alteration in SSc. In the peripheral blood of SSc patients, sufficient evidence indicates the decreased frequency of $IL\text{-}10^{+}$ Bregs which is negatively related to the titers of anti-centromeric and anti-Scl-70 autoantibodies (Matsushita et al., 2016). The possible reasons for the altered quantities consists of TGF-β and IFN-γ both of which inhibited Bregs development (Iwata et al., 2011). In chronic GVHD (cGVHD) patients, Bregs enriched in the $CD19^{+}CD24^{hi}CD38^{hi}$ transitional and $CD19^{+}IgM^{+}CD27^{+}$ memory B cells and exhibited decreased tendencies similar to less-produced IL-10 (Khoder et al., 2014). Recently, $CD24^{hi}CD27^{+}$ Bregs were shown to be involved in the regulation of disease severity due to their reduced frequency in SSc patients with pulmonary arterial hypertension (PAH) (Ricard et al., 2021). Interestingly, T-cell Ig and mucin domain protein 1 (TIM-1), a marker of the Bregs in mice, was also identified in the human $IL\text{-}10^{+}$ Bregs as a unique marker. $TIM\text{-}1^{+}$ B cells in the HC inhibited the pro-inflammatory ability of $CD4^{+}$ T cells when compared with SSc patients (Aravena et al., 2017). Animal experiments yielded similar results. For instance, early adoptive transplantation of $IL\text{-}10^{+}$ Bregs exhibited a suppressive role in the development of sclerodermatous cGVHD (Scl-cGVHD) mice (Le Huu et al., 2013).

5 FIBROBLASTS

The activity of fibroblasts and collagen production is closely related to the pathogenesis and severity of SSc, while there are no specific markers to define fibroblasts. Recently, scRNA-seq emphasized the intrinsic transcriptome changes in fibroblasts in the skin tissues of HC and SSc patients. A total of 10 SSc fibroblast subpopulations were identified by characteristic gene expression, including *SFRP2*^{hi} fibroblasts (*SFRP2*/*WIF* fibroblasts, *SFRP2*/*PRSS23* fibroblasts, *PCOLCE2* fibroblast), *APOE*-defined cells (*MYOC*/*FMO1*/*APOE*^{low} fibroblasts, *CCL19*/*C7*/*APOE*^{hi} fibroblasts), *CRABP1* fibroblasts, *COL11A1* fibroblasts, *POSTN*/*ASPN* fibroblasts, *ANGPTL7* fibroblasts, and proliferating

fibroblasts. The major subpopulation was the *SFRP2*^{hi} [secreted frizzled-related protein (*SFRP*) is related with Wnt signaling] fibroblasts located between the collagen bundles (Tabib et al., 2018). *MYOC*/*FMO1*/*APOE*^{low} fibroblasts were distributed in the MYOC/FMO1/APOElow fibroblasts were distributed in the interstitial regions and around the blood vessels. While *CCL19*/*C7*/*APOE*^{hi} fibroblasts showed a strong trend to SSc fibroblasts which differed from *CCL19*$^{+}$ fibroblasts of HC. The *CRABP1* fibroblasts, *COL11A1* fibroblasts, and *POSTN*/*ASPN* fibroblasts located around hair follicles supported previous finding about papillary dermal fibroblasts regenerating hair follicles (Driskell et al., 2013). Of note, *SFRP2*/*PRSS23* fibroblasts and *ANGPTL7* fibroblasts appeared only in SSc skin lesions. The former was associated with collagen fibril organization and ECM organization by Gene Ontology (GO) analysis, and the latter expressed *SFRP4* and represented myofibroblasts. Myofibroblasts–labeled *SFRP2*, *SFRP4*, and *FNDC1* were converted from *SFRP2*^{hi}*WIF1*$^{+}$ precursor fibroblasts with the upregulation of transcriptome markers *PRSS23* and *THBS1* at the beginning. In addition, the transcription factors of fibroblasts (*RUNX1*, *FOXP1*, *IRF7*, *STAT1*, and *CREB3L1*) promoted the differentiation of fibroblasts into myofibroblasts by bioinformatics analysis (Tabib et al., 2018; Tabib et al., 2021).

The majority of the marker of pulmonary fibroblasts was not shared with dermal fibroblasts. *MFAP5*^{hi}, *SPINT2*^{hi}, few *WIF1*^{hi} fibroblasts, and large proliferating myofibroblasts were identified between the lung tissues of the SSc-ILD and HC groups. It is noteworthy that *MFAP5*^{hi} fibroblasts expressed higher *SFRP*, *PCOLCE2*, and *CD55* than the skin *SFRP2*/*DPP4* fibroblasts, while *WIF1*^{hi} fibroblasts did not express *SFRP2*. In addition, myofibroblasts underwent the greatest phenotypic changes and upregulated the expression of collagen and other pro-fibrotic genes in SSc-ILD, which was pivotal to the pathologic mechanisms of fibrosis in SSc-ILD (Valenzi et al., 2019).

In the lung of bleomycin-induced fibrosis mice, researchers found *ACTA2* was not the only defined marker for activated fibroblasts. For instance, *Ltbp2*, *Col5a2*, and *Sparc* had a stronger correlation with the fibroblast activation signals. This study similarly identified the largest subcluster of fibroblasts exhibiting a myofibroblast-related gene, including muscle contraction and the development of ECM (Peyser et al., 2019). While another study has divided the fibroblasts of the lungs in bleomycin and control mice into 12 clusters, seven clusters expressed higher *COL1A1* and four clusters expressed *ACTA2*. The remaining were proliferative cells, which occupied unique anatomical locations. The study mainly found a unique type of highly expressing collagen triple helix repeat containing-1 (*CTHRC1*), which was a terminal state cluster and was detected in the multiple studies (Peyser et al., 2019; Valenzi et al., 2019; Tsukui et al., 2020). *CTHRC1*$^{+}$ fibroblasts mainly existed in fibrotic lungs of mice and human and expressed the highest level of type I collagen and other ECM-producing genes such as *TNC*, *POSTN*, and *COL3A1*. Purified *CTHRC1*$^{+}$ fibroblasts had better migration ability than other collagen-producing cells and could colonize in the lungs of mice treated with bleomycin (Tsukui et al., 2020).

6 ENDOTHELIAL CELLS

The mechanisms of EC damage and vascular disease progression in SSc are still not clear. ScRNA-seq–determined heparan sulfate proteoglycan 2 (*HSPG2*) and Apelin receptor (*APLNR*) were the two top injury markers of ECs in the skin in SSc. *HSPF2* was implicated in TGF-β signaling (Iozzo et al., 1997; Sharma et al., 1998) and SSc-associated fibrosis (Laplante et al., 2005). Due to the limitation of only one patient and one control biopsy in this study, no specific subtypes of ECs were divided. It is noticeable that enriched genes in ECs of SSc patients were related to ECM formation, vascular injury, and EndMT by the Ingenuity Pathway Analysis (IPA) and Gene Set Enrichment Analysis (GSEA) approaches (Apostolidis et al., 2018). Moreover, scRNA-seq analysis of SSc-ILD implied the active expansion of ECs in the lung tissues due to their increased vasculogenesis, prostaglandin biosynthesis, and PDGFR-signaling (Valenzi et al., 2021).

There are also other possible explanations of endothelial dysfunction. A new study found that neuronal-related characteristics such as dysregulation of the neuronal genes *ETV2* and *NRXN1* in ECs may be a culprit for dysangiogenesis in SSc (Tsou et al., 2021). In addition, sufficient evidence underlined a close liaison between vasculopathy and the metabolism of SSc dermal fibroblasts. Extracellular acidosis derived from the released lactic acid by SSc fibroblasts might lead to the impairment of peripheral capillary networks through acidic upregulated MMP-12 (an inhibitor of angiogenesis) in ECs (Andreucci et al., 2021). Intriguingly, endothelial miR-150 showed a protective effect in an animal experiment which was an independent survival predictor of PAH patients. The possible explanation implicated PTEN-like mitochondrial phosphatase (PTPMT1), which improved mitochondrial function and reduced apoptosis of ECs (Russomanno et al., 2021).

7 CONCLUSION

In SSc, the immune system and stromal cells in the blood and target organs show significant numerical or functional changes leading to the pathogenetic phenotype. ScRNA-seq provides greater insights for identifying new cell subtypes and elaborating their complex roles in disease states, and we need to further explore those subgroups that have no well-characterized functions. With the combination of conventional methods, scRNA-seq analysis, and further integrative multi-omics analysis, we could understand individual cell behavior and cellular variety, and elucidate the pathogenic mechanism of SSc diseases quickly and systematically, significantly propelling precise medical interventions in the near future.

AUTHOR CONTRIBUTIONS

BD wrote the first draft. BD, LD, and LZ revised the manuscript. HZ and HL revised final version and added extra information.

FUNDING

This study was funded by grants from National Natural Science Foundation of China (81671622,81771765, 81701621) and Hunan Provincial Natural Science Foundation (2019JJ40503).

SUPPLEMENTARY MATERIAL

The Supplementary Material for this article can be found online at: https://www.frontiersin.org/articles/10.3389/fphar.2022.826839/full#supplementary-material

REFERENCES

Ah Kioon, M. D., Tripodo, C., Fernandez, D., Kirou, K. A., Spiera, R. F., Crow, M. K., et al. (2018). Plasmacytoid Dendritic Cells Promote Systemic Sclerosis with a Key Role for TLR8. *Sci. Transl Med.* 10 (423), eaam8458. doi:10.1126/scitranslmed.aam8458

Allanore, Y., Simms, R., Distler, O., Trojanowska, M., Pope, J., Denton, C. P., et al. (2015). Systemic Sclerosis. *Nat. Rev. Dis. Primers* 1, 15002. doi:10.1038/nrdp.2015.2

Andreucci, E., Margheri, F., Peppicelli, S., Bianchini, F., Ruzzolini, J., Laurenzana, A., et al. (2021). Glycolysis-derived Acidic Microenvironment as a Driver of Endothelial Dysfunction in Systemic Sclerosis. *Rheumatology (Oxford)* 60 (10), 4508–4519. doi:10.1093/rheumatology/keab022

Annunziato, F., Cosmi, L., Santarlasci, V., Maggi, L., Liotta, F., Mazzinghi, B., et al. (2007). Phenotypic and Functional Features of Human Th17 Cells. *J. Exp. Med.* 204 (8), 1849–1861. doi:10.1084/jem.20070663

Ansel, K. M., Ngo, V. N., Hyman, P. L., Luther, S. A., Förster, R., Sedgwick, J. D., et al. (2000). A Chemokine-Driven Positive Feedback Loop Organizes Lymphoid Follicles. *Nature* 406 (6793), 309–314. doi:10.1038/35018581

Antiga, E., Quaglino, P., Bellandi, S., Volpi, W., Del Bianco, E., Comessatti, A., et al. (2010). Regulatory T Cells in the Skin Lesions and Blood of Patients with Systemic Sclerosis and Morphoea. *Br. J. Dermatol.* 162 (5), 1056–1063. doi:10.1111/j.1365-2133.2010.09633.x

Apostolidis, S. A., Stifano, G., Tabib, T., Rice, L. M., Morse, C. M., Kahaleh, B., et al. (2018). Single Cell RNA Sequencing Identifies HSPG2 and APLNR as Markers of Endothelial Cell Injury in Systemic Sclerosis Skin. *Front. Immunol.* 9, 2191. doi:10.3389/fimmu.2018.02191

Aran, D., Looney, A. P., Liu, L., Wu, E., Fong, V., Hsu, A., et al. (2019). Reference-based Analysis of Lung Single-Cell Sequencing Reveals a Transitional Profibrotic Macrophage. *Nat. Immunol.* 20 (2), 163–172. doi:10.1038/s41590-018-0276-y

Aravena, O., Ferrier, A., Menon, M., Mauri, C., Aguillón, J. C., Soto, L., et al. (2017). TIM-1 Defines a Human Regulatory B Cell Population that Is Altered in Frequency and Function in Systemic Sclerosis Patients. *Arthritis Res. Ther.* 19 (1), 8. doi:10.1186/s13075-016-1213-9

Auffray, C., Fogg, D., Garfa, M., Elain, G., Join-Lambert, O., Kayal, S., et al. (2007). Monitoring of Blood Vessels and Tissues by a Population of Monocytes with Patrolling Behavior. *Science* 317 (5838), 666–670. doi:10.1126/science.1142883

Bettelli, E., Carrier, Y., Gao, W., Korn, T., Strom, T. B., Oukka, M., et al. (2006). Reciprocal Developmental Pathways for the Generation of Pathogenic Effector TH17 and Regulatory T Cells. *Nature* 441 (7090), 235–238. doi:10.1038/nature04753

Bhamidipati, K., Silberstein, J. L., Chaichian, Y., Baker, M. C., Lanz, T. V., Zia, A., et al. (2020). CD52 Is Elevated on B Cells of SLE Patients and Regulates B Cell Function. *Front. Immunol.* 11, 626820. doi:10.3389/fimmu.2020.626820

Bhandari, R., Ball, M. S., Martyanov, V., Popovich, D., Schaafsma, E., Han, S., et al. (2020). Profibrotic Activation of Human Macrophages in Systemic Sclerosis. *Arthritis Rheumatol.* 72 (7), 1160–1169. doi:10.1002/art.41243

Bielecki, M., Kowal, K., Lapinska, A., Chyczewski, L., and Kowal-Bielecka, O. (2013). Increased Release of Soluble CD163 by the Peripheral Blood Mononuclear Cells Is Associated with Worse Prognosis in Patients with Systemic Sclerosis. *Adv. Med. Sci.* 58 (1), 126–133. doi:10.2478/v10039-012-0076-9

Boltjes, A., and van Wijk, F. (2014). Human Dendritic Cell Functional Specialization in Steady-State and Inflammation. *Front. Immunol.* 5, 131. doi:10.3389/fimmu.2014.00131

Bosello, S., Angelucci, C., Lama, G., Alivernini, S., Proietti, G., Tolusso, B., et al. (2018). Characterization of Inflammatory Cell Infiltrate of Scleroderma Skin: B Cells and Skin Score Progression. *Arthritis Res. Ther.* 20 (1), 75. doi:10.1186/s13075-018-1569-0

Brembilla, N. C., Dufour, A. M., Alvarez, M., Hugues, S., Montanari, E., Truchetet, M. E., et al. (2016). IL-22 Capacitates Dermal Fibroblast Responses to TNF in Scleroderma. *Ann. Rheum. Dis.* 75 (9), 1697–1705. doi:10.1136/annrheumdis-2015-207477

Brown Lobbins, M. L., Shivakumar, B. R., Postlethwaite, A. E., and Hasty, K. A. (2018). Chronic Exposure of Interleukin-13 Suppress the Induction of Matrix Metalloproteinase-1 by Tumour Necrosis Factor α in normal and Scleroderma Dermal Fibroblasts through Protein Kinase B/Akt. *Clin. Exp. Immunol.* 191 (1), 84–95. doi:10.1111/cei.13045

Cella, M., Jarrossay, D., Facchetti, F., Alebardi, O., Nakajima, H., Lanzavecchia, A., et al. (1999). Plasmacytoid Monocytes Migrate to Inflamed Lymph Nodes and Produce Large Amounts of Type I Interferon. *Nat. Med.* 5 (8), 919–923. doi:10.1038/11360

Chakarov, S., Lim, H. Y., Tan, L., Lim, S. Y., See, P., Lum, J., et al. (2019). Two Distinct Interstitial Macrophage Populations Coexist across Tissues in Specific Subtissular Niches. *Science* 363 (6432). doi:10.1126/science.aau0964

Chizzolini, C., and Boin, F. (2015). The Role of the Acquired Immune Response in Systemic Sclerosis. *Semin. Immunopathol* 37 (5), 519–528. doi:10.1007/s00281-015-0509-1

Chouri, E., Wang, M., Hillen, M. R., Angiolilli, C., Silva-Cardoso, S. C., Wichers, C. G. K., et al. (2021). Implication of miR-126 and miR-139-5p in Plasmacytoid Dendritic Cell Dysregulation in Systemic Sclerosis. *J. Clin. Med.* 10 (3), 491. doi:10.3390/jcm10030491

Ciechomska, M., Huigens, C. A., Hügle, T., Stanly, T., Gessner, A., Griffiths, B., et al. (2013). Toll-like Receptor-Mediated, Enhanced Production of Profibrotic TIMP-1 in Monocytes from Patients with Systemic Sclerosis: Role of Serum Factors. *Ann. Rheum. Dis.* 72 (8), 1382–1389. doi:10.1136/annrheumdis-2012-201958

Distler, J. H. W., Györfi, A. H., Ramanujam, M., Whitfield, M. L., Königshoff, M., and Lafyatis, R. (2019). Shared and Distinct Mechanisms of Fibrosis. *Nat. Rev. Rheumatol.* 15 (12), 705–730. doi:10.1038/s41584-019-0322-7

Dowson, C., Simpson, N., Duffy, L., and O'Reilly, S. (2017). Innate Immunity in Systemic Sclerosis. *Curr. Rheumatol. Rep.* 19 (1), 2. doi:10.1007/s11926-017-0630-3

Driskell, R. R., Lichtenberger, B. M., Hoste, E., Kretzschmar, K., Simons, B. D., Charalambous, M., et al. (2013). Distinct Fibroblast Lineages Determine Dermal Architecture in Skin Development and Repair. *Nature* 504 (7479), 277–281. doi:10.1038/nature12783

Dufour, A. M., Borowczyk-Michalowska, J., Alvarez, M., Truchetet, M. E., Modarressi, A., Brembilla, N. C., et al. (2020). IL-17A Dissociates Inflammation from Fibrogenesis in Systemic Sclerosis. *J. Invest. Dermatol.* 140 (1), 103–e8. doi:10.1016/j.jid.2019.05.026

Dumoitier, N., Chaigne, B., Régent, A., Lofek, S., Mhibik, M., Dorfmüller, P., et al. (2017). Scleroderma Peripheral B Lymphocytes Secrete Interleukin-6 and Transforming Growth Factor β and Activate Fibroblasts. *Arthritis Rheumatol.* 69 (5), 1078–1089. doi:10.1002/art.40016

Ebmeier, S., and Horsley, V. (2015). Origin of Fibrosing Cells in Systemic Sclerosis. *Curr. Opin. Rheumatol.* 27 (6), 555–562. doi:10.1097/BOR.0000000000000217

Eyerich, S., Eyerich, K., Pennino, D., Carbone, T., Nasorri, F., Pallotta, S., et al. (2009). Th22 Cells Represent a Distinct Human T Cell Subset Involved in Epidermal Immunity and Remodeling. *J. Clin. Invest.* 119 (12), 3573–3585. doi:10.1172/JCI40202

Fleischmajer, R., Perlish, J. S., and Reeves, J. R. (1977). Cellular Infiltrates in Scleroderma Skin. *Arthritis Rheum.* 20 (4), 975–984. doi:10.1002/art.1780200410

Forestier, A., Guerrier, T., Jouvray, M., Giovannelli, J., Lefèvre, G., Sobanski, V., et al. (2018). Altered B Lymphocyte Homeostasis and Functions in Systemic Sclerosis. *Autoimmun. Rev.* 17 (3), 244–255. doi:10.1016/j.autrev.2017.10.015

Fox, D. A., Lundy, S. K., Whitfield, M. L., Berrocal, V., Campbell, P., Rasmussen, S., et al. (2021). Lymphocyte Subset Abnormalities in Early Diffuse Cutaneous Systemic Sclerosis. *Arthritis Res. Ther.* 23 (1), 10. doi:10.1186/s13075-020-02383-w

Fuschiotti, P., Larregina, A. T., Ho, J., Feghali-Bostwick, C., and Medsger, T. A., Jr. (2013). Interleukin-13-producing CD8+ T Cells Mediate Dermal Fibrosis in Patients with Systemic Sclerosis. *Arthritis Rheum.* 65 (1), 236–246. doi:10.1002/art.37706

Gabsi, A., Heim, X., Dlala, A., Gati, A., Sakhri, H., Abidi, A., et al. (2019). TH17 Cells Expressing CD146 Are Significantly Increased in Patients with Systemic Sclerosis. *Sci. Rep.* 9 (1), 17721. doi:10.1038/s41598-019-54132-y

Gao, X., Jia, G., Guttman, A., DePianto, D. J., Morshead, K. B., Sun, K. H., et al. (2020). Osteopontin Links Myeloid Activation and Disease Progression in Systemic Sclerosis. *Cell Rep Med* 1 (8), 100140. doi:10.1016/j.xcrm.2020.100140

Gasparini, G., Cozzani, E., and Parodi, A. (2020). Interleukin-4 and Interleukin-13 as Possible Therapeutic Targets in Systemic Sclerosis. *Cytokine* 125, 154799. doi:10.1016/j.cyto.2019.154799

Gaydosik, A. M., Tabib, T., Domsic, R., Khanna, D., Lafyatis, R., and Fuschiotti, P. (2021). Single-cell Transcriptome Analysis Identifies Skin-specific T-Cell Responses in Systemic Sclerosis. *Ann. Rheum. Dis.* 80 (11), 1453–1460. doi:10.1136/annrheumdis-2021-220209

Giacomelli, R., Matucci-Cerinic, M., Cipriani, P., Ghersetich, I., Lattanzio, R., Pavan, A., et al. (1998). Circulating Vdelta1+ T Cells Are Activated and Accumulate in the Skin of Systemic Sclerosis Patients. *Arthritis Rheum.* 41 (2), 327–334. doi:10.1002/1529-0131(199802)41:2<327:AID-ART17>3.0.CO;2-S

Gordon, J. K., Martyanov, V., Franks, J. M., Bernstein, E. J., Szymonifka, J., Magro, C., et al. (2018). Belimumab for the Treatment of Early Diffuse Systemic Sclerosis: Results of a Randomized, Double-Blind, Placebo-Controlled, Pilot Trial. *Arthritis Rheumatol.* 70 (2), 308–316. doi:10.1002/art.40358

Gordon, S. (2003). Alternative Activation of Macrophages. *Nat. Rev. Immunol.* 3 (1), 23–35. doi:10.1038/nri978

Gourh, P., Agarwal, S. K., Divecha, D., Assassi, S., Paz, G., Arora-Singh, R. K., et al. (2009). Polymorphisms in TBX21 and STAT4 Increase the Risk of Systemic Sclerosis: Evidence of Possible Gene-Gene Interaction and Alterations in Th1/Th2 Cytokines. *Arthritis Rheum.* 60 (12), 3794–3806. doi:10.1002/art.24958

Gu, Y. S., Kong, J., Cheema, G. S., Keen, C. L., Wick, G., and Gershwin, M. E. (2008). The Immunobiology of Systemic Sclerosis. *Semin. Arthritis Rheum.* 38 (2), 132–160. doi:10.1016/j.semarthrit.2007.10.010

Guggino, G., Lo Pizzo, M., Di Liberto, D., Rizzo, A., Cipriani, P., Ruscitti, P., et al. (2017). Interleukin-9 Over-expression and T Helper 9 Polarization in Systemic Sclerosis Patients. *Clin. Exp. Immunol.* 190 (2), 208–216. doi:10.1111/cei.13009

Guiducci, C., Tripodo, C., Gong, M., Sangaletti, S., Colombo, M. P., Coffman, R. L., et al. (2010). Autoimmune Skin Inflammation Is Dependent on Plasmacytoid Dendritic Cell Activation by Nucleic Acids via TLR7 and TLR9. *J. Exp. Med.* 207 (13), 2931–2942. doi:10.1084/jem.20101048

Guilliams, M., Ginhoux, F., Jakubzick, C., Naik, S. H., Onai, N., Schraml, B. U., et al. (2014). Dendritic Cells, Monocytes and Macrophages: a Unified Nomenclature Based on Ontogeny. *Nat. Rev. Immunol.* 14 (8), 571–578. doi:10.1038/nri3712

Hale, G. (2001). The CD52 Antigen and Development of the CAMPATH Antibodies. *Cytotherapy* 3 (3), 137–143. doi:10.1080/146532401753174098

Harrington, L. E., Hatton, R. D., Mangan, P. R., Turner, H., Murphy, T. L., Murphy, K. M., et al. (2005). Interleukin 17-producing CD4+ Effector T Cells Develop via a Lineage Distinct from the T Helper Type 1 and 2 Lineages. *Nat. Immunol.* 6 (11), 1123–1132. doi:10.1038/ni1254

Harris, D. P., Haynes, L., Sayles, P. C., Duso, D. K., Eaton, S. M., Lepak, N. M., et al. (2000). Reciprocal Regulation of Polarized Cytokine Production by Effector B and T Cells. *Nat. Immunol.* 1 (6), 475–482. doi:10.1038/82717

Henriques, A., Silva, C., Santiago, M., Henriques, M. J., Martinho, A., Trindade, H., et al. (2016). Subset-specific Alterations in Frequencies and Functional Signatures of γδ T Cells in Systemic Sclerosis Patients. *Inflamm. Res.* 65 (12), 985–994. doi:10.1007/s00011-016-0982-6

Higashi-Kuwata, N., Jinnin, M., Makino, T., Fukushima, S., Inoue, Y., Muchemwa, F. C., et al. (2010). Characterization of Monocyte/macrophage Subsets in the Skin and Peripheral Blood Derived from Patients with Systemic Sclerosis. *Arthritis Res. Ther.* 12 (4), R128. doi:10.1186/ar3066

Holcombe, R. F., Baethge, B. A., Wolf, R. E., Betzing, K. W., and Stewart, R. M. (1995). Natural Killer Cells and Gamma delta T Cells in Scleroderma: Relationship to Disease Duration and Anti-scl-70 Antibodies. *Ann. Rheum. Dis.* 54 (1), 69–72. doi:10.1136/ard.54.1.69

Hügle, T., O'Reilly, S., Simpson, R., Kraaij, M. D., Bigley, V., Collin, M., et al. (2013). Tumor Necrosis Factor-Costimulated T Lymphocytes from Patients with Systemic Sclerosis Trigger Collagen Production in Fibroblasts. *Arthritis Rheum.* 65 (2), 481–491. doi:10.1002/art.37738

Iozzo, R. V., Pillarisetti, J., Sharma, B., Murdoch, A. D., Danielson, K. G., Uitto, J., et al. (1997). Structural and Functional Characterization of the Human Perlecan Gene Promoter. Transcriptional Activation by Transforming Growth Factor-Beta via a Nuclear Factor 1-binding Element. *J. Biol. Chem.* 272 (8), 5219–5228. doi:10.1074/jbc.272.8.5219

Iwata, Y., Matsushita, T., Horikawa, M., Dilillo, D. J., Yanaba, K., Venturi, G. M., et al. (2011). Characterization of a Rare IL-10-competent B-Cell Subset in Humans that Parallels Mouse Regulatory B10 Cells. *Blood* 117 (2), 530–541. doi:10.1182/blood-2010-07-294249

Jaguin, M., Fardel, O., and Lecureur, V. (2015). AhR-dependent Secretion of PDGF-BB by Human Classically Activated Macrophages Exposed to DEP Extracts Stimulates Lung Fibroblast Proliferation. *Toxicol. Appl. Pharmacol.* 285 (3), 170–178. doi:10.1016/j.taap.2015.04.007

Jimenez, S. A. (2013). Role of Endothelial to Mesenchymal Transition in the Pathogenesis of the Vascular Alterations in Systemic Sclerosis. *ISRN Rheumatol.* 2013, 835948. doi:10.1155/2013/835948

Kahaleh, M. B., and Fan, P. S. (1997). Mechanism of Serum-Mediated Endothelial Injury in Scleroderma: Identification of a Granular Enzyme in Scleroderma Skin and Sera. *Clin. Immunol. Immunopathol* 83 (1), 32–40. doi:10.1006/clin.1996.4322

Kähäri, V. M., Sandberg, M., Kalimo, H., Vuorio, T., and Vuorio, E. (1988). Identification of Fibroblasts Responsible for Increased Collagen Production in Localized Scleroderma by *In Situ* Hybridization. *J. Invest. Dermatol.* 90 (5), 664–670. doi:10.1111/1523-1747.ep12560826

Kaplan, M. H., Hufford, M. M., and Olson, M. R. (2015). The Development and *In Vivo* Function of T Helper 9 Cells. *Nat. Rev. Immunol.* 15 (5), 295–307. doi:10.1038/nri3824

Kataoka, H., Yasuda, S., Fukaya, S., Oku, K., Horita, T., Atsumi, T., et al. (2015). Decreased Expression of Runx1 and Lowered Proportion of Foxp3+ CD25+ CD4+ Regulatory T Cells in Systemic Sclerosis. *Mod. Rheumatol.* 25 (1), 90–95. doi:10.3109/14397595.2014.899736

Khanna, D., Denton, C. P., Lin, C. J. F., van Laar, J. M., Frech, T. M., Anderson, M. E., et al. (2018). Safety and Efficacy of Subcutaneous Tocilizumab in Systemic Sclerosis: Results from the Open-Label Period of a Phase II Randomised Controlled Trial (faSScinate). *Ann. Rheum. Dis.* 77 (2), 212–220. doi:10.1136/annrheumdis-2017-211682

Khanna, D., Lin, C. J. F., Furst, D. E., Wagner, B., Zucchetto, M., Raghu, G., et al. (2021). Long-Term Safety and Efficacy of Tocilizumab in Early Systemic Sclerosis-Interstitial Lung Disease: Open Label Extension of a Phase 3 Randomized Controlled Trial. *Am. J. Respir. Crit. Care Med.* doi:10.1164/rccm.202103-0714OC

Khoder, A., Sarvaria, A., Alsuliman, A., Chew, C., Sekine, T., Cooper, N., et al. (2014). Regulatory B Cells Are Enriched within the IgM Memory and Transitional Subsets in Healthy Donors but Are Deficient in Chronic GVHD. *Blood* 124 (13), 2034–2045. doi:10.1182/blood-2014-04-571125

Klein, S., Kretz, C. C., Ruland, V., Stumpf, C., Haust, M., Hartschuh, W., et al. (2011). Reduction of Regulatory T Cells in Skin Lesions but Not in Peripheral Blood of Patients with Systemic Scleroderma. *Ann. Rheum. Dis.* 70 (8), 1475–1481. doi:10.1136/ard.2009.116525

Kobayashi, S., Nagafuchi, Y., Okubo, M., Sugimori, Y., Shirai, H., Hatano, H., et al. (2021). Integrated Bulk and Single-Cell RNA-Sequencing Identified Disease-Relevant Monocytes and a Gene Network Module Underlying Systemic Sclerosis. *J. Autoimmun.* 116, 102547. doi:10.1016/j.jaut.2020.102547

Korn, T., Bettelli, E., Oukka, M., and Kuchroo, V. K. (2009). IL-17 and Th17 Cells. *Annu. Rev. Immunol.* 27, 485–517. doi:10.1146/annurev.immunol.021908.132710

Kubo, S., Nakayamada, S., Miyazaki, Y., Yoshikawa, M., Yoshinari, H., Satoh, Y., et al. (2019). Distinctive Association of Peripheral Immune Cell Phenotypes with Capillaroscopic Microvascular Patterns in Systemic Sclerosis. *Rheumatology (Oxford)* 58 (12), 2273–2283. doi:10.1093/rheumatology/kez244

Kurasawa, K., Hirose, K., Sano, H., Endo, H., Shinkai, H., Nawata, Y., et al. (2000). Increased Interleukin-17 Production in Patients with Systemic Sclerosis. *Arthritis Rheum.* 43 (11), 2455–2463. doi:10.1002/1529-0131(200011)43:11<2455:AID-ANR12>3.0.CO;2-K

Kuzumi, A., Yoshizaki, A., Matsuda, K. M., Kotani, H., Norimatsu, Y., Fukayama, M., et al. (2021). Interleukin-31 Promotes Fibrosis and T Helper 2 Polarization in Systemic Sclerosis. *Nat. Commun.* 12 (1), 5947. doi:10.1038/s41467-021-26099-w

Lande, R., Mennella, A., Palazzo, R., Pietraforte, I., Stefanantoni, K., Iannace, N., et al. (2020). Anti-CXCL4 Antibody Reactivity Is Present in Systemic Sclerosis (SSc) and Correlates with the SSc Type I Interferon Signature. *Int. J. Mol. Sci.* 21 (14), 5102. doi:10.3390/ijms21145102

Laplante, P., Raymond, M. A., Gagnon, G., Vigneault, N., Sasseville, A. M., Langelier, Y., et al. (2005). Novel Fibrogenic Pathways Are Activated in Response to Endothelial Apoptosis: Implications in the Pathophysiology of Systemic Sclerosis. *J. Immunol.* 174 (9), 5740–5749. doi:10.4049/jimmunol.174.9.5740

Laurent, P., Sisirak, V., Lazaro, E., Richez, C., Duffau, P., Blanco, P., et al. (2018). Innate Immunity in Systemic Sclerosis Fibrosis: Recent Advances. *Front. Immunol.* 9, 1702. doi:10.3389/fimmu.2018.01702

Le Huu, D., Matsushita, T., Jin, G., Hamaguchi, Y., Hasegawa, M., Takehara, K., et al. (2013). Donor-derived Regulatory B Cells Are Important for Suppression of Murine Sclerodermatous Chronic Graft-Versus-Host Disease. *Blood* 121 (16), 3274–3283. doi:10.1182/blood-2012-11-465658

Lech, M., and Anders, H. J. (2013). Macrophages and Fibrosis: How Resident and Infiltrating Mononuclear Phagocytes Orchestrate All Phases of Tissue Injury and Repair. *Biochim. Biophys. Acta* 1832 (7), 989–997. doi:10.1016/j.bbadis.2012.12.001

Lee, D. S. W., Rojas, O. L., and Gommerman, J. L. (2021). B Cell Depletion Therapies in Autoimmune Disease: Advances and Mechanistic Insights. *Nat. Rev. Drug Discov.* 20 (3), 179–199. doi:10.1038/s41573-020-00092-2

Lei, L., Zhao, C., Qin, F., He, Z. Y., Wang, X., and Zhong, X. N. (2016). Th17 Cells and IL-17 Promote the Skin and Lung Inflammation and Fibrosis Process in a Bleomycin-Induced Murine Model of Systemic Sclerosis. *Clin. Exp. Rheumatol.* 34 (5), 14–22.

LeRoy, E. C., Black, C., Fleischmajer, R., Jablonska, S., Krieg, T., Medsger, T. A., Jr., et al. (1988). Scleroderma (Systemic Sclerosis): Classification, Subsets and Pathogenesis. *J. Rheumatol.* 15 (2), 202–205.

Lescoat, A., Lecureur, V., Roussel, M., Sunnaram, B. L., Ballerie, A., Coiffier, G., et al. (2017). CD16-positive Circulating Monocytes and Fibrotic Manifestations of Systemic Sclerosis. *Clin. Rheumatol.* 36 (7), 1649–1654. doi:10.1007/s10067-017-3597-6

Li, G., Larregina, A. T., Domsic, R. T., Stolz, D. B., Medsger, T. A., Jr., Lafyatis, R., et al. (2017). Skin-Resident Effector Memory CD8+CD28- T Cells Exhibit a Profibrotic Phenotype in Patients with Systemic Sclerosis. *J. Invest. Dermatol.* 137 (5), 1042–1050. doi:10.1016/j.jid.2016.11.037

Li, R., Rezk, A., Miyazaki, Y., Hilgenberg, E., Touil, H., Shen, P., et al. (2015). Proinflammatory GM-CSF-Producing B Cells in Multiple Sclerosis and B Cell Depletion Therapy. *Sci. Transl Med.* 7 (310), 310ra166. doi:10.1126/scitranslmed.aab4176

Liu, K., Victora, G. D., Schwickert, T. A., Guermonprez, P., Meredith, M. M., Yao, K., et al. (2009). *In Vivo* analysis of Dendritic Cell Development and Homeostasis. *Science* 324 (5925), 392–397. doi:10.1126/science.1170540

Liu, Q., Zaba, L., Satpathy, A. T., Longmire, M., Zhang, W., Li, K., et al. (2020). Chromatin Accessibility Landscapes of Skin Cells in Systemic Sclerosis Nominate Dendritic Cells in Disease Pathogenesis. *Nat. Commun.* 11 (1), 5843. doi:10.1038/s41467-020-19702-z

Liu, X., Gao, N., Li, M., Xu, D., Hou, Y., Wang, Q., et al. (2013). Elevated Levels of CD4(+)CD25(+)FoxP3(+) T Cells in Systemic Sclerosis Patients Contribute to the Secretion of IL-17 and Immunosuppression Dysfunction. *PLoS One* 8 (6), e64531. doi:10.1371/journal.pone.0064531

Luzina, I. G., Todd, N. W., Nacu, N., Lockatell, V., Choi, J., Hummers, L. K., et al. (2009). Regulation of Pulmonary Inflammation and Fibrosis through Expression of Integrins alphaVbeta3 and alphaVbeta5 on Pulmonary T Lymphocytes. *Arthritis Rheum.* 60 (5), 1530–1539. doi:10.1002/art.24435

Ly, N. T. M., Ueda-Hayakawa, I., Nguyen, C. T. H., Huynh, T. N. M., Kishimoto, I., Fujimoto, M., et al. (2021). Imbalance toward TFH 1 Cells Playing a Role in Aberrant B Cell Differentiation in Systemic Sclerosis. *Rheumatology (Oxford)* 60 (3), 1553–1562. doi:10.1093/rheumatology/keaa669

MacDonald, K. G., Dawson, N. A., Huang, Q., Dunne, J. V., Levings, M. K., and Broady, R. (2015). Regulatory T Cells Produce Profibrotic Cytokines in the Skin of Patients with Systemic Sclerosis. *J. Allergy Clin. Immunol.* 135 (4), 946–e9. doi:10.1016/j.jaci.2014.12.1932

Mackay, F., Schneider, P., Rennert, P., and Browning, J. (2003). BAFF and APRIL: a Tutorial on B Cell Survival. *Annu. Rev. Immunol.* 21, 231–264. doi:10.1146/annurev.immunol.21.120601.141152

Maehara, T., Kaneko, N., Perugino, C. A., Mattoo, H., Kers, J., Allard-Chamard, H., et al. (2020). Cytotoxic CD4+ T Lymphocytes May Induce Endothelial Cell Apoptosis in Systemic Sclerosis. *J. Clin. Invest.* 130 (5), 2451–2464. doi:10.1172/JCI131700

Marrapodi, R., Pellicano, C., Radicchio, G., Leodori, G., Colantuono, S., Iacolare, A., et al. (2020). CD21low B Cells in Systemic Sclerosis: A Possible Marker of Vascular Complications. *Clin. Immunol.* 213, 108364. doi:10.1016/j.clim.2020.108364

Martin, S. F. (2014). Adaptation in the Innate Immune System and Heterologous Innate Immunity. *Cell Mol Life Sci* 71 (21), 4115–4130. doi:10.1007/s00018-014-1676-2

Mathian, A., Parizot, C., Dorgham, K., Trad, S., Arnaud, L., Larsen, M., et al. (2012). Activated and Resting Regulatory T Cell Exhaustion Concurs with High Levels of Interleukin-22 Expression in Systemic Sclerosis Lesions. *Ann. Rheum. Dis.* 71 (7), 1227–1234. doi:10.1136/annrheumdis-2011-200709

Matsushita, T., Hamaguchi, Y., Hasegawa, M., Takehara, K., and Fujimoto, M. (2016). Decreased Levels of Regulatory B Cells in Patients with Systemic Sclerosis: Association with Autoantibody Production and Disease Activity. *Rheumatology (Oxford)* 55 (2), 263–267. doi:10.1093/rheumatology/kev331

Matsushita, T., Kobayashi, T., Mizumaki, K., Kano, M., Sawada, T., Tennichi, M., et al. (2018). BAFF Inhibition Attenuates Fibrosis in Scleroderma by Modulating the Regulatory and Effector B Cell Balance. *Sci. Adv.* 4 (7), eaas9944. doi:10.1126/sciadv.aas9944

Mattoo, H., Mahajan, V. S., Maehara, T., Deshpande, V., Della-Torre, E., Wallace, Z. S., et al. (2016). Clonal Expansion of CD4(+) Cytotoxic T Lymphocytes in Patients with IgG4-Related Disease. *J. Allergy Clin. Immunol.* 138 (3), 825–838. doi:10.1016/j.jaci.2015.12.1330

Mihara, M., Ohsugi, Y., and Kishimoto, T. (2011). Tocilizumab, a Humanized Anti-interleukin-6 Receptor Antibody, for Treatment of Rheumatoid Arthritis. *Open Access Rheumatol.* 3, 19–29. doi:10.2147/OARRR.S17118

Mohamed, M. E., Gamal, R. M., El-Mokhtar, M. A., Hassan, A. T., Abozaid, H. S. M., Ghandour, A. M., et al. (2021). Peripheral Cells from Patients with Systemic Sclerosis Disease Co-expressing M1 and M2 Monocyte/macrophage Surface Markers: Relation to the Degree of Skin Involvement. *Hum. Immunol.* 82 (9), 634–639. doi:10.1016/j.humimm.2021.03.009

Mosser, D. M., and Edwards, J. P. (2008). Exploring the Full Spectrum of Macrophage Activation. *Nat. Rev. Immunol.* 8 (12), 958–969. doi:10.1038/nri2448

Mosser, D. M. (2003). The many Faces of Macrophage Activation. *J. Leukoc. Biol.* 73 (2), 209–212. doi:10.1189/jlb.0602325

Mostmans, Y., Cutolo, M., Giddelo, C., Decuman, S., Melsens, K., Declercq, H., et al. (2017). The Role of Endothelial Cells in the Vasculopathy of Systemic Sclerosis: A Systematic Review. *Autoimmun. Rev.* 16 (8), 774–786. doi:10.1016/j.autrev.2017.05.024

Nakashima, T., Jinnin, M., Yamane, K., Honda, N., Kajihara, I., Makino, T., et al. (2012). Impaired IL-17 Signaling Pathway Contributes to the Increased Collagen Expression in Scleroderma Fibroblasts. *J. Immunol.* 188 (8), 3573–3583. doi:10.4049/jimmunol.1100591

O'Reilly, S., Hügle, T., and van Laar, J. M. (2012). T Cells in Systemic Sclerosis: a Reappraisal. *Rheumatology (Oxford)* 51 (9), 1540–1549. doi:10.1093/rheumatology/kes090

Okamoto, Y., Hasegawa, M., Matsushita, T., Hamaguchi, Y., Huu, D. L., Iwakura, Y., et al. (2012). Potential Roles of interleukin-17A in the Development of Skin Fibrosis in Mice. *Arthritis Rheum.* 64 (11), 3726–3735. doi:10.1002/art.34643

Ototake, Y., Yamaguchi, Y., Asami, M., Komitsu, N., Akita, A., Watanabe, T., et al. (2021). Downregulated IRF8 in Monocytes and Macrophages of Patients with Systemic Sclerosis May Aggravate the Fibrotic Phenotype. *J. Invest. Dermatol.* 141 (8), 1954–1963. doi:10.1016/j.jid.2021.02.015

Park, H., Li, Z., Yang, X. O., Chang, S. H., Nurieva, R., Wang, Y. H., et al. (2005). A Distinct Lineage of CD4 T Cells Regulates Tissue Inflammation by Producing Interleukin 17. *Nat. Immunol.* 6 (11), 1133–1141. doi:10.1038/ni1261

Park, M. J., Moon, S. J., Lee, E. J., Jung, K. A., Kim, E. K., Kim, D. S., et al. (2018). IL-1-IL-17 Signaling Axis Contributes to Fibrosis and Inflammation in Two Different Murine Models of Systemic Sclerosis. *Front. Immunol.* 9, 1611. doi:10.3389/fimmu.2018.01611

Passlick, B., Flieger, D., and Ziegler-Heitbrock, H. W. (1989). Identification and Characterization of a Novel Monocyte Subpopulation in Human Peripheral Blood. *Blood* 74 (7), 2527–2534. doi:10.1182/blood.v74.7.2527.bloodjournal7472527

Perez-Andres, M., Paiva, B., Nieto, W. G., Caraux, A., Schmitz, A., Almeida, J., et al. (2010). Human Peripheral Blood B-Cell Compartments: a Crossroad in B-Cell Traffic. *Cytometry B Clin. Cytom* 78 (Suppl. 1), S47–S60. doi:10.1002/cyto.b.20547

Peyser, R., MacDonnell, S., Gao, Y., Cheng, L., Kim, Y., Kaplan, T., et al. (2019). Defining the Activated Fibroblast Population in Lung Fibrosis Using Single-Cell Sequencing. *Am. J. Respir. Cel Mol Biol* 61 (1), 74–85. doi:10.1165/rcmb.2018-0313OC

Pilling, D., Akbar, A. N., Girdlestone, J., Orteu, C. H., Borthwick, N. J., Amft, N., et al. (1999). Interferon-beta Mediates Stromal Cell rescue of T Cells from Apoptosis. *Eur. J. Immunol.* 29 (3), 1041–1050. doi:10.1002/(SICI)1521-4141(199903)29:03<1041:AID-IMMU1041>3.0.CO;2-#

Pociask, D. A., Chen, K., Choi, S. M., Oury, T. D., Steele, C., and Kolls, J. K. (2011). Γδ T Cells Attenuate Bleomycin-Induced Fibrosis through the Production of CXCL10. *Am. J. Pathol.* 178 (3), 1167–1176. doi:10.1016/j.ajpath.2010.11.055

Radstake, T. R., van Bon, L., Broen, J., Wenink, M., Santegoets, K., Deng, Y., et al. (2009). Increased Frequency and Compromised Function of T Regulatory Cells in Systemic Sclerosis (SSc) Is Related to a Diminished CD69 and TGFbeta Expression. *PLoS One* 4 (6), e5981. doi:10.1371/journal.pone.0005981

Ratzinger, G., Reagan, J. L., Heller, G., Busam, K. J., and Young, J. W. (2003). Differential CD52 Expression by Distinct Myeloid Dendritic Cell Subsets: Implications for Alemtuzumab Activity at the Level of Antigen Presentation in Allogeneic Graft-Host Interactions in Transplantation. *Blood* 101 (4), 1422–1429. doi:10.1182/blood-2002-04-1093

Ricard, L., Jachiet, V., Malard, F., Ye, Y., Stocker, N., Rivière, S., et al. (2019). Circulating Follicular Helper T Cells Are Increased in Systemic Sclerosis and Promote Plasmablast Differentiation through the IL-21 Pathway Which Can Be Inhibited by Ruxolitinib. *Ann. Rheum. Dis.* 78 (4), 539–550. doi:10.1136/annrheumdis-2018-214382

Ricard, L., Malard, F., Riviere, S., Laurent, C., Fain, O., Mohty, M., et al. (2021). Regulatory B Cell Imbalance Correlates with Tfh Expansion in Systemic Sclerosis. *Clin. Exp. Rheumatol.* 39 (4), 20–24.

Rice, L. M., Stifano, G., Ziemek, J., and Lafyatis, R. (2016). Local Skin Gene Expression Reflects Both Local and Systemic Skin Disease in Patients with Systemic Sclerosis. *Rheumatology (Oxford)* 55 (2), 377–379. doi:10.1093/rheumatology/kev335

Robak, E., Gerlicz-Kowalczuk, Z., Dziankowska-Bartkowiak, B., Wozniacka, A., and Bogaczewicz, J. (2019). Serum Concentrations of IL-17A, IL-17B, IL-17E and IL-17F in Patients with Systemic Sclerosis. *Arch. Med. Sci.* 15 (3), 706–712. doi:10.5114/aoms.2019.84738

Rosenbloom, J., Feldman, G., Freundlich, B., and Jimenez, S. A. (1986). Inhibition of Excessive Scleroderma Fibroblast Collagen Production by Recombinant Gamma-Interferon. Association with a Coordinate Decrease in Types I and III Procollagen Messenger RNA Levels. *Arthritis Rheum.* 29 (7), 851–856. doi:10.1002/art.1780290706

Ross, R. L., Corinaldesi, C., Migneco, G., Carr, I. M., Antanaviciute, A., Wasson, C. W., et al. (2021). Targeting Human Plasmacytoid Dendritic Cells through BDCA2 Prevents Skin Inflammation and Fibrosis in a Novel Xenotransplant Mouse Model of Scleroderma. *Ann. Rheum. Dis.* 80 (7), 920–929. doi:10.1136/annrheumdis-2020-218439

Rossato, M., Affandi, A. J., Thordardottir, S., Wichers, C. G. K., Cossu, M., Broen, J. C. A., et al. (2017). Association of MicroRNA-618 Expression with Altered Frequency and Activation of Plasmacytoid Dendritic Cells in Patients with Systemic Sclerosis. *Arthritis Rheumatol.* 69 (9), 1891–1902. doi:10.1002/art.40163

Rudnik, M., Hukara, A., Kocherova, I., Jordan, S., Schniering, J., Milleret, V., et al. (2021). Elevated Fibronectin Levels in Profibrotic CD14+ Monocytes and CD14+ Macrophages in Systemic Sclerosis. *Front. Immunol.* 12, 642891. doi:10.3389/fimmu.2021.642891

Rudnik, M., Rolski, F., Jordan, S., Mertelj, T., Stellato, M., Distler, O., et al. (2021). Regulation of Monocyte Adhesion and Type I Interferon Signaling by CD52 in Patients with Systemic Sclerosis. *Arthritis Rheumatol.* 73 (9), 1720–1730. doi:10.1002/art.41737

Russomanno, G., Jo, K. B., Abdul-Salam, V. B., Morgan, C., Endruschat, J., Schaeper, U., et al. (2021). miR-150-PTPMT1-cardiolipin Signaling in Pulmonary Arterial Hypertension. *Mol. Ther. Nucleic Acids* 23, 142–153. doi:10.1016/j.omtn.2020.10.042

Sato, S., Hasegawa, M., and Takehara, K. (2001). Serum Levels of Interleukin-6 and Interleukin-10 Correlate with Total Skin Thickness Score in Patients with Systemic Sclerosis. *J. Dermatol. Sci.* 27 (2), 140–146. doi:10.1016/s0923-1811(01)00128-1

Satoh, T., Nakagawa, K., Sugihara, F., Kuwahara, R., Ashihara, M., Yamane, F., et al. (2017). Identification of an Atypical Monocyte and Committed Progenitor Involved in Fibrosis. *Nature* 541 (7635), 96–101. doi:10.1038/nature20611

Schneider, L., Marcondes, N. A., Hax, V., da Silva Moreira, I. F., Ueda, C. Y., Piovesan, R. R., et al. (2021). Flow Cytometry Evaluation of CD14/CD16 Monocyte Subpopulations in Systemic Sclerosis Patients: a Cross Sectional Controlled Study. *Adv. Rheumatol.* 61 (1), 27. doi:10.1186/s42358-021-00182-8

Servaas, N. H., Zaaraoui-Boutahar, F., Wichers, C. G. K., Ottria, A., Chouri, E., Affandi, A. J., et al. (2021). Longitudinal Analysis of T-Cell Receptor Repertoires Reveals Persistence of Antigen-Driven CD4+ and CD8+ T-Cell Clusters in Systemic Sclerosis. *J. Autoimmun.* 117, 102574. doi:10.1016/j.jaut.2020.102574

Shapouri-Moghaddam, A., Mohammadian, S., Vazini, H., Taghadosi, M., Esmaeili, S. A., Mardani, F., et al. (2018). Macrophage Plasticity, Polarization, and Function in Health and Disease. *J. Cel Physiol* 233 (9), 6425–6440. doi:10.1002/jcp.26429

Sharma, B., Handler, M., Eichstetter, I., Whitelock, J. M., Nugent, M. A., and Iozzo, R. V. (1998). Antisense Targeting of Perlecan Blocks Tumor Growth and Angiogenesis *In Vivo*. *J. Clin. Invest.* 102 (8), 1599–1608. doi:10.1172/JCI3793

Shen, P., and Fillatreau, S. (2015). Antibody-independent Functions of B Cells: a Focus on Cytokines. *Nat. Rev. Immunol.* 15 (7), 441–451. doi:10.1038/nri3857

Shi, C., and Pamer, E. G. (2011). Monocyte Recruitment during Infection and Inflammation. *Nat. Rev. Immunol.* 11 (11), 762–774. doi:10.1038/nri3070

Siegal, F. P., Kadowaki, N., Shodell, M., Fitzgerald-Bocarsly, P. A., Shah, K., Ho, S., et al. (1999). The Nature of the Principal Type 1 Interferon-Producing Cells in Human Blood. *Science* 284 (5421), 1835–1837. doi:10.1126/science.284.5421.1835

Simon, D., Balogh, P., Erdő-Bonyár, S., Böröcz, K., Minier, T., Czirják, L., et al. (2021). Increased Frequency of Activated Switched Memory B Cells and its Association with the Presence of Pulmonary Fibrosis in Diffuse Cutaneous Systemic Sclerosis Patients. *Front. Immunol.* 12, 686483. doi:10.3389/fimmu.2021.686483

Skaug, B., Khanna, D., Swindell, W. R., Hinchcliff, M. E., Frech, T. M., Steen, V. D., et al. (2020). Global Skin Gene Expression Analysis of Early Diffuse Cutaneous Systemic Sclerosis Shows a Prominent Innate and Adaptive Inflammatory Profile. *Ann. Rheum. Dis.* 79 (3), 379–386. doi:10.1136/annrheumdis-2019-215894

Steen, V. D. (2005). Autoantibodies in Systemic Sclerosis. *Semin. Arthritis Rheum.* 35 (1), 35–42. doi:10.1016/j.semarthrit.2005.03.005

Streicher, K., Sridhar, S., Kuziora, M., Morehouse, C. A., Higgs, B. W., Sebastian, Y., et al. (2018). Baseline Plasma Cell Gene Signature Predicts Improvement in Systemic Sclerosis Skin Scores Following Treatment with Inebilizumab (MEDI-551) and Correlates with Disease Activity in Systemic Lupus Erythematosus and Chronic

Obstructive Pulmonary Disease. *Arthritis Rheumatol.* 70 (12), 2087–2095. doi:10.1002/art.40656

Swiecki, M., and Colonna, M. (2015). The Multifaceted Biology of Plasmacytoid Dendritic Cells. *Nat. Rev. Immunol.* 15 (8), 471–485. doi:10.1038/nri3865

Tabib, T., Huang, M., Morse, N., Papazoglou, A., Behera, R., Jia, M., et al. (2021). Myofibroblast Transcriptome Indicates SFRP2hi Fibroblast Progenitors in Systemic Sclerosis Skin. *Nat. Commun.* 12 (1), 4384. doi:10.1038/s41467-021-24607-6

Tabib, T., Morse, C., Wang, T., Chen, W., and Lafyatis, R. (2018). SFRP2/DPP4 and FMO1/LSP1 Define Major Fibroblast Populations in Human Skin. *J. Invest. Dermatol.* 138 (4), 802–810. doi:10.1016/j.jid.2017.09.045

Taylor, D. K., Mittereder, N., Kuta, E., Delaney, T., Burwell, T., Dacosta, K., et al. (2018). T Follicular Helper-like Cells Contribute to Skin Fibrosis. *Sci. Transl Med.* 10 (431), eaaf5307. doi:10.1126/scitranslmed.aaf5307

Tezcan, D., Sivrikaya, A., Ergün, D., Özer, H., Eryavuz Onmaz, D., Körez, M. K., et al. (2021). Evaluation of Serum Interleukin-6 (IL-6), IL-13, and IL-17 Levels and Computed Tomography Finding in Interstitial Lung Disease Associated with Connective Tissue Disease Patients. *Clin. Rheumatol.* 40 (11), 4713–4724. doi:10.1007/s10067-021-05773-w

Toledo, D. M., and Pioli, P. A. (2019). Macrophages in Systemic Sclerosis: Novel Insights and Therapeutic Implications. *Curr. Rheumatol. Rep.* 21 (7), 31. doi:10.1007/s11926-019-0831-z

Trombetta, A. C., Soldano, S., Contini, P., Tomatis, V., Ruaro, B., Paolino, S., et al. (2018). A Circulating Cell Population Showing Both M1 and M2 Monocyte/macrophage Surface Markers Characterizes Systemic Sclerosis Patients with Lung Involvement. *Respir. Res.* 19 (1), 186. doi:10.1186/s12931-018-0891-z

Truchetet, M. E., Brembilla, N. C., Montanari, E., Allanore, Y., and Chizzolini, C. (2011). Increased Frequency of Circulating Th22 in Addition to Th17 and Th2 Lymphocytes in Systemic Sclerosis: Association with Interstitial Lung Disease. *Arthritis Res. Ther.* 13 (5), R166. doi:10.1186/ar3486

Tsou, P. S., Palisoc, P. J., Ali, M., Khanna, D., and Sawalha, A. H. (2021). Genome-Wide Reduction in Chromatin Accessibility and Unique Transcription Factor Footprints in Endothelial Cells and Fibroblasts in Scleroderma Skin. *Arthritis Rheumatol.* 73 (8), 1501–1513. doi:10.1002/art.41694

Tsukui, T., Sun, K. H., Wetter, J. B., Wilson-Kanamori, J. R., Hazelwood, L. A., Henderson, N. C., et al. (2020). Collagen-producing Lung Cell Atlas Identifies Multiple Subsets with Distinct Localization and Relevance to Fibrosis. *Nat. Commun.* 11 (1), 1920. doi:10.1038/s41467-020-15647-5

Ueda-Hayakawa, I., Hasegawa, M., Hamaguchi, Y., Takehara, K., and Fujimoto, M. (2013). Circulating γ/δ T Cells in Systemic Sclerosis Exhibit Activated Phenotype and Enhance Gene Expression of proalpha2(I) Collagen of Fibroblasts. *J. Dermatol. Sci.* 69 (1), 54–60. doi:10.1016/j.jdermsci.2012.10.003

Ugor, E., Simon, D., Almanzar, G., Pap, R., Najbauer, J., Németh, P., et al. (2017). Increased Proportions of Functionally Impaired Regulatory T Cell Subsets in Systemic Sclerosis. *Clin. Immunol.* 184, 54–62. doi:10.1016/j.clim.2017.05.013

Valenzi, E., Bulik, M., Tabib, T., Morse, C., Sembrat, J., Trejo Bittar, H., et al. (2019). Single-cell Analysis Reveals Fibroblast Heterogeneity and Myofibroblasts in Systemic Sclerosis-Associated Interstitial Lung Disease. *Ann. Rheum. Dis.* 78 (10), 1379–1387. doi:10.1136/annrheumdis-2018-214865

Valenzi, E., Tabib, T., Papazoglou, A., Sembrat, J., Trejo Bittar, H. E., Rojas, M., et al. (2021). Disparate Interferon Signaling and Shared Aberrant Basaloid Cells in Single-Cell Profiling of Idiopathic Pulmonary Fibrosis and Systemic Sclerosis-Associated Interstitial Lung Disease. *Front. Immunol.* 12, 595811. doi:10.3389/fimmu.2021.595811

van Bon, L., Affandi, A. J., Broen, J., Christmann, R. B., Marijnissen, R. J., Stawski, L., et al. (2014). Proteome-wide Analysis and CXCL4 as a Biomarker in Systemic Sclerosis. *N. Engl. J. Med.* 370 (5), 433–443. doi:10.1056/NEJMoa1114576

Veldhoen, M., Uyttenhove, C., van Snick, J., Helmby, H., Westendorf, A., Buer, J., et al. (2008). Transforming Growth Factor-Beta 'reprograms' the Differentiation of T Helper 2 Cells and Promotes an Interleukin 9-producing Subset. *Nat. Immunol.* 9 (12), 1341–1346. doi:10.1038/ni.1659

Visentini, M., Pellicano, C., Leodori, G., Marrapodi, R., Colantuono, S., Gigante, A., et al. (2021). CD21low B Cells Are Predictive Markers of New Digital Ulcers in Systemic Sclerosis. *Clin. Exp. Immunol.* 205 (2), 128–134. doi:10.1111/cei.13604

Whitfield, M. L., Finlay, D. R., Murray, J. I., Troyanskaya, O. G., Chi, J. T., Pergamenschikov, A., et al. (2003). Systemic and Cell Type-specific Gene Expression Patterns in Scleroderma Skin. *Proc. Natl. Acad. Sci. U S A.* 100 (21), 12319–12324. doi:10.1073/pnas.1635114100

Wohlfahrt, T., Rauber, S., Uebe, S., Luber, M., Soare, A., Ekici, A., et al. (2019). PU.1 Controls Fibroblast Polarization and Tissue Fibrosis. *Nature* 566 (7744), 344–349. doi:10.1038/s41586-019-0896-x

Worrell, J. C., and O'Reilly, S. (2020). Bi-directional Communication: Conversations between Fibroblasts and Immune Cells in Systemic Sclerosis. *J. Autoimmun.* 113, 102526. doi:10.1016/j.jaut.2020.102526

Wynn, T. A. (2004). Fibrotic Disease and the T(H)1/T(H)2 Paradigm. *Nat. Rev. Immunol.* 4 (8), 583–594. doi:10.1038/nri1412

Xia, M. Q., Hale, G., Lifely, M. R., Ferguson, M. A., Campbell, D., Packman, L., et al. (1993). Structure of the CAMPATH-1 Antigen, a Glycosylphosphatidylinositol-Anchored Glycoprotein Which Is an Exceptionally Good Target for Complement Lysis. *Biochem. J.* 293 (Pt 3), 633–640. doi:10.1042/bj2930633

Xing, X., Li, A., Tan, H., and Zhou, Y. (2020). IFN-γ+ IL-17+ Th17 Cells Regulate Fibrosis through Secreting IL-21 in Systemic Scleroderma. *J. Cel Mol Med* 24 (23), 13600–13608. doi:10.1111/jcmm.15266

Xing, X., Yang, J., Yang, X., Wei, Y., Zhu, L., Gao, D., et al. (2013). IL-17A Induces Endothelial Inflammation in Systemic Sclerosis via the ERK Signaling Pathway. *PLoS One* 8 (12), e85032. doi:10.1371/journal.pone.0085032

Xu, H., Zaidi, M., Struve, J., Jones, D. W., Krolikowski, J. G., Nandedkar, S., et al. (2011). Abnormal Fibrillin-1 Expression and Chronic Oxidative Stress Mediate Endothelial Mesenchymal Transition in a Murine Model of Systemic Sclerosis. *Am. J. Physiol. Cel Physiol* 300 (3), C550–C556. doi:10.1152/ajpcell.00123.2010

Xue, D., Tabib, T., Morse, C., and Lafyatis, R. (2020). Transcriptome Landscape of Myeloid Cells in Human Skin Reveals Diversity, Rare Populations and Putative DC Progenitors. *J. Dermatol. Sci.* 97 (1), 41–49. doi:10.1016/j.jdermsci.2019.11.012

Xue, D., Tabib, T., Morse, C., Yang, Y., Domsic, R., Khanna, D., et al. (2021). Expansion of FCGR3A + Macrophages, FCN1 + mo-DC, and Plasmacytoid Dendritic Cells Associated with Severe Skin Disease in Systemic Sclerosis. *Arthritis Rheumatol.* doi:10.1002/art.41813

Yanaba, K., Yoshizaki, A., Asano, Y., Kadono, T., and Sato, S. (2011). Serum Interleukin 9 Levels Are Increased in Patients with Systemic Sclerosis: Association with Lower Frequency and Severity of Pulmonary Fibrosis. *J. Rheumatol.* 38 (10), 2193–2197. doi:10.3899/jrheum.110268

Yang, C., Lei, L., Pan, J., Zhao, C., Wen, J., Qin, F., et al. (2021). Altered CD4+ T Cell and Cytokine Levels in Peripheral Blood and Skin Samples from Systemic Sclerosis Patients and IL-35 in CD4+ T Cell Growth. *Rheumatology (Oxford).* doi:10.1093/rheumatology/keab359

Yang, X., Yang, J., Xing, X., Wan, L., and Li, M. (2014). Increased Frequency of Th17 Cells in Systemic Sclerosis Is Related to Disease Activity and Collagen Overproduction. *Arthritis Res. Ther.* 16 (1), R4. doi:10.1186/ar4430

Yao, W., Zhang, Y., Jabeen, R., Nguyen, E. T., Wilkes, D. S., Tepper, R. S., et al. (2013). Interleukin-9 Is Required for Allergic Airway Inflammation Mediated by the Cytokine TSLP. *Immunity* 38 (2), 360–372. doi:10.1016/j.immuni.2013.01.007

Yaseen, B., Lopez, H., Taki, Z., Zafar, S., Rosario, H., Abdi, B. A., et al. (2020). Interleukin-31 Promotes Pathogenic Mechanisms Underlying Skin and Lung Fibrosis in Scleroderma. *Rheumatology (Oxford)* 59 (9), 2625–2636. doi:10.1093/rheumatology/keaa195

Yurovsky, V. V., Wigley, F. M., Wise, R. A., and White, B. (1996). Skewing of the CD8+ T-Cell Repertoire in the Lungs of Patients with Systemic Sclerosis. *Hum. Immunol.* 48 (1-2), 84–97. doi:10.1016/0198-8859(96)00091-2

Zambrano-Zaragoza, J. F., Romo-Martínez, E. J., Durán-Avelar, Mde. J., García-Magallanes, N., and Vibanco-Pérez, N. (2014). Th17 Cells in Autoimmune and Infectious Diseases. *Int. J. Inflam* 2014, 651503. doi:10.1155/2014/651503

Zhang, J. H., Deng, J. H., Yao, X. L., Wang, J. L., and Xiao, J. H. (2020). CD4+CD25+ Tregs as Dependent Factor in the Course of Bleomycin-Induced Pulmonary Fibrosis in Mice. *Exp. Cel Res* 386 (1), 111700. doi:10.1016/j.yexcr.2019.111700

Zhang, M., Srivastava, G., and Lu, L. (2004). The Pre-B Cell Receptor and its Function during B Cell Development. *Cell Mol Immunol* 1 (2), 89–94.

Zhu, J., and Paul, W. E. (2008). CD4 T Cells: Fates, Functions, and Faults. *Blood* 112 (5), 1557–1569. doi:10.1182/blood-2008-05-078154

Zhu, L., Yin, Z., Ju, B., Zhang, J., Wang, Y., Lv, X., et al. (2018). Altered Frequencies of Memory B Cells in New-Onset Systemic Lupus Erythematosus Patients. *Clin. Rheumatol.* 37 (1), 205–212. doi:10.1007/s10067-017-3877-1

Conflict of Interest: The authors declare that the research was conducted in the absence of any commercial or financial relationships that could be construed as a potential conflict of interest.

GLOSSARY

AM alveolar macrophages
anti-Scl-70 anti-topoisomerase I
APLNR Apelin receptor
APRIL A proliferation-inducing ligand
ASM activated switched memory
ATAC-seq assay of transposase accessible chromatin with sequencing
BAFF B-cell–activating-factor
BCRs B-cell receptors
Beffs Effector B cells
Bregs regulatory B cells
cDCs conventional dendritic cells
CDP common DC precursor
CTGF connective tissue growth factor
CTHRC1 collagen triple helix repeat containing 1
DCs Dendritic cells
DN double-negative
ECM extracellular matrix
ECs endothelial cells
EndMT endothelial-to-mesenchymal transition
FGF fibroblast growth factor
FoxP3 forkhead box transcription factor
GO Gene Ontology;
GSEA Gene Set Enrichment Analysis
GVHD graft-versus-host disease
HC healthy control
HDAC IIa histone deacetylase IIa
HSPG2 heparan sulfate proteoglycan 2;
IFN type I interferon;
IM interstitial macrophages
IPA Ingenuity Pathway Analysis
IPF idiopathic pulmonary fibrosis
IRF8 interferon regulatory factor 8
ISH *in situ* hybridization
Lyve1 lymphatic endothelium hyaluronan receptor-1
MDMs monocytes-derived macrophages
MMP-1 matrix metalloproteinase-1
mRSS modified Rodnan skin score
MSR1 macrophage scavenger receptor 1
NOD/SCID nonobese diabetic/severe combined immunodeficiency
OPN osteopontin
PAH pulmonary arterial hypertension
PBMCs peripheral blood mononuclear cells
pDCs plasmacytoid dendritic cells
PTPMT1 PTEN-like mitochondrial phosphatase
Runx1 runt-related transcription factor 1
Scl-cGVHD sclerodermatous cGVHD
scRNA-seq single-cell RNA sequencing
SFRP secreted frizzled–related protein
SLE systemic lupus erythematosus
SNPs single-nucleotide polymorphisms
SSc Systemic sclerosis
SSc-ILD SSc-associated interstitial lung disease
TCRs T-cell receptors
Tfh T follicular helper
TGF-β transforming growth factor-beta
Th T helper
TIM-1 T-cell Ig and mucin domain protein 1
TLOs tertiary lymphoid structures
TLRs toll-like receptors
Tregs regulatory T cells
TSLP thymic stromal lymphopoietin

frontiers | Frontiers in Pharmacology

ORIGINAL RESEARCH
published: 28 April 2022
doi: 10.3389/fphar.2022.866077

Effect of Combined Mycophenolate and Rapamycin Treatment on Kidney Fibrosis in Murine Lupus Nephritis

Chenzhu Zhang, Tsz Wai Tam, Mel KM Chau, Cristina Alexandra García Córdoba, Susan Yung and Tak Mao Chan**

Department of Medicine, The University of Hong Kong, Hong Kong, Hong Kong SAR, China

OPEN ACCESS

Edited by:
Raffaele Strippoli, Sapienza University of Rome, Italy

Reviewed by:
Xiaoshuang Zhou, Shanxi Provincial People's Hospital, China
Katharina Artinger, Medical University of Graz, Austria

***Correspondence:**
Susan Yung
ssyyung@hku.hk
Tak Mao Chan
dtmchan@hku.hk

Specialty section:
This article was submitted to Translational Pharmacology, a section of the journal Frontiers in Pharmacology

Received: *30 January 2022*
Accepted: *28 March 2022*
Published: *28 April 2022*

Citation:
Zhang C, Tam TW, Chau MKM, García Córdoba CA, Yung S and Chan TM (2022) Effect of Combined Mycophenolate and Rapamycin Treatment on Kidney Fibrosis in Murine Lupus Nephritis. Front. Pharmacol. 13:866077. doi: 10.3389/fphar.2022.866077

Background: A significant proportion of lupus nephritis patients develop chronic kidney disease (CKD) and progressive kidney fibrosis, for which there is no specific treatment. We previously reported that mycophenolate or rapamycin monotherapy showed comparable efficacy in suppressing kidney fibrosis in a murine model of lupus nephritis through their direct action on mesangial cells. We extended our study to investigate the effect of combined mycophenolate and rapamycin treatment (MR) on kidney fibrosis in NZBWF1/J mice.

Methods: Female NZBWF1/J mice with active nephritis were randomized to receive vehicle or treatment with mycophenolate (50 mg/kg/day) and rapamycin (1.5 mg/kg/day) (MR) for up to 12 weeks, and the effect of treatment on clinical parameters, kidney histology, and fibrotic processes was investigated.

Results: Progression of nephritis in untreated mice was accompanied by mesangial proliferation, glomerulosclerosis, tubular atrophy, protein cast formation, increased mTOR and ERK phosphorylation, and induction of TGF-β1, IL-6, α-smooth muscle actin, fibronectin, and collagen expression. Combined MR treatment prolonged survival, improved kidney function, decreased anti-dsDNA antibody level, and ameliorated histopathological changes. The effect of combined MR treatment on kidney histology and function was comparable to that of mycophenolate or rapamycin monotherapy. *In vitro* studies in human mesangial cells showed that exogenous TGF-β1 and IL-6 both induced mTOR and ERK phosphorylation and downstream fibrotic processes. Both mycophenolic acid and rapamycin inhibited inflammatory and fibrotic processes induced by TGF-β1 or IL-6 by downregulating mTOR and ERK phosphorylation.

Conclusions: Our findings indicate that combined mycophenolate and rapamycin, at reduced dose, improves kidney fibrosis in murine lupus nephritis through their distinct effect on mTOR and ERK signaling in mesangial cells.

Keywords: lupus nephritis, rapamycin, mycophenolate, mesangial cells, fibrosis

INTRODUCTION

Lupus nephritis is a severe and common manifestation of systemic lupus erythematosus (SLE), a debilitating autoimmune disease characterized by loss of self-tolerance, autoantibody production, aberrant activation of both innate and adaptive immune responses, and immune-mediated kidney injury. Treatment of lupus nephritis is challenging because clinical presentation and response to treatment and prognosis vary considerably between patients and are influenced by genetics, gender, ethnicity, time of presentation, renal reserve, adherence to treatment, and pharmacogenomics. The current standard-of-care treatment for lupus nephritis necessitates high-dose glucocorticoids administered with mycophenolate or cyclophosphamide to induce remission, followed by long-term maintenance with low-dose glucocorticoids and either mycophenolate or azathioprine to prevent relapse (Chan et al., 2005; Mok et al., 2014; Chan, 2015; Yap et al., 2017). Chronic kidney disease (CKD) is prevalent in patients with lupus nephritis due to nephron loss associated with each episode of nephritis flare (Mageau et al., 2019). End-stage renal disease (ESRD) from progressive CKD is the main contributor to inferior patient survival (Yap et al., 2012b; Rijnink et al., 2017; Parikh et al., 2020). The side effects of immunosuppressive agents and inability of some patients to tolerate the target dose of immunosuppressive agents also contribute to failure to induce disease quiescence. There is, therefore, a need to develop new treatment strategies to prevent CKD and preserve long-term kidney and patient survival (Yap et al., 2012b).

CKD is characterized by the accumulation of matrix proteins in the kidney parenchyma, resulting in glomerulosclerosis and interstitial fibrosis (Duffield, 2014). There is currently no treatment for kidney fibrosis. Mycophenolate inhibits lymphocyte proliferation through its effect on inosine monophosphate dehydrogenase (Allison and Eugui, 2000). Emerging evidence suggests that the antiproliferative properties of mycophenolate extend beyond lymphocytes to non-immune cells including mesangial cells, proximal tubular epithelial cells, and fibroblasts, and mycophenolate can also reduce fibrotic processes in these cells (Badid et al., 2000; Dubus et al., 2002; Azzola et al., 2004; Copeland et al., 2007; Yung et al., 2009; Yung et al., 2015a; Yung et al., 2017; Zhang et al., 2019). Dysregulation of the mammalian or mechanistic target of rapamycin (mTOR) signaling pathway is observed in patients and mice with active lupus nephritis, and mTOR activation contributes to inflammatory and fibrotic processes (Warner et al., 1994; Lui et al., 2008a; Lui et al., 2008b; Zhang et al., 2019).

We previously investigated the effect of mTOR inhibitor rapamycin and also mycophenolate on kidney fibrosis in lupus-prone mice and demonstrated comparable efficacy of each in improving renal histopathology including fibrosis and kidney function. Our findings provided original evidence of the antifibrotic effects of monotherapy with mycophenolate or rapamycin in murine lupus nephritis, mediated through their direct actions on mesangial cells (Zhang et al., 2019). Additional potential clinical benefits of mTOR inhibitors include their antiviral effect and decreased incidence of malignancies (Campistol et al., 2006; Tedesco-Silva et al., 2015; Yanik et al., 2015). Studies have shown that SLE patients have an increased incidence of malignancies, attributed to both immune dysregulation and prior exposure to toxic immunosuppressive agents such as cyclophosphamide (Bernatsky et al., 2013; Ladouceur et al., 2018). Therefore, mTOR inhibitors may have a role in the clinical management of lupus nephritis patients, especially in those who cannot tolerate standard-of-care treatments (Chan et al., 2021).

Combination therapy is frequently used in the management of immune-mediated kidney diseases aiming to achieve efficacy, while reducing toxicity associated with individual drugs (Woo et al., 1995). Kidney transplant recipients treated with triple immunosuppression comprising mycophenolate, rapamycin, and corticosteroid showed markedly reduced gene expression of inflammatory and fibrosis mediators and reduced progression rate of chronic allograft nephropathy with better preservation of kidney structure and function compared to patients treated with calcineurin inhibitors and corticosteroids (Flechner et al., 2004). In this study, we investigated the effect of combined mycophenolate and rapamycin at reduced doses compared with that used in monotherapy on kidney fibrosis in active murine lupus nephritis.

MATERIALS AND METHODS

Chemicals, Assays, and Drugs

All chemicals were of the highest purity and were purchased from Sigma Aldrich (Tin Hang Technology Ltd., Hong Kong), unless otherwise stated. QuantiChrom™ Creatinine, Urea and Albumin Assay Kits were purchased from BioAssay Systems, California, United States. Mouse Anti-dsDNA Antibody Quantitative ELISA Kits were purchased from Alpha Diagnostic Inc. (Onwon Trading Ltd., Hong Kong). Primary human mesangial cells (HMCs) were purchased from Lonza Cologne GmbH (Gene Company Limited, Hong Kong). Tissue culture flasks were purchased from Falcon (Becton-Dickenson, Gene Company Limited, Hong Kong). RPMI 1640 culture medium, fetal bovine serum (FBS), L-glutamine, and penicillin/streptomycin were purchased from Life Technologies Ltd. (Thermo Fisher Scientific, Hong Kong). Mouse anti-human fibronectin antibody (clone IST-4), rabbit anti-fibronectin antibody (product no. SAB5700724), mouse anti-human β-actin antibody (clone AC-74), HRP-conjugated rabbit anti-goat IgG antibody (product no. A8919), and FITC-conjugated anti-mouse IgG antibody (product no. AP127F) were purchased from Sigma Aldrich (Tin Hang Technology Ltd., Hong Kong). Rabbit anti-α-smooth muscle actin antibody (product no. ab5694) and rabbit IgG isotype control (product no. ab125938) were purchased from Abcam, Hong Kong). Goat anti-type I collagen (product no. 1310-01) and anti-type III collagen (product no. 1330-01) were purchased from SouthernBiotech (Genetimes Technology International Holding Limited, Hong Kong). Antibodies to TGF-β1 (clone 3C11) and IL-6 (clone M-19) were purchased from Santa Cruz

Biotechnology Inc. (Genetimes Technology International Holding Limited, Hong Kong). Antibodies to phosphorylated (phospho) (Ser^{2448} and Ser^{2481}; product nos. 2971 and 2974, respectively) and total mTOR (product no. 2972), phospho and total AKT (product nos. 9271 and 9272, respectively), phospho and total ERK (product nos. 4370 and 9102, respectively), and HRP-conjugated goat anti-rabbit IgG antibody (product no. 7074) were purchased from Cell Signaling Technology (Gene Company Limited, Hong Kong). Alexa Fluor 488 goat anti-rabbit IgG antibody (product no. A11070), Texas Red-X–conjugated goat anti-rabbit IgG antibody (product no. T6391), HRP-conjugated goat anti-human IgG antibody (product no. 31410), HRP-conjugated goat anti-mouse IgG antibody (product no. A16066), and goat IgG isotype control (product no. 31245) were purchased from ThermoFisher Scientific, Hong Kong. Recombinant human IL-6 and TGF-β1 were purchased from R&D Systems (Gene Company, Hong Kong). The BD OptEIA human IL-6 ELISA kit was purchased from BD Biosciences Pharmigen (Bio-Gene Technology Limited, Hong Kong). Mycophenolate was provided by Roche Diagnostics (Palo Alto, California, United States), and rapamycin (Rapamune) was purchased from Wyeth Hong Kong Limited (animal studies) and provided by Pfizer (New York, United States) (*in vitro* studies).

Animal studies

All animal studies were approved by the Institutional Committee on the Use of Live Animals in Teaching and Research. Female NZBWF1/J mice were purchased from the Jackson Laboratory (Bar Harbor, Maine, United States) and were housed in a specific pathogen-free animal facility at the University of Hong Kong. The mice were placed under normal housing conditions in a 12-h night and day cycle. Water and standard chow were available *ad libitum*. Treatment commenced when mice were 23–25 weeks of age when they developed proteinuria, defined as >300 mg/dl detected on two separate occasions at least 2 days apart. The mice were randomized into four groups to receive vehicle (control group), monotherapy with mycophenolate (100 mg/kg/day) (M group) or rapamycin (3 mg/kg/day) (R group), or combined mycophenolate (50 mg/kg/day) and rapamycin (1.5 mg/kg/day) (MR group) for periods up to 12 weeks. In the MR group, the doses represent the lowest dose of each drug that could be used in combination to reduce proteinuria and collagen expression determined by Masson's trichrome staining after 6–12 weeks of treatment. Treatment was administered by daily oral gavage for 6 and 12 weeks, following which the mice were killed, blood collected and kidneys harvested. Twenty-four hour urine sample was collected prior to sacrifice by placing mice in metabolic cages. After 12 weeks of treatment, some mice had follow-up six or 12 weeks post therapy to determine treatment sustainability (n = 6 mice per treatment per time-point). Six mice with established proteinuria as defined above were killed at the start of the study to obtain baseline clinical, serologic, and histological data (T = 0).

Assays

All samples were measured in duplicate for all assays. Serum creatinine and urea levels were measured using QuantiChrom™ Creatinine and Urea Assay Kits, respectively. Spot urine was collected weekly, and the albumin-to-creatinine ratio (ACR) was determined using QuantiChrom™ Albumin and Creatinine Assay Kits to assess disease progression. Twenty-four hour urine sample was collected prior to sacrifice and albuminuria assessed. The anti-dsDNA antibody level was determined in serum samples using anti-dsDNA IgG quantitative ELISA kits according to the manufacturer's instructions. Lower and upper limits of detection were 50 IU/ml and 1,000 IU/ml, respectively, and values greater than mean +2 SD of the anti-dsDNA antibody level detected in 36-week-old C57BL/6N mice, that is, 15.84 IU/ml [12.04 + (2 × 1.90)] were considered seropositive.

White Blood Cell Count

The number of circulating white blood cells in vehicle and treated mice at the time of sacrifice was assessed by two independent observers without knowledge of the treatment and expressed as number of cells/ml (Yung et al., 2015b).

Renal Histopathology

Paraffin-embedded kidney sections (5 μm) from untreated and treated mice were stained with H&E and Masson's trichome as previously described (Zhang et al., 2019). Renal histology and collagen deposition were scored by two independent observers in a blinded manner. Briefly, kidney lesions relating to inflammation and fibrosis in the glomerular and tubulo-interstitial compartments were graded 0 to 3 (0 = normal, 1 = mild, 2 = moderate, and 3 = severe) and expressed as mean glomerular and tubulo-interstitial lesion scores for each group (Zhang et al., 2019). For each mouse, approximately 20 glomeruli, tubular, interstitial, and vascular areas were evaluated for glomerular hypercellularity, mesangial matrix expansion, crescent formation, influx of mononuclear cells, fibrinoid necrosis, hyaline deposits, tubular atrophy, protein cast deposition, and vasculopathy (Moreth et al., 2010; Yung et al., 2015b). Glomerular tuft area was assessed using Axiovision software. For semi-quantitative assessment of Masson's trichrome staining, the images of approximately 15 glomeruli and tubules per mouse kidney were captured and graded as follows: 0 = 0–5% staining; 1 = 6–25% staining; 2 = 26–50% staining; 3 = 51–75% staining; 4 = >75% staining (Janssen et al., 2003).

Cytochemical and Immunohistochemical Staining

Paraffin-embedded kidney sections (8 μm) from untreated and treated mice were stained for IL-6, TGF-β1, α-smooth muscle actin, fibronectin, and collagen I and collagen III, as previously described (Yung et al., 2009; Yung et al., 2015b; Zhang et al., 2019). Signal detection and visualization was performed by the peroxidase-anti-peroxidase method, and specimens were counterstained with hematoxylin (Yung et al., 2009). Staining of fibrotic mediators in the capillary loops, mesangium, and tubulo-interstitium was assessed semi-quantitatively in a blinded manner in approximately 15

glomeruli and tubules per mouse kidney and graded as previously described (Janssen et al., 2003). IgG deposition and phosphorylated mTOR and ERK were assessed in frozen renal sections (8 μm) from control and MR-treated mice using indirect immunofluorescence staining (Zhang et al., 2019). Briefly, to assess mTOR and ERK phosphorylation, sections were incubated with phospho-mTOR or anti–phospho-ERK antibodies followed by Texas Red or Alexa Fluor 488 conjugated goat anti-rabbit secondary antibodies, respectively. To determine IgG deposition, the kidney sections were incubated with FITC-conjugated anti-mouse IgG. The sections were mounted in a fluorescent mountant and epifluorescence viewed using a Nikon 80i upright fluorescent microscope and Spot RT3 slider digital camera system (Chintek Scientific (China) Ltd., Hong Kong). Fifteen glomeruli per kidney section were analyzed, and fluorescent staining in the glomerular capillary walls and mesangium was scored blindly on a scale of 0–3 (0 = no staining; 1 = weak staining; 2 = moderate staining, 3 = strong staining) (Herber et al., 2007; Yung et al., 2010).

Human Mesangial Cells

Primary HMCs were maintained in RPMI 1640 medium supplemented with L-glutamine (2 μM), penicillin (100 U/ml), streptomycin (100 μg/ml), insulin (5 μg/ml), transferrin (5 μg/ml), and 10% FBS. All experiments were performed on the cells of the fifth to seventh passage that has been growth-arrested for 48 h. To identify signaling pathways and matrix proteins induced by IL-6 and TGF-β1, HMCs were pre-incubated with inhibitors to mTOR (rapamycin, 3 ng/ml), ERK (PD98059, 10 μM) and PI3K (LY294002, 25 μM), or rapamycin in combination with either PD98059 or LY294002 for 1 h at 37°C prior to incubation with serum-free medium (SFM), IL-6, or TGF-β1 (10 ng/ml final concentration, for both) for 24 h, after which time the supernatants were collected and the cells washed with PBS and lysed with 20 mM sodium acetate, pH 6.0, containing 4 M urea, 1% Triton X-100, and a cocktail of proteinase inhibitors (200 μl) (Yung et al., 2010; Yung et al., 2015a). We have chosen to stimulate HMCs with IL-6 and TGF-β1 since renal expression of both is increased in patients, and mice with active lupus nephritis and both drive tissue fibrosis (Yamamoto et al., 1996; Fielding et al., 2014). To determine the effect of mycophenolic acid (MPA) or rapamycin on inflammatory and fibrotic processes, HMCs were incubated with MPA (1 and 5 μg/ml) or rapamycin (1 and 3 ng/ml) for 1 h at 37°C followed by incubation with SFM, IL-6, or TGF-β1 (10 ng/ml, for both) for periods up to 72 h and samples processed as described above. The concentrations of MPA and rapamycin used in these studies represent blood trough levels in lupus nephritis patients and renal transplant recipients when given a daily dose of 2–3 g mycophenolate and 2–5 mg rapamycin, respectively (Hauser et al., 1999; Kahan et al., 2000; Borrows et al., 2006; Yap et al., 2018; Yap et al., 2020). The supernatants were used to determine the effect of MPA and rapamycin on IL-6 secretion, and cell lysates were used to assess phosphorylation of signaling pathways, α-smooth muscle actin, and matrix protein expression.

Measurement of IL-6 in the Culture Supernatant

HMCs were incubated with SFM or TGF-β1 in the presence or absence of MPA or rapamycin for up to 72 h, after which time the supernatant was collected and centrifuged at 3,000 rpm for 10 min to remove any cell debris. Secreted IL-6 was determined using the IL-6 OptEIA™ ELISA kit according to the manufacturer's instructions. Lower and upper limits of detection were 5 pg/ml and 300 pg/ml, respectively. All samples were measured in duplicate in serial dilution and normalized to their cellular protein content.

Western Blot Analysis

Aliquots of cell lysates (20 μg total protein content) were separated under denaturing conditions on 8% polyacrylamide gels to determine fibronectin and collagen III expression and on 10% polyacrylamide gels to determine the expression of phospho- and total mTOR, phospho- and total ERK, phospho- and total AKT, α-smooth muscle actin, and β-actin. The samples were transferred onto nitrocellulose membranes and incubated with the relevant primary antibodies followed by the addition of secondary antibodies as previously described (Yung et al., 2009; Yung et al., 2010; Zhang et al., 2019). The bands were visualized with ECL, semi-quantitated by densitometry using ImageJ (NIH, United States), and expressed as arbitrary densitometric units (DU). Phospho-mTOR, phospho-ERK, and phospho-AKT were normalized to total mTOR, ERK, and AKT, respectively, and α-smooth muscle actin, fibronectin, and collagen III expression were normalized to β-actin.

Statistical Analyses

The results from our animal studies were expressed as mean ± SEM (n = six to eight for each time-point per group). All *in vitro* studies were repeated at least three times and data expressed as mean ± SD. Statistical analysis was performed using Prism 6.0 for Windows (GraphPad Software, Inc., California, United States). Mouse survival was determined using Fisher's exact test. The D'Agostino–Pearson normality test was used to assess normal distribution. Repeated measures ANOVA followed by Bonferroni's multiple comparison post-test was used to assess intragroup and intergroup comparisons with three groups or more. Ordinary ANOVA followed by Bonferroni's multiple comparison post-test was used to assess intergroup comparison for *in vitro* studies. Two-tailed $p < 0.05$ was considered statistically significant.

RESULTS

Effect of Combined Mycophenolate and Rapamycin on Survival Rate, Kidney Function, and anti-dsDNA Antibody Titer in NZBWF1/J Mice

After 12 weeks of treatment, peripheral blood lymphocyte count in M, R, and MR groups was significantly lower than that in

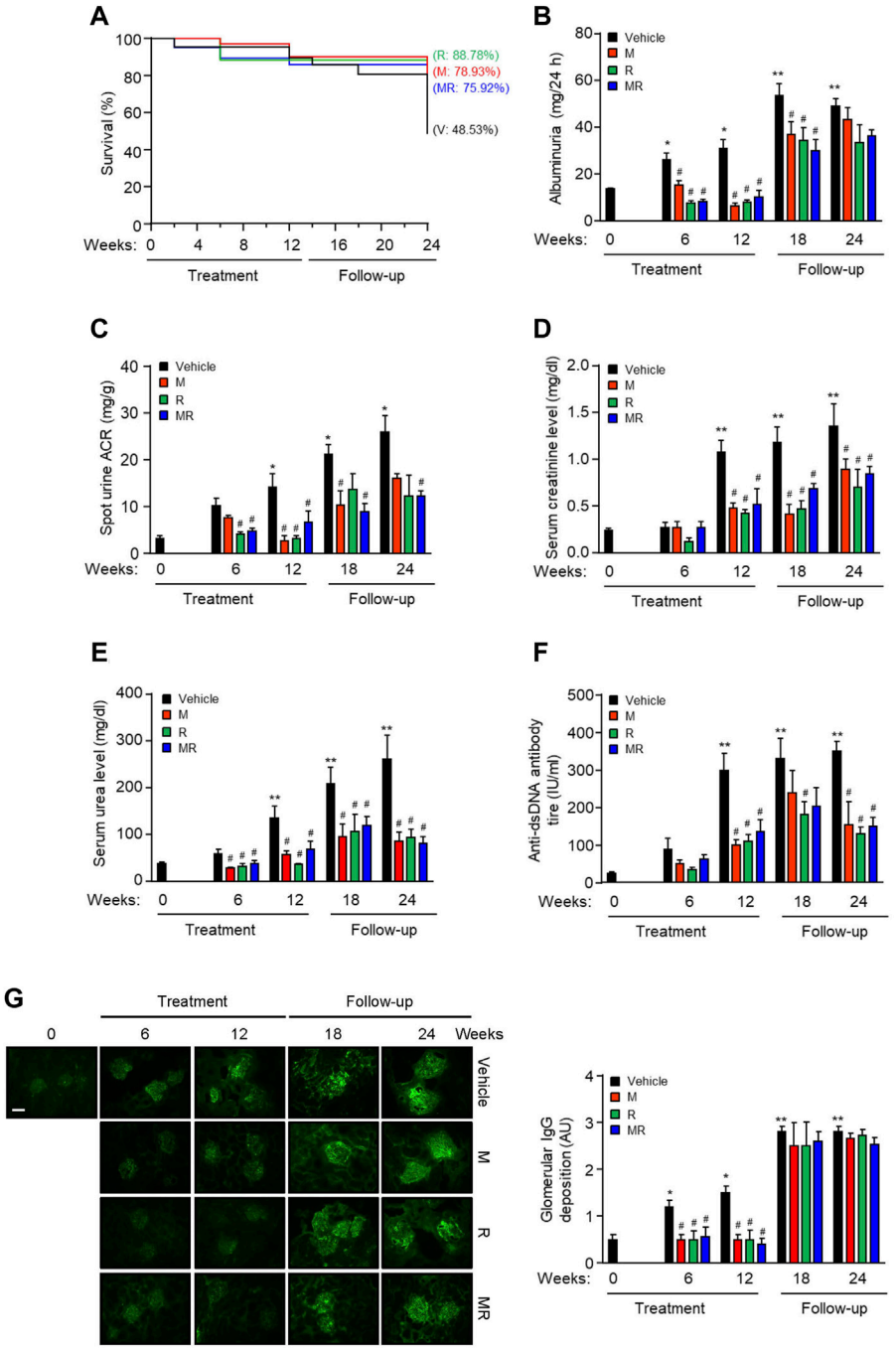

FIGURE 1 | Effect of combined mycophenolate and rapamycin on survival, clinical, and serological parameters and IgG deposition in NZBWF1/J mice. The effect of vehicle (V), monotherapy mycophenolate (M) or rapamycin (R), or combined mycophenolate and rapamycin (MR) on **(A)** survival curves, **(B)** albuminuria, **(C)** spot urine albumin-to-creatinine ratio (ACR), **(D)** serum creatinine level, **(E)** serum urea level, and **(F)** circulating anti-dsDNA antibody titer in NZBWF1/J mice. **(G)** Representative images showing IgG deposition in vehicle-, M-, R-, and combined MR-treated mice at baseline (T = 0), 6, 12, 18, and 24 weeks. Original magnification x 200; Scale bar: 20 μm. Glomerular IgG deposition was graded as described in the *Materials and Methods* and data expressed as mean ± SEM (right panels). AU, arbitrary units. Data expressed as mean ± SEM (n = 6 mice per time-point per group). Data analyzed using Fisher's exact test for panel A and repeated measures ANOVA with Bonferroni's multiple comparison post-test for panels B–G. $^{*}p < 0.05$, $^{**}p < 0.01$, compared to baseline; $^{\#}p < 0.05$, compared to vehicle for the same time-point.

untreated mice (12.60 ± 0.81, 6.73 ± 0.35, 6.00 ± 0.72 and 6.20 ± 1.01 × 10^6 lymphocyte count per ml blood for vehicle, M, R, and MR groups, respectively, $p < 0.01$, Vehicle vs. M, R, or MR). The immunosuppressive actions of M, R, and combined MR were comparable between all treated groups. None of the mice in the treatment groups developed infection, and body weight did not

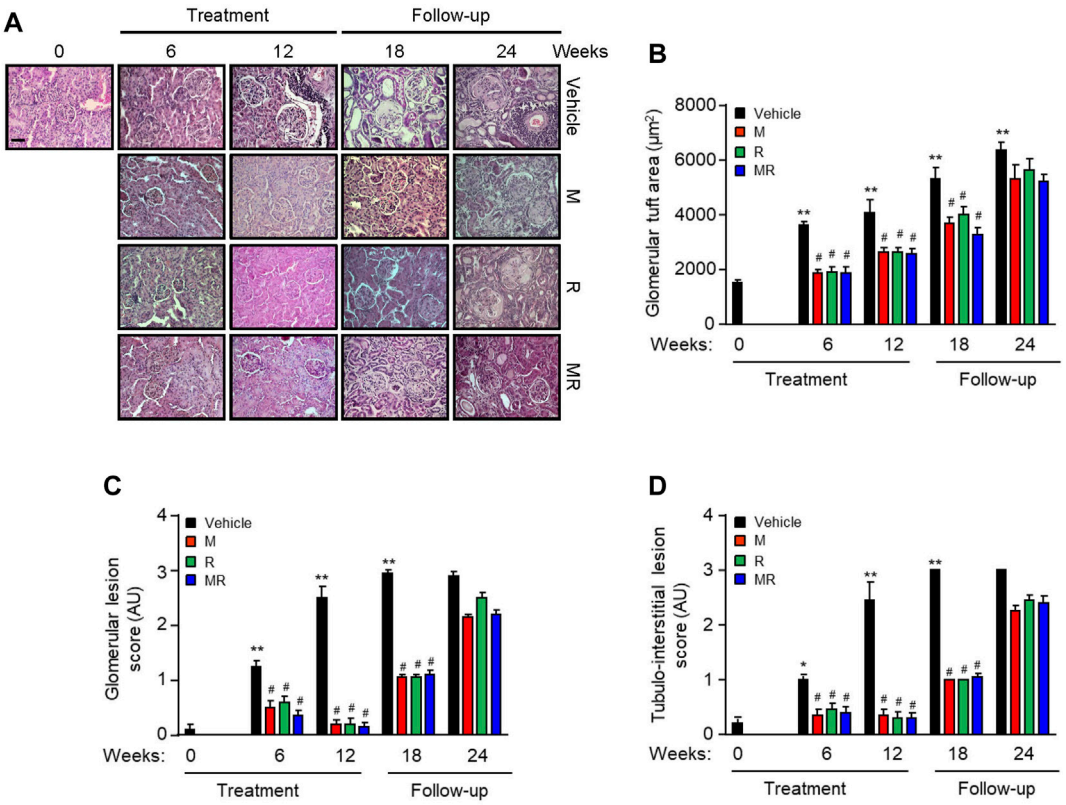

FIGURE 2 | Effect of combined mycophenolate and rapamycin on kidney histology in NZBWF1/J mice **(A)** Representative images showing renal histopathology in vehicle-, M-, R-, and MR-treated mice as determined by H&E staining at baseline, 6, 12, 18, and 24 weeks. Original magnification x 200; Scale bar: 20 μm. **(B)** Glomerular tuft area, **(C)** glomerular lesion score, and **(D)** tubulo-interstitial lesion score for each group were graded as described in the *Materials and Methods*, and mean scores ±SEM are shown (n = 6 mice per time-point per group). AU, arbitrary units. Data analyzed using repeated measures ANOVA with Bonferroni's multiple comparison post-test. $^{*}p < 0.05$, $^{**}p < 0.01$, compared to baseline; $^{\#}p < 0.05$, vehicle vs. treated groups for the same time-point.

differ between the groups throughout the course of the study (data not shown).

The survival rate for vehicle-, M-, R-, and MR-treated mice was similar after 12 weeks treatment (*P*=NS). Twelve weeks after cessation of treatment, the survival rate was 48.53, 78.93, 88.78, and 75.92%, respectively ($p < 0.05$, vehicle vs. M, R, or MR). There was no statistical difference in the survival rate for M-, R-, and MR-treated mice (**Figure 1A**). Albuminuria and serum creatinine, urea, and anti-dsDNA antibody levels increased with progressive nephritis in untreated mice, whereas M, R, and MR treatment significantly reduced these clinical and serological parameters of disease after 6–12 weeks and was sustained for 12 weeks after cessation of treatment (**Figure 1B–F**).

Effect of Combined Mycophenolate and Rapamycin on IgG Deposition and Kidney Histology

Glomerular IgG deposition increased with progressive nephritis, whereas treatment with M, R, or MR significantly reduced IgG deposition after 6 weeks of treatment and was sustained for 12 weeks. IgG deposition increased in M, R, and combined MR groups once treatment was stopped (**Figure 1G**). Progression of nephritis in untreated mice was accompanied by mesangial expansion, glomerular hypertrophy, and infiltration of inflammatory cells in the periglomerular and tubulo-interstitial compartments (**Figure 2**). As disease progressed, tubular atrophy, cast formation, glomerulosclerosis, and interstitial fibrosis were detected 18–24 weeks after commencement of the study. M, R, and MR treatment attenuated histopathological changes after 12 weeks, but these abnormalities appeared 12 weeks after cessation of treatment (**Figure 2**).

Effect of Combined Mycophenolate and Rapamycin on Glomerular mTOR and ERK Phosphorylation, and Expression of TGF-β1, IL-6, α-smooth Muscle Actin, Fibronectin, and Collagen

Since MR treatment showed comparable efficacy as that for monotherapy M or R in improving kidney histopathology, we next focused on the effect of combined MR on mediators of fibrosis. Increased mTOR phosphorylation at Ser^{2448}, but not at Ser^{2481}, and ERK phosphorylation were observed in the

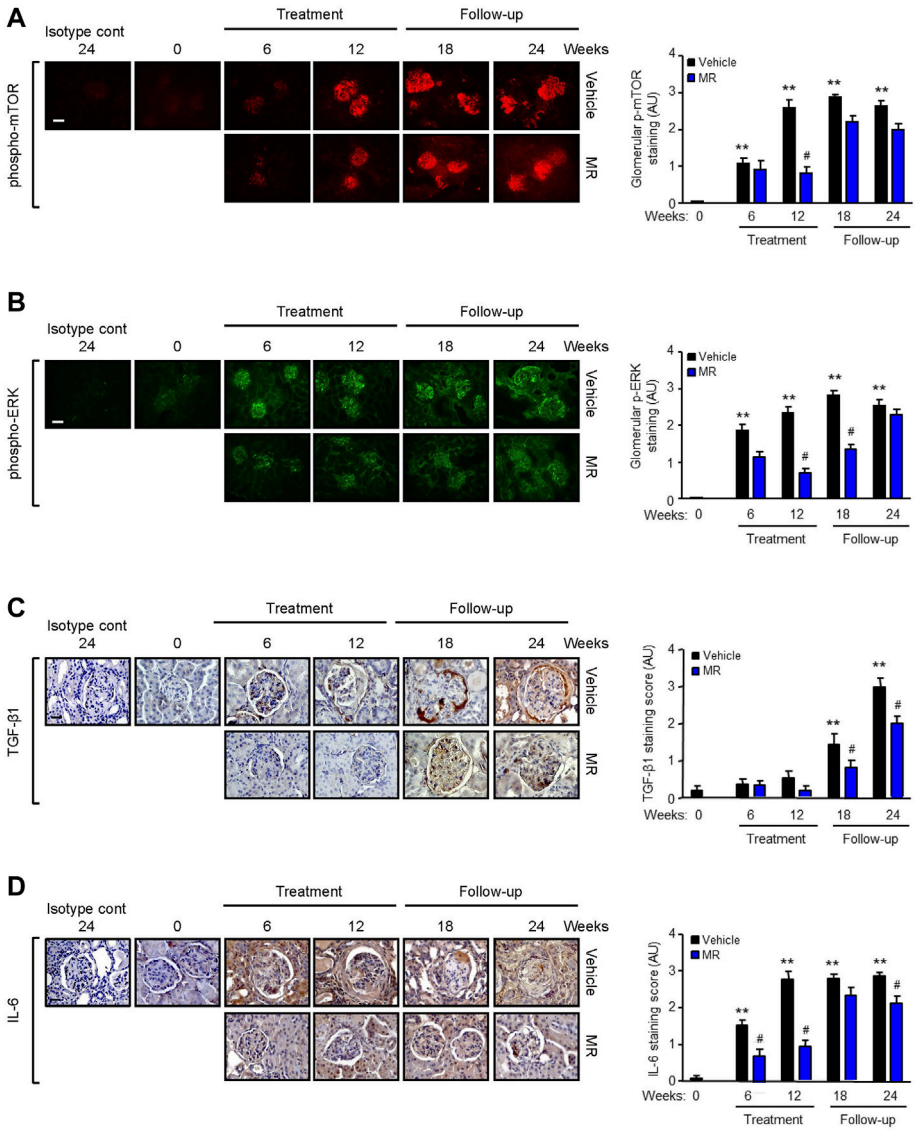

FIGURE 3 | Effect of mycophenolate and rapamycin on mTOR and ERK phosphorylation and TGF-β1 and IL-6 expression in NZBWF1/J mice. Representative images showing **(A)** mTOR phosphorylation at Ser^{2448}, **(B)** ERK phosphorylation, **(C)** TGF-β1, and **(D)** IL-6 expression in the kidneys of vehicle- and MR-treated mice at baseline (T = 0), 6, 12, 18, and 24 weeks. Isotype cont: isotype control. Original magnification x 200; Scale bar: 20 μm for panels A and B and original magnification x 400; Scale bar; 50 μm for panels C and D. mTOR and ERK phosphorylation and TGF-β1 and IL-6 expression were graded as described in the *Materials and Methods* and data expressed as mean ± SEM (right panels) (n = 6 mice per time-point per group). AU, arbitrary units. Data analyzed using repeated measures ANOVA with Bonferroni's multiple comparison post-test. $^{**}p < 0.01$, compared to baseline; $^{\#}p < 0.05$, vehicle vs. MR for the same time-point.

glomeruli of NZBWF1/J mice with active nephritis. As disease progressed, ERK phosphorylation was also detected in the tubulo-interstitium. Treatment with combined MR for 12 weeks resulted in marked reduction in mTOR and ERK phosphorylation, whereas activation of both signaling pathways increased when treatment was stopped (**Figure 3A,B**).

TGF-β1 is a well-established mediator of kidney fibrosis, and long-term exposure to IL-6 has been reported to induce tissue fibrosis in unresolved inflammation (Yamamoto et al., 1993; Fielding et al., 2014). TGF-β1 expression was detected in the glomerulus and tubulo-interstitium after 18 and 24 weeks, respectively, and MR treatment reduced TGF-β1 expression (**Figure 3C**). Renal IL-6 expression increased progressively in control mice and was detected in the glomerulus and tubulo-interstitium after 6 weeks and in crescents and areas of interstitial fibrosis after 12 weeks. MR treatment significantly decreased glomerular and tubulo-interstitial IL-6 expression after 6 weeks of treatment, which was sustained for 12 weeks after cessation of treatment (**Figure 3D**). Increased collagen deposition, attributed at least in part to increased collagen I and III expression, was detected in the

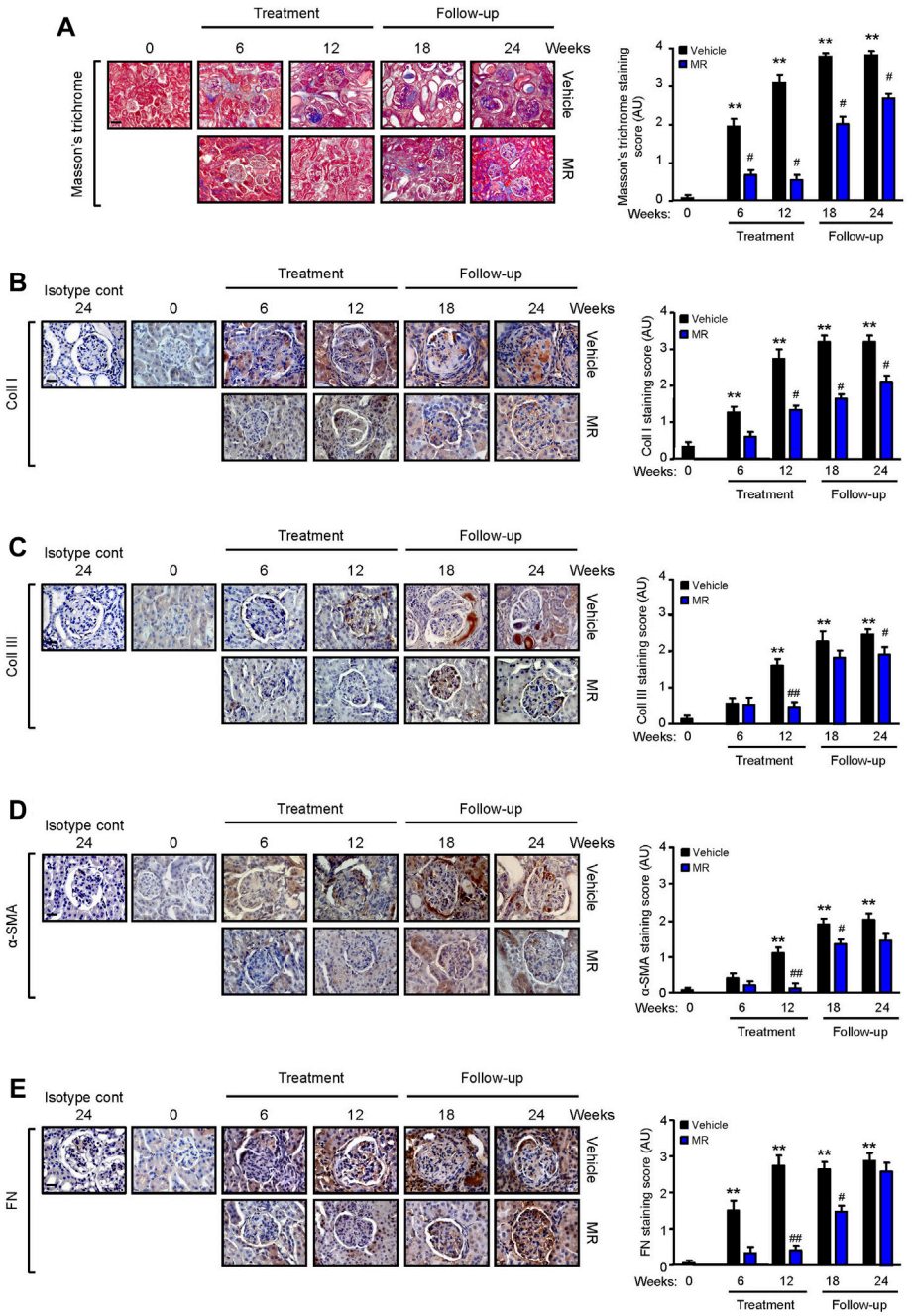

FIGURE 4 | Effect of combined mycophenolate and rapamycin on collagen deposition, α-smooth muscle actin, and fibronectin expression in NZBWF1/J mice. Representative images showing **(A)** total collagen deposition as determined by Masson's trichrome staining, **(B)** collagen I (Coll I), **(C)** collagen III (Coll III), **(D)** α-smooth muscle actin (α-SMA), and **(E)** fibronectin (FN) expression in the kidneys of vehicle- and MR-treated mice at baseline, 6, 12, 18, and 24 weeks. Original magnification x 200; Scale bar: 20 μm for panel A, and original magnification x 400; Scale bars 50 μm for panels B–E. Collagen, α-SMA, and FN expression in the kidneys of control and treated mice was graded as described in the *Materials and Methods*, and mean scores ±SEM are shown (n = 6 mice per time-point per group). AU, arbitrary units. Data analyzed using repeated measures ANOVA with Bonferroni's multiple comparison post-test. $^{**}p < 0.01$, compared to baseline; $^{\#}p < 0.05$; $^{\#\#}p < 0.01$, vehicle vs. MR for the same time-point.

glomerulus and tubulo-interstitium of untreated mice at 6 weeks after commencement of the study, and this was accompanied by increased α-smooth muscle actin expression and fibronectin expression (**Figure 4**). Treatment with combined MR reduced these fibrotic markers after 6–12 weeks. Decreased α-smooth muscle actin and fibronectin expression was sustained for 6 weeks after cessation of treatment, whereas suppression of collagen I

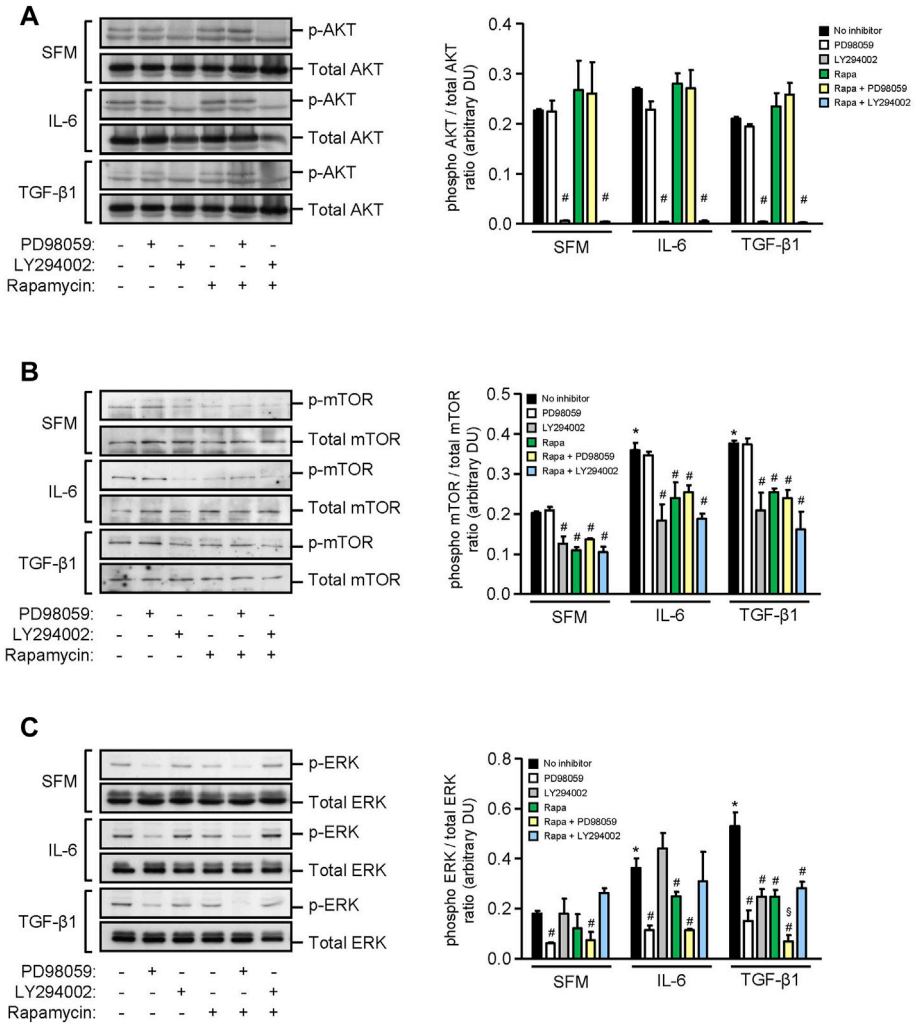

FIGURE 5 | Effect of IL-6 or TGF-β1 on AKT, mTOR, and ERK phosphorylation in human mesangial cells. Representative Western blots showing the effect of SFM, IL-6, or TGF-β1 in the presence or absence of PD98059, LY294002, or rapamycin with or without PD98059 or LY294002 on **(A)** AKT phosphorylation, **(B)** mTOR phosphorylation at Ser^{2448}, and **(C)** ERK phosphorylation, after 24 h (left panels). The intensity of each band was semi-quantitated using ImageJ, normalized to total AKT, total mTOR, and total ERK, and values expressed as mean ± SD for three separate experiments (right panels). DU, densitometric units. All data analyzed using ordinary ANOVA with Bonferroni's multiple comparison post-test. $^{*}p < 0.05$, SFM vs. IL-6 or TGF-β1; $^{\#}p < 0.05$, with vs. without inhibitor for the same stimulus; $^{\S}p < 0.05$, compared to rapamycin alone for the same stimulus.

and III deposition was sustained to the cessation of the study (**Figure 4**).

Effect of IL-6 and TGF-β1 on mTOR, PI3K, and ERK Phosphorylation and IL-6 Secretion in Human Mesangial Cells

We next investigated the signaling pathways that induced inflammatory and fibrotic mediators in HMCs. Under basal conditions, HMCs showed weak expression of AKT, mTOR, and ERK phosphorylation. Exogenous IL-6 increased mTOR and ERK phosphorylation by 1.80-fold and 2.01-fold, respectively, whereas TGF-β1 increased mTOR and ERK phosphorylation by 1.85-fold and 2.38-fold, respectively, in HMCs after 24 h stimulation. Neither IL-6 nor TGF-β1 had any effect on AKT phosphorylation after 24 h (**Figure 5**). Rapamycin and LY294002 (PI3K inhibitor) significantly decreased IL-6– and TGF-β1–induced mTOR phosphorylation, whereas PD98059 (ERK inhibitor) had no effect (**Figure 5**). PD98059, rapamycin, and LY294002 significantly decreased ERK phosphorylation that was induced by IL-6 or TGF-β1. Inhibition of ERK activation was more pronounced when combined rapamycin and PD98059 was used in cells stimulated with TGF-β1 (64.84, 42.44, and 83.73% reduction in cells incubated with PD98059, rapamycin, and combined rapamycin and PD98059, respectively) (**Figure 5**).

Stimulation of HMCs with TGF-β1 for 24 h increased IL-6 secretion by 4.36-fold compared with that of cells incubated with SFM ($p < 0.01$, **Figure 6**). The results from experiments using specific inhibitors to ERK, mTOR, and PI3K showed that constitutive IL-6 secretion was mediated through PI3K since

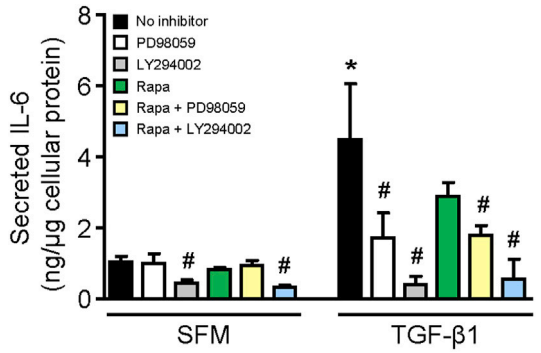

FIGURE 6 | Effect of TGF-β1 on IL-6 secretion in human mesangial cells. Effect of TGF-β1 in the presence or absence of PD98059, LY294002, or rapamycin with or without PD98059 or LY29400 on IL-6 secretion in HMCs after 24-h incubation. Results are expressed as mean ± SD from three separate experiments. Data analyzed using ordinary ANOVA with Bonferroni's multiple comparison post-test. *$p < 0.05$, SFM vs. TGF-β1; #$p < 0.05$, with vs. without inhibitor for the same stimulation.

LY294002 reduced IL-6 secretion by 57.50%, whereas inhibition of ERK or mTOR had no effect (**Figure 6**). IL-6 secretion induced by TGF-β1 was mediated through ERK and PI3K since incubation of cells with PD98059 and LY294002 reduced IL-6 secretion by 61.72 and 91.14%, respectively (**Figure 6**). Rapamycin also decreased IL-6 secretion in HMCs stimulated with TGF-β1 (35.48% reduction), but it did not reach statistical significance.

Effect of IL-6 and TGF-β1 on α-smooth Muscle Actin, Fibronectin, and Collagen III Expression in Human Mesangial Cells

HMCs constitutively expressed α-smooth muscle actin and soluble and cell-associated fibronectin and collagen III. IL-6 significantly increased α-smooth muscle actin, soluble fibronectin, and soluble and cell-associated collagen III expression after 24 h when compared to SFM. mTOR phosphorylation, but not PI3K or ERK phosphorylation, contributed to IL-6–induced α-smooth muscle actin since incubation of HMCs with rapamycin reduced α-smooth muscle actin expression by 35.51% ($p < 0.05$, **Figure 7**). Accumulation of fibronectin in the extracellular matrix is dependent on the activation and polymerization of soluble fibronectin monomers to form activated dimers (Wierzbicka-Patynowski and Schwarzbauer, 2003). Constitutive and IL-6–induced soluble fibronectin expression was mediated through PI3K, mTOR, and ERK phosphorylation since incubation with LY294002, rapamycin, and PD98059 significantly reduced soluble fibronectin expression, whereas PI3K, mTOR, and ERK phosphorylation had no apparent effect on cell-association fibronectin. Constitutive and IL-6–induced soluble and cell-associated collagen III were mediated through PI3K and mTOR phosphorylation. IL-6 induction of soluble but not cell-associated collagen III was also mediated through ERK phosphorylation (**Figure 7**).

TGF-β1 significantly increased α-smooth muscle actin, soluble fibronectin, and soluble and cell-associated collagen III expression in HMCs, and the increase of all three mediators of fibrosis was comparable to that observed with IL-6. Induction of α-smooth muscle actin by TGF-β1 was mediated, in part, through mTOR activation since incubation with rapamycin decreased α-smooth muscle actin by 38.65%. Induction of soluble fibronectin was mediated through PI3K, mTOR, and ERK phosphorylation since incubation with LY294002, rapamycin, and PD98059 decreased soluble fibronectin expression by 68.93, 61.62, and 42.15%, respectively. HMC co-incubated with rapamycin and PD98059 or rapamycin and LY294002 further reduced soluble fibronectin expression (82.19 and 88.53% reduction, respectively, **Figure 7**). Soluble and cell-associated collagen III induced by TGF-β1 was mediated through PI3K and mTOR phosphorylation since pre-incubation with LY294002 and rapamycin decreased soluble collagen III by 94.40 and 78.36%, respectively, and cell-associated collagen III by 92.28 and 75.85%, respectively (**Figure 7**).

Effect of MPA and Rapamycin on Inflammatory and Fibrotic Processes Induced by IL-6 and TGF-β1 in Human Mesangial Cells

We next compared the effect of MPA and rapamycin on mediators of inflammation and fibrosis that were induced by IL-6 and TGF-β1 in HMCs. MPA at 5 µg/ml decreased constitutive IL-6 secretion after 24 h and was sustained for 72 h ($p < 0.05$). Rapamycin at 3 ng/ml also reduced constitutive IL-6 secretion, but the inhibitory effect was not apparent until after 48 h and was sustained up to 72 h. TGF-β1 induced IL-6 secretion in a time-dependent manner. MPA reduced TGF-β1–induced IL-6 secretion after 48 h, whereas rapamycin decreased IL-6 secretion after 72 h ($p < 0.05$, for both) (**Figure 8**).

IL-6 and TGF-β1 induced AKT, mTOR, and ERK phosphorylation in a time-dependent manner. Rapamycin decreased IL-6- and TGF-β-induced mTOR phosphorylation after 24 h, which was sustained for 72 h. MPA decreased IL-6- but not TGF-β1-induced mTOR phosphorylation after 72 h (**Figure 9B**). MPA and rapamycin also reduced ERK phosphorylation that was induced by IL-6, whereas rapamycin but not MPA transiently decreased TGF-β1–induced ERK phosphorylation (**Figure 9C**). Both drugs had no effect on AKT phosphorylation (**Figure 9A**). IL-6 and TGF-β1 induced α-smooth muscle actin and soluble fibronectin in a time-dependent manner. Both MPA and rapamycin reduced IL-6– and TGF-β1–induced α-smooth muscle and soluble fibronectin actin after 24 h, and this reduction was sustained for 72 h (**Figure 10**).

DISCUSSION

The main objective of immunosuppressive treatment in patients with active lupus nephritis is to suppress acute inflammatory processes and prevent nephron loss (Chan, 2015; Parodis and

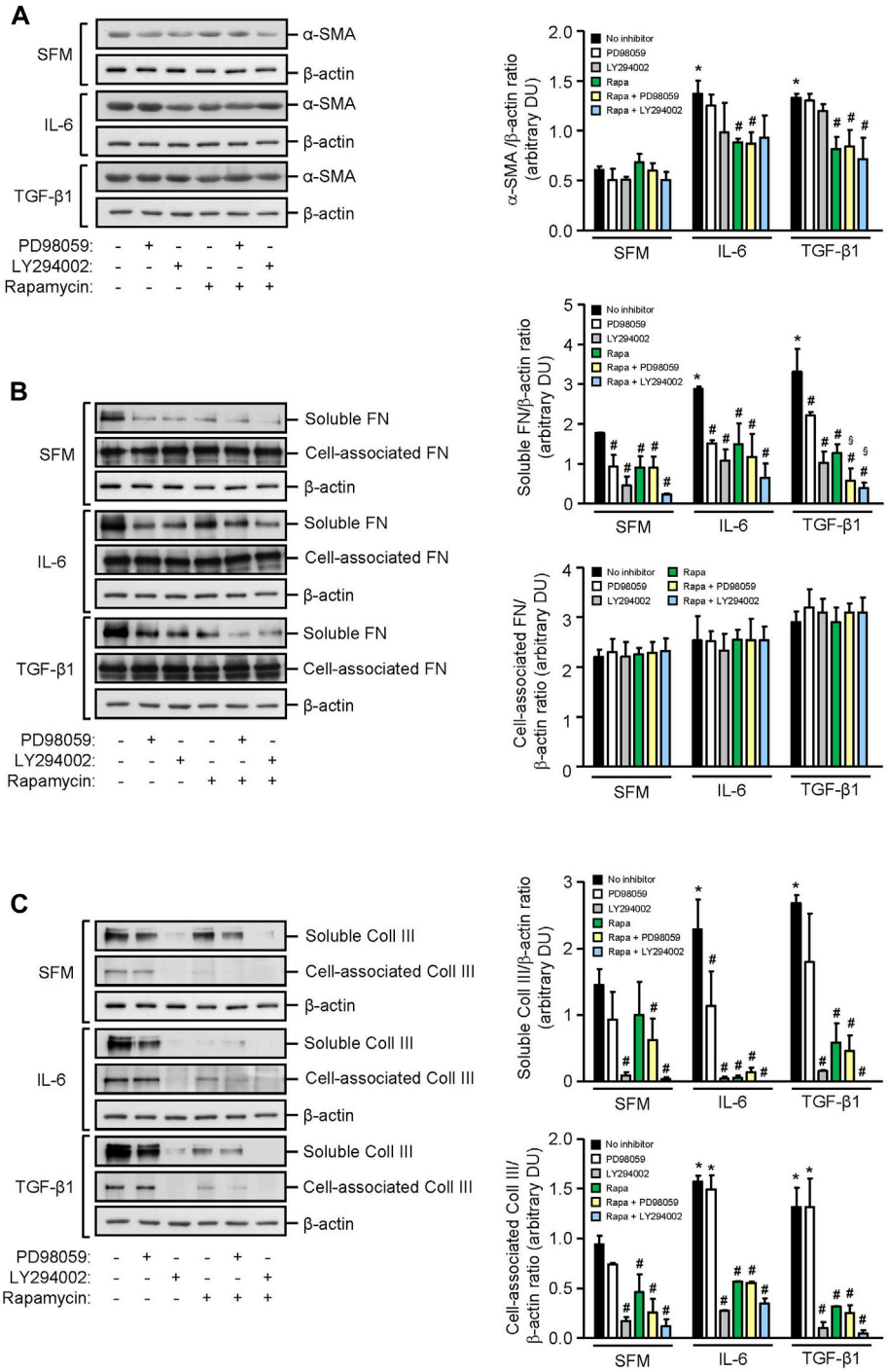

FIGURE 7 | Effect of IL-6 or TGF-β1 on α-smooth muscle actin, fibronectin, and collagen III expression in human mesangial cells. Representative Western blots showing the effect of SFM, IL-6, or TGF-β1 in the presence or absence of PD98059, LY294002, or rapamycin with or without PD98059 or LY294002 on **(A)** α-smooth muscle actin (α-SMA), **(B)** soluble and cell-associated fibronectin (FN), and **(C)** soluble and cell-associated collagen III (Coll III) after 24 h (left panels). The intensity of each band was semi-quantitated using ImageJ, normalized to β-actin, and values expressed as mean ± SD for three separate experiments (right panels). DU, densitometric units. All data analyzed using ordinary ANOVA with Bonferroni's multiple comparison post-test. $^{*}p < 0.05$, SFM vs. IL-6 or TGF-β1; $^{\#}p < 0.05$, with vs. without inhibitor for the same stimulus; $^{\S}p < 0.05$, compared to rapamycin alone for the same stimulus.

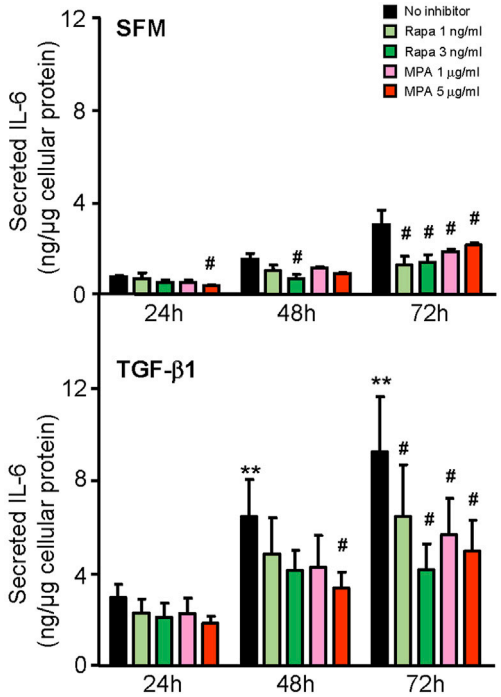

FIGURE 8 | Effect of MPA or rapamycin on IL-6 secretion induced by TGF-β1 in human mesangial cells. Effect of SFM (upper panel) or TGF-β1 (lower panel) in the presence or absence of rapamycin (1 or 3 ng/ml) or MPA (1 or 5 μg/ml) on IL-6 secretion in HMCs. Results are expressed as mean ± SD from three separate experiments. Data analyzed using ordinary ANOVA with Bonferroni's multiple comparison post-test. $^{**}p < 0.01$, SFM vs. TGF-β1 for the same time-point; $^{\#}p < 0.05$, with vs. without rapamycin or MPA for the same stimulation and time-point.

Houssiau, 2022). Current treatment regimens for lupus nephritis comprise an induction phase aimed at inducing remission and a maintenance phase to prevent disease flares. Despite improvement in the management of lupus nephritis patients over the past 3 decades, a significant proportion of patients develop CKD and progress to ESRD (Maroz and Segal, 2013; Zhang et al., 2016; Parodis and Houssiau, 2022). There is, therefore, a need to develop new treatment strategies to prevent progressive kidney fibrosis and preserve long-term kidney function (Yap et al., 2012b).

Combination therapy is often used in the treatment of lupus nephritis with the aim of achieving efficacy, while reducing toxicity associated with individual drugs. We previously reported that mycophenolate at 100 mg/kg/day and rapamycin at 3 mg/kg/day showed comparable immunosuppressive effects and efficacy in preventing kidney function deterioration and fibrosis in murine lupus nephritis (Zhang et al., 2019). We extended our study to investigate the effect of combined mycophenolate and rapamycin on kidney fibrosis in active murine lupus nephritis. When used in combination, the dose of each immunosuppressive agent could be halved to provide the same level of immunosuppression as mycophenolate or rapamycin monotherapy, and combined MR treatment maintained the antifibrotic properties of the drugs. Peripheral white blood cell count was comparable between monotherapy and combination therapy, and none of the treatment groups showed signs of infection. The advantages of using mTOR inhibitors are that unlike calcineurin inhibitors, they do not possess nephrotoxicity and they also exert anti-neoplastic effect. While there had been concerns that mTOR inhibitors may induce proteinuria and onset of glomerulonephritis in some kidney transplant patients, this was not observed in our study.

Although treatment was initiated at the onset of albuminuria, renal histopathological changes were relatively modest at baseline. Progressive lupus nephritis was characterized by the production of anti-dsDNA antibodies, immune complex deposition in the glomerulus, mesangial expansion, glomerulosclerosis, increased tubulo-interstitial inflammatory cell infiltration, tubular atrophy, interstitial fibrosis, and deterioration of kidney function. mTOR and ERK phosphorylation increased with progressive disease and was predominantly localized to the glomerulus, and this was accompanied by induction of TGF-β1, IL-6, α-smooth muscle actin, fibronectin, and collagen I and III. Combined MR treatment improved kidney histology and fibrotic processes and phenotypic disease manifestations after 12 weeks and was sustained up to 6–12 weeks after cessation of treatment. Combined MR treatment showed comparable efficacy as that of monotherapy in improving kidney histology and fibrotic processes, with comparable reduction in mTOR and ERK phosphorylation and mediators of fibrosis. MR treatment reduced TGF-β1, IL-6, collagen I, collagen III, α-smooth muscle actin, and fibronectin expression. When treatment was stopped, the inhibitory effect of MR on α-smooth muscle actin and fibronectin expression was sustained for 6 weeks, whereas the inhibitory effect on TGF-β1, IL-6, and collagen I and collagen III expression persisted until the cessation of the study. It is possible that the sustained reduction in TGF-β1 and IL-6 expression may result in a concomitant downstream reduction in collagen expression, although further studies are warranted to confirm this, whereas the regulation of fibronectin and α-smooth muscle actin may be through additional mediators such as TNF-α or MCP-1 (Yung et al., 2015a), the levels of which may be increased following cessation of treatment.

TGF-β1 is a key mediator of kidney fibrosis, and IL-6 has been reported to drive tissue fibrosis in unresolved inflammation (Fielding et al., 2014). Increased IL-6, α-smooth muscle actin, fibronectin, and collagen I and III expression in the kidney was detected before TGF-β1 expression, suggesting that TGF-β1 may amplify fibrotic processes once fibrosis is established, but it does not appear to play a role in the initiation of kidney fibrosis in lupus nephritis. The role of TGF-β1 in fibrogenesis in lupus nephritis is controversial. Independent researchers have reported an increase in TGF-β1 expression, which was associated with increased fibronectin expression in renal specimens from patients and mice with active lupus nephritis (Yamamoto et al., 1994; Yamamoto et al., 1996; Yamamoto and Loskutoff, 2000), whereas other investigators suggested that kidney fibrosis in lupus nephritis patients occurred through proinflammatory mediators such as MCP-1 and not TGF-β1 since microarray analysis of glomeruli that were isolated from lupus nephritis

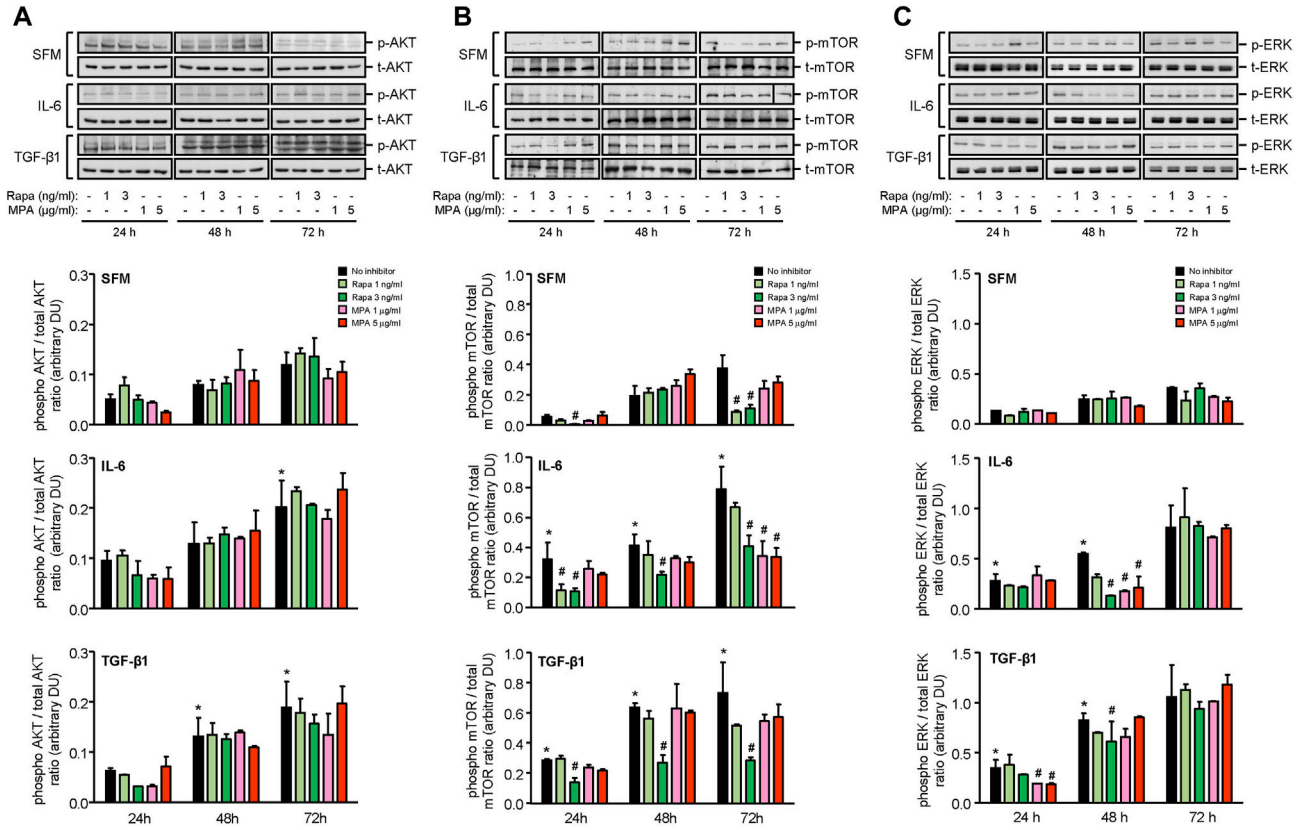

FIGURE 9 | Effect of MPA or rapamycin on AKT, mTOR, and ERK phosphorylation in human mesangial cells.Representative Western blots showing the effect of SFM, IL-6, or TGF-β1 in the presence or absence of rapamycin (1 or 3 ng/ml) or MPA (1 or 5 μg/ml) on **(A)** AKT phosphorylation, **(B)** mTOR phosphorylation at Ser^{2448}, and **(C)** ERK phosphorylation. The intensity of each band was semi-quantitated using ImageJ and normalized to total AKT, total mTOR, or total ERK. Values are expressed as mean ± SD for three separate experiments. DU, densitometric units. All data analyzed using ordinary ANOVA with Bonferroni's multiple comparison post-test. $^{*}p < 0.05$, SFM vs. IL-6 or TGF-β1; $^{\#}p < 0.05$, with vs. without rapamycin or MPA for the same stimulation and time-point.

patients showed reduced TGF-β1 expression, whereas MCP-1 expression clustered with genes related to fibrogenesis (Peterson et al., 2004).

Data from our *in vitro* studies demonstrated that induction of mTOR and ERK phosphorylation, α-smooth muscle actin, and mediators of fibrosis by IL-6 was comparable to that observed with TGF-β1, and it is plausible to suggest that IL-6 may contribute to kidney fibrosis in lupus nephritis. TGF-β1 was shown to increase IL-6 secretion in HMCs, which was mediated through increased PI3K, mTOR, and ERK phosphorylation and suggests that TGF-β1 may amplify the fibrotic effects of IL-6. We previously reported that IL-6 induced soluble fibronectin in proximal tubular epithelial cells (Yung et al., 2015a). In this study, we demonstrated that IL-6 induced α-smooth muscle actin, fibronectin, and collagen III in HMCs, and this underscores the contribution of proinflammatory mediators in kidney fibrosis. In line with our studies, Chen et al. reported on the role of IL-6 trans-signaling in murine models of kidney fibrosis (Chen et al., 2019). The importance of IL-6 in lupus nephritis pathogenesis is underscored in murine studies, whereby disruption of IL-6 signaling in lupus-prone mice was associated with reduced anti-dsDNA antibody production and proteinuria and improvement in kidney function (Kiberd, 1993; Finck et al., 1994). Mycophenolate has been shown to decrease IL-6 secretion in cultured proximal and distal tubular epithelial cells (Baer et al., 2004), whereas there are conflicting data on the effect of rapamycin on renal IL-6 expression. In a murine model of anti-GBM glomerulonephritis, mice treated with rapamycin at the time of immunization were protected from glomerulonephritis and renal IL-6 expression was reduced, whereas rapamycin treatment given 14 days after immunization resulted in a significant increase in both albuminuria and renal IL-6 expression, suggesting that the time when rapamycin treatment is initiated determines whether the drug exerts a beneficial or otherwise effect (Hochegger et al., 2008). In this study, we demonstrated that both MPA and rapamycin reduced IL-6 secretion in HMCs following TGF-β1 stimulation, although the anti-inflammatory/antifibrotic effect of MPA appeared earlier than that of rapamycin. In our animal studies, mycophenolate and rapamycin, whether administered as monotherapy or combination therapy to NZBWF1/J mice with active nephritis, showed comparable efficacy in suppressing IL-6 expression in the kidney (unpublished data). It is plausible that decreased IL-6

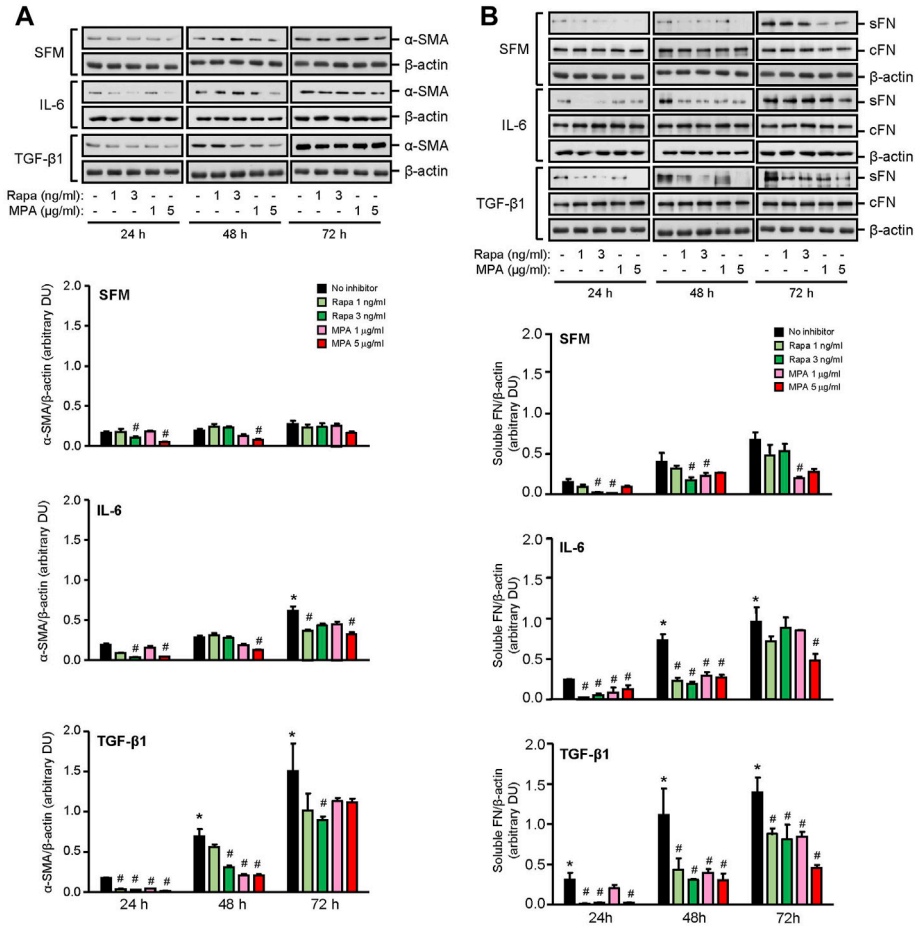

FIGURE 10 | Effect of MPA or rapamycin on α-smooth muscle actin and fibronectin expression in human mesangial cells. Representative Western blots showing the effect of SFM, IL-6, or TGF-β1 in the presence or absence of rapamycin (1 or 3 ng/ml) or MPA (1 or 5 μg/ml) on **(A)** α-smooth muscle actin (α-SMA) and **(B)** soluble (sFN) and cell-associated FN (cFN). The intensity of each band for α-SMA and sFN was semi-quantitated using ImageJ and normalized to β-actin. Values are expressed as mean ± SD for three separate experiments. DU, densitometric units. All data analyzed using ordinary ANOVA with Bonferroni's multiple comparison post-test. $^{*}p < 0.05$, SFM vs. IL-6 or TGF-β1; $^{\#}p < 0.05$, with vs. without rapamycin or MPA for the same stimulation.

expression in the glomeruli and tubulo-interstitium following MR treatment was attributed to both immunosuppressive agents.

Activation of PKC, TGF-β/SMAD, mTOR, and MAPK signaling pathways has been shown to contribute to kidney fibrosis (Yung et al., 2009; Yung et al., 2015a; Yung et al., 2017; Feng et al., 2018). IL-6 and TGF-β1 induced PI3K, mTOR, and ERK phosphorylation in HMCs, which was accompanied by downstream induction of IL-6 secretion and α-smooth muscle actin, fibronectin, and collagen III expression. IL-6 and TGF-β1 induced α-smooth muscle actin through mTOR phosphorylation. Induction of fibronectin was mediated through ERK, PI3K, and mTOR activation, and induction of collagen III was mediated through PI3K/mTOR signaling. Mycophenolate can decrease fibrotic processes in the kidney through downregulation of TGF-β1 expression and PKC, ERK, p38 MAPK, JNK, and mTOR activation (Yung et al., 2009; Yung et al., 2017; Zhang et al., 2019). In this study, mycophenolate and rapamycin decreased ERK phosphorylation that was induced by IL-6 and TGF-β1, and the inhibitory effect was comparable between both drugs. Mycophenolate and rapamycin also decreased mTOR activation, although the suppressive effect of mycophenolate on mTOR activation was less rapid and less effective than that of rapamycin. In animal models of CKD and tubulo-interstitial fibrosis, inhibition of ERK signaling using trametinib attenuated mTORC1 activation, suggesting that the ERK signaling pathway is upstream of mTORC1 (Andrikopoulos et al., 2019). In this study, we demonstrated that ERK phosphorylation was downstream of mTOR signaling in HMCs since inhibition of mTOR signaling with rapamycin resulted in a decrease in ERK phosphorylation, whereas PD98059 had no effect on mTOR phosphorylation. This discrepancy may be due to the cell-type, mediator that induced injury, disease model, and the time of sample collection. It is possible that mycophenolate reduced mTOR phosphorylation through downregulation of ERK phosphorylation, although further studies are necessary to confirm this. Neither mycophenolate nor rapamycin has any effect on PI3K phosphorylation, suggesting that PI3K activation

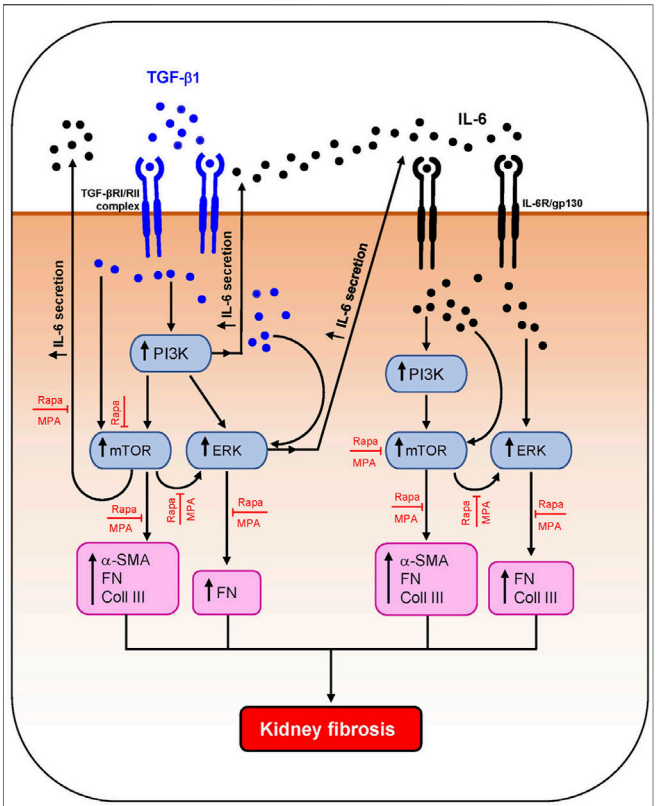

FIGURE 11 | Schematic diagram summarizing the effect of MPA and rapamycin on TGF-β1– and IL-6–induced inflammatory and fibrotic processes in human mesangial cells. TGF-β1 induced AKT/PI3K, mTOR, and ERK phosphorylation and downstream IL-6 secretion and α-smooth muscle actin (α-SMA), collagen III (Coll III), and fibronectin (FN) expression in HMCs. IL-6 also induced the aforementioned signaling pathways and mediators of fibrosis in HMCs. Both mycophenolic acid (MPA) and rapamycin (Rapa) significantly decreased mTOR and ERK phosphorylation and downstream inflammatory and fibrotic processes but had no effect on AKT/PI3K phosphorylation.

is upstream of the actions of these immunosuppressive agents. Mycophenolate and rapamycin reduced α-smooth muscle actin expression in HMCs through inhibition of mTOR but not ERK phosphorylation, whereas suppression of fibronectin expression by both drugs was likely mediated through the inhibition of ERK and mTOR phosphorylation. Although mesangial cells are key mediators of kidney fibrosis, other resident renal cells and immune cells such as proximal tubular epithelial cells, fibroblasts/myofibroblasts, and macrophages also contribute to kidney fibrosis. We and others have shown that mycophenolate and rapamycin can exert anti-inflammatory and antifibrotic effects on proximal tubular epithelial cells and fibroblasts, which may also contribute to the improvement in kidney structure and fibrotic processes (Badid et al., 2000; Copeland et al., 2007; Yung et al., 2015a; Yung et al., 2017). **Figure 11** summarizes the effect of MPA and rapamycin on signaling pathways and inflammatory and fibrotic processes induced by TGF-β1 and IL-6 in HMCs. Our findings demonstrated that both MPA and rapamycin can exert direct anti-inflammatory and antifibrotic effects in HMCs.

Our animal studies demonstrated that treatment of NZBWF1/J mice with combined mycophenolate and rapamycin at half the doses used in monotherapy improved the structural integrity of the kidney and prevented deterioration of kidney function. Both immunosuppressive agents exerted their antifibrotic effects directly on mesangial cells. Our clinical evidence suggests efficacy and safety of using mTOR inhibitors in the treatment of lupus nephritis patients (Yap et al., 2012a; Yap et al., 2018). Based on the findings from our translational and clinical studies, further studies may be warranted to investigate the combined use of mycophenolate and rapamycin in the clinical management of lupus nephritis, which would be helpful when tailoring treatment according to the specific characteristics of each patient with the objective of maximizing the benefits of the medication, while minimizing the side effects of each drug.

In conclusion, data from our animal studies demonstrated that combined mycophenolate and rapamycin reduced kidney fibrosis and improved kidney function. The suppressive effect on fibrotic processes in HMCs suggests a direct effect on resident kidney cells that was most likely independent of their immunosuppressive actions. The antifibrotic effects of mycophenolate and rapamycin were mediated, at least in part, through their ability to inhibit mTOR and ERK phosphorylation. We also demonstrated the importance of proinflammatory mediators in kidney fibrosis and the contribution of IL-6 in inducing fibrogenesis in lupus nephritis.

DATA AVAILABILITY STATEMENT

The original contributions presented in the study are included in the article/Supplementary Material; further inquiries can be directed to the corresponding authors.

ETHICS STATEMENT

The animal study was reviewed and approved by the Institutional Committee on the Use of Live Animals in Teaching and Research at the University of Hong Kong.

AUTHOR CONTRIBUTIONS

Study conception and design: SY and TMC. Acquisition of data: CZ, TWT, MKC, and CGC. Analysis and interpretation of the data: SY, CZ, and TMC. Drafting the article: CZ, SY, and TMC. Approval of the final version for submission: CZ, TWT, MKC, CGC, SY, and TMC.

FUNDING

This study received funding from the Hong Kong Research Grant Council General Research Fund (grant number HKU

7550/06M), Health and Medical Research Fund (06172656), UGC Matching Grant Scheme, the Department of Medicine Academic Activities Fund and kind donations from C. S. Yung, S. Ho, and Hui Hoy and Chow Sin Lan Charity Fund and the Family of Hui Ming. SY is supported by the Endowment Fund established for the "Yu Chiu Kwong Professorship in Medicine" awarded to TMC, the Wai Hung Charitable Foundation Limited and Tam Wing Fan Edmund Renal Research Fund. The funders were not involved in the study design, collection, analysis, interpretation of data, the writing of this article or the decision to submit it for publication. All authors declare no other competing interests.

REFERENCES

Allison, A. C., and Eugui, E. M. (2000). Mycophenolate Mofetil and its Mechanisms of Action. *Immunopharmacology* 47, 85–118. doi:10.1016/s0162-3109(00)00188-0

Andrikopoulos, P., Kieswich, J., Pacheco, S., Nadarajah, L., Harwood, S. M., O'riordan, C. E., et al. (2019). The MEK Inhibitor Trametinib Ameliorates Kidney Fibrosis by Suppressing ERK1/2 and mTORC1 Signaling. *J. Am. Soc. Nephrol.* 30, 33–49. doi:10.1681/ASN.2018020209

Azzola, A., Havryk, A., Chhajed, P., Hostettler, K., Black, J., Johnson, P., et al. (2004). Everolimus and Mycophenolate Mofetil Are Potent Inhibitors of Fibroblast Proliferation after Lung Transplantation. *Transplantation* 77, 275–280. doi:10.1097/01.TP.0000101822.50960.AB

Badid, C., Vincent, M., Mcgregor, B., Melin, M., Hadj-Aissa, A., Veysseyre, C., et al. (2000). Mycophenolate Mofetil Reduces Myofibroblast Infiltration and Collagen III Deposition in Rat Remnant Kidney. *Kidney Int.* 58, 51–61. doi:10.1046/j.1523-1755.2000.00140.x

Baer, P. C., Wegner, B., and Geiger, H. (2004). Effects of Mycophenolic Acid on IL-6 Expression of Human Renal Proximal and Distal Tubular Cells *In Vitro*. *Nephrol. Dial. Transpl.* 19, 47–52. doi:10.1093/ndt/gfg429

Bernatsky, S., Ramsey-Goldman, R., Labrecque, J., Joseph, L., Boivin, J. F., Petri, M., et al. (2013). Cancer Risk in Systemic Lupus: an Updated International Multi-centre Cohort Study. *J. Autoimmun.* 42, 130–135. doi:10.1016/j.jaut.2012.12.009

Borrows, R., Chusney, G., Loucaidou, M., James, A., Lee, J., Tromp, J. V., et al. (2006). Mycophenolic Acid 12-h Trough Level Monitoring in Renal Transplantation: Association with Acute Rejection and Toxicity. *Am. J. Transpl.* 6, 121–128. doi:10.1111/j.1600-6143.2005.01151.x

Campistol, J. M., Eris, J., Oberbauer, R., Friend, P., Hutchison, B., Morales, J. M., et al. (2006). Sirolimus Therapy after Early Cyclosporine Withdrawal Reduces the Risk for Cancer in Adult Renal Transplantation. *J. Am. Soc. Nephrol.* 17, 581–589. doi:10.1681/ASN.2005090993

Chan, T. M. (2015). Treatment of Severe Lupus Nephritis: the New Horizon. *Nat. Rev. Nephrol.* 11, 46–61. doi:10.1038/nrneph.2014.215

Chan, T. M., Tse, K. C., Tang, C. S., Mok, M. Y., and Li, F. K.Hong Kong Nephrology Study Group (2005). Long-term Study of Mycophenolate Mofetil as Continuous Induction and Maintenance Treatment for Diffuse Proliferative Lupus Nephritis. *J. Am. Soc. Nephrol.* 16, 1076–1084. doi:10.1681/ASN.2004080686

Chan, T. M., Mejia-Vilet, J. M., and Liu, Z. H. (2021). Chapter 10. Lupus Nephritis, in KDIGO 2021 Clinical Practice Guideline for the Management of Glomerular Diseases. *Kidney Int.* 100, S207–S230. doi:10.1016/j.kint.2021.05.021

Chen, W., Yuan, H., Cao, W., Wang, T., Chen, W., Yu, H., et al. (2019). Blocking Interleukin-6 Trans-signaling Protects against Renal Fibrosis by Suppressing STAT3 Activation. *Theranostics* 9, 3980–3991. doi:10.7150/thno.32352

Copeland, J. W., Beaumont, B. W., Merrilees, M. J., and Pilmore, H. L. (2007). Epithelial-to-mesenchymal Transition of Human Proximal Tubular Epithelial Cells: Effects of Rapamycin, Mycophenolate, Cyclosporin, Azathioprine, and Methylprednisolone. *Transplantation* 83, 809–814. doi:10.1097/01.tp.0000255680.71816.aa

Dubus, I., Vendrely, B., Christophe, I., Labouyrie, J. P., Delmas, Y., Bonnet, J., et al. (2002). Mycophenolic Acid Antagonizes the Activation of Cultured Human Mesangial Cells. *Kidney Int.* 62, 857–867. doi:10.1046/j.1523-1755.2002.00514.x

Duffield, J. S. (2014). Cellular and Molecular Mechanisms in Kidney Fibrosis. *J. Clin. Invest.* 124, 2299–2306. doi:10.1172/JCI72267

Feng, M., Tang, P. M., Huang, X. R., Sun, S. F., You, Y. K., Xiao, J., et al. (2018). TGF-β Mediates Renal Fibrosis via the Smad3-Erbb4-IR Long Noncoding RNA Axis. *Mol. Ther.* 26, 148–161. doi:10.1016/j.ymthe.2017.09.024

Fielding, C. A., Jones, G. W., Mcloughlin, R. M., Mcleod, L., Hammond, V. J., Uceda, J., et al. (2014). Interleukin-6 Signaling Drives Fibrosis in Unresolved Inflammation. *Immunity* 40, 40–50. doi:10.1016/j.immuni.2013.10.022

Finck, B. K., Chan, B., and Wofsy, D. (1994). Interleukin 6 Promotes Murine Lupus in NZB/NZW F1 Mice. *J. Clin. Invest.* 94, 585–591. doi:10.1172/JCI117373

Flechner, S. M., Kurian, S. M., Solez, K., Cook, D. J., Burke, J. T., Rollin, H., et al. (2004). De Novo kidney Transplantation without Use of Calcineurin Inhibitors Preserves Renal Structure and Function at Two Years. *Am. J. Transpl.* 4, 1776–1785. doi:10.1111/j.1600-6143.2004.00627.x

Hauser, I. A., Renders, L., Radeke, H. H., Sterzel, R. B., and Goppelt-Struebe, M. (1999). Mycophenolate Mofetil Inhibits Rat and Human Mesangial Cell Proliferation by Guanosine Depletion. *Nephrol. Dial. Transpl.* 14, 58–63. doi:10.1093/ndt/14.1.58

Herber, D., Brown, T. P., Liang, S., Young, D. A., Collins, M., and Dunussi-Joannopoulos, K. (2007). IL-21 Has a Pathogenic Role in a Lupus-Prone Mouse Model and its Blockade with IL-21R.Fc Reduces Disease Progression. *J. Immunol.* 178, 3822–3830. doi:10.4049/jimmunol.178.6.3822

Hochegger, K., Jansky, G. L., Soleiman, A., Wolf, A. M., Tagwerker, A., Seger, C., et al. (2008). Differential Effects of Rapamycin in Anti-GBM Glomerulonephritis. *J. Am. Soc. Nephrol.* 19, 1520–1529. doi:10.1681/ASN.2007121375

Janssen, U., Riley, S. G., Vassiliadou, A., Floege, J., and Phillips, A. O. (2003). Hypertension Superimposed on Type II Diabetes in Goto Kakizaki Rats Induces Progressive Nephropathy. *Kidney Int.* 63, 2162–2170. doi:10.1046/j.1523-1755.2003.00007.x

Kahan, B. D., Napoli, K. L., Kelly, P. A., Podbielski, J., Hussein, I., Urbauer, D. L., et al. (2000). Therapeutic Drug Monitoring of Sirolimus: Correlations with Efficacy and Toxicity. *Clin. Transpl.* 14, 97–109. doi:10.1034/j.1399-0012.2000.140201.x

Kiberd, B. A. (1993). Interleukin-6 Receptor Blockage Ameliorates Murine Lupus Nephritis. *J. Am. Soc. Nephrol.* 4, 58–61. doi:10.1681/ASN.V4158

Ladouceur, A., Bernatsky, S., Ramsey-Goldman, R., and Clarke, A. E. (2018). Managing Cancer Risk in Patients with Systemic Lupus Erythematous. *Expert Rev. Clin. Immunol.* 14, 793–802. doi:10.1080/1744666X.2018.1519394

Lui, S. L., Tsang, R., Chan, K. W., Zhang, F., Tam, S., Yung, S., et al. (2008a). Rapamycin Attenuates the Severity of Established Nephritis in Lupus-Prone NZB/W F1 Mice. *Nephrol. Dial. Transpl.* 23, 2768–2776. doi:10.1093/ndt/gfn216

Lui, S. L., Yung, S., Tsang, R., Zhang, F., Chan, K. W., Tam, S., et al. (2008b). Rapamycin Prevents the Development of Nephritis in Lupus-Prone NZB/W F1 Mice. *Lupus* 17, 305–313. doi:10.1177/0961203307088289

Mageau, A., Timsit, J. F., Perrozziello, A., Ruckly, S., Dupuis, C., Bouadma, L., et al. (2019). The burden of Chronic Kidney Disease in Systemic Lupus Erythematosus: A Nationwide Epidemiologic Study. *Autoimmun. Rev.* 18, 733–737. doi:10.1016/j.autrev.2019.05.011

Maroz, N., and Segal, M. S. (2013). Lupus Nephritis and End-Stage Kidney Disease. *Am. J. Med. Sci.* 346, 319–323. doi:10.1097/MAJ.0b013e31827f4ee3

Mok, C. C., Yap, D. Y., Navarra, S. V., Liu, Z. H., Zhao, M. H., Lu, L., et al. (2014). Overview of Lupus Nephritis Management Guidelines and Perspective from Asia. *Nephrology (Carlton)* 19, 11–20. doi:10.1111/nep.12136

Moreth, K., Brodbeck, R., Babelova, A., Gretz, N., Spieker, T., Zeng-Brouwers, J., et al. (2010). The Proteoglycan Biglycan Regulates Expression of the B Cell Chemoattractant CXCL13 and Aggravates Murine Lupus Nephritis. *J. Clin. Invest.* 120, 4251–4272. doi:10.1172/JCI42213

Parikh, S. V., Almaani, S., Brodsky, S., and Rovin, B. H. (2020). Update on Lupus Nephritis: Core Curriculum 2020. *Am. J. Kidney Dis.* 76, 265–281. doi:10.1053/j.ajkd.2019.10.017

Parodis, I., and Houssiau, F. A. (2022). From Sequential to Combination and Personalised Therapy in Lupus Nephritis: Moving towards a Paradigm Shift? *Ann. Rheum. Dis.* 81, 15–19. doi:10.1136/annrheumdis-2021-221270

Peterson, K. S., Huang, J. F., Zhu, J., D'agati, V., Liu, X., Miller, N., et al. (2004). Characterization of Heterogeneity in the Molecular Pathogenesis of Lupus Nephritis from Transcriptional Profiles of Laser-Captured Glomeruli. *J. Clin. Invest.* 113, 1722–1733. doi:10.1172/JCI19139

Rijnink, E. C., Teng, Y. K. O., Wilhelmus, S., Almekinders, M., Wolterbeek, R., Cransberg, K., et al. (2017). Clinical and Histopathologic Characteristics Associated with Renal Outcomes in Lupus Nephritis. *Clin. J. Am. Soc. Nephrol.* 12, 734–743. doi:10.2215/CJN.10601016

Tedesco-Silva, H., Felipe, C., Ferreira, A., Cristelli, M., Oliveira, N., Sandes-Freitas, T., et al. (2015). Reduced Incidence of Cytomegalovirus Infection in Kidney Transplant Recipients Receiving Everolimus and Reduced Tacrolimus Doses. *Am. J. Transpl.* 15, 2655–2664. doi:10.1111/ajt.13327

Warner, L. M., Adams, L. M., and Sehgal, S. N. (1994). Rapamycin Prolongs Survival and Arrests Pathophysiologic Changes in Murine Systemic Lupus Erythematosus. *Arthritis Rheum.* 37, 289–297. doi:10.1002/art.1780370219

Wierzbicka-Patynowski, I., and Schwarzbauer, J. E. (2003). The Ins and Outs of Fibronectin Matrix Assembly. *J. Cel Sci* 116, 3269–3276. doi:10.1242/jcs.00670

Woo, J., Wright, T. M., Lemster, B., Borochovitz, D., Nalesnik, M. A., and Thomson, A. W. (1995). Combined Effects of FK506 (Tacrolimus) and Cyclophosphamide on Atypical B220+ T Cells, Cytokine Gene Expression and Disease Activity in MRL/MpJ-lpr/lpr Mice. *Clin. Exp. Immunol.* 100, 118–125. doi:10.1111/j.1365-2249.1995.tb03612.x

Yamamoto, K., and Loskutoff, D. J. (2000). Expression of Transforming Growth Factor-Beta and Tumor Necrosis Factor-Alpha in the Plasma and Tissues of Mice with Lupus Nephritis. *Lab. Invest.* 80, 1561–1570. doi:10.1038/labinvest.3780166

Yamamoto, T., Nakamura, T., Noble, N. A., Ruoslahti, E., and Border, W. A. (1993). Expression of Transforming Growth Factor Beta Is Elevated in Human and Experimental Diabetic Nephropathy. *Proc. Natl. Acad. Sci. U S A.* 90, 1814–1818. doi:10.1073/pnas.90.5.1814

Yamamoto, T., Noble, N. A., Cohen, A. H., Nast, C. C., Hishida, A., Gold, L. I., et al. (1996). Expression of Transforming Growth Factor-Beta Isoforms in Human Glomerular Diseases. *Kidney Int.* 49, 461–469. doi:10.1038/ki.1996.65

Yamamoto, T., Noble, N. A., Miller, D. E., and Border, W. A. (1994). Sustained Expression of TGF-Beta 1 Underlies Development of Progressive Kidney Fibrosis. *Kidney Int.* 45, 916–927. doi:10.1038/ki.1994.122

Yanik, E. L., Siddiqui, K., and Engels, E. A. (2015). Sirolimus Effects on Cancer Incidence after Kidney Transplantation: a Meta-Analysis. *Cancer Med.* 4, 1448–1459. doi:10.1002/cam4.487

Yap, D. Y., Ma, M. K., Tang, C. S., and Chan, T. M. (2012a). Proliferation Signal Inhibitors in the Treatment of Lupus Nephritis: Preliminary Experience. *Nephrology (Carlton)* 17, 676–680. doi:10.1111/j.1440-1797.2012.01646.x

Yap, D. Y., Tang, C. S., Ma, M. K., Lam, M. F., and Chan, T. M. (2012b). Survival Analysis and Causes of Mortality in Patients with Lupus Nephritis. *Nephrol. Dial. Transpl.* 27, 3248–3254. doi:10.1093/ndt/gfs073

Yap, D. Y. H., Tam, C. H., Yung, S., Wong, S., Tang, C. S. O., Mok, T. M. Y., et al. (2020). Pharmacokinetics and Pharmacogenomics of Mycophenolic Acid and its Clinical Correlations in Maintenance Immunosuppression for Lupus Nephritis. *Nephrol. Dial. Transpl.* 35, 810–818. doi:10.1093/ndt/gfy284

Yap, D. Y. H., Tang, C., Chan, G. C. W., Kwan, L. P. Y., Ma, M. K. M., Mok, M. M. Y., et al. (2018). Longterm Data on Sirolimus Treatment in Patients with Lupus Nephritis. *J. Rheumatol.* 45, 1663–1670. doi:10.3899/jrheum.180507

Yap, D. Y. H., Tang, C., Ma, M. K. M., Mok, M. M. Y., Chan, G. C. W., Kwan, L. P. Y., et al. (2017). Longterm Data on Disease Flares in Patients with Proliferative Lupus Nephritis in Recent Years. *J. Rheumatol.* 44, 1375–1383. doi:10.3899/jrheum.170226

Yung, S., Cheung, K. F., Zhang, Q., and Chan, T. M. (2010). Anti-dsDNA Antibodies Bind to Mesangial Annexin II in Lupus Nephritis. *J. Am. Soc. Nephrol.* 21, 1912–1927. doi:10.1681/ASN.2009080805

Yung, S., Ng, C. Y., Au, K. Y., Cheung, K. F., Zhang, Q., Zhang, C., et al. (2017). Binding of Anti-dsDNA Antibodies to Proximal Tubular Epithelial Cells Contributes to Renal Tubulointerstitial Inflammation. *Clin. Sci. (Lond)* 131, 49–67. doi:10.1042/CS20160421

Yung, S., Ng, C. Y., Ho, S. K., Cheung, K. F., Chan, K. W., Zhang, Q., et al. (2015a). Anti-dsDNA Antibody Induces Soluble Fibronectin Secretion by Proximal Renal Tubular Epithelial Cells and Downstream Increase of TGF-B1 and Collagen Synthesis. *J. Autoimmun.* 58, 111–122. doi:10.1016/j.jaut.2015.01.008

Yung, S., Zhang, Q., Chau, M. K., and Chan, T. M. (2015b). Distinct Effects of Mycophenolate Mofetil and Cyclophosphamide on Renal Fibrosis in NZBWF1/J Mice. *Autoimmunity* 48, 471–487. doi:10.3109/08916934.2015.1054027

Yung, S., Zhang, Q., Zhang, C. Z., Chan, K. W., Lui, S. L., and Chan, T. M. (2009). Anti-DNA Antibody Induction of Protein Kinase C Phosphorylation and Fibronectin Synthesis in Human and Murine Lupus and the Effect of Mycophenolic Acid. *Arthritis Rheum.* 60, 2071–2082. doi:10.1002/art.24573

Zhang, C., Chan, C. C. Y., Cheung, K. F., Chau, M. K. M., Yap, D. Y. H., Ma, M. K. M., et al. (2019). Effect of Mycophenolate and Rapamycin on Renal Fibrosis in Lupus Nephritis. *Clin. Sci. (Lond)* 133, 1721–1744. doi:10.1042/CS20190536

Zhang, L., Lee, G., Liu, X., Pascoe, E. M., Badve, S. V., Boudville, N. C., et al. (2016). Long-term Outcomes of End-Stage Kidney Disease for Patients with Lupus Nephritis. *Kidney Int.* 89, 1337–1345. doi:10.1016/j.kint.2016.02.014

Conflict of Interest: The authors declare that the research was conducted in the absence of any commercial or financial relationships that could be construed as a potential conflict of interest.

Publisher's Note: All claims expressed in this article are solely those of the authors and do not necessarily represent those of their affiliated organizations, or those of the publisher, the editors, and the reviewers. Any product that may be evaluated in this article, or claim that may be made by its manufacturer, is not guaranteed or endorsed by the publisher.

frontiers | Frontiers in Pharmacology

ORIGINAL RESEARCH
published: 13 June 2022
doi: 10.3389/fphar.2022.843732

Endothelial Activin Receptor-Like Kinase 1 (ALK1) Regulates Myofibroblast Emergence and Peritubular Capillary Stability in the Early Stages of Kidney Fibrosis

Carlos Martínez-Salgado[1,2]*, *Fernando Sánchez-Juanes*[2,3], *Francisco J. López-Hernández*[1,2] *and José M. Muñoz-Félix*[2,3]*

[1]Department of Physiology and Pharmacology, Translational Research on Renal and Cardiovascular Diseases (TRECARD)-REDINREN (ISCIII), University of Salamanca, Salamanca, Spain, [2]Institute of Biomedical Research of Salamanca (IBSAL), Salamanca, Spain, [3]Department of Biochemistry and Molecular Biology, University of Salamanca, Salamanca, Spain

OPEN ACCESS

Edited by:
Raffaele Strippoli,
Sapienza University of Rome, Italy

Reviewed by:
Marta Ruiz-Ortega,
Autonomous University of Madrid, Spain
Jie Qing,
Southwest Medical University, China
Carmelo Bernabeu,
Spanish National Research Council (CSIC), Spain

***Correspondence:**
Carlos Martínez-Salgado
carlosms@usal.es
José M. Muñoz-Félix
jmmb@usal.es

Specialty section:
This article was submitted to Inflammation Pharmacology, a section of the journal Frontiers in Pharmacology

Received: 26 December 2021
Accepted: 04 May 2022
Published: 13 June 2022

Citation:
Martínez-Salgado C, Sánchez-Juanes F, López-Hernández FJ and Muñoz-Félix JM (2022) Endothelial Activin Receptor-Like Kinase 1 (ALK1) Regulates Myofibroblast Emergence and Peritubular Capillary Stability in the Early Stages of Kidney Fibrosis. Front. Pharmacol. 13:843732. doi: 10.3389/fphar.2022.843732

Renal tubulo-interstitial fibrosis is characterized by the excessive accumulation of extracellular matrix (ECM) in the tubular interstitium during chronic kidney disease. The main source of ECM proteins are emerging and proliferating myofibroblasts. The sources of myofibroblasts in the renal tubular interstitium have been studied during decades, in which the epithelial contribution of the myofibroblast population through the epithelial-to-mesenchymal (EMT) process was assumed to be the major mechanism. However, it is now accepted that the EMT contribution is very limited and other mechanisms such as the proliferation of local resident fibroblasts or the transdifferentiation of endothelial cells seem to be more relevant. Activin receptor-like kinase 1 (ALK1) is a type I receptor which belongs to the transforming growth factor beta (TGF-β) superfamily, with a key role in tissue fibrosis and production of ECM by myofibroblast. Predominantly expressed in endothelial cells, ALK1 also plays an important role in angiogenesis and vessel maturation, but the relation of these processes with kidney fibrosis is not fully understood. We show that after 3 days of unilateral ureteral obstruction (UUO), ALK1 heterozygous mice (*Alk1*$^{+/-}$) display lower levels of kidney fibrosis associated to a lower number of myofibroblasts. Moreover, *Alk1*$^{+/-}$ mice have a lower degree of vascular rarefaction, showing improved peritubular microvasculature after UUO. All these data suggest an important role of ALK1 in regulating vascular rarefaction and emergence of myofibroblasts.

Keywords: ALK1, Angiogenesis, peritubular capillaries, myofibroblasts, fibrosis, chronic kidney disease

INTRODUCTION

Tissue fibrosis is a common process to several chronic diseases of the liver, lungs, and kidneys, characterized by loss of tissue parenchyma (hepatocytes, pneumocytes and tubular epithelial cells, respectively), abundance of myofibroblasts, increased secretion of extracellular matrix proteins (ECM) and capillary rarefaction (Zeisberg and Kalluri, 2013). Specifically, in chronic kidney disease (CKD), a progressive and irreversible loss of renal function and renal tissue integrity, is associated with tubulo-interstitial fibrosis resulting from excessive deposition of ECM proteins by

myofibroblasts. Different sources of myofibroblasts contribute to renal fibrosis (Grande and López-Novoa, 2009; Munoz-Felix and Martinez-Salgado, 2021). During years, the epithelial-to-mesenchymal transition (EMT) was considered the main source (Sato et al., 2003; Zeisberg et al., 2003; Grande and López-Novoa, 2009; Grande et al., 2010) (of myofibroblasts). However, it was demonstrated that the epithelial contribution to myofibroblast abundance was around 5%, and other mechanisms such as the proliferation of local resident fibroblasts, the endothelial-to-mesenchymal transition (EndMT) and other mechanisms were involved (LeBleu et al., 2013; Grande et al., 2015).

Loss of the renal microcirculation due to blood vessel dropout is a major feature of chronic kidney disease (CKD) which also correlates with the progression of renal injury and tissue regeneration (Ishii et al., 2005). The loss of peritubular capillaries (PTC) also correlates with hypoxia and the development of fibrosis (Goligorsky, 2010; Gewin, 2019). Multiple mechanisms contribute to microvascular rarefaction such as "drive in reverse" or anti-angiogenic reprogramming due to the induction of anti-angiogenic programs promoted by angiostatin or endostatin (Goligorsky, 2010). In renal fibrosis, PTC undergo rarefaction after kidney injury (Kida et al., 2014). In an early phase, angiogenic factors are upregulated, endothelial cells proliferate and pericytes migrate away from the capillary area. Subsequently, a progression phase ensues with vascular regression, endothelial cell disfunction and apoptosis (Kida et al., 2014).

Activin receptor-like kinase 1 (ALK1) is a type I receptor from the TGF-β1 superfamily with a documented role in regulating ECM deposition and thus tissue fibrosis in the skin (Morris et al., 2011), liver (Breitkopf-Heinlein et al., 2017; Desroches-Castan et al., 2019a), heart (Morine et al., 2017a) and kidneys (Muñoz-Félix et al., 2014a). We previously showed that the increased renal fibrosis associated to ALK1 heterozygosity after 15 days of unilateral ureteral obstruction (UUO) was due to the promotion of ECM protein synthesis in myofibroblasts, the major source of fibrotic matrix (Muñoz-Félix et al., 2014a). ALK1 is also involved in the regulation of endothelial cell activation (Lamouille et al., 2002; Jonker, 2014), which impinges on vascular homeostatic processes. ALK1 seems to have a dual role in angiogenesis. While some studies show a pro-angiogenic role (Goumans et al., 2002; Lebrin et al., 2005), some others have demonstrated that ALK1 inhibits the activation phase of angiogenesis (Lamouille et al., 2002; Larrivée et al., 2012), especially when activated by its high affinity ligand bone morphogenetic protein 9 (BMP9), a quiescent factor promoting the normalization of the vasculature (David et al., 2007a; David et al., 2008; Ouarné et al., 2018; Viallard et al., 2020). Apart from our previous studies, it has been recently shown the protective role of ALK1 in diabetic nephropathy due to its effect in blood vessel integrity maintenance (Lora Gil et al., 2020; Gil et al., 2021). Yet, the contribution of alterations in vascular homeostasis to tissue fibrosis is not completely understood.

In this manuscript we aim to elucidate the role of ALK1 in renal vascular rarefaction and integrity in a fibrotic scenario produced by UUO.

MATERIALS AND METHODS

Mice

We used ALK1 heterozygous mice to evaluate the role of ALK1 in the early changes of the ureteral obstruction. *Alk1*$^{+/-}$ mice were generated as previously described (Oh et al., 2000). Adult *Alk1*$^{+/-}$ mice were kept in the pathogen-free facilities for genetically modified mice of the Animal Experimentation Service, University of Salamanca. Genotype analysis was performed by PCR with DNA isolated from mouse tail biopsies and using the primers previously reported (Oh et al., 2000).

In vivo Experimental Model of Tubulointerstitial Fibrosis

Unilateral ureteral obstruction (UUO) is an experimental model of renal injury, which causes tubular cell injury, inflammation and fibrosis. UUO has been used as a model for the events that take place during chronic kidney disease (Ucero et al., 2014).

UUO was performed during 3 days, as we aim to evaluate the early changes of this experimental approach. The unilateral ureteral obstruction (UUO) was performed as previously described (Rodríguez-Peña et al., 2002; Grande et al., 2009). In brief, 8 weeks old male mice were anesthetized with Isoflurane (Schering-Plough, Madrid, Spain). After laparatomy, we used non-reabsorbable 5-0 silk to ligate the left ureter. To generate sham operated mice (SO), we manipulated the left kidney ureter without ligation.

In this study, 5 mice were included in each experimental group. Animals were kept under controlled ambient conditions in a temperature controlled-room with a 12 h light/dark cycle, and were reared on standard chow (Panlab, Barcelona, Spain) and water *ad libitum*. In all procedures, mice were treated in accordance with the Recommendations of the Helsinki Declaration on the Advice on Care and Use of Animals referred to in: law 14\/2 007 (3 July) on Biomedical Research, Conseil de l´Europe (published in Official Daily N. L358/1-358/6, 18-12-1986), Government Spanish (Royal Decree 223/1 988, (14 March) and Order of 13-10-1989, and Official Bulletin of the State b. 256, pp. 31349-31362, 28-10-1990). The procedure was approved for the Bioethics committee of the University of Salamanca and Consejería de Agricultura y Pesca (Junta de Castilla y León).

Renal Tissue Preparation

Obstructed (O) and contralateral kidneys (NO), as well as kidneys of sham operated mice (SO), were removed 3 days after surgery after perfusion with heparinized saline solution at 37°C in order to eliminate red blood cells from the tissue and to avoid endogenous peroxidase signals in immunohistochemistry procedures. Next, kidneys were halved longitudinally in order to use one half for protein extraction and analysis and the other half for stainings and immunohistochemistry. Renal samples for protein extraction were frozen in liquid nitrogen and stored at −80°C. Renal samples for histological studies were fixed for 24 h in formaldehyde, transferred to ethanol 70% and then embedded in paraffin.

Western Blot

Western blot was performed for protein levels analysis in mouse kidney tissue. Tissue protein extracts were homogenized in lysis buffer (150 mmol/L NaCl, 1% Igepal CA-630, 10 mmol/L $MgCl_2$, 1 mmol/L EDTA, 10% glycerol, 1 mmol/L Na_3VO_4, 25 mmol/L NaF, l mmol/L PMSF, 10 mg/ml aprotinin and 10 mg/ml leupeptin) containing 25 mmol/L HEPES, pH 7.5 and centrifuged at 14000 g during 20 min at 4°C. Supernatants were recovered and the protein concentration was quantified using Lowry Method (BioRad). Lysates (100 µg per lane) were loaded onto polyacrylamide gels and the proteins were transferred to PVDF membranes (Millipore, Billerica, MA, United States) by electroblotting. Next, membranes were blocked in bovine serum albumin (BSA) 3% and were incubated overnight at 4°C with the following antibodies: rabbit anti-collagen type I (dilution 1:1,000) and rabbit anti-fibronectin (1:1,000) from Chemicon International (Temecula, CA, United States); rabbit anti-ACVRL1 (ALK1) (1:1,000) from Abgent (Derio, Spain); mouse anti-α-SMA (1:5,000) from Sigma-Aldrich (Madrid, Spain); mouse anti-PCNA (1:1,000) from Transduction Laboratories (Madrid, Spain); and mouse anti-GAPDH (1:40000) from Ambion (Barcelona, Spain). After overnight incubation with the primary antibodies, membranes were incubated with the corresponding horseradish peroxidase-conjugated secondary antibodies during 60 min (1:10000) and were developed using ECL chemiluminescence reagent (Amersham Biosciences, Barcelona, Spain). Developed signals were recorded on X-ray films (Fujifilm Spain, Barcelona, Spain) for densitometric analysis (Scion Image software, Frederick, MD, United States). GAPDH (Ambion, Barcelona, Spain) was used as loading control. GAPDH was incubated in the same membrane that the protein of interest when it was possible.

Histochemistry and Immunohistochemistry

3 µm sections were cut from paraffin-embedded samples and stained with haematoxylin-eosin, picrosirius, and Masson's trichrome. Sirius red staining was evaluated by a quantitative scoring system, Fiji (https://imagej.net/software/fiji/), released as open source under the GNU General Public License in 12 randomly selected fields (200X) per experimental group.

Immunohistochemistry was performed on buffered formalin-fixed, paraffin-embedded tissues as previously described (Rodríguez-Peña et al., 2002; Grande et al., 2010) Briefly, 3 µm sections were deparaffinized in xylene and rehydrated in graded ethanols (100, 80, 70 and 50%) before antigen retrieval with sodium citrate buffer pH = 6.0, Then, primary antibodies were incubated overninght. Primary antibodies were: mouse anti-alpha smooth muscle actin (α-SMA, dilution 1:100, from Sigma-Aldrich), CD31 (Abcam) and rabbit anti-S100A4 (1:100 from Chemicon International, Temecula, CA, United States), mouse anti-VEGF (1: 100 from Santa Cruz Biotechnology. After that staining continued with the peroxidase-antiperoxidase method. Tissue sections were incubated with the corresponding horseradish peroxidase-conjugated secondary antibodies during 60 min (1:250). After three washes in phosphate-buffered saline (PBS: 0.81% NaCl, 2.6 mM H_2KPO_4, 4.1 mM HNa_2PO_4), sections were sequentially incubated with the Novolink Polymer Detection System (Novocastra, Newcastle, United Kingdom) using 3,3′-diaminobenzidine (Biogenez, San Ramón CA, United States) as chromogen. Sections were counterstained with haematoxylin and were dehydrated and cover slipped. Endogenous peroxidase was blocked by incubation in 3% hydrogen peroxide. For an adequate optimization of the method, negative controls were prepared without primary antibodies. VEGF staining was evaluated using Fiji as mentioned above in 10–15 randomly selected fields (400X) per experimental group.

Immunofluorescence Staining

Paraffin-embedded tissues were cut in 3 µm sections. Heat-induced antigen retrieval was performed in sodium citrate buffer pH 6.00 in a microwave owen, and washed with PBS. Sections were incubated with endomucin (Santa Cruz Biotechnology) in combination or not with anti-α-SMA (Sigma Aldrich) overnight at 4°. Following three washes in PBS, sections were incubated with anti-rat 488 Alexa and anti-mouse 546 (Molecular Probes, Barcelona, Spain), diluted 1:200 for 60 min at room temperature, washed in PBS, and stained with 2 µM Hoechst 33258 (Molecular Probes, Barcelona, Spain). Slides were rinsed in PBS and mounted in Prolong anti-fade (Invitrogen, Barcelona, Spain). Confocal images were photographed using a Zeiss Axiovert 200 M microscope and a Zeiss LSM 510 confocal module. All images were obtained with identical parameters for intensity, pinhole aperture, etc. Image manipulation of immunofluorescence analysis was performed using the same settings in all the samples and pictures shown in this manuscript, and following the image manipulation guidelines from the journal.

Blood Vessel Density Analysis

Abundance of peritubular capillaries was assessed by counting the number of CD31 or endomucin-positive microvessels in peritubular areas in the kidney cortex across 5 different fields per kidney. Glomerular capillaries were not considered for the analysis.

Vascular Rarefaction and Endothelial-Myofibroblast Transition Analysis

Apart from the blood vessel density analysis, vascular rarefaction was assessed by the individual quantitation of endomucin+ endothelial cells across 5 different fields per kidney (SO and O kidneys form $Alk1^{+/+}$ and $Alk1^{+/-}$ mice). Myofibroblast emergence was also assessed by the individual number of α-SMA+ cells excluding vascular smooth muscle cells. Hoechst counterstaining helped us to identify individual cells. Endothelial-myofibroblast transition was assessed by counting the double endomucin+ and α-smooth muscle actin α-SMA+ cells versus total endomucin + cells across 5 fields per kidney.

Statistical Analysis

Data are expressed as mean ± standard error of the mean (SEM). The Kolmogorov-Smirnov test was used to assess the normality of the data distribution. Comparison of means was performed by two way analysis of variance (ANOVA) with Tukey's HSC post hoc test. Data was analyzed using Graph Pad Prism software 9.0. A "p" value lower than 0.05 was considered statistically significant.

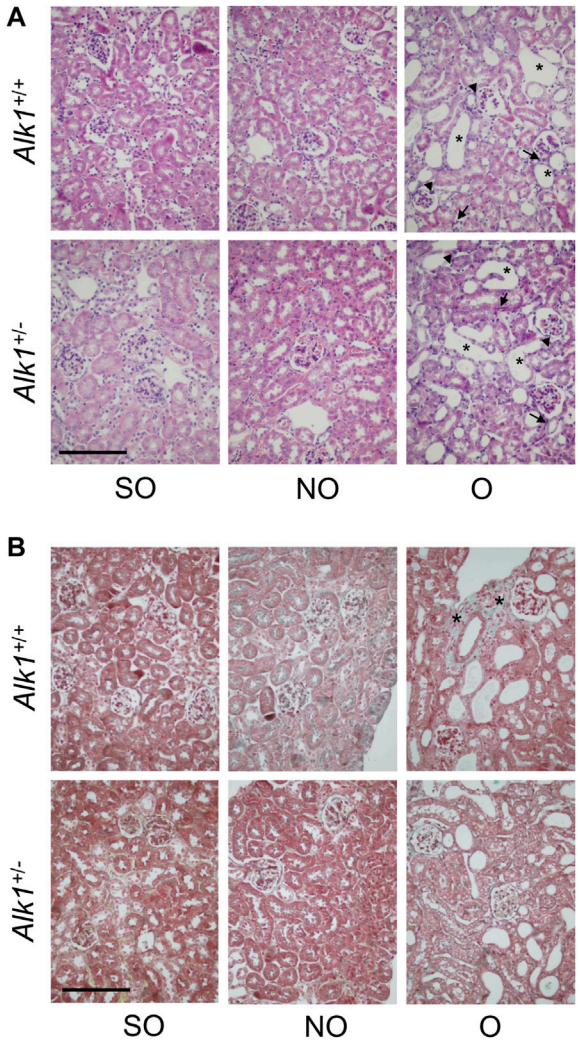

FIGURE 1 | UUO modifies the renal ultrastructure after 3 days in *Alk1*$^{+/+}$ and *Alk1*$^{+/-}$ mice. **(A)** Haematoxylin-eosin staining in SO, NO and O kidneys from *Alk1*$^{+/+}$ and *Alk1*$^{+/-}$ mice show the typical features of the early stages of UUO such as tubular dilatation (asterisk), interstitial cell proliferation (arrow) or immune cell infiltration (arrowhead), being these features similar in O kidneys from *Alk1*$^{+/+}$ and *Alk1*$^{+/-}$ mice. **(B)** Masson's trichrome staining in SO, NO and O kidneys from *Alk1*$^{+/+}$ and *Alk1*$^{+/-}$ mice showing lower ECM deposition (asterisk) in O kidneys from *Alk1*$^{+/-}$. Scale bar = 200 microns in both panels.

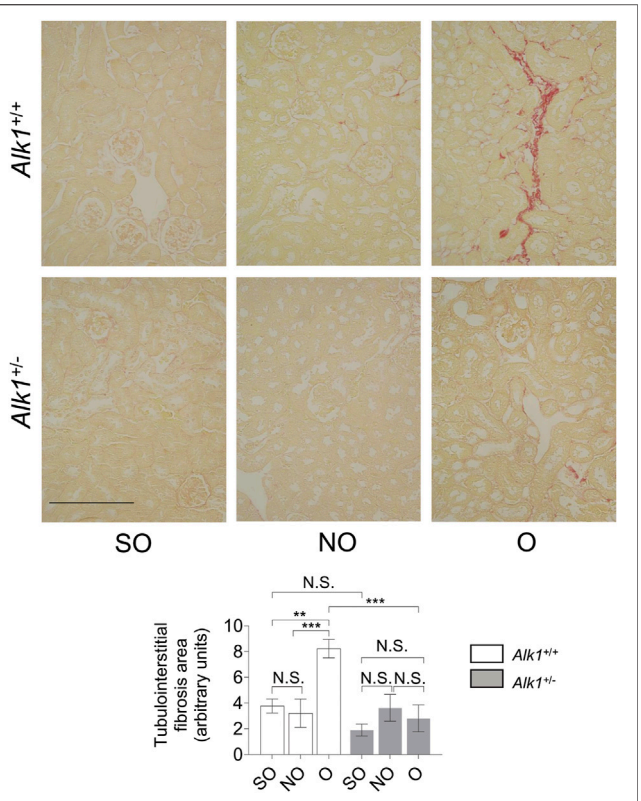

FIGURE 2 | *Alk1*$^{+/-}$ mice show lower kidney fibrosis after 3 days UUO. Sirius red staining in SO, NO and O kidneys from *Alk1*$^{+/+}$ and *Alk1*$^{+/-}$ mice (N = 5) (upper panel). Analysis of tubule-interstitial fibrosis area in SO, NO and O kidneys from *Alk1*$^{+/+}$ and *Alk1*$^{+/-}$ mice, assessed by Fiji (ImageJ) software. $^{**}p < 0.01$; $^{***}p < 0.001$ (Two-way ANOVA); N.S = Not statistically significant. Scale bar = 250 microns.

RESULTS

Renal Injury and Kidney Fibrosis After 3 days UUO in *Alk1*$^{+/+}$ and *Alk1*$^{+/-}$ Mice

O kidneys from both *Alk1*$^{+/+}$ and *Alk1*$^{+/-}$ mice show the histological events that take place after the UUO: Tubular cell injury, tubular dilation, inflammation; as shown with the Haematoxylin-eosin staining (**Figure 1A**) and tubule-interstitial fibrosis, as shown with the Masson's trichrome staining (**Figure 1B**). While we observed no differences in kidney injury between both genotypes, we detected lower tubule-interstitial fibrosis in *Alk1*$^{+/-}$ mice.

Alk1$^{+/-}$ Mice Show Decreased Tubulo-Interstitial Fibrosis After 3 days of Unilateral Ureteral Obstruction (UUO)

One of the most representative features of obstructive nephropathy is the accumulation of ECM proteins in the tubular interstitium, such as collagens (collagen I or collagen III), fibronectin or laminin. After our analysis of the picrosirius red staining, we observed increased levels of collagens in O kidneys form *Alk1*$^{+/+}$ mice but not in O kidneys from *Alk1*$^{+/-}$ mice (**Figure 2**).

There is also an increase in the expression of ECM proteins (collagen I, fibronectin) in O kidneys from *Alk1*$^{+/+}$ but not in O kidneys from *Alk1*$^{+/-}$ mice evaluated by western blot (**Figure 3**).

Reduced Renal Myofibroblast Emergence and Proliferation in *Alk1*$^{+/-}$ Mice

Renal myofibroblasts emerge and proliferate in the first steps of obstructive nephropathy. After 3 days of UUO we observe an increase in the presence of myofibroblasts in the tubular initerstitium of *Alk1*$^{+/+}$ mice, evaluated by immunostaining of the myofibroblast markers α-smooth muscle actin (α-SMA) (**Figure 4A**) and FSP1/S100A4 (**Figure 4C**) and by α-SMA

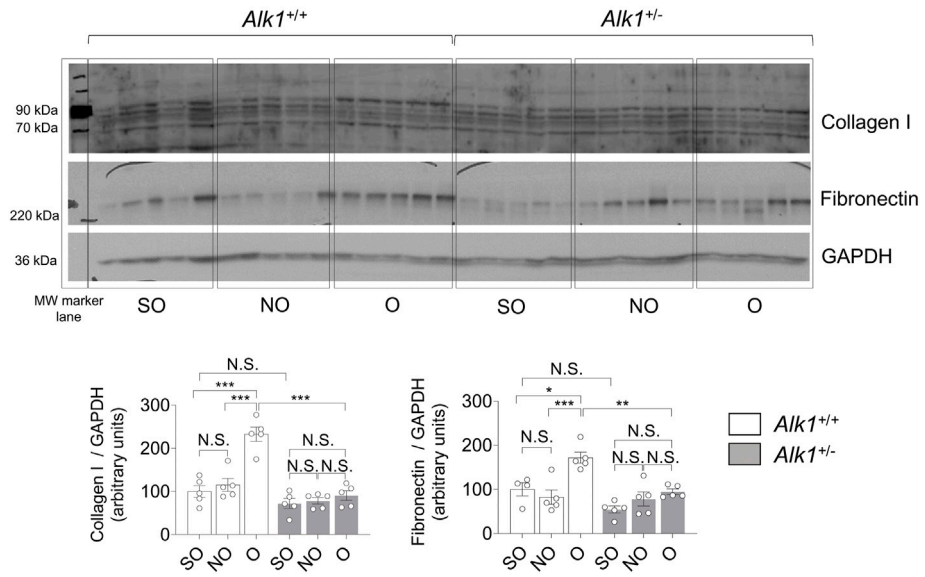

FIGURE 3 | Obstructed kidneys from *Alk1*$^{+/-}$ mice show reduced ECM protein levels after 3 days UUO. Western blot analysis of collagen I and fibronectin protein expression in SO, NO and O kidneys from *Alk1*$^{+/+}$ and *Alk1*$^{+/-}$ mice, and quantification of the corresponding densitometry. Bars represent the ratio between the proteins and GAPDH, used as loading control. *$p < 0.05$; **$p < 0.01$; ***$p < 0.001$; N.S = Not statistically significant (Two-way ANOVA). One statistical outlier was removed from the analysis of fibronectin in a SO mice from *Alk1*$^{+/+}$ mice.

western blot analysis (**Figure 4B**) in O kidneys from *Alk1*$^{+/+}$ mice. However, we barely observe those increases in O kidneys from *Alk1*$^{+/-}$ mice. (**Figures 4A–C**). As α-SMA is not only a specific maker for myofibroblasts, because it is highly expressed in vascular smooth muscle cells (VSMCs) we quantified the α-SMA+ individual cells by immunofluorescence with Hoechst counterstaining excluding VSMCs, and we show that O kidneys from *Alk1*$^{+/+}$ mice show a higher number of α-SMA+ myofibroblasts than O kidneys from *Alk1*$^{+/-}$ mice (**Figure 5**). In O kidneys from *Alk1*$^{+/-}$ mice the presence of α-SMA positive cells is reduced and correlates with the lower ECM deposition observed in these animals. Moreover, the increase in cell proliferation is lower in O kidneys from *Alk1*$^{+/-}$ mice, assessed by proliferating cell nuclear antigen (PCNA) expression (**Figure 4D**). Taken all these together, we can suggest that ALK1 heterozygosity leads to a lower kidney fibrosis due to a reduced abundance and proliferation of myofibroblasts.

ALK1 Deficiency Ameliorates the Microvascular Damage Early Produced by UUO

As mentioned before, microvascular rarefaction is a feature of tubule-interstitial fibrosis and it contributes to the progression of hypoxia and tissue fibrosis. In the early stages of UUO, there is a vessel regression phase in which endothelial cells undergo apoptosis and pericyte adhesion is disrupted (Kida et al., 2014). Several studies show that ALK1 is involved in vessel maturation and quiescence (Akla et al., 2018; Viallard et al., 2020).

We observe a decrease in blood vessel density in O kidneys from *Alk1*$^{+/+}$ mice, assessed by immunostaining of the endothelial markers CD31 (**Figure 6A**) and endomucin (**Figure 6B**), similar to that previously described in other studies performed in the UUO model (Kida et al., 2014). However, blood vessel density was maintained in *Alk1*$^{+/-}$ mice after UUO, suggesting that ALK1 heterozygosity protects from vascular rarefaction in the UUO early stages.

Impaired Emergence of Myofibroblasts From Endothelial Cell Origin in *Alk1*$^{+/-}$ Mice

As stated before, myofibroblasts in the obstructed kidney emerge from different origins such as proliferating local resident fibroblasts, bone marrow derived cells or vascular cells. Vascular endothelial cells and pericytes can transdifferentiate into myofibroblasts. To dissect the myofibroblast cells that arise from endothelial cells we have double-immunostained kidney sections with an endothelial marker (endomucin) and a myofibroblast marker (α-SMA). Thus, cells with double positive staining for endomucin and α-SMA are endothelial cells being transdifferentiated into myofibroblasts. We observed that these double stained cells are more abundant in O kidneys from *Alk1*$^{+/+}$ mice than in O kidneys from *Alk1*$^{+/-}$ mice (**Figure 7**). This finding indicates that the lower abundance of myofibroblasts observed in ALK1 heterozygous mice is due to a lower transdifferentiation from endothelial cells and this correlates with the PTC stability after 3 days UUO in *Alk1*$^{+/-}$ mice.

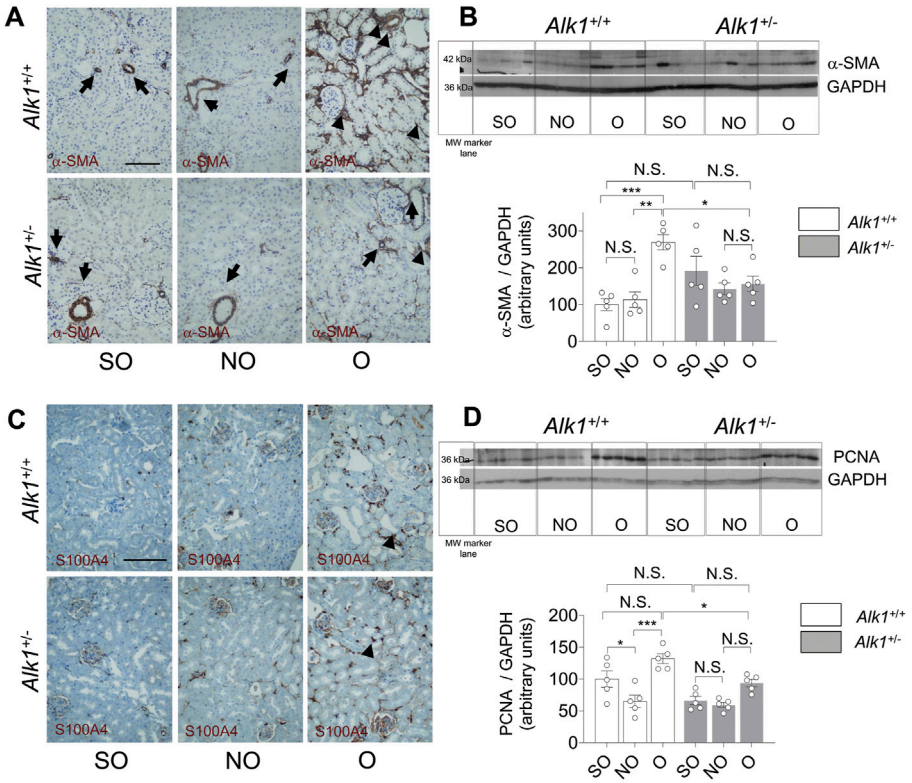

FIGURE 4 | Reduced myofibroblast abundance and proliferation in obstructed kidneys from *Alk1*$^{+/-}$ mice after 3 days UUO. **(A)** α-SMA immunostaining in SO, NO and O kidneys from *Alk1*$^{+/+}$ and *Alk1*$^{+/-}$ mice. **(B)** Western blot analysis of α-SMA protein expression in SO, NO and O kidneys from *Alk1*$^{+/+}$ and *Alk1*$^{+/-}$ mice and quantification of the corresponding densitometry analysis ($N = 5$). Bars represent the ratio between α-SMA and GAPDH, used as loading control. **(C)** FSP1/S100A4 immunostaining in SO, NO and O kidneys from *Alk1*$^{+/+}$ and *Alk1*$^{+/-}$ mice. **(D)** Western blot analysis of PCNA protein expression in SO, NO and O kidneys from *Alk1*$^{+/+}$ and *Alk1*$^{+/-}$ mice and quantification of the corresponding densitometry analysis. Bars represent the ratio between PCNA and GAPDH, used as loading control. $^{*}p < 0.05$; $^{**}p < 0.01$; $^{***}p < 0.001$; N.S = Not statistically significant (Two-way ANOVA). The loading control for PCNA is the same as that used in **Figure 3**, as both Collagen I and PCNA were incubated in the same membrane. Arrows in **(A)** identify VSMCs. Arrowheads in **(A)** and **(B)** identify tubulo-interstitial myofibroblasts. Scale bar = 100 microns in A, 150 microns in **(C)**.

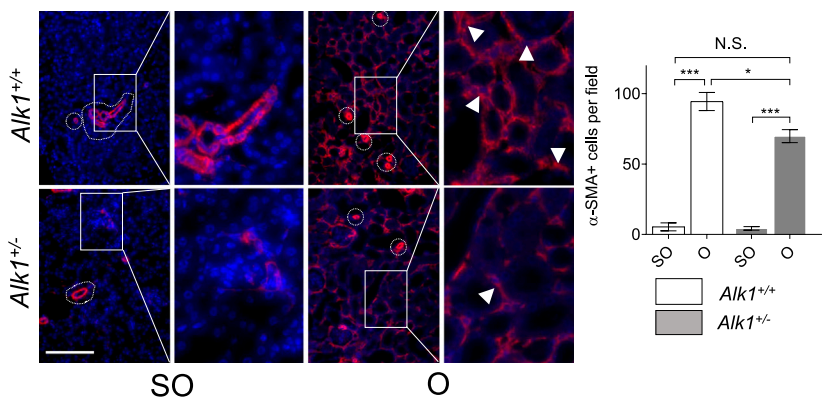

FIGURE 5 | Analysis of α-SMA + myofibroblasts. Identification of α-SMA+ myofibroblasts by immunofluorescence of α-SMA with Hoechst counterstaining in SO and O kidneys from *Alk1*$^{+/+}$ and *Alk1*$^{+/-}$ mice. Squares identify zoomed areas $^{*}p < 0.05$; $^{***}p < 0.001$; N.S = Not statistically significant. (Two-way ANOVA). Cropped areas identify α-SMA+ VSMCs from small vessels. Arrowheads identify α-SMA+ tubulo-interstitial myofibroblasts. Scale bar = 150 microns.

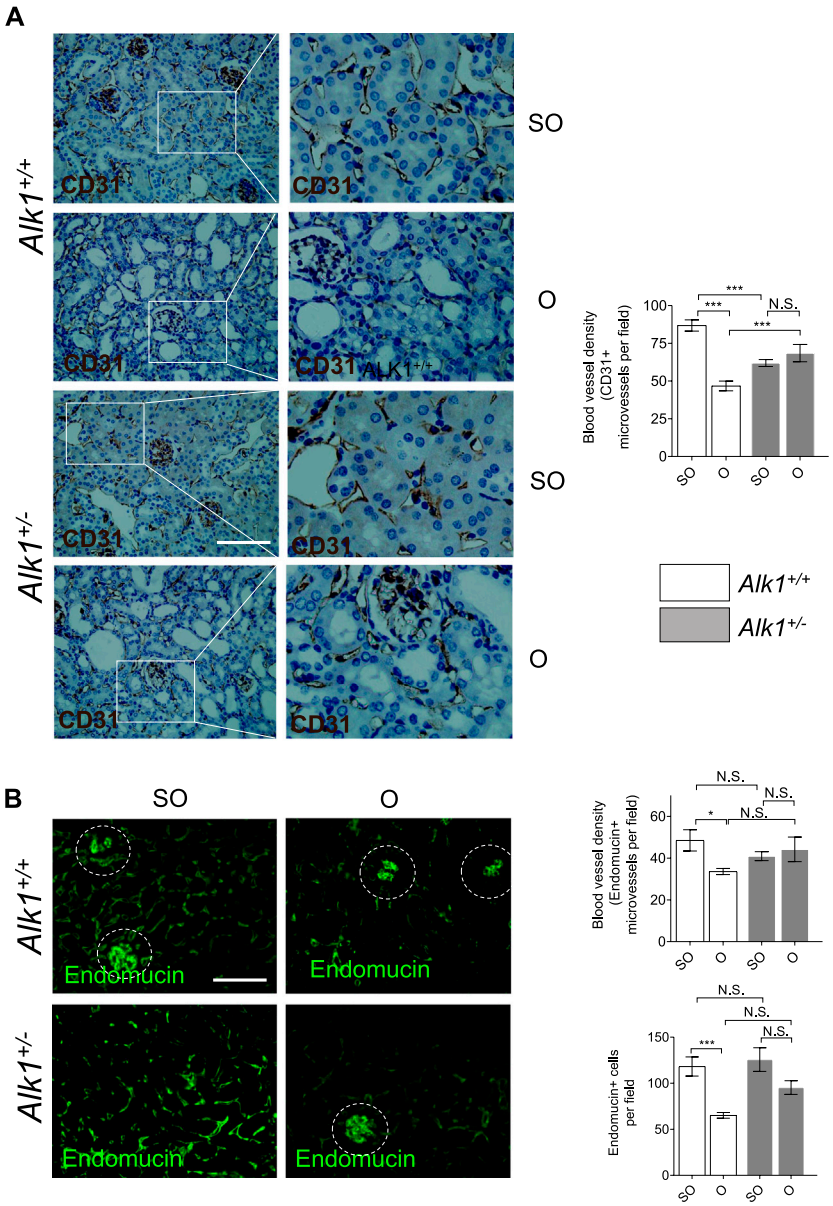

FIGURE 6 | Impaired peritubular capillaries rarefaction in *Alk1*$^{+/-}$ mice. **(A)** CD31 immunostaining in SO and O kidneys from *Alk1*$^{+/+}$ and *Alk1*$^{+/-}$ mice and blood vessel density analysis, represented as CD31 $^{+}$ vessels per field. **(B)** Endomucin immunofluorescence staining in SO and O kidneys from *Alk1*$^{+/+}$ and *Alk1*$^{+/-}$ mice and blood vessel density quantification from endomucin staining, represented as microvessels per field (upper graph) and endomucin+ cells per field (lower graph) in SO and O kidneys from *Alk1*$^{+/+}$ and *Alk1*$^{+/-}$ mice. *$p < 0.05$; ***$p < 0.001$; N.S. Not statistically significant (Two-way ANOVA). Squares in **(A)** indicate the zoomed areas. Scale bar = 200 microns in both panels. Blood vessels from the glomeruli in **(B)** (highlighted as cropped áreas) were not counted.

Alk1$^{+/-}$ Mice Are Protected From Vessel Regression After 3 days UUO

ALK1 was described by David et al. (2008) as a molecule which induces quiescence and inhibits endothelial cell proliferation and migration (Lamouille et al., 2002; David et al., 2008). Angiogenesis is a process linked with the development of tubule-interstitial fibrosis after UUO. We found an increase of ALK1 expression in O kidneys from both *Alk1*$^{+/+}$ mice which may indicate the beginning of the regression phase of angiogenesis after obstruction. As expected, we do not observe increased levels of ALK1 receptor in *Alk1*$^{+/-}$ mice after UUO, suggesting a pro-angiogenic effect in these animals (**Figure 8A**). To elucidate the differences in the angiogenic process during vascular rarefaction after UUO, we have analyzed the levels of one of the most important angiogenic factors, vascular endothelial growth factor (VEGF). We detected no differences in VEGF expression after UUO in *Alk1*$^{+/+}$ mice but we observed a

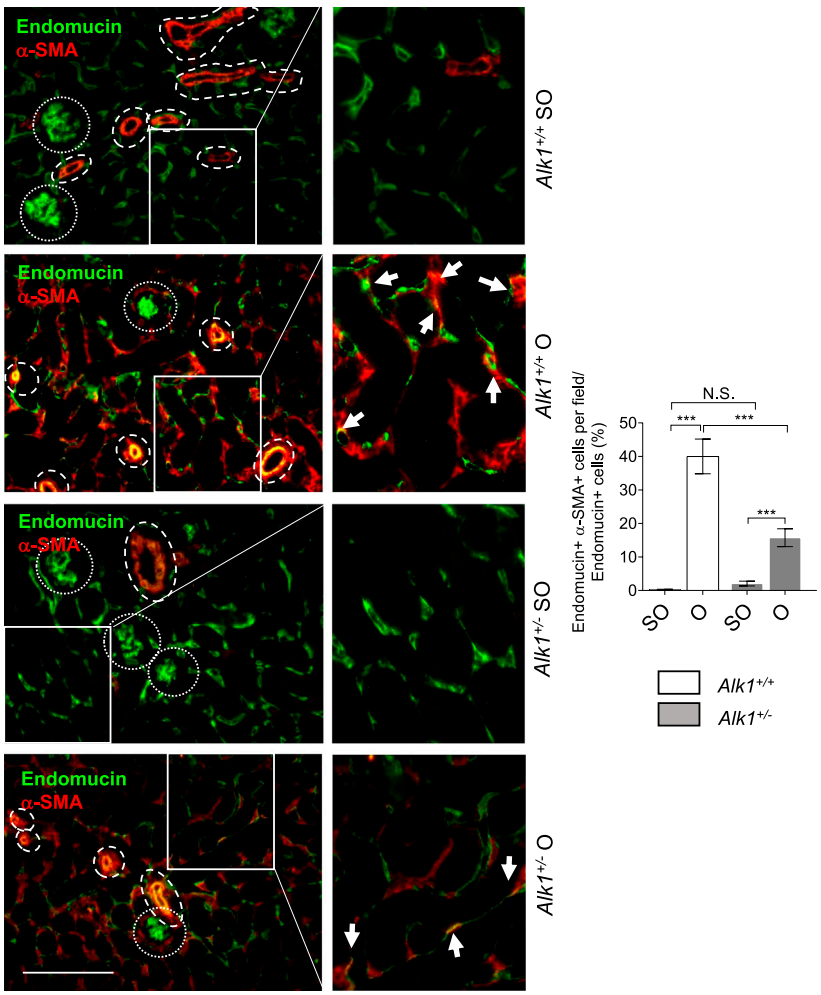

FIGURE 7 | Endothelial-to-myofibroblast transdifferentiation after UUO in *Alk1*$^{+/+}$ and *Alk1*$^{+/-}$ mice. Double immunofluorescence of endomucin (endothelial marker) and α-SMA (myofibroblast marker) in SO and O kidneys from *Alk1*$^{+/+}$ and *Alk1*$^{+/-}$ mice and quantification of double endomucin and α-SMA positive cells. Cropped areas with small dashed line are glomeruli, not considered for the analysis. Cropped areas with large dashed lines are small vessels, also not considered for the analysis. ***$p <$ 0.001; N.S. Not statistically significant (Two-way ANOVA). Arrows identify double endomucin+—α-SMA+ cells. Scale bar = 200 microns.

higher expression in O kidneys from *Alk1*$^{+/-}$ mice (**Figure 8B**). Taken all these together, we suggest that the lower ALK1 levels and increased levels of VEGF in O kidneys from *Alk1*$^{+/-}$ mice may correlate with a delay of the regression phase of angiogenesis that prevents endothelial-pericyte detachment, contributing to microvascular preservation and impaired endothelial to myofibroblast transdifferentiation.

DISCUSSION

Renal myofibroblasts are the main source of ECM proteins during tubule-interstitial fibrosis (LeBleu and Kalluri, 2011). Myofibroblasts are activated fibroblasts with high contractile capacity, and with a high capacity to synthesize ECM proteins such as collagens, fibronectin or laminin (Munoz-Felix and Martinez-Salgado, 2021). These cells emerge during the first steps of the fibrotic process from different origins. Numerous studies attributed their origin to the epithelial-to-mesenchymal transition (EMT) program (Grande and López-Novoa, 2009). However, although the EMT process has been validated in renal cells *in vitro* (Docherty et al., 2006a), the contribution of the epithelial components to myofibroblast abundance is very limited, as it has been demonstrated *in vivo* (Picard et al., 2008; Grande et al., 2015). The most important origins and mechanisms of myofibroblast emergence are proliferating local resident fibroblasts and the transdifferentiation from endothelial cells or and pericytes (LeBleu et al., 2013).

In this study we observe a lower kidney fibrosis after 3 days UUO which correlates with a lower myofibroblast abundance in *Alk1*$^{+/-}$ mice. Moreover, we show a lower microvascular rarefaction in these mice. Vascular rarefaction is involved in

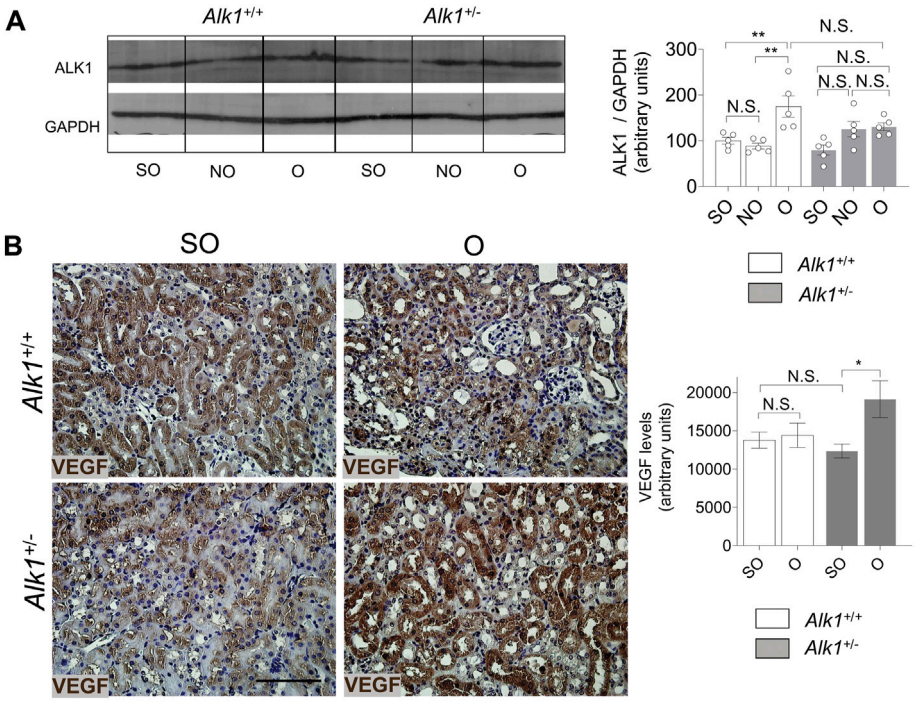

FIGURE 8 | ALK1 and VEGF protein expression after UUO. **(A)** Western blot analysis of ALK1 protein in SO, NO and O kidneys from *Alk1*$^{+/+}$ and *Alk1*$^{+/-}$ mice (N = 5), and quantification of the corresponding densitometry analysis. Bars represent the ratio between the proteins and GAPDH, used as loading control. **(B)** VEGF immunohistochemistry representative pictures and quantification of VEGF levels (using Fiji software) in SO, NO and O kidneys from *Alk1*$^{+/+}$ and *Alk1*$^{+/-}$ mice. *$p < 0.05$; **$p < 0.01$ N.S. Non statistically significant (Two-way ANOVA). Scale bar = 150 microns.

myofibroblast emergence by different mechanisms. In the early phases of UUO, endothelial cells undergo an apoptotic program which lead to the detachment of endothelial cells from pericytes (Kida et al., 2014). Endothelial cells can transdifferentiate into myofibroblasts *via* the endothelial to mesenchymal transition program (Zeisberg et al., 2008). On the other hand, pericytes can migrate from the basement membrane and transdifferentiate into myofibroblasts (Kida et al., 2014). Our data suggest that the maintenance of the microvascular architecture observed in *Alk1*$^{+/-}$ may be related with the lower emergence of myofibroblasts observed in these mice and the lower ECM deposition as a possible consequence of the reduced number of myofibroblasts (**Figure 9**).

The process by which PTC undergo rarefaction comprises two different stages: Initially, there is an angiogenic phase where angiogenic factors such as VEGF are upregulated and inflammatory cell infiltration happens. Later, the vascular regression phase occurs when a decrease of angiogenic factors and an increase of anti-angiogenic factors takes place in the obstructed kidney (Kida et al., 2014). Endothelial cells and pericytes are detached in the regression phase and can be transdifferentiated to myofibroblasts. Our data suggest that ALK1 is regulating this phenomenon. We observed lower vascular rarefaction in *Alk1*$^{+/-}$ mice after 3 days of UUO. ALK1 regulates negatively the activation phase of angiogenesis (Ayuso-Inigo et al., 2021) and it is expected that lower levels of ALK1 in *Alk1*$^{+/-}$ mice lead to a maintained angiogenic phase or an impaired vessel regression phase, which also correlates with the higher VEGF levels observed in O kidneys from *Alk1*$^{+/-}$ mice. Our observations are in concordance with those of Sharpfenecker et al. (2011), who demonstrated in a kidney fibrosis model after irradiation that *Alk1*$^{+/-}$ mice show lower vascular injury after 20 weeks of irradiation, and this correlated with higher levels of VEGF and VEGFR2 at that time point (Scharpfenecker et al., 2011).

Years ago, we demonstrated a role of ALK1 in counteracting TGF-β1-induced kidney fibrosis at 15 days UUO (Muñoz-Félix et al., 2014a). In that context, both *Alk1*$^{+/-}$ and *Alk1*$^{+/+}$ mice showed same myofibroblast abundance but *Alk1*$^{+/-}$ myofibroblasts produced higher amounts of ECM proteins (Muñoz-Félix et al., 2014b; Oujo et al., 2014). In this manuscript we demonstrate that after 3 days UUO ALK1 heterozygosity is associated with a lower myofibroblast emergence, due to a higher microvessel stability, and this lower number of myofibroblasts results in a decrease in tubulo-interstitial fibrosis. We suggest that in the early stages of UUO, ALK1 function is mainly related with its effect on endothelial cells. The different effects of ALK1 receptor in kidney fibrosis at different time points following UUO can be explained by the different cellular players in these different stages of fibrosis progression. We suggest that in the early stages of the ureteral obstruction ALK1 is regulating the myofibroblast emergence from endothelial cells while after 15 days UUO the fibrotic program is completely established and myofibroblast

TABLE 1 | ALK1, BMP9 and Endoglin effects in tissue fibrosis.

ALK1				BMP9				Endoglin			
Profibrotic effect		**Antifibrotic effect**		**Profibrotic effect**		**Antifibrotic effect**		**Profibrotic effect**		**Antifibrotic effect**	
Ref.	**Experimental model**	**Ref.**	**Experimental model**	**Ref.**	**Experimental model**	**Ref.**	**Experimental model**	**Ref.**	**Experimental model**	**Ref.**	**Experimental model**
Scharpfenecker et al. (2011)	Kidney fibrosis by irradiation in *Alk1*$^{+/-}$ mice	Muñoz-Félix et al. (2014a)	Unilateral Ureteral Obstruction (UUO) during 15 days in *Alk1*$^{+/-}$ mice	Muñoz-Félix et al. (2016a)	Cultured mouse embryo fibroblasts	Morine et al. (2018)	Transverse aortic constriction (TAC) in Bmp9-KO mice.	Scharpfenecker et al. (2012)	Kidney fibrosis by irradiation in *Eng*$^{+/-}$ mice	Muñoz-Félix et al. (2016b)	UUO in *S-Eng*$^{+}$ mice (mice overexpressing human Short endoglin).
Morine et al. (2017b)	Deletion of ALK1 with conditional knockout mice	Morine et al. (2017a)	Transverse aortic constriction (TAC) in *Alk1*$^{+/-}$ mice	Li et al. (2018)	CCl_4 induced liver fibrosis Bile duct ligation (BDL) induced liver fibrosis	Desroches-Castan et al. (2019a)	*Bmp9*-KO mice	Scharpfenecker et al. (2009)	Kidney fibrosis by irradiation in *Eng*$^{+/-}$ mice	Pericacho et al. (2013)	Cutured dermal fibroblasts from *Eng*$^{+/-}$ mice
Wiercinska et al. (2006)	Cultured hepatic stellate cells	Muñoz-Félix et al. (2014b)	Cultured mouse embryo fibroblasts form *Alk1*$^{+/-}$ mice	Breitkopf-Heinlein et al. (2017)	CCL_4 and LPS induced liver fibrosis. BMP9 inactivated with adenoviruses	Desroches-Castan et al. (2019b)	*Bmp9*-KO mice	Scharpfenecker et al. (2013)	Kidney fibrosis by irradiation in *Eng*$^{+/-}$ mice	Velasco et al. (2008)	Cultured L6E9 rat myoblasts overexpressing L-Endoglin
Breitkopf-Heinlein et al. (2017)	CCL_4 and LPS induced liver fibrosis. BMP9 inactivated with adenoviruses	Finnson et al. (2008)	Cultured human chondrocytes			Jiang et al. (2021)	Bleomycin-induced pulmonary fibrosis	Docherty et al. (2006b)	Kidney fibrosis induced by Ischaemia-reperfusion injury in *Eng*$^{+/-}$ mice	Finnson et al. (2010)	Cultured human chondrocytes
This current manuscript	UUO during 3 days in *Alk1*$^{+/-}$ mice					Chen et al. (2017)	BMP9 treatment in neonatal rats	Kapur et al. (2012)	TAC in *Eng*$^{+/-}$ mice	Alzahrani et al. (2018)	Skin fibrosis induced by bleomycin
								Oujo et al. (2014)	UUO in *L-Eng*$^{+}$ mice (mice overexpressing human Large endoglin).	Obreo et al. (2004)	Cultured L6E9 myoblasts
								Gerrits et al. (2020)	cultured human renal myofibroblasts	Diez-Marques et al. (2002)	Cultured human mesangial cells
								Owen et al. (2020)	Patients with cirrhosis	Rodríguez-Barbero et al. (2006)	Cultured L6E9 myoblasts
								Morris et al. (2011)	Cultured scleroderma (SSc) fibroblasts		
								Meurer et al. (2011)	Cultured Hepatic stellate cells		

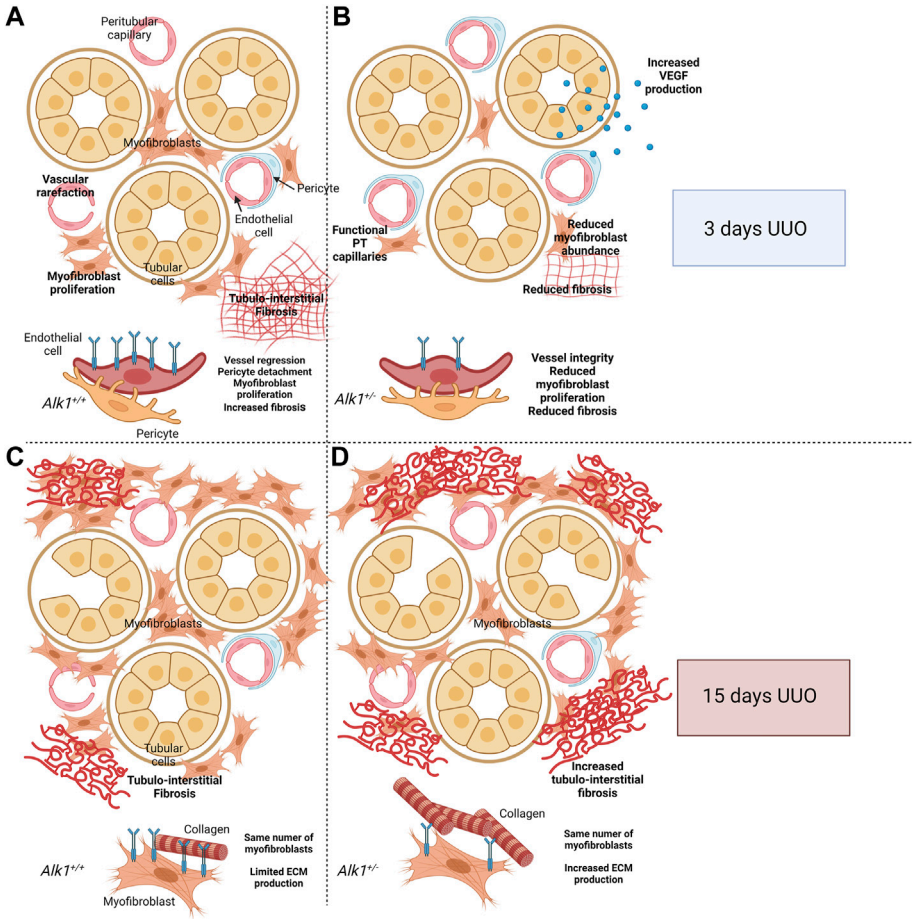

FIGURE 9 | Proposed cellular mechanism. After 3 days of Unilateral Ureteral Obstruction (UUO), myofibroblasts emerge in the renal tubular interstitium and synthesize ECM proteins. At the same time, peritubular capillaries (PTC) undergo vascular rarefaction. This process starts with an angiogenic phase followed by a regression phase in which endothelial cells detach from pericytes and basement membrane, followed by apoptosis and leading to loss of functional capillaries. Both endothelial cells and pericytes can transdifferentiate into myofibroblasts and act as a source of extracellular matrix (ECM) components **(A,C)**. ALK1 heterozygosity is associated with PTC stability linked to an angiogenic process VEGF-dependent and the reduction of myofibroblast abundance, leading to reduced tubule-interstitial fibrosis **(A,B)** Previous results from our laboratory demonstrated that after 15 days of UUO, *Alk1*$^{+/+}$ and *Alk1*$^{+/-}$ mice show the same number of myofibroblasts but those from *Alk1*$^{+/-}$ mice produce higher amounts of ECM proteins leading to increased tubulointerstitial fibrosis **(C,D)**. Figure 9 was created using BioRender.com.

number is elevated and ALK1 regulates negatively ECM protein synthesis by myofibroblasts through an inhibition of TGF-β1/Smad2/3 pathway (Muñoz-Félix et al., 2014b).

Although our previous studies demonstrate a role of ALK1 in regulating ECM production by ECM producing cells like fibroblasts, the biological role of ALK1 has been traditionally considered more relevant in the regulation of endothelial cell balance during development, cardiovascular diseases and tumor angiogenesis (Ayuso-Inigo et al., 2021). To understand ALK1 function in tissue fibrosis is very important to consider two molecular players that regulate ALK1 activity: Its high affinity ligand BMP9 (David et al., 2007b) and the coreceptor endoglin (Lebrin et al., 2004; López-Novoa and Bernabeu, 2010). Both molecules have been studied in depth as regulators of vascular homeostasis and tissue fibrosis (**Table 1**).

However, the link of the ALK1-mediated endothelial effects and tissue fibrosis has not been studied in depth so far. Nevertheless, new functions have been recently described in different tissues such as liver and kidney. In the liver, ALK1 is involved in capillary fenestration and prevents the development of liver fibrosis (Desroches-Castan et al., 2019a). In this study, the authors show that mice lacking BMP9, a high affinity receptor for ALK1, show enlarged sinusoidal vessels and a reduced number of fenestrae. This suggests an interesting role of the BMP9-ALK1 axis in liver fibrosis protection. In renal tissue, a role for ALK1 in vascular cells has been described in diabetic nephropathy. ALK1 levels decrease in diabetic mice, being ALK1 expression circumscribed to glomerular capillaries. ALK1 heterozygous mice display albuminuria, as a result of changes in endothelial cells and podocytes, leading to exacerbated levels of collagen IV

and thickening of the glomerular basement membrane (Lora Gil et al., 2020).

Our study shows that ALK1 is involved in the regulation of the stability of renal peritubular capillaries. In the same circumstances we observe a lower number of myofibroblasts in mice with lower expression of ALK1, which also show lower tubule-interstitial fibrosis. With these results, we suggest that both processes may be linked. Reduced levels of ALK1 together with an increase in VEGF levels maintains the stability of peritubular capillaries protecting kidney from myofibroblast emergence and ECM deposition. Considering all these facts, ALK1 seems to regulate the endothelial activation and quiescence in the context of UUO. Endothelial activation in kidney fibrosis occurs in the early steps of vascular rarefaction, and it is accompanied of endothelial and pericyte detachments. Both cell types might be the source of the increased number of myofibroblasts, as it has been demonstrated during the last years (Zeisberg and Kalluri, 2013).

CONCLUSION

ALK1 is involved in the early changes of UUO, promoting the development of vascular rarefaction. $Alk1^{+/-}$ mice maintain the stability of the peritubular capillaries network after UUO, leading to a decrease of myofibroblasts emergence and ECM deposition.

DATA AVAILABILITY STATEMENT

The raw data supporting the conclusion of this article will be made available by the authors, without undue reservation.

ETHICS STATEMENT

The animal study was reviewed and approved by The procedure was approved for the Bioethics committee of the University of Salamanca and Consejería de Agricultura y Pesca (Junta de Castilla y León).

AUTHOR CONTRIBUTIONS

CM-S, FS-J, FL-H, and JM-F conceived the idea, design the experiments, carried out the experimental research, analyzed the data and wrote the manuscript.

FUNDING

This work was supported by grants from Instituto de Salud Carlos III, Ministerio de Ciencia e Innovación: PI18/00996 and RETICS RD016/0009/0025 (REDINREN), co-funded by FEDER funds, and from Consejeria de Educación, Junta de Castilla y León: IES160P20 and Universidad de Salamanca (Programas Propios de la Agencia de Gestión de la Investigación).

ACKNOWLEDGMENTS

We thank Annette Düwel and Lucía Martín for their technical assistance, especially in genotyping the animals. **Figure 9** was created using BioRender.com, with the agreement number JJ23WW3A8X (License granted to JM-F).

REFERENCES

Akla, N., Viallard, C., Popovic, N., Lora Gil, C., Sapieha, P., and Larrivée, B. (2018). BMP9 (Bone Morphogenetic Protein-9)/Alk1 (Activin-like Kinase Receptor Type I) Signaling Prevents Hyperglycemia-Induced Vascular Permeability. *Arterioscler. Thromb. Vasc. Biol.* 38, 1821–1836. doi:10.1161/ATVBAHA.118.310733

Alzahrani, A., Chi, Y., Finnson, K. W., Blati, M., Lussier, B., Kapoor, M., et al. (2018). Endoglin Haploinsufficiency Is Associated with Differential Regulation of Extracellular Matrix Production during Skin Fibrosis and Cartilage Repair in Mice. *J. Cell Commun. Signal* 12, 379–388. doi:10.1007/s12079-018-0461-7

Ayuso-Inigo, B., Mendez-Garcia, L., Pericacho, M., and Munoz-Felix, J. M. (2021). The Dual Effect of the BMP9-ALK1 Pathway in Blood Vessels: An Opportunity for Cancer Therapy Improvement? *Cancers (Basel)* 13. 5412, doi:10.3390/cancers13215412

Breitkopf-Heinlein, K., Meyer, C., König, C., Gaitantzi, H., Addante, A., Thomas, M., et al. (2017). BMP-9 Interferes with Liver Regeneration and Promotes Liver Fibrosis. *Gut* 66, 939–954. doi:10.1136/gutjnl-2016-313314

Chen, X., Orriols, M., Walther, F. J., Laghmani, E. H., Hoogeboom, A. M., Hogen-Esch, A. C. B., et al. (2017). Bone Morphogenetic Protein 9 Protects against Neonatal Hyperoxia-Induced Impairment of Alveolarization and Pulmonary Inflammation. *Front. Physiol.* 8, 486. doi:10.3389/fphys.2017.00486

David, L., Mallet, C., Keramidas, M., Lamandé, N., Gasc, J. M., Dupuis-Girod, S., et al. (2008). Bone Morphogenetic Protein-9 Is a Circulating Vascular Quiescence Factor. *Circ. Res.* 102, 914–922. doi:10.1161/CIRCRESAHA.107.165530

David, L., Mallet, C., Mazerbourg, S., Feige, J. J., and Bailly, S. (2007). Identification of BMP9 and BMP10 as Functional Activators of the Orphan Activin Receptor-like Kinase 1 (ALK1) in Endothelial Cells. *Blood* 109, 1953–1961. doi:10.1182/blood-2006-07-034124

David, L., Mallet, C., Vailhé, B., Lamouille, S., Feige, J. J., and Bailly, S. (2007). Activin Receptor-like Kinase 1 Inhibits Human Microvascular Endothelial Cell Migration: Potential Roles for JNK and ERK. *J. Cell Physiol.* 213, 484–489. doi:10.1002/jcp.21126

Desroches-Castan, A., Tillet, E., Ricard, N., Ouarné, M., Mallet, C., Belmudes, L., et al. (2019). Bone Morphogenetic Protein 9 Is a Paracrine Factor Controlling Liver Sinusoidal Endothelial Cell Fenestration and Protecting against Hepatic Fibrosis. *Hepatology* 70, 1392–1408. doi:10.1002/hep.30655

Desroches-Castan, A., Tillet, E., Ricard, N., Ouarné, M., Mallet, C., Feige, J. J., et al. (2019). Differential Consequences of Bmp9 Deletion on Sinusoidal Endothelial Cell Differentiation and Liver Fibrosis in 129/Ola and C57BL/6 Mice. *Cells* 8. 1079, doi:10.3390/cells8091079

Diez-Marques, L., Ortega-Velazquez, R., Langa, C., Rodriguez-Barbero, A., Lopez-Novoa, J. M., Lamas, S., et al. (2002). Expression of Endoglin in Human Mesangial Cells: Modulation of Extracellular Matrix Synthesis. *Biochim. Biophys. Acta* 1587, 36–44. doi:10.1016/s0925-4439(02)00051-0

Docherty, N. G., López-Novoa, J. M., Arevalo, M., Düwel, A., Rodriguez-Peña, A., Pérez-Barriocanal, F., et al. (2006). Endoglin Regulates Renal Ischaemia-Reperfusion Injury. *Nephrol. Dial. Transpl.* 21, 2106–2119. doi:10.1093/ndt/gfl179

Docherty, N. G., O'Sullivan, O. E., Healy, D. A., Murphy, M., O'neill, A. J. A., Fitzpatrick, J. M., et al. (2006). TGF-beta1-induced EMT Can Occur Independently of its Proapoptotic Effects and Is Aided by EGF Receptor Activation. *Am. J. Physiol. Ren. Physiol.* 290, F1202–F1212. doi:10.1152/ajprenal.00406.2005

Finnson, K. W., Parker, W. L., Chi, Y., Hoemann, C. D., Goldring, M. B., Antoniou, J., et al. (2010). Endoglin Differentially Regulates TGF-β-Induced Smad2/3 and Smad1/5 Signalling and its Expression Correlates with Extracellular Matrix Production and Cellular Differentiation State in Human Chondrocytes. *Osteoarthr. Cartil.* 18, 1518–1527. doi:10.1016/j.joca.2010.09.002

Finnson, K. W., Parker, W. L., ten Dijke, P., Thorikay, M., and Philip, A. (2008). ALK1 Opposes ALK5/Smad3 Signaling and Expression of Extracellular Matrix Components in Human Chondrocytes. *J. Bone Min. Res.* 23, 896–906. doi:10.1359/jbmr.080209

Gerrits, T., Zandbergen, M., Wolterbeek, R., Bruijn, J. A., Baelde, H. J., and Scharpfenecker, M. (2020). Endoglin Promotes Myofibroblast Differentiation and Extracellular Matrix Production in Diabetic Nephropathy. *Int. J. Mol. Sci.* 21. 7713, doi:10.3390/ijms21207713

Gewin, L. S. (2019). Transforming Growth Factor-β in the Acute Kidney Injury to Chronic Kidney Disease Transition. *Nephron* 143, 154–157. doi:10.1159/000500093

Gil, C. L., Hooker, E., and Larrivée, B. (2021). Diabetic Kidney Disease, Endothelial Damage, and Podocyte-Endothelial Crosstalk. *Kidney Med.* 3, 105–115. doi:10.1016/j.xkme.2020.10.005

Goligorsky, M. S. (2010). Microvascular Rarefaction: the Decline and Fall of Blood Vessels. *Organogenesis* 6, 1–10. doi:10.4161/org.6.1.10427

Goumans, M. J., Valdimarsdottir, G., Itoh, S., Rosendahl, A., Sideras, P., and ten Dijke, P. (2002). Balancing the Activation State of the Endothelium via Two Distinct TGF-Beta Type I Receptors. *EMBO J.* 21, 1743–1753. doi:10.1093/emboj/21.7.1743

Grande, M. T., Arévalo, M., Núñez, A., Cannata-Andía, J. B., Santos, E., and López-Novoa, J. M. (2009). Targeted Genomic Disruption of H-Ras and N-Ras Has No Effect on Early Renal Changes after Unilateral Ureteral Ligation. *World J. Urol.* 27, 787–797. doi:10.1007/s00345-009-0399-8

Grande, M. T., Fuentes-Calvo, I., Arévalo, M., Heredia, F., Santos, E., Martínez-Salgado, C., et al. (2010). Deletion of H-Ras Decreases Renal Fibrosis and Myofibroblast Activation Following Ureteral Obstruction in Mice. *Kidney Int.* 77, 509–518. doi:10.1038/ki.2009.498

Grande, M. T., and López-Novoa, J. M. (2009). Fibroblast Activation and Myofibroblast Generation in Obstructive Nephropathy. *Nat. Rev. Nephrol.* 5, 319–328. doi:10.1038/nrneph.2009.74

Grande, M. T., Sánchez-Laorden, B., López-Blau, C., De Frutos, C. A., Boutet, A., Arévalo, M., et al. (2015). Snail1-induced Partial Epithelial-To-Mesenchymal Transition Drives Renal Fibrosis in Mice and Can Be Targeted to Reverse Established Disease. *Nat. Med.* 21, 989–997. doi:10.1038/nm.3901

Ishii, Y., Sawada, T., Kubota, K., Fuchinoue, S., Teraoka, S., and Shimizu, A. (2005). Injury and Progressive Loss of Peritubular Capillaries in the Development of Chronic Allograft Nephropathy. *Kidney Int.* 67, 321–332. doi:10.1111/j.1523-1755.2005.00085.x

Jiang, Q., Liu, C., Liu, S., Lu, W., Li, Y., Luo, X., et al. (2021). Dysregulation of BMP9/BMPR2/SMAD Signalling Pathway Contributes to Pulmonary Fibrosis and Pulmonary Hypertension Induced by Bleomycin in Rats. *Br. J. Pharmacol.* 178, 203–216. doi:10.1111/bph.15285

Jonker, L. (2014). TGF-β & BMP Receptors Endoglin and ALK1: Overview of Their Functional Role and Status as Antiangiogenic Targets. *Microcirculation* 21, 93–103. doi:10.1111/micc.12099

Kapur, N. K., Wilson, S., Yunis, A. A., Qiao, X., Mackey, E., Paruchuri, V., et al. (2012). Reduced Endoglin Activity Limits Cardiac Fibrosis and Improves Survival in Heart Failure. *Circulation* 125, 2728–2738. doi:10.1161/CIRCULATIONAHA.111.080002

Kida, Y., Tchao, B. N., and Yamaguchi, I. (2014). Peritubular Capillary Rarefaction: a New Therapeutic Target in Chronic Kidney Disease. *Pediatr. Nephrol.* 29, 333–342. doi:10.1007/s00467-013-2430-y

Lamouille, S., Mallet, C., Feige, J. J., and Bailly, S. (2002). Activin Receptor-like Kinase 1 Is Implicated in the Maturation Phase of Angiogenesis. *Blood* 100, 4495–4501. doi:10.1182/blood.V100.13.4495

Larrivée, B., Prahst, C., Gordon, E., del Toro, R., Mathivet, T., Duarte, A., et al. (2012). ALK1 Signaling Inhibits Angiogenesis by Cooperating with the Notch Pathway. *Dev. Cell* 22, 489–500. doi:10.1016/j.devcel.2012.02.005

LeBleu, V. S., and Kalluri, R. (2011). Blockade of PDGF Receptor Signaling Reduces Myofibroblast Number and Attenuates Renal Fibrosis. *Kidney Int.* 80, 1119–1121. doi:10.1038/ki.2011.300

LeBleu, V. S., Taduri, G., O'Connell, J., Teng, Y., Cooke, V. G., Woda, C., et al. (2013). Origin and Function of Myofibroblasts in Kidney Fibrosis. *Nat. Med.* 19, 1047–1053. doi:10.1038/nm.3218

Lebrin, F., Deckers, M., Bertolino, P., and Ten Dijke, P. (2005). TGF-beta Receptor Function in the Endothelium. *Cardiovasc Res.* 65, 599–608. doi:10.1016/j.cardiores.2004.10.036

Lebrin, F., Goumans, M. J., Jonker, L., Carvalho, R. L., Valdimarsdottir, G., Thorikay, M., et al. (2004). Endoglin Promotes Endothelial Cell Proliferation and TGF-beta/ALK1 Signal Transduction. *EMBO J.* 23, 4018–4028. doi:10.1038/sj.emboj.7600386

Li, P., Li, Y., Zhu, L., Yang, Z., He, J., Wang, L., et al. (2018). Targeting Secreted Cytokine BMP9 Gates the Attenuation of Hepatic Fibrosis. *Biochim. Biophys. Acta Mol. Basis Dis.* 1864, 709–720. doi:10.1016/j.bbadis.2017.12.008

López-Novoa, J. M., and Bernabeu, C. (2010). The Physiological Role of Endoglin in the Cardiovascular System. *Am. J. Physiol. Heart Circ. Physiol.* 299, H959–H974. doi:10.1152/ajpheart.01251.2009

Lora Gil, C., Henley, N., Leblond, F. A., Akla, N., Laurin, L. P., Royal, V., et al. (2020). Alk1 Haploinsufficiency Causes Glomerular Dysfunction and Microalbuminuria in Diabetic Mice. *Sci. Rep.* 10, 13136. doi:10.1038/s41598-020-68515-z

Meurer, S. K., Tihaa, L., Borkham-Kamphorst, E., and Weiskirchen, R. (2011). Expression and Functional Analysis of Endoglin in Isolated Liver Cells and its Involvement in Fibrogenic Smad Signalling. *Cell Signal* 23, 683–699. doi:10.1016/j.cellsig.2010.12.002

Morine, K. J., Qiao, X., Paruchuri, V., Aronovitz, M. J., Mackey, E. E., Buiten, L., et al. (2017). Conditional Knockout of Activin like Kinase-1 (ALK-1) Leads to Heart Failure without Maladaptive Remodeling. *Heart Vessels* 32, 628–636. doi:10.1007/s00380-017-0955-x

Morine, K. J., Qiao, X., Paruchuri, V., Aronovitz, M. J., Mackey, E. E., Buiten, L., et al. (2017). Reduced Activin Receptor-like Kinase 1 Activity Promotes Cardiac Fibrosis in Heart Failure. *Cardiovasc Pathol.* 31, 26–33. doi:10.1016/j.carpath.2017.07.004

Morine, K. J., Qiao, X., York, S., Natov, P. S., Paruchuri, V., Zhang, Y., et al. (2018). Bone Morphogenetic Protein 9 Reduces Cardiac Fibrosis and Improves Cardiac Function in Heart Failure. *Circulation* 138, 513–526. doi:10.1161/CIRCULATIONAHA.117.031635

Morris, E., Chrobak, I., Bujor, A., Hant, F., Mummery, C., Ten Dijke, P., et al. (2011). Endoglin Promotes TGF-β/Smad1 Signaling in Scleroderma Fibroblasts. *J. Cell Physiol.* 226, 3340–3348. doi:10.1002/jcp.22690

Muñoz-Félix, J. M., Cuesta, C., Perretta-Tejedor, N., Subileau, M., López-Hernández, F. J., López-Novoa, J. M., et al. (2016). Identification of Bone Morphogenetic Protein 9 (BMP9) as a Novel Profibrotic Factor *In Vitro*. *Cell Signal* 28, 1252–1261. doi:10.1016/j.cellsig.2016.05.015

Muñoz-Félix, J. M., López-Novoa, J. M., and Martínez-Salgado, C. (2014). Heterozygous Disruption of Activin Receptor-like Kinase 1 Is Associated with Increased Renal Fibrosis in a Mouse Model of Obstructive Nephropathy. *Kidney Int.* 85, 319–332. doi:10.1038/ki.2013.292

Muñoz-Félix, J. M., Pérez-Roque, L., Núñez-Gómez, E., Oujo, B., Arévalo, M., Ruiz-Remolina, L., et al. (2016). Overexpression of the Short Endoglin Isoform Reduces Renal Fibrosis and Inflammation after Unilateral Ureteral Obstruction. *Biochim. Biophys. Acta* 1862, 1801–1814. doi:10.1016/j.bbadis.2016.06.010

Muñoz-Félix, J. M., Perretta-Tejedor, N., Eleno, N., López-Novoa, J. M., and Martínez-Salgado, C. (2014). ALK1 Heterozygosity Increases Extracellular Matrix Protein Expression, Proliferation and Migration in Fibroblasts. *Biochim. Biophys. Acta* 1843, 1111–1122. doi:10.1016/j.bbamcr.2014.02.017

Munoz-Felix, J. M., and Martinez-Salgado, C. (2021). Dissecting the Involvement of Ras GTPases in Kidney Fibrosis. *Genes (Basel)* 12, 800, doi:10.3390/genes12060800

Obreo, J., Díez-Marques, L., Lamas, S., Düwell, A., Eleno, N., Bernabéu, C., et al. (2004). Endoglin Expression Regulates Basal and TGF-Beta1-Induced Extracellular Matrix Synthesis in Cultured L6E9 Myoblasts. *Cell Physiol. Biochem.* 14, 301–310. doi:10.1159/000080340

Oh, S. P., Seki, T., Goss, K. A., Imamura, T., Yi, Y., Donahoe, P. K., et al. (2000). Activin Receptor-like Kinase 1 Modulates Transforming Growth Factor-Beta 1 Signaling in the Regulation of Angiogenesis. *Proc. Natl. Acad. Sci. U. S. A.* 97, 2626–2631. doi:10.1073/pnas.97.6.2626

Ouarné, M., Bouvard, C., Boneva, G., Mallet, C., Ribeiro, J., Desroches-Castan, A., et al. (2018). BMP9, but Not BMP10, Acts as a Quiescence Factor on Tumor Growth, Vessel Normalization and Metastasis in a Mouse Model of Breast Cancer. *J. Exp. Clin. Cancer Res.* 37, 209. doi:10.1186/s13046-018-0885-1

Oujo, B., Muñoz-Félix, J. M., Arévalo, M., Núñez-Gómez, E., Pérez-Roque, L., Pericacho, M., et al. (2014). L-endoglin Overexpression Increases Renal Fibrosis after Unilateral Ureteral Obstruction. *PLoS One* 9, e110365. doi:10.1371/journal.pone.0110365

Owen, N. E., Alexander, G. J., Sen, S., Bunclark, K., Polwarth, G., Pepke-Zaba, J., et al. (2020). Reduced Circulating BMP10 and BMP9 and Elevated Endoglin Are Associated with Disease Severity, Decompensation and Pulmonary Vascular Syndromes in Patients with Cirrhosis. *EBioMedicine* 56, 102794. doi:10.1016/j.ebiom.2020.102794

Pericacho, M., Velasco, S., Prieto, M., Llano, E., López-Novoa, J. M., and Rodríguez-Barbero, A. (2013). Endoglin Haploinsufficiency Promotes Fibroblast Accumulation during Wound Healing through Akt Activation. *PLoS One* 8, e54687. doi:10.1371/journal.pone.0054687

Picard, N., Baum, O., Vogetseder, A., Kaissling, B., and Le Hir, M. (2008). Origin of Renal Myofibroblasts in the Model of Unilateral Ureter Obstruction in the Rat. *Histochem Cell Biol.* 130, 141–155. doi:10.1007/s00418-008-0433-8

Rodríguez-Barbero, A., Obreo, J., Alvarez-Munoz, P., Pandiella, A., Bernabéu, C., and López-Novoa, J. M. (2006). Endoglin Modulation of TGF-Beta1-Induced Collagen Synthesis Is Dependent on ERK1/2 MAPK Activation. *Cell Physiol. Biochem.* 18, 135–142. doi:10.1159/000095181

Rodríguez-Peña, A., Eleno, N., Düwell, A., Arévalo, M., Pérez-Barriocanal, F., Flores, O., et al. (2002). Endoglin Upregulation during Experimental Renal Interstitial Fibrosis in Mice. *Hypertension* 40, 713–720. doi:10.1161/01.hyp.0000037429.73954.27

Sato, M., Muragaki, Y., Saika, S., Roberts, A. B., and Ooshima, A. (2003). Targeted Disruption of TGF-beta1/Smad3 Signaling Protects against Renal Tubulointerstitial Fibrosis Induced by Unilateral Ureteral Obstruction. *J. Clin. Invest.* 112, 1486–1494. doi:10.1172/JCI19270

Scharpfenecker, M., Floot, B., Korlaar, R., Russell, N. S., and Stewart, F. A. (2011). ALK1 Heterozygosity Delays Development of Late Normal Tissue Damage in the Irradiated Mouse Kidney. *Radiother. Oncol.* 99, 349–355. doi:10.1016/j.radonc.2011.05.061

Scharpfenecker, M., Floot, B., Russell, N. S., Coppes, R. P., and Stewart, F. A. (2013). Endoglin Haploinsufficiency Attenuates Radiation-Induced Deterioration of Kidney Function in Mice. *Radiother. Oncol.* 108, 464–468. doi:10.1016/j.radonc.2013.06.016

Scharpfenecker, M., Floot, B., Russell, N. S., and Stewart, F. A. (2012). The TGF-β Co-receptor Endoglin Regulates Macrophage Infiltration and Cytokine Production in the Irradiated Mouse Kidney. *Radiother. Oncol.* 105, 313–320. doi:10.1016/j.radonc.2012.08.021

Scharpfenecker, M., Floot, B., Russell, N. S., Ten Dijke, P., and Stewart, F. A. (2009). Endoglin Haploinsufficiency Reduces Radiation-Induced Fibrosis and Telangiectasia Formation in Mouse Kidneys. *Radiother. Oncol.* 92, 484–491. doi:10.1016/j.radonc.2009.06.013

Ucero, A. C., Benito-Martin, A., Izquierdo, M. C., Sanchez-Niño, M. D., Sanz, A. B., Ramos, A. M., et al. (2014). Unilateral Ureteral Obstruction: beyond Obstruction. *Int. Urol. Nephrol.* 46, 765–776. doi:10.1007/s11255-013-0520-1

Velasco, S., Alvarez-Muñoz, P., Pericacho, M., Dijke, P. T., Bernabéu, C., López-Novoa, J. M., et al. (2008). L- and S-Endoglin Differentially Modulate TGFbeta1 Signaling Mediated by ALK1 and ALK5 in L6E9 Myoblasts. *J. Cell Sci.* 121, 913–919. doi:10.1242/jcs.023283

Viallard, C., Audiger, C., Popovic, N., Akla, N., Lanthier, K., Legault-Navarrete, I., et al. (2020). BMP9 Signaling Promotes the Normalization of Tumor Blood Vessels. *Oncogene* 39, 2996–3014. doi:10.1038/s41388-020-1200-0

Wiercinska, E., Wickert, L., Denecke, B., Said, H. M., Hamzavi, J., Gressner, A. M., et al. (2006). Id1 Is a Critical Mediator in TGF-Beta-Induced Transdifferentiation of Rat Hepatic Stellate Cells. *Hepatology* 43, 1032–1041. doi:10.1002/hep.21135

Zeisberg, E. M., Potenta, S. E., Sugimoto, H., Zeisberg, M., and Kalluri, R. (2008). Fibroblasts in Kidney Fibrosis Emerge via Endothelial-To-Mesenchymal Transition. *J. Am. Soc. Nephrol.* 19, 2282–2287. doi:10.1681/ASN.2008050513

Zeisberg, M., Bottiglio, C., Kumar, N., Maeshima, Y., Strutz, F., Müller, G. A., et al. (2003). Bone Morphogenic Protein-7 Inhibits Progression of Chronic Renal Fibrosis Associated with Two Genetic Mouse Models. *Am. J. Physiol. Ren. Physiol.* 285, F1060–F1067. doi:10.1152/ajprenal.00191.2002

Zeisberg, M., and Kalluri, R. (2013). Cellular Mechanisms of Tissue Fibrosis. 1. Common and Organ-specific Mechanisms Associated with Tissue Fibrosis. *Am. J. Physiol. Cell Physiol.* 304, C216–C225. doi:10.1152/ajpcell.00328.2012

Conflict of Interest: The authors declare that the research was conducted in the absence of any commercial or financial relationships that could be construed as a potential conflict of interest.

Publisher's Note: All claims expressed in this article are solely those of the authors and do not necessarily represent those of their affiliated organizations, or those of the publisher, the editors and the reviewers. Any product that may be evaluated in this article, or claim that may be made by its manufacturer, is not guaranteed or endorsed by the publisher.

frontiers | Frontiers in Pharmacology

ORIGINAL RESEARCH
published: 21 June 2022
doi: 10.3389/fphar.2022.890881

Elabela Attenuates the TGF-β1-Induced Epithelial-Mesenchymal Transition of Peritoneal Mesothelial Cells in Patients Receiving Peritoneal Dialysis

Shunyun Xie, Feng Xu, Yue Lu, Yixian Zhang, Xinyang Li, Mengyuan Yu and Wenpeng Cui[*†]

Department of Nephrology, The Second Hospital of Jilin University, Changchun, China

OPEN ACCESS

Edited by:
Cecilia Battistelli,
Sapienza University of Rome, Italy

Reviewed by:
Na Liu,
Tongji University, China
Kunyi Wu,
The Second Affiliated Hospital of Xi'an Jiaotong University, China

***Correspondence:**
Wenpeng Cui
wenpengcui@163.com

†ORCID:
Wenpeng Cui
orcid.org/0000-0001-6637-7255

Specialty section:
This article was submitted to Experimental Pharmacology and Drug Discovery, a section of the journal Frontiers in Pharmacology

Received: *06 March 2022*
Accepted: *20 May 2022*
Published: *21 June 2022*

Citation:
Xie S, Xu F, Lu Y, Zhang Y, Li X, Yu M and Cui W (2022) Elabela Attenuates the TGF-β1-Induced Epithelial-Mesenchymal Transition of Peritoneal Mesothelial Cells in Patients Receiving Peritoneal Dialysis. Front. Pharmacol. 13:890881. doi: 10.3389/fphar.2022.890881

Peritoneal fibrosis (PF), a common complication in patients receiving peritoneal dialysis (PD), is primarily caused by the epithelial-mesenchymal transition (EMT) of human peritoneal mesothelial cells (HPMCs). PF is the main reason for patients on PD to withdraw from PD. Effective treatment is unavailable for this complication at present. Elabela (ELA) is a polypeptide hormone secreted by the vascular endothelium and kidney. Peptide hormones ELA and apelin (APLN) have various protective effects on the cardiovascular and urinary systems and have potential therapeutic effects on organ fibrosis. ELA and APLN are less studied in PD population. Here, we aimed to investigate the clinical significance of ELA in patients on PD and to evaluate the therapeutic effect of ELA on EMT of HPMCs. Compared with those in patients with stage 5 chronic kidney disease who are not on dialysis, serum ELA levels in patients on PD increased with the improvement of residual renal function at PD duration <36 months and decreased to pre-dialysis levels at PD duration ≥36 months, suggesting that dialysis duration is the main risk factor affecting serum ELA levels in patients on PD. In addition, serum APLN levels decreased in the early stage of PD and recovered to the pre-dialysis level with the prolongation of dialysis time. Notably, serum APLN levels were positively correlated with dialysis duration in patients undergoing PD. To establish the EMT model, we stimulated HPMCs using transforming growth factor-beta 1 (TGF-β1) in cell experiments performed *in vitro*. ELA-32 treatment reversed the TGF-β1-induced reduction in the expression of the epithelial cell marker and suppressed the expression of mesenchymal cell markers by inhibiting the phosphorylation of SMAD2/3, ERK1/2, and AKT. Therefore, our findings imply that ELA-32 can interfere with the EMT of HPMCs by inhibiting the activation of the TGF-β/SMAD2/3, ERK1/2, and AKT pathways, providing novel insights on the potential therapeutic use of ELA for treating PD-related PF.

Keywords: peritoneal fibrosis, apelin, HPMCs, EMT, chronic kidney disease, TGF-beta/SMAD/ERK/AKT pathway, elabela, peritoneal dialysis

INTRODUCTION

As one of the most common renal replacement therapies for patients with stage 5 chronic kidney disease (CKD5), peritoneal dialysis (PD) is more effective than hemodialysis in maintaining residual renal function, hemodynamic stability, and improving quality of life (Mehrotra et al., 2016). PD uses the peritoneal tissue to remove metabolic waste and excess fluid from the body. Peritoneal function often affects the duration of treatment in patients receiving PD treatment. The main cause of peritoneal dysfunction is peritoneal fibrosis (PF), which is caused by various factors including the stimulation of non-physiological peritoneal dialysate and increased glycosylation product formation and TGF-β1 secretion (Balzer, 2020). The clinicopathological manifestations of PF include the epithelial-mesenchymal transition (EMT) of human peritoneal mesothelial cells (HPMCs), submesothelial thickening, increased blood vessel formation, and elevated autocrine activity. EMT plays a central role in initiating and accelerating PF (Selgas et al., 2006). The above changes eventually lead to ultrafiltration failure and decrease in dialysis adequacy when patients receive PD treatment, which, in severe cases, cause patients to withdraw from PD (Aroeira et al., 2007). Currently, effective treatment for PF is unavailable in clinical settings.

For treatment of PF, the addition of peptides showed a significant therapeutic effect on the treatment of PD-related PF. For example, Ferrantelli et al. (2016) reported that the intraperitoneal administration of alanyl-glutamine can reduce peritoneal thickness, alpha-smooth muscle actin (α-SMA) expression, and local angiogenesis by regulating the expression of the inflammatory cytokine interleukin (IL)-17. In addition, the use of peptides can attenuate the production of protein glycosylation products (Alhamdani et al., 2007), which contributes to protection of the peritoneal structure (Honda et al., 1999). However, no peptides have yet been successfully applied in clinical treatment. Therefore, we sought to identify a similar polypeptide that could play a role in inhibiting PF.

APJ is a G protein-coupled receptor with 30% homology to angiotensin receptor 1 (O'Dowd et al., 1993). Apelin (APLN) is the first discovered ligand of the APJ receptor (Tatemoto et al., 1998). Based on its distribution level in the body, APLN is commonly regarded as a fat factor because its content in the surrounding tissue is significantly higher than that in the serum (Boucher et al., 2005). Elabela (ELA) was discovered as the second endogenous ligand of APJ in 2013 (Chng et al., 2013). The ELA gene, located in the autosomal chromosome, transcribes and translates into a 54-amino acid precursor polypeptide with a signal peptide fragment, and its active end product is ELA-32 peptide. The ELA-32 peptide chain has two potential protease cleavage sites, which can be further metabolized to ELA-21 and ELA-11 (Yang et al., 2017). The three peptides have similar biological effects, but mainly, ELA-32 exhibits biological activity and has a longer half-life in terms of metabolism (Nyimanu et al., 2021). In adulthood, ELA is mainly expressed in the human heart, vascular endothelial cells, and kidneys (Wang et al., 2015). The axis composed of APLN, ELA, and APJ receptors has shown beneficial effects in the pathophysiological process of cardiovascular diseases and renal diseases (Chapman et al., 2021). The ELA/APLN-APJ axis is involved in regulating the metabolism of vascular endothelial cells and renal tubular epithelial cells under various pathological conditions, such as ischemia and hypoxia, and has shown good anti-EMT performance. However, the regulatory mechanisms by which it exerts protective effects are complex and vary in different pathological conditions.

The serum levels of APLN and ELA in the human body are affected by renal function (Dogan et al., 2018; Lu et al., 2020). Moreover, in patients undergoing PD, the changes in serum levels of ELA and APLN and factors influencing these changes remain unclear. Therefore, we detected the serum levels of ELA and APLN in patients on PD to explore the connection between the ligands and PD. We further studied whether ELA has an anti-EMT effect on HPMCs stimulated *in vitro* and its therapeutic potential when added to the peritoneal dialysate for PF treatment.

MATERIALS AND METHODS

Study Subjects

From September 2020 to September 2021, patients with CKD5 who were on PD and patients with CKD5 who were not on dialysis admitted to the Department of Nephrology, the Second Hospital of Jilin University (Changchun, China) were screened. The inclusion criteria were as follows: 1) patients with PD as the only renal replacement therapy; and 2) patients with CKD5 who had not received renal replacement therapy. The exclusion criteria were as follows: 1) patients aged ≤18 years; 2) patients undergoing regular hemodialysis combined with PD; 3) patients with history of abdominal surgery in the past 2 weeks; 4) patients with severe heart failure and/or brain natriuretic peptide (BNP) levels >500 pg/ml; 5) patients with pulmonary infection, peritonitis, and other infectious diseases; 6) patients with severe liver diseases, hematological diseases, malignant tumors, and other consumptive diseases affecting the whole body; and 7) patients with incomplete or no clinical data. In total, we collected fasting serum samples from 20 patients with CKD5 and 60 patients on PD. Among them, the patients on PD were divided into long-term and short-term dialysis groups based on whether the treatment time exceeded 36 months. Furthermore, patients were divided into three groups: CKD5 group, eGFR < 15 (ml/min/1.73 m^2) without renal replacement therapy; PD < 36 group, patients who received PD with PD treatment time <36 months; and PD ≥ 36 group, patients who received PD with PD treatment time ≥36 months. Informed consent was obtained from the subjects before the collection of all serum samples; the study was approved by the Ethics Committee of the Second Hospital of Jilin University (approval number: 2020010).

Clinical Data Collection

The age, sex, body mass index (BMI), dialysis duration, primary disease, history of hypertension and diabetes, systolic and diastolic blood pressure, residual urine volume, 24 h ultrafiltration volume of peritoneal dialysate, and routine

laboratory indicators of the patients on PD were collected. The residual glomerular filtration rate (rGFR) in the patients on PD was calculated using the following formula: (Qin et al., 2020).

$$rGFR = (residual\ creatine\ clearance + residual\ urea\ clearance)/2$$

Enzyme-Linked Immunosorbent Assay (ELISA)

Fasting venous blood samples were collected from the patients on PD and patients with CKD5 in the morning and placed in a vacuum tube filled with separation gel-coagulant. The upper serum was extracted *via* centrifugation at 3,000 rpm for 10 min at 4°C and frozen in the refrigerator at −80°C. Human ELA Elisa Kit (S-1508; Peninsula Laboratories International, BMA Biomedicals, Basel, Switzerland) and human APLN Elisa Kit (E-EL-H0456C; Elabscience, Wuhan, China) were used to determine the serum ELA and APLN levels, respectively.

Chemicals

ELA-32 (amino acid sequence: QRPVNLTMRRKLRK HNCLQRRCMPLHSRVPFP) was synthesized by GenStar (Beijing, China) and stored at −20°C. The ELA-32 powder was dissolved in aseptic deionized water to the cryopreservation concentration, sub-packed, and stored at −80°C.

Cell Culture and Treatment

The immortalized HPMC line HMrSv5 (Jennio Biotech Co., Ltd., Guangzhou, China) was cultured in high-glucose (4.5 g/L) Dulbecco's Modified Eagle Medium (DMEM; Gibco, Thermo Fisher Scientific, Waltham, MA, United States) supplemented with 10% fetal bovine serum (FBS; Gibco) and incubated at 37°C and 5% CO_2. All experiments were performed after 24 h of treatment using serum-free media. To induce EMT, cells were treated with 10 ng/ml TGF-β1 (cat:100-21, Peprotech, Rocky Hill, CT, United States) for 24 h. HMrSv5 was divided into four groups according to different treatments: 1) Control group where cells were cultured with DMEM medium containing 10% FBS after 24 h of synchronization; 2) ELA group where cells were treated with ELA-32 (10 μM) for 24 h; 3) TGF-β1 group where cells were treated with TGF-β1 (10 ng/ml) for 24 h; and TGF-β1 + ELA group where cells were co-treated with TGF-β1 (10 ng/ml) and ELA-32 (10 μM) for 24 h.

Transwell Assay

The HPMCs in logarithmic growth phase were subjected to TGF-β1 (10 ng/ml) treatment with or without ELA-32 for 24 h. After stimulation, the cells were digested with trypsin, and the sample was centrifuged (1,000 rpm, 5 min). The supernatant was discarded, and the cells were resuscitated with serum-free DMEM. The number of terminal cells was adjusted to 5×10^5/ml. DMEM (800 μl) containing 10% FBS was added to the lower chamber of the 24-well plate; a 200-μl cell suspension was added to the upper chamber, and the culture was maintained in the aseptic cell incubator for 24 h. The chamber was taken out, and the cells were washed with 1 × phosphate buffered saline (PBS, 548117; Sangon Biotech, Shanghai, China), fixed with 4% paraformaldehyde, and stained with 0.1% crystal violet. The chambers were dried and analyzed using an inverted microscope. The average count from the fields was calculated, and the experiments were independently repeated four times.

Wounding Healing Assay

The HPMCs in the logarithmic growth phase were subcultured in a 6-well plate and cultured in DMEM containing 10% FBS when the cell fusion rate reached 100%. A 200-μl sterile liquid transfer gun head was used to scratch the cells perpendicular to the cell plane and to the line marked in advance at the back of the plate. The cells were washed thrice with aseptic 1 × PBS (B548117; Sangon Biotech), and the remaining non-adherent cells were washed out. The medium was replaced with serum-free DMEM and treated with or without TGF-β1 and ELA-32 for 24 h. Before and after the experiment, the scratch width was measured, and the cells were observed under a light microscope. The experiments were independently repeated four times.

Immunofluorescence Assay

The HPMCs (1×10^5/ml) were inoculated in 25-mm aseptic cell climbing tablets, cultured for 24 h, and synchronized with serum-free DMEM for 24 h. The cells were treated TGF-β1 (10 ng/ml) with or without ELA-32 for 24 h. After stimulation,the cells were washed with 1 × PBS (B548117; Sangon Biotech). Then, the cells were fixed with 4% paraformaldehyde, incubated with 0.1% Triton X-100 for 15 min at 27°C, and blocked with goat serum for 30 min. The primary antibodies of α-SMA (ab7817; Abcam), E-cadherin [14472; Cell Signaling Technology (CST), Danvers, MA, United States], and fibronectin (ab45688; Abcam) diluted to 1: 200 in PBS were added and covered on the cell slides, and incubated overnight at 4°C. After washing with 1 × PBS (5 min, 3 times), the cells were incubated with Anti-Rabbit IgG (P0176, Beyotime Biotechnology, Jiangsu, China) for 1 h at 27°C in the dark. Finally, the cells were washed with 1 × PBS in the dark (5 min, 3 times), mounted on a sealing tablet containing 4′,6-diamidino-2-phenylindole (DAPI; ab104139; Abcam, Cambridge, UK), and observed under a laser scanning confocal microscope (Olympus, Japan). For the fluorescence results, mean immunofluorescence intensity measurements on cell climbing tablets were performed using ImageJ (National Institutes of Health, Bethesda, MD, United States).

Western Blot Analysis

The cells were incubated in radioimmunoprecipitation assay cleavage buffer (P0013B; Beyotime) containing 0.1 mM phenylmethylsulfonyl fluoride. The lysate was centrifuged, and the supernatant was collected. The protein concentration was determined using BCA Protein Detection Kit (P0010; Beyotime). The protein was resolved and separated on a gel, with a mass of 20 μg per lane. The extracted cleavage products were transferred to a PVDF membrane *via* sodium dodecyl sulfate–polyacrylamide gel electrophoresis and electroporation. After blocking with 5% milk in tris buffered saline with Tween (A100777; Sangon Biotech), the sample was incubated with the

TABLE 1 | Individual baseline characteristics in different groups.

	CKD5 group (n = 20)	PD < 36 group (n = 40)	PD ≥ 36 group (n = 20)	p-value
Age (year)	47.95 ± 15.54	44.98 ± 12.59	45.80 ± 9.11	0.763
Sex (male/female)	9/11	28/12	8/12	0.044
BMI (kg/m^2)	24.06 ± 2.92	24.04 ± 3.74	23.98 ± 2.65	0.996
Hypertension, n (%)	17 (85)	38 (95)	20 (100)	0.132
Diabetes, n (%)	5 (25)	8 (20)	3 (15)	0.732
SBP (mmHg)	147.75 ± 19.79	148.99 ± 12.95	146.53 ± 24.18	0.899
DBP (mmHg)	88.85 ± 11.93	94.70 ± 11.26	91.89 ± 13.92	0.211
PD duration(month)	—	9.00 (3.25, 18.75)	49.50 (37.25, 70.50)	<0.001
Primary renal disease, n (%)				0.611
Glomerulonephritis	11 (55)	23 (57.5)	12 (60)	
Diabetic nephropathy	5 (25)	7 (17.5)	2 (10)	
Interstitial nephropathy	4 (20)	10 (25)	5 (25)	
Others	0 (0)	0 (0)	1 (5)	
Laboratory data				
Hb (g/L)	94.60 ± 19.30	111.03 ± 17.71[a]	95.55 ± 15.94[b]	0.001
Albumin (g/L)	37.74 ± 5.72	38.59 ± 3.81	35.73 ± 4.94	0.148
CO_2P (mM)	19.31 ± 2.86	24.01 ± 4.11[a]	26.31 ± 4.45[a]	<0.001
BUN (mM)	27.96 ± 13.06	19.40 ± 5.73[a]	21.13 ± 4.47	0.024
Cre (μM)	788.65 ± 353.33	920.46 ± 360.13	1,134.70 ± 260.94[a,b]	0.003
β2-MG (mg/L)	16.59 ± 4.99	25.75 ± 8.48[a]	33.45 ± 6.55[a,b]	<0.001
eGFR(ml/min/1.73m^2)/rGFR(ml/min)	6.56 ± 3.13	14.44 (5.13, 36.13)[a]	2.37 (0.10, 5.25)[a,b]	<0.001
PTH (pg/ml)	390.35 (256.78, 452.13)	392.00 (180.80, 533.13)	320.90 (168.20, 652.75)	0.985
CRP (mg/L)	1.37 (0.34, 2.39)	4.32 (2.22, 7.58)[a]	3.84 (1.15, 11.48)[a]	0.001
FBG (mM)	5.44 ± 1.29	6.35 ± 1.53	6.29 ± 3.06	0.222
BNP (ng/ml)	104.50 (20.50, 313.75)	112.50 (67.00,246.25)	191.00 (56.25, 464.00)	0.314
Dialysis parameters				
Peritoneal Kt/V	—	1.42 ± 0.49	1.54 ± 0.35	0.350
Renal Kt/V	—	0.57 (0.22, 1.00)	0.09 (0.01, 0.17)	<0.001
Total Kt/V	—	2.10 ± 0.79	1.79 ± 0.22	0.097
4h D/P	—	0.61 ± 0.16	0.64 ± 0.09	0.456
4h D/Do	—	0.45 ± 0.28	0.41 ± 0.08	0.577

ELA, elabela; CKD5, stage 5 chronic kidney disease; PD, peritoneal dialysis; BMI, body mass index; SBP, systolic blood pressure; DBP, diastolic blood pressure; Hb, hemoglobin; CO_2P, carbon dioxide binding capacity; BUN, blood urine nitrogen; β2-MG, β2-microglobulin; Cre, serum creatinine; eGFR, estimated glomerular filtration rate; PTH, parathyroid hormone; rGFR, residual glomerular filtration rate; CRP, c-reaction protein; FBG, fasting blood glucose; BNP, brain natriuretic peptide; Kt/V, urea removal index; D/P, dialysate-to-plasma creatinine; D/Do, glucose uptake ratio. Data are expressed as mean ± SD.

[a]p < *0.05, vs. the CKD5 group.*

[b]p <*0.05, vs. the PD < 36 group.*

first antibody overnight at 4°C and then with the HRP-coupled anti-mouse/rabbit IgG secondary antibody for 1 h. After soaking in HRP Substrate (Millipore, Burlington, MA, United States) hypersensitive to electro-chemi-luminescence, the protein bands were observed using ChemiDoc™ MP Imaging System (Bio-Rad Laboratories, Hercules, CA, United States). The following antibodies were used for immunoblotting: α-SMA (ab7817; Abcam), fibronectin (ab45688; Abcam), E-cadherin (14472; CST), vimentin (5741; CST), p-SMAD2/3 (8828; CST), SMAD2/3 (8685; CST), AKT (AF6261; Affinity Biosciences, Cincinnati, OH, United States), p-AKT (AF0016; Affinity), ERK1/2 (4695; CST), p-ERK1/2 (9101S; CST), GAPDH (D190090; Sangon Biotech, Shanghai, China), HRP-coupled rabbit secondary antibody (ZB-2301; ZSGB-Bio, Beijing, China), and HRP-coupled anti-mouse secondary antibody (ZB-2305; ZSGB-Bio).

Statistical Analysis

The data were analyzed using SPSS 25.0 statistical software (SPSS Inc., Chicago, IL, United States). For data with normal or approximately normal distribution (presented as mean ± SD), Student's t-test was used to compare two groups, whereas single-factor analysis of variance (ANOVA) was used to compare among groups. For comparison among more than two groups and between any two groups, Mann–Whitney and Kruskal–Wallis tests, respectively, were used. The adoption rates or constituent ratio of the count data was also expressed, and chi-square test or Fisher exact probability test was performed to compare among groups. Finally, Pearson correlation, Spearman correlation, and multiple linear regression analyses were conducted to determine the correlation between variables. Differences with $p < 0.05$ were statistically significant.

RESULTS

Serum Elabela and Apelin Levels Significantly Correlate With Dialysis Duration

In total, 20, 40, and 20 patients were included in the CKD5 group, the PD < 36 group, and the PD ≥ 36 group, respectively. In this

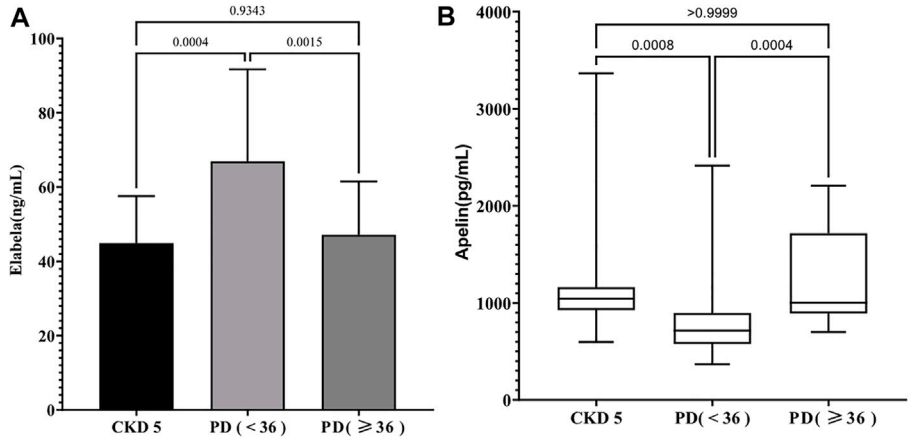

FIGURE 1 | (A) The level of serum ELA in different groups; **(B)** The level of serum Apelin in different groups.

study, no significant differences in age, history of hypertension and diabetes, primary glomerular diseases, and blood pressure were found in the CKD5 group, the PD < 36 group, or the PD ≥ 36 group. The dialysis duration of the PD < 36 group and PD ≥ 36 group was 9.00 (3.25, 18.75) and 49.50 (37.25, 70.50) months, respectively (**Table 1**). The three groups were analyzed based on the clinical laboratory tests of the serum. Compared with CKD5 group, the patients in PD < 36 group exhibited significantly higher levels of hemoglobin (Hb) and C-reactive protein (CRP), glomerular filtration rate (GFR), and carbon dioxide binding capacity (CO_2P) ($p < 0.05$) (**Table 1**); levels of CRP, serum creatinine (Cre), and β2 microglobulin were further increased in PD ≥ 36 group ($p < 0.05$). However, no differences in the levels of Hb, blood urea nitrogen (BUN), and GFR were found between the CKD5 group and PD ≥ 36 group. In addition, no differences in the levels of serum albumin, parathyroid hormone, fasting venous blood glucose, and BNP among the three groups were observed (**Table 1**).

Compared with serum ELA levels of patients in the CKD5 group (44.92 ± 12.61 ng/ml), that of patients in the PD < 36 group was noted to be significantly higher (66.95 ± 24.73 ng/ml) ($p < 0.05$), but no significant difference (47.14 ± 14.34 ng/ml) ($p > 0.05$) was observed in that of patients in the PD ≥ 36 group (**Figure 1A**). In contrast, serum APLN levels of the patients in PD < 36 group [717.10 (575.95, 896.38) pg/ml] were decreased compared with that in the CKD5 group [1,042.84 (927.02, 1,164.62) pg/ml], but there were no similar differences between the CKD5 group and PD ≥ 36 group [1,003.09 (890.24, 1,718.88) pg/ml] ($p > 0.05$) (**Figure 1B**). In summary, serum ELA and APLN levels were different in PD patients at different periods.

Dialysis Duration is the Risk Factor Influencing Serum Elabela Levels in Patients on Peritoneal Dialysis

To further analyze the effects of serum ELA and APLN in patients on PD, Spearman correlation analysis was performed using the clinical data obtained. We included the PD duration, age, and levels of Hb, CO_2P, BUN, Cre, rGFR, BNP, CRP, and serum ELA and APLN levels for the correlation analysis. The results showed a negative correlation of serum ELA level with dialysis duration ($r = -0.525$, $p < 0.05$) and a positive correlation between serum ELA level and rGFR ($r = 0.322$, $p < 0.05$). At the same time, serum APLN level positively correlated with dialysis duration ($r = 0.355$, $p < 0.05$) (**Table 2**). Multiple linear regression was not possible because APLN positively correlated only with dialysis duration. After PD, an irreversible loss of renal function is commonly observed in patients. To determine the specific factors affecting the serum ELA level in patients on PD, stepwise multiple linear regression analysis was conducted using serum ELA concentration as the dependent variable. Notably, the results revealed that dialysis duration was the major risk factor affecting serum ELA levels in patients on PD ($r = -0.412$, $p < 0.05$) (**Table 3**).

ELA-32 Reduces TGF-β1-Induced Epithelial-Mesenchymal Transition of Human Peritoneal Mesothelial Cells

PMCs are one of the main components of the peritoneal tissue (Selgas et al., 2006). To determine whether ELA-32 holds significance in PD when added to the peritoneal dialysate, we established the EMT model using TGF-β1 (10 ng/ml) and treated the HPMCs with ELA-32 (10 μM). After 24 h, we discovered that compared with untreated cells (control group), the TGF-β1-group HPMCs lost their pebble-like appearance and became elongated spindles. Notably, ELA-32 treatment reduced the proportion of spindle cells, suggesting that the combined treatment with ELA-32 and TGF-β1 can inhibit the morphological changes induced by the previous TGF-β1 treatment (**Figure 2A**). Based on the Western blot assay, the TGF-β1 treatment significantly upregulated the expression of mesenchymal cell markers α-SMA, fibronectin, and vimentin and downregulated the expression of the epithelial cell marker E-cadherin. However, the combined treatment with ELA-32

TABLE 2 | *R*-values and *p*-values of correlations among the study variables.

	ELA	Apelin	PD duration	Age	Hb	CO_2P	BUN	Cre	rGFR	BNP
Apelin	–0.193									
	0.139									
PD	–0.525	0.355								
Duration	<0.001	0.005								
Age	–0.001	0.069	0.087							
	0.996	0.602	0.509							
Hb	0.148	–0.019	–0.249	–0.059						
	0.261	0.886	0.055	0.655						
CO_2P	–0.010	0.198	0.032	–0.263	0.116					
	0.941	0.129	0.808	0.042	0.379					
BUN	0.013	–0.078	0.120	0.157	–0.183	–0.028				
	0.920	0.552	0.361	0.232	0.162	0.830				
Cre	–0.286	0.003	0.407	0.004	–0.345	0.041	0.500			
	0.027	0.984	0.001	0.977	0.007	0.754	<0.001			
rGFR	0.322	–0.173	–0.622	–0.048	0.352	–0.036	–0.223	–0.755		
	0.012	0.187	<0.001	0.715	0.006	0.786	0.086	<0.001		
BNP	–0.129	–0.006	0.033	0.187	–0.327	0.004	0.128	–0.022	–0.061	
	0.327	0.967	0.802	0.153	0.011	0.978	0.330	0.867	0.643	
CRP	0.070	0.037	–0.051	–0.050	–0.161	–0.152	–0.042	0.126	–0.258	0.240
	0.593	0.781	0.699	0.706	0.219	0.248	0.750	0.336	0.047	0.062

ELA, elabela; Hb, hemoglobin; PD, peritoneal dialysis; CO_2P, carbon dioxide combining power; BUN, blood urine nitrogen; Cre, serum creatinine; rGFR, residual glomerular filtration rate; BNP, brain natriuretic peptide; CRP, c-reaction protein. The first row for each variable represents the r value, and the second row represents the p value.

TABLE 3 | Stepwise multiple linear regression analysis of ELA.

Variables	Partial regression coefficient	SE	Standard partial regression coefficient	*t*	*p*	95% CI of partial regression coefficient
Constant	70.985	4.000		17.744	0.001	(62.977, 78.993)
PD duration	–0.412	0.112	–0.436	–3.687	0.001	(–0.636, –0.188)

ELA, elabela; SE, standard error; CI, confidence interval. Multiple R-squared: 0.190; adjusted R-squared: 0.176.

and TGF-β1 significantly inhibited the expression of mesenchymal protein markers and restored the expression of E-cadherin (**Figure 2B**). To further confirm the anti-EMT effect of ELA-32, immunofluorescence staining was performed using E-cadherin, α-SMA, and fibronectin. Compared with the control group, the intracellular distribution of α-SMA and fibronectin in the TGF-β1 group increased, when observed under confocal fluorescence microscope, while the content of the protein E-cadherin decreased in the cell membrane; however, after ELA-32 treatment, the expression of the three markers were restored (**Figure 2C**). Taken together, these results suggest that ELA-32 inhibited HMrSv5 EMT induced by TGF-β1.

ELA-32 Attenuates the TGF-β1-Induced Migration of Human Peritoneal Mesothelial Cells

In addition to the recovery of EMT marker expression, ELA-32 treatment also inhibited the TGF-β1-induced increase in migration capacity of the HPMCs. In wound healing assays and Transwell assays, the migration and invasion abilities of HMPCs were increased after administering TGF-β1 (10 ng/ml) but were attenuated on administering ELA-32 (10 μM) (**Figure 3**). These data suggest that ELA-32 effectively inhibited EMT progress.

ELA-32 Inhibits the TGF-β1-Induced Activation of the SMAD/ERK1/2/AKT Pathway

As the activation of the TGF-β/SMAD pathway is the main cause of PF (Balzer, 2020), we investigated the total SMAD2/3 content and its phosphorylation level in the HPMCs after TGF-β1 treatment to elucidate the mechanism underlying the ELA-32 mediated inhibition of EMT. After TGF-β1 stimulation of HPMCs for 24 h, phosphorylation of SMAD2/3 was increased in the TGF-β1 group, while that of SMAD2/3 was attenuated in the TGF-β1 + ELA group (**Figure 4**). ELA plays a protective role mainly by activating the ERK1/2 and AKT pathways (Chapman et al., 2021). However, the activation of the AKT and ERK1/2 pathways promotes EMT of HPMCs (Balzer, 2020). Therefore, we examined whether ELA-32 treatment influenced the ERK1/2 and AKT pathways. Interestingly, TGF-β1 treatment enhanced the phosphorylation levels of ERK1/2 and AKT in HPMCs, but these levels decreased after the addition of ELA-32 (**Figure 4**). These findings indicate that ELA-32 could reduce TGF-β1-induced EMT by suppressing SAMD/ERK/AKT pathway in HPMCs.

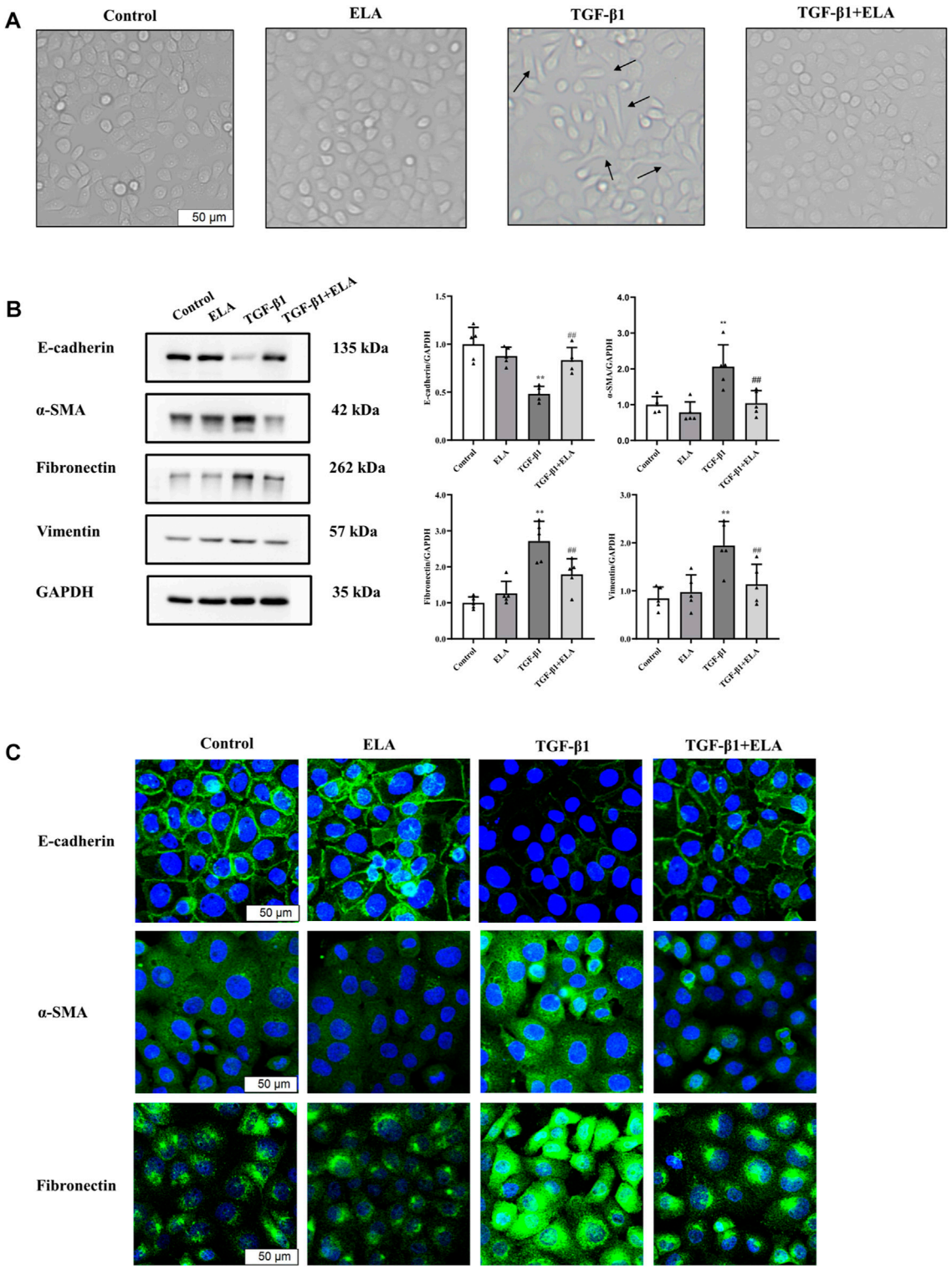

FIGURE 2 | The role of ELA in TGF-β1-induced EMT in HMrSv5. HMrSv5 was divided into four groups according to different treatments: 1) Control group where cells were cultured with DMEM medium containing 10% FBS after 24 h of synchronization; 2) ELA group where cells were treated with ELA-32 (10 μM) for 24 h; 3) TGF-β1 group where cells were treated with TGF-β1 (10 ng/ml) for 24 h; and TGF-β1+ELA group where cells were co-treated with TGF-β1 (10 ng/ml) and ELA-32 (10 μM) for 24 h. Notes **(A)** Light microscope was used to observe the morphological changes of human peritoneal mesenchymal cells. **(B)** The expression of E-cadherin, α-SMA, fibronectin, and vimentin proteins were detected by Western blotting. The experiments were repeated five times. **(C)** The E-cadherin, α-SMA, Fibronectin were observed by immunofluorescence; cell nuclei were stained with DAPI (blue fluorescence) (scale bar = 50 μm). In HMrSv5, E-cadherin is a green fluorescence located in the cell membrane, α-SMA, fibronectin is a green fluorescence distributed in the cytoplasm. Data are expressed as mean ± SD, $^{**}p < 0.05$ vs. control group; $^{\#\#}p < 0.05$ vs. TGF-β1 group. Abbreviations: ELA, elabela; TGF-β1, transforming growth factor-β1.

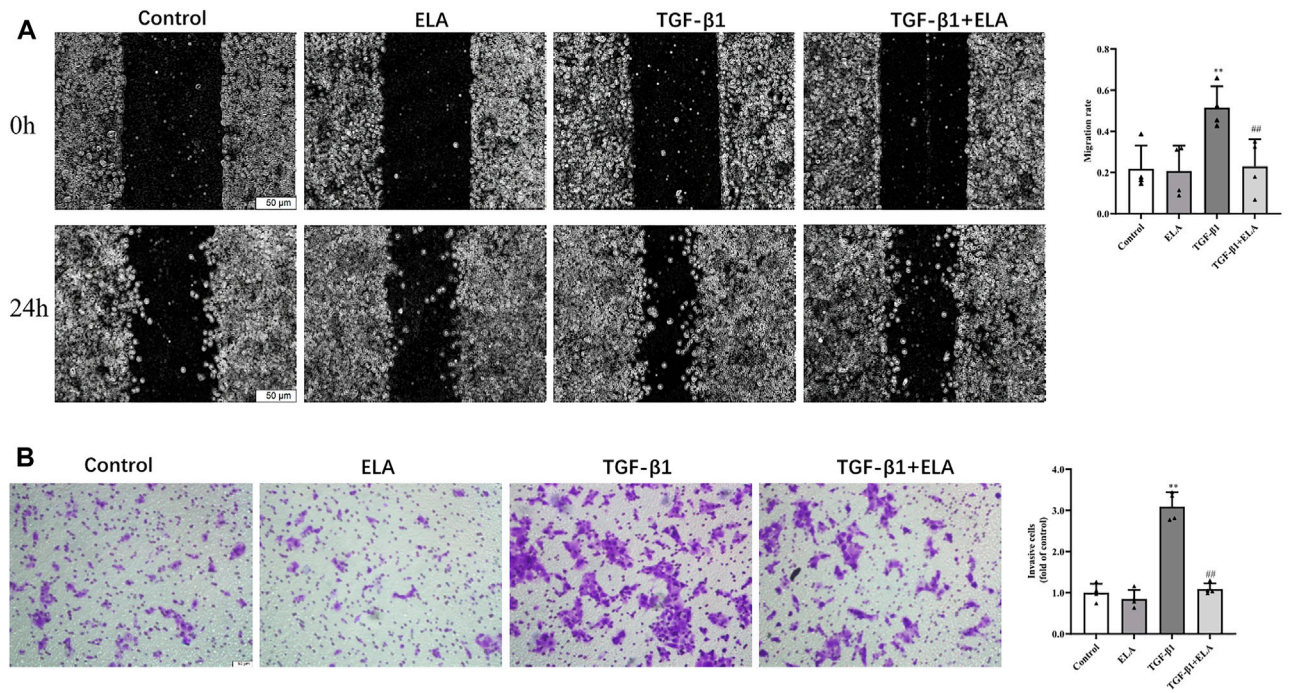

FIGURE 3 | Effects of ELA-32 on TGF-β1-induced migration of HMrSv5. HMrSv5 was divided into four groups according to different treatments: 1) Control group where cells were cultured with DMEM medium containing 10% FBS after 24 h of synchronization; 2) ELA group where cells were treated with ELA-32 (10 μM) for 24 h; 3) TGF-β1 group where cells were treated with TGF-β1 (10 ng/ml) for 24 h; and TGF-β1+ELA group where cells were co-treated with TGF-β1 (10 ng/ml) and ELA-32 (10 μM) for 24 h. Wound healing **(A)** and Transwell **(B)** was observed under optical microscope (scale bar = 50 μm). ImageJ software was used for data statistical analysis. The experiments were repeated four times. Data are expressed as mean ± SD, $^{**}p < 0.05$ vs. control group; $^{\#\#}p < 0.05$ vs. TGF-β1 group. Abbreviations: ELA, elabela; TGF-β1, transforming growth factor-β1.

DISCUSSION

In this study, we discovered that serum ELA levels increased and serum APLN levels decreased in patients with CKD5 entering the early stage of PD. With the extension of dialysis duration, serum ELA level decreased to the pre-dialysis level, whereas the serum APLN level increased to the pre-dialysis level. Notably, the major risk factor affecting the serum ELA levels in patients undergoing PD was dialysis duration. In addition, serum APLN level positively correlated with dialysis duration. Based on our *in vitro* experimental findings, we found that ELA-32 attenuates the TGF-β1-induced EMT of HPMCs by inhibiting the activation of the TGF-β/SAMD/ERK and AKT pathways (**Figure 5**).

In the circulatory system, ELA dilates the blood vessels, lowers blood pressure, alters renal blood flow, and increases diuresis (Hus-Citharel et al., 2008; Murza et al., 2016). Since ELA is distributed in the kidney and vascular endothelium in adults, the main factors affecting serum ELA levels are circulatory and renal system diseases. During acute myocardial infarction, compared with healthy people, the serum ELA level of patients showed an acute increase, and it positively correlated with myocardial injury markers troponin I and NT-pro BNP (Dönmez and Acele, 2019). In patients with stable angina pectoris and atrial fibrillation in stable disease, ELA levels will be reduced (Cui et al., 2021; Diakowska et al., 2021). Further, compared with healthy people, serum ELA is lower in patients with diabetic nephropathy (Onalan et al., 2020). In patients with CKD, the serum ELA level gradually decreases with the reduced GFR level, with the lowest values observed in patients with CKD5 (Lu et al., 2020). In our study, we used rGFR to evaluate the residual renal function in patients on PD in comparison with that in patients with CKD5. Our results suggest that after entering the early stage of PD, the serum ELA levels increased in patients with CKD5, corroborating previous results (Lu et al., 2020). Early PD treatment improves residual renal function in some patients with CKD5 (Kuo et al., 2022). We speculate that after patients with CKD5 enter the early stage of PD, the anemia and acidosis of the body will improve to a certain extent, which may promote the transient increase of ELA in the circulatory system. The decrease in peritoneal function leads to the accumulation of uremic toxins in the body, which is accompanied by the continuous aggravation of vascular endothelial damage, which may also lead to the reduction of ELA levels. However, the serum concentration of ELA in patients suggested that with the extension of PD treatment time, patients with PD will lose the protective effect of ELA on the body.

In patients with CKD, the distribution of serum APLN is controversial. Lu et al. (2020) indicated that there is no difference in the serum APLN levels between healthy people and patients with CKD at stages 1–5 without renal replacement therapy. In another study, non-diabetic patients on hemodialysis (HD) had lower serum APLN levels than healthy individuals (Małyszko et al., 2006). On the contrary, the detection of serum APLN level in patients on HD and PD indicated that the level of APLN was higher than that in the normal population (Büyükbakkal et al.,

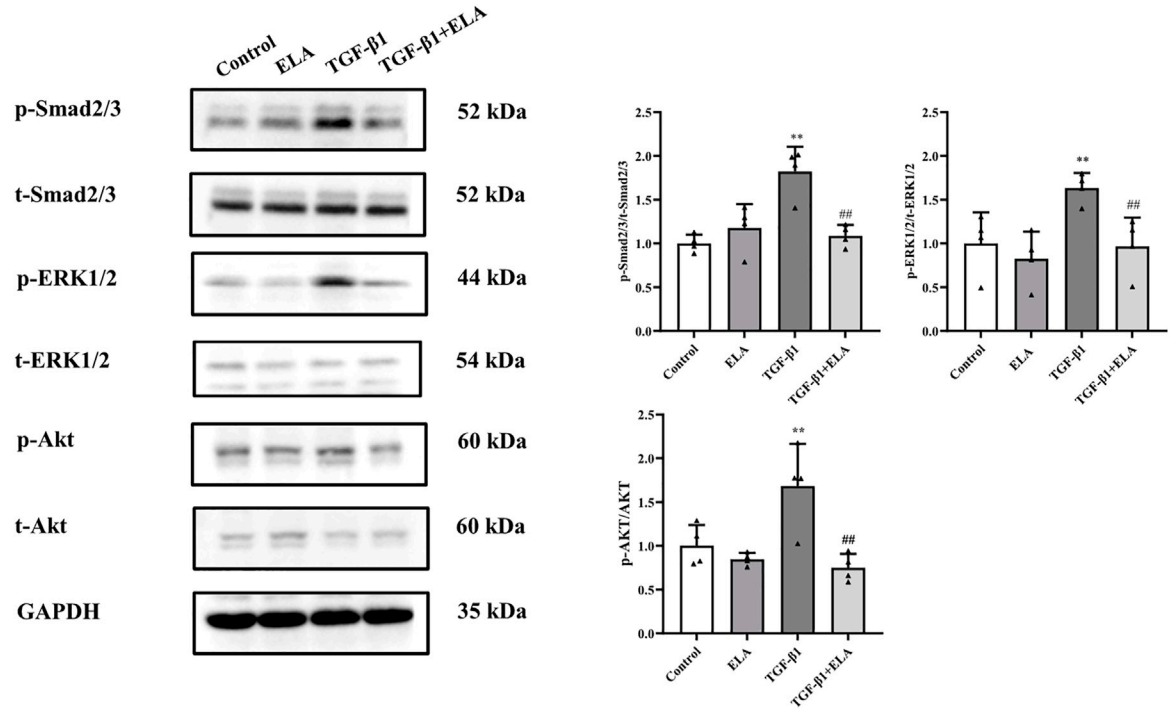

FIGURE 4 | Effects of ELA on TGF-β1-induced activation of the SMAD/ERK/AKT Pathway. HMrSv5 was divided into four groups according to different treatments: 1) Control group where cells were cultured with DMEM medium containing 10% FBS after 24 h of synchronization; 2) ELA group where cells were treated with ELA-32 (10 μM) for 24 h; 3) TGF-β1 group where cells were treated with TGF-β1 (10 ng/ml) for 24 h; and TGF-β1+ELA group where cells were co-treated with TGF-β1 (10 ng/ml) and ELA-32 (10 μM) for 24 h. After stimulate for 24 h, the expression of p-SMAD2/3, p-ERK1/2, and p-AKT were detected by Western blotting. Four independent experiments were carried out in each group. Data are expressed as mean ± SD, $^{**}p < 0.05$ vs. control group; $^{\#\#}p < 0.05$ vs. TGF-β1 group. Abbreviations: ELA, elabela; TGF-β1, transforming growth factor-β1.

2015; Dogan et al., 2018). The latest detection of serum APLN levels in patients with PD also indicated that APLN levels in this set of patients were higher than those in the normal population (Karaer Büberci et al., 2022). APLN is mainly catabolized by the angiotensin converting enzyme 2. The increase in APLN levels in patients with CKD may be caused by the decrease in the expression of angiotensin converting enzyme 2 due to the uremic microenvironment in patients with CKD that leads to decreased APLN degradation (Wang et al., 2016). The exact role of APLN in EMT is unknown. However, the relationship between APLN and inflammation, which is known to promote EMT (Li et al., 2014), has been studied. Some scholars suggested that APLN can evaluate inflammation and prevent the occurrence of atherosclerotic cardiovascular disease in patients undergoing both PD and HD (Dogan et al., 2018; Trojanowicz et al., 2020; Karaer Büberci et al., 2022). However, some studies have also indicated that APLN induces the expression of inflammatory factors MCP-1, VCAM-1, and ICAM-1 in human umbilical vein endothelial cells by activating the NF-kB/JNK signaling pathway (Trojanowicz et al., 2020). In addition, Sumi et al. (2021) found a weak negative correlation between serum APLN level and dialysis duration, leading them to speculate that APLN promotes peritoneal vascular proliferation. However, in our experiment, the serum APLN levels positively correlated with dialysis duration in patients on PD, contrary to the findings of Sumi et al. (2021). Furthermore, the other factors involved still remain unclear. Therefore, more studies are needed to clarify the role of APLN in EMT.

As the key cytokine-promoting PD-associated PF, TGF-β plays an important role in promoting fibrosis through the classical SMAD2/3 and non-classical ERK1/2 and AKT pathways (Balzer, 2020). First, we chose to use TGF-β1 to establish an EMT model of HPMCs, and then administered ELA-32 (10 μM) treatment. Our results found that ELA-32 could treat TGF-β1-induced EMT of HPMCs from the aspects of morphology and protein expression. The ELA-mediated activation of the PI3K/AKT pathway produces protective effects in kidney disease (Dagamajalu et al., 2022). However, the activation of this pathway promotes the occurrence of PF in the peritoneal tissues of patients on PD. Notably, our *in vitro* results showed that it did not have a significant effect on activating ERK1/2 and AKT in HPMCs in the ELA-32 treated group. On the contrary, ELA-32 could reduce TGF-β1-induced EMT by suppressing the SAMD/ERK/AKT pathway in HPMCs. Hence, we suggested that ELA-32 may be added as a protective peptide to peritoneal dialysate during PD; when absorbed into the blood through the peritoneum, it may improve the state of ELA deficiency in late PD. ELA-32 may be a potential therapeutic target for future studies on the prevention and treatment of PD-related PF.

However, the current study had some limitations. First, due to the small sample size, the results were limited, which mandates further studies with a large sample size. Second, other factors that influence

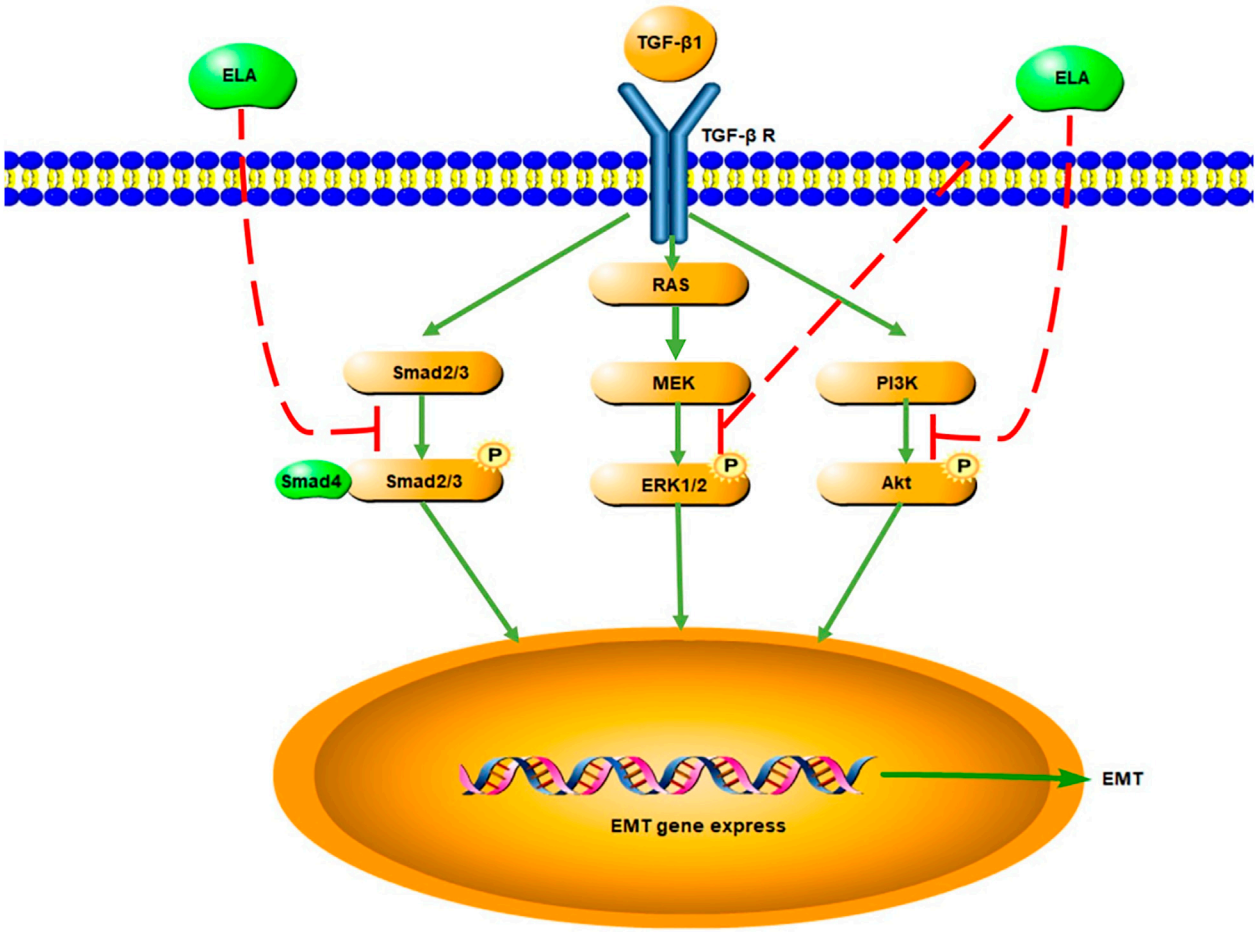

FIGURE 5 | Signaling pathway diagram of ELA inhibiting EMT in HMrSv5.

the serum levels of ELA and APLN in patients on PD need to be further explored. Third, we mainly detected the serum levels of ELA and APLN in patients without assessing whether ELA and APLN were expressed in the dialysate effluent and peritoneal tissue of patients on PD during different dialysis time periods and whether the two were consistent with the serological test results. Finally, the effect of ELA-32 in inhibiting the EMT of HMPCs was observed *in vitro*; further *in vivo* experiments are necessary to verify the results.

In conclusion, our findings demonstrated that the serum ELA level decreased in patients receiving PD after prolonged dialysis time. Furthermore, ELA-32 effectively inhibited the TGF-β1-induced EMT of HPMCs by inhibiting the TGF-β/SMAD/ERK and AKT signaling pathways.

DATA AVAILABILITY STATEMENT

The original contributions presented in the study are included in the article/Supplementary Material, further inquiries can be directed to the corresponding author.

ETHICS STATEMENT

The studies involving human participants were reviewed and approved by the Ethics Committee of the Second Hospital of Jilin University. The patients/participants provided their written informed consent to participate in this study.

AUTHOR CONTRIBUTIONS

WPC designed the experiments. SYX, FX, and YL performed the experiments and prepared the figures. SYX wrote the manuscript. YXZ, XYL, and MYY reviewed the manuscript.

FUNDING

This study was supported by the Research Project of the Branch of Blood Purification Center of the Chinese Hospital Association (Project No. CHABP 2021-20).

REFERENCES

Alhamdani, M. S., Al-Azzawie, H. F., and Abbas, F. K. (2007). Decreased Formation of Advanced Glycation End-Products in Peritoneal Fluid by Carnosine and Related Peptides. *Perit. Dial. Int.* 27, 86–89. doi:10.1177/089686080702700118

Aroeira, L. S., Aguilera, A., Sánchez-Tomero, J. A., Bajo, M. A., del Peso, G., Jiménez-Heffernan, J. A., et al. (2007). Epithelial to Mesenchymal Transition and Peritoneal Membrane Failure in Peritoneal Dialysis Patients: Pathologic Significance and Potential Therapeutic Interventions. *J. Am. Soc. Nephrol.* 18, 2004–2013. doi:10.1681/ASN.2006111292

Balzer, M. S. (2020). Molecular Pathways in Peritoneal Fibrosis. *Cell Signal* 75, 109778. doi:10.1016/j.cellsig.2020.109778

Boucher, J., Masri, B., Daviaud, D., Gesta, S., Guigné, C., Mazzucotelli, A., et al. (2005). Apelin, a Newly Identified Adipokine Up-Regulated by Insulin and Obesity. *Endocrinology* 146, 1764–1771. doi:10.1210/en.2004-1427

Büyükbakkal, M., Canbakan, B., Eser, B., Yayar, Ö., Ercan, Z., Merhametsiz, Ö., et al. (2015). The Relation between Apelin Levels, Echocardiographic Findings and Carotid Intima Media Thickness in Peritoneal Dialysis Patients. *Ren. Fail* 37, 433–438. doi:10.3109/0886022X.2014.996108

Chapman, F. A., Nyimanu, D., Maguire, J. J., Davenport, A. P., Newby, D. E., and Dhaun, N. (2021). The Therapeutic Potential of Apelin in Kidney Disease. *Nat. Rev. Nephrol.* 17, 840–853. doi:10.1038/s41581-021-00461-z

Chng, S. C., Ho, L., Tian, J., and Reversade, B. (2013). Elabela: A Hormone Essential for Heart Development Signals via the Apelin Receptor. *Dev. Cell* 27, 672–680. doi:10.1016/j.devcel.2013.11.002

Cui, C., Zhou, H., and Xu, J. (2021). Elabela Acts as a Protective Biomarker in Patients with Atrial Fibrillation. *J. Thorac. Dis.* 13, 6876–6884. doi:10.21037/jtd-21-1728

Dagamajalu, S., Rex, D. A. B., Suchitha, G. P., Rai, A. B., Rainey, J. K., and Prasad, T. S. K. (2022). The Network Map of Elabela Signaling Pathway in Physiological and Pathological Conditions. *J. Cell Commun. Signal* 16, 145–154. doi:10.1007/s12079-021-00640-4

Diakowska, D., Wyderka, R., Krzystek-Korpacka, M., Osuch, Ł., Leśków, A., Sołtowska, A., et al. (2021). Plasma Levels of Apelinergic System Components in Patients with Chronic and Acute Coronary Syndromes-A Pilot Study. *J. Clin. Med.* 10 (19), 4420. doi:10.3390/jcm10194420

Dogan, I., Dogan, T., Yetim, M., Kayadibi, H., Yilmaz, M. B., Eser, B., et al. (2018). Relation of Serum Adma, Apelin-13 and Lox-1 Levels with Inflammatory and Echocardiographic Parameters in Hemodialysis Patients. *Ther. Apher. Dial.* 22, 109–117. doi:10.1111/1744-9987.12613

Dönmez, Y., and Acele, A. (2019). Increased Elabela Levels in the Acute St Segment Elevation Myocardial Infarction Patients. *Med. Baltim.* 98, e17645. doi:10.1097/md.0000000000017645

Ferrantelli, E., Liappas, G., Vila Cuenca, M., Keuning, E. D., Foster, T. L., Vervloet, M. G., et al. (2016). The Dipeptide Alanyl-Glutamine Ameliorates Peritoneal Fibrosis and Attenuates Il-17 Dependent Pathways during Peritoneal Dialysis. *Kidney Int.* 89, 625–635. doi:10.1016/j.kint.2015.12.005

Honda, K., Nitta, K., Horita, S., Yumura, W., Nihei, H., Nagai, R., et al. (1999). Accumulation of Advanced Glycation End Products in the Peritoneal Vasculature of Continuous Ambulatory Peritoneal Dialysis Patients with Low Ultra-filtration. *Nephrol. Dial. Transpl.* 14, 1541–1549. doi:10.1093/ndt/14.6.1541

Hus-Citharel, A., Bouby, N., Frugière, A., Bodineau, L., Gasc, J. M., and Llorens-Cortes, C. (2008). Effect of Apelin on Glomerular Hemodynamic Function in the Rat Kidney. *Kidney Int.* 74, 486–494. doi:10.1038/ki.2008.199

Karaer Büberci, R., Öztekin, P. S., and Duranay, M. (2022). The Relationship between Apelin and Carotid Intima Media Thickness, and the Presence of Plaque in Dialysis Patients. *Seminars Dialysis*. doi:10.1111/sdi.13052

Kuo, G., Chen, J. J., Cheng, Y. L., Fan, P. C., Lee, C. C., and Chang, C. H. (2022). Comparison between Peritoneal Dialysis and Hemodialysis on Kidney Function Recovery in Incident Kidney Failure: A Nationwide Cohort Study. *Semin. Dial.* 35 (3), 278–286. doi:10.1111/sdi.13050

Li, Z., Zhang, L., He, W., Zhu, C., Yang, J., and Sheng, M. (2014). Astragalus Membranaceus Inhibits Peritoneal Fibrosis via Monocyte Chemoattractant Protein (MCP)-1 and the Transforming Growth Factor-B1 (TGF-B1) Pathway in Rats Submitted to Peritoneal Dialysis. *Int. J. Mol. Sci.* 15, 12959–12971. doi:10.3390/ijms150712959

Lu, X., Liu, S., Luan, R., Cui, W., Chen, Y., Zhang, Y., et al. (2020). Serum Elabela and Apelin Levels during Different Stages of Chronic Kidney Disease. *Ren. Fail* 42, 667–672. doi:10.1080/0886022X.2020.1792926

Małyszko, J., Małyszko, J. S., Koźminski, P., and Myśliwiec, M. (2006). Apelin and Cardiac Function in Hemodialyzed Patients: Possible Relations? *Am. J. Nephrol.* 26, 121–126. doi:10.1159/000092122

Mehrotra, R., Devuyst, O., Davies, S. J., and Johnson, D. W. (2016). The Current State of Peritoneal Dialysis. *J. Am. Soc. Nephrol.* 27, 3238–3252. doi:10.1681/ASN.2016010112

Murza, A., Sainsily, X., Coquerel, D., Côté, J., Marx, P., Besserer-Offroy, É., et al. (2016). Discovery and Structure-Activity Relationship of a Bioactive Fragment of Elabela that Modulates Vascular and Cardiac Functions. *J. Med. Chem.* 59, 2962–2972. doi:10.1021/acs.jmedchem.5b01549

Nyimanu, D., Kay, R. G., Kuc, R. E., Brown, A. J. H., Gribble, F. M., Maguire, J. J., et al. (2021). *In Vitro* metabolism of Synthetic Elabela/toddler (Ela-32) Peptide in Human Plasma and Kidney Homogenates Analyzed with Mass Spectrometry and Validation of Endogenous Peptide Quantification in Tissues by Elisa. *Peptides* 145, 170642. doi:10.1016/j.peptides.2021.170642

O'Dowd, B. F., Heiber, M., Chan, A., Heng, H. H., Tsui, L. C., Kennedy, J. L., et al. (1993). A Human Gene that Shows Identity with the Gene Encoding the Angiotensin Receptor Is Located on Chromosome 11. *Gene* 136, 355–360. doi:10.1016/0378-1119(93)90495-o

Onalan, E., Doğan, Y., Onalan, E., Gozel, N., Buran, I., and Donder, E. (2020). Elabela Levels in Patients with Type 2 Diabetes: Can it Be a Marker for Diabetic Nephropathy? *Afr. Health Sci.* 20, 833–840. doi:10.4314/ahs.v20i2.37

Qin, A., Liu, X., Yin, X., Zhou, H., Tang, Y., and Qin, W. (2020). Normalized Protein Catabolic Rate Is a Superior Nutritional Marker Associated with Dialysis Adequacy in Continuous Ambulatory Peritoneal Dialysis Patients. *Front. Med. (Lausanne)* 7, 603725. doi:10.3389/fmed.2020.603725

Selgas, R., Bajo, A., Jiménez-Heffernan, J. A., Sánchez-Tomero, J. A., Del Peso, G., Aguilera, A., et al. (2006). Epithelial-to-mesenchymal Transition of the Mesothelial Cell-Iits Role in the Response of the Peritoneum to Dialysis. *Nephrol. Dial. Transpl.* 21 (Suppl. 2), ii2–7. doi:10.1093/ndt/gfl183

Sumi, Y., Sakai, Y., Terada, K., Otsuka, Y., Otsuka, T., and Tsuruoka, S. (2021). Association of Adipocytokines with Peritoneal Function. *Perit. Dial. Int.* 41, 79–85. doi:10.1177/0896860819896133

Tatemoto, K., Hosoya, M., Habata, Y., Fujii, R., Kakegawa, T., Zou, M. X., et al. (1998). Isolation and Characterization of a Novel Endogenous Peptide Ligand for the Human Apj Receptor. *Biochem. Biophys. Res. Commun.* 251, 471–476. doi:10.1006/bbrc.1998.9489

Trojanowicz, B., Ulrich, C., and Girndt, M. (2020). Uremic Apelin and Leucocytic Angiotensin-Converting Enzyme 2 in Ckd Patients. *Toxins* 12 (12), 742. doi:10.3390/toxins12120742

Wang, Z., Yu, D., Wang, M., Wang, Q., Kouznetsova, J., Yang, R., et al. (2015). Elabela-apelin Receptor Signaling Pathway Is Functional in Mammalian Systems. *Sci. Rep.* 5, 8170. doi:10.1038/srep08170

Wang, W., McKinnie, S. M., Farhan, M., Paul, M., McDonald, T., McLean, B., et al. (2016). Angiotensin-converting Enzyme 2 Metabolizes and Partially Inactivates Pyr-Apelin-13 and Apelin-17: Physiological Effects in the Cardiovascular System. *Hypertension* 68, 365–377. doi:10.1161/HYPERTENSIONAHA.115.06892

Yang, P., Read, C., Kuc, R. E., Buonincontri, G., Southwood, M., Torella, R., et al. (2017). Elabela/toddler Is an Endogenous Agonist of the Apelin Apj Receptor in

the Adult Cardiovascular System, and Exogenous Administration of the Peptide Compensates for the Downregulation of its Expression in Pulmonary Arterial Hypertension. *Circulation* 135, 1160–1173. doi:10.1161/CIRCULATIONAHA.116.023218

Conflict of Interest: The authors declare that the research was conducted in the absence of any commercial or financial relationships that could be construed as a potential conflict of interest.

Publisher's Note: All claims expressed in this article are solely those of the authors and do not necessarily represent those of their affiliated organizations, or those of the publisher, the editors and the reviewers. Any product that may be evaluated in this article, or claim that may be made by its manufacturer, is not guaranteed or endorsed by the publisher.

frontiers | Frontiers in Pharmacology

TYPE Original Research
PUBLISHED 16 August 2022
DOI 10.3389/fphar.2022.868374

OPEN ACCESS

EDITED BY
Timothy Joseph Keane,
Imperial College London,
United Kingdom

REVIEWED BY
Valentina Masola,
University of Verona, Italy
Isaac Teitelbaum,
University of Colorado Anschutz Medical Campus, United States

*CORRESPONDENCE
Manuel López-Cabrera,
mlcabrera@cbm.csic.es
Guadalupe-Tirma González-Mateo,
gtirma@cbm.csic.es

SPECIALTY SECTION
This article was submitted to Experimental Pharmacology and Drug Discovery, a section of the journal Frontiers in Pharmacology

RECEIVED 02 February 2022
ACCEPTED 13 July 2022
PUBLISHED 16 August 2022

CITATION
Kopytina V, Pascual-Antón L, Toggweiler N, Arriero-País E-M, Strahl L, Albar-Vizcaíno P, Sucunza D, Vaquero JJ, Steppan S, Piecha D, López-Cabrera M and González-Mateo G-T (2022), Steviol glycosides as an alternative osmotic agent for peritoneal dialysis fluid. *Front. Pharmacol.* 13:868374. doi: 10.3389/fphar.2022.868374

Steviol glycosides as an alternative osmotic agent for peritoneal dialysis fluid

Valeria Kopytina[1], Lucía Pascual-Antón[1], Nora Toggweiler[2], Eva-María Arriero-País[1], Lisa Strahl[2], Patricia Albar-Vizcaíno[3], David Sucunza[4], Juan J. Vaquero[4], Sonja Steppan[5], Dorothea Piecha[5], Manuel López-Cabrera[1]* and Guadalupe-Tirma González-Mateo[1,3]*

[1]Department of Immunology, Molecular Biology Research Center Severo Ochoa (CBMSO), Spanish National Research Council (CSIC), Madrid, Spain, [2]Fresenius Medical Care Deutschland GmbH, Frankfurter, St. Wendel, Germany, [3]Department of Nephrology, IdiPAZ Research Institute, La Paz University Hospital, Madrid, Spain, [4]Department of Organic and Inorganic Chemistry, Faculty of Pharmacy, University of Alcalá (IRYCIS), Madrid, Spain, [5]Fresenius Medical Care Deutschland GmbH, St. Wendel, Germany

Background: Peritoneal dialysis (PD) is a renal replacement technique that requires repeated exposure of the peritoneum to hyperosmolar PD fluids (PDFs). Unfortunately, it promotes alterations of the peritoneal membrane (PM) that affects its functionality, including mesothelial-mesenchymal transition (MMT) of mesothelial cells (MCs), inflammation, angiogenesis, and fibrosis. Glucose is the most used osmotic agent, but it is known to be at least partially responsible, together with its degradation products (GDP), for those changes. Therefore, there is a need for more biocompatible osmotic agents to better maintain the PM. Herein we evaluated the biocompatibility of Steviol glycosides (SG)-based fluids.

Methods: The ultrafiltration and transport capacities of SG-containing and glucose-based fluids were analyzed using artificial membranes and an *in vivo* mouse model, respectively. To investigate the biocompatibility of the fluids, Met-5A and human omental peritoneal MCs (HOMCs) were exposed *in vitro* to different types of glucose-based PDFs (conventional 4.25% glucose solution with high-GDP level and biocompatible 2.3% glucose solution with low-GDP level), SG-based fluids or treated with TGF-β1. Mice submitted to surgery of intraperitoneal catheter insertion were treated for 40 days with SG- or glucose-based fluids. Peritoneal tissues were collected to determine thickness, MMT, angiogenesis, as well as peritoneal washings to analyze inflammation.

Results: Dialysis membrane experiments demonstrated that SG-based fluids at 1.5%, 1%, and 0.75% had a similar trend in weight gain, based on curve slope, as glucose-based fluids. Analyzing transport capacity *in vivo*, 1% and 0.75% SG-based fluid-exposed nephrectomized mice extracted a similar amount of urea as the glucose 2.3% group. *In vitro*, PDF with high-glucose (4.25%) and high-GDP content induced mesenchymal markers and angiogenic factors (Snail1, Fibronectin, VEGF-A, FGF-2) and downregulates the epithelial marker E-Cadherin. In contrast, exposition

to low-glucose-based fluids with low-GDP content or SG-based fluids showed higher viability and had less MMT. *In vivo,* SG-based fluids preserved MC monolayer, induced less PM thickness, angiogenesis, leukocyte infiltration, inflammatory cytokines release, and MMT compared with glucose-based fluids.

Conclusion: SG showed better biocompatibility as an osmotic agent than glucose *in vitro* and *in vivo*, therefore, it could alternatively substitute glucose in PDF.

KEYWORDS

biocompatibility, dialysis solutions, fibrosis, osmotic agents, peritoneal dialysis (PD), chronic inflammation

Introduction

Peritoneal dialysis (PD) is a well-established kidney replacement therapy that allows the elimination of toxic metabolic products and excess water from the body, through a process known as ultrafiltration (UF). However, continuous exposure to PD fluids (PDFs) triggers a series of processes associated with the appearance of morphological and functional alterations in the peritoneal membrane (PM), leading to the development of fibrosis, angiogenesis, hyalinizing vasculopathy, and a deterioration of the membrane UF capacity (Krediet, 1999). These alterations are attributed to the lack of biocompatibility of PDFs, which generally use glucose as an osmotic agent. In addition, heat sterilization of glucose-based PDFs generates glucose degradation products (GDP) (Welten et al., 2003), which in turn raises the formation of advanced glycation end-products (AGEs). AGEs, together with GDP, promote the synthesis of cytokines related to inflammation, fibrosis, vascular alterations, and angiogenesis, driving UF failure (Qayyum et al., 2015).

Moreover, PDFs cause damage to the mesothelial cells (MCs) monolayer that lines the whole PM and is in direct contact with the PDFs. As a consequence of these damages, MCs undergo a process called mesothelial-mesenchymal transition (MMT). MMT is a normal tissue repair process by which cells acquire the ability to migrate, invade the submesothelial stroma and synthesize large amounts of extracellular matrix as well as inflammatory and angiogenic factors (Yáñez-Mó et al., 2003; López-Cabrera, 2014). PDF exposure leads to tissue damage and consequently generates inflammation, inducing pathological MMT that plays a key role in the peritoneal injury. Bio-incompatible PDFs also alter the peritoneal leukocytes population, which constitutes the first line of defense against peritoneal infection (McIntyre, 2007; García-López et al., 2012). The repeated metabolic and biomechanical damages arising from serial PDF exposures lead to smoldering inflammation and reduced host defense in the peritoneal cavity (Jörres et al., 1992; Brulez et al., 1999; Devuyst et al., 2002; Mackenzie et al., 2003; Schilte et al., 2009). The interplay of PDF cytotoxicity and intermittent bacterial infections contribute to clinical complications of PD therapy, such as UF failure and peritonitis (Davies et al., 1998).

During the last decades, new and more biocompatible PDFs have been developed to correct the problems associated with PD by using either different osmotic agents such as icodextrin or amino acids, or other sterilization techniques to avoid the generation of GDP or more physiological pH. However, a definitive solution has not been found yet. Glucose is still the most widely used agent since other commercialized substitutes (icodextrin and aminoacids) can only be used in one exchange per day, so it is mandatory to use glucose in the rest of the exchanges. The constant use of a high amount of glucose not only causes local problems in the peritoneum but also systemic alterations, such as diabetes, dyslipidemia, hydrocarbon intolerance (Delarue and Maingourd, 2001), and cardiovascular disease (Balafa and Krediet, 2012). Meta-analyses revealed no significant improvement of newer varieties of biocompatible PDFs on peritonitis rate or PM function (Cho et al., 2013, 2014). Therefore, the greatest challenge since the development of PD as a treatment for chronic kidney disease (CKD) is to find a definitive alternative to glucose.

Stevia rebaudiana is a plant that is used as a sweetener (Goyal et al., 2010). The leaves of *stevia rebaudiana* contain Steviol glycosides (SG) which are active compounds responsible for their sweet taste. Many plant-based glycosides are used as medicines. Beyond sweetening value, SG have therapeutic effects against cancer, inflammation, cystic fibrosis, obesity, and dental caries (López et al., 2016; Momtazi-Borojeni et al., 2017; Ramos-Tovar et al., 2018; Casas-Grajales et al., 2019). Another aspect that makes it even more attractive is that it acts as an antioxidant (Bender et al., 2015), anti-hypertensive (Hsieh et al., 2003), anti-diabetic, improving hydrocarbon resistance (Mohd-Radzman et al., 2013; Periche et al., 2015), and protects against kidney damage (Ozbayer et al., 2011; Shivanna et al., 2013). Hypertension, hydrocarbon

intolerance, and a pro-oxidative environment frequently accompany central obesity, being cardiovascular risk factors commonly found in uremia (a syndrome caused by the accumulation of toxic products in the blood that the kidneys are not able to eliminate) (Podkowińska and Formanowicz, 2020), therefore SG properties could help to control these illnesses.

An optimal osmotic agent for PD should have some specific characteristics, such as a molecular weight (MW) that permits using it in several exchanges per day, an osmotic and UF capacity, no absorption, no interference with tissue repair ability nor immunocompetence, and no toxicity (Khanna et al., 1986). This is important as part of it can be absorbed or degraded, thus constituting an additional problem (Lee et al., 2005). Moreover, it has been determined that an ideal osmotic agent should weigh around 1 kDa (Rippe and CarlssOn, 1996). According to this background, we selected a pure *stevia* extract composed of SG (≥ 95%), which contains Rebaudioside A as the main compound (62.6%) and Stevioside (21.3%) to be tested as an osmotic agent for PDFs. The components of the *stevia* extract do not contain glucose and have MW ranging from 950 to 1,050 Da.

Materials and methods

Peritoneal dialysis fluids

A mixture of SG (≥95%) that contains Rebaudioside A (62.6%) and Stevioside (21.3%) was bought from AgriStevia (SG95RA60, Spain). The total composition and theoretical osmolarity of SG extract are indicated in the Supplementary Figure SA,B. SG solutions were prepared at different concentrations (0.75%: pH = 6.29; 1%: pH = 6.24, 1.5%: pH = 6.17) in a lactate buffer that contains: 1.25 mmol/L calcium, 134 mmol/L sodium, 0.5 mmol/L magnesium, 100.5 mmol/L chloride, 25 mmol/L lactate. SG solutions have been heat sterilized at 121°C for 1 h for *in vitro* and *in vivo* experiments. PDFs containing 1.5%, 2.3%, and 4.25% dextrose (glucose monohydrate, Mass Weight 198.20 Da) are commercially available and labeled as such in North America. The true anhydrous dextrose or glucose concentrations (Mass Weight 180.15 Da) in these solutions are 1.36%, 2.27%, and 3.86%, respectively, and this is how they are typically labeled in Europe. We used American nomenclature in this work (Daugirdas et al., 2015). A commercial standard PDF with 4.25% of glucose, pH = 5.5, and a high concentration of GDP (Stay Safe®; Fresenius Medical Care) was used as a positive control (named SS 4.25%), and a more biocompatible PDF with 2.3% glucose, pH = 7.0, and low-GDP concentration (Balance®, Fresenius Medical Care) (named Bl 2.3%) was employed to compare its effects *in vitro* and *in vivo* with SG.

Osmotic capacity measurements

Glucose-based PDFs at 1.5%, 2.3%, and 4.25% concentrations have been used as commercial dialysis solutions to compare their osmotic capacity with SG solutions. The solutions contain glucose solved in different concentrations in a lactate matrix with the same composition as in commercial SS 4.25% and Bl 2.3% PDFs. Glucose-based solutions have been heat sterilized at 121°C for 1 h. SG-based fluids were used at 1.5%, 1%, and 0.75% concentrations. pH-value of all test solutions was adjusted to 6.4 ± 0.2 using hydrochloride acid or sodium hydroxide before performing the experiments.

Osmotic capacity experiments were performed using dialysis membranes (ZelluTrans/Roth V-series) with a molecular weight cutoff 25 kDa purchased from Carl Roth. Dialysis tubing length of 8 cm was used in all experiments. The filling volume of dialysis tubes at the beginning of the experiments was 10 ml, closed by two clamps, each system with a sinker and swimmer. Dialysis tubing bags were placed in a beaker filled with 1,100 ± 0.1 g of lactate matrix which is tempered to 37°C and the weight of each bag was measured to determine the mass change all 30 min over a period of 24 h. The mass increase was calculated for each dwelling time interval. Experiments were carried out 3-times, and the mean value with the respective standard deviation was calculated. Determination of the concentration of the osmotic agent was made by measuring the refraction index (Refractometer DR 6300-T, KRÜSS Optronic). A calibration curve was prepared for each substance, and the test solution was measured after 24 h' test.

The reflection coefficient of the SG mixture was calculated using the relation between reflection coefficients (σ) of low molecular weight solutes (urea, glycerol, glucose, sucrose) as well as insulin, icodextrin, and albumin and their molecular weights.

Isolation, culture, and treatments of human omental peritoneal MCs

HOMCs were obtained from omental samples taken from patients undergoing elective abdominal surgery as described previously (Stylianou et al., 1990; Aroeira et al., 2005). Cells were cultured in Earle's M199 medium (Biological Industries, Kibbutz Beit Haemek, Israel) supplemented with 20% fetal bovine serum (FBS; Thermo Scientific, Cramlington, United Kingdom), 50 U/ml penicillin, 50 µg/ml streptomycin (PPA Laboratories GmbH, Pasching, Austria), 2% HEPES 1 M (Lonza™ BioWhittaker™), 2% Biogro-2 (Biological Industries). These cells were used and remained stable for one to two passages.

HOMCs were incubated with glucose-based PDFs (SS 4.25%, or Bl 2.3%, Fresenius Medical Care) diluted 1:1 with a culture medium for 48 h. In addition, HOMCs were

incubated with SG 1% or 0.75% in the same conditions. HOMCs were also treated with recombinant human TGF-β1 (1 ng/ml) (R&D Systems Inc., Minneapolis, MN, United States) to induce MMT *in vitro* (Aroeira et al., 2005). The control (CTRL) group was incubated with a lactate buffer 1:1 with a culture medium. Each experiment was carried out in duplicate, and at least five experiments were performed.

Culture of Met-5A and viability assay

The stable tetrazolium salt MTT is converted by active mitochondrial dehydrogenases of living cells to MTT Formazan. Therefore, the amount of formazan dye formed directly correlates to the number of metabolically active cells in the culture.

Met-5A cells were grown in a 96-well tissue culture plate in Earle's M199 medium (Biological Industries, Kibbutz Beit Haemek, Israel) supplemented with 10% fetal bovine serum (FBS; Thermo Scientific, Cramlington, United Kingdom), 50 U/ml penicillin, 50 µg/ml streptomycin (PPA Laboratories GmbH, Pasching, Austria), 2% HEPES 1 M (Lonza™ BioWhittaker™), 2% Biogro-2 (Biological Industries). The cells were incubated with glucose-based PDFs (SS 4.25%, or Bl 2.3%, Fresenius Medical Care) and SG solutions 1% or 0.75%, as well as with TGF-beta (1 ng/ml) and DMSO 5% as controls, diluted 1:1 with a culture medium for 96 h. The cells were incubated subsequently with the MTT reagent (Invitrogen, reference M6494) at 0.5 mg/ml for 4 h. Then, DMSO was added to solubilize the formazan dye formed and it was quantitated with a scanning multi-well spectrophotometer at 570 nm (ClarioStar Plus reader). The measured absorbance directly correlates to the number of viable cells.

Real-time qPCR

Cell lysis and RNA extraction were done using TRI Reagent® Solution (Ambion, Austin, TX) according to the manufacturer's instructions. cDNA for RT-qPCR was generated from 1 µg total RNA using the High Capacity cDNA Reverse Transcription Kit (Applied Biosystems, Foster City, CA, United States). Quantitative PCR was carried out on a LightCycler 480 using a SYBR Green labeling kit (Roche, Mannheim, Germany) and specific primers sets for human histone H3, Snail1, Fibronectin, VEGF-A and E-Cadherin. The data were analyzed by using the comparative Ct method (ΔΔCt). The x-fold change in RNA expression was quantified relative to control samples from the same experiment. Samples were normalized with respect to the value obtained for H3.

FGF-2 and VEGF-A detection in supernatants

The supernatants were collected and stored at −80°C. The secreted Fibroblast Growth Factor 2 (FGF-2) and VEGF-A by HOMCs were determined using a simplex kit (EPX01A-12074-901, EPX01A-10277-901, Invitrogen) by Luminex 100 technology.

Animals

Female C57BL/6JRccHsd mice, from 18 weeks of age, were purchased from ENVIGO (Barcelona, Spain) and maintained in conventional conditions at the CBMSO animal facilities. All animal procedures were approved by the ethics committee of the CSIC, authorized by the Comunidad Autónoma de Madrid according to RD 53/2013, with affiliation number PROEX 273/19, and conducted in accordance with the institutional guidelines that comply with the Directive of the European Parliament and of the Council on the Protection of Animals Used for Scientific Purposes.

Urea removal capacity and surgery

For urea removal capacity analysis, mice were submitted for surgery to induce uremia (González-Mateo et al., 2018). Briefly, 5/6 nephrectomy was performed under isoflurane anesthesia (4% for induction and 2%–3% for maintenance); 0.05–0.1 mg/kg buprenorphine (Temgesic) was injected intramuscularly 15–30 min preoperatively, and eye drops were given. The animal was shaved in the abdomen, and it was placed on a heating pad. An incision of approximately 0.5 cm in the skin was performed, on the right side, close to the ribs, to have direct access to the right kidney. A small incision was opened in the muscle to take the right kidney out of the peritoneum, removing the capsule and the adrenal gland. At this point, the kidney could be easily positioned on top of the peritoneum and was placed on a wound pad. A total ligation with insoluble suture was applied that included the kidney vein, artery, and urethra. After the ligation, the right kidney was totally removed from the body. After 1 week of recovery, the left kidney was also removed from the abdominal cavity following the same procedure and released from the capsule. The anterior one-third and posterior one-third parts of the kidney were impaired by using a monopolar electric blade. The remaining functional one-third of the left kidney is placed back into its original position in the abdominal cavity. To allow the mice to fully recover, transport analyses were performed 2 weeks after surgery.

The mice were euthanized 10, 40, and 60 min after receiving 2 ml of each tested fluid (Bl 2.3%, SG 1%, and SG 0.75%, $n = 4$ or 5 per group), and the total peritoneal volume was drained and urea concentration was measured. To confirm uremia, a volume of 200–400 µl blood was drawn via facial vein puncture 2 days before the surgery and at the end point, analyzing serum samples for urea levels (Ab83362; Abcam).

PD fluid exposure and surgery

Catheter implantation was performed as previously described (Aroeira et al., 2009; González-Mateo et al., 2018). The control group received physiologic saline (605,137.5, Grifols, n = 5 per group). The glucose-based PDF groups received a commercial solution with high glucose and high-GDP concentration or low glucose and low-GDP concentration (PDF-4.25% glucose; pH 5.5; Stay Safe®; and PDF-2.3% glucose, pH 7.0; Balance®, respectively, from Fresenius Medical Care) (n = 6 per group). The SG groups received SG at 1% and 0.75% concentrations diluted a lactate buffer (n = 6 per group). All mice received 2 ml of the solution corresponding to their treatment group, twice a day through the catheter, for 40 days. Before starting the 40 days-treatment, animals were injected with increasing concentrations of the corresponding fluid, starting at a 5 times-diluted concentration and increasing proportionally every 3 days for 12 days until the final concentration was reached for each group. This methodology was designed in order to avoid possible undesirable reactions due to a high-concentrated initial exposition, as we have previously observed that animals need to gradually adapt to SG intraperitoneal (i.p.) exposition.

Cytokines detection in peritoneal washings

Peritoneal washings were collected at the end of the experiment, stored at −80°C, and analyzed by Luminex 100 technology using simplex kits for IL-6 (EPX01A-20603-901, Invitrogen), IL-22 (EPX01A-26022-901, Invitrogen), IL-1β (EPX01A-26002-901, Invitrogen), TNF-α (EPX01A-20607-90, Invitrogen), IL-17 (EPX01A-26001-901, Invitrogen).

FACS analyses

Cell suspensions obtained from peritoneal washing were counted with a Scepter handheld automatic cell counter (Millipore) and stained with fluorochrome-conjugated mouse-specific antibodies against CD3, CD4, CD8α, CD11b, Ly6G, F4/80 (BD Biosciences Pharmingen, San Diego, CA, United States) following manufacturer's instructions. Samples were analyzed in a BD FACS Canto II (BD Biosciences, San Jose, CA) flow cytometer, and data analyses were performed using FlowJo software.

Histological analyses

Parietal peritoneal biopsies were collected from the opposite side of the catheter installation. For thickness analyses, biopsies were fixed in Bouin solution, embedded in paraffin, cut into 5 µm sections, and stained with Trichrome Stain (Masson) kit (HT15, Sigma-Aldrich, United States). PM thickness of submesothelial tissue was determined by blinded microscope analysis using a metric ocular. The peritoneal thickness in each mouse was calculated by the median of measurements taken every 50 µm from one extreme to the other of the biopsy. The result was used to calculate the group thickness.

For immunofluorescence staining, biopsies of mice were frozen in optimal cutting temperature (OCT) compound and cut into 5 µm sections. To identify the mesothelial cells, we used a mouse anti-cytokeratin (CK) 8/18 (clone 5D3; Novocastra, Newcastle, United Kingdom), which was stained with anti-IgG1–specific Zenon Fab Fragments (Zenon Alexa Fluor 555, Invitrogen) according to the manufacturer's instructions. The $CD45^+$ cells were identified using a rat anti-mouse $CD45^+$ (Clone 16A; Biotin Rat Anti-Mouse CD45RB, BD Biosciences) and stained with goat anti-rat antibody (Alexa Fluor 488, A11006, Invitrogen). Fibroblastoid cells were marked with rabbit anti-mouse FSP-1 (Polyclonal Rabbit Anti-Human S100A4, Dako, Denmark) and stained with goat anti-rabbit antibody (Alexa Fluor 647, A31573, Invitrogen). The nuclei were stained with DAPI (268,298, MERCK). The images were made with a confocal microscope (Laser Scanning Confocal Microscope LSM710 ZEISS).

For immunohistochemistry staining, biopsies were fixed in paraformaldehyde, embedded in paraffin, and cut into 3 µm sections. After paraffin removal with xylol treatment, samples were heated to expose any masked antigens using a Real Target Retrieval Solution containing citrate buffer (pH 6.0, Dako). Samples were pre-treated with Real Peroxidase-Blocking Solution (Dako) to block the endogenous peroxidase. Tissue sections were stained with anti-von Willebrand factor (VWF) (ab6994, Abcam) and counterstained with nuclear hematoxylin. Positive staining was counted and expressed as the mean of 10 independent counts for each animal, quantified at 20x using the analysis program Image-J 1.53 g (National Institute of Health, United States).

The analyses of these staining were done completely blinded, associating a number to each sample that could not be related to the type of treatment.

Rebaudioside A degradation and reabsorption analyses

Since Rebaudioside A is the most abundant compound (62.6%) present in the SG extract, a solution containing Rebaudioside A at 1% was analyzed before and after 40 min of its injection (2 ml) to two C57BL/6JRccHsd mice not submitted to any treatment. The analysis was carried out using HPLC equipment coupled to Q Exacmemtive hybrid quadrupole-orbitrap mass spectrometer (MS) from Thermo

Scientific (Waltham, Massachusetts, United States) with electrospray ionization (ESI) interface in negative mode. For chromatographic separation, an omega Polar C18 column (100 mm × 2.1 mm, particle size 3 µm) from Phenomenex, Madrid, Spain. The mobile phases and separation gradient were used at a flow rate of 0.4 ml/min. Ultrapure water with 0.1% (v/v) of formic acid (solvent A) and ACN with 0.1% (v/v) of formic acid (solvent B), applying a gradient from 0 % to 100% B during 15 min and 100% B were maintained for 2 min and the post-run equilibration time was 5 min. The temperature of the columns was kept at 40°C and the injection volume was 20 µl. MS analyses were performed using the full scan mode of 200–3,000 m/z.

Statistical analyses

All statistical analyses were carried out with GraphPad Prism 8 (GraphPad Software, La Jolla, CA). Comparisons between the groups were performed using the unpaired *t* test or the nonparametric Mann-Whitney U test. The means of the experimental groups were compared by using one-way ANOVA. p values < 0.05 were considered significant.

Results

Steviol glycosides solutions showed ultrafiltration and transport capacities *in vitro*

The dialysis tubing bags containing different solutions were placed in a beaker filled with electrolytes (Na^+, Mg^{2+}, Ca^{2+}, Cl^-) in a lactate buffer and the mass change using artificial membranes was measured up to 24 h. Then, the weight increase (g) of each bag was calculated. SG-based fluids demonstrated a maintained and prolonged weight increase similar to glucose-based fluids, as indicated by the trend of their curves (Figure 1A).

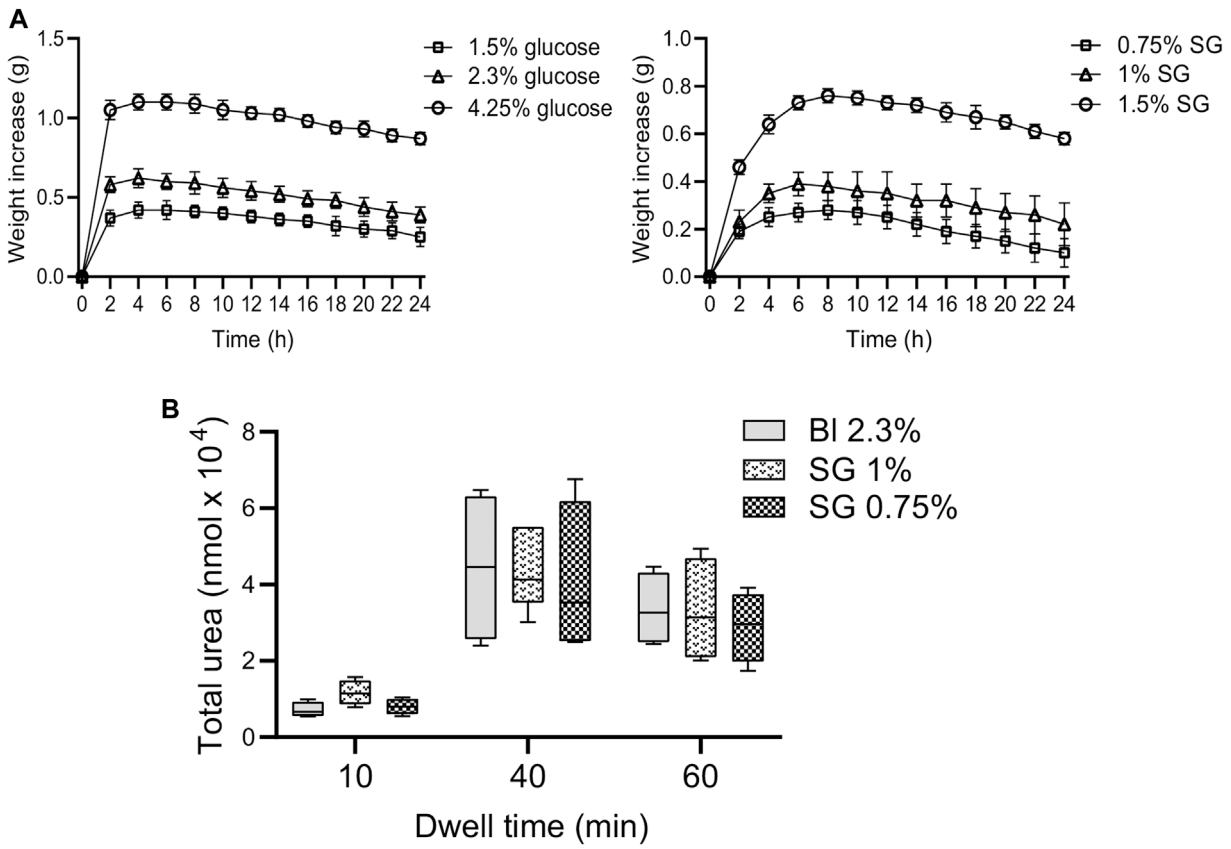

FIGURE 1
Trend curves of glucose and SG-based solutions and total urea measured in effluents. **(A)** Weight change curves of glucose 4.25%, 2.3%, and 1.5%, and SG solutions at 1.5%, 1%, and 0.75% measured at different time points using artificial membranes. Data are represented as mean ± SD of three independent experiments. **(B)** Total urea measured in drained effluents and extracted after 10, 40, and 60 min of dwell. Data are represented as median, maximum, minimum and the first and third quartiles. The analysis of variance results in a non-significant (NS) p-value (two-way ANOVA test).

Calculated crystalloid pressures exerted by SGs at the employed concentrations resulted isotonic to the blood, but the average MW of SG (905.50 Da) resulted in a value of 0.3183 for the reflection coefficient (σ), demonstrating that this compound has colloidal/oncotic osmotic capacity. (Supplementary Figure SC). Results *in vivo* indicated that SG 1% and 0.75% extracted urea from the blood to the peritoneal cavity in a similar-manner as Bl 2.3% after 10, 40, and 60 min (Figure 1B).

Steviol glycosides has less impact on mesothelial cells alterations *in vitro*

Sub-confluents HOMCs cultures were exposed for 48 h to glucose-based PDFs (SS 4.25%, as a positive control, or Bl 2.3%) and SG-based fluids (1% and 0.75%). The control group was incubated with a lactate buffer diluted one-half with a culture medium. MCs were lysed and RNA extracted for analysis by RT-qPCR. Exposure of HOMCs to SS 4.25% resulted in cell death and in changed morphology, becoming elongated after 48 h (Figure 2A). The morphology of HOMCs incubated with Bl 2.3% was slightly changed, which was confirmed by the measurement of levels of standard epithelial and mesenchymal markers by RT-qPCR. Glucose-based PDFs significantly upregulate the expression of Snail1, VEGF-A, and Fibronectin, whereas SG did not show regulation of these markers (Figure 2B). Angiogenic factors FGF-2 and VEGF-A were mainly affected by glucose treatment (Figure 2C). In addition, the expression of E-Cadherin was preserved with SG and Bl 2.3% fluids, while SS 4.25% showed a tendency to decrease this epithelial marker (Figure 2B). In agreement with these results, incubation of Met-5A cell line with Bl 2.3% or SG-based fluids did not have an effect on cellular viability,

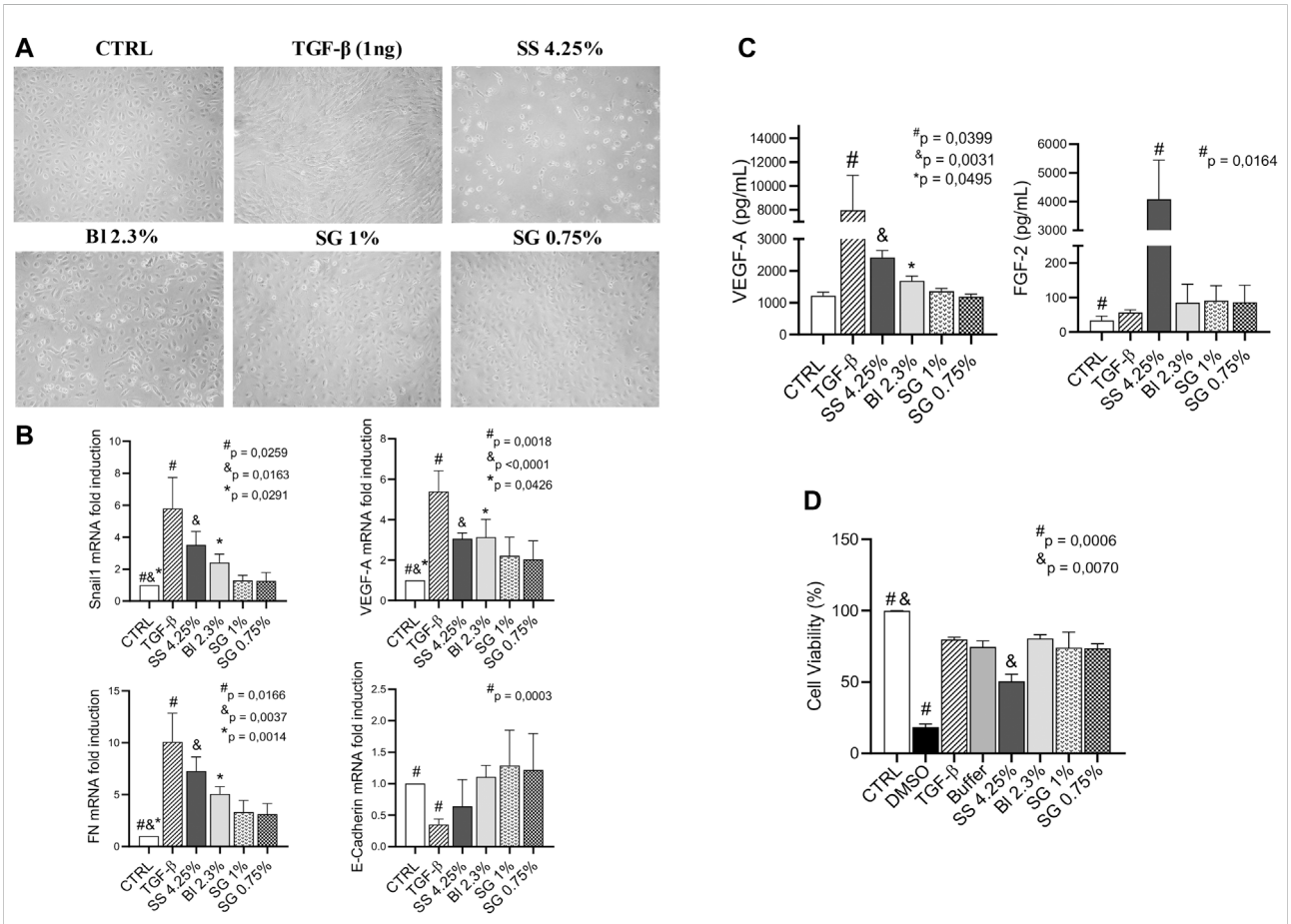

FIGURE 2
Effect of PDFs on HOMCs. **(A)** Effects of lactate buffer (CTRL), TGF-β1 (1 ng/ml), and different PD solutions (glucose and SG-based) on HOMCs morphology at 48 h. Pictures are representative of five independent experiments. **(B)** mRNA levels of different MMT markers analyzed by quantitative RT–qPCR. The results represent the relative expression of Snail1, VEGF-A, Fibronectin (FN), and E-Cadherin. The data are depicted as a mean ± SEM of five independent experiments. The analysis of variance results in a p-value = 0.0028; 0.0044; 0.0011 and NS respectively (one-way ANOVA test). **(C)** VEGF-A and FGF-2 concentration in supernatants analyzed by Luminex 100 (p-value = 0.0009 and 0.0154 respectively, one-way ANOVA). **(D)** Cellular viability of Met-5A incubated with DMSO 5%, TGF-β1 (1 ng/ml), lactate buffer, glucose, and SG-based solutions. The analysis of variance results in a p-value = 0.01 (one-way ANOVA test). Symbols show statistical differences between groups analyzed by the unpaired t test.

whereas incubation with SS 4.25 significantly reduced the cellular viability (Figure 2D).

Steviol glycosides-based PD fluids did not induce significant mesothelial-mesenchymal transition, fibrosis, inflammatory response, or angiogenesis at the peritoneal tissue *in vivo*

The mice were treated with glucose-based and SG-based fluids (2 ml twice per day) for 40 days and the thickness of the PM was evaluated. Masson's trichrome staining of the peritoneal biopsies showed that SG groups had less submesothelial matrix deposition and cell infiltration than glucose-based PDFs (Figure 3A). Morphometric analysis showed that glucose-based PDFs had thicker PMs as compared with SG groups (Figure 3B).

In addition, the number of blood vessels in the submesothelial zone was counted. It was observed that the blood vessels increased in glucose-based PDFs and were not significantly affected in SG groups as compared with control mice (Figure 3C).

Immunofluorescence analysis of peritoneal tissues showed that SS 4.25% induced high recruitment of $CD45^+$ cells (green) in the submesothelial zone and that the MCs layer was not well preserved. Furthermore, it showed an accumulation of fibroblastoid cells expressing FSP-1 (cyan), some of them co-expressed cytokeratin (CK, yellow) that indicates MCs undergo the MMT process; some of them co-expressed $CD45^+$ (gray arrow) showing myofibroblasts originated from bone-marrow-derived circulating cells (fibrocytes). In the Bl 2.3% group, the MC layer was better preserved and $FSP\text{-}1^+$ and $CD45^+$ cells were found in lower numbers than in SS 4.25%. The SG groups showed even better preservation of the mesothelium and $FSP\text{-}1^+$ and $CD45^+$ cells were less abundant (Figure 4).

Steviol glycosides-based solutions induced a milder inflammatory response *in vivo*

Thereafter, the levels of the infiltrating leukocytes were analyzed within the peritoneal cavity after the treatments. The total number of nucleated cells was not affected by SG solutions, while increased in glucose-based PDF in comparison with control (saline-treated) mice (Figure 5A). The level of macrophages was significantly increased in glucose-based groups, whereas the increment was less pronounced in SG groups, although they did not show a significant reduction

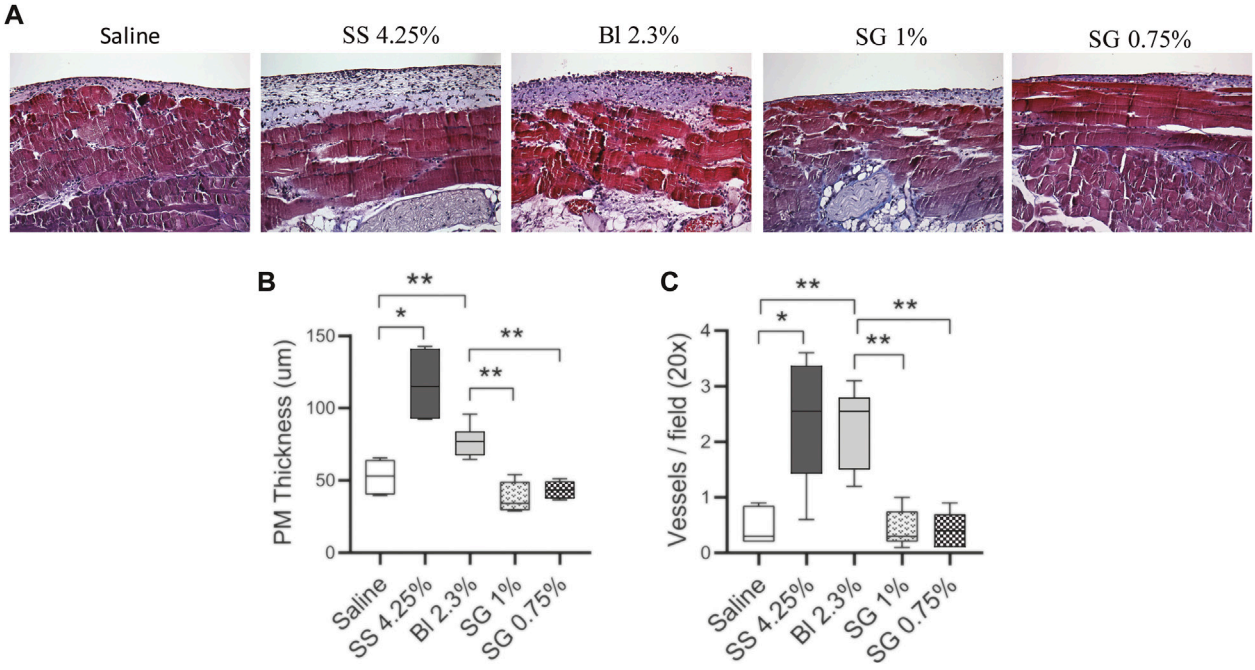

FIGURE 3
Peritoneal membrane alterations in mice. **(A)** Paraffin sections of the PM from all the groups were stained with Masson's trichrome (20X). **(B)** The thickening of PM was determined by morphometric analysis. One-way ANOVA test results in a p-value < 0.0001. **(C)** Quantification of the total VWF positive cells in the PM (p-value < 0.0001, one-way ANOVA). Box plots graphics represent the median, minimum, and maximum values. Symbols represent the statistical differences between the groups analyzed by Mann-Whitney U test (*p < 0.05, **p < 0.01).

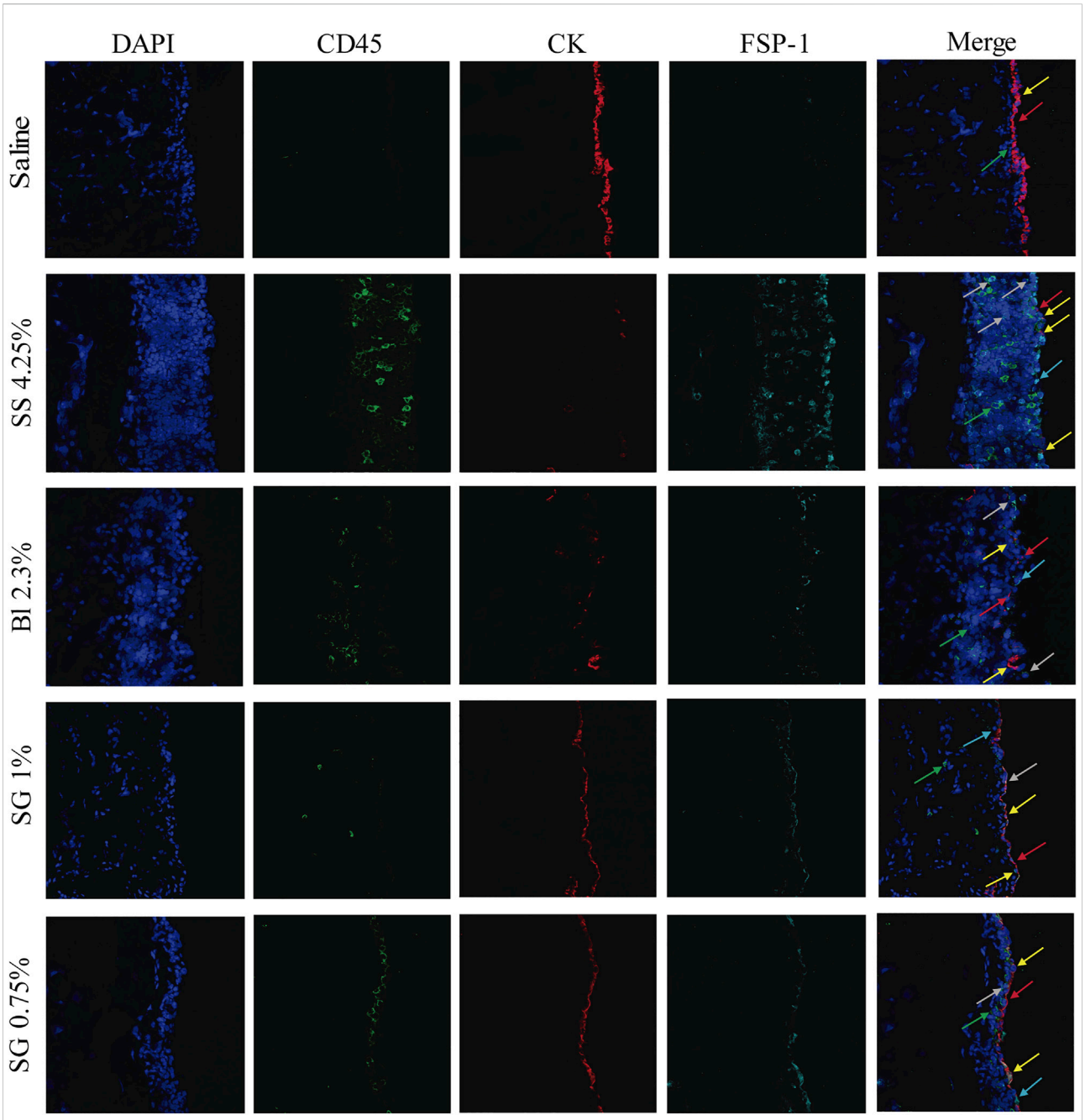

FIGURE 4
Immunofluorescence microscopy analysis of parietal peritoneal tissue sections. The presence of inflammatory (CD45, green), fibroblastoid cells (FSP-1, cyan), and mesothelial cells (Cytokeratin (CK), red) were determined in frozen sections of the PM. Yellow arrows show co-expression of FSP-1 and CK indicating MCs convert into myofibroblast by MMT process. Gray arrows show co-expression of FSP-1 with CD45$^+$ indicating fibrocytes origin. The color balance was equally adjusted by using Image-J 1.53 g. The pictures are representative of each group.

when compared with Bl 2.3% (Figure 5B). Moreover, granulocytes, agents of the innate immune system, tended to increase in glucose-based PDF groups compared with saline and SG solutions (Figure 5C).

In addition, the presence of T cells was analyzed in the peritoneal cavity. The mice group treated with Bl 2.3% had a higher number of CD4$^+$ and CD8$^+$ T cells compared with control, SS 4.25%, and SG-treated mice (Figure 5D).

Regarding soluble factors analyzed in peritoneal washings, IL-6 concentrations do not show differences between groups, while there is an increase of IL-1β in SS 4.25% compared with the other groups, and of TNF-α, IL-17, and IL-22 in Bl 2.3% (Figure 6).

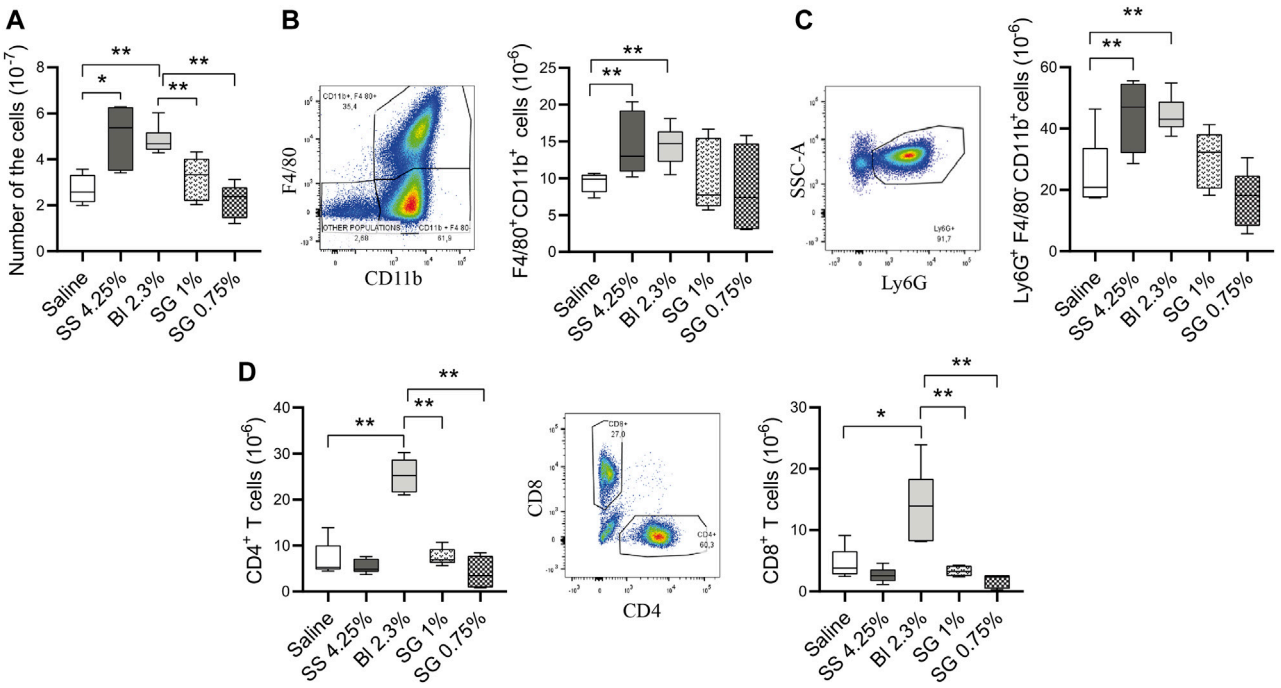

FIGURE 5
Cell populations and inflammatory status at the peritoneal washings. **(A)** Total numbers of nucleated cells. One-way ANOVA test results in a p-value of 0.0033. **(B)** Total numbers of macrophages ($CD11b^+F4/80^+$ cells) (p = NS, one-way ANOVA). **(C)** Total numbers of granulocytes ($Ly6G^+F4/80^-CD11b^+$ cells). One-way ANOVA test results in a p-value of 0.0008. **(D)** Total numbers of $CD3^+CD4^+$ and $CD3^+CD8^+$ T cells (p-value < 0.0001, one-way ANOVA test). Box plots represent the median, minimum, and maximum values. Symbols represent the statistical differences between the groups analyzed by Mann-Whitney U test (*p < 0.05, **p < 0.01).

Rebaudioside A did not degrade in the peritoneal cavity

The main components of the SG extract (Rebaudioside A and Stevioside) were preserved when compared with a pattern sample (data not shown). To explore the possible degradation of SG fluid i.p., its main compound was analyzed by HPLC equipment before and after 40 min dwell in mice. For that, its main compound (Rebaudioside A) was used to facilitate the measurement of degradation products. Rebaudioside A solution at 1% (weight/volume) was analyzed before being injected into mice, and we observed a purity of 96%, with a small amount of Rebaudioside B. Two mice were injected with this solution, and we observed that the proportion of both components remained equally constant after 40 min of dwelling. Therefore, no degradation was observed (data not shown).

Discussion

Using glucose as an osmotic agent in PD has the advantage of being relatively safe and inexpensive, and is a source of calories. However, an increase in glucose absorption leads to worsening control of blood sugar (Daugirdas et al., 2015). The instillation of large amounts of glucose into the peritoneal cavity predisposes patients to hyperglycemia, dyslipidemia, obesity and cardiovascular alterations (Delarue and Maingourd, 2001; Balafa and Krediet, 2012). Long-term PM damage is caused, leastwise partially, by glucose or via GDP and the formation of AGEs, impairing UF (Witowski et al., 2003). The fact that severe peritoneal damage is still observed in patients infused with low-GDP PDFs solutions, suggests that glucose per se has a deteriorating effect on the PM. Moreover, glucose-based PDFs are not very effective in high transporters patients, and inadequate UF may result. High osmolarity itself is also a key factor affecting the biocompatibility of PDFs (Cendoroglo et al., 1998; Wong et al., 2003; Piccapane et al., 2020). Clinical studies have determined that patients who use large concentrations of glucose during the day are at the highest risk for developing a loss of UF capacity (Daugirdas et al., 2015). Continued use of the SS 4.25% PDF could theoretically result in the removal of 7.2–9.6 L per day and cause marked hypernatremia. In practice, this degree of fluid removal is rarely required (Daugirdas et al., 2015). Moreover, glucose-based PDFs are associated with reduced immunological defenses in the peritoneal cavity, since analyses

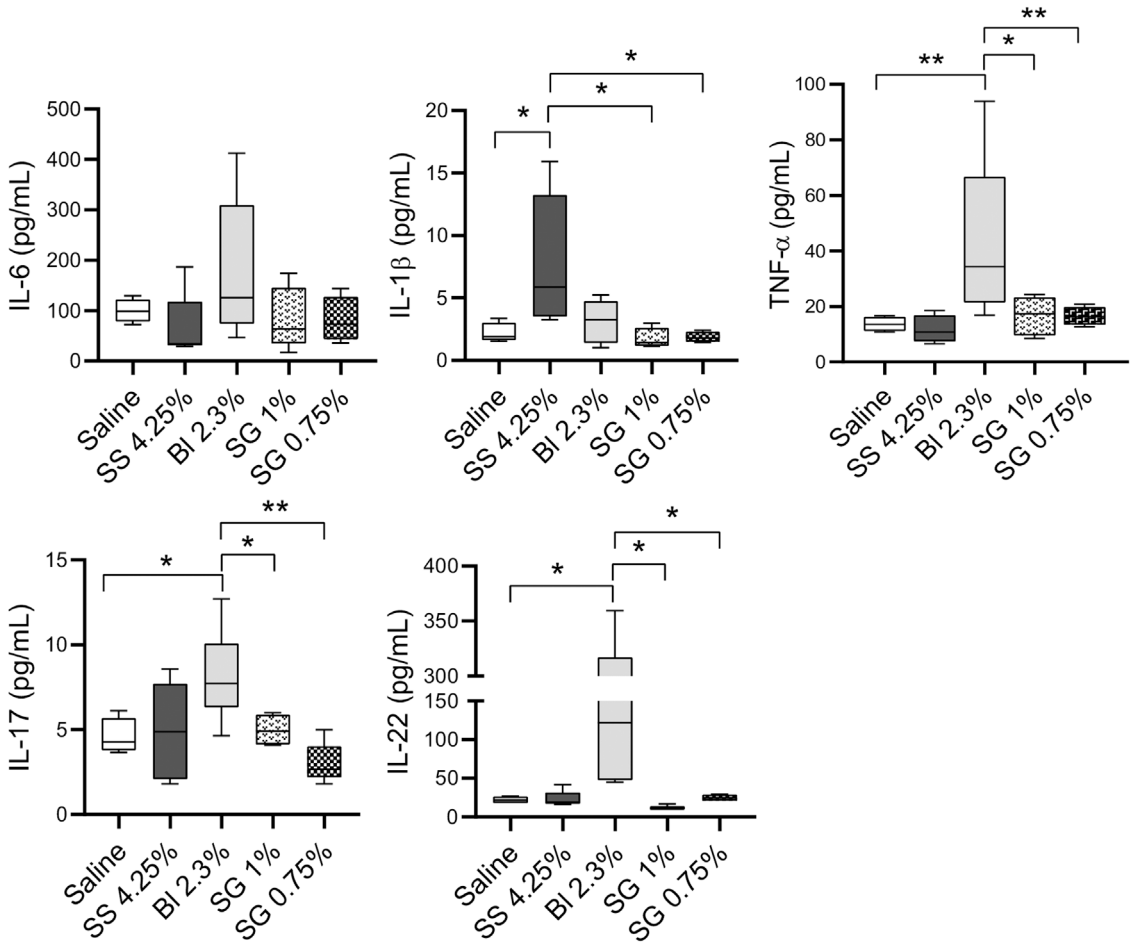

FIGURE 6
Cell populations and inflammatory status at the peritoneal washings. IL-6, IL-1β, TNF-α, IL-17, and IL-22 concentrations at peritoneal washings. One-way ANOVA test results in a *p*-value of 0.0042 for IL-1β, 0.0205 of TNF-α, 0.0059 for IL-17, and NS for IL-6 and IL-22. Box plots represent the median, minimum, and maximum values. Symbols represent the statistical differences between the groups analyzed by Mann-Whitney U test (*$p < 0.05$, **$p < 0.01$)

on leukocytes demonstrate impairment of peritoneal immunocompetence, potentially contributing to an increased risk of PD-related peritonitis (Herzog et al., 2017). Therefore, the use of SS 4.25% glucose-based PDF, which contains high amounts of GDP, is decreasing nowadays worldwide at least for regular exchanges. For these reasons, we selected a glucose concentration of 2.3% (Bl 2.3%) to compare it with the candidate compound.

Regarding the ideal osmotic agent for PDFs, it has been determined that there is an optimal MW balancing the benefits of increasing molecular size (and the increased osmotic efficiency associated with this size increment) and the disadvantage of the increases in solute mass per molecule, (the increasing concentration in g/L). This seems to occur already at MW of around 1,000 Da (Rippe and CarlssOn, 1996). Thereby, given its therapeutic effects and its average MW (905 Da, while glucose is 180 Da), the SG mixture was considered a very interesting candidate for a PDF osmotic agent. In the case of high MW agents, colloid osmotic pressure is particularly relevant. Net ultrafiltration flux is the result of crystalloid and colloid/oncotic pressures (Devuyst and Rippe, 2014). The relationship between these pressures is determined by the Starling equation, which takes into account the reflection coefficient (σ) of the molecules. It indicates the probability of not being reabsorbed through three types of pores (large, small, and ultrasmall) (Rippe and CarlssOn, 1996) into the microvessel blood torrent and is an inherent property of the molecule given the charges, the size, and the topology. The estimated reflection coefficient (σ) of the SG mixture is ten times higher than glucose. It has been demonstrated with icodextrin (average MW = 5,000) that

substances of about 4 nm are expected to be actively reflected by the pores to the peritoneal cavity (Rippe and Levin, 2000; Morelle et al., 2018). Icodextrin entails a mean hydrodynamic radius of 4 nm (1–23 nm), forming 25%–30% of colloidal fractions of highest MW (Morelle et al., 2018). Rebaudioside A, the major SG component, has self-nanomicellizing properties of up to nearly 4 nm (Hou et al., 2019; Song et al., 2020). Micelles are a type of colloid. Thereby, SG osmotic capacity is dependent on oncotic forces.

Using artificial membranes, we observed that 1.5%, 1%, and 0.75% SG-based fluids display prolonged and maintained ability to attract water *in vitro*. Checking *in vivo,* these concentrations (Bl 2.3%, 1% and 0.75% SG) were able to extract the same amount of urea after 10, 40, and 60 min in the peritoneal cavity. Based on the results, these concentrations were chosen for all further experiments.

The next step to determine SG benefits to be used for PDFs was to test the peritoneal status after SG exposure. MCs are the first line of contact of the body with PDFs, suffering alterations related to functional and structural peritoneal damages (Yáñez-Mó et al., 2003). To analyze their behavior in the presence of SG, HOMCs were exposed to the selected concentrations of SG for 48 h and their effects were compared with Bl 2.3% since longer exposition periods strongly affect the viability of cells treated with SS 4.25%. SG solutions did not affect morphology and ameliorate cellular viability in contrast with the deleterious effect of SS 4.25%. The morphology of MCs incubated with Bl 2.3% was slightly changed, as confirmed by standard mesenchymal markers measured by RT-qPCR. Glucose-based fluids induced mesenchymal markers (Snail1, VEGF-A, Fibronectin), while downregulated the epithelial marker (E-Cadherin) in the case of the highest concentration of glucose and GDP (SS 4.25%), which indicates the induction of an MMT process. This agrees with previous observations from our group in which we observed that low-GDP PDFs have less impact *in vitro* on MMT of MCs than a standard PDF (Bajo et al., 2011). None of the mentioned markers were significantly affected by SG treatment. An increasing number of studies indicate direct adverse effects of high glucose concentrations on cellular function. In line with Lee et al. (2004) we have also demonstrated the induction of the fibronectin expression in human peritoneal MCs upon exposure to high glucose in conventional PDF, thus favoring the pathogenesis of peritoneal fibrosis.

We have previously described that VEGF-A levels had marked differences between early (epithelioid phenotype) and advanced (non-epithelioid phenotype) stages of MMT, which in turn correlated with the elliptical factor values of effluent-derived MCs (Ruiz-Carpio et al., 2017). Here, we observed that VEGF-A levels measured by RT-qPCR and ELISA significantly increased when treating cells with glucose-based PDFs, but not with SG solutions. Since MMT plays a central role in the pathogenesis of peritoneal decline during PD (Yáñez-Mó et al., 2003), these results are very promising, as they demonstrate that SG is able to better preserve the epithelial morphology of MCs *in vitro* compared with glucose. In previous studies, it was suggested that FGF-2 and VEGF-A are the most potent angiogenesis inducers and have a synergistic effect on this process (Pepper et al., 1992; Asahara et al., 1995). Here we observed that angiogenic growth factor FGF-2 was mainly affected by SS 4.25% treatment. Previously, it was demonstrated that exposure to high glucose levels caused a concentration-dependent increase of FGF-2 mRNA expression and secretion by HOMCs, indicating that MCs are one of the peritoneal sources of this factor (Ogata et al., 2001).

To go further to unravel the biological effects of SG, we analyzed them *in vivo* in a mice model of peritoneal PDF exposition. It has been previously described that glucose-based PDFs induce fibrosis, angiogenesis, MMT, and leukocyte infiltration within the peritoneum (González-Mateo et al., 2014; Liappas et al., 2016). All these biomarkers are clearly reduced when administering SG solutions in comparison with glucose-based PDFs, which demonstrates that SG is a much more biocompatible solution.

During the peritoneal thickening process, there is a progressive accumulation of myofibroblasts. Here, we show that the accumulation of myofibroblasts is greater in the peritoneal samples from glucose-based PDFs exposed animals than in SG-based PDF treatments. Concretely, in the SS 4.25% group, there is a remarkable infiltration of $CD45^+$ cells, and many of these cells co-express FSP-1, a fibroblastoid cell marker, suggesting that these cells are fibrocytes generated from progenitors of hematopoietic origin that are recruited to the injured tissues (Loureiro et al., 2011). Besides this, SG maintains the integrity of the mesothelial layer, while glucose disrupts it in a concentration-dependent manner. Although the mesothelial layer deteriorates in the SS 4.25% group and most MCs are lost, a significant proportion of the ones that remain in the tissue express FSP-1, indicating that these fibroblastic cells derive from mesothelial cells via MMT (Loureiro et al., 2011).

Moreover, intact mesothelium provides *in vivo* resistance against solute permeation. Damage of intercellular junctions leads to an increase in solute permeability. High glucose concentration, along with high osmolarity, has been probed to damage intercellular junctions in HOMCs (Ito et al., 2000; Ito and Yorioka, 2008). The high paracellular permeability is a characteristic of the so-called “high transporters” PD patients (Correa-Rotter and Cueto-Manzano, 2001), in which the osmotic gradient between the PDF and the blood is rapidly dissipated, leading to poor UF. Taking this into account, SG-based PDF, while preserving the integrity of the mesothelial layer as observed *in vitro* and *in vivo*, and given that its bigger MW reduces the

diffusion speed to the blood of the compound, would guarantee a better UF capacity.

Another fact directly implicated in UF capacity is the number of capillaries. Angiogenesis is an important component of PM failure and it has been associated with alterations in the peritoneal water transport (Krediet et al., 2000). In this study, an increase in the number of vessels per field is observed in the glucose-based PDFs groups compared with control, whereas in SG-based fluids such increase is not produced. This data agrees with the induction of the pro-angiogenic factors VEGF-A and FGF-2 by HOMCs treated with glucose-based PDFs in contrast with cells treated with SG-based fluids, previously observed *in vitro*. This fact indicates again that SG would better maintain UF capacity.

Peritoneal effluent is a source of inflammatory cells recruited to the peritoneal cavity and of biomarkers produced by both, these cells and the ones present in the tissue. Inflammatory processes are key in modulating wound healing, angiogenesis, and fibrosis. It is known that macrophages play an important role in the fibrotic process through the secretion of growth factors. T cells are responsible for the orchestration of inflammatory responses through the secretion of cytokines that play a role in fibrosis by the activation of fibroblasts (Theiss et al., 2005; Doucet et al., 2008) and recruitment of fibrocytes (Shao et al., 2008). Here we observed that peritoneal exposure to glucose-based PDF tended to increase cell numbers in the peritoneal cavity, mainly macrophages ($CD11b^+F4/80^+$ cells). To a lesser extent, there is also a tendency to increase the number of granulocytes ($CD11b^+F4/80^-Ly6G^+$ cells), while SG-based fluids maintained a low number of these cells, similar to the control group.

The numbers of $CD4^+$ and $CD8^+$ T cells increased as well in the Bl 2.3% group as observed before (Aroeira et al., 2009; González-Mateo et al., 2014). Bl 2.3% demonstrated to better maintain HOMCs viability compared with SS 4.25%. Therefore, it could additionally preserve the viability of other cell types and thus exert better immunocompetence than SS 4.25%. It has been suggested that $CD4^+$ T cells are the primary source of IL-17 in the peritoneum of mice treated with PDF and that this cytokine plays an important role in the generation of PDF-induced peritoneal fibrosis in patients and mice exposed to PDF (Rodrigues-Díez et al., 2014). Here there is an increase of IL-17 in the Bl 2.3% group, but not in the others.

In the case of IL-22, is produced by several populations of immune cells at the site of inflammation. Producers are $\alpha\beta$ T cells classes Th1, Th22, and Th17 along with γδ T cells, NKT, ILC3, neutrophil granulocytes, and macrophages (Dudakov et al., 2015). As commented above, T cells and macrophages do significantly increase and total granulocytes tend to enhance in the Bl 2.3% injected mice. Here, IL-22 concentrations in peritoneal washings increase in the Bl 2.3% group compared with the control. IL-22 exerts its effect on non-hematopoietic cells, mainly stromal and epithelial cells, stimulating cell survival and participating in wound healing, and proliferation and synthesis of antimicrobials (Dudakov et al., 2015). It has been described that IL-22 might protect from fibrosis (Gu et al., 2021) and MMT of MCs (Ye et al., 2015). Thus, we hypothesized that this cytokine protects the Bl 2.3% treated group from MMT and fibrosis, counteracting the effect of IL-17.

Moreover, *Stevia* extracts have been proven to downregulate inflammatory-related response markers such as IL-1β and TNF-α (Mehmood et al., 2020; Mostafa et al., 2020). Here we have observed an increase of IL-1β and TNF-α in washings of mice treated with SS 4.25% and Bl 2.3% PDFs respectively, while it is not observed in SG-based fluids-treated mice. Regarding other cytokine production, we have previously observed that IL-6 could slightly increase during long-term PDF exposure, without reaching statistical significance (González-Mateo et al., 2014; Liappas et al., 2016). Here, we also observed no differences among groups in peritoneal washings concentrations.

In addition, it has been described that Rebaudioside A and Stevioside do not undergo browning or caramelization when heated (Joint Expert Committee on Food Additives, 2005). Considering its safety to be used *in vivo*, we evaluated the absorption of SG into the body and its degradation to discard toxicity. It has been shown that the mean absorption rate when using 4.25% and 2.3% of glucose dwelled for 4 h was 64.4% in humans, ranging from 30.6% to 92.4%, (Zuo et al., 2015). Another study revealed absorption of 75% of the initial glucose concentration at the end of a 6 h dwell. The percentage of glucose absorbed overtime was almost identical for the 3 different concentrations used in the clinical practice (1.5%, 2.3%, or 4.25%) (Heimbürger et al., 1992). Studying in isolation Rebaudioside A (with a 3.6% of Rebaudioside B), the majority component of the SGs mixture, we observed absorption of 40%–60% in 40 min in mice exposed to 1% concentration. This component has self-nanomicellizing properties, so it **can** be hypothesized that a percentage of it will form aggregates of bigger size (Hou et al., 2019), leading to a slow absorption rate. Most important is that no degradation was observed, since no other compounds were detected in effluents and the percentages of the Rebaudioside A and B remain invariables, indicating that there is no generation of any toxic metabolic product. Further analyses regarding the possible accumulation of these compounds in the body and their implications should be done in the future.

In this regard, it has been reported that, after oral administration, SG are not modified during their way through the digestive system until the colon. In the colon the Stevioside and the Rebaudioside A are hydrolyzed to Steviol (318.45 Da), although the hydrolysis of Rebaudioside A is slower than that of Stevioside. It has been confirmed that Rebaudioside A showed stability when exposed to *in vitro* matrices simulating stomach and small intestine fluids, with susceptibility to hydrolytic degradation by enteric bacteria

collected from the cecum (Nikiforov et al., 2013). Incubations with rat liver microsomes indicated that it is not expected to be metabolized by the liver enzymes. Plasma concentrations of Rebaudioside A and/or its final hydrolysis product, free/conjugated Steviol, were consistent between animals administered Rebaudioside A in the diet. In humans treated orally with Stevioside, small amounts of Steviol were detected in the plasma, with considerable interindividual variability. A dietary toxicity study (repeated exposure 2000 mg/kg/d Rebaudioside A) observed that there were no treatment-related effects on the general condition and behavior of the animals and no toxicologically relevant, treatment-related effects on hematology, serum chemistry, or urinalysis. Macroscopic and microscopic findings revealed no treatment-related effects on any organ evaluated (Nikiforov et al., 2013). Together with our results, these findings confirm that this compound seems to be free of toxicity at tested concentrations.

Stevioside and/or Steviol affected a variety of biochemical parameters in *in vitro* models, indicating possible anti-hypertensive and anti-glycemic effects. Stevioside and Rebaudioside A have not shown evidence of genotoxicity *in vitro* or *in vivo*. (Joint Expert Committee on Food Additives, 2005).

Novel osmotic agents have also been recently proposed as substitutes for glucose in PDFs, such as xylitol and L-carnitine (Bazzato et al., 1982; Rago et al., 2021). These compounds showed as well interesting properties, and their behavior corresponds to crystalloid osmosis since they have a MW similar to glucose.

Recent studies about glucose sparing (Piccapane et al., 2020; Masola et al., 2021) suggested a combination of two or three osmotic agents replacing a substantial part of glucose to improve the PD solution biocompatibility. The authors maintained some glucose in the PD solution affirming that it is still a key nutrient for patients affected by malnutrition. The suggestion of mixing two or even more osmotic agents for PDFs is not novel, as it was already proposed more than 40 years ago (Khanna et al., 1986). In this regard, to achieve higher osmotic capacities for special requirements, it could be interesting to combine SG and glucose, so that none of the two osmotic agents needs to be present at high concentrations.

A large body of evidence tends to show that *stevia* and SG are safe for human consumption at the dietary level. Nevertheless, their clinical efficacy and safety for PD still require further pre-clinical studies. Therefore, the results of the present report are preliminary and the usefulness of SG as an osmotic agent advocates for more studies to provide in-depth insights into its safety, health benefits, and physiological mechanisms. In any case, this study opens a new door toward a possible new substitute for glucose as an osmotic agent. In conclusion, SG has demonstrated good qualities to be used as an osmotic agent for PDF, with fewer side effects compared with glucose.

Data availability statement

The raw data supporting the conclusions of this article will be made available by the authors, without undue reservation.

Ethics statement

The studies involving human participants were reviewed and approved by Comité de Ética de la Investigación con medicamentos del Hospital Universitario La Paz, HULP: PI-4600. The patients/participants provided their written informed consent to participate in this study. The animal study was reviewed and approved by Consejo Superior de Investigaciones Científicas (CSIC), Ref: PROEX 273/19.

Author contributions

Conceived and designed the experiments: ML-C, JV, DP, and G-TG-M. Performed osmotic capacity analyses: NT, LS, and SS. Molecular stability analyses: DS. Conducted *in vitro* experiments: VK, LP-A, and PA-V. Performed *in vivo* experiments: VK, LP-A, and G-TG-M. Analyzed the data: VK and G-TG-M. Mathematical calculations: E-MA-P. Wrote the paper: VK, ML-C, and G-TG-M. All the authors reviewed the manuscript.

Funding

This project has received funding from the European Union's Horizon 2020 research and innovation program under the Marie Skłodowska-Curie grant agreement No 812699. This work was also supported by a grant (PID 2019-110132RB-I00/AEI/10.13039/501100011033) from the Spanish Ministry of Science and Innovation/Fondo Europeo de Desarrollo Regional (MICINN/FEDER) to ML-C, and the Spanish Ministry of Economy and Competitivity (CTQ 2017-85263-R MINECO/FEDER) to JV. In addition, it was supported by Instituto de Salud Carlos III and FEDER funds (RD16/0009/0015) and Redes de Investigación Cooperativa orientadas al Resultado en Salud (Red RICORS from ISCIII RD21/0005/0018).

Acknowledgments

We would like to specially acknowledge Dr. Abelardo Aguilera Peralta, the person who started this project putting all his efforts to achieve a better quality of life for PD patients, who unfortunately passed away before finishing this work. We thank Carmen Moreno Ortiz (National Center of Biotechnology,

Madrid, Spain) for her help with Luminex technology, and Leonor Nozal Martínez (Center for Applied Chemistry and Biotechnology, Alcalá de Henares, Madrid, Spain) for her help with HPLC-orbitrap equipment.

Conflict of interest

NT, LS, SS, and DP are employers of Fresenius Medical Care D GmbH. The collaboration study has received financial support by FME.

The remaining authors declare that the research was conducted in the absence of any commercial or financial relationships that could be construed as a potential conflict of interest.

Publisher's note

Supplementary material

The Supplementary Material for this article can be found online at: https://www.frontiersin.org/articles/10.3389/fphar.2022.868374/full#supplementary-material

References

Asahara, T., Bauters, C., Zheng, L. P., Takeshita, S., Bunting, S., Ferrara, N., et al. (1995). Synergistic effect of vascular endothelial growth factor and basic fibroblast growth factor on angiogenesis *in vivo*. *Circulation* 92, II365–371. doi:10.1161/01.cir.92.9.365

Aroeira, L. S., Aguilera, A., Selgas, R., Ramírez-Huesca, M., Pérez-Lozano, M. L., Cirugeda, A., et al. (2005). Mesenchymal conversion of mesothelial cells as a mechanism responsible for high solute transport rate in peritoneal dialysis: Role of vascular endothelial growth factor. *Am. J. Kidney Dis.* 46, 938–948. doi:10.1053/j.ajkd.2005.08.011

Aroeira, L. S., Lara-Pezzi, E., Loureiro, J., Aguilera, A., Ramírez-Huesca, M., González-Mateo, G., et al. (2009). Cyclooxygenase-2 mediates dialysate-induced alterations of the peritoneal membrane. *J. Am. Soc. Nephrol.* 20, 582–592. doi:10.1681/ASN.2008020211

Bajo, M. A., Pérez-Lozano, M. L., Albar-Vizcaino, P., del Peso, G., Castro, M.-J., Gonzalez-Mateo, G., et al. (2011). Low-GDP peritoneal dialysis fluid ('balance') has less impact *in vitro* and *ex vivo* on epithelial-to-mesenchymal transition (EMT) of mesothelial cells than a standard fluid. *Nephrol. Dial. Transpl.* 26, 282–291. doi:10.1093/ndt/gfq357

Balafa, O., and Krediet, R. T. (2012). Peritoneal dialysis and cardiovascular disease. *Minerva Urol. E Nefrol. Ital. J. Urol. Nephrol.* 64, 153–162.

Bazzato, G., Coli, U., Landini, S., Fracasso, A., Morachiello, P., Righetto, F., et al. (1982). Xylitol as osmotic agent in CAPD: An alternative to glucose for uremic diabetic patients? *Trans. Am. Soc. Artif. Intern. Organs* 28, 280–286.

Bender, C., Graziano, S., and Zimmermann, B. F. (2015). Study of Stevia rebaudiana Bertoni antioxidant activities and cellular properties. *Int. J. Food Sci. Nutr.* 66, 553–558. doi:10.3109/09637486.2015.1038223

Brulez, H. F., ter Wee, P. M., Snijders, S. V., Donker, A. J., and Verbrugh, H. A. (1999). Mononuclear leucocyte function tests in the assessment of the biocompatibility of peritoneal dialysis fluids. *J. Clin. Pathol.* 52, 901–909. doi:10.1136/jcp.52.12.901

Casas-Grajales, S., Ramos-Tovar, E., Chávez-Estrada, E., Alvarez-Suarez, D., Hernández-Aquino, E., Reyes-Gordillo, K., et al. (2019). Antioxidant and immunomodulatory activity induced by stevioside in liver damage: *In vivo*, *in vitro* and *in silico* assays. *Life Sci.* 224, 187–196. doi:10.1016/j.lfs.2019.03.035

Cendoroglo, M., Sundaram, S., Jaber, B. L., and Pereira, B. J. (1998). Effect of glucose concentration, osmolality, and sterilization process of peritoneal dialysis fluids on cytokine production by peripheral blood mononuclear cells and polymorphonuclear cell functions *in vitro*. *Am. J. Kidney Dis.* 31, 273–282. doi:10.1053/ajkd.1998.v31.pm9469498

Cho, Y., Johnson, D. W., Badve, S. V., Craig, J. C., Strippoli, G. F. M., Wiggins, K. J., et al. (2013). The impact of neutral-pH peritoneal dialysates with reduced glucose degradation products on clinical outcomes in peritoneal dialysis patients. *Kidney Int.* 84, 969–979. doi:10.1038/ki.2013.190

Cho, Y., Johnson, D. W., Craig, J. C., Strippoli, G. F. M., Badve, S. V., Wiggins, K. J., et al. (2014). Biocompatible dialysis fluids for peritoneal dialysis. *Cochrane Database Syst. Rev.* 1, CD007554. doi:10.1002/14651858.CD007554.pub2

Correa-Rotter, R., and Cueto-Manzano, A. (2001). The problem of the high transporter: Is survival decreased? *Perit. Dial. Int.* 21 (3), S75–S79. doi:10.1177/089686080102103s13

Daugirdas, J., Blake, P., and Ing, T. (2015). *Handbook of dialysis*. 5th ed. Philadelphia, PA: Fac. Bookshelf. Available at: https://hsrc.himmelfarb.gwu.edu/books/23.

Davies, S. J., Phillips, L., Griffiths, A. M., Russell, L. H., Naish, P. F., Russell, G. I., et al. (1998). What really happens to people on long-term peritoneal dialysis? *Kidney Int.* 54, 2207–2217. doi:10.1046/j.1523-1755.1998.00180.x

Delarue, J., and Maingourd, C. (2001). Acute metabolic effects of dialysis fluids during CAPD. *Am. J. Kidney Dis.* 37, 103–107. doi:10.1053/ajkd.2001.20762

Devuyst, O., and Rippe, B. (2014). Water transport across the peritoneal membrane. *Kidney Int.* 85, 750–758. doi:10.1038/ki.2013.250

Devuyst, O., Topley, N., and Williams, J. D. (2002). Morphological and functional changes in the dialysed peritoneal cavity: Impact of more biocompatible solutions. *Nephrol. Dial. Transpl.* 17 (3), 12–15. doi:10.1093/ndt/17.suppl_3.12

Doucet, C., Milin, S., Favreau, F., Desurmont, T., Manguy, E., Hébrard, W., et al. (2008). A p38 mitogen-activated protein kinase inhibitor protects against renal damage in a non-heart-beating donor model. *Am. J. Physiol. Ren. Physiol.* 295, F179–F191. doi:10.1152/ajprenal.00252.2007

Dudakov, J. A., Hanash, A. M., and van den Brink, M. R. M. (2015). Interleukin-22: Immunobiology and pathology. *Annu. Rev. Immunol.* 33, 747–785. doi:10.1146/annurev-immunol-032414-112123

García-López, E., Lindholm, B., and Davies, S. (2012). An update on peritoneal dialysis solutions. *Nat. Rev. Nephrol.* 8, 224–233. doi:10.1038/nrneph.2012.13

González-Mateo, G. T., Fernández-Míllara, V., Bellón, T., Liappas, G., Ruiz-Ortega, M., López-Cabrera, M., et al. (2014). Paricalcitol reduces peritoneal fibrosis in mice through the activation of regulatory T cells and reduction in IL-17 production. *PloS One* 9, e108477. doi:10.1371/journal.pone.0108477

González-Mateo, G. T., Pascual-Antón, L., Sandoval, P., Aguilera Peralta, A., and López-Cabrera, M. (2018). Surgical techniques for catheter placement and 5/6 nephrectomy in murine models of peritoneal dialysis. *J. Vis. Exp.* 1, 56746. doi:10.3791/56746

Goyal, S. K., Samsher, null, and Goyal, R. K. (2010). Stevia (Stevia rebaudiana) a bio-sweetener: A review. *Int. J. Food Sci. Nutr.* 61, 1–10. doi:10.3109/09637480903193049

Gu, P., Wang, D., Zhang, J., Wang, X., Chen, Z., Gu, L., et al. (2021). Protective function of interleukin-22 in pulmonary fibrosis. *Clin. Transl. Med.* 11, e509. doi:10.1002/ctm2.509

Heimbürger, O., Waniewski, J., Werynski, A., and Lindholm, B. (1992). A quantitative description of solute and fluid transport during peritoneal dialysis. *Kidney Int.* 41, 1320–1332. doi:10.1038/ki.1992.196

Herzog, R., Kuster, L., Becker, J., Gluexam, T., Pils, D., Spittler, A., et al. (2017). Functional and transcriptomic characterization of peritoneal immune-modulation by

addition of alanyl-glutamine to dialysis fluid. *Sci. Rep.* 7, 6229. doi:10.1038/s41598-017-05872-2

Hou, Y., Wang, H., Zhang, F., Sun, F., Xin, M., Li, M., et al. (2019). Novel self-nanomicellizing solid dispersion based on rebaudioside A: A potential nanoplatform for oral delivery of curcumin. *Int. J. Nanomedicine* 14, 557–571. doi:10.2147/IJN.S191337

Hsieh, M.-H., Chan, P., Sue, Y.-M., Liu, J.-C., Liang, T. H., Huang, T.-Y., et al. (2003). Efficacy and tolerability of oral stevioside in patients with mild essential hypertension: A two-year, randomized, placebo-controlled study. *Clin. Ther.* 25, 2797–2808. doi:10.1016/s0149-2918(03)80334-x

Ito, T., and Yorioka, N. (2008). Peritoneal damage by peritoneal dialysis solutions. *Clin. Exp. Nephrol.* 12, 243–249. doi:10.1007/s10157-008-0032-y

Ito, T., Yorioka, N., Yamamoto, M., Kataoka, K., and Yamakido, M. (2000). Effect of glucose on intercellular junctions of cultured human peritoneal mesothelial cells. *J. Am. Soc. Nephrol.* 11, 1969–1979. doi:10.1681/ASN.V11111969

Joint Expert Committee on Food Additives (2005). in *Evaluation of certain veterinary drug residues in food: Geneva, 8 - 17 June 2004* (Geneva: World Health Organization).

Jörres, A., Topley, N., Gahl, G. M., and Jorres, A. (1992). Biocompatibility of peritoneal dialysis fluids. *Int. J. Artif. Organs* 15, 79–83. doi:10.1177/039139889201500203

Khanna, R., Twardowski, Z. J., and Oreopoulos, D. G. (1986). Osmotic agents for peritoneal dialysis. *Int. J. Artif. Organs* 9, 387–390. doi:10.1177/039139888600900604

Krediet, R. T., Lindholm, B., and Rippe, B. (2000). Pathophysiology of peritoneal membrane failure. *Perit. Dial. Int.* 20 (4), S22–S42. doi:10.1177/089686080002004s03

Krediet, R. T. (1999). The peritoneal membrane in chronic peritoneal dialysis. *Kidney Int.* 55, 341–356. doi:10.1046/j.1523-1755.1999.00264.x

Lee, H. B., Yu, M. R., Song, J. S., and Ha, H. (2004). Reactive oxygen species amplify protein kinase C signaling in high glucose-induced fibronectin expression by human peritoneal mesothelial cells. *Kidney Int.* 65, 1170–1179. doi:10.1111/j.1523-1755.2004.00491.x

Lee, H. Y., Park, H. C., Seo, B. J., Do, J. Y., Yun, S. R., Song, H. Y., et al. (2005). Superior patient survival for continuous ambulatory peritoneal dialysis patients treated with a peritoneal dialysis fluid with neutral pH and low glucose degradation product concentration (Balance). *Perit. Dial. Int.* 25, 248–255. doi:10.1177/089686080502500308

Liappas, G., González-Mateo, G. T., Sánchez-Díaz, R., Lazcano, J. J., Lasarte, S., Matesanz-Marín, A., et al. (2016). Immune-Regulatory molecule CD69 controls peritoneal fibrosis. *J. Am. Soc. Nephrol.* 27, 3561–3576. doi:10.1681/ASN.2015080909

López, V., Pérez, S., Vinuesa, A., Zorzetto, C., and Abian, O. (2016). Stevia rebaudiana ethanolic extract exerts better antioxidant properties and antiproliferative effects in tumour cells than its diterpene glycoside stevioside. *Food Funct.* 7, 2107–2113. doi:10.1039/c5fo01586c

López-Cabrera, M. (2014). Mesenchymal conversion of mesothelial cells is a key event in the pathophysiology of the peritoneum during peritoneal dialysis. *Adv. Med.* 2014, 473134. doi:10.1155/2014/473134

Loureiro, J., Aguilera, A., Selgas, R., Sandoval, P., Albar-Vizcaíno, P., Pérez-Lozano, M. L., et al. (2011). Blocking TGF-β1 protects the peritoneal membrane from dialysate-induced damage. *J. Am. Soc. Nephrol.* 22, 1682–1695. doi:10.1681/ASN.2010111197

Mackenzie, R., Holmes, C. J., Jones, S., Williams, J. D., and Topley, N. (2003). Clinical indices of *in vivo* biocompatibility: The role of *ex vivo* cell function studies and effluent markers in peritoneal dialysis patients. *Kidney Int.* 64, S84–S93. doi:10.1046/j.1523-1755.2003.08809.x

Masola, V., Bonomini, M., Onisto, M., Ferraro, P. M., Arduini, A., and Gambaro, G. (2021). Biological Effects of XyloCore, a Glucose Sparing PD solution, on Mesothelial cells: Focus on Mesothelial-Mesenchymal transition, inflammation and angiogenesis. *Nutrients* 13, 2282. doi:10.3390/nu13072282

McIntyre, C. W. (2007). Update on peritoneal dialysis solutions. *Kidney Int.* 71, 486–490. doi:10.1038/sj.ki.5002109

Mehmood, A., Zhao, L., Ishaq, M., Xin, W., Zhao, L., Wang, C., et al. (2020). Anti-hyperuricemic potential of stevia (Stevia rebaudiana Bertoni) residue extract in hyperuricemic mice. *Food Funct.* 11, 6387–6406. doi:10.1039/c9fo02246e

Mohd-Radzman, N. H., Ismail, W. I. W., Adam, Z., Jaapar, S. S., and Adam, A. (2013). Potential roles of Stevia rebaudiana bertoni in abrogating insulin resistance and diabetes: A review. *Evid. Based. Complement. Altern. Med.* 2013, 718049. doi:10.1155/2013/718049

Momtazi-Borojeni, A. A., Esmaeili, S.-A., Abdollahi, E., and Sahebkar, A. (2017). A review on the Pharmacology and toxicology of steviol glycosides extracted from Stevia rebaudiana. *Curr. Pharm. Des.* 23, 1616–1622. doi:10.2174/1381612822666161021142835

Morelle, J., Sow, A., Fustin, C. A., Fillée, C., Garcia-Lopez, E., Lindholm, B., et al. (2018). Mechanisms of crystalloid versus colloid osmosis across the peritoneal membrane. *J. Am. Soc. Nephrol.* 29, 1875–1886. doi:10.1681/ASN.2017080828

Mostafa, A. F., Elalfy, M. M., Shata, A., and Elhadidy, M. G. (2020). Prophylactic effect of aquatic extract of stevia on acetic acid induced-ulcerative colitis in male rats: A possible role of Nrf2 and PPARγ. *J. Basic Clin. Physiol. Pharmacol.* 32, 1093–1104. doi:10.1515/jbcpp-2020-0039

Nikiforov, A. I., Rihner, M. O., Eapen, A. K., and Thomas, J. A. (2013). Metabolism and toxicity studies supporting the safety of rebaudioside D. *Int. J. Toxicol.* 32, 261–273. doi:10.1177/1091581813492828

Ogata, S., Yorioka, N., and Kohno, N. (2001). Glucose and prednisolone alter basic fibroblast growth factor expression in peritoneal mesothelial cells and fibroblasts. *J. Am. Soc. Nephrol.* 12, 2787–2796. doi:10.1681/ASN.V12122787

Ozbayer, C., Kurt, H., Kalender, S., Ozden, H., Gunes, H. V., Basaran, A., et al. (2011). Effects of Stevia rebaudiana (Bertoni) extract and N-nitro-L-arginine on renal function and ultrastructure of kidney cells in experimental type 2 Diabetes. *J. Med. Food* 14, 1215–1222. doi:10.1089/jmf.2010.0280

Pepper, M. S., Ferrara, N., Orci, L., and Montesano, R. (1992). Potent synergism between vascular endothelial growth factor and basic fibroblast growth factor in the induction of angiogenesis *in vitro*. *Biochem. Biophys. Res. Commun.* 189, 824–831. doi:10.1016/0006-291x(92)92277-5

Periche, A., Castelló, M. L., Heredia, A., and Escriche, I. (2015). Influence of drying method on steviol glycosides and antioxidants in Stevia rebaudiana leaves. *Food Chem.* 172, 1–6. doi:10.1016/j.foodchem.2014.09.029

Piccapane, F., Bonomini, M., Castellano, G., Gerbino, A., Carmosino, M., Svelto, M., et al. (2020). A novel formulation of glucose-sparing peritoneal dialysis solutions with l-carnitine improves biocompatibility on human mesothelial cells. *Int. J. Mol. Sci.* 22, 123. doi:10.3390/ijms22010123

Podkowińska, A., and Formanowicz, D. (2020). Chronic kidney disease as oxidative stress- and inflammatory-mediated cardiovascular disease. *Antioxidants* 9, E752. doi:10.3390/antiox9080752

Qayyum, A., Oei, E. L., Paudel, K., and Fan, S. L. (2015). Increasing the use of biocompatible, glucose-free peritoneal dialysis solutions. *World J. Nephrol.* 4, 92–97. doi:10.5527/wjn.v4.i1.92

Rago, C., Lombardi, T., Di Fulvio, G., Di Liberato, L., Arduini, A., Divino-Filho, J. C., et al. (2021). A new peritoneal dialysis solution containing L-carnitine and xylitol for patients on continuous ambulatory peritoneal dialysis: First clinical experience. *Toxins* 13, 174. doi:10.3390/toxins13030174

Ramos-Tovar, E., Flores-Beltrán, R. E., Galindo-Gómez, S., Vera-Aguilar, E., Diaz-Ruiz, A., Montes, S., et al. (2018). Stevia rebaudiana tea prevents experimental cirrhosis via regulation of NF-κB, Nrf2, transforming growth factor beta, Smad7, and hepatic stellate cell activation. *Phytother. Res.* 32, 2568–2576. doi:10.1002/ptr.6197

Rippe, B., and CarlssOn, O. (1996). Zakaria el-R, null, and Carlsson, OTheoretical analysis of osmotic agents in peritoneal dialysis. What size is an ideal osmotic agent? *Perit. Dial. Int.* 16 (1), 97–103. doi:10.1177/089686089601601s17

Rippe, B., and Levin, L. (2000). Computer simulations of ultrafiltration profiles for an icodextrin-based peritoneal fluid in CAPD. *Kidney Int.* 57, 2546–2556. doi:10.1046/J.1523-1755.2000.00114.X

Rodrigues-Díez, R., Aroeira, L. S., Orejudo, M., Bajo, M.-A., Heffernan, J. J., Rodrigues-Díez, R. R., et al. (2014). IL-17A is a novel player in dialysis-induced peritoneal damage. *Kidney Int.* 86, 303–315. doi:10.1038/ki.2014.33

Ruiz-Carpio, V., Sandoval, P., Aguilera, A., Albar-Vizcaíno, P., Perez-Lozano, M. L., González-Mateo, G. T., et al. (2017). Genomic reprograming analysis of the Mesothelial to Mesenchymal Transition identifies biomarkers in peritoneal dialysis patients. *Sci. Rep.* 7, 44941. doi:10.1038/srep44941

Schilte, M. N., Celie, J. W. A. M., Wee, P. M. ter, Beelen, R. H. J., and van den Born, J. (2009). Factors contributing to peritoneal tissue remodeling in peritoneal dialysis. *Perit. Dial. Int.* 29, 605–617. doi:10.1177/089686080902900604

Shao, D. D., Suresh, R., Vakil, V., Gomer, R. H., and Pilling, D. (2008). Pivotal advance: Th-1 cytokines inhibit, and Th-2 cytokines promote fibrocyte differentiation. *J. Leukoc. Biol.* 83, 1323–1333. doi:10.1189/jlb.1107782

Shivanna, N., Naika, M., Khanum, F., and Kaul, V. K. (2013). Antioxidant, anti-diabetic and renal protective properties of Stevia rebaudiana. *J. Diabetes Complicat.* 27, 103–113. doi:10.1016/j.jdiacomp.2012.10.001

Song, K., Xin, M., Zhang, F., Xie, W., Sun, M., and Wu, X. (2020). Novel ultrasmall nanomicelles based on rebaudioside A: A potential nanoplatform for the ocular delivery of pterostilbene. *Int. J. Pharm.* 577, 119035. doi:10.1016/j.ijpharm.2020.119035

Stylianou, E., Jenner, L. A., Davies, M., Coles, G. A., and Williams, J. D. (1990). Isolation, culture and characterization of human peritoneal mesothelial cells. *Kidney Int.* 37, 1563–1570. doi:10.1038/ki.1990.150

Theiss, A. L., Fuller, C. R., Simmons, J. G., Liu, B., Sartor, R. B., Lund, P. K., et al. (2005). Growth hormone reduces the severity of fibrosis associated with chronic intestinal inflammation. *Gastroenterology* 129, 204–219. doi:10.1053/j.gastro.2005.05.019

Welten, A. G. A., Schalkwijk, C. G., ter Wee, P. M., Meijer, S., van den Born, J., Beelen, R. J. H., et al. (2003). Single exposure of mesothelial cells to glucose degradation products (GDPs) yields early advanced glycation end-products (AGEs) and a proinflammatory response. *Perit. Dial. Int.* 23, 213–221. doi:10.1177/089686080302300301

Witowski, J., Jörres, A., Korybalska, K., Ksiazek, K., Wisniewska-Elnur, J., Bender, T. O., et al. (2003). Glucose degradation products in peritoneal dialysis fluids: Do they harm? *Kidney Int.* 63, S148–S151. doi:10.1046/j.1523-1755.63.s84.18.x

Wong, T. Y. H., Phillips, A. O., Witowski, J., and Topley, N. (2003). Glucose-mediated induction of TGF-beta 1 and MCP-1 in mesothelial cells *in vitro* is osmolality and polyol pathway dependent. *Kidney Int.* 63, 1404–1416. doi:10.1046/j.1523-1755.2003.00883.x

Yáñez-Mó, M., Lara-Pezzi, E., Selgas, R., Ramírez-Huesca, M., Domínguez-Jiménez, C., Jiménez-Heffernan, J. A., et al. (2003). Peritoneal dialysis and epithelial-to-mesenchymal transition of mesothelial cells. *N. Engl. J. Med.* 348, 403–413. doi:10.1056/NEJMoa020809

Ye, Z., Li, M., Mei, Z., Zhen, G., and Zhang, P. (2015). [The effects and mechanisms of interleukin-22 and interferon-γ on epithelial-mesenchymal transition of pleural mesothelial cells]. *Zhonghua Jie He He Hu Xi Za Zhi Zhonghua Jiehe He Huxi Zazhi Chin. J. Tuberc. Respir. Dis.* 38, 501–506.

Zuo, X., Ye, X., Sun, F., Qian, K., Xiang, S., Liang, W., et al. (2015). Glucose absorption in nephropathy patients receiving continuous ambulatory peritoneal dialysis. *Asia Pac. J. Clin. Nutr.* 24, 394–402. doi:10.6133/apjcn.2015.24.3.16

Advantages of publishing in Frontiers

OPEN ACCESS
Articles are free to read for greatest visibility and readership

FAST PUBLICATION
Around 90 days from submission to decision

HIGH QUALITY PEER-REVIEW
Rigorous, collaborative, and constructive peer-review

TRANSPARENT PEER-REVIEW
Editors and reviewers acknowledged by name on published articles

Frontiers
Avenue du Tribunal-Fédéral 34
1005 Lausanne | Switzerland

Visit us: www.frontiersin.org
Contact us: frontiersin.org/about/contact

REPRODUCIBILITY OF RESEARCH
Support open data and methods to enhance research reproducibility

DIGITAL PUBLISHING
Articles designed for optimal readership across devices

FOLLOW US
@frontiersin

IMPACT METRICS
Advanced article metrics track visibility across digital media

EXTENSIVE PROMOTION
Marketing and promotion of impactful research

LOOP RESEARCH NETWORK
Our network increases your article's readership